Methods in Molecular Biology 1174

Springer Protocols

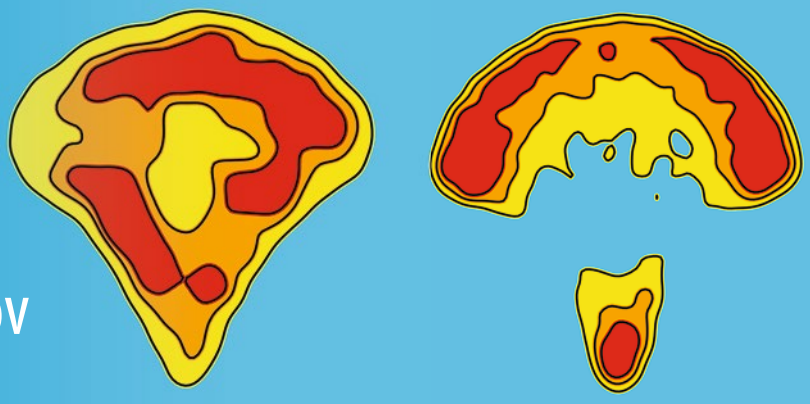

Andrei I. Ivanov
Editor

Exocytosis and Endocytosis

Second Edition

Humana Press

METHODS IN MOLECULAR BIOLOGY

Series Editor
John M. Walker
School of Life Sciences
University of Hertfordshire
Hatfield, Hertfordshire, AL10 9AB, UK

For further volumes:
http://www.springer.com/series/7651

Exocytosis and Endocytosis

Second Edition

Edited by

Andrei I. Ivanov

Department of Human and Molecular Genetics, VCU Institute of Molecular Medicine, Virginia Commonwealth University, Richmond, VA, USA

Humana Press

Editor
Andrei I. Ivanov
Department of Human and Molecular Genetics
VCU Institute of Molecular Medicine
Virginia Commonwealth University
Richmond, VA, USA

ISSN 1064-3745 ISSN 1940-6029 (electronic)
ISBN 978-1-4939-0943-8 ISBN 978-1-4939-0944-5 (eBook)
DOI 10.1007/978-1-4939-0944-5
Springer New York Heidelberg Dordrecht London

Library of Congress Control Number: 2014940962

Printed on acid-free paper

Humana Press is a brand of Springer
Springer is part of Springer Science+Business Media (www.springer.com)

Preface

Studies of membrane trafficking, including vesicle exocytosis and endocytosis, comprise one of the most important and fascinating fields of modern biology. This field was born 50 years ago with the first application of electron microscopy in examining biological samples and it remains an exciting endeavor to this day, as reflected by the 2013 Novel Prize in Physiology and Medicine for the discovery of mechanisms of vesicle fusion. Exocytosis and endocytosis are essential for establishing the complex internal architecture of the cell and for mediating communication between the cell and its environment. At the cellular level, membrane trafficking has many housekeeping and specialized functions including nutrient uptake, regulation of receptor signaling, release of different molecules to the environment, cytokinesis, and cell migration. At the tissue and organ level, exocytosis and endocytosis underlie fundamental physiological processes such as tissue morphogenesis, neuronal synaptic transmission, innate and adaptive immune responses, and secretion of hormones and mediators. This comprehensive role of membrane trafficking yields a diverse and multidisciplinary arena of study, which is driven by consistent progress and cross talk between different areas of biology, chemistry, and physics.

Exocytosis and Endocytosis II is the second edition of a successful collection of methods and protocols published by the Humana Press in 2008. However, this is a completely new book that includes only two updated chapters from the previous edition. While the first edition of Exocytosis and Endocytosis presents classic techniques for examining membrane trafficking and fusion, the present book focuses on recently developed methods of studying exocytosis and endocytosis in vitro and in vivo. The volume begins with two reviews summarizing recent strategies for examining common endocytic and exocytic pathways. Part II (Chapters 3–7) describes cell-free and biochemical assays of exocytosis and endocytosis including unbiased proteome-based analysis of protein ubiquitination and secretion. Part III (Chapters 8–21) presents assays of exocytosis and endocytosis in cultured cells. It focuses on live cell imaging and ultrastructural analysis of membrane trafficking and describes novel protein tags, fixation protocols, and computational approaches to monitor intracellular vesicles and organelles. Part IV (Chapters 22–29) describes how to examine endocytosis and exocytosis in model organisms. These chapters outline powerful in vivo imaging approaches to investigate different physiological processes involving vesicle trafficking.

Exocytosis and Endocytosis II targets a large variety of researchers including cell biologists studying the mechanisms of membrane trafficking, along with physiologists, developmental biologists, immunologists, and neurobiologists, whose research interests focus on cellular processes regulated by exocytosis and endocytosis. This volume contains comprehensive and easy to follow protocols that should be helpful to both seasoned researchers as well as newcomers to the field.

I would like to thank all the contributors for sharing their expertise and carefully guiding readers through all the nuanced details of their techniques. I am very grateful to the series editor, Dr. John Walker, for his help during the editing process. I would also like to acknowledge Alex Feygin for his valuable assistance in proofreading and organizing this volume.

Richmond, VA, USA ***Andrei I. Ivanov***

Contents

Contributors

Arun Anantharam • *Department of Biological Sciences, Wayne State University, Detroit, MI, USA*

Arianna Bellucci • *Division of Pharmacology, Department of Molecular and Translational Medicine, University of Brescia, Brescia, Italy*

Gaelle Boncompain • *Institut Curie, Paris, France*

Michael J. Caplan • *Department of Cellular and Molecular Physiology, Yale University School of Medicine, New Haven, CT, USA*

Milton P. Charlton • *Department of Physiology, University of Toronto, Toronto, ON, Canada*

Jeffrey S. Dason • *Department of Physiology, University of Toronto, Toronto, ON, Canada*

Alessia Deglincerti • *Department of Pharmacology, Weill Medical College, Cornell University, New York, NY, USA*

Mark Donowitz • *GI Division, Department of Medicine, Johns Hopkins University School of Medicine, Baltimore, MD, USA*

Francesca Di Nunzio • *Unité de Virologie Moléculaire et Vaccination, Institut Pasteur, Paris, France*

Katrin Eichelbaum • *Genome Biology Unit, European Molecular Biology Laboratory, Heidelberg, Germany*

Glen A. Farr • *Department of Cellular & Molecular Physiology, Yale University School of Medicine, New Haven, CT, USA*

Chiara Fiorentini • *Division of Pharmacology, Department of Molecular and Translational Medicine, University of Brescia, Brescia, Italy*

Marc Fransen • *Laboratory of Lipid Biochemistry and Protein Interactions, Department of Cellular and Molecular Medicine, Faculty of Medicine, Katholieke Universiteit Leuven, Leuven, Belgium*

Milos Galic • *Department of Chemical and Systems Biology, Stanford University, Stanford, CA, USA; Institute of Medical Physics and Biophysics, University of Münster, Münster, Germany; Cluster of Excellence EXC 1003, Cells in Motion, Münster, Germany*

Bruno Goud • *Unité Mixte de Recherche, Institut Curie, Paris, France*

Jean-Philippe Grossier • *Unité Mixte de Recherche, Institut Curie, Paris, France*

Yoshimi Haga • *Glycometabolome Team, Systems Glycobiology Research Group, RIKEN-Max Planck Joint Research Center for Systems Chemical Biology, RIKEN Global Research Cluster, Wako, Saitama, Japan*

Glenn R. Hicks • *Department of Botany and Plant Sciences, Institute for Integrative Genome Biology, University of California, Riverside, CA, USA*

Michael Hull • *Department of Cellular and Molecular Physiology, Yale University School of Medicine, New Haven, CT, USA*

Takanari Inoue • *Department of Cell Biology, Center for Cell Dynamics, Johns Hopkins University, Baltimore, MD, USA*

Andrei I. Ivanov • *Department of Human and Molecular Genetics, VCU Institute of Molecular Medicine, Virginia Commonwealth University, Richmond, VA, USA*

Samie R. Jaffrey • *Department of Pharmacology, Weill Medical College, Cornell University, New York, NY, USA*
Sangmoo Jeong • *Department of Electrical Engineering, Stanford University, Stanford, CA, USA*
Anupma Jha • *Department of Cell Biology, University of Pittsburgh School of Medicine, Pittsburgh, PA, USA*
Nuria Jiménez • *Biology Department, Faculty of Science, Utrecht University, Utrecht, The Netherlands*
Matthia A. Karreman • *Cell Biology and Biophysics Unit, European Molecular Biology Laboratory, Heidelberg, Germany*
Anton Khmelinskii • *Zentrum für Molekulare Biologie der Universität Heidelberg, Heidelberg, Germany*
Michael Knop • *Zentrum für Molekulare Biologie der Universität Heidelberg, DKFZ-ZMBH Alliance, Heidelberg, Germany*
Toru Komatsu • *Graduate School of Pharmaceutical Sciences, The University of Tokyo, Tokyo, Japan*
Sandhya P. Koushika • *Department of Biological Sciences, DBS-TIFR, Tata Institute of Fundamental Research, Mumbai, Maharashtra, India*
Jeroen Krijgsveld • *Genome Biology Unit, European Molecular Biology Laboratory, Heidelberg, Germany*
Lena Kühling • *Emmy Noether Group: Virus Endocytosis, Institutes of Molecular Virology and Medical Biochemistry, ZMBE, University of Münster, Münster, Germany*
Mickaël Lelek • *Unité Imagerie et Modélisation, Institut Pasteur, Paris, France*
Xuhang Li • *GI Division, Department of Medicine, Johns Hopkins University School of Medicine, Baltimore, MD, USA*
Andrius Masedunskas • *Oral and Pharyngeal Cancer Branch, National Institute of Dental and Craniofacial Research, National Institutes of Health, Bethesda, MD, USA*
Oleg Milberg • *Oral and Pharyngeal Cancer Branch, National Institute of Dental and Craniofacial Research, National Institutes of Health, Bethesda, MD, USA*
Cristina Missale • *Division of Pharmacology, Department of Molecular and Translational Medicine, University of Brescia, Brescia, Italy*
Kensaku Mizuno • *Department of Biomolecular Sciences, Graduate School of Life Sciences, Tohoku University, Sendai, Miyagi, Japan*
Sudip Mondal • *Department of Mechanical Engineering, University of Texas at Austin, Austin, TX, USA*
Lorena Norambuena • *Plant Molecular Biology Laboratory, Department of Biology, Faculty of Sciences, University of Chile, Santiago, Chile*
Kazumasa Ohashi • *Graduate School of Life Sciences, Tohoku University, Sendai, Miyagi, Japan*
Jeremy S. Paige • *Department of Pharmacology, Weill Medical College, Cornell University, New York, NY, USA*
Daniel R. Passmore • *Department of Biological Sciences, Wayne State University, Detroit, MI, USA*
Franck Perez • *Institut Curie, CNRS UMR144, Paris, France*
Hidde L.Ploegh • *Whitehead Institute for Biomedical Research, Cambridge, MA, USA*
Jan A. Post • *Cell Biology, Biology Department, Science Faculty, Utrecht University, Utrecht, The Netherlands*
Dmitry Poteryaev • *Biozentrum, University of Basel, Basel, Switzerland*

Tejeshwar Rao • *Department of Biological Sciences, Wayne State University, Detroit, MI, USA*
Cecilia Rodriguez-Furlán • *Department of Biology, Faculty of Sciences, University of Chile, Santiago, Chile*
Kristine Schauer • *Molecular Mechanisms of Intracellular Transport, Institut Curie/ CNRS UMR 144, Paris, France*
Mario Schelhaas • *Emmy Noether Group: Virus Endocytosis, Institutes of Molecular Virology and Medical Biochemistry, ZMBE, Westphalian Wilhelms University of Münster, Münster, Germany*
Antje Schmidt • *Leibniz-Institut für Molekulare Pharmacologie, Berlin, Germany*
Ralf Schülen • *Leibniz-Institut für Molekulare Pharmacologie, Berlin, Germany*
Akiko Shitara • *Division of Biochemistry, Department of Oral Biology, School of Dentistry, Health Sciences University of Hokkaido, Ishikari, Hokkaido, Japan*
Jachen A. Solinger • *Biozentrum, University of Basel, Basel, Switzerland*
Anne Spang • *Biozentrum, University of Basel, Basel, Switzerland*
PierFranco Spano • *Division of Pharmacology, Department of Molecular and Translational Medicine, University of Brescia, Brescia, Italy*
Emily H. Stoops • *Department of Cellular and Molecular Physiology, Yale University School of Medicine, New Haven, CT, USA*
Karin Strijbis • *Department of Infectious Diseases & Immunology, Utrecht University, Utrecht, The Netherlands*
Tadashi Suzuki • *Glycometabolome Team, Systems Glycobiology Research Group, RIKEN-Max Planck Joint Research Center for Systems Chemical Biology, RIKEN Global Research Cluster, Wako, Saitama, Japan*
Taishin Takuma • *Division of Biochemistry, Department of Oral Biology, School of Dentistry, Health Sciences University of Hokkaido, Ishikari, Hokkaido, Japan*
Anke Teichmann • *Leibniz-Institut für Molekulare Pharmacologie, Berlin, Germany*
Peter Thorn • *School of Biomedical Sciences, University of Queensland, St. Lucia, QLD, Australia*
Muhibullah Tora • *Oral and Pharyngeal Cancer Branch, National Institute of Dental and Craniofacial Research, National Institutes of Health, Bethesda, MD, USA*
Linton M. Traub • *Department of Cell Biology, University of Pittsburgh School of Medicine, Pittsburgh, PA, USA*
Elly G. Van Donselaar • *Faculty of Science, Utrecht University, Utrecht, The Netherlands*
Oleg Varlamov • *Division of Diabetes, Obesity, & Metabolism, Oregon National Primate Research Center, Beaverton, OR, USA*
Roberto Weigert • *Oral and Pharyngeal Cancer Branch, Intracellular Membrane Trafficking Unit, National Institute of Dental and Craniofacial Research, National Institutes of Health, Bethesda, MD, USA*
Burkhard Wiesner • *Leibniz-Institut für Molekulare Pharmacologie, Berlin, Germany*
Guoqiang Xu • *Jiangsu Key Laboratory of Translational Research and Therapy for Neuro-Psycho-Diseases and College of Pharmaceutical Sciences, Soochow University, Suzhou, Jiangsu, China*
Michela Zaltieri • *Division of Pharmacology, Department of Molecular and Translational Medicine, University of Brescia, Brescia, Italy*
Christophe Zimmer • *Unité Imagerie et Modélisation, CNRS URA 2582, Institut Pasteur, Paris, France*

Part I

An Overview of Methods for Analyzing Vesicular Trafficking

Chapter 1

Pharmacological Inhibitors of Exocytosis and Endocytosis: Novel Bullets for Old Targets

Andrei I. Ivanov

Abstract

Pharmacological inhibitors of vesicle trafficking possess great promise as valuable analytical tools for the study of a variety of biological processes and as potential therapeutic agents to fight microbial infections and cancer. However, many commonly used trafficking inhibitors are characterized by poor selectivity that diminishes their use in solving basic problems of cell biology or drug development. Recent high-throughput chemical screens intensified the search for novel modulators of vesicle trafficking, and successfully identified a number of small molecules that inhibit exocytosis and endocytosis in different types of mammalian cells. This chapter provides a systematic overview of recently discovered inhibitors of vesicle trafficking. It describes cellular effects and mechanisms of action of novel inhibitors of exocytosis and endocytosis. Furthermore, it pays special attention to the selectivity and possible off-target effects of these inhibitors.

Key words Endoplasmic reticulum, Golgi, Endosomes, Lysosomes, Clathrin, Dynamin, ARF GTPases, High-throughput screen, Selectivity

1 Introduction

Vesicle trafficking is a fundamental feature of eukaryotic cells that plays key roles in creating the complex interior architecture of the cell and mediating communication between the cell and its environment. This process involves bidirectional fluxes of membrane-coated vesicles transitioning in and out of the cell surface. The process of delivery and fusion of intracellular vesicles with the plasma membrane is known as exocytosis, whereas inward cytosolic movement of plasma membrane derived vesicles is termed endocytosis. Exocytosis and endocytosis serve a variety of housekeeping and specialized cellular functions. The former includes formation of different intracellular organelles, nutrient uptake and processing, modulation of cell surface receptor signaling, regulation of cell shape and volume, while the latter encompasses neuronal synaptic transmission, secretion of enzymes, hormones, and other bioactive molecules, regulation of cell migration, and immune defense functions.

Andrei I. Ivanov (ed.), *Exocytosis and Endocytosis*, Methods in Molecular Biology, vol. 1174,
DOI 10.1007/978-1-4939-0944-5_1,

Vesicular trafficking is controlled by a large number of specialized structural, signaling, and motor proteins that mediate bending, fission, and fusion of phospholipid membranes as well as movement and docking of vesicles to different intracellular compartments [1, 2]. Studies that targeted individual trafficking regulators markedly improved our understanding of many molecular events involved in the biogenesis of transport vesicles. The most common strategy of studying exocytosis and endocytosis involves inactivation of trafficking proteins using gene deletion, overexpression of dominant-negative mutants, or expressional downregulation via RNA interference. However, these genetic approaches have two potential drawbacks. One is a frequent lack of functional effects after inhibition of individual trafficking regulators that reflects redundancy within the exocytic and endocytic pathways [3]. The opposite problem arises from the fact that some trafficking proteins control vital cellular functions and their prolonged inactivation results in cell death [4]. One can then surmise that the aforementioned problems with the various genetic approaches can be avoided if small molecules are used to inhibit specific steps of exocytosis and endocytosis. Indeed, pharmacological inhibitors are usually effective against different members of the same protein family, thereby overcoming any functional redundancy. Furthermore, small molecules can be efficient during short-term treatments that do not affect long-term cell viability. However, despite these advantages, application of small molecules to study exocytosis and endocytosis is still limited by their poor selectivity. For example, a comprehensive analysis of the available literature published in the first edition of this book clearly demonstrated that classical pharmacological inhibitors of three major endocytosis pathways lack genuine selectivity due to cross-inhibition of alternative internalization pathways and effects on the cellular cytoskeleton [5].

Recent development of large-scale chemical compound screens provides a unique opportunity to identify novel inhibitors of vesicle trafficking. There are two major types of chemical genetic screens, forward and reverse [6]. The forward screen involves unbiased monitoring for a specific cellular phenotype such as inhibition of a trafficking pathway or disruption of a specific cellular organelle. For example, trafficking of GFP-fused vesicular stomatitis virus (VSVG-GFP) is commonly used in high-throughput screens for exocytosis inhibitors [6]. Reverse chemical genetics aims to biochemically identify compounds that inactivate known regulators of membrane trafficking with subsequent verification of their activity in cell-based assays. Recently conducted forward and reverse chemical genetic screens significantly expanded our repertoire of small molecular compounds that interfere with vesicle trafficking [6, 7]. The present chapter provides a systematic overview of these new pharmacological tools ability to inhibit exocytosis and endocytosis in mammalian cells. Cellular effects and molecular

targets of these compounds are discussed while also addressing the question of their specificity to help rationalize the application of new inhibitors in studies of mechanisms and biological roles of vesicle trafficking.

2 Small Molecular Inhibitors of Exocytosis

Exocytosis is a key mechanism involved in the formation and maintenance of different intracellular compartments and the release of various substances from the cell. Protein secretion is a classic example of exocytosis [2]. This process starts in the endoplasmic reticulum (ER) where newly synthesized proteins are packaged into coat protein (COP)II-covered vesicles that bud from ER exit sites (ERES) and deliver their cargo to the Golgi complex. Next, the proteins travel through the Golgi to reach the compartment that faces the plasma membrane; this is called a *trans*-Golgi network (TGN). In TGN, secreted proteins are packed into clathrin-coated vesicles that are delivered to the plasma membrane either directly or via intermediate steps involving fusion with endosomal compartments [2]. The plasma membrane is not the only destination for TGN-derived vesicles, since TGN is also involved in the sorting of proteins and lipid destined for different intracellular organelles such as lysosomes and mitochondria.

2.1 Inhibitors of the ER and ER-to-Golgi Trafficking

Processing of newly synthesized protein cargo in the ER cisternae and subsequent packaging into ER-derived vesicles are crucial initial stages in exocytosis. These stages have been subjected to numerous genetic manipulations, yet only a few chemical compounds are known to inhibit vesicle trafficking at the ER (Table 1).

For example, a small molecule, Eeyarestatin I (ESI), blocks protein secretion in mammalian cells by attenuating translocation of newly synthesized polypeptides from the cytosolic face of the ER membrane into the ER lumen [8]. Evidence suggests that ESI inhibits functions of the Sec61 complex that forms the membrane pore used for the translocation of ER-targeted nascent polypeptides [8]. It is of note that ESI does not possess absolute selectivity toward Sec61. This small molecule was initially discovered as an inhibitor of ER-associated protein degradation [32]. Subsequent studies demonstrated that ESI affects this process by binding to p97 large ATPase and blocking its activity toward polyubiquitinated substrates targeted for proteosomal degradation [33]. ESI demonstrates substantial toxicity for different cancer cells and is considered a potential anticancer agent [34]. However, it remains unclear which of two targets, Sec61 or p97, is responsible for the described antitumor activity of this compound.

Sec61 also was found to be a primary target of "cotransins"; a class of cyclic heptadepsipeptides that inhibit processing of different

Table 1
Novel pharmacological inhibitors of vesicle trafficking pathways

Trafficking step	Inhibitor	Molecular target	Other effects	References
ER	Eeyarestatin I	Sec61 complex	p97 Inhibition	[8]
ER	Cotransins	Sec61 complex		[9, 10]
ER-to-Golgi	CI-976	Lysophospholipid transferases		[11]
ER-to-Golgi	Dispergo	Unknown		[12]
ER-to-Golgi	Apogossypol	Unknown	Bcl-2 inhibition	[13]
ER-to-Golgi	FLI-06	Unknown		[14]
Golgi	AMF-26	ARF1	Disruption of recycling endosomes	[15]
Golgi	Golgicide A	GBF1		[16]
Golgi	Exo2 and LG186	GBF1		[17, 18]
Golgi	Exo1	Unknown		[18]
Golgi	AG1478	GBF1 (?)	EGF receptor inhibition	[19]
Golgi	LM11	ARF1-ARNO complex		[20]
Golgi	Secramine A	Cdc42	Effects on the actin cytoskeleton	[21]
Golgi	ZCL278	Cdc42	Effects on the actin cytoskeleton	[22]
Clathrin-mediated endocytosis	Pitstop-1 and pitstop-2	Clathrin heavy chain	Inhibition of non-clathrin endocytosis	[23]
Endocytosis	Dynasore	Dynamin	Disruption of the actin cytoskeleton	[24]
Endocytosis	MiTMAB	Dynamin		[25]
Endosomes to cell surface	16D10	Endosomal V-ATPase		[26]
TGN to endosomes	Compound A5	AP-1 (?)		[27]
Lysosomal exocytosis	Vacuolin-1	Unknown		[28]
Endosomes to TGN	Retro-1 and Retro-2	Unknown		[29]
Endosomes to TGN or cell surface	Compounds 75 and 134	Unknown		[30]
Early to late endosomes	YM201636	PIKfyve	Effects on autophagy	[31]

secreted and transmembrane proteins [9, 10]. It is believed that cotransins prevent recognition of the signaling sequence of newly synthesized proteins by the Sec61 complex. Interestingly, small modification to cotransin structure has a dramatic effect on their specificity. For example, a so-called CT09 cotransin potently inhibits secretion of 25 tested proteins, whereas a related substance, CT08, demonstrates a high selectivity toward vascular cellular adhesive molecule-1 and tumor necrosis factor-alpha [35]. Since studies of cotransins were narrowly focused on protein translocation in the ER, it remains unclear if these inhibitors also affect general ER structure or trafficking of ER-derived vesicles. Some small molecular compounds block late stages of ER-dependent membrane transport that involve assembly of COPII coated vesicles. One example is CI-976, an inhibitor of phospholipid-generating enzymes, lysophospholipid transferases [11]. CI-976 inhibits the processing and transport of VSVG-GFP from the ER and induces retention of COPII-coated vesicles at the ERES. Interestingly, recent high-throughput screens yielded several new compounds that block the assembly of Golgi-directed vesicles at the ER. One such compound is a derivative of a natural product, carpanone, named "dispergo" [12]. Dispergo was shown to attenuate protein secretion by selectively inhibiting cargo recruitment to the ERES. This compound causes early ER tubulation with subsequent formation of dense ER patches, which can be explained by inhibition of anterograde trafficking of ER-derived vesicles [12]. Such traffic blockage induces Golgi fragmentation but does not alter endocytosis or the morphology of different endosomal compartments. Formation of dense ER membrane patches is also induced by other chemical agents including a Bcl inhibitor, apogossypol, store-operated calcium channel blockers, and an inhibitor of sphingolipid synthesis, phenyl-2-decanoyl-amino-3-morpholino-1-propanol hydrochloride [13, 36, 37]. Although the exact mechanisms of such reorganizations of the ER membrane remain unclear, they have been linked to altered homeostasis of calcium and sodium ions [13, 37]. Formation of dense membrane patches is not the only phenotype caused by chemical inhibitors of ER trafficking. A recent compound screen of Notch signaling inhibitors identified a dihydropyridine compound, FLI-06 that converts ER tubules into large sheet-like structures [14]. Since FLI-06 blocks cargo recruitment to the ERES, the observed formation of membrane sheets is likely to represent another morphological manifestation of the gain in ER membrane due to inhibition of vesicle export from the ER.

2.2 Inhibitors of Golgi Structure and Functions

The Golgi complex was the first organelle involved in exocytosis whose functions were probed with small molecules. The most known Golgi inhibitor is the fungal macrocyclic lactone, Brefeldin A (BFA), which inhibits exocytic trafficking and markedly alters Golgi morphology. BFA treatment induces Golgi tubulation with

eventual redistribution of Golgi membranes into the ER [38–40]. This inhibitor also disrupts different endosomal compartments resulting in their fusion with the TGN [41]. BFA is a popular tool to examine Golgi structure, and dynamics and mechanisms of its action have been extensively investigated. This agent interferes with the activity of Golgi-resident ARF small GTPases [38] that are critical for anterograde intra-Golgi vesicle trafficking [42, 43]. As with other small GTPases, ARFs exist in active, GTP-bound and inactive, GDP-bound forms and their activation involves interactions with specific guanine exchange factors (GEF). BFA targets a complex of ARF-GDP with GEFs possessing the Sec7 domain. This results in complex stabilization thereby inhibiting GDP/GTP exchange and ARF activation [44]. There are three different Sec7 domains containing GEFs, BIG1 (BFA-inhibited 1), BIG2 (BFA-inhibited 2), and GBF1 (Golgi-associated BFA-resistant 1), that are sensitive to BFA inhibition [45–47]. Selective inhibition of ARF-dependent anterograde membrane flux by BFA results in fragmentation of the Golgi ribbon and retrograde relocalization of the Golgi contents into the ER.

For a long period BFA remained the unique pharmacological tool to directly probe Golgi dynamics and functions. Other known Golgi-disrupting agents such as monensin, bafilomycin, okadaic acids, and nocodazole affect this organelle indirectly by inhibiting different non-Golgi targets [48]. However, high-throughput compound screens conducted over the last decade have identified several new molecules that target Golgi-dependent trafficking by mechanisms that are either similar or different from BFA actions. One compound that mimics the major effects of BFA is a structurally unrelated octahydronaphthalene derivative, AMF-26 [15]. A side by side comparison of AMF-26 and BFA revealed that both compounds disrupt the Golgi, the ER-Golgi intermediate compartment (ERGIC), and recycling endosomes, with similar potency. Similarly to BFA, AMF-26 inactivates ARF1 but mechanisms of this inactivation have not been elucidated [15]. Another recently discovered compound is a selective inhibitor of GBF1, Golgicide A (GA) [16]. GA was shown to bind within the intercellular cleft formed between ARF1 and the Sec7 domain of GBF1. Importantly, this binding involves unique amino acid residues of GBF1 that are lacking in other ARF GEFs. GA induces dislocation of markers of *cis*-Golgi and TGN without affecting morphology of the ERGIC and endocytic pathways [16]. GA exerts multiple functional effects in mammalian cells including inhibition of protein secretion [16], arrest of Shiga toxin trafficking in the endosomal compartment [16], disruption of epithelial apical junctions [49], and perturbation of autophagic flux [50].

Other small molecules that disperse Golgi by inhibiting GBF1 activity include Exo2 and its derivative LG186 [17, 18, 51], as well as structurally unrelated compound, AG1478 [19].

Unlike BFA, neither Exo2 nor LG186 tubulates recycling endosomes, which indicates their higher selectivity toward the Golgi [17]. Interestingly, LG186 possesses the unique ability to inhibit canine GBF1 possessing a single amino acid M832L substitution in the Sec7domain that renders this protein insensitive to BFA, GA, and Exo2 [17]. Another GBF1 inhibitor, AG1478, was shown to more potently disperse *cis*-Golgi markers compared to those for TGN without altering morphology of endosomal compartments [19]. Of note, AG1478 is a known inhibitor of epidermal growth factor (EGF) receptor; however, the Golgi-disruption activity of this compound is unrelated to EGF signaling [19]. A recent study reports a side-by-side comparison of GA and AG1478 activity in epithelial cells [52]. While both inhibitors similarly disrupt Golgi and block protein secretion, they also demonstrate differences in their cellular effects. For example, GA effectively inhibits enterovirus replication in GBF1-dependent fashion. By contrast, AG1478 does not affect viral replication. Furthermore, overexpression of ARF1 attenuates the effects of AG1478, but not GA, on Golgi morphology. Together this data suggests that AG1478 may not be a selective inhibitor of GBF1 and may target ARF1 via an as yet to be defined mechanism.

Some small molecules disrupt Golgi by inhibiting ARF1 activity independently of GBF1. For example, an in silico screening discovered a compound, name LM11 that produces inactive complexes of Golgi-resident ARFs with their BFA-insensitive small GEF, ARNO [20]. LM11 causes dispersion of both *cis*-Golgi and TGN and blocks ARNO-dependent epithelial cell migration. Furthermore, an Exo1 compound identified in a high-throughput phenotypic screen disperses Golgi ribbon and releases ARF1 from the Golgi membrane without inhibiting ARF1-GDP/GTP exchange [18]. Mechanisms of Exo1 action have not been elucidated but one model suggests that this agent blocks the formation of the ARF-vesicular coat complexes involved in intra-Golgi trafficking [18].

Inactivation of ARF small GTPases is not the only mechanism by which small molecules interfere with Golgi dynamics and functions. Similar effects can be achieved by inhibiting a member of the Rho family of small GTPases, Cdc42. Thus, Secramine A, the first discovered Cdc42 inhibitor, was shown to arrest VSVG trafficking in the Golgi and attenuate exocytosis of basolateral but not apical plasma membrane proteins in polarized epithelial cells [21]. Interestingly, Secramine A does not induce Golgi fragmentation but blocks reorientation of the Golgi in migrating cells. Contrary to this data, a recent study observed that pharmacological inhibition of Cdc42 can disrupt Golgi integrity. This study has identified ZCL278, a small molecular inhibitor of Cdc42 interactions with its GEF, intersectin [22]. ZCL278 has multiple effects on mammalian cells that include disruption of the Golgi ribbon. Importantly, such

Golgi fragmentation appears to be a specific consequence of Cdc42 inactivation since pharmacological inhibition of a closely related Rac1 GTPase does not affect Golgi integrity [22].

3 Recent Developments in Endocytosis Inhibitors

Endocytosis is a key mechanism by which cells communicate with the environment. It involves formation of plasma membrane vesicles with subsequent internalization and fusion with intracellular endosomes. Cells use endocytosis for various reasons, from nutrient uptake to initiation or termination of signaling, therefore endocytic vesicles can be formed via different mechanisms. Although classification of internalization pathways is constantly evolving, there are at least three major pathways to generate endocytic carriers: assembly of clathrin-coated vesicles, internalization via lipid raft plasma membrane domains followed by formation of large vacuoles mediating phagocytosis, and micropinocytosis [1]. Endocytosis is governed by sophisticated multiprotein machinery composed of components that are either common or unique for each internalization pathway. Genetic or pharmacological inhibition of these unique molecular components is used to probe biological roles of individual routes of endocytosis. Pharmacological inhibition of different endocytic pathways has a long history and remains popular nowadays despite the fact that commonly used inhibitors of different internalization pathways lack genuine specificity [5]. The following subchapter discusses recent progress toward discovering novel small molecular inhibitors of endocytosis.

3.1 Inhibitors of Clathrin-Dependent Endocytosis

Endocytosis via clathrin-coated pits has been extensively studied by utilizing various tools such as pharmacological inhibitors, RNA interference, and expression of dominant negative mutants [5, 53, 54]. Recently, an ELISA-based screen has been conducted to identify small molecules that block interactions between the clathrin N-terminal domain and its endocytic adaptor, amphiphysin. This screen identified two structurally unrelated compounds, pitstop 1 and pitstop 2, that inhibit clathrin domain interactions in low micromolar concentrations [23]. In the initial study, pitstop 2 demonstrated superior cell membrane permeability and was thus highlighted as a preferred selective inhibitor of clathrin-mediated endocytosis that does not affect internalization of the lipid raft ligand, Shiga toxin. Pitstops 2 blocks a wide range of clathrin-dependent processes such as transferrin and EGF uptake [23, 55], cell entry of HIV and hemorrhagic fever viruses [23, 56], and synaptic vesicle cycling [23]. However, initial enthusiasm regarding pitstop as a selective inhibitor of clathrin-dependent endocytosis was tempered by two recent studies that identified additional activities of this compound. One study has found that pitstop 2

inhibits growth and induces apoptosis of dividing HeLa cells [57]. These effects were due to loss of mitotic spindle integrity and activation of the spindle assembly checkpoint, consistent with the known role of clathrin in stabilizing mitotic spindle. Another report demonstrated that pitstop 2 also inhibits clathrin independent endocytosis [58]. This study shows that pitstop 2 blocks internalization of different plasma membrane proteins (major histocompatibility complex, CD44, CD98, and CD147) that are known cargo for clathrin-independent pathways. It is noteworthy that pitstop 2 inhibits endocytosis of this clathrin-independent cargo with even higher potency as compared with inhibition of transferrin internalization [58]. It has been suggested that pitstop 2 may block the majority of internalization events by inducing global alterations of plasma membrane structure. Overall, this data indicates that pitstop lacks the desired specificity and cannot be recommended as a tool to selectively probe clathrin-mediated endocytosis.

3.2 Dynamin Inhibitors

Endocytic activity of the plasma membrane eventuates in the formation of intracellular vesicles, which requires membrane fission. This step is controlled by members of the evolutionarily conserved dynamin family [59, 60]. Dynamin is a large GTPase that has the ability to oligomerize on lipid membranes and interact with different protein effectors. Although its role in clathrin-mediated endocytosis has been most extensively characterized, dynamin is also essential for internalization of many clathrin-independent ligands [59, 60]. The first small molecular dynamin inhibitor, called "dynasore," was identified by chemical screen almost a decade ago [24]. Dynasore is a relatively low affinity dynamin inhibitor that targets the GTPase domain of this protein. It potently blocks internalization of classical ligands of clathrin mediated endocytosis, such as transferrin and low-density lipoprotein receptor, by interfering with invagination and fission of clathrin-coated vesicles [24]. Likewise, dynasore inhibits other internalization pathways such as caveolae-mediated and fluid phase endocytosis. These effects are consistent with known roles of dynamin in regulating different modes of membrane internalization. Recent attempts to improve dynasore activity yielded derivatives such as DD and Dyngo; compounds that block transferrin uptake at low micromolar concentrations [61]. In addition to dynasore, several other chemical inhibitors of dynamin have been identified [25, 62, 63]. The majority of these small molecules are non-competitive inhibitors of dynamin GTPase activity, although the so-called MiTMAB inhibitors bind to the pleckstrin homology domain thereby blocking dynamin interactions with membrane phospholipids [25]. Despite the common belief that pharmacological inhibitors of dynamin are selective tools to interrupt membrane fission, data obtained with these compounds should be viewed with caution.

In addition to its key roles in membrane fission, dynamin was found to be a potent regulator of the actomyosin cytoskeleton. For example, it interacts with actin-binding protein, cortactin, and stabilizes/cross-links actin filaments [64]. Furthermore, overexpression of dynamin mutants causes myosin activation and actomyosin driven apical constriction of polarized epithelial cells [65]. Since siRNA-mediated depletion of dynamin results in dramatic disorganization of actin filaments [64, 65] it is expectable that its pharmacological inhibitors may also disrupt cytoskeletal organization. This suggestion is supported by two recent studies that report rapid and profound disorganization of actin filaments in mammalian cells treated with dynasore [66, 67]. Given the essential role of the actomyosin cytoskeleton in mediating stability and dynamics of the plasma membrane it is possible that many previously observed effects of dynamin inhibitors on endocytosis are indirect consequences of disorganization of submembranous actin filaments. Importantly, a recent report indicates off-target effects of common dynamin inhibitors. In this study, effects of dynasore or Dyngo-4a were tested in cells with triple knockdown of all dynamin isoforms. Despite complete lack of dynamin expression, both dynasore and Dyngo impaired fluid phase marker uptake and inhibited cell motility [68]. Given these results the conclusions involving dynamin-dependence of a particular cellular process should not be based solely on the effects of pharmacological inhibitors and should be verified by alternative approaches.

4 Inhibitors of Endosomal Trafficking

Bidirectional trafficking in and out of the plasma membrane involves cargo delivery into different endosomal populations that serve as processing centers determining the final destinations of transported molecules. For example, recycling endosomes are essential for delivery of internalized proteins back to the cell surface as well as for the anterograde trafficking of TGN-derived vesicles to the plasma membrane [69]. In contrast, late endosomes mediate the retrograde transport of proteins that are destined for lysosomal degradation [70, 71]. In addition, retrograde trafficking from endosomal compartments to the Golgi is essential for returning important Golgi enzymes and structural and regulatory proteins depleted during exocytosis [72]. Several studies have described small molecular compounds that selectively block either the anterograde or the retrograde trafficking through endosomes. For example, a sulfonamide compound, 16D10, inhibits transferrin receptor recycling without affecting protein endocytosis or ER-to-Golgi trafficking [26]. 16D10 appears to have dual function both acting as inhibitor of endosomal V-ATPase and a direct proton ionophore leading to increase in endosomal pH. Another inhibitor of anterograde transport through endosomes is a compound, A5,

that was shown to attenuate adaptor protein 1 (AP-1)-dependent trafficking between the TGN and endosomes in yeast [27]. This compound also disrupts normal AP-1 localization and inhibits trafficking of Usher proteins in mammalian cells, which indicates an evolutionarily conserved mechanism of action [27, 73]. A peculiar example of anterograde endosomal trafficking is lysosomal exocytosis. This process involves calcium-stimulated fusion of lysosomes to the plasma membrane and serves as an important mechanism to repair membrane damage [74]. Lysosomal exocytosis can be prevented by a small molecular compound, vacuolin-1, that inhibits the appearance of lysosomal markers at the plasma membrane and releases lysosomal enzymes into the extracellular space [28]. Vacuolin-1 reportedly attenuates such lysosome-dependent processes as glioma cell invasion [75] and superoxide anion radical production by endothelial cells [76]. Furthermore, this compound induces the formation of large endosome and lysosome-derived vacuoles and may promote erythropoesis by enhancing vacuole-driven enucleation of erythroblasts [77].

The retrograde route through endosomes to the Golgi and ER has recently been targeted in several high-throughput screens aimed at identifying small-molecular inhibitors of pathogen trafficking and toxicity [78]. These screens discovered a number of inhibitors of retrograde endosomal trafficking with varying specificity. One notable example is the so-called Retro compounds that block transport of ricin and Shiga-like toxins from early endosomes to the TGN without affecting other trafficking steps or the morphology of many intracellular organelles [29]. The Retro compounds are characterized by different biological activities that involve inhibition of cellular entry of papillomavirus in vitro [79] and protection of mice from lethal ricin exposure in vivo [29]. Interestingly, Retro-1 affects intracellular distribution of exogenously added oligonucleotides and promotes their accumulation in the nucleus [80]. This makes Retro compounds attractive agents to enhance the efficiency of oligonucleotide-dependent gene targeting as well as nuclear delivery of pharmacological agents. Another high-throughput screen characterized two small molecular compounds (compounds 75 and 134) that also inhibit various stages of retrograde endosomal transport of bacterial toxins [30]. These compounds arrest Cholera toxin or Shiga toxin trafficking in the early endosomes by blocking their delivery to either TGN or the recycling compartment. The relative specificity of these inhibitors is established by the fact that neither compound 75 nor compound 134 inhibit anterograde ER-to-Golgi trafficking of VSVG [30]. Since the majority of inhibitors of retrograde endosomal trafficking were discovered by searching for specific cellular phenotypes, molecular targets of these inhibitors remain unknown. A notable exception is YM201636, a pyridofuropyrimidine compound, identified by a drug discovery program that targeted phosphoinositide synthesis [31]. This molecule is a selective inhibitor

of the mammalian phosphatidylinositol phosphate kinase PIKfyve, which synthesizes phosphatidylinositol 3,5-biphosphate. YM201636 inactivates its target at nanomolar concentrations leading to multiple defects in cellular trafficking. For example, it induces formation of swollen vesicles in fibroblast, a specific phenotype that is recapitulated by siRNA-mediated knockdown of PIKfyve [31]. The swollen vesicles in YM201636-treated cells contain protein markers of early endosomes and are likely to originate due to interrupted membrane flux toward late endosomal and lysosomal compartments. This suggestion is supported by recent data showing inhibition of lysosomal targeting of internalized ologonucleoties in leukocytes after exposure to YM201636. Since early endosomes are important hubs that may direct cargo trafficking toward various intracellular destinations, blocking early endosomal membrane sorting is expected to affect diverse trafficking events. Consistent with this notion, YM201636 has recently been shown to attenuate recycling of cell adhesion proteins in epithelial cells [81] and to disregulate autophagy in neurons [82].

5 Conclusion and Perspectives

High-throughput screening of chemical compound libraries has proven to be a fruitful approach to identifying novel inhibitors of both exocytosis and endocytosis. It has yielded a diverse array of small molecules that blocks different steps of vesicle trafficking in cultured mammalian cells. Since the majority of these compounds were identified by selecting for specific cellular phenotypes, their exact molecular targets remain to be elucidated. Furthermore, the specificity of these newly discovered chemical inhibitors is not absolute, as they can frequently interfere with multiple trafficking events. Hence, the quest for more specific chemical inhibitors of membrane trafficking is far from completion. Future discoveries of such inhibitors are likely to be accelerated by recent advances in the drug discovery and chemoinformatics fields, including various chemical genetic-based approaches and computational tools to predict targets for bioactive compounds. Another driving force for the discovery of novel trafficking inhibitors is their potential application as therapeutic agents. Indeed, inhibitors of endocytosis and retrograde endosomal trafficking can be used to protect human patients against bacterial and viral infection. On the other hand, inhibitors of ER-Golgi trafficking frequently lead to cell death and therefore can be used for the development of novel antitumor agents. There can be little doubt that future studies will discover more highly selective chemical inhibitors of exocytosis and endocytosis that can be used for experimental and clinical applications.

Acknowledgments

The author thanks Alex Feygin for excellent editorial assistance. This work was supported by National Institute of Health grants RO1 DK083968 and R01 DK084953.

References

1. Doherty GJ, McMahon HT (2009) Mechanisms of endocytosis. Annu Rev Biochem 78:857–902
2. Kasai H, Takahashi N, Tokumaru H (2012) Distinct initial SNARE configurations underlying the diversity of exocytosis. Physiol Rev 92:1915–1964
3. Gordon DE, Bond LM, Sahlender DA, Peden AA (2010) A targeted siRNA screen to identify SNAREs required for constitutive secretion in mammalian cells. Traffic 11: 1191–1204
4. Naydenov NG, Harris G, Brown B, Schaefer KL, Das SK, Fisher PB, Ivanov AI (2012) Loss of soluble N-ethylmaleimide-sensitive factor attachment protein alpha (αSNAP) induces epithelial cell apoptosis via down-regulation of Bcl-2 expression and disruption of the Golgi. J Biol Chem 287:5928–5941
5. Ivanov AI (2008) Pharmacological inhibition of endocytic pathways: is it specific enough to be useful? Methods Mol Biol 440:15–33
6. Mishev K, Dejonghe W, Russinova E (2013) Small molecules for dissecting endomembrane trafficking: a cross-systems view. Chem Biol 20:475–486
7. von Kleist L, Haucke V (2012) At the crossroads of chemistry and cell biology: inhibiting membrane traffic by small molecules. Traffic 13:495–504
8. Cross BC, McKibbin C, Callan AC et al (2009) Eeyarestatin I inhibits Sec61-mediated protein translocation at the endoplasmic reticulum. J Cell Sci 122:4393–4400
9. Besemer J, Harant H, Wang S et al (2005) Selective inhibition of cotranslational translocation of vascular cell adhesion molecule 1. Nature 436:290–293
10. Garrison JL, Kunkel EJ, Hegde RS, Taunton J (2005) A substrate-specific inhibitor of protein translocation into the endoplasmic reticulum. Nature 436:285–289
11. Brown WJ, Plutner H, Drecktrah D, Judson BL, Balch WE (2008) The lysophospholipid acyltransferase antagonist CI-976 inhibits a late step in COPII vesicle budding. Traffic 9: 786–797
12. Lu L, Hannoush RN, Goess BC, Varadarajan S, Shair MD, Kirchhausen T (2013) The small molecule dispergo tubulates the endoplasmic reticulum and inhibits export. Mol Biol Cell 24:1020–1029
13. Sprocati T, Ronchi P, Raimondi A, Francolini M, Borgese N (2006) Dynamic and reversible restructuring of the ER induced by PDMP in cultured cells. J Cell Sci 119:3249–3260
14. Kramer A, Mentrup T, Kleizen B et al (2013) Small molecules intercept Notch signaling and the early secretory pathway. Nat Chem Biol 9:731–738
15. Ohashi Y, Iijima H, Yamaotsu N et al (2012) AMF-26, a novel inhibitor of the Golgi system, targeting ADP-ribosylation factor 1 (Arf1) with potential for cancer therapy. J Biol Chem 287:3885–3897
16. Saenz JB, Sun WJ, Chang JW et al (2009) Golgicide A reveals essential roles for GBF1 in Golgi assembly and function. Nat Chem Biol 5:157–165
17. Boal F, Guetzoyan L, Sessions RB et al (2010) LG186: an inhibitor of GBF1 function that causes Golgi disassembly in human and canine cells. Traffic 11:1537–1551
18. Feng Y, Yu S, Lasell TK et al (2003) Exo1: a new chemical inhibitor of the exocytic pathway. Proc Natl Acad Sci U S A 100:6469–6474
19. Pan H, Yu J, Zhang L et al (2008) A novel small molecule regulator of guanine nucleotide exchange activity of the ADP-ribosylation factor and golgi membrane trafficking. J Biol Chem 283:31087–31096
20. Viaud J, Zeghouf M, Barelli H et al (2007) Structure-based discovery of an inhibitor of Arf activation by Sec7 domains through targeting of protein–protein complexes. Proc Natl Acad Sci U S A 104:10370–10375
21. Pelish HE, Peterson JR, Salvarezza SB et al (2006) Secramine inhibits Cdc42-dependent functions in cells and Cdc42 activation in vitro. Nat Chem Biol 2:39–46

22. Friesland A, Zhao Y, Chen YH, Wang L, Zhou H, Lu Q (2013) Small molecule targeting Cdc42-intersectin interaction disrupts Golgi organization and suppresses cell motility. Proc Natl Acad Sci U S A 110:1261–1266
23. von Kleist L, Stahlschmidt W, Bulut H et al (2011) Role of the clathrin terminal domain in regulating coated pit dynamics revealed by small molecule inhibition. Cell 146:471–484
24. Macia E, Ehrlich M, Massol R, Boucrot E, Brunner C, Kirchhausen T (2006) Dynasore, a cell-permeable inhibitor of dynamin. Dev Cell 10:839–850
25. Quan A, McGeachie AB, Keating DJ et al (2007) Myristyl trimethyl ammonium bromide and octadecyl trimethyl ammonium bromide are surface-active small molecule dynamin inhibitors that block endocytosis mediated by dynamin I or dynamin II. Mol Pharmacol 72:1425–1439
26. Nieland TJ, Feng Y, Brown JX et al (2004) Chemical genetic screening identifies sulfonamides that raise organellar pH and interfere with membrane traffic. Traffic 5:478–492
27. Duncan MC, Ho DG, Huang J, Jung ME, Payne GS (2007) Composite synthetic lethal identification of membrane traffic inhibitors. Proc Natl Acad Sci U S A 104:6235–6240
28. Cerny J, Feng Y, Yu A et al (2004) The small chemical vacuolin-1 inhibits Ca(2+)-dependent lysosomal exocytosis but not cell resealing. EMBO Rep 5:883–888
29. Stechmann B, Bai SK, Gobbo E et al (2010) Inhibition of retrograde transport protects mice from lethal ricin challenge. Cell 141: 231–242
30. Saenz JB, Doggett TA, Haslam DB (2007) Identification and characterization of small molecules that inhibit intracellular toxin transport. Infect Immun 75:4552–4561
31. Jefferies HB, Cooke FT, Jat P et al (2008) A selective PIKfyve inhibitor blocks PtdIns(3,5) P(2) production and disrupts endomembrane transport and retroviral budding. EMBO Rep 9:164–170
32. Fiebiger E, Hirsch C, Vyas JM, Gordon E, Ploegh HL, Tortorella D (2004) Dissection of the dislocation pathway for type I membrane proteins with a new small molecule inhibitor, eeyarestatin. Mol Biol Cell 15:1635–1646
33. Wang Q, Li L, Ye Y (2008) Inhibition of p97-dependent protein degradation by Eeyarestatin I. J Biol Chem 283:7445–7454
34. Magnaghi P, D'Alessio R, Valsasina B et al (2013) Covalent and allosteric inhibitors of the ATPase VCP/p97 induce cancer cell death. Nat Chem Biol 9:548–556
35. Maifeld SV, MacKinnon AL, Garrison JL et al (2011) Secretory protein profiling reveals TNF-alpha inactivation by selective and promiscuous Sec61 modulators. Chem Biol 18:1082–1088
36. Varadarajan S, Bampton ET, Smalley JL et al (2012) A novel cellular stress response characterised by a rapid reorganisation of membranes of the endoplasmic reticulum. Cell Death Differ 19:1896–1907
37. Varadarajan S, Tanaka K, Smalley JL et al (2013) Endoplasmic reticulum membrane reorganization is regulated by ionic homeostasis. PLoS One 8:e56603
38. Helms JB, Rothman JE (1992) Inhibition by brefeldin A of a Golgi membrane enzyme that catalyses exchange of guanine nucleotide bound to ARF. Nature 360:352–354
39. Jackson CL (2000) Brefeldin A revealing the fundamental principles governing membrane dynamics and protein transport. Subcell Biochem 34:233–272
40. Lippincott-Schwartz J, Yuan LC, Bonifacino JS, Klausner RD (1989) Rapid redistribution of Golgi proteins into the ER in cells treated with brefeldin A: evidence for membrane cycling from Golgi to ER. Cell 56:801–813
41. Lippincott-Schwartz J, Yuan L, Tipper C, Amherdt M, Orci L, Klausner RD (1991) Brefeldin A's effects on endosomes, lysosomes, and the TGN suggest a general mechanism for regulating organelle structure and membrane traffic. Cell 67:601–616
42. Donaldson JG, Jackson CL (2011) ARF family G proteins and their regulators: roles in membrane transport, development and disease. Nat Rev Mol Cell Biol 12:362–375
43. Kahn RA (2009) Toward a model for Arf GTPases as regulators of traffic at the Golgi. FEBS Lett 583:3872–3879
44. Zeghouf M, Guibert B, Zeeh JC, Cherfils J (2005) Arf, Sec7 and Brefeldin A: a model towards the therapeutic inhibition of guanine nucleotide-exchange factors. Biochem Soc Trans 33:1265–1268
45. Morinaga N, Tsai SC, Moss J, Vaughan M (1996) Isolation of a brefeldin A-inhibited guanine nucleotide-exchange protein for ADP ribosylation factor (ARF) 1 and ARF3 that contains a Sec7-like domain. Proc Natl Acad Sci U S A 93:12856–12860
46. Niu TK, Pfeifer AC, Lippincott-Schwartz J, Jackson CL (2005) Dynamics of GBF1, a Brefeldin A-sensitive Arf1 exchange factor at the Golgi. Mol Biol Cell 16:1213–1222
47. Togawa A, Morinaga N, Ogasawara M, Moss J, Vaughan M (1999) Purification and cloning of

a brefeldin A-inhibited guanine nucleotide-exchange protein for ADP-ribosylation factors. J Biol Chem 274:12308–12315

48. Dinter A, Berger EG (1998) Golgi-disturbing agents. Histochem Cell Biol 109:571–590
49. Naydenov NG, Brown B, Harris G et al (2012) A membrane fusion protein αSNAP is a novel regulator of epithelial apical junctions. PLoS One 7:e34320
50. Naydenov NG, Harris G, Morales V, Ivanov AI (2012) Loss of a membrane trafficking protein αSNAP induces non-canonical autophagy in human epithelia. Cell Cycle 11:4613–4625
51. Spooner RA, Watson P, Smith DC et al (2008) The secretion inhibitor Exo2 perturbs trafficking of Shiga toxin between endosomes and the trans-Golgi network. Biochem J 414: 471–484
52. van der Linden L, van der Schaar HM, Lanke KH, Neyts J, van Kuppeveld FJ (2010) Differential effects of the putative GBF1 inhibitors Golgicide A and AG1478 on enterovirus replication. J Virol 84:7535–7542
53. Huang F, Khvorova A, Marshall W, Sorkin A (2004) Analysis of clathrin-mediated endocytosis of epidermal growth factor receptor by RNA interference. J Biol Chem 279:16657–16661
54. Vassilieva EV, Nusrat A (2008) Vesicular trafficking: molecular tools and targets. Methods Mol Biol 440:3–14
55. Gourlaouen M, Welti JC, Vasudev NS, Reynolds AR (2013) Essential role for endocytosis in the growth factor-stimulated activation of ERK1/2 in endothelial cells. J Biol Chem 288:7467–7480
56. Garrison AR, Radoshitzky SR, Kota KP et al (2013) Crimean-Congo hemorrhagic fever virus utilizes a clathrin- and early endosome-dependent entry pathway. Virology 444:45–54
57. Smith CM, Haucke V, McCluskey A, Robinson PJ, Chircop M (2013) Inhibition of clathrin by pitstop 2 activates the spindle assembly checkpoint and induces cell death in dividing HeLa cancer cells. Mol Cancer 12:4
58. Dutta D, Williamson CD, Cole NB, Donaldson JG (2012) Pitstop 2 is a potent inhibitor of clathrin-independent endocytosis. PLoS One 7:e45799
59. Hinshaw JE (2000) Dynamin and its role in membrane fission. Annu Rev Cell Dev Biol 16:483–519
60. Mettlen M, Pucadyil T, Ramachandran R, Schmid SL (2009) Dissecting dynamin's role in clathrin-mediated endocytosis. Biochem Soc Trans 37:1022–1026
61. McCluskey A, Daniel JA, Hadzic G et al (2013) Building a better dynasore: the dyngo compounds potently inhibit dynamin and endocytosis. Traffic 14:1272–1289
62. Gordon CP, Venn-Brown B, Robertson MJ et al (2013) Development of second-generation indole-based dynamin GTPase inhibitors. J Med Chem 56:46–59
63. Hill TA, Gordon CP, McGeachie AB et al (2009) Inhibition of dynamin mediated endocytosis by the dynoles – synthesis and functional activity of a family of indoles. J Med Chem 52:3762–3773
64. Mooren OL, Kotova TI, Moore AJ, Schafer DA (2009) Dynamin2 GTPase and cortactin remodel actin filaments. J Biol Chem 284: 23995–24005
65. Chua J, Rikhy R, Lippincott-Schwartz J (2009) Dynamin 2 orchestrates the global actomyosin cytoskeleton for epithelial maintenance and apical constriction. Proc Natl Acad Sci U S A 106:20770–20775
66. Yamada H, Abe T, Li SA et al (2009) Dynasore, a dynamin inhibitor, suppresses lamellipodia formation and cancer cell invasion by destabilizing actin filaments. Biochem Biophys Res Commun 390:1142–1148
67. Yamada H, Abe T, Satoh A et al (2013) Stabilization of actin bundles by a dynamin 1/cortactin ring complex is necessary for growth cone filopodia. J Neurosci 33:4514–4526
68. Park RJ, Shen H, Liu L, Liu X, Ferguson SM, De Camilli P (2013) Dynamin triple knockout cells reveal off target effects of commonly used dynamin inhibitors. J Cell Sci 126:5305–5312
69. Taguchi T (2013) Emerging roles of recycling endosomes. J Biochem 153:505–510
70. Epp N, Rethmeier R, Kramer L, Ungermann C (2011) Membrane dynamics and fusion at late endosomes and vacuoles–Rab regulation, multisubunit tethering complexes and SNAREs. Eur J Cell Biol 90:779–785
71. Rainero E, Norman JC (2013) Late endosomal and lysosomal trafficking during integrin-mediated cell migration and invasion: cell matrix receptors are trafficked through the late endosomal pathway in a way that dictates how cells migrate. Bioessays 35:523–532
72. Burd CG (2011) Physiology and pathology of endosome-to-Golgi retrograde sorting. Traffic 12:948–955
73. Zallocchi M, Delimont D, Meehan DT, Cosgrove D (2012) Regulated vesicular trafficking of specific PCDH15 and VLGR1 variants in auditory hair cells. J Neurosci 32: 13841–13859
74. McNeil PL (2002) Repairing a torn cell surface: make way, lysosomes to the rescue. J Cell Sci 115:873–879

75. Liu Y, Zhou Y, Zhu K (2012) Inhibition of glioma cell lysosome exocytosis inhibits glioma invasion. PLoS One 7:e45910
76. Bao JX, Chang H, Lv YG et al (2012) Lysosome-membrane fusion mediated superoxide production in hyperglycaemia-induced endothelial dysfunction. PLoS One 7:e30387
77. Keerthivasan G, Small S, Liu H, Wickrema A, Crispino JD (2010) Vesicle trafficking plays a novel role in erythroblast enucleation. Blood 116:3331–3340
78. Barbier J, Bouclier C, Johannes L, Gillet D (2012) Inhibitors of the cellular trafficking of ricin. Toxins 4:15–27
79. Lipovsky A, Popa A, Pimienta G et al (2013) Genome-wide siRNA screen identifies the retromer as a cellular entry factor for human papillomavirus. Proc Natl Acad Sci U S A 110: 7452–7457
80. Ming X, Carver K, Fisher M et al (2013) The small molecule Retro-1 enhances the pharmacological actions of antisense and splice switching oligonucleotides. Nucleic Acids Res 41: 3673–3687
81. Dukes JD, Whitley P, Chalmers AD (2012) The PIKfyve inhibitor YM201636 blocks the continuous recycling of the tight junction proteins claudin-1 and claudin-2 in MDCK cells. PLoS One 7:e28659
82. Martin S, Harper CB, May LM, Coulson EJ, Meunier FA, Osborne SL (2013) Inhibition of PIKfyve by YM-201636 dysregulates autophagy and leads to apoptosis-independent neuronal cell death. PLoS One 8:e60152

Chapter 2

Systematic Analysis of Endocytosis by Cellular Perturbations

Lena Kühling and Mario Schelhaas

Abstract

Endocytosis is an essential process of eukaryotic cells that facilitates numerous cellular and organismal functions. The formation of vesicles from the plasma membrane serves the internalization of ligands and receptors and leads to their degradation or recycling. A number of distinct mechanisms have been described over the years, several of which are only partially characterized in terms of mechanism and function. These are often referred to as novel endocytic pathways. The pathways differ in their mode of uptake and in their intracellular destination. Here, an overview of the set of cellular proteins that facilitate the different pathways is provided. Further, the approaches to distinguish between the pathways by different modes of perturbation are critically discussed, emphasizing the use of genetic tools such as dominant negative mutant proteins.

Key words Endocytosis, Membrane transport, Recycling, Degradation, Novel pathways

1 Introduction

1.1 Endocytosis

Endocytosis is an essential process of eukaryotic cells that is needed to internalize extracellular particles and solutes [1]. Phagocytosis, the uptake of large particles, is typically restricted to specialized cells. In contrast, the uptake of small particles and solutes (pinocytosis) occurs virtually in all eukaryotic cells. There is considerable interest to study this process due to the implications of endocytosis in many biological processes such as development, the immune response, neurotransmission, intercellular communication, signal transduction, and cellular and organismal homeostasis as well as in the pathogenesis of viral and bacterial infections.

For a long time it has been thought, that pinocytosis is mainly comprised of clathrin-mediated endocytosis (CME). However, current research indicates a complex network of diverse ongoing and triggered endocytic mechanisms [2]. These have been differentiated

Andrei I. Ivanov (ed.), *Exocytosis and Endocytosis*, Methods in Molecular Biology, vol. 1174,
DOI 10.1007/978-1-4939-0944-5_2,

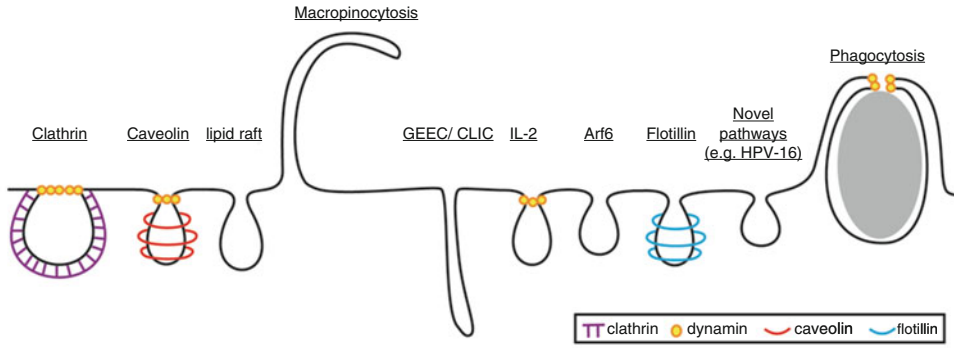

coat	clathrin	caveolin-1/2			GRAF1			Flotillin-1/2		
pit forming factors	PI(4,5)P_2 FCHO1/2 epsin1 AP-2 eps15 amphiphysin endophiln sorting nexin 9	cholesterol cavin-1 cavin-2 cavin-3 EHD2	cholesterol	cholesterol PI(3,4,5)P_3	cholesterol	cholesterol	cholesterol Arf6 EHD1	cholesterol		cholesterol FcyR CR3
scission	dynamin-2 actin	dynamin-2 actin	actin	CtBP1/BARs	actin	dynamin-2 actin	actin		actin	
regulatory factors	synaptojanin HSC70 auxillin N-WASP Arp2/3 cortactin	tyrosine kinases RhoA PKC	tyrosine kinases RhoA	Na^+/H^+-exch. PAK1, PI3K PLC, PKC Rac1 or Cdc42 Ras, Src Arf6, Rab34	Arf1 ARHGAP10 Cdc42 N-WASP	PAK1 cortactin PI3K Vav2 ubiquitin	PIP5K PI3K	Fyn-Kinase	PAK1 PI3K PKC Na^+/H^+-exchanger	Cdc42 RhoA Rac RhoG dynamin-2 PI3K, PKC Ras Arf6

Fig. 1 Factors required for endocytic uptake. Overview of the different endocytic mechanisms with important contributing factors. *Bold letters* denote key factors. *PI(4,5)P_2* phosphatidyl-inositol (4,5) bisphosphate, *Eps15* epidermal growth factor receptor pathway substrate, *HSC70* heat shock protein 70, *N-WASP* neural Wiskott–Aldrich syndrome protein, *Arp2/3* actin related protein, *PKC* protein kinase C, *PI(3,4,5)P_3* phosphatidylinositol 3,4,5-trisphosphate, *PAK1* p21 activated kinase, *PI3K* phosphatidyl-inositol 3 kinase, *PLC* phospholipase C, *PKC* protein kinase C, *Cdc42* cell division cycle 42, *Arf* ADP ribosylation factor, *GRAF1* GTPase regulator associated with focal adhesion kinase-1, *ARHGAP10* Rho GTPase activating protein 10, *EHD1* eps15 homology domain, *PIP5K* phosphatidylinositol 4-phosphate 5 kinase, *CR3* complement receptor 3

by the different morphologies of endocytic pits or vesicles, by the kinetics of uptake, and most importantly by the cellular machinery that generates the endocytic vesicle.

The classical mechanisms include phagocytosis, macropinocytosis, i.e., the uptake of large amounts of fluid, and CME, originally thought to be the sole mechanism of receptor-mediated endocytosis. In the past decade, a number of mechanisms have been emerging from the literature (summarized in [2–4], for an overview *see* Fig. 1), which will be discussed in more detail below.

This chapter introduces experimental approaches to differentiate between the known mechanisms. With a focus on mammalian cell culture systems, we emphasize the use of genetic tools such as mutant proteins and further loss of function strategies to systematically analyze the requirements for endocytic uptake of receptors and ligands.

1.2 Endocytosis Assays

In order to functionally study endocytosis, it is essential to develop a robust uptake and/or recycling assay that allows a quantitative distinction between cell surface and intracellular pools of ligands

and receptors. A number of protocols are available in the literature that could be used (e.g., [5, 6]). Most protocols rely on a labeling strategy of the ligand or receptor that allows selective removal or detection of the label on the cell surface. The label of choice (e.g., a fluorophore or biotin) may be linked to the ligand by a cleavable disulfide bond, which in turn allows to determine the accessibility either to avidin or to small membrane-impermeant thiol-reducing reagent on the cell surface of intact cells. The readout may then include fluorescence or ELISA measurements.

1.3 Perturbation Approaches to Study Endocytosis

To identify the endocytic mechanism of a certain ligand or receptor, it is necessary to comprehensively analyze the contribution of a number of key factors involved in the various mechanisms. This is best carried out by multiple approaches to perturb endocytosis such as depletion of factors required for uptake, perturbation by overexpression of functional mutant proteins (the so-called dominant negative (DN) proteins), and inhibition by small compound inhibitors. Since these approaches are associated with specific caveats, we advice to combine approaches and to use appropriate controls for the efficiency and specificity of the perturbations. After the initial characterization of endocytosis described in this review, morphological and kinetic assays will help to substantiate these findings.

1.4 RNAi to Study Endocytosis

The advent of RNA interference (RNAi) technologies allows to apply loss-of-function analysis of virtually any cellular genes. As tools small interfering RNAs (siRNAs) or short hairpin RNAs (shRNAs) can be used [7–9]. The RNAi approach may be performed in a genome-wide scale or as a targeted screen. Genome-wide screening provides the most comprehensive and unbiased view of the cellular factors that impact endocytosis. However, a targeted small-scale screen may be advantageous. Firstly, genome-wide screens are costly, difficult to execute, and thus are typically performed only in duplicate using simple assays. By contrast, small-scale screens focus on a particular biology (here endocytosis and vesicular trafficking). They can be performed more robustly with more complex assays. In any case, significant results rely on a robust assay that can be miniaturized, and on controls for false-positives and false-negatives, which are the most important caveats of this technology. False positives are typically derived from the off-target effects of siRNAs and from the assay noise [10, 11], whereas false-negatives are typically derived from insufficient silencing. The first may be alleviated by using multiple independent siRNAs, of which the majority phenocopies the same result. The second can be verified in targeted screens by functional controls, e.g., uptake of a ligand that should be perturbed.

1.5 Knockout Models and Targeted Genome Editing

The use of cell lines derived from knockout animals may be used as an additional approach to investigate any role of a cellular factor. However, this approach might not be feasible for endocytic factors, if the knockout may is detrimental or compensated for by other proteins. Knockout cell lines can still be useful to study nonessential endocytic factors in detail, e.g., by reexpression of mutants and the wild-type protein.

Another loss-of-function strategy that is potentially very useful for studying endocytosis is targeted genome editing. This approach uses genetically engineered nucleases to create specific double stranded breaks at desired locations in the genome, and harnesses the cell's endogenous mechanisms to repair the induced break. The engineered nucleases include Zink finger nucleases (ZFNs), transcription activator like effector nucleases (TALENs), and reengineered homing endonucleases [12, 13]. These nucleases allow site-specific removal, insertion, or replacement of DNA into the genome of cells. Although not yet widely used in the analysis of endocytosis, this approach may become an important tool to study the function of endocytic proteins and their mutants at an endogenous level of expression [14].

1.6 Mutant Proteins as Functional Dominant Negative Regulators

A powerful approach to study the involvement of particular factors in endocytosis is the use of dominant negative (DN) mutations. DN mutations abolish the function of the protein of interest. The overexpressed dominant mutant thereby inhibits the function of the endogenous wild-type protein [15]. There is a variety of mutations and deletions that serve this purpose. DN mutations of structural proteins often involve deletion of interaction sites, which renders them dysfunctional for interaction with further components of the machinery. Alternatively, an interaction domain may—when expressed on its own—sequester interaction partners. Dominant mutations of regulatory factors such as kinases or GTPases cause the protein to become inactive or hyperactive. The hyperactive mutants such as the constitutive active Rho or Rab GTPases often functionally act as dominant negatives in endocytosis, as they are globally activated not locally.

One of the key limitations for the use of dominant mutants may be the often poorly defined level of overexpression that is required to exert a dominant function. A low level of DN proteins may not perturb the function of the endogenous wild-type protein, whereas an extremely high level of overexpression may perturb the function of related members of the same protein family. Thus, positive as well as negative controls are highly recommended. A list of useful mutant proteins is provided in Table 1.

1.7 Pharmacological Inhibitors

Small compound inhibitors have proven to be valuable tools for the analysis of endocytosis. Their ease of use makes them a primary choice for initial analysis. However, the value of the information is

Table 1
Genetic tools to perturb endocytic pathways

	Protein	Mutant	Effect	Reference
Pit forming factors	Dynamin	K44A	Defective in GTP binding and hydrolysis	[35]
		K206	Defective in GTP binding and hydrolysis	[35]
		S45N	Lacks GTPase activity	[60]
		T65F	Lacks GTPase activity, less effective	[60]
		K562E	Charcot–Marie–Tooth disease associated	[61]
	Clathrin	T7Hub	Prevents triskelion formation	[54]
	AP-2	μ2-D176A	Disrupts interaction with internalization signal	[65]
		μ2-W421A	Disrupts interaction with internalization signal	[65]
		α-PPI$^-$	Lacks PI(4,5)P_2 binding	[66]
		FKBP-tagged AP-2	Can be redirected upon rapamycin addition	[67]
	Eps-15	Eps15-DIII	Cannot bind AP-2	[72]
		Eps15-EΔ29/295	Cannot bind AP-2	[204]
	Intersectin	SH3 domain	Sequesters dynamin	[73]
	Epsin1	R63L+H73L	Sequesters AP-2	[205]
	Syndapin I, II	SH3 domain	Sequesters dynamin	[74]
	Abp1	SH3 domain	Sequesters dynamin	[75]
	FCHO	F38E+W37E	Dimerization impaired	[27]
		K146E+K163E	Cannot bind membranes	[27]
	CtBP1/BARs	D355A	Defective in fission	[206]
	GRAF1	BAR-PH-domain	Prevents GEEC endocytosis	[152]
		KK131/132EE	Redistributes to the cytosol	[152]
	EHD1	G65R	Dissociates from Arf6 tubules	[162]
		K220N	Dissociates from Arf6 tubules	[162]
		ΔEH	Redistribution to vesicles	[162]
	Flotillin-1	Y160F	Phosphorylation deficient	[119]
		Y163F	Perturbs interaction with flotillin-2	[119]
Actin reg. factors	WAVE2	WAVE2ΔV	Cannot associate with actin	[138]
		Scar-WA	Sequesters Arp2/3	[139]
	N-WASP	CRIB-motif	Prevents interaction with Cdc42	[153]

(continued)

Table 1
(continued)

	Protein	Mutant	Effect	Reference
Rho-like GTPases	Cdc42	T17N	Dominant negative	[140]
		G12V	Constitutively active	[140, 207]
		Q61L	Constitutively active (less potent)	[207]
	RhoA	T19N	Dominant negative	[208]
		G14V	Constitutively active	[209]
		Q63L	Constitutively active (less potent)	[210]
	Rac1	T17N	Dominant negative	[128]
		G14V	Constitutively active	[211]
		Q61L	Constitutively active (less potent)	[210]
Arf-GTPases	Arf1	T31N	Dominant negative	[212]
		N126I	Dominant negative	[212]
		D129N	Dominant negative	[212]
		Q71L	Constitutively active	[212]
	Arf6	T27N	Dominant negative	[167]
		Q67L	Constitutively active	[167]
Kinases	PAK1	PID	Inhibitory domain	[213]
		K299R	Dominant negative	[214]
		T423E	Constitutively active	[215]
	PI3K	Δp85α	Dominant negative	[216, 126]
		p85	Constitutively active	[216, 126]
	PKCδ	T505A[1]	Dominant negative	[217]
	Src	M6	Dominant negative	[218]
		M9	Dominant negative	[218]
		Y527F	Constitutively active	[218]
	PIP5K	D270A	Lacks kinase activity	[165, 219]

In this table, several dominant negative mutants are listed that are useful to study endocytosis. Amino-acid exchanges denote the wild-type amino-acid followed by the mutant replacement

FKBP FK506 binding protein, *PI(4,5)P*$_2$ phosphatidyl-inositol (4,5) bisphosphate, *Eps15* epidermal growth factor receptor pathway substrate, *SH3* Src homology 3, *Abp1* amiloride binding protein 1, *FCHO* Fer/Cip4 homology domain-only, *CtBP1/BARs* C-terminal binding protein 1/brefeldin A-ribosylated substrate, *GRAF1* GTPase regulator associated with focal adhesion kinase-1, *GEEC* GPI-anchored-protein-enriched endosomal compartment, *EHD1* Eps15 homology domain 1, *Arf* ADP ribosylation factor, *Arp2/3* actin related protein, *N-WASP* neural Wiskott–Aldrich syndrome protein, *CRIB* Cdc42/Rac1 interactive binding, *Cdc42* Cell division cycle 42, *Rac1* Ras related C3 botulinum toxin substrate, *PAK1* p21 activated kinase, *PI3K* phosphatidyl-inositol 3 kinase; *PKC* protein kinase C, *PIP5K* phosphatidylinositol 4-phosphate 5 kinase

[a]Analogous mutants exist for other isoforms of PKC, *see* [217]

diminished by potential pleiotropic effects of the drugs that depend on the specificity and efficacy of a certain inhibitor. These are discussed in more detail elsewhere [16]. As an example, we highlight the use of cholesterol depleting drugs below.

In the following sections, we briefly discuss how the various cellular proteins contribute to endocytosis by a specific pathway, and how these factors can be perturbed.

1.8 The Different Endocytic Mechanisms

1.8.1 Clathrin-Mediated Endocytosis

Basic Mechanisms of CME

CME was one of the first pathways to be described. Already 1964, "bristle-coated" vesicles were observed in electron micrographs [17]. Since then, great many details of endocytic vesicle formation have been unraveled, so that CME is now the best-understood mechanism of receptor-mediated pathways.

CME is responsible for uptake of a variety of plasma membrane receptors and thereby regulates many cellular functions, e.g., growth control [18] and synaptic transmission [19]. The classical example of receptor endocytosis is internalization of the transferrin receptor, which is often used as a model cargo [20, 21]. Also, many pathogens exploit CME for internalization [4, 22]. Cargo in CME is first routed to a Rab5 positive early endosomal compartment from where it is either recycled to the plasma membrane or targeted for degradation [23]. CME occurs constitutively, and recycles receptors after ligand engagement or targets them for degradation [24]. However, certain cargoes also stimulate the formation of clathrin-coated vesicles (CCV) [25].

The formation of a clathrin-coated pit (CCP) is a multistep process, during which each step is mediated by distinct sets of factors that have been termed modules [26]. Initiation of pit formation is mediated by a nucleation module, which includes F-BAR domain-containing Fer/Cip4 homology domain-only (FCHO) proteins such as epidermal growth factor receptor pathway substrate (Eps15) and intersectins [27]. FCHO proteins bind initially to phosphatidyl-inositol (4,5) bisphosphate ($PI(4,5)P_2$) in the membrane through their F-BAR domain. By means of their intrinsic curvature, FCHO proteins are thought to facilitate initial membrane curvature formation [27]. Subsequently, the adaptor protein AP-2 is recruited to the nucleation module. Together with further cargo-specific adaptors, AP-2 mediates the selection of cargo into the forming pit [28]. AP-2 recognizes endocytic motifs such as an YXXØ or dileucine sequence in the cytoplasmic tail of receptors [28]. It interacts with clathrin and many further adaptor proteins [29]. Thus, AP-2 appears to be a major hub of interactions in CME. The recruitment of clathrin by AP-2 initiates the assembly of the characteristic coat. Triskelia of clathrin light and heavy chain form a basket around the maturing pit, stabilizing the membrane curvature [30]. This process leads to displacement of certain accessory proteins such as Eps15 and epsin to the edge of the forming vesicle [31]. BAR-domain containing proteins such as

amphiphysin, endophilin, and sorting nexin 9 bind to the curvature at the vesicle neck and recruit dynamin [32, 33]. The src homology 3 (SH3) domain of the recruiters interacts with the proline-rich region of dynamin.

Dynamin is a large GTPase essential for scission of CCP from the plasma membrane [34–36]. Self-assembly into ring-like structures of dynamin multimers is required to stimulate its GTPase activity [5, 37]. How dynamin mechanistically mediates scission is a subject of debate [38]. The two classical models describe dynamin either as a "pinchase" or a "poppase". The "pinchase" model suggests that reorganization upon GTP-hydrolysis leads to constriction of the vesicle neck until the vesicle pinches off [36, 39, 40]. In the "poppase" model GTP-hydrolysis leads to stretching of the dynamin structure in a spring-like manner, elongating the vesicle neck until the connection to the plasma membrane disrupts [41]. Recently, alternative models including a "wringing" motion are also discussed [42]. It is noteworthy that dynamin acts as scission factor not only during CME but also in a number of other pathways (see below). Actin contributes to the scission process of CCPs, which is particularly apparent in yeast [43]. However, often it is not essential for CME. It appears that actin polymerization assists in the process if large forces are required [44], or if large cargo is internalized [45].

AP-2 is one of several adaptor proteins available for cargo recognition in CME. Several different adaptors are used to distinguish between internalization sequences [46]. While AP-2 is involved in most instances of CME, internalization of certain cargoes (e.g., low density lipoprotein receptor) is possible in the absence of AP-2 [47]. This suggests that a specific cargo recognizing adaptor protein may not be always essential for CME, but may facilitate fine-tuning the endocytosis.

Uncoating of the CCV is initiated by the phosphatase synaptojanin that dephosphorylates PI(4,5)P_2 and phosphatidylinositol 3,4,5-trisphosphate (PI(3,4,5)P_3) [48]. Subsequently, heat shock protein 70 (HSC70) together with its cofactor auxillin disassemble the coat into clathrin triskelia [49, 50].

Experimental Approaches to Perturb CME

Despite the plethora of proteins facilitating CME, only a few can be used to decisively implicate CME. Rather crude, early methods to implicate CME in uptake of a ligand include treatment with hypertonic sucrose, acidification of the cytosol, or injection of clathrin antibodies into the cytosol [51–53]. The identification of disease-related mutations in proteins implicated in CME allows utilizing a diverse set of DN proteins for a more specific analysis.

The key identifier is the name-giving clathrin triskelion. Overexpression of the clathrin hub domain, the central portion of the triskelion, affects the interactions of clathrin light and heavy chains and exerts a dominant negative effect on CME [54].

A functional perturbation of CME by RNAi is achieved by targeting clathrin heavy chains. Since the half-life of the protein is about 50 h [55], a repeated transfection of the siRNA oligos is required for an efficient knockdown [56]. Depletion experiments may need sensitive controls, as low levels of clathrin can be sufficient to allow a substantial CME to occur [57]. Recently, a novel set of inhibitors has been identified that target specifically the clathrin terminal domain. These compounds, named Pitstop 1 and 2, interfere with the association of accessory proteins with clathrin [58].

Dynamin provides another prime target for perturbation, since it is indispensable for CME [59]. Please remember, however, that dynamin is required for other mechanisms as well. A common approach to interfere with dynamin function is overexpression of the DN K44A mutant [35]. This mutant is defective in GTP binding and hydrolysis and is most often used in functional assays. However, a number of further mutants have been used: the K206D mutant acts in the same manner as the K44A mutant [35]. The S45N and T65F mutants lack the GTPase activity required for scission. Of note, the T65F mutant appears to perturb endocytosis less efficiently [60]. Several mutations in dynamin-2 are also found associated with neuropathy (Charcot–Marie–Tooth disease). Of those, the K562E mutant showed similar effects on endocytosis to the K44A mutant [61]. Dynamin function can also be blocked with inhibitors, the most widely used being dynasore [62]. Other, novel inhibitors include pyrimidyn or dyngo compounds [63, 64], which were only recently introduced. Dyngo compounds are analogous to dynasore but show increased potency and reduced cytotoxicity [63]. Pyrimidyn competitively inhibits GTP and phospholipid binding, thereby limiting the activity of dynamin and its membrane recruitment [64].

In addition to the major coat component, clathrin, further coat-associated factors can be targeted. The multimeric adaptor complex AP-2 is required in CME for sorting cargo into the growing pit. The point mutations D176A and W421A of the μ2 subunit of AP-2 impair the interaction with internalization signals [65]. In addition, the α-subunit lacking the $PI(4,5)P_2$-binding domain acts as a DN if highly overexpressed [66]. Besides depleting AP-2 over several days by RNAi, AP-2 may be sequestered quickly from the plasma membrane by a “knocksideways” approach. This method relies on tagging the target protein with a FK506 binding protein (FKBP) domain. If the endogenous protein is depleted, and the tagged construct expressed instead together with a rapamycin-binding domain-containing construct that is for example targeted to the mitochondrial membrane, the addition of rapamycin reroutes the tagged protein such as AP-2 rapidly to mitochondria, thereby blocking CME [67]. This approach allows a rapid depletion of the protein from the plasma membrane. However, interacting proteins may be depleted from the membrane as well, as observed

in the case of AP-2 [67]. Chlorpromazine is widely used as an inhibitor for CME, as it interferes with recruitment of AP-2 to the plasma membrane [68]. However, it can also alter membrane fluidity [69], and it may act as an inhibitor of phospholipase C [70]. Thus, chlorpromazine has the potential to inhibit clathrin-independent endocytosis [71].

Eps15 binds to AP-2 and can thus be employed as well to identify CME. To perturb Eps15, the C-terminal AP-2 binding site of Eps15 has been used as DN construct to impair CME. It has been suggested that it acts by sequestering AP-2 [72].

Although AP-2 has been a useful target to block internalization of many cargoes by CME, it is important to remember that CME may occur independent of AP-2 [46, 47].

SH3 domain containing proteins provide another approach to block CME. Overexpression of the intersectin SH3A domain prevents CME presumably by preventing dynamin recruitment [73]. Similarly, the SH3 domains of Syndapin I, II and amiloride binding protein 1 (Abp1) inhibit uptake of transferrin [74, 75].

Several mutants of FCHO2 are incapable in rescuing CME after depletion of endogenous FCHO [27]. Although certain deletion mutants of auxillin are no longer capable of being recruited to CCPs, it is unclear whether this affects the uptake of cargo [76].

Since many adaptor proteins are likely not essential for CME but rather appear to influence the efficiency and the kinetics of CME, the most reliable determinants are clathrin and dynamin. The adaptor proteins may, however, be helpful to study details of the uptake and sorting of certain receptors (reviewed in [77, 78].

1.8.2 Caveolar/Lipid Raft-Mediated Endocytosis

Basic Mechanisms of Caveolar/Lipid Raft-Mediated Endocytosis

Besides CME, which is the most prominent pathway, a number of further mechanisms exist. Many are only rudimentarily understood. Of those, caveolar/lipid raft endocytosis is probably the best studied.

Caveolae are flask-shaped invaginations of the plasma membrane. Rich in cholesterol, these microdomain-like structures of the plasma membrane were suggested early on to play a role as a clathrin-independent endocytic mechanism [79]. The cave-like shape gave those domains the name caveolae, which in turn suggested the major protein associated with them, caveolin-1 (Cav1) [80]. Three isoforms of caveolin are found, besides Cav1, there is caveolin-2 (Cav2) and caveolin-3 (Cav3). Cav2 is expressed abundantly in several cell types and is part of caveolin oligomers as a minor component; however, it cannot form caveolae on its own [81]. Cav3 exhibits a similar subcellular localization to Cav1 but is exclusively expressed in muscle cells [82]. In addition to the caveolins, cavins play an important role in shaping caveolae. Four different cavins exist, cavin-1–4. With the exception of the muscle-specific cavin-4 they are expressed ubiquitously and aid the formation of caveolae, as described below [16].

Caveolae internalize glycolipid receptors and their ligands. Cholera toxin and further bacterial toxins have been widely used as a model cargo, as they bind to glycolipids [79]. In addition, caveolae are exploited by polyomaviruses for cell entry [83–86]. Cargo is typically routed via the endosomal pathway to the ER [87].

Caveolae differ from CCPs in that caveolae function as preformed cargo containers. Assembly of these containers already starts upon expression in the ER membrane, where oligomers of 7–14 Cav1 molecules form [88]. In cells expressing Cav2, Cav2 is incorporated as a minor component into these oligomers [89]. Upon secretory transport to the Golgi, higher molecular weight complexes are formed, and the oligomers associate with cholesterol [89]. From there, the Cav1 scaffolds are transported to the plasma membrane. In a final assembly step, cavins associate with the Cav1-scaffold [90]. The resulting caveolar coat complex consists of Cav1/Cav2 and cavin-1. Cavin-2 and cavin-3 associate indirectly with the complex via cavin-1 [91]. Cavin-1 and cavin-2 are required to shape flat Cav1 scaffolds into caveolae, while cavin-3 has a role in budding [16, 92, 93].

Caveolae can be stationary for extended periods of time. They are linked to the underlying actin cytoskeleton by the ATPase Eps-15 homology domain containing protein 2 (EHD2) [94]. Cargo is sorted into these containers. Upon receptor clustering, internalization is triggered by activation of tyrosine kinases [95–97].

Scission of caveolae depends on dynamin and actin polymerization [95, 97, 98]. The guanine nucleotide exchange factor (GEF) intersectin-2L is located at the neck of caveolae and activates Cell division cylce 42 (Cdc42), which in turn induces actin polymerization via the neural Wiskott–Aldrich syndrome protein (N-WASP) [99]. Dynamin complexes with intersectin at the vesicle neck and is strictly required for scission [97, 98, 100].

Experimental Approaches to Study Caveolar/Lipid Raft-Mediated Endocytosis

Only few proteins have been targeted to implicate caveolar endocytosis in uptake of ligands. One of the diagnostic hallmarks of caveolar endocytosis is its dependency on cholesterol. Different pharmacological inhibitors are used to perturb membrane cholesterol. Methyl-β-cyclodextrin (MβCD) extracts cholesterol from membranes. However, it is a rather harsh treatment, which at higher doses will also affect cholesterol-independent pathways, as shown with CME [101, 102]. Filipin binds cholesterol within membranes and is often used to visualize cholesterol distribution. Filipin leads to a disruption of lipid raft domains and can thereby perturb caveolar endocytosis [103]. The effects of filipin are sometimes difficult to interpret, since the absence of perturbation does not necessarily exclude the requirement for cholesterol. Nystatin and progesteron perturb cholesterol levels by sequestration and inhibition of de novo synthesis, respectively. This combination

of drugs may be the best way to analyze the requirement for cholesterol-rich membranes for endocytosis. In any case, we suggest to include positive and negative controls for the effect of cholesterol depletion, to determine whether cholesterol was efficiently depleted and whether general membrane trafficking was unaffected [57].

Like CME, caveolar endocytosis depends on dynamin for scission [98]. Therefore, the tools for dynamin perturbation described above will also affect uptake by this pathway.

Interfering with the dynamic actin cytoskeleton provides further means by which caveolar endocytosis is perturbed. This is typically achieved by pharmacological inhibitors. Cytochalasin D binds to barbed ends of growing filaments and prevents the addition of new monomers [104]. Latrunculin A binds to free monomers and similarly prevents growth of actin filaments [105]. In contrast, jasplakinolide stabilizes the actin cytoskeleton, although it often leads to a disruption of filaments upon longer treatments [106].

Like clathrin in CME, the coat protein caveolin can also be targeted. Depletion of caveolin by RNAi or the use of caveolin knockout cell lines (e.g., from the $Cav^{-/-}$ mouse model [107]) may be used to assess caveolar endocytosis.

Tyrosine phosphorylation regulates caveolar dynamics. Phosphatase inhibitors such as okadaic acid trigger internalization, whereas kinase inhibitors such as genistein and staurosporine prevent it [95, 108, 109]. More specifically, depletion of Src causes the formation of immobile multi-caveolar assemblies on the cell surface [109]. In addition, overexpression of the anchoring protein EHD2 blocks caveolar endocytosis [94].

A mechanism closely related to caveolar endocytosis was described by following SV40 internalization in $Cav1^{-/-}$ cells. This pathway is referred to as lipid raft-mediated endocytosis in this review. The mechanism of virus uptake does not require caveolin and dynamin, but cholesterol-rich membranes, tyrosine phosphorylation and actin polymerization [110]. This mechanism is similar in many ways, but exhibits faster kinetics, which highlights the role of the caveolar coat as a regulatory as well as a structural component [111, 112].

1.8.3 Flotillin

Basic Mechanisms of Flotillin Endocytosis

A mechanism potentially related to caveolar endocytosis is flotillin endocytosis, where flotillin supposedly functions similarly as caveolin [113]. Flotillin forms microdomains of flotillin-1 and flotillin-2 in a 1:1 stoichiometric ratio. Flotillins localize to membrane invaginations distinct from caveolae [114]. The pathway is used for example for the uptake of glutamate and dopamine receptors [115], the GPI-linked CD59, and cholera toxin B [113]. Additional functions besides their role in endocytosis have been described, such as sensing membrane cholesterol or the interaction with cortical actin during neutrophil migration [116, 117].

Experimental Approaches to Perturb Flotillin Endocytosis

There is limited mechanistic detail available for this mechanism besides the role of flotillin microdomains. Flotillin is phosphorylated in response to epidermal growth factor (EGF) stimulation and this phosphorylation is important for endocytosis [118, 119]. Accordingly, flotillin-1 mutations of the phosphorylation sites Y160 and Y163 perturb flotillin-dependent endocytosis [119]. In addition mutation of Y163 also interferes with heterooligomerization with flotillin-2 [120]. Knockdown of flotillins by RNAi is another possibility to assess their involvement. It is important to note, however, that siRNA-mediated depletion of flotillin-1 reduces additionally the levels of caveolin-1 [121]. Flotillin-microdomains require cholesterol. Perturbation of cholesterol levels leads to disruption of the microdomains, and prevents endocytic uptake by this pathway [122].

1.8.4 Macropinocytosis

Basic Mechanisms of Macropinocytosis

Macropinocytosis is in many regards different than the other pinocytic pathways, as the mechanism of vesicle formations is quite distinct. It was described early on by the extensive remodeling of the plasma membrane that is observable by light microscopy [123]: large membrane extensions (ruffles or blebs) fuse back with the plasma membrane, which in turn create large endocytic vacuoles, the macropinosomes. These large vacuoles are not smaller than 0.2 μm but often about 1 μm in diameter [124]. In contrast to CME and caveolar/lipid raft-mediated endocytosis, bulk uptake of extracellular fluids and plasma membrane occurs rather than a selective uptake of receptors and ligands.

Macropinocytosis is activated for example through growth factor binding to receptor tyrosine kinases [125]. Activated receptor-tyrosine kinases recruit phosphatidylinositol-4,5-bisphosphate 3-kinase (PI3K) to the plasma membrane, where it generates $PI(3,4,5)P_3$. $PI(3,4,5)P_3$ serves as a docking site for effectors such as phospholipase C (PLC), exchange factors for Rho-like GTPases, and actin-regulatory proteins [126]. PLC can further amplify the signal, by cleaving PIP_2 into diacylglycerol (DAG) and inositol-trisphosphate (IP3) [126]. DAG activates protein kinase C (PKC), which has been shown to promote ruffling and macropinosome formation [127].

Ras-related C3 botulinum toxin substrate 1 (Rac1) and Cdc42 are the main GTPases regulating macropinocytosis. They relay the signaling to downstream effectors such as the WAVE complex that acts as a nucleation promotion factor. WAVE promotes actin polymerization through activation of the actin-related protein complex (Arp2/3) [128–130]. In addition, essential Na^+/H^+-exchangers influence the local, submembranous pH, which affects the activation of Cdc42/Rac1 [131]. P21 protein (Cdc42/Rac)-activated kinase 1 (PAK1) acts downstream of Rac1, and regulates uptake and recycling [132]. Its target, the C-terminal binding

protein 1/brefeldin A-ribosylated substrate (CtBP1/BARs), has been shown to play an important role in macropinosome closure [133]. A number of additional factors are involved in macropinocytosis, several of which are acting in a cell-type dependent manner (for a more detailed overview *see* [134, 135]).

Experimental Approaches to Perturb Macropinocytosis

Despite the many proteins of the macropinocytic machinery that are used to functionally implicate macropinocytosis, only few if any are exclusive to macropinocytosis. Traditionally, induction of macropinocytosis has been analyzed morphologically by the appearance of membrane ruffles and the transient increase of fluid-phase uptake into cells [136]. Fluid-phase uptake is typically assessed by the uptake of fluorescently labeled, high molecular weight dextrans. In addition, dextran may be used transiently to localize cargo intracellularly to marcopinosomes. As a caveat, macropinosomes fuse quickly with the endosomal pathway, i.e., within 5–20 min of their formation [137], which may lead to erroneous interpretation of the colocalization data.

Actin polymerization drives the formation of the membrane extensions and is therefore indispensable for macropinocytosis. As described above, inhibitors of actin polymerization can be used to block this mechanism. Genetic tools such as mutant proteins are mainly used to decipher details of actin polymerization in macropinocytosis. Examples include a deletion mutant for WAVE2 (WAVE2ΔV) that reduces macropinosome numbers [138], and the carboxy-terminal domain of WAVE (Scar-WA) that sequesters the Arp2/3 complex and prevents growth factor induced ruffle formation [139].

Rac1 or Cdc42 initiate actin polymerization in macropinocytosis. DN mutants of these Rho-like GTPases interfere with uptake, and constitutively active forms may enhance or block macropinocytosis [128, 140–142]. Blocking Na^+/H^+-exchangers by amiloride and its derivative EIPA will affect macropinocytosis [143]. As such, it has been used as the key criterion to ascertain uptake by macropinocytosis. Although it is still an important line of evidence towards macropinocytic uptake, pleiotropic effects such as reorganization of the actin cytoskeleton have been described [144, 145].

Several kinases involved in macropinocytosis have been targeted to block this pathway. Interfering with PAK1 function by overexpression of the autoinhibitory domain or by using the inhibitor IPA-3 reduces fluid phase uptake significantly [132, 146]. The formation of $PI(3,4,5)P_3$ can be blocked by wortmannin, or LY294002 [147, 148]. As a genetic tool, overexpression of a truncated version of the PI3K-subunit p85 that lacks the interaction domain for the catalytic subunit serves as DN and reduces the formation of macropinosomes [126]. The inhibitors rottlerin, calphostin C, and bisindolylmaleimide block PKC and reduce membrane ruffling [127].

1.8.5 GEEC/CLIC Pathway

Basic Mechanisms of the GEEC/CLIC Pathway

The GEEC/CLIC pathway represents a more recently described process. Endocytosis of glycophosphatidyl-anchored proteins (GPI-AP) occurs by a cholesterol-dependent, clathrin-, caveolin-, and dynamin-independent mechanism [149]. The pathway is named after the primary endocytic structures formed, i.e., GPI-anchored-protein-enriched endosomal compartment (GEEC) [149] or clathrin-independent carriers (CLIC) [150] denominating the same structures. Cargo is routed to the endosomal recycling pathway. Interestingly this route appears to bypass the Rab5-positive sorting endosomes [149]. After induction, this pathway mediates a substantial amount of fluid uptake into cells. Endocytic pits present as tubular structures in electron micrographs, which give rise to long tubular endocytic vacuoles [151]. The tubular structures are marked by the presence of the GTPase Regulator Associated with Focal Adhesion Kinase-1 (GRAF1), implicating this GTPase as a coat protein [152]. Actin dynamics, regulated by Cdc42 and its downstream target N-WASP, are required for GEEC endocytosis [153]. Cdc42 is activated by the Rho GTPase activating protein 10 (ARHGAP10), which is recruited to the plasma membrane by Arf1 [154].

Experimental Approaches to Perturb the GEEC/CLIC Pathway

Most of the described factors affect uptake by the GEEC/CLIC pathway when perturbed. The requirement for cholesterol is a key feature of this pathway. Perturbations of cholesterol will therefore block GEEC endocytosis [155].

The regulation of actin polymerization by specific factors may additionally be helpful to address any role of GEEC endocytosis. Overexpression of the DN Cdc42-T17N or the Cdc42/Rac1 interactive binding (CRIB) motif of N-WASP prevents activation of N-WASP and reduces fluid phase uptake by GEEC endocytosis [153]. The DN mutant Arf1-T31N targets the regulation more upstream by preventing recruitment of the GEF ARHGAP10 [154]. In addition, inhibitors of actin polymerization dynamics as described above may be helpful.

GRAF1 provides a more specific target. GRAF1 consists of a BAR-domain, a pleckstrin homology (PH) domain, a Rho-GTPases activating (RhoGAP) domain, a proline-rich domain, and a C-terminal SH3 domain. A mutant consisting of the BAR and the PH domain binds to the endocytic tubules that become less mobile, and whose endocytosis is blocked [152]. The exchange of lysine to glutamate residues in the BAR domain (KK131/132EE) redistributes the protein to the cytosol. Both mutants therefore act as DN [152]. In addition, colocalization/comigration of cargo with GRAF-1 in the tubular structures is characteristic for this pathway.

1.8.6 IL-2 Endocytosis

Basic Mechanisms of IL-2 Endocytosis

Another cholesterol-dependent pathway is observed in the endocytosis of interleukin-2 (IL-2). This pathway is also clathrin- and caveolin-independent [156, 157]. Unlike lipid raft-mediated endocytosis, however, internalization depends on dynamin for scission of the endocytic pit [157]. The scission process is also linked to actin polymerization [158]. PAK-1-activated cortactin is recruited to the vesicle neck via dynamin [158, 159], which in turn recruits the Arp2/3 complex [158]. The Arp2/3 complex requires activation by Rac1. The activational cascade involves PI3K generating PI(3,4,5)P_3. The RhoGEF Vav2 binds to PI(3,4,5)P_3, activating Rac1. Rac1 activation of Arp2/3 via N-WASP induces the actin polymerization [159, 160].

Experimental Approaches to Perturb IL-2 Endocytosis

The IL-2 pathway belongs in the group of dynamin-dependent pathways rendering it sensitive to the overexpression of Dyn-K44A or other perturbations of dynamin as described above [158].

The involvement of detergent-resistant membrane domains suggests the potential for perturbation by cholesterol depletion [157].

Perturbation of the actin polymerization step may involve overexpression of the DN Rac1-T17N, and of the truncated cortactin, Cort^{SH3}, [159], or the use of actin inhibitors (see above). A mutated form of the PI3K subunit p85α (p85Δ85) lacking the Bcl-homology (BH) domain required to recruit Rac1 will block activation of actin polymerization [160]. Overexpression of the phosphatase synaptojanin 2 reduces PI(3,4,5)P_3 levels at the plasma membrane, thereby preventing the recruitment of Vav2 and activation of Rac1 [160].

1.8.7 Arf6-Dependent Endocytosis

Basic Mechanisms of Arf6-Dependent Endocytosis

The literature references a further clathrin-independent endocytic mechanism defined by Arf6, which so far has been exclusively observed in HeLa cells [161]. Arf6 endocytosis is responsible for recycling plasma membrane proteins such as the IL-2 receptor α subunit Tac or MHC-I [161, 162]. This mechanism differs from macropinocytosis as it recruits only specific cargoes [163]. Vesicle formation is independent of dynamin but requires cholesterol [163, 164]. Its morphological hallmark is a tubular system. The tubular network depends on intact microtubules. The tubules are decorated with the Eps15 homology domain-containing protein EHD1. EHD1 influences the rate of recycling [162]. Importantly, recycling requires the GTPase activity of Arf6 and the subsequent activation of the phosphatidylinositol 4-phosphate 5 kinase (PIP5K) [165].

Experimental Approaches to Perturb Arf6-Dependent Endocytosis

The limited amount of knowledge about this pathway and its detection in limited mammalian cells systems allows only few options for perturbation analysis. The existing literature has studied the recycling rather than the endocytosis of cargo. Thus, colocalization or cointernalization with existing cargoes or EHD1 may be

used to imply Arf6 endocytosis for uptake of a protein. However, internalized cargo merges with traffic from clathrin-mediated endocytosis at about 20 min after internalization, so that the experimental timing needs to be well controlled [164].

For certain cargoes, association with cholesterol is important for endocytosis by the Arf6 pathway (e.g., CD59), while others show no association with lipid rafts (e.g., Tac, MHC-I) [164, 163].

Of note, overexpression of the DN Arf6-T27N that is deficient in GTP binding does not affect internalization but rather recycling of cargo [163]. The constitutively active Arf6-Q67L will alter the trafficking of proteins and abrogate the formation of EHD1-positive tubules [162, 164]. As a caveat, Arf6 is involved in the regulation of many actin-based processes such as spreading and migration [166]. In addition, Arf6 is required for uptake through clathrin-mediated endocytosis and Fcγ-receptor (FcγR)-mediated phagocytosis [167, 168]. Other perturbations used previously include mutants of PIP5K and EHD1 but neither blocks internalization of cargo [162, 165, 169].

1.8.8 Novel Endocytic Pathways

In addition to the endocytic mechanisms mentioned above, several further mechanisms exist that have been termed "novel pathways" in the literature [4]. They commonly fail to match the requirements laid out above. Also, they have been mostly described using viruses as cargo molecules. As the receptors responsible for virus uptake by these mechanisms have not been clearly identified, the cellular function remains unknown.

Influenza A virus typically enters cells via CME [170]. In addition, influenza viruses use a second, alternative mechanism simultaneously in the same cells [171–173]. It appears that the spherical influenza particles use CME whereas larger filamentous particles use the alternate mechanism [174].

The alternative pathway for IAV internalization is clathrin-, caveolin-, and dynamin-independent [171], but shares similarities with macropinocytosis [172]. Virus uptake requires an intact actomyosin network, and signal transduction by the kinases PAK1, PI3K Src family kinases and PKC [172].

The uptake mechanisms for the human papillomavirus (HPV) [71, 175] and the lymphocytic choriomeningitis virus (LCMV) [57, 176] are additional examples for viruses that use further mechanisms.

HPV uses a mechanism that is independent of clathrin, caveolin, lipid rafts, and dynamin but requires actin dynamics and a set of kinases similar to those involved in macropinocytosis [71]. However, unlike macropinocytosis, it is independent of cholesterol and Rho-GTPases. Ultrastructural imaging shows the virus particle in small membrane indentations and pits that share no resemblance to the outward protrusions typical for macropinocytosis [71].

LCMV is another virus that, like influenza, can enter to a small extent via CME, but mainly uses an alternative route of internalization [57]. The requirements for this route do not match the pathways described above, as it does not require clathrin, caveolin, dynamin, or actin dynamics. Although lipid rafts have been implied, carefully controlled experiments exclude a need for cholesterol [57, 176].

1.8.9 Phagocytosis

Basic Mechanisms of Phagocytosis

As opposed to the preceding pathways, phagocytosis is a mechanism employed only by specialized cells of the immune system for uptake of large particles, such as bacteria or apoptotic bodies [177]. Two mechanisms of phagocytosis can be distinguished. Type I phagocytosis is mediated by the FcγR that allows recognition of particles coated with immunoglobulins [178]. Here, membrane extensions wrap around the particle to engulf it [179, 180]. Type II phagocytosis is initiated by the complement receptor 3 (CR3) [181]. In this process the opsonized particles appear to sink into the plasma membrane and little membrane protrusive activity is observed [182]. The resulting phagosome matures in both cases and acquires lysosomal properties that allow degradation of the cargo. Type I phagocytosis additionally initiates an inflammatory response [183, 184].

The mechanism of phagocytosis has been researched extensively since its discovery over a century ago. Phagocytosis starts with the clustering of the phagocytic receptor. While this most likely occurs by diffusion of receptor molecules in the membrane, RhoA may facilitate this process [185]. RhoA function may be required for the formation of clusters between FcγRs and associated β2 integrins [186].

After clustering, immune-receptor tyrosine activation motifs (ITAMs) of the receptors are phosphorylated [187]. Src family kinases play an important role in this process although knockdown experiments indicate some redundancy in the system [188]. The kinase Syk is recruited to phosphorylated ITAMs, upon which it is activated by autophosphorylation and possibly further kinase activity [189, 190]. In addition, increased levels of Ca^{2+} and reactive oxygen species play a role in the activation of this kinase [191, 192].

Downstream of the immune-receptor signaling, actin polymerization is activated.

Both types of phagocytosis employ Rho-like GTPases to mediate actin rearrangement. Type I and type II phagocytosis require Cdc42/Rac1 and RhoA, respectively [182, 193, 194].

Arf6 is another GTPase with a role in actin rearrangements and is required in type I phagocytosis [168]. The phenotype observed upon Arf6 perturbation implies that Rac1 and Arf6 rely on the same effector pathway.

The size of particles internalized by phagocytosis necessitates extensive membrane rearrangements. The surface area of cells undergoing phagocytosis however remains largely unchanged, indicating the insertion of additional membrane for pseudopod formation [195]. The origin of this membrane is likely derived from endosomal organelles [196]. Exertion requires exocytosis [197]. PI3K is involved in the regulation of this process making it an important mediator of pseudopod formation [198].

Dynamin is also required for phagocytosis [199]. Here, it aids the efficient exocytosis of vesicles to allow pseudopod extension rather than vesicle scission [199, 200]. In addition, dynamin also plays a role in the maturation of phagosomes [201].

Experimental Approaches to Perturb Phagocytosis

As actin plays a major role in mediating the membrane extension, perturbing its function has detrimental effects on phagocytosis. Actin polymerization can be targeted upstream at the regulatory steps, with DN mutants of the Rho-like GTPases Rho, Rac1, or Cdc42, depending on the type of phagocytosis [182]. Inhibitors (see above), provide another easy and universal tool to disrupt actin polymerization.

Another common target that is found again in phagocytosis is dynamin. Despite the fact that the role for dynamin in phagocytosis differs from that in other pathways of endocytosis, the same tools can be applied for perturbation. Gold et al. [199] showed that the DN Dyn-K44A is sufficient to effectively block particle uptake.

To analyze Arf6 involvement, cells transfected with Arf6-Q67L and Arf6-T27N no longer show proper formation of a phagocytic cup, resulting in a block in phagocytosis [168].

Src kinases were shown to play a role in phosphorylation of ITAMs and in activation of Syk. However, even in cells lacking Src family kinases, phagocytosis is merely reduced, not blocked [188]. Targeting the downstream kinase Syk may be more efficient. In Syk-deficient cells phagocytosis is abrogated, a phenotype that can be reproduced with siRNA depletion of Syk [188, 191, 202, 203].

The role of PI3K in phagocytosis was unraveled by the use of inhibitors [198]. Other tools described above that target PI3K should block pseudopod formation and thereby phagocytosis as well.

2 Conclusions

In a nutshell, it is obvious that the complexity of endocytic mechanisms revealed over the last decade does not allow easy conclusions from isolated perturbation experiments. A number of factors participate in several different pathways, sometimes even in a mechanistically distinct fashion. Thus, only a comprehensive perturbation

strategy enables the identification of the endocytic machinery that a particular ligand or receptor requires. Due to the specific limitations of the different perturbation strategies, a combination of approaches will allow a better view on the mechanism that is being analyzed.

However, it is important to note that the definition of endocytic mechanisms by sets of defined factors may be somewhat arbitrary and should be treated with caution. If applied rigorously, mechanisms such as CME would have to be split up into several different mechanisms, since sets of adaptor proteins are essential or dispensable for endocytosis of one cargo but not another. In addition, the adaptors may also substitute for one another. In turn, this may mean that upon closer analysis pathways that are considered as distinct entities as yet might be in fact variations of a single mechanism. Nevertheless, the perturbations laid our above will provide an initial characterization of the mechanism involved and will allow a more detailed characterization.

Acknowledgements

We would like to thank members of the Schelhaas laboratory for helpful comments and suggestions on the manuscript. Work in the Schelhaas laboratory is supported by the German Research Foundation (DFG) (grant SCHE 1552/2-1, Collaborative Research Centre SFB629/A16, International Graduate School GRK1409/C2, and partly by EXC 1003).

References

1. Conner SD, Schmid SL (2003) Regulated portals of entry into the cell. Nature 422:37–44
2. Doherty GJ, McMahon HT (2009) Mechanisms of endocytosis. Annu Rev Biochem 78:857–902
3. Hansen CG, Nichols BJ (2009) Molecular mechanisms of clathrin-independent endocytosis. J Cell Sci 122:1713–1721
4. Mercer J, Schelhaas M, Helenius A (2010) Virus entry by endocytosis. Annu Rev Biochem 79:803–833
5. Osborne A, Flett A, Smythe E (2005) Endocytosis assays in intact and permeabilized cells. *Current Prot Cell Biol* Chapter 11, Unit 11 18
6. Knisely JM, Lee J, Bu G (2008) Measurement of receptor endocytosis and recycling. Methods Mol Biol 457:319–332
7. Pan Q, van der Laan LJ, Janssen HL, Peppelenbosch MP (2012) A dynamic perspective of RNAi library development. Trends Biotechnol 30:206–215
8. Rao DD, Senzer N, Cleary MA, Nemunaitis J (2009) Comparative assessment of siRNA and shRNA off target effects: what is slowing clinical development. Cancer Gene Ther 16:807–809
9. Rao DD, Vorhies JS, Senzer N, Nemunaitis J (2009) siRNA vs. shRNA: similarities and differences. Adv Drug Deliv Rev 61:746–759
10. Echeverri CJ, Beachy PA, Baum B et al (2006) Minimizing the risk of reporting false positives in large-scale RNAi screens. Nat Methods 3:777–779
11. Echeverri CJ, Perrimon N (2006) High-throughput RNAi screening in cultured cells: a user's guide. Nat Rev Genet 7:373–384

12. Esvelt KM, Wang HH (2013) Genome-scale engineering for systems and synthetic biology. Mol Syst Biol 9:641
13. Tan WS, Carlson DF, Walton MW, Fahrenkrug SC, Hackett PB (2012) Precision editing of large animal genomes. Adv Genet 80:37–97
14. Doyon JB, Zeitler B, Cheng J et al (2011) Rapid and efficient clathrin-mediated endocytosis revealed in genome-edited mammalian cells. Nat Cell Biol 13:331–337
15. Herskowitz I (1987) Functional inactivation of genes by dominant negative mutations. Nature 329:219–222
16. Ivanov AI (2008) Pharmacological inhibition of endocytic pathways: is it specific enough to be useful? Methods Mol Biol 440:15–33
17. Roth TF, Porter KR (1964) Yolk protein uptake in the oocyte of the mosquito *Aedes aegypti* L. J Cell Biol 20:313–332
18. Huang F, Khvorova A, Marshall W, Sorkin A (2004) Analysis of clathrin-mediated endocytosis of epidermal growth factor receptor by RNA interference. J Biol Chem 279: 16657–16661
19. Saheki Y, De Camilli P (2012) Synaptic vesicle endocytosis. Cold Spring Harb Perspect Biol 4:a005645
20. Pearse BM (1982) Coated vesicles from human placenta carry ferritin, transferrin, and immunoglobulin G. Proc Natl Acad Sci U S A 79:451–455
21. Jing SQ, Spencer T, Miller K, Hopkins C, Trowbridge IS (1990) Role of the human transferrin receptor cytoplasmic domain in endocytosis: localization of a specific signal sequence for internalization. J Cell Biol 110:283–294
22. Pizarro-Cerda J, Bonazzi M, Cossart P (2010) Clathrin-mediated endocytosis: what works for small, also works for big. Bioessays 32:496–504
23. Yamashiro DJ, Tycko B, Fluss SR, Maxfield FR (1984) Segregation of transferrin to a mildly acidic (pH 6.5) para-Golgi compartment in the recycling pathway. Cell 37: 789–800
24. Grant BD, Donaldson JG (2009) Pathways and mechanisms of endocytic recycling. Nat Rev Mol Cell Biol 10:597–608
25. Hopkins CR, Miller K, Beardmore JM (1985) Receptor-mediated endocytosis of transferrin and epidermal growth factor receptors: a comparison of constitutive and ligand-induced uptake. J Cell Sci 3:173–186
26. Taylor MJ, Perrais D, Merrifield CJ (2011) A high precision survey of the molecular dynamics of mammalian clathrin-mediated endocytosis. PLoS Biol 9:e1000604
27. Henne WM, Boucrot E, Meinecke M et al (2010) FCHo proteins are nucleators of clathrin-mediated endocytosis. Science 328:1281–1284
28. Traub LM (2009) Tickets to ride: selecting cargo for clathrin-regulated internalization. Nat Rev Mol Cell Biol 10:583–596
29. Brett TJ, Traub LM, Fremont DH (2002) Accessory protein recruitment motifs in clathrin-mediated endocytosis. Structure 10: 797–809
30. Kirchhausen T (2000) Clathrin. Annu Rev Biochem 69:699–727
31. Tebar F, Sorkina T, Sorkin A, Ericsson M, Kirchhausen T (1996) Eps15 is a component of clathrin-coated pits and vesicles and is located at the rim of coated pits. J Biol Chem 271:28727–28730
32. Ferguson SM, Raimondi A, Paradise S (2009) Coordinated actions of actin and BAR proteins upstream of dynamin at endocytic clathrin-coated pits. Dev Cell 17: 811–822
33. Wigge P, Kohler K, Vallis Y et al (1997) Amphiphysin heterodimers: potential role in clathrin-mediated endocytosis. Mol Biol Cell 8:2003–2015
34. Hinshaw JE (2000) Dynamin and its role in membrane fission. Annu Rev Cell Dev Biol 16:483–519
35. Damke H, Baba T, Warnock DE, Schmid SL (1994) Induction of mutant dynamin specifically blocks endocytic coated vesicle formation. J Cell Biol 127:915–934
36. Hinshaw JE, Schmid SL (1995) Dynamin self-assembles into rings suggesting a mechanism for coated vesicle budding. Nature 374 (6518):190–192
37. Warnock DE, Hinshaw JE, Schmid SL (1996) Dynamin self-assembly stimulates its GTPase activity. J Biol Chem 271:22310–22314
38. Sever S, Damke H, Schmid SL (2000) Garrotes, springs, ratchets, and whips: putting dynamin models to the test. Traffic 1:385–392
39. Kozlov MM (1999) Dynamin: possible mechanism of "Pinchase" action. Biophys J 77: 604–616
40. Bashkirov PV, Akimov SA, Evseev AI et al (2008) GTPase cycle of dynamin is coupled to membrane squeeze and release, leading to spontaneous fission. Cell 135:1276–1286
41. Stowell MH, Marks B, Wigge P, McMahon HT (1999) Nucleotide-dependent conformational changes in dynamin: evidence for a

mechanochemical molecular spring. Nat Cell Biol 1(1):27–32

42. Faelber K, Held M, Gao S et al (2012) Structural insights into dynamin-mediated membrane fission. Structure 20:1621–1628
43. Kaksonen M, Sun Y, Drubin DG (2003) A pathway for association of receptors, adaptors, and actin during endocytic internalization. Cell 115:475–487
44. Boulant S, Kural C, Zeeh JC, Ubelmann F, Kirchhausen T (2011) Actin dynamics counteract membrane tension during clathrin-mediated endocytosis. Nat Cell Biol 13: 1124–1131
45. Cureton DK, Massol RH, Whelan SP, Kirchhausen T (2010) The length of vesicular stomatitis virus particles dictates a need for actin assembly during clathrin-dependent endocytosis. PLoS Pathog 6:e1001127
46. Warren RA, Green FA, Stenberg PE, Enns CA (1998) Distinct saturable pathways for the endocytosis of different tyrosine motifs. J Biol Chem 273:17056–17063
47. Hinrichsen L, Harborth J, Andrees L, Weber K, Ungewickell EJ (2003) Effect of clathrin heavy chain- and alpha-adaptin-specific small inhibitory RNAs on endocytic accessory proteins and receptor trafficking in HeLa cells. J Biol Chem 278:45160–45170
48. Cremona O, Di Paolo G, Wenk MR et al (1999) Essential role of phosphoinositide metabolism in synaptic vesicle recycling. Cell 99:179–188
49. Schlossman DM, Schmid SL, Braell W, Rothman JE (1984) An enzyme that removes clathrin coats: purification of an uncoating ATPase. J Cell Biol 99:723–733
50. Ungewickell E, Ungewickell H, Holstein SE et al (1995) Role of auxilin in uncoating clathrin-coated vesicles. Nature 378: 632–635
51. Cosson P, de Curtis I, Pouysségur J, Griffiths G, Davoust J (1989) Low cytoplasmic pH inhibits endocytosis and transport from the trans-Golgi network to the cell surface. J Cell Biol 108:377–387
52. Heuser JE, Anderson RG (1989) Hypertonic media inhibit receptor-mediated endocytosis by blocking clathrin-coated pit formation. J Cell Biol 108:389–400
53. Doxsey SJ, Brodsky FM, Blank GS, Helenius A (1987) Inhibition of endocytosis by anti-clathrin antibodies. Cell 50:453–463
54. Liu SH, Marks MS, Brodsky FM (1998) A dominant-negative clathrin mutant differentially affects trafficking of molecules with distinct sorting motifs in the class II major histocompatibility complex (MHC) pathway. J Cell Biol 140:1023–1037
55. Acton SL, Brodsky FM (1990) Predominance of clathrin light chain LCb correlates with the presence of a regulated secretory pathway. J Cell Biol 111:1419–1426
56. Motley A, Bright NA, Seaman MN, Robinson MS (2003) Clathrin-mediated endocytosis in AP-2-depleted cells. J Cell Biol 162:909–918
57. Quirin K, Eschli B, Scheu I et al (2008) Lymphocytic choriomeningitis virus uses a novel endocytic pathway for infectious entry via late endosomes. Virology 378:21–33
58. von Kleist L, Stahlschmidt W, Bulut H et al (2011) Role of the clathrin terminal domain in regulating coated pit dynamics revealed by small molecule inhibition. Cell 146:471–484
59. van der Bliek AM, Redelmeier TE, Damke H et al (1993) Mutations in human dynamin block an intermediate stage in coated vesicle formation. J Cell Biol 122:553–563
60. Damke H, Binns DD, Ueda H et al (2001) Dynamin GTPase domain mutants block endocytic vesicle formation at morphologically distinct stages. Mol Biol Cell 12:2578–2589
61. Sidiropoulos PN, Miehe M, Bock T et al (2012) Dynamin 2 mutations in Charcot-Marie-Tooth neuropathy highlight the importance of clathrin-mediated endocytosis in myelination. Brain 135:1395–1411
62. Macia E, Ehrlich M, Massol R et al (2006) Dynasore, a cell-permeable inhibitor of dynamin. Dev Cell 10:839–850
63. McCluskey A, Daniel JA, Hadzic G et al (2013) Building a better dynasore: the dyngo compounds potently inhibit dynamin and endocytosis. Traffic 14:1272–1289
64. McGeachie AB, Odell LR, Quan A et al (2013) Pyrimidyn compounds: dual-action small molecule pyrimidine-based dynamin inhibitors. ACS Chem Biol 8(7):1507–1518
65. Nesterov A, Carter RE, Sorkina T, Gill GN, Sorkin A (1999) Inhibition of the receptor-binding function of clathrin adaptor protein AP-2 by dominant-negative mutant mu2 subunit and its effects on endocytosis. EMBO J 18:2489–2499
66. Gaidarov I, Keen JH (1999) Phosphoinositide-AP-2 interactions required for targeting to plasma membrane clathrin-coated pits. J Cell Biol 146:755–764
67. Robinson MS, Sahlender DA, Foster SD (2010) Rapid inactivation of proteins by rapamycin-induced rerouting to mitochondria. Dev Cell 18:324–331
68. Wang L-H, Rothberg KG, Anderson RGW (1993) Mis-assembly of clathrin lattices on

endosomes reveals a regulatory switch for coated pit formation materials and methods. J Cell Biol 123:1107–1117

69. Ogiso T, Iwaki M, Mori K (1981) Fluidity of human erythrocyte membrane and effect of chlorpromazine on fluidity and phase separation of membrane. Biochim Biophys Acta 649:325–335
70. Walenga RW, Opas EE, Feinstein MB (1981) Differential effects of calmodulin antagonists on phospholipases A2 and C in thrombin-stimulated platelets. J Biol Chem 256: 12523–12528
71. Schelhaas M, Shah B, Holzer M (2012) Entry of human papillomavirus type 16 by actin-dependent, clathrin- and lipid raft-independent endocytosis. PLoS Pathog 8:e1002657
72. Benmerah A, Lamaze C, Bègue B (1998) AP-2/Eps15 interaction is required for receptor-mediated endocytosis. J Cell Biol 140:1055–1062
73. Simpson F, Hussain NK, Qualmann B et al (1999) SH3-domain-containing proteins function at distinct steps in clathrin-coated vesicle formation. Nat Cell Biol 1:119–124
74. Qualmann B, Kelly RB (2000) Syndapin isoforms participate in receptor-mediated endocytosis and actin organization. J Cell Biol 148:1047–1062
75. Kessels MM, Engqvist-Goldstein AE, Drubin DG, Qualmann B (2001) Mammalian Abp1, a signal-responsive F-actin-binding protein, links the actin cytoskeleton to endocytosis via the GTPase dynamin. J Cell Biol 153:351–366
76. Massol RH, Boll W, Griffin AM, Kirchhausen T (2006) A burst of auxilin recruitment determines the onset of clathrin-coated vesicle uncoating. Proc Natl Acad Sci U S A 103: 10265–10270
77. Maldonado-Baez L, Wendland B (2006) Endocytic adaptors: recruiters, coordinators and regulators. Trends Cell Biol 16:505–513
78. Szymkiewicz I, Shupliakov O, Dikic I (2004) Cargo- and compartment-selective endocytic scaffold proteins. Biochem J 383(Pt 1):1–11
79. Montesano R, Roth J, Robert A, Orci L (1982) Non-coated membrane invaginations are involved in binding and internalization of cholera and tetanus toxins. Nature 296:651–653
80. Rothberg KG, Heuser JE, Donzell WC et al (1992) Caveolin, a protein component of caveolae membrane coats. Cell 68:673–682
81. Scherer PE, Lewis RY, Volonte D et al (1997) Cell-type and tissue-specific expression of caveolin-2. Caveolins 1 and 2 co-localize and form a stable hetero-oligomeric complex in vivo. J Biol Chem 272:29337–29346
82. Song KS, Scherer PE, Tang Z et al (1996) Expression of caveolin-3 in skeletal, cardiac, and smooth muscle cells. Caveolin-3 is a component of the sarcolemma and co-fractionates with dystrophin and dystrophin-associated glycoproteins. J Biol Chem 271:15160–15165
83. Anderson HA, Chen Y, Norkin LC (1996) Bound simian virus 40 translocates to caveolin-enriched membrane domains, and its entry is inhibited by drugs that selectively disrupt caveolae. Mol Biol Cell 7:1825–1834
84. Gilbert J, Benjamin T (2004) Uptake pathway of polyomavirus via ganglioside GD1a. J Virol 78:12259–12267
85. Eash S, Querbes W, Atwood WJ (2004) Infection of vero cells by BK virus is dependent on caveolae. J Virol 78:11583–11590
86. Pelkmans L, Kartenbeck J, Helenius A (2001) Caveolar endocytosis of simian virus 40 reveals a new two-step vesicular-transport pathway to the ER. Nat Cell Biol 3:473–483
87. Engel S, Heger T, Mancini R et al (2011) Role of endosomes in simian virus 40 entry and infection. J Virol 85:4198–4211
88. Monier S, Parton RG, Vogel F et al (1995) VIP21-caveolin, a membrane protein constituent of the caveolar coat, oligomerizes in vivo and in vitro. Mol Biol Cell 6:911–927
89. Scheiffele P, Verkade P, Fra AM et al (1998) Caveolin-1 and -2 in the exocytic pathway of MDCK cells. J Cell Biol 140:795–806
90. Hayer A, Stoeber M, Bissig C, Helenius A (2010) Biogenesis of caveolae: stepwise assembly of large caveolin and cavin complexes. Traffic 11:361–382
91. Ludwig A, Howard G, Mendoza-Topaz C et al (2013) Molecular composition and ultrastructure of the caveolar coat complex. PLoS Biol 11:e1001640
92. Hansen CG, Bright NA, Howard G, Nichols BJ (2009) SDPR induces membrane curvature and functions in the formation of caveolae. Nat Cell Biol 11:807–814
93. McMahon KA, Zajicek H, Li WP et al (2009) SRBC/cavin-3 is a caveolin adapter protein that regulates caveolae function. EMBO J 28:1001–1015
94. Stoeber M, Stoeck IK, Hanni C et al (2012) Oligomers of the ATPase EHD2 confine caveolae to the plasma membrane through association with actin. EMBO J 31: 2350–2364
95. Parton RG, Joggerst B, Simons K (1994) Regulated internalization of caveolae. J Cell Biol 127:1199–1215
96. Minshall RD, Tiruppathi C, Vogel SM et al (2000) Endothelial cell-surface gp60 activates

vesicle formation and trafficking via G(i)-coupled Src kinase signaling pathway. J Cell Biol 150:1057–1070

97. Pelkmans L, Puntener D, Helenius A (2002) Local actin polymerization and dynamin recruitment in SV40-induced internalization of caveolae. Science 296:535–539
98. McIntosh PO, Schnitzer A (1998) Dynamin at the neck of caveolae mediates their budding to form transport vesicles by GTP-driven fission from the plasma membrane of endothelium. J Cell Biol 141:101–114
99. Klein IK, Predescu DN, Sharma T (2009) Intersectin-2L regulates caveola endocytosis secondary to Cdc42-mediated actin polymerization. J Biol Chem 284:25953–25961
100. Predescu SA, Predescu DN, Malik AB (2007) Molecular determinants of endothelial transcytosis and their role in endothelial permeability. Am J Physiol Lung Cell Mol Physiol 293:L823–L842
101. Rodal SK, Skretting G, Garred O et al (1999) Extraction of cholesterol with methyl-beta-cyclodextrin perturbs formation of clathrin-coated endocytic vesicles. Mol Biol Cell 10:961–974
102. Subtil A, Gaidarov I, Kobylarz K et al (1999) Acute cholesterol depletion inhibits clathrin-coated pit budding. Proc Natl Acad Sci U S A 96:6775–6780
103. Orlandi PA, Fishman PH (1998) Filipin-dependent inhibition of cholera toxin: evidence for toxin internalization and activation through caveolae-like domains. J Cell Biol 141:905–915
104. Cooper JA (1987) Effects of cytochalasin and phalloidin on actin. J Cell Biol 105:1473–1478
105. Coue M, Brenner SL, Spector I, Korn ED (1987) Inhibition of actin polymerization by latrunculin A. FEBS Lett 213:316–318
106. Bubb MR, Spector I, Beyer BB, Fosen KM (2000) Effects of jasplakinolide on the kinetics of actin polymerization. An explanation for certain in vivo observations. J Biol Chem 275:5163–5170
107. Drab M, Verkade P, Elger M (2001) Loss of caveolae, vascular dysfunction, and pulmonary defects in caveolin-1 gene-disrupted mice. Science 293:2449–2452
108. Chen Y, Norkin LC (1999) Extracellular simian virus 40 transmits a signal that promotes virus enclosure within caveolae. Exp Cell Res 246:83–90
109. Pelkmans L, Zerial M (2005) Kinase-regulated quantal assemblies and kiss-and-run recycling of caveolae. Nature 436:128–133
110. Damm E-M, Pelkmans L, Kartenbeck J et al (2005) Clathrin- and caveolin-1-independent endocytosis: entry of simian virus 40 into cells devoid of caveolae. J Cell Biol 168:477–488
111. Le PU, Guay G, Altschuler Y, Nabi IR (2002) Caveolin-1 is a negative regulator of caveolae-mediated endocytosis to the endoplasmic reticulum. J Biol Chem 277:3371–3379
112. Pelkmans L, Bürli T, Zerial M, Helenius A (2004) Caveolin-stabilized membrane domains as multifunctional transport and sorting devices in endocytic membrane traffic. Cell 118:767–780
113. Glebov OO, Bright NA, Nichols BJ (2006) Flotillin-1 defines a clathrin-independent endocytic pathway in mammalian cells. Nat Cell Biol 8:46–54
114. Frick M, Bright NA, Riento K et al (2007) Coassembly of flotillins induces formation of membrane microdomains, membrane curvature, and vesicle budding. Curr Biol 17:1151–1156
115. Cremona ML, Matthies HJ, Pau K et al (2011) Flotillin-1 is essential for PKC-triggered endocytosis and membrane microdomain localization of DAT. Nat Neurosci 14:469–477
116. Ge L, Qi W, Wang LJ et al (2011) Flotillins play an essential role in Niemann-Pick C1-like 1-mediated cholesterol uptake. Proc Natl Acad Sci U S A 108:551–556
117. Ludwig A, Otto GP, Riento K et al (2010) Flotillin microdomains interact with the cortical cytoskeleton to control uropod formation and neutrophil recruitment. J Cell Biol 191:771–781
118. Neumann-Giesen C, Fernow I, Amaddii M, Tikkanen R (2007) Role of EGF-induced tyrosine phosphorylation of reggie-1/flotillin-2 in cell spreading and signaling to the actin cytoskeleton. J Cell Sci 120:395–406
119. Riento K, Frick M, Schafer I, Nichols BJ (2009) Endocytosis of flotillin-1 and flotillin-2 is regulated by Fyn kinase. J Cell Sci 122:912–918
120. Babuke T, Ruonala M, Meister M et al (2009) Hetero-oligomerization of reggie-1/flotillin-2 and reggie-2/flotillin-1 is required for their endocytosis. Cell Signal 21:1287–1297
121. Vassilieva EV, Ivanov AI, Nusrat A (2009) Flotillin-1 stabilizes caveolin-1 in intestinal epithelial cells. Biochem Biophys Res Commun 379:460–465
122. Kokubo H, Helms JB, Ohno-Iwashita Y et al (2003) Ultrastructural localization of flotillin-1 to cholesterol-rich membrane microdo-

mains, rafts, in rat brain tissue. Brain Res 965:83–90

123. Lewis WH (1931) Pinocytosis. Bull Johns Hopkins Hosp 49:17
124. Swanson JA, Watts C (1995) Macropinocytosis. Trends Cell Biol 5:424–428
125. Haigler HT, McKanna JA, Cohen S (1979) Rapid stimulation of pinocytosis in human carcinoma cells A-431 by epidermal growth factor. J Cell Biol 83:82–90
126. Amyere M, Payrastre B, Krause U (2000) Constitutive macropinocytosis in oncogene-transformed fibroblasts depends on sequential permanent activation of phosphoinositide 3-kinase and phospholipase C. Mol Biol Cell 11:3453–3467
127. Miyata Y, Nishida E, Koyasu S, Yahara I, Sakai H (1989) Protein kinase C-dependent and -independent pathways in the growth factor-induced cytoskeletal reorganization. J Biol Chem 264:15565–15568
128. Ridley AJ, Paterson HF, Johnston CL, Diekmann D, Hall A (1992) The small GTP-binding protein rac regulates growth factor-induced membrane ruffling. Cell 70: 401–410
129. Suetsugu S, Yamazaki D, Kurisu S, Takenawa T (2003) Differential roles of WAVE1 and WAVE2 in dorsal and peripheral ruffle formation for fibroblast cell migration. Dev Cell 5:595–609
130. Krueger EW, Orth JD, Cao H, McNiven MA (2003) A dynamin-cortactin-Arp2/3 complex mediates actin reorganization in growth factor-stimulated cells. Mol Biol Cell 14: 1085–1096
131. Koivusalo M, Welch C, Hayashi H et al (2010) Amiloride inhibits macropinocytosis by lowering submembranous pH and preventing Rac1 and Cdc42 signaling. J Cell Biol 188:547–563
132. Dharmawardhane S, Schurmann A, Sells MA (2000) Regulation of macropinocytosis by p21-activated kinase-1. Mol Biol Cell 11: 3341–3352
133. Liberali P, Kakkonen E, Turacchio G et al (2008) The closure of Pak1-dependent macropinosomes requires the phosphorylation of CtBP1/BARS. EMBO J 27:970–981
134. Lim JP, Gleeson PA (2011) Macropinocytosis: an endocytic pathway for internalising large gulps. Immunol Cell Biol 89:836–843
135. Mercer J, Helenius A (2012) Gulping rather than sipping: macropinocytosis as a way of virus entry. Curr Opin Microbiol 15: 490–499
136. Steinman RM, Silver JM, Cohn ZA (1974) Pinocytosis in fibroblasts. Quantitative studies in vitro. J Cell Biol 63:949–969
137. Kerr MC, Lindsay MR, Luetterforst R et al (2006) Visualisation of macropinosome maturation by the recruitment of sorting nexins. J Cell Sci 119:3967–3980
138. Suetsugu S, Miki H, Takenawa T (1999) Identification of two human WAVE/SCAR homologues as general actin regulatory molecules which associate with the Arp2/3 complex. Biochem Biophys Res Commun 260:296–302
139. Machesky LM, Insall RH (1998) Scar1 and the related Wiskott-Aldrich syndrome protein, WASP, regulate the actin cytoskeleton through the Arp2/3 complex. Curr Biol 8:1347–1356
140. Chen LM, Hobbie S, Galan JE (1996) Requirement of CDC42 for Salmonella-induced cytoskeletal and nuclear responses. Science 274:2115–2118
141. Mercer J, Knebel S, Schmidt FI et al (2010) Vaccinia virus strains use distinct forms of macropinocytosis for host-cell entry. Proc Natl Acad Sci USA 107:9346–9351
142. Mercer J, Helenius A (2008) Vaccinia virus uses macropinocytosis and apoptotic mimicry to enter host cells. Science 320:531–535
143. Dowrick P, Kenworthy P, McCann B, Warn R (1993) Circular ruffle formation and closure lead to macropinocytosis in hepatocyte growth factor/scatter factor-treated cells. Eur J Cell Biol 61:44–53
144. Fretz M, Jin J, Conibere R et al (2006) Effects of Na+/H+ exchanger inhibitors on subcellular localisation of endocytic organelles and intracellular dynamics of protein transduction domains HIV-TAT peptide and octaarginine. J Control Release 116:247–254
145. Lagana A, Vadnais J, Le PU et al (2000) Regulation of the formation of tumor cell pseudopodia by the Na(+)/H(+) exchanger NHE1. J Cell Sci 113:3649–3662
146. Deacon SW, Beeser A, Fukui JA et al (2008) An isoform-selective, small-molecule inhibitor targets the autoregulatory mechanism of p21-activated kinase. Chem Biol 15:322–331
147. Arcaro A, Wymann MP (1993) Wortmannin is a potent phosphatidylinositol 3-kinase inhibitor : the role of phosphatidylinositol 3,4,5-trisphosphate in neutrophil responses. Biochem J 301:297–301
148. Vlahos CJ, Matter WF, Hui KY, Brown RF (1994) A specific inhibitor of phosphatidylinositol 3-kinase, 2-(4-morpholinyl)-8-phenyl-

4H-1-benzopyran-4-one (LY294002). J Biol Chem 269:5241–5248

149. Sabharanjak S, Sharma P, Parton RG, Mayor S (2002) GPI-anchored proteins are delivered to recycling endosomes via a distinct cdc42-regulated, clathrin-independent pinocytic pathway. Dev Cell 2:411–423
150. Kirkham M, Parton RG (2005) Clathrin -independent endocytosis: new insights into caveolae and non-caveolar lipid raft carriers. Biochim Biophys Acta 1746:349–363
151. Kirkham M, Fujita A, Chadda R et al (2005) Ultrastructural identification of uncoated caveolin-independent early endocytic vehicles. J Cell Biol 168:465–476
152. Lundmark R, Doherty GJ, Howes MT et al (2008) The GTPase-activating protein GRAF1 regulates the CLIC/GEEC endocytic pathway. Curr Biol 18:1802–1808
153. Chadda R, Howes MT, Plowman SJ et al (2007) Cholesterol-sensitive Cdc42 activation regulates actin polymerization for endocytosis via the GEEC pathway. Traffic 8: 702–717
154. Kumari S, Mayor S (2008) ARF1 is directly involved in dynamin-independent endocytosis. Nat Cell Biol 10:30–41
155. Nonnenmacher M, Weber T (2011) Adeno-associated virus 2 infection requires endocytosis through the CLIC/GEEC pathway. Cell Host Microbe 10:563–576
156. Subtil A, Hémar A, Dautry-Varsat A (1994) Rapid endocytosis of interleukin 2 receptors when clathrin-coated pit endocytosis is inhibited. J Cell Sci 107:3461–3468
157. Lamaze C, Dujeancourt A, Baba T et al (2001) Interleukin 2 receptors and detergent-resistant membrane domains define a clathrin-independent endocytic pathway. Mol Cell 7:661–671
158. Sauvonnet N, Dujeancourt A, Dautry-Varsat A (2005) Cortactin and dynamin are required for the clathrin-independent endocytosis of gammac cytokine receptor. J Cell Biol 168:155–163
159. Grassart A, Dujeancourt A, Lazarow PB, Dautry-Varsat A, Sauvonnet N (2008) Clathrin-independent endocytosis used by the IL-2 receptor is regulated by Rac1, Pak1 and Pak2. EMBO Rep 9:356–362
160. Basquin C, Malarde V, Mellor P et al (2013) The signalling factor PI3K is a specific regulator of the clathrin-independent dynamin-dependent endocytosis of IL-2 receptors. J Cell Sci 126:1099–1108
161. Radhakrishna H, Donaldson JG (1997) ADP-ribosylation factor 6 regulates a novel plasma membrane recycling pathway. J Cell Biol 139:49–61
162. Caplan S, Naslavsky N, Hartnell LM et al (2002) A tubular EHD1-containing compartment involved in the recycling of major histocompatibility complex class I molecules to the plasma membrane. EMBO J 21:2557–2567
163. Naslavsky N, Weigert R, Donaldson JG (2004) Characterization of a nonclathrin endocytic pathway: membrane cargo and lipid requirements. Mol Biol Cell 15:3542–3552
164. Naslavsky N, Weigert R, Donaldson JG (2003) Convergence of non-clathrin- and clathrin-derived endosomes involves Arf6 inactivation and changes in phosphoinositides. Mol Biol Cell 14:417–431
165. Brown FD, Rozelle AL, Yin HL, Balla T, Donaldson JG (2001) Phosphatidylinositol 4,5-bisphosphate and Arf6-regulated membrane traffic. J Cell Biol 154:1007–1017
166. Donaldson JG (2003) Multiple roles for Arf6: sorting, structuring, and signaling at the plasma membrane. J Biol Chem 278:41573–41576
167. D'Souza-Schorey C, Li G, Colombo MI, Stahl PD (1995) A regulatory role for ARF6 in receptor-mediated endocytosis. Science 267:1175–1178
168. Zhang Q, Cox D, Tseng CC, Donaldson JG, Greenberg S (1998) A requirement for ARF6 in Fcgamma receptor-mediated phagocytosis in macrophages. J Biol Chem 273:19977–19981
169. Vidal-Quadras M, Gelabert-Baldrich M, Soriano-Castell D et al (2011) Rac1 and calmodulin interactions modulate dynamics of ARF6-dependent endocytosis. Traffic 12:1879–1896
170. Matlin KS, Reggio H, Helenius A, Simons K (1981) Infectious entry pathway of influenza virus in a canine kidney cell line. J Cell Biol 91:601–613
171. Sieczkarski SB, Whittaker GR (2002) Influenza virus can enter and infect cells in the absence of clathrin-mediated endocytosis. J Virol 76:10455–10464
172. de Vries E, Tscherne DM, Wienholts MJ et al (2011) Dissection of the influenza A virus endocytic routes reveals macropinocytosis as an alternative entry pathway. PLoS Pathog 7:e1001329
173. Rust MJ, Lakadamyali M, Zhang F, Zhuang X (2004) Assembly of endocytic machinery around individual influenza viruses during viral entry. Nat Struct Mol Biol 11:567–573
174. Sieczkarski SB, Whittaker GR (2005) Characterization of the host cell entry of

filamentous influenza virus. Arch Virol 150:1783–1796

175. Spoden G, Kuhling L, Cordes N et al (2013) Human papillomavirus types 16, 18, and 31 share similar endocytic requirements for entry. J Virol 87:7765–7773
176. Rojek JM, Perez M, Kunz S (2008) Cellular entry of lymphocytic choriomeningitis virus. J Virol 82:1505–1517
177. Aderem A, Underhill DM (1999) Mechanisms of phagocytosis in macrophages. Annu Rev Immunol 17:593–623
178. Karakawa WW, Sutton A, Schneerson R, Karpas A, Vann WF (1988) Capsular antibodies induce type-specific phagocytosis of capsulated Staphylococcus aureus by human polymorphonuclear leukocytes. Infect Immun 56:1090–1095
179. Doshi N, Mitragotri S (2010) Macrophages recognize size and shape of their targets. PLoS One 5:e10051
180. Champion JA, Mitragotri S (2006) Role of target geometry in phagocytosis. Proc Natl Acad Sci U S A 103:4930–4934
181. Kaplan G (1977) Differences in the mode of phagocytosis with Fc and C3 receptors in macrophages. Scand J Immunol 6:797–807
182. Caron E, Hall A (1998) Identification of two distinct mechanisms of phagocytosis controlled by different Rho GTPases. Science 282:1717–1721
183. Wright SD, Silverstein SC (1983) Receptors for C3b and C3bi promote phagocytosis but not the release of toxic oxygen from human phagocytes. J Exp Med 158:2016–2023
184. Stein M, Gordon S (1991) Regulation of tumor necrosis factor (TNF) release by murine peritoneal macrophages: role of cell stimulation and specific phagocytic plasma membrane receptors. Eur J Immunol 21: 431–437
185. Hackam DJ, Rotstein OD, Schreiber A, Zhang WJ, Grinstein S (1997) Rho is required for the initiation of calcium signaling and phagocytosis by Fcgamma receptors in macrophages. J Exp Med 186:955–966
186. Laudanna C, Campbell JJ, Butcher EC (1996) Role of Rho in chemoattractant-activated leukocyte adhesion through integrins. Science 271:981–983
187. Paolini R, Jouvin MH, Kinet JP (1991) Phosphorylation and dephosphorylation of the high-affinity receptor for immunoglobulin E immediately after receptor engagement and disengagement. Nature 353:855–858
188. Crowley MT, Costello PS, Fitzer-Attas CJ et al (1997) A critical role for Syk in signal transduction and phagocytosis mediated by Fcgamma receptors on macrophages. J Exp Med 186:1027–1039
189. Rowley RB, Burkhardt AL, Chao HG, Matsueda GR, Bolen JB (1995) Syk protein-tyrosine kinase is regulated by tyrosine-phosphorylated Ig alpha/Ig beta immunoreceptor tyrosine activation motif binding and autophosphorylation. J Biol Chem 270:11590–11594
190. Kurosaki T, Takata M, Yamanashi Y et al (1994) Syk activation by the Src-family tyrosine kinase in the B cell receptor signaling. J Exp Med 179:1725–1729
191. Matsuda M, Park JG, Wang DC et al (1996) Abrogation of the Fc gamma receptor IIA-mediated phagocytic signal by stem-loop Syk antisense oligonucleotides. Mol Biol Cell 7:1095–1106
192. Schieven GL, Kirihara JM, Burg DL, Geahlen RL, Ledbetter JA (1993) p72syk tyrosine kinase is activated by oxidizing conditions that induce lymphocyte tyrosine phosphorylation and Ca2+ signals. J Biol Chem 268:16688–16692
193. Cox D, Chang P, Zhang Q et al (1997) Requirements for both Rac1 and Cdc42 in membrane ruffling and phagocytosis in leukocytes. J Exp Med 186:1487–1494
194. Massol P, Montcourrier P, Guillemot JC, Chavrier P (1998) Fc receptor-mediated phagocytosis requires CDC42 and Rac1. EMBO J 17:6219–6229
195. Bowers B, Olszewski TE, Hyde J (1981) Morphometric analysis of volumes and surface areas in membrane compartments during endocytosis in Acanthamoeba. J Cell Biol 88:509–515
196. Lennartz MR, Yuen AF, Masi SM et al (1997) Phospholipase A2 inhibition results in sequestration of plasma membrane into electronlucent vesicles during IgG-mediated phagocytosis. J Cell Sci 110:2041–2052
197. Hackam DJ, Rotstein OD, Sjolin C et al (1998) v-SNARE-dependent secretion is required for phagocytosis. Proc Natl Acad Sci U S A 95:11691–11696
198. Cox D, Tseng CC, Bjekic G, Greenberg S (1999) A requirement for phosphatidylinositol 3-kinase in pseudopod extension. J Biol Chem 274:1240–1247
199. Gold ES, Underhill DM, Morrissette NS et al (1999) Dynamin 2 is required for phagocytosis in macrophages. J Exp Med 190: 1849–1856
200. Di A, Nelson DJ, Bindokas V et al (2003) Dynamin regulates focal exocytosis in phago-

cytosing macrophages. Mol Biol Cell 14:2016–2028

201. Kinchen JM, Doukoumetzidis K, Almendinger J et al (2008) A pathway for phagosome maturation during engulfment of apoptotic cells. Nat Cell Biol 10:556–566
202. Cox D, Chang P, Kurosaki T, Greenberg S (1996) Syk tyrosine kinase is required for immunoreceptor tyrosine activation motif-dependent actin assembly. J Biol Chem 271:16597–16602
203. Zhang J, Berenstein EH, Evans RL, Siraganian RP (1996) Transfection of Syk protein tyrosine kinase reconstitutes high affinity IgE receptor-mediated degranulation in a Syk-negative variant of rat basophilic leukemia RBL-2H3 cells. J Exp Med 184:71–79
204. Benmerah A, Bayrou M, Cerf-Bensussan N, Dautry-Varsa A (1999) Inhibition of clathrin-coated pit assembly by an Eps15 mutant. J Cell Sci 112:1303–1311
205. Ford MGJ, Mills IG, Peter BJ et al (2002) Curvature of clathrin-coated pits driven by epsin. Nature 419:361–366
206. Bonazzi M, Spano S, Turacchio G et al (2005) CtBP3/BARS drives membrane fission in dynamin-independent transport pathways. Nat Cell Biol 7:570–580
207. Miller PJ, Johnson DI (1994) Cdc42p GTPase is involved in controlling polarized cell growth in Schizosaccharomyces pombe. Mol Cell Biol 14:1075–1083
208. Madaule P, Axel R, Myers AM (1987) Characterization of two members of the rho gene family from the yeast Saccharomyces cerevisiae. Proc Natl Acad Sci U S A 84: 779–783
209. Ridley AJ, Hall A (1992) The small GTP-binding protein rho regulates the assembly of focal adhesions and actin stress fibers in response to growth factors. Cell 70:389–399
210. Zhang S, Han J, Sells MA et al (1995) Rho family GTPases regulate p38 mitogen-activated protein kinase through the downstream mediator Pak1. J Biol Chem 270:23934–23936
211. Ridley AJ, Hall A (1994) Signal transduction pathways regulating Rho-mediated stress fibre formation: requirement for a tyrosine kinase. EMBO J 13:2600–2610
212. Dascher C, Balch WE (1994) Dominant inhibitory mutants of ARF1 block endoplasmic reticulum to Golgi transport and trigger disassembly of the Golgi apparatus. J Biol Chem 269:1437–1448
213. Zhao Z, Manser E, Chen X et al (1998) A conserved negative regulatory region in α PAK: inhibition of PAK kinases reveals their morphological roles downstream of Cdc42. Mol Cell Biol 18:2153–2163
214. Tang Y, Chen Z, Ambrose D et al (1997) Kinase-deficient Pak1 mutants inhibit Ras transformation of Rat-1 fibroblasts. Mol Cell Biol 17:4454–4464
215. Vadlamudi RK, Adam L, Wang RA et al (2000) Regulatable expression of p21-activated kinase-1 promotes anchorage-independent growth and abnormal organization of mitotic spindles in human epithelial breast cancer cells. J Biol Chem 275:36238–36244
216. Hara K, Yonezawa K, Sakaue H et al (1994) 1-Phosphatidylinositol 3-kinase activity is required for insulin-stimulated glucose transport but not for RAS activation in CHO cells. Proc Natl Acad Sci U S A 91:7415–7419
217. Garcia-Paramio P, Cabrerizo Y, Bornancin F, Parker PJ (1998) The broad specificity of dominant inhibitory protein kinase C mutants infers a common step in phosphorylation. Biochem J 333:631–636
218. Hirai H, Varmus HE (1990) SH2 mutants of c-src that are host dependent for transformation are trans-dominant inhibitors of mouse cell transformation by activated c-src. Gene Dev 4:2342–2352
219. Mejillano M, Yamamoto M, Rozelle AL (2001) Regulation of apoptosis by phosphatidylinositol 4,5-bisphosphate inhibition of caspases, and caspase inactivation of phosphatidylinositol phosphate 5-kinases. J Biol Chem 276:1865–1872

Part II

Cell-Free and Biochemical Assays of Exocytosis and Endocytosis

Chapter 3

Real-Time Detection of SNARE Complex Assembly with FRET Using the Tetracysteine System

Oleg Varlamov

Abstract

Small tetracysteine insertions are more suitable for fluorescence resonance energy transfer (FRET) studies of protein folding and small complex assembly than bulky GFP-based fluorophores. Here, we describe a procedure for expression, purification, and fluorescent labeling of a FRET-based probe, called CSNAC that can track the conformational changes undergone by SNAP-25 as it folds in the exocytic complex. The fluorescent protein Cerulean was attached to the N-terminus and served as a FRET donor. The biarsenical dye FlAsH, served as a FRET acceptor, was bound to a short tetracysteine motif positioned in the linker domain of SNAP-25. CSNAC can report real-time FRET changes when the Syntaxin soluble domain is added in vitro.

Key words CSNAC, FRET, SNARE, GFP, FlAsH, Tetracysteine, Folding

1 Introduction

The soluble N-ethylmaleimide-sensitive fusion protein attachment protein receptors (SNAREs), Syntaxin-1a, VAMP-2, and SNAP-25 form the complex required for exocytosis [1]. SNAP-25 is unstructured in solution, but when it binds Syntaxin and VAMP, the two N-terminals of the SNARE domains of SNAP-25 (H1 and H2) are brought together by intramolecular folding [2, 3]. By attaching appropriate fluorophores near the two terminals of SNAP-25, SNARE complex assembly can be studied by intramolecular fluorescence resonance energy transfer (FRET). This strategy was employed by labeling of a pair of cysteines (Cys) in the C-terminal ends of the two SNARE domains of SNAP-25 with Cy3, a donor, and Cy5, an acceptor of fluorescence [4]. Another FRET reporter, SCORE, used a brighter version of the cyan fluorescent protein Cerulean [5, 6] as a FRET donor and the yellow fluorescent protein Venus as a FRET acceptor. A similar reporter used Citrine in the place of Venus [7].

Andrei I. Ivanov (ed.), *Exocytosis and Endocytosis*, Methods in Molecular Biology, vol. 1174,
DOI 10.1007/978-1-4939-0944-5_3,

Because SNAP-25 complexes interact with regulatory factors [8–10], large fluorophores such as Venus and Citrine positioned in the middle of the coding region of SNAP-25 may disrupt protein–protein interactions. To overcome this problem we used genetically encoded Cerulean as a FRET donor and the membrane-permeable biarsenical dye FlAsH, a small fluorophore that is expected to have less steric hindrance than Venus as a FRET acceptor. Here, we describe a procedure for expression, purification, and fluorescent labeling of a FRET-based probe, called CSNAC that can track the conformational changes undergone by SNAP-25 as it folds in the exocytic complex. We propose that this SNAP-25 probe can be used for real-time studies of SNARE complex assembly in vitro.

2 Materials

2.1 Protein Expression and Purification Reagents

1. BL21 (DE3) bacterial strain (*see* **Note 1**). Store at −80 °C.
2. Super-pure XL10-Gold β-mercaptoethanol (Agilent Technology, Santa Clara, CA). Store at −80 °C.
3. Super Optimal Broth with Catabolite repression (SOC) medium. Store at 4 °C.
4. LBA medium: Suspend 20 g LB broth in 1 L deionized H_2O, autoclave for 20 min at 121 °C to sterilize, cool to room temperature, and add 1 mL of filter-sterilized ampicillin solution (1 mg/mL). Store at 4 °C.
5. LB-ampicillin agar plates. Store at 4 °C.
6. Isopropyl β-D-1 thiogalactopyranoside (IPTG): 0.5 M stock solution in water, filter-sterilized.
7. Breaking buffer: 25 mM HEPES, 0.1 M KCl, 10 % glycerol, 1 mM β-mercaptoethanol, complete cocktail of protease inhibitors (Roche Diagnostics), pH 7.4. Store at 4 °C.
8. Washing buffer: 25 mM HEPES, 0.1 M KCl, 10 % glycerol, 1 mM β-mercaptoethanol, 1 % octyl-β-D-Glucopyranoside (Anatrace, Santa Clara, CA, USA), pH 7.4.
9. Glutathione agarose beads. Wash with the washing buffer before use. Store at 4 °C.
10. GST cleavage buffer: 1 mL 25 mM HEPES, 0.1 M KCl, 10 % glycerol, 1 mM β-mercaptoethanol, 0.5 % octyl-β-D-Glucopyranoside, pH 7.4, and 4 μL of human thrombin (Haematologic Technologies Inc, Essex Junction, VA, USA).
11. 4-Benzenesulfonyl fluoride hydrochloride (AEBSF): 20 mM AEBSF solution in dH_2O. Prepare fresh.
12. Bradford protein assay reagent.
13. EmulsiFlex cell disruptor (Avestin, Canada).

2.2 FlAsH Labeling Regents

1. 2 mM FlAsH reagent in DMSO (Life technologies, Grand Island, NY, USA, Cat# T34561).
2. Dialysis buffer (25 mM HEPES, 0.1 M KCl, 10 % glycerol, 0.25 % octyl-β-D-Glucopyranoside, 0.5 mM Tris-[2-carboxyethyl] phosphine (TCEP), pH 7.4.
3. Dialysis cassettes, Slide-A-Lyzer Dialysis Cassette Kit, 7K MWCO, 3 mL (Thermo Fisher Scientific Ins, Rockford, IL, USA, Cat# 66372).
4. 2,3-Dimercaptopropanol.

2.3 Fluorescence Analysis Equipment

5. PTI spectrofluorometer (Photon Technology International, Canada) supplied with Felix-32 software or any other spectrofluorometer.
6. 10-mm quartz cuvette (Starna Cells, Inc, Atascadero, CA, USA) supplied with a stir bar.

3 Methods

3.1 Protein Expression and Purification

3.1.1 Bacterial Transformation

1. Thaw two 100-μL aliquots of the competent cells on ice.
2. Dilute β-mercaptoethanol 1:10 with dH_2O and add 2 μL to each of the 100-μL aliquots of competent cells. Incubate the cells on ice for 10 min, swirling gently every 2 min.
3. Add 10–25 ng (2–5 μL) of CSNAC expression plasmid [11] or 2–5 μL of dH_2O (negative control) to the tubes of cells and swirl gently. Incubate the reactions on ice for 30 min.
4. Preheat SOC medium in a 42 °C water bath. Heat-shock each transformation reaction in the 42 °C water bath for 20 s. Incubate the reactions on ice for 2 min.
5. Add 0.9 mL of preheated SOC medium to each transformation reaction and incubate the reactions at 37 °C for 1 h with shaking at 250 rpm.
6. Spread 100 μL of the cells transformed with CSNAC or control cells onto LB-ampicillin agar plates and incubate overnight at 37 °C (*see* **Note 2**).

3.1.2 Bacterial Culture Inoculation and Propagation

1. Inoculate a single bacterial colony in 2 mL of LBA media in a 14-mL BD Falcon polypropylene round-bottom tube. Incubate the tube at 37 °C for 6 h with shaking at 250 rpm (Fig. 1a).
2. Transfer 1 mL of the starter bacterial culture into 200 mL of sterile TBA media in a 1 L glass flask at 37 °C and grow for 6–8 h with shaking at 250 rpm to OD_{600} 0.8 (*see* **Note 3**).
3. Quickly chill the flask to 20 °C in a water bath for 5–10 min. Add 0.2 mL of 0.5 M IPTG and 0.2 mL 0.5 M ampicillin (*see* **Note 4**). Incubate overnight at 20 °C with shaking at 250 rpm.

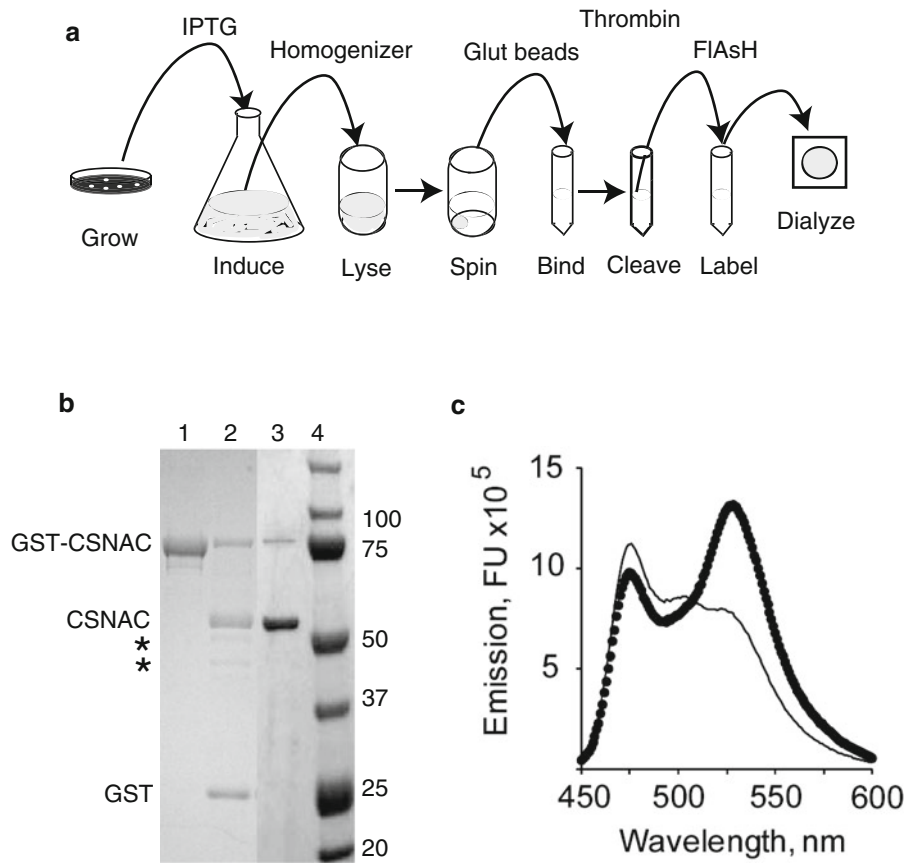

Fig. 1 Purification and FlAsH-labeling of CSNAC. (**a**) The schematic diagram showing bacterial growth on the selective media, large-scale protein induction with IPTG, cell disruption and lysis, binding to the glutathione agarose beads, cleavage of GST-CSNAC with thrombin, labeling of CSNAC with FlAsH, and dialysis. (**b**) SDS-PAGE analysis of the CSNAC protein. *Lane 1*, uncleaved GST-CSNAC; *lane 2*, thrombin-cleaved GST-CSNAC (GST-protein was exposed to thrombin cleavage in solution and then analyzed on the 10 % gel); *lane 3*, thrombin-cleaved GST-CSNAC (GST-CSNAC protein was immobilized on glutathione agarose beads, and exposed to thrombin cleavage; unbound material was analyzed on the 10 % gel); *lane 4*, protein standard, molecular weights in kDa and the position of individual proteins are indicated. The *asterisks* show the position of nonspecific cleavage products of GST-CSNAC. (**c**) Effect of Syntaxin on the fluorescence of CSNAC. 0.2 μM CSNAC was incubated at room temperature for 60 min with or without 10 μM of Syntaxin as described [11]. Fluorescence of Cerulean was excited at 433 nm and emission spectra in the absence (*thin line*) or the presence of Syntaxin (*circles*) were collected. Emission spectra are shown in arbitrary fluorescence units (FU)

3.1.3 Protein Extraction and Purification

1. Transfer bacterial culture into a 500-mL polypropylene centrifuge bottle and collect cells by centrifugation for 10 min at 2,500×*g*. Remove the residual amounts of TBA media by rinsing bacterial pellets with cold PBS.
2. Add 40 mL of ice-cold breaking buffer to the bacterial pellet and resuspend by repeated pipetting on ice. Pass cell suspension three times through the EmulsiFlex cell disruptor (*see* **Note 5**).

3. Remove unbroken cells by centrifugation at 4 °C for 1 h at 20,000 × *g*.
4. Transfer the supernatant into a 50-mL polypropylene conical tube, add 0.5 mL of glutathione agarose beads and incubate the tube for 2–4 h at 4 °C with slow rotation.
5. Transfer the beads into a 15-mL polypropylene conical tube and wash the beads via centrifugation 5 × 10 mL of the cold washing buffer.
6. Transfer the beads into a 1.5-mL Eppendorf tube containing 1 mL of the GST cleavage buffer. Incubate the tube for 2 h at room temperature with slow rotation. Inactivate thrombin by adding 10 μL AEBSF to the tube.
7. Determine protein concentration and purity using Bradford reagent and SDS-PAGE (*see* **Note 6** and Fig. 1b).

3.2 FlAsH-Labeling

1. Mix 200 μL of CSNAC protein solution (2 mg/mL) with 4 μL FlAsH in a 1.5-mL Eppendorf tube and incubate in the dark at room temperature for 1 h. Transfer labeling reaction to 4 °C and continue incubation overnight. Stop labeling by addition of 25 μM 2,3-dimercaptopropanol.
2. Transfer protein solution into a dialysis cassette and dialyze for 6 h against 3 L of the cold breaking buffer. Replace 3 L of the breaking buffer and continue dialysis for additional 16 h (*see* **Note 7** and Fig. 1a).
3. Carefully remove CSNAC protein solution from a dialysis cassette with a 18 × 1.5 needle and a 1-mL syringe and transfer into a 1.5-mL Eppendorf tube on ice (*see* **Note 8**).
4. Make 20 μL aliquots in 0.5-mL Eppendorf tubes and snap-freeze them in liquid nitrogen. Stored the tubes protected from light at −80 °C (*see* **Note 9**).

3.3 Fluorimetry

1. Thaw a single aliquot of the FlAsH-labeled CSNAC protein on ice, protecting from the direct light (*see* **Note 10**).
2. Transfer 5 μL of CSNAC protein sample in the 10 mm quartz cuvette supplied with a spinning stir bar and 1 mL of 20 mM HEPES, 0.1 M KCl pH 7.4 at room temperature (*see* **Note 11**).
3. Excite Cerulean fluorescence at 433 nm and collect emission spectra in the range of 450–600 nm with the integration time 0.1 s (*see* **Note 12** and Fig. 1c).
4. Add 10 μL of the Syntaxin soluble domain to the cuvette (*see* **Note 13**), incubate for 20 min mixing, and collect the emission spectra again (Fig. 1c).

4 Notes

1. Aliquot the stock of the competent cells in 100-μL aliquots in 1.5-mL sterile Eppendorf tubes and store at −80 °C. Keep the competent cells on ice at all times while aliquoting. Do not freeze competent cells more than once.
2. Do not allow colonies to grow for more than 16 h, as it may result in the appearance of small, ampicillin-sensitive false-positive colonies.
3. Do not allow bacterial culture to grow pass OD_{600} 0.9, as it may result in inefficient protein induction and lower expression levels.
4. Because ampicillin is not stable in bacterial cultures, additional dose is required to maintain antibiotic-resistant cells in overnight cultures.
5. Before use, chill a cell disrupter on ice. To prevent clogging, it is helpful to repeatedly pass bacterial suspension through the 1.2 mm × 40 mm needle. Complete cell homogenization results in a transparent solution.
6. The expected protein concentration of the cleaved CSNAC product is 2 mg/mL. Protein solution can be aliquoted and snap-frozen in liquid nitrogen.
7. Protect the dialysis container from a direct light with the aluminum foil. Allow proper mixing with a stir bar.
8. Position a dialysis cassette at a 45° angle and puncture a corner of a cassette with a needle. Carefully remove protein solution without touching the walls of a dialysis cassette with a needle which may result in tearing and sample loss.
9. Do not allow more than five freeze–thaw cycles which may result in partial loss of FRET activity. FlAsH-labeled recombinant proteins remain stable at 4 °C for at least 24 h, and at −80 °C for up to 6 months.
10. Protein samples can be thawed and frozen at least four times without loss of activity.
11. Final CSNAC protein concentration in the cuvette is 0.2 μM.
12. To verify FlAsH labeling of the protein, perform the direct excitation of FlAsH at 500 nm and collect emission spectra in the range of 510–600 nm with the integration time 0.1 s. Set excitation and emission slits to 5 nm.
13. Final Syntaxin soluble domain protein concentration in the cuvette is 20 μM.

References

1. Jahn R, Lang T, Sudhof TC (2003) Membrane fusion. Cell 112:519–533
2. Sutton RB, Fasshauer D, Jahn R, Brunger AT (1998) Crystal structure of a SNARE complex involved in synaptic exocytosis at 2.4 A resolution. Nature 395:347–353
3. Stein A, Weber G, Wahl MC, Jahn R (2009) Helical extension of the neuronal SNARE complex into the membrane. Nature 460: 525–528
4. Sakon JJ, Weninger KR (2010) Detecting the conformation of individual proteins in live cells. Nat Methods 7:203–205
5. An SJ, Almers W (2004) Tracking SNARE complex formation in live endocrine cells. Science 306:1042–1046
6. Takahashi N, Hatakeyama H, Okado H, Noguchi J, Ohno M, Kasai H (2010) SNARE conformational changes that prepare vesicles for exocytosis. Cell Metab 12:19–29
7. Wang L, Bittner MA, Axelrod D, Holz RW (2008) The structural and functional implications of linked SNARE motifs in SNAP25. Mol Biol Cell 19:3944–3955
8. Jahn R, Scheller RH (2006) SNAREs – engines for membrane fusion. Nat Rev Mol Cell Biol 7:631–643
9. Sorensen JB (2009) Conflicting views on the membrane fusion machinery and the fusion pore. Annu Rev Cell Dev Biol 25:513–537
10. Pang ZP, Sudhof TC (2010) Cell biology of Ca^{2+}-triggered exocytosis. Curr Opin Cell Biol 22:496–505
11. Varlamov O (2012) Detection of SNARE complexes with FRET using the tetracysteine system. Biotechniques 52:103–108

Chapter 4

Profiling Lysine Ubiquitination by Selective Enrichment of Ubiquitin Remnant-Containing Peptides

Guoqiang Xu, Alessia Deglincerti, Jeremy S. Paige, and Samie R. Jaffrey

Abstract

Protein ubiquitination plays critical roles in many biological processes. However, functional studies of protein ubiquitination in eukaryotic cells are limited by the ability to identify protein ubiquitination sites. Unbiased high-throughput screening methods are necessary to discover novel ubiquitination sites that play important roles in cellular regulation. Here, we describe an immunopurification approach that enriches ubiquitin remnant-containing peptides to facilitate downstream mass spectrometry (MS) identification of lysine ubiquitination sites. This approach can be utilized to identify ubiquitination sites from proteins in a complex mixture.

Key words Ubiquitination, Ubiquitin remnant-containing peptides, Anti-diglycyl lysine antibody, Ubiquitin remnant profiling, Mass spectrometry, Proteomics

1 Introduction

Ubiquitin (Ub) is a 76-amino-acid protein that is highly conserved from yeast to human. The C-terminus of Ub can be conjugated to the ε-amine of a lysine residue of a protein to form an isopeptide bond through an enzymatic cascade involving E1 activating enzymes, E2 conjugating enzymes, and E3 Ub ligases [1]. Ub itself has seven lysines, and each of them can be modified by another Ub molecule [2]. Versatile Ub topologies, such as monoubiquitination, multi-monoubiquitination, K48- and K63-linked polyubiquitination, can be formed on substrates. The fate of the ubiquitinated protein is, at least partially, determined by the topology of the Ub chain. Protein ubiquitination affects many cellular processes, through its ability to affect protein trafficking, protein degradation, and protein–protein interactions [1]. The identification of the ubiquitination sites on target proteins is necessary to generate ubiquitination-resistant mutants which can provide critical insight into the role of ubiquitination in protein function.

Andrei I. Ivanov (ed.), *Exocytosis and Endocytosis*, Methods in Molecular Biology, vol. 1174,
DOI 10.1007/978-1-4939-0944-5_4,

Furthermore, detection of a Ub remnant-containing peptide provides strong proof that a protein is indeed ubiquitinated.

The C-terminus of Ub ends with the amino acids Arg-Gly-Gly, in which the last Gly can be conjugated to the ε-amine of a lysine residue on a target protein [1]. Since trypsin cleaves peptide bonds at the carboxyl side of Arg and Lys, trypsin digestion of ubiquitinated proteins will generate peptides from both the substrate and the conjugated Ub. The majority of these peptides are "regular" tryptic peptides that bear no information about the ubiquitination site(s). However, a small fraction of peptides, which are derived from the portion of the protein that is modified by Ub, will contain Lys residue(s) modified by a diglycine on their ε-amines (Fig. 1). These peptides are termed as Ub remnant-containing peptides [3] or Ub signature peptides [2]. Their detection unambiguously identifies sites of protein ubiquitination.

Several MS approaches [2, 4–12] have been used to identify ubiquitinated proteins and/or ubiquitination sites. In these approaches, ubiquitinated proteins are first isolated by immobilized Ub-interacting proteins such as S5a [7, 11], by anti-Ub antibodies [8, 13], or by tagged Ub (in particular hexahistidine [2] or biotin acceptor peptide [9] tagged Ub). The purified proteins are then digested by trypsin and further fractionated by strong cationic exchange (SCX) chromatography for tandem MS identification [2]. Multidimensional protein identification technology (MudPIT), which fractionates tryptic peptides in an online SCX column prior to a reverse-phase separation of peptides for MS identification, has also been applied to identify ubiquitinated proteins in plants and yeast [14, 15]. However, these methods identify proteins based on the presence of regular tryptic peptides, not Ub remnant-containing peptides, raising the question of whether these proteins are indeed ubiquitinated or are co-precipitated with the ubiquitinated proteins. In order to reduce the background derived from unmodified peptides and increase the efficiency of the identification of ubiquitination sites by tandem MS, we developed a method to enrich for Ub remnant-containing peptides [3].

In this article, we describe an immunoaffinity purification approach, which uses an anti-diglycyl lysine (GG-ε-K) antibody to immunoprecipitate Ub remnant-containing peptides after trypsin digestion of the Ub conjugates. Because of the direct isolation of Ub remnant-containing peptides, unmodified tryptic peptides are removed. The peptides containing Gly-Gly-modified lysines are then identified by tandem MS, which allows for precise determination of the position of Ub modification. This enrichment approach can significantly increase the efficiency of the identification of ubiquitination sites for a complex protein mixture in a high-throughput manner.

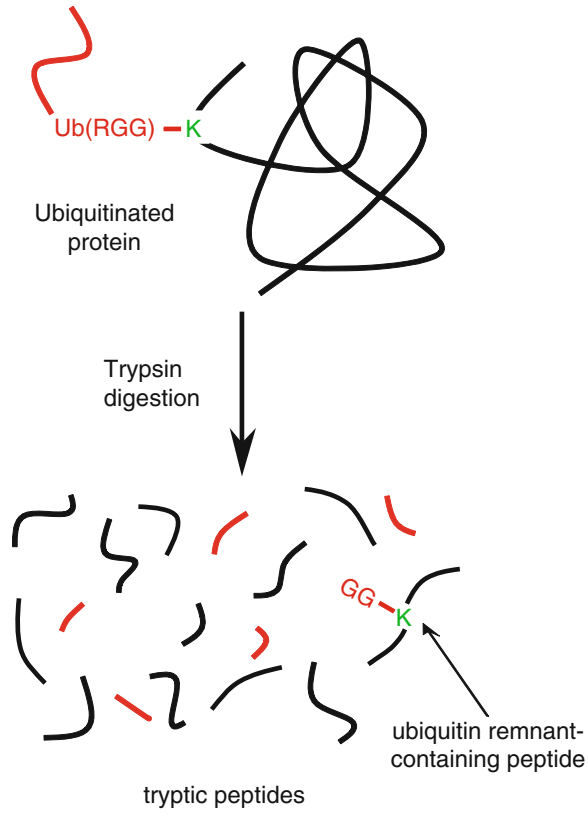

Fig. 1 Ubiquitin remnant-containing peptides. After immobilized metal affinity chromatography purification, the ubiquitinated proteins are digested with trypsin, which cleaves on the carboxyl side of Arg and Lys in both the target protein and the conjugated Ub. The majority of peptides obtained from the Ub conjugate are "regular" tryptic peptides, i.e., lacking any diglycine-modified lysine residues, because only one or a few lysines are ubiquitinated in a protein. However, a small percentage of peptides are derived from ubiquitinated portions of the target protein. These peptides have a diglycine modification on their lysine residues and are termed Ub remnant-containing peptides or Ub signature peptides. The identification of Ub remnant-containing peptides can unambiguously determine the ubiquitination sites

2 Materials

2.1 Cell Culture and Transfection

1. Growth medium: Dulbecco's Modified Eagle Medium (DMEM) supplemented with 10 % fetal bovine serum (FBS), 100 unit/mL penicillin G, and 100 μg/mL streptomycin and filtered through a 0.22 μm filter.
2. Proteasome inhibitor: N-Acetyl-Leu-Leu-Nle-CHO (LLnL, 25 μM) or MG132 (10 μM) in DMSO (Store at −20 °C).

3. Transfection reagent: Calcium phosphate transfection reagent or other suitable transfection reagents for cells of interest.
4. 10-cm petri dishes.

2.2 Cell Lysis and Purification of Ubiquitinated Proteins

1. Lysis buffer: 8 M urea, 0.3 M NaCl, 50 mM phosphate, 0.5 % NP-40 (vol/vol), pH 8.0. Add freshly made 5 mM chloroacetamide before use.
2. Ni-NTA washing buffer A: 8 M urea, 0.3 M NaCl, 50 mM phosphate, 0.5 % NP-40 (vol/vol), pH 8.0.
3. Ni-NTA agarose resin (Qiagen, Valencia, CA, USA): Wash Ni-NTA resin three times with Ni-NTA washing buffer A.
4. Ni-NTA washing buffer B: 8 M urea, 0.3 M NaCl, 50 mM phosphate, 0.5 % NP-40 (vol/vol), pH 6.5.
5. Ni-NTA elution buffer: 8 M urea, 0.3 M NaCl, 50 mM phosphate, 250 mM imidazole, 0.5 % NP-40 (vol/vol), pH 8.0.
6. 5″ polystyrene disposable columns with coarse (90–130 μm) filters (Evergreen Scientific, Los Angeles, CA, USA).
7. TALON metal affinity resin (Clontech, Mountain View, CA).
8. Sonifier and water bath sonicator.

2.3 SDS-PAGE and Trypsin Digestion

1. NuPAGE® LDS sample buffer (4×) or SDS sample buffer.
2. Precision Plus Protein™ All Blue Standards.
3. SimplyBlue™ SafeStain or Coomassie stain reagents.
4. NuPage 4–12 % Tris-Glycine mini-gel or homemade polyacrylamide gel for gel electrophoresis.
5. Gel washing buffer: 50 % acetonitrile (vol/vol) in 25 mM ammonium bicarbonate (freshly made, *see* **Note 1**).
6. Protein reduction solution: 10 mM dithiothreitol in 25 mM ammonium bicarbonate (freshly made).
7. Protein alkylation solution: 55 mM chloroacetamide in 25 mM ammonium bicarbonate (freshly made).
8. Protein digestion solution: 12.5 μg/mL sequencing grade modified trypsin (Promega, Madison, WI, USA, catalog number V5111) solution in 25 mM ammonium bicarbonate and 1 mM $CaCl_2$ (aliquot and store at –20 °C; minimize freeze–thaw cycles up to three times).
9. Peptide extraction solvent: 5 % formic acid (vol/vol)/50 % acetonitrile (vol/vol) (can be stored at room temperature for 1 month).
10. Thermomixer: Eppendorf Thermomixer® (Hauppauge, NY, USA, catalog number 022670107).

2.4 Antibody Conjugation and Immunoprecipitation of Ubiquitin Remnant-Containing Peptides

1. Anti-diglycyl lysine (anti-GG-ε-K) antibody (Lucerna Technologies, New York, NY, USA, catalog numbers 30-1000 or 30-0100, or Millipore, Billerica, MA, USA, catalog number MABS27).
2. Affi-gel 10 resin.
3. Phosphate buffered saline (PBS): Make 1 L PBS with 8 g of NaCl, 0.2 g of KCl, 1.15 g of Na_2HPO_4, 0.262 g of $NaH_2PO_4 \cdot H_2O$, adjust pH to 7.4 and sterilize by autoclaving or filtering through a 0.45 μm filter.
4. Peptide elution buffer: 10 mM sodium citrate, pH 3.0 (adjust pH with 5 M HCl in distilled H_2O) or 0.1 % trifluoroacetic acid.

2.5 LC-MS/MS Analysis

1. MS instrument Q-TOF or LTQ Orbitrap mass spectrometer (Thermo Scientific) equipped with a nano high performance liquid chromatography (HPLC) system.
2. LC-MS grade water and LC-MS grade acetonitrile.
3. LC Buffer A: 0.1 % formic acid (vol/vol) in LC-MS grade water (can be stored at room temperature for 1–4 months).
4. LC Buffer B: 90 % acetonitrile (vol/vol)/0.1 % formic acid (vol/vol) in LC-MS grade water (can be stored at room temperature for 1–4 months).
5. Software for MS/MS data analysis.

3 Methods

In this approach, hexahistidine-tagged Ub (His_6-Ub) is expressed in human embryo kidney (HEK) 293 cells and the ubiquitinated proteins are purified under denaturing conditions using immobilized metal affinity chromatography prior to trypsin digestion in the polyacrylamide gel. The Ub remnant-containing peptides are immunoprecipitated with the anti-diglycyl lysine antibody and identified by mass spectrometry. A flowchart of the method is shown in Fig. 2. The detailed experimental procedure is discussed below.

3.1 Cell Culture and Transfection

1. Grow HEK293 cells in growth medium in a 5 % CO_2 cell culture incubator with 95 % humidity. Split HEK293 cells the day before transfection to twenty 10-cm petri dishes. Adjust the splitting ratio so that the cells are approximately 50 % confluent on the day of transfection.
2. Replace the medium with pre-warmed fresh medium 1–3 h before transfection.

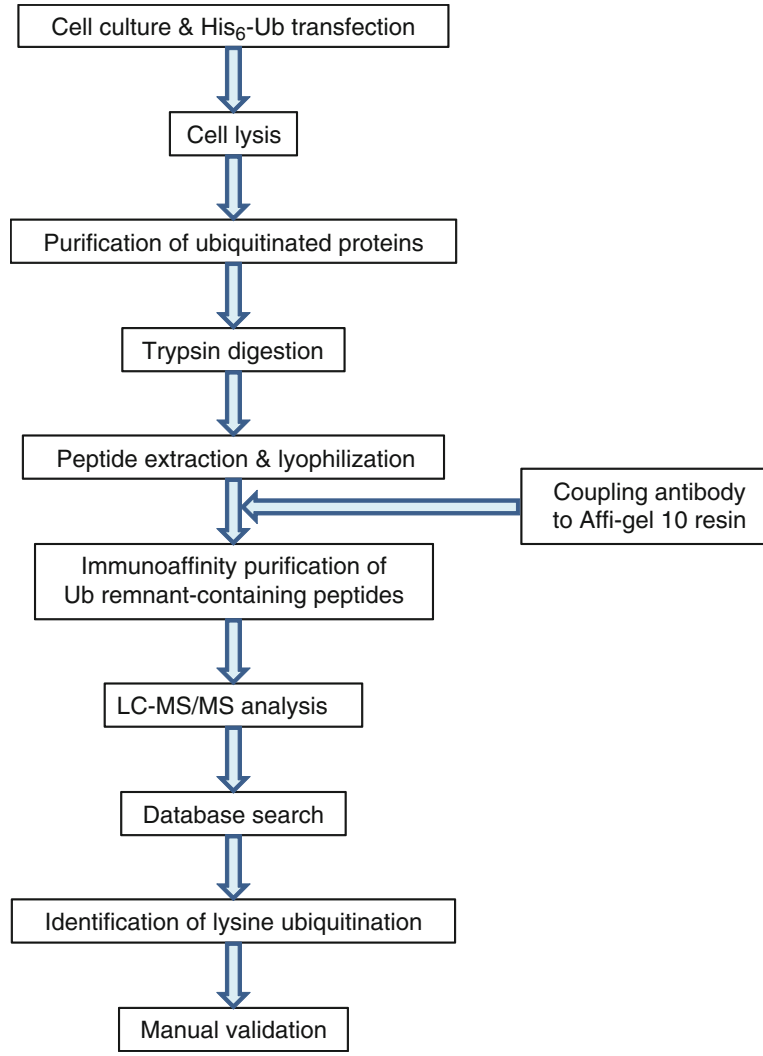

Fig. 2 A flowchart for the identification of lysine ubiquitination sites

3. Transfect the cells with 10 μg His_6-Ub plasmid for each 10-cm petri dish using the calcium phosphate transfection method [16] (*see* **Note 2**).
4. Replace the medium with fresh, pre-warmed medium the morning after transfection.
5. (Optional) On the evening of the 2nd day post transfection, treat cells with 25 μM LLnL or a suitable proteasome inhibitor and incubate the cells for 16 h to allow ubiquitinated proteins, which are targeted for proteasome degradation, to accumulate.

3.2 Purification of Ubiquitinated Proteins

1. Wash the cells twice with 5 mL ice-cold PBS per petri dish.
2. Detach the cells with 5 mL ice-cold PBS per dish by pipetting up and down several times and transfer the cells to four 50 mL conical tubes.
3. Centrifuge at 2,000 × *g* for 5 min at 4 °C in a swing-bucket centrifuge. Decant PBS and transfer the cells to a 1.6 mL eppendorf tube with 1 mL ice-cold PBS for each 50 mL conical tube. Centrifuge at 2,000 × *g* for 5 min at 4 °C in a benchtop centrifuge and decant PBS. The cells can be flash-frozen in liquid nitrogen and kept at –80 °C for several weeks.
4. Lyse cells with 1 mL lysis buffer per 1.5 mL tube (*see* **Note 3**).
5. Sonicate samples on ice at 40 % output in a Branson sonifier four times for 10 s. Alternatively, lyse the cells by grinding in liquid nitrogen to maximally preserve protein ubiquitination [17]. Avoid sample heating during sonication.
6. Centrifuge the samples at 21,000 × *g* for 10 min at 25 °C. It is recommended that 5 μL of sample is saved for an anti-Ub western blot. This western blot is useful because it can monitor ubiquitinated proteins at each step of the sample preparation. The sample should be diluted 1:1 or more with double distilled H_2O to reduce the concentration of salt and urea in the buffer. The high concentration of salt and urea can adversely affect protein mobility in SDS-PAGE. His_6-Ub has a slower mobility than the endogenous Ub due to the increase in molecular weight and charge. In an anti-Ub western blot, two bands at about ~8.5 and ~10 kDa are visible, which confirms the expression of His_6-Ub (~10 kDa band). Make sure that His_6-Ub is expressed at a low level compared with endogenous Ub (*see* Fig. 3 and **Note 4**). This ensures that the overall cellular ubiquitin levels are not substantially altered.
7. Transfer 500 μL of a 50 % slurry of Ni-NTA agarose beads to a 1.6 mL eppendorf tube.
8. Wash the Ni-NTA agarose beads three times with 5 column bed volumes (CVs) of lysis buffer.
9. Transfer 500 μL Ni-NTA beads to a 15 mL conical tube.
10. Filter the lysate from **step 6** through a 0.45 μm filter and transfer the lysate to the 15 mL conical tube with Ni-NTA beads.
11. Incubate the lysate with Ni-NTA agarose beads on an end-over-end rotator at 25 °C for 2 h. Alternatively, run the lysate over Ni-NTA agarose beads in a 5″ polystyrene disposable column 3–5 times.
12. Transfer the lysate to a disposable column and let the lysate drain. Make sure not to let the column dry.

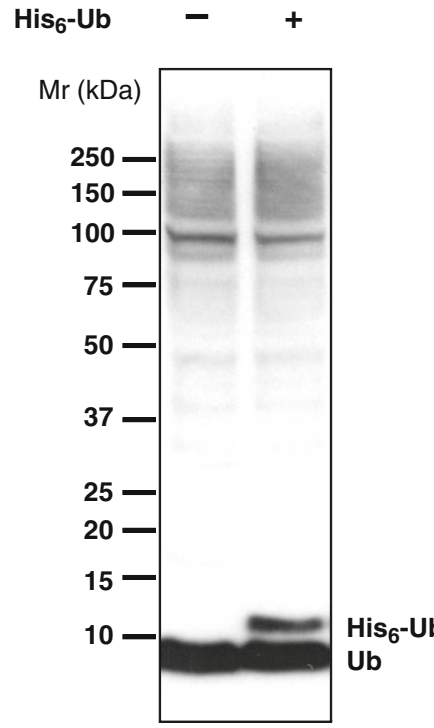

Fig. 3 Expression of His_6-Ub does not significantly affect total cellular Ub levels. Untransfected and His_6-Ub-transfected HEK293 cells (both treated with LLnL) were lysed and the lysates were separated by SDS-PAGE followed by blotting with an anti-Ub antibody. In the low molecular weight region, only a small amount of His_6-Ub is expressed compared to the amount of endogenous Ub. Both untransfected and His_6-Ub transfected cells show similar amount of Ub conjugated to the substrates, as seen in the higher molecular weight portion of the blot. This result demonstrates that expression of His_6-Ub does not significantly perturb endogenous Ub pathways

13. Wash the beads twice with 5 CVs of Ni-NTA washing buffer A (pH 8.0).
14. Wash the beads twice with 5 CVs of Ni-NTA washing buffer B (pH 6.5).
15. Elute His_6-Ub and ubiquitinated proteins in five 250 μL fractions of Ni-NTA elution buffer and combine the eluate in a 1.6 mL eppendorf tube. Save 5 μL sample for anti-Ub western blotting analysis to ensure that the ubiquitinated proteins are eluted. Alternatively, measure protein concentration using the Bradford or BCA protein assay. The ubiquitinated proteins can also be eluted with 1× LDS (or SDS) sample buffer at elevated temperature, such as 100 °C for 5 min (*see* **Note 5**).
16. Alternatively, the ubiquitinated proteins can also be purified using TALON metal affinity resin (*see* Fig. 4 and **Note 6**).

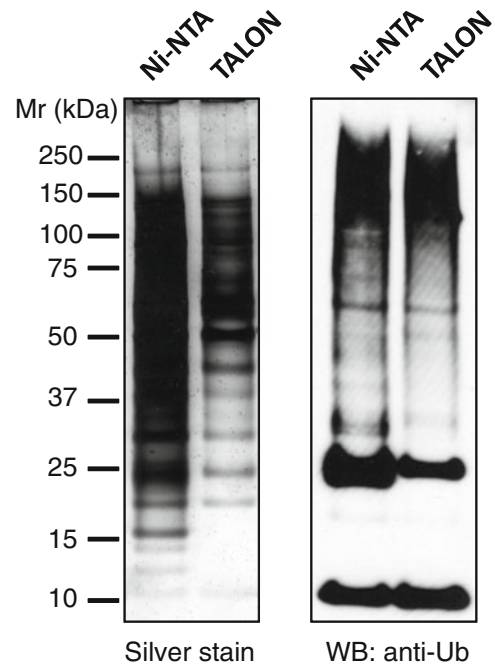

Fig. 4 TALON resin purification results in purer ubiquitinated proteins than Ni-NTA resin purification. His_6-tagged Ub and ubiquitinated proteins from HEK 293 cells expressing His_6-Ub were purified in parallel using either Ni-NTA resin or TALON resin. The samples were visualized by silver staining and by an anti-Ub western blot. The results showed that TALON resin yielded almost same amount of ubiquitinated proteins (anti-Ub western blot: *right panel*) as Ni-NTA resin, while it pulled down much less nonspecific bound proteins (silver stain: *left panel*). The results suggested that use of TALON resin may increase the efficiency in the identification of lysine ubiquitination sites due to the reduction of non-ubiquitinated proteins

3.3 Trypsin Digestion of Ubiquitinated Proteins

We use the in-gel trypsin digestion protocol [18] to digest ubiquitinated proteins because this procedure is compatible with small amounts of detergent in the purified Ub conjugates and produces peptide samples with little salt and denaturant, which are suitable for the downstream immunopurification of Ub remnant-containing peptides and MS analysis. The purified ubiquitinated proteins are first separated by sodium dodecyl sulfate-polyacrylamide gel electrophoresis (SDS-PAGE). Then, the bands above 25 kDa are excised, disulfide bonds are reduced and thiols are alkylated. In the alkylation step, chloroacetamide is used instead of iodoacetamide that has been used in the majority of proteomics studies to avoid the risk of introducing two $-CH_2CONH_2$ modification on one lysine residue. This modification generates a moiety with exactly the same chemical formula but different structure as a diglycine modification on lysines and would therefore interfere

with proper identification of Ub-remnant containing peptides in mass spectrometer [19]. Alternative digestion approaches, such as in-solution digestion [20] and on-bead digestion [21], can also be adapted to this method.

1. Run a short SDS-PAGE and separate proteins on a NuPAGE 4–12 % Tris-Glycine mini-gel (1.5 mm in thickness) (*see* **Note 7**).
2. (Optional) Stain gel with SimplyBlue™ SafeStain for 1 h and destain gel with distilled H_2O. Alternatively, the gel can be stained with silver stain. This step is optional and is used to confirm that the ubiquitinated proteins are resolved on the polyacrylamide gel.
3. Cut the gel above 25 kDa into ~1 mm × 1 mm gel pieces.
4. Destain or wash the gel pieces with gel washing buffer with constant shaking (1,000 rpm) in a thermomixer at 25 °C. If the gel is stained with SimplyBlue, change gel washing buffer every 30 min until the gel is destained. The gel pieces can be stored in gel washing buffer overnight at 4 °C.
5. Dehydrate the gel pieces with 200 µL of 100 % acetonitrile for 5 min and carefully remove acetonitrile using a gel loading tip.
6. Dry the gel pieces completely by SpeedVac at 25 °C for 5 min.
7. Add 100 µL (or suitable amount) of protein reduction solution to wet and cover the gel pieces and incubate at 50 °C for 30 min with constant shaking in a thermomixer.
8. Wash the gel pieces once with freshly made 25 mM ammonium bicarbonate.
9. Add 100 µL (or suitable amount) of protein alkylation solution to cover gel pieces and incubate at 25 °C for 45 min with constant shaking in the dark.
10. Remove alkylation solution from the gel pieces using a gel loading tip.
11. Incubate the gel pieces twice with gel washing buffer at 25 °C for 20 min with constant shaking and carefully remove gel washing buffer using a gel loading tip.
12. Dehydrate the gel pieces with 200 µL of 100 % acetonitrile at 25 °C for 5 min with constant shaking and carefully remove acetonitrile using a gel loading tip.
13. Dry the gel pieces completely by SpeedVac at 25 °C for 5 min.
14. Add three gel volumes of protein digestion solution to the gel pieces and wait for 10 min to ensure that the gel pieces are covered by protein digestion solution.
15. Perform digestion at 37 °C for 16 h with constant shaking in a thermomixer (600 rpm) or in a incubator.
16. Transfer digestion solution to a 15 mL conical tube.

17. Extract tryptic peptides from the gel pieces with peptide extraction solution (200 µL) at 25 °C by constant shaking for 30 min and sonicate in a water bath sonicator for 20 min. Combine the extracts with the digestion solution in **step 16**.
18. Repeat **step 17** once.
19. Extract peptides with 200 µL of 100 % acetonitrile once at 25 °C by constant shaking for 5 min.
20. Combine the extracted peptide solution and lyophilize overnight.

3.4 Conjugation of Anti-diglycyl Lysine Antibody

In this method, the anti-diglycyl lysine antibody is coupled to the Affi-gel 10 resin for immunopurification of Ub remnant-containing peptides. Alternatively, protein G beads can be used to bind and couple the monoclonal antibody by dimethyl pimelimidate [22] or bis(sulfosuccinimidyl) suberate [23] under slightly basic conditions. Our experiments show that protein G retains more nonspecific peptides than Affi-gel 10 resin. Therefore, we prefer to use Affi-gel in this method.

1. Transfer 50 µL of 50 % Affi-gel 10 resin to a 1.6 mL eppendorf tube.
2. Wash the Affi-gel 10 resin twice with 1 mL of ice-cold 1 mM HCl.
3. Adjust pH of 500 µL of anti-diglycyl lysine antibody (>1 mg/mL) to ~8.5 with 1 M HEPES (pH 9) (*see* **Note 8**).
4. Add antibody solution to the Affi-gel 10 resin and incubate at 25 °C for 4 h or at 4 °C overnight.
5. Wash beads with 500 µL of 1 M Tris–HCl (pH 8.0) and incubate with 500 µL of 1 M Tris–HCl solution on an end-over-end rotator at 25 °C for 2 h or at 4 °C overnight to block the remaining NHS active groups.
6. Briefly wash the beads twice with 500 µL of 0.1 M glycine (pH 2.7) to remove the unbound antibodies, and twice with 0.1 M Tris–HCl (pH 8.0) to neutralize pH.
7. Resuspend Affi-gel 10 resin with PBS containing 0.02 % sodium azide and store at 4 °C. The immobilized antibody can be kept at 4 °C for more than 4 weeks (*see* **Note 9**).

3.5 Immunoprecipitation of Ubiquitin Remnant-Containing Peptides

1. Dissolve lyophilized peptides in 300 µL of 150 mM NaCl, 50 mM Tris–HCl (pH 7.4) and 2 mM EDTA. Make sure that the pH of the solution is ~7.4.
2. Incubate the sample in boiling water for 10 min to inactivate residual trypsin. Cool sample to 4 °C on ice.
3. Incubate peptide sample with 20 µL of Affi-gel 10 resin coupled with anti-diglycyl lysine antibody for at least 4 h at 4 °C

on an end-over-end rotator. Alternatively, the incubation can be extended to overnight at 4 °C. The Affi-gel 10 resin is chemically reactive and hydrolyzes when exposed to water for long periods. Fresh Affi-gel 10 resin typically gives best coupling results.

4. Transfer beads to a Pierce micro-spin column. Wash the beads three times with 0.5 mL 2× PBS and three times with 0.5 mL 1× PBS.
5. Elute Ub remnant-containing peptides six times with 20 μL of 10 mM sodium citrate solution (pH 3.0). Alternatively, 0.1 % TFA can be used to elute the Ub remnant-containing peptides, which can improve the yield up to 20 % (*see* **Note 10**).
6. Reduce the volume of the eluate to ~20 μL by SpeedVac at 25 °C. Samples can be stored overnight or longer at −20 °C.

3.6 Mass Spectrometry Measurement and Data Analysis

1. Centrifuge the samples at 21,000 × *g* in a benchtop centrifuge for 10 min at 4 °C.
2. Transfer 10 μL of sample to an LC-MS/MS sample vial and load 8 μL sample to LC-MS/MS (Q-TOF or Orbitrap) instruments with a 1 h gradient (*see* **Note 11**). Run LC-MS/MS to analyze peptide complex (*see* **Note 12**).
3. Perform database search of MS/MS spectra using Mascot [24], X!Tandem [25], OMSSA [26], Sequest [27], Spectrum Mill [28], or other database search programs, using the appropriate protein sequence database, such as Swiss-Prot [29], NCBI [30], or IPI [31]. Select fixed modification for cysteine (carbamidomethylation, the same as chloroacetamide modification), and variable modifications for lysines (Gly-Gly-) and methionine (oxidation). Set appropriate mass accuracy for precursor ions (20 ppm for Q-TOF) and fragment ions (40 ppm for Q-TOF) (*see* **Note 13**).
4. Manually validate the Ub remnant-containing peptides. Make sure that no peptide with a sequence containing isobaric modification to the diglycine modification [32] matches MS/MS spectra of Ub remnant-containing peptides. Confirm all the major ions in the MS/MS spectra match the theoretical masses of fragment ions, such as *b*- and *y*-ions. Confirm the fragmentation of identified peptides fits the common rules, such as preferred cleavages at the proline residues.

4 Notes

1. The pH of the solution is determined by the 25 mM ammonium bicarbonate (~8.0).
2. Ensure that the pH of the 2× HBS reagent is ~7.2. Check cells after transfection under microscope and make sure that calcium phosphate precipitates in the form of small particles are

visible over the cells in the petri dishes. These particles are a sign of effective transfection. For other type of cells, it is important to identify appropriate transfection methods that reach satisfactory transfection efficiency.

3. Make sure that there is no dithiothreitol or EDTA in the lysis buffer because they can interfere with immobilized metal affinity chromatography during the purification of ubiquitinated proteins.
4. If the western blotting does not detect the His_6-Ub, try to expose the blot for a longer time or use ECL Plus Western Blotting Substrate or SuperSignal West Pico Chemiluminescent Substrate for western blotting. To improve the transfection efficiency, consider using other transfection reagent (such as Lipofectamine and FuGENE) for higher expression of His_6-Ub in cells.
5. If the elution of ubiquitinated protein is not efficient, increase the concentration of imidazole in the elution buffer to ≥250 mM. Alternatively, ubiquitinated proteins can be eluted by EDTA or low pH from Ni-NTA resin.
6. TALON resin has much lower nonspecific binding to proteins without hexahistidine tags than Ni-NTA resin [19]. Additionally, it binds strongly to hexahistidine-tagged proteins, such as, in our case, free His_6-Ub and His_6-tagged ubiquitinated proteins. The downstream immunoaffinity purification of Ub remnant-containing peptides may be improved if TALON resin is used for the purification of ubiquitinated proteins (Fig. 4). It should be noted that the washing step at pH 6.5 should be skipped if TALON resin is used for the purification of ubiquitinated proteins because Ni-NTA washing buffer B (pH 6.5) can elute ubiquitinated proteins from TALON resin.
7. If the sample volume is too large, concentrate the sample with an Amicon filter (10 kDa molecular weight cutoff) or use multiple lanes of a mini-gel for each sample. Dilute the eluate 2× with double distilled water before running SDS-PAGE to reduce the concentration of salt and urea. Otherwise, the sample runs irregularly due to the presence of high concentration of salts and urea.
8. The antibody used in this experiment is stored in PBS. If the antibody solution contains bovine serum albumin or free amines, such as Tris–HCl and glycine, protein G should be used to immobilize the antibody [22].
9. It is critical that the antibody is efficiently conjugated to the Affi-gel 10. Make sure that the pH of the antibody solution is about 8.5, the concentration of the antibody is ≥1 mg/mL, and the Affi-gel 10 is not hydrolyzed before antibody coupling.
10. In order to efficiently elute the Ub remnant-containing peptides, make sure that the pH of the peptide solution is about 7.4, the pH of the elution solution is below 3, and the

volume of the elution solution is 6× of the resin volume. Alternatively, Ub remnant-containing peptides can be eluted by 0.1 % TFA from the Affi-gel 10.

11. A typical LC gradient uses 5–40 % acetonitrile. The length of the LC gradient depends on the complexity of the sample. Longer gradients are required for very complex samples. Repeated runs with an exclusion list during MS/MS fragmentation may be required to identify more Ub remnant-containing peptides [33].
12. If no peptide is detected in LC-MS/MS analysis, make sure that MS instrument is working properly. Use standard peptide samples or a bovine serum albumin digest to diagnose problems associated with LC-MS/MS [34].
13. It may be required to convert LC-MS/MS data file to a format, such as mzXML and MGF, which a specific search program recognizes. The number of trypsin missed-cleavages is set up to four since trypsin does not efficiently cleave lysines after diglycine modification. The mass accuracy for the precursor and fragment ions is determined by the mass spectrometers and the MS operation condition.

Acknowledgements

The work was supported by the National Natural Science Foundation of China (Grant 31270874), Jiangsu Key Laboratory of Translational Research and Therapy for Neuro-Psycho-Diseases (BM2013003), a project funded by the Priority Academic Program Development (PAPD) of Jiangsu Higher Education Institutions (GX), NIH-NIMH (MH086128) (SRJ), Boehringer Ingelheim Fonds predoctoral fellowship (AD).

References

1. Hershko A, Ciechanover A (1998) The ubiquitin system. Annu Rev Biochem 67:425–479
2. Peng J, Schwartz D, Elias JE et al (2003) A proteomics approach to understanding protein ubiquitination. Nat Biotechnol 21: 921–926
3. Xu G, Paige JS, Jaffrey SR (2010) Global analysis of lysine ubiquitination by ubiquitin remnant immunoaffinity profiling. Nat Biotechnol 28:868–873
4. Beers EP, Callis J (1993) Utility of polyhistidine-tagged ubiquitin in the purification of ubiquitin-protein conjugates and as an affinity ligand for the purification of ubiquitin-specific hydrolases. J Biol Chem 268:21645–21649
5. Cooper HJ, Heath JK, Jaffray E, Hay RT, Lam TT, Marshall AG (2004) Identification of sites of ubiquitination in proteins: a fourier transform ion cyclotron resonance mass spectrometry approach. Anal Chem 76:6982–6988
6. Jeon HB, Choi ES, Yoon JH et al (2007) A proteomics approach to identify the ubiquitinated proteins in mouse heart. Biochem Biophys Res Commun 357:731–736
7. Layfield R, Tooth D, Landon M, Dawson S, Mayer J, Alban A (2001) Purification of polyubiquitinated proteins by S5a-affinity chromatography. Proteomics 1:773–777
8. Matsumoto M, Hatakeyama S, Oyamada K, Oda Y, Nishimura T, Nakayama KI (2005) Large-scale analysis of the human ubiquitin-related proteome. Proteomics 5:4145–4151
9. Tagwerker C, Flick K, Cui M, Guerrero C, Dou Y, Auer B et al (2006) A tandem affinity

tag for two-step purification under fully denaturing conditions: application in ubiquitin profiling and protein complex identification combined with in vivo cross-linking. Mol Cell Proteomics 5:737–748

10. Srikumar T, Jeram SM, Lam H, Raught B (2010) A ubiquitin and ubiquitin-like protein spectral library. Proteomics 10:337–342
11. Tomlinson E, Palaniyappan N, Tooth D, Layfield R (2007) Methods for the purification of ubiquitinated proteins. Proteomics 7: 1016–1022
12. Xu P, Peng J (2006) Dissecting the ubiquitin pathway by mass spectrometry. Biochim Biophys Acta 1764:1940–1947
13. Vasilescu J, Smith JC, Ethier M, Figeys D (2005) Proteomic analysis of ubiquitinated proteins from human MCF-7 breast cancer cells by immunoaffinity purification and mass spectrometry. J Proteome Res 4:2192–2200
14. Radivojac P, Vacic V, Haynes C, Cocklin RR, Mohan A, Heyen JW et al (2010) Identification, analysis, and prediction of protein ubiquitination sites. Proteins 78:365–380
15. Maor R, Jones A, Nuhse TS, Studholme DJ, Peck SC, Shirasu K (2007) Multidimensional protein identification technology (MudPIT) analysis of ubiquitinated proteins in plants. Mol Cell Proteomics 6:601–610
16. Smale ST (2010) Calcium phosphate transfection of 3T3 fibroblasts. Cold Spring Harb Protoc. doi:10.1101/pdb.prot5372
17. Kaiser P, Wohlschlegel J (2005) Identification of ubiquitination sites and determination of ubiquitin-chain architectures by mass spectrometry. Methods Enzymol 399:266–277
18. Shevchenko A, Tomas H, Havlis J, Olsen JV, Mann M (2006) In-gel digestion for mass spectrometric characterization of proteins and proteomes. Nat Protoc 1:2856–2860
19. Nielsen ML, Vermeulen M, Bonaldi T, Cox J, Moroder L, Mann M (2008) Iodoacetamide-induced artifact mimics ubiquitination in mass spectrometry. Nat Methods 5:459–460
20. Link AJ, LaBaer J (2011) Solution protein digest. Cold Spring Harb Protoc. doi:10.1101/pdb.prot5569
21. Parker CE, Warren MR, Mocanu V, Greer SF, Borchers CH (2008) Mass spectrometric determination of protein ubiquitination. Methods Mol Biol 446:109–130
22. Harlow E, Lane D (2006) Immunoaffinity purification: coupling antibodies to protein A or G bead columns. Cold Spring Harb Protoc. doi: 10.1101/pdb.prot4303
23. Mattson G, Conklin E, Desai S, Nielander G, Savage MD, Morgensen S (1993) A practical approach to crosslinking. Mol Biol Rep 17: 167–183
24. Perkins DN, Pappin DJ, Creasy DM, Cottrell JS (1999) Probability-based protein identification by searching sequence databases using mass spectrometry data. Electrophoresis 20: 3551–3567
25. Craig R, Beavis RC (2004) TANDEM: matching proteins with tandem mass spectra. Bioinformatics 20:1466–1467
26. Geer LY, Markey SP, Kowalak JA, Wagner L, Xu M, Maynard DM et al (2004) Open mass spectrometry search algorithm. J Proteome Res 3:958–964
27. MacCoss MJ, Wu CC, Yates JR 3rd (2002) Probability-based validation of protein identifications using a modified SEQUEST algorithm. Anal Chem 74:5593–5599
28. Palagi PM, Hernandez P, Walther D, Appel RD (2006) Proteome informatics I: bioinformatics tools for processing experimental data. Proteomics 6:5435–5444
29. Boeckmann B, Bairoch A, Apweiler R, Blatter MC, Estreicher A, Gasteiger E et al (2003) The SWISS-PROT protein knowledgebase and its supplement TrEMBL in 2003. Nucleic Acids Res 31:365–370
30. Pruitt KD, Tatusova T, Maglott DR (2007) NCBI reference sequences (RefSeq): a curated non-redundant sequence database of genomes, transcripts and proteins. Nucleic Acids Res 35:D61–D65
31. Kersey PJ, Duarte J, Williams A, Karavidopoulou Y, Birney E, Apweiler R (2004) The International Protein Index: an integrated database for proteomics experiments. Proteomics 4:1985–1988
32. Xu G, Jaffrey SR (2013) Proteomic identification of protein ubiquitination events. Biotechnol Genet Eng Rev 29:73–109
33. Seo J, Jeong J, Kim YM, Hwang N, Paek E, Lee KJ (2008) Strategy for comprehensive identification of post-translational modifications in cellular proteins, including low abundant modifications: application to glyceraldehyde-3-phosphate dehydrogenase. J Proteome Res 7:587–602
34. Xu H, Freitas MA (2009) Automated diagnosis of LC-MS/MS performance. Bioinformatics 25: 1341–1343

Chapter 5

Secretion of Circular Proteins Using Sortase

Karin Strijbis and Hidde L. Ploegh

Abstract

Circular proteins occur naturally and have been found in microorganisms, plants, and eukaryotes where they are commonly involved in host defense. Properties of circular proteins include enhanced resistance to exoproteases, increased thermostability, longer life spans, and increased activity. Using an enzymatic approach based on the bacterial sortase A (SrtA) transpeptidase, N- and C-termini of conventional linear proteins can be linked resulting in a circular protein. Circularization of bioengineered linear substrate proteins can indeed confer the desirable properties associated with circular proteins. Here, we describe how cells can be manipulated to secrete circularized proteins for substrates of choice via sortase-mediated circularization in the lumen of the endoplasmic reticulum.

Key words Sortase (SrtA), Protein circularization, Intracellular sortagging, Endoplasmic reticulum, Secretion

1 Introduction

Circular proteins have evolved as an important component of host defense in microorganisms, plants, and eukaryotes [1, 2]. Compared to conventional linear proteins, circular proteins display decreased sensitivity to proteolytic attack as no N- or C-termini are exposed. Circular proteins are therefore often more stable, especially in a protease-rich inflammatory milieu. In addition, circular proteins may also display improved refolding kinetics, improved stability and higher activity than their linear counterparts. Examples of naturally occurring circular proteins include the pore-forming *Enterococcus faecalis* bacteriocin AS-48 [3], *Escherichia coli* microcin J25 (MccJ25) which interferes with cell division of related species [4], plant cyclotides with antibacterial, antifungal, or insecticidal properties [5–7], amatoxins and phallotoxins of lethal mushrooms [7], and the antibacterial Rhesus theta defensin-1 (RTD-1) secreted by rhesus macaque leukocytes [8–10]. While the biosynthetic pathways of circular proteins remain to be deciphered in detail, most are produced by posttranslational modification of linear precursors.

Andrei I. Ivanov (ed.), *Exocytosis and Endocytosis*, Methods in Molecular Biology, vol. 1174,
DOI 10.1007/978-1-4939-0944-5_5,

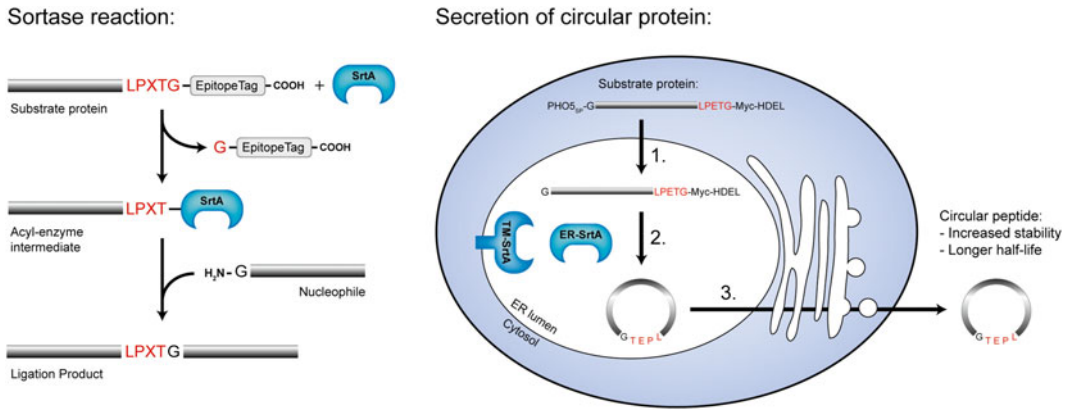

Fig. 1 Secretion of circular proteins using sortase-mediated protein ligation in the endoplasmic reticulum. *Left*: The sortase protein-ligation reaction. A substrate protein is equipped with a LPXTG sortase recognition motif followed by an epitope tag of choice. Sortase (SrtA) binds to the LPXTG motif resulting in formation of an acyl-enzyme intermediate and release of the G-epitope tag fraction of the substrate protein. A nucleophile protein with an N-terminal glycine can resolve the acyl-enzyme intermediate thereby forming the ligation product through a regular peptide bond. *Right*: Secretion of circular protein using ER-luminal sortagging. A substrate protein with an N-terminal Pho5 signal peptide (SP) and C-terminal LPETG-Myc-HDEL motif is expressed in the cytosol. The Pho5 SP induces import into the ER (1) and the HDEL motif prevents the substrate protein from exiting the ER. Cleavage of the Pho5 signal peptide exposes an N-terminal glycine (G). Induction of soluble ER-SrtA or transmembrane-bound TM_{Sec66}-SrtA initiates the protein ligation reaction that forms the circular protein (2). The loss of the Myc epitope tag can be used as a readout for successful substrate recognition by the SrtA enzyme. The circularized protein no longer contains the HDEL ER retention signal and therefore enters the secretory pathway resulting in secretion

Synthetic methods for the production of cyclic polypeptides include modified solid phase peptide synthesis, native chemical ligation, intein-based methods, and a method based on the bacterial transpeptidase sortase A (SrtA) [11, 12]. SrtA is an enzyme of gram-positive bacterial origin involved in covalent attachment of proteins to the bacterial cell wall. Protein ligation by SrtA has been used in a number of in vitro protein-engineering applications (reviewed in ref. 13). The SrtA enzyme binds to and cleaves within a C-terminal 5-residue sortase motif (LPXTG), forming an acyl-enzyme intermediate (Fig. 1). This structure can be resolved by an incoming nucleophile, for example a protein with N-terminal glycines, resulting in ligation of the nucleophile to the sortase motif. Sortase-mediated circularization requires only minimal modifications of the substrate protein; a C-terminal LPXTG sortase tag and suitably exposed N-terminal glycine residue(s). Using SrtA, in vitro circularization of proteins such as enhanced green fluorescent protein (eGFP) [12], Cre recombinase [12], four-helix bundle cytokines interferon α3 (IFNα3) and granulocyte colony-stimulating factor-3 (GCSF-3) [14], human erythropoietin (EPO) [14], and the wound-healing peptide Histatin-1 [15] was accomplished. In line with the properties of naturally occurring cyclic

polypeptides, the synthetic polypeptides also displayed increased stability and activity compared to their linear counterparts [12, 14, 15]. In addition to such SrtA applications in vitro, we showed that the Ca^{2+}-independent *Streptococcus pyogenes* SrtA enzyme can be used for intracellular protein ligation in living cells [16]. Using *S. pyogenes* SrtA, eGFP circularization could be accomplished in the cytosol and endoplasmic reticulum (ER) lumen of both *S. cerevisiae* and mammalian HEK293T cells [16].

In this chapter we describe a method for the secretion of circular proteins of choice making use of ER-luminal sortagging (Fig. 1). The method involves the design of a linear substrate protein equipped with an N-terminal signal peptide (SP) that exposes a glycine residue after cleavage and a C-terminal sortase recognition motif (LPETG) followed by a Myc epitope tag and an ER retention signal (HDEL). The next step is transformation of *Saccharomyces cerevisiae* with the substrate protein expression plasmid and the pGAL-ER-SrtA plasmid. Sortase activity in the ER lumen will result in circularization of this substrate protein and loss of the Myc-HDEL portion of the protein. Subsequently, the circular protein advances in the secretory system and is ultimately secreted. Regulated secretion of the circular protein product is obtained by galactose-inducible ER-SrtA expression. Our method can be employed to investigate the functions of circular proteins in complex systems or for the biosynthesis of circular proteins with minimal purification.

2 Materials

2.1 Generation of Circularization Substrate and Sortase Expression Vectors

1. ER-SrtA plasmid (pKS82; pRS303-pGAL-$PHO5_{SP}$-G-$SrtA_{strep}$-HA-HDEL) or TM_{Sec66}-SrtA plasmid (pKS105; pRS303-pGAL-HA-TMSec66-SrtA). Plasmids are available at Addgene (www.addgene.org) (*see* **Note 1**).
2. DNA primers for PCR amplification (*see* **Note 2**).

   Forward primer with 5′ adaptor introducing ***Xba*I**-$PHO5_{SP}$-G-***BamH*I**:

   5′-ga**TCTAGA**ATGTTTAAATCTGTTGTTTATTCAATT TTAGCCGCTTCTTTGGCCAATGCAGGTACC ATTCCCTTA**GGATCC**C… (introduce gene-specific sequence after ATG start codon)-3′.

   Reverse primer with 5′ adaptor introducing ***Sal*I**-LPETG-Myc-HDEL-***Xho*I**:

   5′-ga**CTCGAG**CCTACAGCTCGTCATGCTCGCTTG CGGCCCCATTCAGATCCTCTTCTGAG ATGAGTTTTTGTTCTGCGGCCGCACCAGTT TCAGGAAG**GTCGAC** (introduce gene-specific sequence before STOP codon)-3′.

3. DNA template for gene of choice (plasmid, cDNA, genomic DNA).
4. A yeast expression plasmid with a constitutive promoter, here pRS306 with *pCIT1*.
5. A high-fidelity polymerase like Phusion DNA polymerase (Finnzyme), and its specific buffer and dNTP mix.
6. A PCR purification kit, here QIAquick PCR purification kit (Qiagen).
7. Standard restriction enzymes and their related buffers, here *Xba*I and *Xho*I (New England Biolabs).
8. A gel extraction kit, here QIAquick Gel Extraction kit (Qiagen).
9. A T4 DNA ligase and its accompanying buffer (New England Biolabs).
10. *E. coli* competent cells, here DH5α competent *E. coli* cells.
11. Sterile LB medium and LB agar plates (1 % tryptone, 0.5 % yeast extract, 1 % NaCl).
12. Antibiotic stocks for plasmid selection (100 mg/ml ampicillin or 50 mg/ml kanamycin).
13. Nucleic acid extraction and purification kit, here QIAprep spin Miniprep kit (Qiagen).
14. Standard equipment, consumables, and chemicals for routine molecular biology techniques including PCR amplification of DNA fragments, DNA separation and visualization, UV spectrophotometry, and *E. coli* culturing.
15. DNA sequence primers.

2.2 Plasmid Isolation

1. Bacterial stock (typically *E. coli* DH5α) transformed with the substrate or sortase plasmids.
2. Sterile LB medium and LB agar plates (1 % tryptone, 0.5 % yeast extract, 1 % NaCl).
3. High-speed plasmid Maxi kit (QIAGEN).

2.3 Yeast Transformation with Substrate and Sortase Plasmids

1. All yeast reagents are listed in Table 1.
2. Freshly plated auxotrophic *S. cerevisiae* strain, here W303-K700.
3. Salmon sperm carrier DNA (Sigma-Aldrich), store at –20 °C.
4. 50 % polyethylene glycol 4000 solution in water, stable at room temperature.
5. 1 M lithium acetate solution in water, stable at room temperature.
6. YPDA medium: 1 % yeast extract, 2 % Bacto Peptone, 2 % glucose, 1× adenine, stable at room temperature.

Table 1
Yeast solutions and media

S. cerevisiae strain W303-K700	*MATalpha, ade2-1, leu2-3, ura3, trp1-1, his3-11,15, can1-100, GAL, psi+*
YP	10 g yeast extract and 20 g Bacto Peptone in 900 ml deionized water, autoclave and cool down
20 % glucose	20 g/100 ml, filter-sterilize
20 % galactose	20 g/100 ml, filter-sterilize
10× YNB	134 g yeast nitrogen base with ammonium sulfate without amino acids /1 L, filter-sterilize
100× Adenine	0.55 g/100 ml, filter-sterilize
100× Uracil	0.224 g/100 ml, filter-sterilize
100× Tryptophan	0.8 g/100 ml, filter-sterilize, protect from light
60× Leucine	1.31 g/100 ml, filter-sterilize
100× Histidine	2.09 g/100 ml, filter-sterilize, protect from light
1 M LiAc	6.6 g Lithium Acetate/100 ml, autoclave
0.1 M LiAc	0.66 g/100 ml, autoclave
50 % PEG	50 ml polyethylene glycol 4000/100 ml, autoclave
TRAFO mix	240 µl 50 % PEG, 36 µl 1.0 M LiAc, 10 µl salmon sperm carrier DNA, 1 µg, H_2O up to 360 µl for each transformation
YPDA	To 900 ml YP stock medium, add 100 ml 20× glucose and 10 ml 100× Adenine
YPGA	To 900 ml YP stock medium, add 100 ml 20× galactose and 10 ml 100× Adenine
YNB 2 % glucose	20 g/900 ml D-glucose, autoclave and cool down, add 100 ml 10× YNB
YNB 0.3 % glucose	3 g/900 ml D-glucose, autoclave and cool down, add 100 ml 10× YNB
Selection plates	4 g D-glucose and 4 g agar in 180 ml, autoclave and cool down, add 20 ml 10× YNB and all amino acids (adenine, uracil, tryptophan, leucine, histidine) except for the selection marker(s) of the transformed plasmids

7. 100× Adenine, Uracil, Tryptophan, Leucine, Histidine amino acid solutions in water, stable at room temperature.
8. Selection plates lacking the amino acid selective marker(s).

2.4 Galactose Induction to Initiate Sortase Expression and Substrate Circularization

1. *S. cerevisiae* isolates transformed with the substrate and sortase plasmids.
2. YNB 2 % glucose medium: 1× YNB, 2 % glucose.
3. YNB 2 % glucose medium: 1× YNB, 2 % glucose.
4. YPGA medium: 2 % Bacto Peptone, 1 % yeast extract, 2 % galactose and 1× adenine.

2.5 Detection of Circular Protein

1. Optional: antibody for immunoprecipitation.
2. Optional: 100 % trichloroacetic acid (TCA) solution for protein precipitation.
3. Optional: Amicon Ultra Centrifugal Filters (Millipore) for protein concentration.
4. Equipment and materials for SDS-PAGE gels and Coomassie staining.
5. MS/MS facilities for sample analysis.

3 Methods

3.1 Generation of Circularization Substrate and Sortase Expression Vectors

1. Prepare the PCR reaction mix on ice: typically 1–10 ng of the template DNA, 5 μl each of the 10 μM stock solution of the forward and reverse primers, 10 μl of 5× PCR buffer, 5 μl of dNTP mixture (2.5 mM each), 1 U of high fidelity Phusion polymerase, and sterile water to a final volume of 50 μl.
2. Run the PCR reaction in a thermocycler with a 25-cycle protocol alternating 15 s at 98 °C, 15 s at 56 °C, and 1 min at 72 °C.
3. Pipette 5 μl of the PCR reaction, add DNA loading dye, and load the mixture on a 1 % agarose gel to analyze the amplified product (*see* **Note 3**).
4. Purify the remaining 45 μl of the substrate PCR reaction using the protocol detailed in the PCR purification kit.
5. In individual eppendorf tubes, cut the amplified DNA fragment coding for the circularization substrate and the expression vector of choice (pRS306 or other) with the appropriate restriction enzymes, in this case *Xba*I and *Xho*I. Typically, 1 μg of plasmid DNA is used.
6. Load the digestion products on a 1 % agarose gel and following separation extract the cut insert and vector fragments separately (*see* **Note 4**).
7. Isolate the DNA from the gel pieces using the protocol detailed in the QIAquick Gel Extraction kit.
8. Prepare the ligation reaction with a 5:1 ratio of insert–plasmid. Always include a control ligation reaction without the insert and a control reaction with T4 DNA ligase. Add 1 U of T4 DNA ligase together with the ligase buffer and add sterile water to a final volume to 20 μl.
9. Incubate the ligation reaction 1–2 h at room temperature or overnight at 16 °C (preferred, *see* **Note 5**).
10. For bacterial transformation, add 10 μl of the ligation mixture to 50 μl of DH5α competent cells. Incubate on ice for 30 min to allow for DNA uptake.

11. Heat-shock the cells for 45 s at 42 °C and immediately transfer the tubes on ice.
12. Add 1 ml of LB medium without antibiotics and let the cells regenerate in the shaker for 1 h at 37 °C.
13. Spread 100 μl of the transformation mixture on LB agar plates supplemented with ampicillin or kanamycin and incubate overnight at 37 °C. The remainder of the transformed bacteria can be stored at 4 °C for up to 1 week.
14. The following day, pick colonies and use to inoculate 2 ml LB supplemented with ampicillin. Grow the cultures overnight in the shaker at 37 °C.
15. Purify the plasmid DNA of each clone using the plasmid purification kit following the manufacturer's instructions.
16. Take 2 μl of each plasmid preparation and perform restriction digest analysis using the *Xba*I and *Xho*I enzymes to confirm the presence of the insert.
17. Final check the insert by DNA sequencing and select a plasmid containing the correct insert sequence (*see* **Note 6**).
18. Store the plasmid at –20 °C.

3.2 Plasmid Isolation

1. Transform DH5α competent cells with the correct substrate plasmid and the obtained ER-SrtA and TM_{Sec66}-SrtA plasmids.
2. Isolate DNA by following the protocol detailed in the High-speed plasmid Maxi kit.

3.3 Yeast Transformation with Substrate and Sortase Plasmids

1. Aseptically pick a single *S. cerevisiae* colony from a freshly streaked YPD agar plate in to 5 ml of YPD medium with 1× adenine and culture overnight in the shaker at 30 °C.
2. The next day, dilute the culture to $OD_{600} = 0.2$ in 50 ml YPDA medium. Incubate in the shaker at 30 °C until $OD_{600} = 0.4–0.7$ (this will take about 4 h).
3. Spin down at 3,000 × *g* for 5 min. Wash the pellet with 25 ml H_2O, spin at 3,000 × *g* for 5 min. Resuspend in 1 ml 0.1 M lithium acetate and transfer to an eppendorf tube.
4. Spin down at 3,000 × *g* for 5 min and aspirate the supernatant. Take the pellet up in 400 μl of 0.1 M lithium acetate (total volume ~500 μl).
5. Set up tubes for transformation with the substrate plasmid, the sortase plasmid, and the combined plasmids (*see* **Note 7**).
6. For each transformation, aliquot 50 μl of the cell suspension in an eppendorf tube. Spin down and remove lithium acetate.
7. Add 360 μl of TRAFO mix to each cell pellet.
8. Incubate with rotation at 30 °C for 30 min.

9. Heat-shock at 42 °C for 15 min (*see* **Note 8**).
10. Spin down and resuspend the pellet in 100 μl H_2O.
11. Plate on appropriate selective YNB 2 % glucose plates (-His/-Ura/-Leu/-Tryp) and grow for 2–3 days at 30 °C.
12. Restreak single colonies on fresh selective plates and grow for 2–3 days at 30 °C (*see* **Note 9**).
13. Pick single colonies to make glycerol stocks and/or do the experiment.

3.4 Galactose Induction to Initiate Sortase Expression and Substrate Circularization

1. Inoculate a yeast colony in 25 ml of YNB 2 % glucose medium with necessary amino acids (add Leu, Trp, Ade, His, Ura, with exception of selection markers on transformed plasmids). Grow overnight in the shaker at 30 °C.
2. Next day late afternoon, inoculate the culture in 25 ml YNB 0.3 % glucose + amino acids. Grow for about 16 h in the shaker at 30 °C.
3. Next day morning, inoculate cells in YPGA medium at an OD_{600} of 0.2.
4. Harvest supernatant and cell pellets after 2, 4, and 8 h. The circular protein is secreted in the media.

3.5 Detection of Circular Protein

1. If an antibody is available for the substrate of choice, the circular protein can be isolated from the media by immunoprecipitation. Otherwise, precipitate the protein fraction from the media by TCA precipitation or concentrate the protein fraction using spin columns (for example Amicon Ultra Centrifugal Filters from Millipore).
2. Analyze the immunoprecipitate or protein fraction by SDS-PAGE gel and immunoblotting and/or Coomassie staining. The circular protein usually runs at a lower molecular weight compared to its linear counterpart. In addition, the linear substrate protein contains a Myc tag that is lost upon circularization.
3. Cut the area containing the circular protein from the Coomassie-stained gel and perform MS/MS analysis to confirm the molecular weight of the circularized protein.

4 Notes

1. The insert sequences of the sortase plasmids are as follows:

   Sol. ER-SrtA

   ATGTTTAAATCTGTTGTTTATTCAATTTTAGCCGCTT
   CTTTGGCCAATGCAGGTACCATTCCCTTAGGAT
   CC AGTGTCTT

GCAAGCACAAATGGCGGCTCAGCAACTTCCTGTT
ATAGGGGGCATTGCCATACCAGAGCTTGGCAT
TAATTT ACCAATTT

TTAAAGGTTTAGGAAATACTGAGCTTATTTAT
GGCGCAGGAACGATGAAAGAAGAACAAGT
TATGGGA GGA GAAAATAAT

TATTCTCTTGCCAGTCATCATATTTTTGGAATTACA
GGTTCATCTCAAATGCTCTTTTCGCCGCTTGA
AAGA GCACAAAA

TGGGATGTCCATCTATTTAACAGATAAAGAAAAAA
TTTACGAATACATCATAAAAGATGTTTTCAC
GGTAGC TCCTGAAC

GCGTTGATGTTATCGATGATACAGCTGGTCTCAAAG
AAGTGACTTTAGTGACTTGTACAGATATCGA
AGCAA CAGAACGT

ATTATTGTCAAAGGAGAACTAAAAACAGAATACGAC
TTTGATAAAGCGCCCGCCGATGTATTGAAAGC
TTTTAATCATTC

TTATAACCAAGTATCTACCGTCGACGCGGCCGCA
TACCCATACGACGTACCAGACTACGCAAATGGGG
CCGCAAGCGAGC

ATGACGAGCTGTAG

TM_{Sec66}-SrtA ATGTACCCATACGACGTACCAGACTACGC
AGAGACGAAATCAATCTCCGTTTATACCCCA
CTCATATATGTCTTTATTCT

GGTGGTGTCCCTTGTGATGTTTGCTTCAAGCGGAT
CCGAGCCAGTTAGTACAGAGAGTGTCTTGCA
AGCACAAATGGCGG

CTCAGCAACTTCCTGTTATAGGGGGCATTGCCATAC
CAGAGCTTGGCATTAATTTACCAATTTTTAAA
GGTTTAGGAAAT

ACTGAGCTTATTTATGGCGCAGGAACGATGAAAGAA
GAACAAGTTATGGGAGGAGAAAATAATTATTC
TCTTGCCAGTCA

TCATATTTTTGGAATTACAGGTTCATCTCAAATGCTC
TTTTCGCCGCTTGAAAGAGCACAAAATGGGATGT
CCATCTATT

TAACAGATAAAGAAAA AATTTACGAATACATCATAAAA
GATGTTTTCACGGTAGCTCCTGAACGCGTTG
ATGTTATCGAT

GATACAGCTGGTCTCAAAGAAGTGACTTTAGTGAC
TTGTACAGATATCGAAGCAACAGAACGTATT
ATTGTCAAAGGAGA

ACTAAAAACAGAATACGACTTTGATAAAGCGCCCG
CCGATGTATTGAAAGCTTTTAATCATTCTTATAA
CC AAGTATCTA

CCTAG

2. The termini of most proteins are unstructured and accessible for modification by SrtA. The proximity of N- and C-terminus depends on the protein of choice and can be studied when a crystal structure is available. A longer linker sequence can be introduced when it is expected that the termini are not in close proximity. We have found that also termini that are buried within a structure can be accessible for sortagging like in the case of UCHL3 [12] and HUWE1 (unpublished results).
3. Problem solving in case the PCR reaction does not yield a product: the template concentration might be too low (especially when cDNA is used). Increase the number of cycles from 25 to 35. When increasing the number of cycles does not yield a product, a two-step PCR protocol can be performed. First step: perform the primary PCR with the long primers for 5 rounds. Second amplification step: add short primers (covering the 5′ ends of the long primers) to the reaction and perform an additional 25 rounds.
4. Before and during cutting of the fragments from the 1 % agarose gel, use low wavelength UV irradiation as high wavelength can introduce DNA mutations.
5. The 20 μl ligation reaction can be split in two: 10 μl can be incubated for 1–2 h at RT, the other 10 μl of the reaction can be incubated overnight at 10 °C.
6. For cloning and expression of other substrate(s), the *BamHI* and *SalI* restriction sites can be used bypassing the need for long primers.
7. Always set up a transformation with the single plasmids as a control for unmodified substrate and sortase expression.
8. The timing of the heat shock treatment is important.
9. Restreaking is important as amino acid selection is not lethal and non-transformed cells might still be present. Try to restreak the colonies so that one ends up with single colonies. A tree shape is commonly used.

References

1. Trabi M, Craik DJ (2002) Circular proteins – no end in sight. Trends Biochem Sci 27:132–138
2. Craik DJ, Allewell NM (2012) Thematic minireview series on circular proteins. J Biol Chem 287:26999–27000
3. Martinez-Bueno M, Maqueda M, Galvez A et al (1994) Determination of the gene sequence and the molecular structure of the enterococcal peptide antibiotic AS-48. J Bacteriol 176:6334–6339

4. Salomon RA, Farias RN (1992) Microcin 25, a novel antimicrobial peptide produced by Escherichia coli. J Bacteriol 174:7428–7435
5. Jennings C, West J, Waine C, Craik D, Anderson M (2001) Biosynthesis and insecticidal properties of plant cyclotides: the cyclic knotted proteins from Oldenlandia affinis. Proc Natl Acad Sci U S A 98:10614–10619
6. Tam JP, Lu YA, Yang JL, Chiu KW (1999) An unusual structural motif of antimicrobial peptides containing end-to-end macrocycle and cystine-knot disulfides. Proc Natl Acad Sci U S A 96:8913–8918
7. Goransson U, Burman R, Gunasekera S, Stromstedt AA, Rosengren KJ (2012) Circular proteins from plants and fungi. J Biol Chem 287:27001–27006
8. Tang YQ, Yuan J, Osapay G et al (1999) A cyclic antimicrobial peptide produced in primate leukocytes by the ligation of two truncated alpha-defensins. Science 286:498–502
9. Trabi M, Schirra HJ, Craik DJ (2001) Three-dimensional structure of RTD-1, a cyclic antimicrobial defensin from Rhesus macaque leukocytes. Biochemistry 40:4211–4221
10. Lehrer RI, Cole AM, Selsted ME (2012) theta-Defensins: cyclic peptides with endless potential. J Biol Chem 287:27014–27019
11. Aboye TL, Camarero JA (2012) Biological synthesis of circular polypeptides. J Biol Chem 287:27026–27032
12. Antos JM, Popp MW, Ernst R et al (2009) A straight path to circular proteins. J Biol Chem 284:16028–16036
13. Popp MW, Ploegh HL (2011) Making and breaking peptide bonds: protein engineering using sortase. Angew Chem Int Ed Engl 50: 5024–5032
14. Popp MW, Dougan SK, Chuang TY, Spooner E, Ploegh HL (2011) Sortase-catalyzed transformations that improve the properties of cytokines. Proc Natl Acad Sci U S A 108: 3169–3174
15. Bolscher JG, Oudhoff MJ, Nazmi K et al (2011) Sortase A as a tool for high-yield histatin cyclization. FASEB J 25: 2650–2658
16. Strijbis K, Spooner E, Ploegh HL (2012) Protein ligation in living cells using sortase. Traffic 13:780–789

Chapter 6

Fractionation of Subcellular Membrane Vesicles of Epithelial and Non-epithelial Cells by OptiPrep™ Density Gradient Ultracentrifugation

Xuhang Li and Mark Donowitz

Abstract

Density gradient ultracentrifugation (DGUC) is widely used for physical isolation (enrichment rather than purification) of subcellular membrane vesicles. It has been a valuable tool to study specific subcellular localization and dynamic trafficking of proteins. While sucrose has been the main component of density gradients, several years ago, synthetic OptiPrep™ (iodixanol) began being used for separation of organelles due to its iso-osmotic property. Here, we describe a detailed protocol for density gradient fractionation of various mammalian subcellular vesicles, including endoplasmic reticulum (ER), Golgi apparatus, endosomes, and lipid rafts, as well as apical and basolateral membranes of polarized epithelial cells.

Key words Density gradient ultracentrifugation, OptiPrep, Subcellular membrane vesicles, Organelles, Lipid rafts, Epithelia

1 Introduction

Density gradient ultracentrifugation (DGUC) is a common separation technique that is used in separation of both protein complexes and subcellular membrane vesicles based on size and density. The principle of DGUC is based on the difference in terminal velocities ($\mathbf{V_t}$) of different particles (proteins or vesicles in this case) as defined by Stoke's law: $\mathbf{V_t} = 2R^2(Ps-P)a/(9\mu)$, where R is the radius of the particle, Ps the density of the particle, P the density of the medium, a the centrifugal acceleration of the centrifuge, and μ the viscosity of the medium. At a given centrifugal force (a), $\mathbf{V_t}$ is essentially a function of radius (R) and density (Ps) of the particles for a particular separation medium of fixed density and viscosity. The other important variable in this equation is the density of the medium (P), which is the key to separate different particles when a gradual density gradient is present along the path of particle sedimentation. Typically, larger (in size) and heavier (in density)

Andrei I. Ivanov (ed.), *Exocytosis and Endocytosis*, Methods in Molecular Biology, vol. 1174,
DOI 10.1007/978-1-4939-0944-5_6,

particles will travel through a gradient faster and settle further down the gradient In the case of membrane vesicle separation by a density gradient, at equilibrium a particular vesicle species will remain in a specific fraction where the density of this fraction is equal to the density of the vesicles. At this stage, $\mathbf{V_t}$ is zero (no vesicle movement) (For more information on principles and applications of centrifugation methods, *see* ref. 1).

Sucrose has always been a major component of density gradient centrifugation for separation of both organelles and subcellular vesicles from various sources [1–4]. A simple search of PubMed with key words "sucrose density gradient" yields 10,192 publications (as of December 30, 2013), indicating its extensive biological application. In 1994, Rickwood's group [5, 6] first introduced a new nonionic density gradient medium, iodixanol, which is a dimer of Nycodenz. Iodixanol has a significant advantage over previously iodinated density gradient media (such as sucrose): Its aqueous solutions are iso-osmotic up to a density of 1.32 g/m [5]. Iodixanol has been marketed as OptiPrep™ by the Diagnostic Division of Nycomed Pharma (Norway), which was later acquired by Axis-Shield in 2000. We are among the earliest groups to use OptiPrep to separate apical, basolateral, and endosomal membrane vesicles of polarized epithelial cells [7, 8]. Due primarily to the attractive iso-osmotic property of OptiPrep, the new medium has become widely used for separating cells and subcellular membrane vesicles, in spite of a higher price than sucrose (see Axis-Shield Web site for extensive references: http://www.axis-shield.com/density/optiHome.htm).

In this chapter, we focus on the application of OptiPrep density gradient ultracentrifucation in separation of organelles and/or subcellular membrane vesicles, including lipid rafts.

2 Materials

2.1 Density Gradient Preparation

OptiPrep™: 60 % of Iodixanol as original package available from Axis-Shield.

2.2 Animals, Cell Culture, and Lysis Buffer

1. Male New Zealand white rabbits, weighing 2.5–5 kg.
2. Caco-2 cell (Human colon cancer cell) and PS120/E3V cell [a Na+/H+exchanger-deficient derivative of the Chinese hamster lung fibroblast CCL39 cell line; E3V denotes that this PS120 cell line was stably transfected with VSV-G-tagged NHE3 (rabbit *Na*$^+$/*H*$^+$ *e*xchanger *3*)].
3. *Cell culture media:* All cells were grown in 5 % CO_2/95 % O_2 at 37 °C in the following media: *Caco-2 cells*: DMEM supplemented 10 % fetal bovine serum (FBS) (vol/vol), 0.1 mM

nonessential amino acids, 1 mM pyruvate, 100 U/ml penicillin, 100 μg/ml streptomycin; *PS120 cells*: DMEM supplemented with 10 % FBS, 100 U/ml penicillin, and 100 μg/ml streptomycin.

4. Costar Brand Transwell dish inserts (Corning, Cat#: 3419).
5. *Cell lysis buffers:* all buffers contain 1 mM Na_3VO_4, 1 mM PMSF, and a protease inhibitor cocktail (Sigma, 1:500 dilution).
   (a) *HEPES buffer:* 25 mM HEPES bis-tris propane (HEPES-BTP) (pH 7.4), containing 150 mM NaCl, 1 mM DTT, 2 mM EGTA.
   (b) *TNE buffer*: 25 mM Tris–HCl, pH 7.4, 150 mM NaCl, 5 mM EDTA, 5 mM DTT, 1 mM Na_3VO_4.

2.3 Buffers for Ileal Mucosal Total Membranes and Brush Border Preparation

1. *BB isolation buffers:* All three BB isolation buffers contain the following protease inhibitors: 1 mM PMSF, a protease inhibitor cocktail, and phosphoramidon (10 μg/ml).
   (a) BB Isolation Buffer # 1, pH 7.1

	Final concentration	For 500 ml	For 250 ml
Mannitol	300 mM	27.33 g	13.67 g
Tris–HCl	12 mM	0.726 g	0.363 g
EGTA	5 mM	0.950 g	0.475 g
Na_3VO_4	10 mM	50 ml (100 mM stock)	25 ml
β-Glycerophosphate	5 mM	0.540 g	0.27 g
Phenylalanine	5 mM	0.4125 g	0.21 g

(b) BB Isolation Buffer # 2, pH 7.1

	Final concentration	For 500 ml	For 250 ml
Mannitol	60 mM	5.468 g	2.734 g
EGTA	5 mM	0.950 g	0.475 g
β-Glycerophosphate	1 mM	0.108 g	0.05 g
Phenylalanine	1 mM	0.0825 g	0.041 g
Na_3VO_4	1 mM	5 ml (100 mM stock)	2.5 ml

(Adjust pH with 1 M Tris)

(c) BB Isolation Buffer # 3, pH 7.1

	Final concentration	For 500 ml	For 250 ml
Mannitol	300 mM	27.32 g	13.67 g
HEPES	20 mM	2.382 g	1.19 g
Mg-gluconate	5 mM	0.515 g	0.257 g
β-Glycerophosphate	1 mM	0.108 g	0.05 g
Phenylalanine	1 mM	0.0825 g	0.04 g
Na_3VO_4	1 mM	5 ml (100 mM stock)	2.5 ml

(Adjust pH with 1 M Tris)

2. *Saline:* 36 g NaCl dissolved in 4,000 ml DI H_2O.

2.4 SDS-PAGE (SDS–Polyacrylamide Gel Electrophoresis)

1. Polyacrylamide–Bis solution (29 %/1 %) (Bio-Rad).
2. 5× Sample buffer [prepare as a 5× stock (*see* **Note 1**); use 1× as final concentration):

	Final concentration at 1× after dilution	For 50 ml	For 200 ml
Tris–HCl (1 M stock, pH 6.8)	44.0 mM	11 ml	22 ml
EDTA-2Na	4.33 mM	0.403 g	1.612 g
SDS	1.8 %	4.5 g	18 g
Glycerol	10 %	25 ml	100 ml
β-Mercaptoethanol	2 %	5 ml	20 ml
Bromophenol blue	0.012 %	24 mg	96 mg

3. 5× Running buffer (Prepare as a 5× stock; use 1× as final concentration):

	Final concentration at 1× after dilution	For 1 l	For 10 l
Tris-base	24.8 mM	15 g	150 g
Glycine	192 mM	72 g	720 g
SDS (w/v)	0.1 %	5 g	50 g

2.5 Western Blotting: 10× Transfer Buffer (Prepare as a 10× Stock; Use 1× as Final Concentration)

	Final concentration at 1× after dilution	For 1 l	For 10 l
Tris-base	34.3 mM	41.53 g	415.3 g
Glycine	39 mM	39 g	390 g
SDS (w/v)	0.0357 %	0.357 g	3.57 g

3 Methods

3.1 Preparation of Total Cellular Membranes (See Note 2)

3.1.1 Total Cellular Membrane Preparation from Caco-2 Cells for Isolation of Lipid Rafts (All Procedures Were Performed at 4 °C, Except **Step 1**)

1. Caco-2/E3V cells, which were transfected with NHE3 epitope-tagged at the C-terminus with VSVG [9], were grown on 100 mm Costar Brand Transwell dish inserts. After 1 or 2 weeks post-confluence, the Caco-2 cells were incubated with serum-free medium overnight before being used for experiments.
2. Rinse both sides of each Transwell 3–4 times with cold (4 °C) PBS buffer. Use 15–20 ml per rinse. Completely remove the HEPES buffer with aspiration after the last rinse.
3. Add 1 ml of cold TNE buffer PBS in the upper chamber of the Transwell, and gently scrape cells in each Transwell into a 1.5 ml Eppendorf tube using a disposable plastic scraper. To avoid breaking the Transwell membranes, place the Transwell onto the lid of the housing petri dish. Avoid bubbles trapped under the Transwell.
4. Remove the TNE buffer by centrifuging cells at 3,000 × *g* for 3 min.
5. Resuspend cells in TNE buffer (1.5–2 ml per 10 cm Transwell dish).
6. Sonicate at 4 °C for 10 pulses and repeat two more times, using Sonicator with output and cycle set at 30 %. Allow 10 s between each 10 pulses. Note: All samples should be sonicated in exactly the same way. Otherwise, resulting membrane vesicles may be different.
7. Pass each sonicated cell lysate through a 23G (or 25G) syringe (3 ml max volume) 10 times. This step helps break additional unbroken cells through shear forces generated by forced passage of cells through the needle.
8. Centrifuge homogenates at 3,000 × *g* for 15 min to remove unbroken cells, cell debris and nucleus. Each resulting supernatant, which consist of total cellular membranes and cytosol, is referred to as total cell lysate.
9. Ultracentrifuge each cell lysate for 45 min at 200,000 × *g*. Each resulting pellet is referred to as total membrane, and this supernatant is called cytosol.
10. Resuspend each membrane pellet with 1 ml of TNE buffer. The membrane pellet is usually quite sticky, and therefore hard to be resuspended. Pass each resuspension through a 23G syringe needle/syringe (1 ml max volume) 5 times until a milky solution is formed without any visible particulate matter. The total membrane suspension usually used immediately for lipid raft analysis by density gradient floatation (*see* Subheading 3.4).

*3.1.2 Total Cellular Membrane Preparation from PS120 Cells for Subcellular Fractionation of Organelles (All Procedures Were Performed at 4 °C, Except **step 1**)*

1. PS120/E3V cells grown to confluence were rinsed 3–4 times with cold (4 °C) PBS buffer. Use ~15 ml per rinse. Completely remove the HEPES buffer with aspiration after the last rinse.
2. Add 1 ml of cold HEPES buffer over the cell layer and gently scrape the cells in each dish into an 1.5 ml eppendorf tube using a disposable plastic scraper.
3. Remove the HEPES buffer by centrifuging the cells at 3,000 × *g* for 2–3 min.
4. Resuspend the cells in HEPES buffer (1 ml per 10 cm dish)
5. Homogenize the cells by passing through a 23G syringe (3 ml max volume) 15 times.
6. The rest of the procedure is the same as described in Subheading 3.1.1, **steps 8–10** (see above), except resuspension of the membrane pellets was done with HEPES buffer instead of TNE buffer.

3.1.3 Total Cellular Membrane Preparation from Rabbit Ileal Mucosa

1. Ileal mucosa (villous cells) were obtained from New Zealand White rabbits as described in detail in Subheading 3.2 (see below) [7, 10].
2. Isolated mucosa was transferred directly into a 50 ml plastic tube containing 30 ml of BB Isolation Buffer #3.
3. The mucosa is homogenized with a Polytron (at speed of 5) for 10 times, 10 s burst each time followed by a 20 s interval in a cold room.
4. The rest of the procedure is the same as described in Subheading 3.1.1, **steps 8–10** (see above), except that resuspension of the membrane pellets was done with BB Isolation Buffer #3 instead of TNE buffer.

3.2 Preparation of Rabbit Ileal Brush Border Membranes (BBM) (See Note 2)

Male New Zealand White rabbits weighing 2.5–5 kg were sacrificed by overdose of IV Nembutal (according to JHUSOM approved animal protocol), and distal half of the small intestine, referred to as ileum, was obtained. The rest of the procedure was as described below (All procedures were performed at 4 °C).

1. Dissect out ileum (~4 feet) and remove all the fat.
2. Cut the ileum into equal halves and flush out waste in the lumen with ice-cold saline twice (3 or more times until no visible waste in the lumen) using a 100 ml syringe, then transfer the ileum in a beaker containing cold saline (4 °C).
3. In cold room (4 °C), blot the ileal segments on Kimwipe to remove excess saline, open the ileum along the mesenteric border with a pair of scissors, and scrape ileal mucosa (predominantly villous cells) with glass slides by using one to hold one end of the ileum and the other to scrape against a glass or

plastic plate. Deposit mucosa into 60 ml BB Isolation Buffer #1 on ice. If necessary, pool all the scraped mucosa, blot with filter paper to remove the excess of saline, and weigh (want ~6–8 g).

4. Homogenize with a Polytron (at speed of 5 out of 10) for 10 times, 10 s burst each time followed by a 20 s interval on wet ice in a cold room. Take 100 μl homogenate into Eppendorf tube for total protein estimate. This total protein fraction can be used for estimating the enrichment (purity) of BBM preparation when necessary.
5. Divide each homogenate equally into two centrifuge tubes (for Sorvall SS-34 rotor; ~35 ml per tube). Add 350 μl of 1 M $MgCl_2$ into each centrifuge tube (final concentration of $MgCl_2$: 10 mM). Incubate on ice for 15 min. This is a magnesium precipitation step [also in **step 10** below] that will remove cellular membranes other than BBM, particularly basolateral membranes.
6. Remove the foam at the top of the tube by suction. Centrifuge for 15 min at 3,000 × *g* at 4 °C. Discard the pellets.
7. Remove the lipids floating on the top of the centrifuge tube and transfer the supernatant into another centrifuge tube of the same kind. Discard the pellets.
8. Centrifuge for 30 min at 23,000 × *g* at 4 °C. Discard the supernatant.
9. Resuspend the pellets in 25 ml (each tube) of BB Isolation Buffer #2. Homogenize in a glass-teflon homogenizer on wet ice for 10 times (One complete up and down is counted as one time, voltage at 100 V). Allow a 20 s interval after first 5 times to avoid over-heating.
10. Add 250 μl of 1 M $MgCl_2$ into each tube and mix well. Incubate on ice for 15 min.
11. Pour each homogenate into a centrifuge tube and centrifuge for 15 min at 3,000 × *g*. Discard the pellets.
12. Centrifuge each supernatant at 23,000 × *g* for 30 min. Discard the supernatant. Homogenize each pellet in 15 ml BB Isolation Buffer #3 in a glass-teflon homogenizer on ice as stated in the previous step.
13. Centrifuge at 23,000 × *g* for 40 min. Discard the supernatant.
14. Resuspend and homogenize each pellet in 300–500 μl of Isolation Buffer BB #3 with a 23G syringe (1 ml volume) to yield Brush Border Membrane (BBM).
15. Measure protein concentration and adjust the final protein concentration to ~10 μg/μl. The suspension should be milky. Store the BBM preparation in 100 μl aliquots in –80 °C freezer or liquid nitrogen for long-term storage.

3.3 Preparation and Fractionation of OptiPrep Density Gradients for Membrane Vesicle Fractionation (See Notes 3 and 4)

As a personal favorite, we use a rotor with swinging buckets rather than a fixed angle rotor. The longer the centrifuge tubes, the better the expected separation. An 11-step OptiPrep gradient of 10–30 % (2.5 % increments) is described here and previously [8].

3.3.1 Preparation of a Good Step Gradient

1. Make a thin-cut (~1 mm thick) of a cork from a wine or champagne bottle. The cork is sliced and soaked in DI water for a week with several changes of water (to remove the alcohol and sugar). Trim the cork slice round to make it fit well inside the centrifuge tube. The cork has to be able to float smoothly inside the centrifuge tube when each step of the gradient was overlaid.
2. Load the first step gradient with the highest density (30 %) at the bottom of the centrifuge tube, then drop the cork into the tube. The cork should float flat on the top of the gradient.
3. Load the rest of the step gradient one by one slowly from the highest density to the lowest. There should be at least 1.5 ml volume of space left at the top of the gradient for the loading of the total membrane preparation to be fractionated. Once the gradient is made, care must be taken to avoid disturbing the gradient.
4. Load the sample (0.5–1 ml in volume, total protein 1 mg) at the top of gradient (*see* **Note 5**).
5. Gently remove the cork before centrifugation. *Note: Each centrifuge tube has to be at least 90 % full to avoid collapse of the tube at the top.*
6. Centrifuge at 100,000 × *g* for 16 h at 4 °C.

3.3.2 Fractionation of a Gradient

The best way to collect fractions is to use a *peristaltic pump* that is connected with appropriate tubing (Fig. 1). A capillary tube, which is connected to one end of the tubing, is vertically inserted (slowly) to the bottom of the centrifuge tube, so that the fractionation starts from the bottom of the gradient. Normally, 20 fractions are collected (for subcellular fractionation of membrane vesicles) from an ultracentrifuge tube that fits into a SW40 swinging bucket (Beckman, 0.6 ml each fraction). As many fractions as necessary can be collected. More fractions are done only if the vesicles one is trying to separate are close in density. After fractionation, proteins of interest in each fraction (use 60–80 μl) can be analyzed by SDS-PAGE using Bio-Rad Protein IIxi gel system and western blot (Figs. 2 and 3). Alternatively, vesicles in each fraction can be used directly for other assays.

3.4 Isolation of Lipid Rafts by Density Gradient Floatation (All Procedures Were Performed at 4 °C Unless Described Otherwise)

To achieve the specificity of each signaling pathway, in addition to maintaining spatial separation of various molecules through specialized subcellular membranes/organelles, cells also employ a recently identified mechanism of compartmentation via lipid rafts (LR). LR, also known as lipid microdomains and referred to as DRM (*d*etergent *r*esistant *m*embranes), are defined as dynamic lipid membrane structures that are enriched in glycosphingolipids

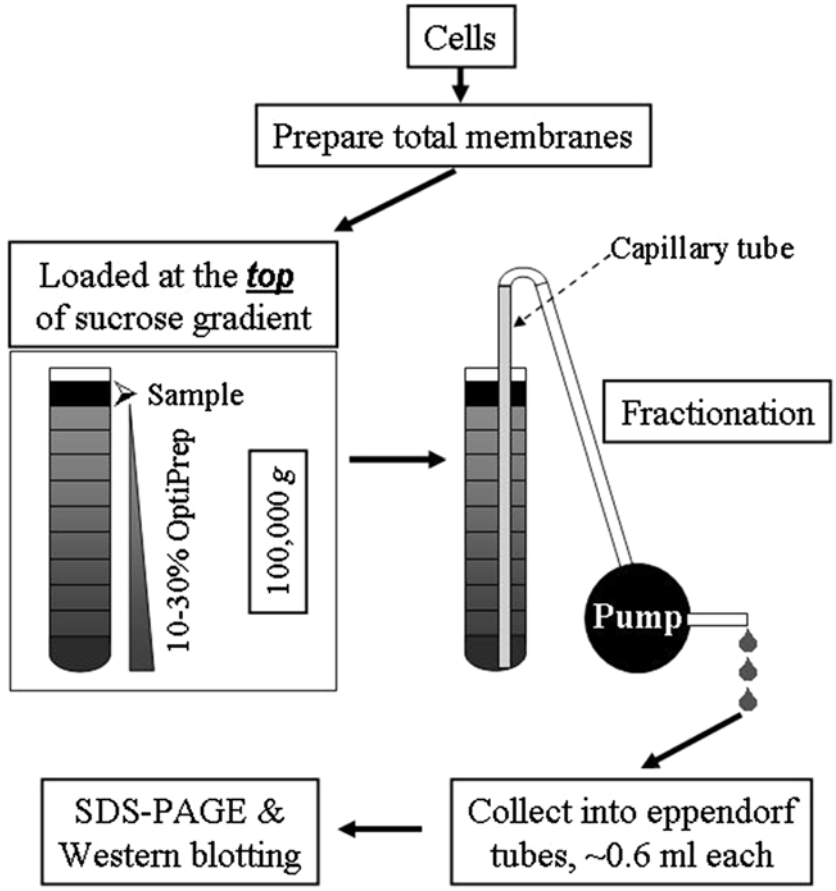

Fig. 1 Flow chart illustrating the process of fractionation of membrane vesicles by density gradient fractionation. Total membranes were isolated from cells and then loaded on to an OptiPrep gradient. After centrifuged at 100,000 × *g* for 16 h, the gradient was fractionated using a peristaltic pump from the *bottom* of the tube. Proteins in each fraction were then analyzed by SDS-PAGE and western blotting. Different gray scales indicate the gradual decrease of the OptiPrep density from the *bottom* to the *top* of the centrifuge tube

and cholesterol [11–13]. LR have been suggested as being involved in many cellular processes, including signal transduction, apical membrane protein trafficking in epithelial cells, endocytosis, and exocytosis [11, 14–17]. LR also function as signaling platforms that cluster certain cell surface receptors, membrane proteins, and signaling molecules to confined regions, while excluding others. LR can be isolated to a high purity (or at least highly enriched) by density gradient floatation, which is based on the strategy that low density membrane vesicles, including LR, will float to low density fractions during centrifugation when detergent-treated cell membranes are placed at the bottom of a

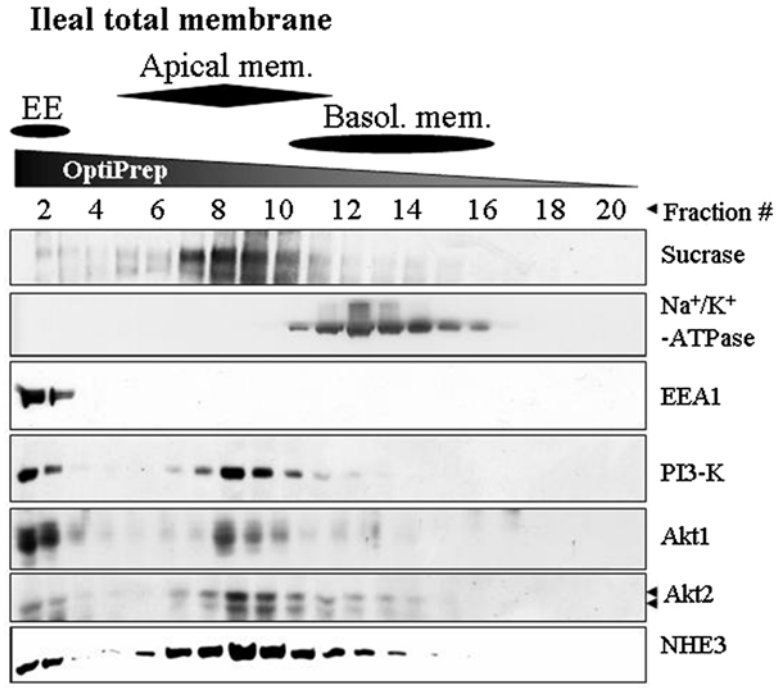

Fig. 2 OptiPrep density gradient fractionation of rabbit ileal villus Na absorptive cells results in efficient separation of early endosomes, apical and basolateral membranes. Total membranes (1.5 mg proteins) prepared from ileal villus cells were loaded on the *top* of the gradient and subjected to fractionation using OptiPrep gradients (10–30 %) as illustrated in Fig. 1. Proteins in each fraction were analyzed by SDS-PAGE and western-blotted with antibodies against the proteins indicated. Established membrane markers used include: the apical marker sucrase, early endosomal marker EEA1 and Na^+/K^+-ATPase, a marker of basolateral membranes. Both PI-3K and Akt2 were mainly localized at the apical membrane of ileal villus cells (*lanes 7–10*). A portion of PI-3K and Akt2 was also present at the basolateral membrane (*lanes 11–14*) and endosomes (*lanes 1* and *2*). In contrast, more than 50 % of Akt1 was present in the endosomal compartment. The double bands of Akt2 indicated by the double arrows are likely the representation of different states of Akt2 phosphorylation. Adapted from Li et al., 2004, Gastroenterology, 126:122–135 (Courtesy of the Elsevier Inc.)

density gradient. Here, we describe the use of OptiPrep™ density gradients for LR isolation. Sucrose density gradients are also widely used for this purpose.

1. Ileal BBM and the total membranes of Caco-2 cells were incubated or not (Control) with10 mM MβCD (Sigma) at 37 °C for 30 min (*see* **Notes 5** and **6**).
2. Untreated and MβCD-treated total membranes were solubilized with 0.5 % Triton X-100 for 30 min on a rotary shaker at 4 °C.

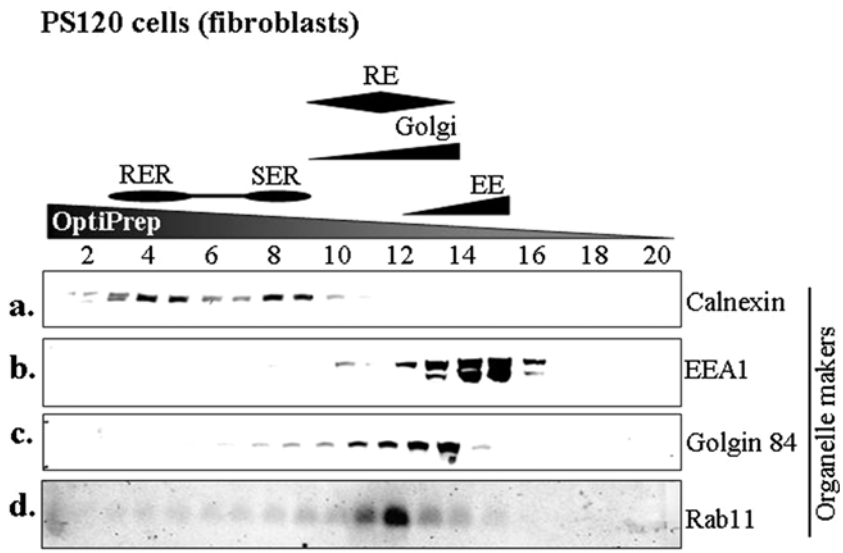

Fig. 3 Separation of different intracellular organelles from PS120 cells by OptiPrep density gradient fractionation. Residential marker proteins, for different membrane vesicles, including calnexin for the ER (**a**), EEA1 for early endosomes (**b**), Golgin 84 for Golgi (**c**), and Rab11 for recycling endosomes (**d**), were used to locate the migration of these membrane vesicles along the density gradients. The enrichment and location of each marker were indicated at the *top*. Total membranes (~1 mg proteins) were loaded on the *top* of the gradient and fractionated as illustrated in Fig. 1

3. Adjust each sample to 35 % of OptiPrep with 60 % original stock (final volume: 1 ml). Transfer each sample to the bottom of an ultracentrifuge tube (fits Beckman SW40 rotor).
4. Overlay each sample with 30, 20, 10, and 5 % OptiPrep. Each step gradient contains 0.1 % Triton X-100.
5. Centrifuge in Beckman SW40 rotor at 100,000 × *g* at 4 °C for 4 h.
6. Fractionate each sample into 11 fractions (1 ml per fraction) from the bottom of each tube, as described in Fig. 1 and Subheading 3.3.2.
7. Analyze one ninth of each fraction with SDS/PAGE and western blotting for proteins of interest (as shown Fig. 4 for Akt2 and PI-3K).

3.5 SDS-PAGE and Western Blotting

Proteins in each density fraction were mixed with 5× SDS-PAGE sample buffer (*see* Subheading 2.4) to make final sample buffer concentration to 1×, separated on 10 % SDS polyacrylamide gels using Bio-Rad Protein IIxi Cell, and then electro-blotted onto nitrocellulose membranes using Bio-Rad gel transfer system (See running buffer and transfer buffer in Subheadings 2.4 and 2.5, respectively). Immunofluorescent detection of proteins of interests was performed at room temperature. Briefly, nitrocellulose membranes were incubated first in PBST-milk (*PBS* buffer containing

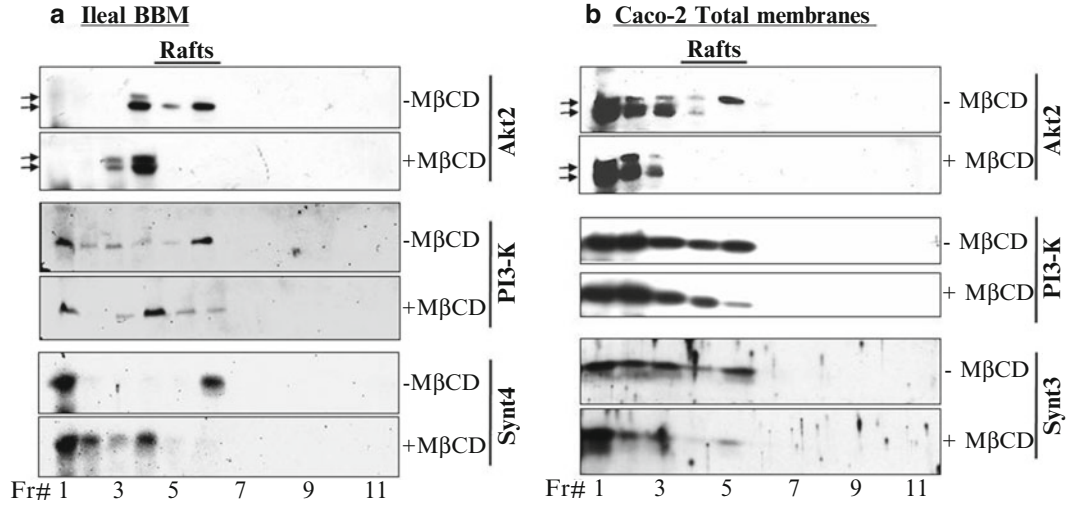

Fig. 4 Akt2 and PI-3K are Associated with LR in Both Rabbit Ileal BBM and Caco-2 Cells. Ileal BBM (**a**) and the total membranes of Caco-2 cells (**b**) (~1 mg protein each) were solubilized with 1 % Triton X-100 at 4 °C with or without MβCD pretreatment at 37 °C for 30 min. Samples were then subjected to Opti-Prep density gradient floatation and fractionated into 11 fractions as illustrated in Fig. 1 (with an exception that sample was loaded at the *bottom* of the gradient instead of on the *top*). Proteins in each fraction were analyzed by SDS-PAGE and western-blotted with different antibodies as indicated. Fractions 1–11 were fractions from the highest (35 %) (Fraction 1) to the lowest density (5 %) (Fraction 11). Significant amounts of Akt2 and PI-3K were in the LR fractions that were shifted from lighter fractions (**a**: fractions 5–6; **b**: lanes 4–5) to heavier fractions (**a**: fractions 3–4; **b**: fraction 1–3) after MβCD treatment. This was similar to syntaxin 4, a marker for LR of BBM (shifted from fraction 6 to fractions 1–4; **a**) and syntaxin 3, a marker for LR of Caco-2 cells (shifted from fractions 4 and 5 to fractions 1–3; **b**). *Double arrows* on the *left* indicate the doublet of Akt2 recognized by Akt antibodies. Representative of 3 similar experiments were shown. Adapted from Li et al., 2004, Gastroenterology, 126:122–135 (Courtesy of the Elsevier Inc.)

0.1 % *T*ween-20 and 5 % non-fat *milk*) for 1 h and then with primary antibodies diluted with PBST-milk for another 1 h, with constant rocking on a shaker. At the end of incubation, the blots were washed 3 times, 10 min each with PBST, and subsequently incubated with HRP-conjugated secondary antibodies diluted in PBST-milk for 1 h. After 3 washes, 10 min each, the blots were incubated with Renaissance Enhanced Luminol Reagent (NEN™ Life Science Products) for 20 s and exposed to Hyperfilm™ MP film.

4 Notes

1. Making 5× sample buffer stock for SDS-PAGE can be difficult because of high concentration of each component, particularly SDS and glycerol. Here is a little trick: Dissolve EDTA-2Na first and then SDS in Tris stock on a heated stir plate (heat but not boil!). Add glycerol, stir mixed and let cool to room temperature.

Add β-mercaptoethanol and adjust pH with HCl to 6.8. Add double de-ionized water to desired volume before bromophenol blue being added at last. The entire preparation should be done in a fume hood due to the strong odor of β-mercaptoethanol. Store in 0.5 or 1 ml aliquots at −20 °C. The stock is good for at least 6 months.

2. When considering the choices how to lyse cells for total membranes, different approaches may be applied according to what cell types to be dealt with. To isolate total membranes, cells have to be broken mechanically in a detergent-free buffer. PS120 cell, which is a fibroblast cell line, can be lysed much more easily than epithelial cells, particularly intestinal epithelial cells such as Caco-2 cells, of which <50 % of cells can be lysed by "syringing" alone. Therefore, sonication is not necessary for PS120 cell lysis. To achieve a maximum yield, sonication may be used. However, sonication may significantly change the properties of membrane vesicles. Therefore, if cells of several experimental conditions are to be compared and sonication is to be used, sonication should be used for cells under all experimental conditions for consistency. If cell membranes are to be prepared from tissues or organs, a Polytron homogenizer and a glass-teflon homogenizer are recommended.
3. Select a right range of OptiPrep densities and appropriate number of fractions for purifying the vesicles of interest: If you have no idea what range to use for the best separation of your vesicles, an 11-step OptiPrep gradient of 10–30 % (2.5 % increments, as we described previously and here [8] or 10–40 % (3 % increment) should be tried. We found that these ranges are suitable for separation of several types of vesicles including early endosomes, plasma membrane (apical membranes, basolateral membranes), and TGN. We tested preparations of membrane vesicles from several tissues (including kidney cortex and small intestine) and cell lines (including PS120 fibroblasts and the human colon cancer cell line, Caco-2). If there is extensive overlapping between two types of vesicles you want to separately isolate, use smaller increments of densities that will cover the fractions in which the two types of vesicles equilibrate. The increments can be as small as 0.5 % if one uses a simple device (a thin slice wine cork) to make an excellent gradient. Try to prepare each step gradient with the same buffer that is used for the membrane vesicle preparation. Furthermore, in general the more fractions collected, the better separation between different membrane populations achieved.
4. Accurate pipetting is very important to generate reproducible density gradients. The step density gradients prepared as described here are very simple and highly reproducible.

Such reproducibility is almost impossible to achieve if continuous density gradients are to be manually prepared. To achieve reproducible density gradients, pipetting is most critical. Since the higher density fractions contain Opti-Prep up to 40 %, pipette tips with low-resistance or coated with silicone are recommended.

5. Amount of proteins loaded on the gradient: To achieve a best separation of different populations of cellular membranes/organelles, the amount of total membranes loaded on a gradient should be kept to the minimum (as long as enough quantity of the membranes of interest can be obtained for subsequent analysis). The more proteins (total membranes) are used, the poorer resolution (more overlaps) of different membrane vesicles will be. We prefer to use the term "enrichment," rather than "purification," of a particular subcellular membrane population/organelle when using the density gradient fractionation approach, since generally there will probably always be small degree of contamination of other unwanted membrane vesicles.
6. In all buffers described in this chapter, protease inhibitors, including PMSF (1 mM), and a protease inhibitor cocktail (Sigma; use as manufacturer suggested), must be added freshly (right before use). When treating cell membranes with MβCD described in lipid rafts isolation, to prevent protein from degradation at 37 °C, those protease inhibitors (See above) should be added freshly again even though they are already present in buffers used in total cellular membrane preparation. For ileal total membrane and BBM isolation, as well as subsequent use of these membranes in density gradient fractionation or lipid raft isolation, phosphoramidon (10 μg/ml) should always be added for inhibition of intestinal specific proteases. Phosphoramidon is not required in membrane analysis of non-intestinal epithelial cells.

Acknowledgments

This work is supported by in part by the National Institutes of Health, NIDDK Grants KO1-DK62264, RO1-DK26523, RO1-DK61765, PO1-DK44484, PO1-DK72084, R24-DK64388, Broad Medical Research Program Grant (IBD-0119R2), and the Hopkins Center for Epithelial Disorders. We thank the Elsevier Inc. for permission to reuse the figures originally published in its journal Gastroenterology.

References

1. Ngsee JK, Trimble WS, Elferink LA et al (1990) Molecular analysis of proteins associated with the synaptic vesicle membrane. Cold Spring Harb Symp Quant Biol 55: 111–118
2. Li X, Sze H (1999) A 100 kDa polypeptide associates with the V0 membrane sector but not with the active oat vacuolar H(+)-ATPase, suggesting a role in assembly. Plant J 17:19–30
3. Huber LA, Pfaller K, Vietor I (2003) Organelle proteomics: implications for subcellular fractionation in proteomics. Circ Res 92:962–968
4. Gutwein P, Stoeck A, Riedle S et al (2005) Cleavage of L1 in exosomes and apoptotic membrane vesicles released from ovarian carcinoma cells. Clin Cancer Res 11:2492–2501
5. Ford T, Graham J, Rickwood D (1994) Iodixanol: a nonionic iso-osmotic centrifugation medium for the formation of self-generated gradients. Anal Biochem 220:360–366
6. Graham J, Ford T, Rickwood D (1994) The preparation of subcellular organelles from mouse liver in self-generated gradients of iodixanol. Anal Biochem 220:367–373
7. Li X, Galli T, Leu S et al (2001) Na+-H+exchanger 3 (NHE3) is present in lipid rafts in the rabbit ileal brush border: a role for rafts in trafficking and rapid stimulation of NHE3. J Physiol 537:537–552
8. Li X, Leu S, Cheong A et al (2004) Akt2, phosphatidylinositol 3-kinase, and PTEN are in lipid rafts of intestinal cells: role in absorption and differentiation. Gastroenterology 126:122–135
9. Janecki AJ, Montrose MH, Tse CM, de Medina FS, Zweibaum A, Donowitz M (1999) Development of an endogenous epithelial Na(+)/H(+) exchanger (NHE3) in three clones of caco-2 cells. Am J Physiol 277:G292–G305
10. Cohen ME, Wesolek J, McCullen J et al (1991) Carbachol- and elevated Ca(2+)-induced translocation of functionally active protein kinase C to the brush border of rabbit ileal Na+absorbing cells. J Clin Invest 88: 855–863
11. Simons K, Toomre D (2000) Lipid rafts and signal transduction. Nat Rev Mol Cell Biol 1:31–39
12. Simons K, Vaz WL (2004) Model systems, lipid rafts, and cell membranes. Annu Rev Biophys Biomol Struct 33:269–295
13. Brown DA (2006) Lipid rafts, detergent-resistant membranes, and raft targeting signals. Physiology (Bethesda) 21:430–439
14. Lusa S, Blom TS, Eskelinen EL et al (2001) Depletion of rafts in late endocytic membranes is controlled by NPC1- dependent recycling of cholesterol to the plasma membrane. J Cell Sci 114:1893–1900
15. Lafont F, Verkade P, Galli T, Wimmer C, Louvard D, Simons K (1999) Raft association of SNAP receptors acting in apical trafficking in Madin-Darby canine kidney cells. Proc Natl Acad Sci U S A 96:3734–3738
16. Bagnat M, Keranen S, Shevchenko A, Shevchenko A, Simons K (2000) Lipid rafts function in biosynthetic delivery of proteins to the cell surface in yeast. Proc Natl Acad Sci U S A 97:3254–3259
17. Fullekrug J, Simons K (2004) Lipid rafts and apical membrane traffic. Ann N Y Acad Sci 1014:164–169

Chapter 7

Combining Pulsed SILAC Labeling and Click-Chemistry for Quantitative Secretome Analysis

Katrin Eichelbaum and Jeroen Krijgsveld

Abstract

Secreted proteins, such as cytokines, chemokines, and hormones, exhibit central functions in intercellular communication, which is crucial to maintain homeostasis in every multicellular organism. A common approach to identify secreted proteins is by proteomic analysis of culture media after conditioning with a cell type of interest. This is preferably done in serum-free conditions to enable the detection of low-abundance secretory factors that would otherwise be masked by serum proteins. However, serum starvation introduces the risk of bringing cells in a stressed or perturbed state. A superior approach employs the enrichment of newly synthesized and secreted proteins from serum-containing growth medium. This is achieved by the combination of two metabolic labels: stable isotope-labeled amino acids for reliable quantification, and azidohomoalanine (AHA), an azide-bearing analogue of methionine, for the enrichment of newly synthesized and secreted proteins. This approach has been used to compare secretomes of multiple cell lines or to analyze proteins that are secreted upon a specific stimulation. Here we describe in detail the enrichment and quantification of newly synthesized and secreted proteins.

Key words Secretome, Secreted proteins, Biomarker, Quantitative proteomics, Protein synthesis

1 Introduction

Secretome analysis using conditioned culture media has become a central method for the detection of biomarkers, e.g., to indicate different stages of cancer progression [1]. While ELISA assays and microarrays depend on the availability of specific antibodies, mass spectrometry is an unbiased method, allowing in theory the detection of all proteins present in a sample [2]. In practice this is limited by the measurable dynamic abundance range. Since most cells are grown using media supplemented with bovine serum (10 %), the serious challenge of secretome analysis using mass spectrometry lies in the detection of low-abundant secreted proteins (ng/ml range) against a background of 1,000s of high-abundant serum proteins (mg/ml). It has been shown that, even when reducing the concentration of serum to 0.5 %, the detection of secreted proteins

Andrei I. Ivanov (ed.), *Exocytosis and Endocytosis*, Methods in Molecular Biology, vol. 1174,
DOI 10.1007/978-1-4939-0944-5_7,

is complicated [1]. An additional source of contamination is intracellular proteins originating from cells that die during collection [3]. Hence, mass spectrometric analysis of conditioned media is done in either of two ways. First, serum is omitted to reduce analytical interference and facilitate the detection of secreted proteins [1], although serum starvation can have several unintended consequences in protein expression and phosphorylation levels [4–7]. Alternatively, to distinguish cellular from serum proteins in serum-containing secretome samples, isotope labeling strategies have been used. Examples are the labeling of newly synthesized proteins with radioactive isotopes, followed by gel electrophoresis and autoradiographic visualization of secreted proteins [8], as well as approaches using stable isotopes, like stable isotope labeling with amino acids in cell culture (SILAC) [9, 10]. An increase in sensitivity has been achieved by protein equalization using Proteominer beads [11] or by the enrichment of newly synthesized and glycosylated proteins after pulse labeling with noncanonical sugars bearing an azide functionality, which was used for the enrichment of glycosylated proteins from cell growth medium [12]. Since 66 % of all secreted proteins are glycosylated, this method addresses a high proportion of the secretome but not all secreted proteins.

The method presented here allows an unbiased enrichment of secreted proteins from culture medium by the metabolic incorporation of azidohomoalanine (AHA), an azide-bearing analogue of methionine, into proteins as they are synthesized in cells of interest (Fig. 1) [13]. To enrich newly synthesized and secreted proteins from serum-containing medium, these azide-containing proteins are covalently coupled to an alkyne-activated resin via click-chemistry, allowing stringent washing to remove serum and other background proteins (Fig. 1). For reliable identification and quantification using mass spectrometry of secreted proteins, AHA incorporation is combined with pulse labeling with SILAC amino acids (Fig. 1) [13]. This serves the additional benefit that newly synthesized proteins can be distinguished from any remaining serum proteins. This method allows cells to be grown in the presence of serum, while preserving the capacity to identify a large repertoire of low-abundant secreted proteins. We previously demonstrated various applications of this approach including the comparison of secretomes of several (cancer) cell lines and primary cells, and the analysis of secretome composition under different growth conditions, partly in a time-series manner [13]. Here, we provide a stepwise protocol for the enrichment of secreted and newly synthesized proteins from complete cell growth medium, along with procedures for reliable comparative quantification of secretomes.

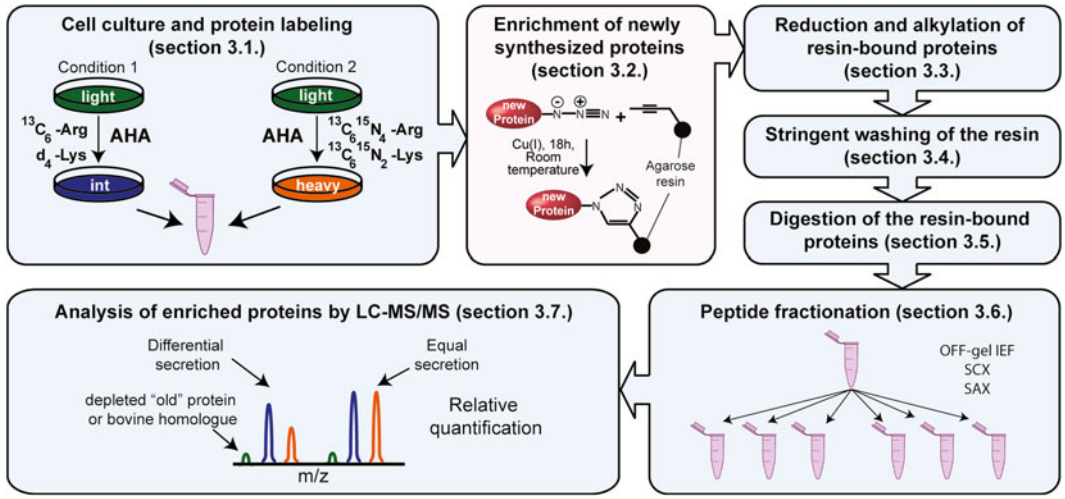

Fig. 1 Workflow for the analysis of secreted proteins. Simultaneous pulse labeling with SILAC amino acids and AHA, followed by selective enrichment of AHA-containing proteins using click-chemistry, allows selective enrichment and detection of secreted proteins by LC-MS/MS. (int: intermediate)

2 Materials

Deionized water, 18 MΩ, needs to be used for all solutions and buffers.

2.1 Cell Culture

1. Phosphate buffered saline (PBS): 137 mM NaCl, 2.7 mM KCl, 2 mM KH_2PO_4, 10 mM Na_2HPO_4, pH 7.4.
2. Petri dishes (preferably 10 cm diameter) or cell culture flasks (preferably 75 cm^2).
3. Cell culture medium (optimized medium for the cell type used), warmed to cell culture temperature (usually 37 °C).
4. Cell viability test (e.g., trypan blue).
5. Depletion medium: cell culture medium without methionine, arginine, and lysine (custom production) but containing all other usual additions (e.g., fetal bovine serum, antibiotics, L-glutamine). Warm to cell culture temperature (usually 37 °C). Store at 4 °C.
6. Labeling medium "intermediate": depletion medium containing 0.1 mM L-azidohomoalanine (AHA) (AnaSpec, Inc., Fremont, CA, USA); 84 μg/ml [$^{13}C_6$] L-arginine and 146 μg/ml [4,4,5,5-D_4] L-lysine (Cambridge Isotope Laboratories, Inc., Tewksbury, MA, USA). Add 0.2 μl of 500 mM AHA (dissolved in DMSO), 1 μl of 84 mg/ml [$^{13}C_6$] L-arginine, and 1 μl of 146 mg/ml [4,4,5,5-D_4] L-lysine (both dissolved in

water) per 1 ml of medium. Warm to cell culture temperature (usually 37 °C) (*see* **Note 1**).

7. Labeling medium "heavy": depletion medium containing 0.1 mM L-azidohomoalanine (AHA) (AnaSpec, Inc.), 84 μg/ml [$^{13}C_6$,$^{15}N_4$] L-arginine, and 146 μg/ml [$^{13}C_6$,$^{15}N_2$] L-lysine (Cambridge Isotope Laboratories, Inc.). Add 0.2 μl of 500 mM AHA (dissolved in DMSO) and 1 μl of 84 mg/ml [$^{13}C_6$,$^{15}N_4$] L-arginine and 1 μl of 146 mg/ml [$^{13}C_6$,$^{15}N_2$] L-lysine (both dissolved in water) per 1 ml of medium. Warm to cell culture temperature (usually 37 °C) (*see* **Note 1**).
8. Protease inhibitor diluted in water to a 50× solution. Store at −20 °C.

2.2 Enrichment of Newly Synthesized Proteins

1. 15 ml ultrafiltration tubes 3 kDa cut off.
2. Click-iT® Protein Enrichment Kit (C10416, Life Technologies, Grand Island, NY, USA). The kit comes with component A-F. Stock solutions need to be prepared and stored according to the manufacturer's instructions.

   2× catalyst solution: Prepare fresh at the day of use. For 1 ml combine 835 μl of 18 megaOhm water, 125 μl of Reaction Additive 1 (Component D), 20 μl of 100 mM Copper (II) sulfate (Component E); Vortex the solution, then add 20 μl of dissolved Reaction Additive 2 (Component F) and vortex again.

2.3 Washing and Digestion of Resin-Bound Proteins

1. SDS wash buffer: 100 mM Tris–HCl pH 8, 1 % SDS, 250 mM NaCl, 5 mM EDTA. Store at 4 °C. The amount of SDS wash buffer provided with the kit is not sufficient, since higher amounts than proposed by the manufacturer are used (*see* **Note 2**).
2. 1 M Dithiothreitol in water (DTT). Store at −20 °C.
3. 40 mM Iodoacetamide, dissolved in SDS wash buffer: 0.5 ml needed per enrichment reaction. Dissolve 7.4 mg/ml SDS wash buffer. Prepare fresh at the day of use and keep in the dark.
4. Spin columns (Bio-Spin Chromatography Columns 732-6008EDU BioRad, München, Germany) (10 columns are provided with the Click-iT® Protein Enrichment Kit, but since just half of one reaction is used per sample additional columns are needed).
5. 8 M urea in 100 mM Tris–HCl, pH 8.
6. 20 % isopropanol in water.
7. 20 % acetonitrile in water.
8. Digestion buffer: 100 mM Tris–HCl pH 8, 2 mM $CaCl_2$, 10 % acetonitrile.

9. Trypsin (sequencing-grade modified trypsin, Promega). 5 µl aliquots of 1 µg/µl trypsin dissolved in 50 mM acetic acid. Store at −80 °C.
10. 10 % (v/v) trifluoroacetic acid (TFA) (ULC/MS grade).
11. Sep-Pak® cartridges (Vac 1 cc (50 mg) tC18) (Waters, Milford, MA, USA).
12. 50 % (v/v) acetonitrile (ULC/MS grade), 0.5 % (v/v) acetic acid (ULC/MS grade).
13. 0.1 % (v/v) TFA.
14. 0.5 % (v/v) acetic acid.
15. 4 % (v/v) acetonitrile, 0.1 % (v/v) formic acid (FA)(ULC/MS grade).

2.4 Separation and Analysis of Peptide Samples

1. Nanoflow liquid chromatography system.
2. Reversed-phase C18 analytical column, e.g., nanoAcquity BEH C18, 1.7 µm, 75 µm × 200 mm (Waters). Other columns (50–100 µm internal diameter, packed or monolithic) will work as well.
3. Reversed-phase C18 trap column, e.g., nanoAcquity Symmetry C_{18}, 5 µm, 180 µm × 20 mm (Waters).
4. HPLC buffer A: 0.1 % (v/v) formic acid (ULC/MS grade) in water.
5. HPLC buffer B: 0.1 % (v/v) formic acid (ULC/MS grade) in acetonitrile.
6. High-resolution electrospray hybrid mass spectrometer (e.g., Q-TOF, LTQ-Orbitrap, LTQ-FT).
7. The HPLC, columns, and mass spectrometer are connected essentially as described previously [14].

3 Methods

Carry out all procedures at room temperature unless specified otherwise.

3.1 Cell Culture and Protein Labeling

1. Viability test: Perform only when using a new cell line.

   Since AHA is incorporated into proteins at a slower rate than methionine [15], it is advised to perform a viability test in AHA and custom medium for each cell line to be used. Therefore perform **steps 2–7** below, using regular instead of stable isotope-labeled amino acids, collect the cells at different times covering the desired treatment times, and measure cell viability. As controls, use cells grown in conventional medium as well as cells grown in custom medium supplemented with methionine instead of AHA.

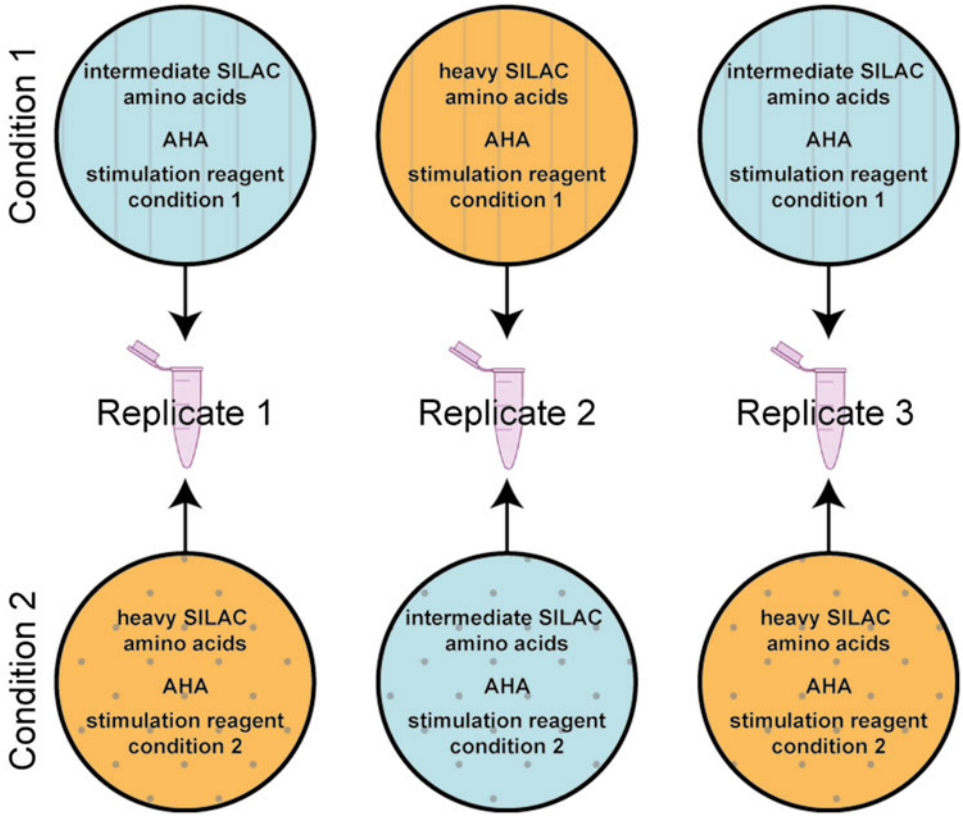

Fig. 2 Example of the experimental setup. Two conditions (or cell types) are compared in biological triplicate. *Circles* indicate cell culture dishes and their growth conditions

2. Grow the cells under optimized conditions to 60–70 % confluency. Optimally, two or three biological replicates are performed for each condition with reversed SILAC labels (Fig. 2). Therefore, a minimum of 4 or 6 dishes of cells are required. The dish size depends on the type of cells, their seed density, their secretion capacity, and the duration of the treatment (if applicable) (*see* **Note 3**).
3. Completely remove the cell medium. Wash once with warm PBS (*see* **Note 4**).
4. To remove remaining methionine, lysine, and arginine incubate the cells with depletion medium for 30–60 min (*see* **Note 5**).
5. During the depletion prepare the labeling medium by adding AHA, SILAC amino acids, and the stimulation reagents (if applicable) to a fresh lot of depletion media according to the scheme in Fig. 2 (*see* **Note 5**).
6. Remove the depletion medium from the cells and add the media prepared in **step 5**.

7. Incubate the cells for the desired time (*see* **Note 3**).
8. Collect the media and immediately combine oppositely SILAC-labeled medium of the conditions to be compared into properly labeled falcon tubes (i.e., intermediate condition 1 and heavy condition 2) (Fig. 2).
9. Centrifuge the collected media for 5 min at 1,000×*g* (or another appropriate speed) to pellet remaining cells. Transfer the supernatant to fresh tubes without transferring the cell pellet (if any), add the appropriate amount of protease inhibitor, and freeze at −80 °C.
10. If desirable, the cells can be collected separately after washing 3 times with warm PBS. If no secreted proteins are detected in the secretome, the cells can be used to check if newly synthesized proteins were properly labeled. Furthermore, the cells may be used for parallel measurement of intracellular protein synthesis.
11. Detach the cells and collect them in an Eppendorf tube. Spin down the cells and freeze them at −80 °C after removing the remaining PBS.

3.2 Enrichment of Newly Synthesized Proteins

The Click-iT® Protein Enrichment Kit contains 10 reactions with 200 µl of bead slurry. For the enrichment of secreted proteins only 100 µl of slurry is used.

1. Thaw the medium containing AHA and SILAC-labeled secreted proteins.
2. Concentrate it in 15 ml ultrafiltration tubes to ~250 µl at 4 °C.
3. Add 250 µl urea buffer (provided in the kit) and keep the sample on ice until further use.
4. Prepare the resin: Thoroughly mix the resin slurry by rocking or rotating the vial until the resin is completely resuspended. Use a 200 µl pipet with 4–5 mm of the tip cut off with a razor blade to pipet 100 µl of slurry into a 2 ml tube. Add 0.9 ml water to the resin. Pellet the resin by centrifugation for 5 min at 1,000×*g*. Aspirate the supernatant to waste, leaving approximately 100 µl in the tube and taking care not to aspirate the resin.
5. Prepare 0.5 ml of 2× catalyst solution per sample.
6. Set up the Click Reaction: To the 2 ml tube containing the 100 µl of washed resin slurry, add 500 µl of concentrated medium and 500 µl of 2× catalyst solution.
7. Rotate end-over-end at room temperature for 18 ± 2 h.

3.3 Reduction and Alkylation of Resin-Bound Proteins

1. Warm the SDS wash buffer to room temperature at least 30 min before starting. Invert the bottle and ensure that the solution is homogenous and not cloudy before use.

2. Centrifuge the reaction mixture from Subheading 3.2, **step 7** for 1 min at 1,000 × *g*. Aspirate the reaction supernatant to waste, taking care not to aspirate the resin.
3. Add 0.9 ml water to the resin and repeat the centrifugation and aspiration of the supernatant to waste. This step prevents clumping of the resin caused by the interaction of the residual lysis buffer with the SDS Wash Buffer.
4. Add 0.5 ml of SDS wash buffer and 5 µl of 1 M DTT to the resin. Vortex briefly to resuspend the resin. Heat the resin at 70 °C on a heating block for 15 min, and then cool at room temperature for 15 min. Centrifuge the resin for 5 min at 1,000 × *g*, then aspirate the supernatant to waste.
5. Add 0.5 ml of the iodoacetamide solution to the resin. Vortex briefly to resuspend the resin, and then shake it in the dark at 500 rpm for 30 min (*see* **Note 6**).

3.4 Stringent Washing of the Resin

1. Snap off the outlet closure from a spin column and place the column on a syringe needle in the lid of a 50 ml falcon tube (Fig. 3). Use a 1 ml pipette with 4–5 mm of the tip cut off with a razor blade to resuspend the resin solution and transfer it to the column. Rinse the resin tube with 0.5 ml water and add the rinse to the column (*see* **Note 7**).

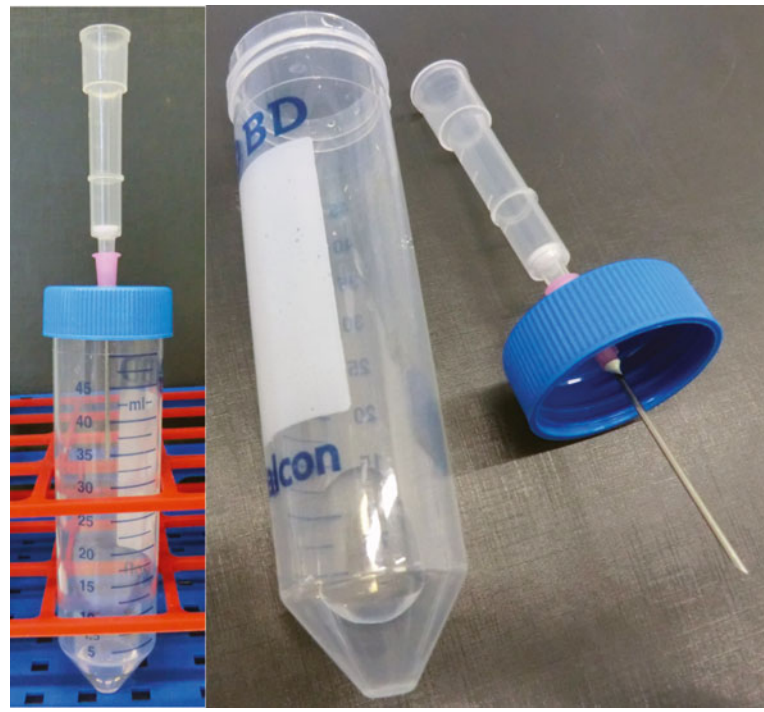

Fig. 3 Setup for stringent resin washing. The syringe needle causes a capillary flow that increases the flow speed compared to simple gravity flow

2. Wash the resin by applying in total 20 ml of SDS wash buffer. Let it run through the column by gravity flow.
3. Wash the resin by applying in total 20 ml of 8 M urea/100 mM Tris–HCl, pH 8 to the column and allow it to flow to waste.
4. Wash the resin by applying in total 20 ml of 20 % isopropanol to the column and allow it to flow to waste.
5. Wash the resin by applying in total 20 ml of 20 % acetonitrile to the column and allow it to flow to waste.

3.5 Digestion of the Resin-Bound Proteins

1. Cap the bottom of the column and add 500 µL of digestion buffer to the resin. Use a 1 ml pipette with 4–5 mm of the tip cut off with a razor blade to resuspend the resin and transfer it to a clean tube. Rinse the column with 0.5 ml of digestion buffer and add the rinse to the transferred resin.
2. Pellet the resin by centrifugation for 5 min at 1,000 × *g*. Aspirate the supernatant to waste, leaving approximately 200 µl of digestion buffer in the tube with the resin, taking care not to aspirate the resin.
3. Add 0.5 µg of trypsin to the resin slurry, vortex briefly to mix the slurry, and shake it at 37 °C overnight.
4. Pellet the resin by centrifugation for 5 min at 1,000 × *g*, and then transfer the supernatant containing the peptides to a clean tube.
5. Add 500 µl of water to the resin. Pellet the resin by centrifugation for 5 min at 1,000 × *g*. Add the rinse supernatant to the supernatant collected in **step 4** of Subheading 3.5. Add additional water to the digest to a final volume of 1 ml to dilute the acetonitrile to 2 %.
6. Acidify the diluted digest with 20 µl of 10 % TFA.
7. Desalt the digest on a Sep-Pak® cartridge (Vac 1 cc (50 mg) tC18) as described by Villen et al. [16]: Wash and condition the cartridge using 0.9 ml of acetonitrile. Wash with 0.3 ml of 50 % acetonitrile and 0.5 % acetic acid. Equilibrate with 0.9 ml of 0.1 % TFA and load the sample. Wash and desalt with 0.9 ml of 0.1 % TFA. Remove the TFA with 0.9 ml of 0.5 % acetic acid. Elute with 0.5 ml of 50 % acetonitrile, 0.5 % acetic acid and collect eluate in an Eppendorf tube. Keep 5 % of the sample separate for a test measurement. Dry (by vacuum) both samples and store them at –20 °C.
8. Resuspend the test sample in 20 µl 4 % acetonitrile, 0.1 % formic acid and analyze 4 µl by nanoLC-MS/MS (*see* Subheading 3.7 and **Note 8**).
9. Search the data in a database search engine using the SwissProt database and a triple labeling method in the quantification option (*see* **Note 9**).

10. Check in the result files, if intermediate or heavy labeled peptides are detected and if the proteins identified based on these peptides are likely to be secreted proteins. At least a few secreted proteins with intermediate or heavy labeled peptides should be identified (the number depends on the resolution and speed of the instrument used).

3.6 Peptide Fractionation

This step is optional and serves to increase the number of quantified proteins. Multiple peptide fractionation strategies are available, e.g., off-gel isoelectric focusing (OFF-Gel IEF), strong cation exchange-HPLC (SCX-HPLC), or stage tip-based strong anion exchange [17]. We used off-gel isoelectric focusing as well as stage tip-based strong anion exchange and find slightly higher numbers of identified proteins when using OFF-Gel IEF, but stage tip-based strong anion exchange allows for higher throughput of samples, since up to 24 samples can be fractionated in parallel (*see* **Note 10**).

3.7 Analysis of Enriched Proteins by LC-MS/MS

Peptide samples are best analyzed by liquid chromatography coupled to tandem mass spectrometry (LC-MS/MS) for protein identification and quantification. This process involves the online separation of peptides by reversed phase LC, electrospray ionization of peptides, and fragmentation of detected peptides in the mass spectrometer. This setup can be achieved on multiple platforms (i.e., various types of LC systems coupled to a range of mass spectrometers), and the exact protocol depends on available instrumentation (for reviews, *see* [18, 19]). Therefore, we will describe the workflow only in general terms, highlighting some aspects that should be kept in mind for optimal performance for a quantitative analysis.

1. A chromatographic system should be chosen that can deliver flow rates at 100–300 nl/min, either as a splitless nanoflow system or as a conventional system running at 100–300 μl/min and passive splitting to the desired flow rate.
2. Choose a reversed-phase column (either prepacked or homemade) that efficiently captures both hydrophilic and hydrophobic peptides. The internal diameter should be in the range of 50–100 μm; length can vary between 10 and 40 cm depending on gradient length and flow rate, but 15–20 cm is a good starting point. Slope and length of the gradient should be optimized for the sample and column system. For secretome samples without pre-fractionation, a typical gradient can be generated by raising the concentration of acetonitrile from 5 % to approximately 40 % over a 4 h period. With pre-fractionation a 2 h long gradient is sufficient.
3. The amount of sample (peptide mixture) injected into the system should not exceed but be near the capacity of the column. Overloading will cause peak broadening and (potentially)

saturation of the detector in the mass spectrometer. Both will compromise proper quantification.

4. Ideally, a high-resolution mass spectrometer should be used. Resolution should be sufficient to determine the charge state of the peptide and the mass of the mono-isotopic peak. High resolution (such as in TOF, Orbitrap, or FT instruments) is usually coupled to high mass accuracy, aiding in the identification process.
5. After processing raw data to peaklists (often by vendor-specific software), proteins can be identified by a range of database search algorithms. It is important to supplement the database with contaminating proteins expected in fetal bovine serum (e.g., contaminant list provided with MaxQuant [20]). To exclude serum-derived proteins from the list of identified proteins the list needs to be filtered, removing proteins that are only detected based on peptides containing the light versions of SILAC amino acids (meaning that they are not newly synthesized during the collection time) (*see* **Note 11**).
6. Protein quantification is a critical process that is supported by a number of software packages. MSQuant [21] and Census [22] support a range of data formats and are available free of charge. MaxQuant [20] is widely used for data derived from instruments manufactured by Thermo Scientific. Mascot distiller (www.matrixscience.com) is a commercial package supporting nearly all data formats.
7. Determine the average protein ratios, if a protein was quantified in at least two biological replicates each based on at least two ratio counts.
8. Perform the statistical analysis using the Limma package in R/Bioconductor [23, 24] (*see* **Note 12**).
9. The quality of the final data set is determined by the percentage of established secretory proteins compared to all identified proteins. Use UniProt annotations [25] as well as SignalP predictions [26] to define which proteins are expected to be secreted.

4 Notes

1. We store the diluted amino acids and AHA in 50 µl aliquots at −20 °C and prepare the labeling medium fresh at the day of use.
2. We use a 20 % SDS solution (BioRad). It happens that SDS precipitates, then the solution has to be heated by placing the bottle in warm water to fully dissolve the SDS before preparing the SDS wash buffer.

3. For most cell types tested, we retrieved good results by using 10 cm cell culture dishes (~2–4 × 10^6 cells) or 75 cm^2 cell culture flasks (~1 × 10^7 cells) for AHA incorporation times of 4–24 h. We tested the enrichment of secreted proteins from down to 1 × 10^6 cells (mouse macrophages), still resulting in good numbers of identifications even after only 2 h of AHA incorporation.
4. Tilting the dish for a few seconds helps to completely remove the medium.
5. For depletion and labeling medium we use half of the volume of medium we would normally use for cell culture (e.g., 4 ml for a 10 cm dish; 7 ml for a 75 cm^2 cell culture flask). This serves to increase the ratio of secreted proteins to proteins contained in the growth medium (derived from fetal bovine serum), thus raising the chance to detect secreted proteins. Since the duration of the treatment (hours) is usually shorter than the time cells are usually kept in the medium (days) this does not harm the cells.
6. Cover the shaker containing the samples with aluminum foil.
7. It is very difficult to prevent the resin to dry out completely at this point, when multiple samples are processed in parallel. If this happens, resupply washing solution as quickly as possible, although we did not experience a reduction in identifications when the resin gets dry.
8. At this point this does not need to be an instrument with high resolution (e.g., ion trap or similar will suffice).
9. There are several search algorithms that allow the identification of SILAC-labeled proteins. In Mascot (http://www.matricscience.com/), define the label combinations used in a quantification method. In MaxQuant [20], check the boxes defining the labels in the "modification & labels" tab.
10. For isoelectric focusing an Agilent 3100 OFFGEL Fractionator is used in combination with Immobiline™ DryStrips (pH 3–10 NL, 13 cm, GE Healthcare). Resuspend the dried samples in 360 µl H_2O and dilute them in 1.44 ml 1.25 × IEF stock solution (6 % glycerol, 2 % Ampholytes pH 3–10 (1:50) (BioRad)). Perform focusing at a constant current of 50 mA with a maximum Voltage of 4,000 V. Collect the samples after reaching 20 kVh. Acidify the samples with CF_3COOH and desalt them using StageTips [27]. Combine the 12 fractions to 6 fractions. Dry the peptide samples and dissolve them in 4 % acetonitrile, 0.1 % formic acid. Alternatively, strong anion exchange can be used for the fractionation of the samples into 6 fractions, as described elsewhere [17] with minor adaptations. Briefly, desalted peptide samples are dissolved in 200 µl Britton & Robinson Universal Buffer pH 12 and loaded on the anion

exchange stage tip which is placed into a C18-stage tip. Peptides are successively eluted to new C18-stage tips each with Britton & Robinson Universal Buffer pH 12, pH 8, pH 6, pH 4, and pH 2. The flow through is reloaded to the C18-stage tips and desalted.

11. We only keep a protein group for further analysis, if the number of identified peptide species carrying an intermediate or heavy label (the sum of these) divided by the total number of labeled peptide species detected (with intermediate or heavy label) is higher than 0.2.
12. We fit a linear model to the data and use an empirical Bayes moderated *t*-test followed by adjustment of the *p*-values for multiple testing with Benjamini and Hochberg's method. In most cases we consider protein groups with adjusted *p*-value lower than 0.01 as differentially secreted, but this value can be adjusted depending on the quality of the data set and the biological question.

Acknowledgements

We thank Itahisa Hernandez, Sophia Föhr, and Jenny Hansson for careful reading of the manuscript.

References

1. Dowling P, Clynes M (2011) Conditioned media from cell lines: a complementary model to clinical specimens for the discovery of disease-specific biomarkers. Proteomics 11:794–804
2. Mustafa SA, Hoheisel JD, Alhamdani MS (2011) Secretome profiling with antibody microarrays. Mol Biosyst 7:1795–1801
3. Raimondo F, Morosi L, Chinello C, Magni F, Pitto M (2011) Advances in membranous vesicle and exosome proteomics improving biological understanding and biomarker discovery. Proteomics 11:709–720
4. Pirkmajer S, Chibalin AV (2011) Serum starvation: caveat emptor. Am J Physiol Cell Physiol 301:C272–C279
5. Hasan NM, Adams GE, Joiner MC (1999) Effect of serum starvation on expression and phosphorylation of PKC-alpha and p53 in V79 cells: implications for cell death. Int J Cancer 80:400–405
6. Levin VA, Panchabhai SC, Shen L, Kornblau SM, Qiu Y, Baggerly KA (2010) Different changes in protein and phosphoprotein levels result from serum starvation of high-grade glioma and adenocarcinoma cell lines. J Proteome Res 9:179–191
7. Cooper S (2003) Reappraisal of serum starvation, the restriction point, G0, and G1 phase arrest points. FASEB J 17:333–340
8. Zwickl H, Traxler E, Staettner S, Parzefall W, Grasl-Kraupp B, Karner J, Schulte-Hermann R, Gerner C (2005) A novel technique to specifically analyze the secretome of cells and tissues. Electrophoresis 26:2779–2785
9. Henningsen J, Pedersen BK, Kratchmarova I (2011) Quantitative analysis of the secretion of the MCP family of chemokines by muscle cells. Mol Biosyst 7:311–321
10. Kristensen LP, Chen L, Nielsen MO, Qanie DW, Kratchmarova I, Kassem M, Andersen JS (2012) Temporal profiling and pulsed SILAC labeling identify novel secreted proteins during ex vivo osteoblast differentiation of human stromal stem cells. Mol Cell Proteomics 11:989–1007
11. Colzani M, Waridel P, Laurent J, Faes E, Ruegg C, Quadroni M (2009) Metabolic labeling and protein linearization technology allow the study of proteins secreted by cul-

tured cells in serum-containing media. J Proteome Res 8:4779–4788

12. Kuhn PH, Koroniak K, Hogl S et al (2012) Secretome protein enrichment identifies physiological BACE1 protease substrates in neurons. EMBO J 31:3157–3168
13. Eichelbaum K, Winter M, Diaz MB, Herzig S, Krijgsveld J (2012) Selective enrichment of newly synthesized proteins for quantitative secretome analysis. Nat Biotechnol 30:984–990
14. Meiring HD, van der Heeft E, ten Hove GJ, de Jong A (2002) Nanoscale LC-MS(n): technical design and applications to peptide and protein analysis. J Separat Sci 25:557–568
15. Kiick KL, Saxon E, Tirrell DA, Bertozzi CR (2002) Incorporation of azides into recombinant proteins for chemoselective modification by the Staudinger ligation. Proc Natl Acad Sci U S A 99:19–24
16. Villen J, Gygi SP (2008) The SCX/IMAC enrichment approach for global phosphorylation analysis by mass spectrometry. Nat Protoc 3:1630–1638
17. Wisniewski JR, Zougman A, Mann M (2009) Combination of FASP and StageTip-based fractionation allows in-depth analysis of the hippocampal membrane proteome. J Proteome Res 8:5674–5678
18. Motoyama A, Yates JR 3rd (2008) Multidimensional LC separation in shotgun proteomics. Anal Chem 80:7187–7193
19. Qian WJ, Jacobs JM, Liu T, Camp DG 2nd, Smith RD (2006) Advances and challenges in liquid chromatography-mass spectrometry-based proteomics profiling for clinical applications. Mol Cell Proteomics 5:1727–1744
20. Cox J, Mann M (2008) MaxQuant enables high peptide identification rates, individualized p.p.b.-range mass accuracies and proteome-wide protein quantification. Nat Biotechnol 26:1367–1372
21. Mortensen P, Gouw JW, Olsen JV et al (2010) MSQuant, an open source platform for mass spectrometry-based quantitative proteomics. J Proteome Res 9:393–403
22. Park SK, Venable JD, Xu T, Yates JR 3rd (2008) A quantitative analysis software tool for mass spectrometry-based proteomics. Nat Methods 5:319–322
23. Gentleman RC, Carey VJ, Bates DM et al (2004) Bioconductor: open software development for computational biology and bioinformatics. Genome Biol 5:R80
24. Smyth GK (2004) Linear models and empirical bayes methods for assessing differential expression in microarray experiments. Stat Appl Genet Mol Biol 3, Article 3
25. Jain E, Bairoch A, Duvaud S, Phan I, Redaschi N, Suzek BE, Martin MJ, McGarvey P, Gasteiger E (2009) Infrastructure for the life sciences: design and implementation of the UniProt website. BMC Bioinformat 10:136
26. Petersen TN, Brunak S, von Heijne G, Nielsen H (2011) SignalP 4.0: discriminating signal peptides from transmembrane regions. Nat Methods 8:785–786
27. Rappsilber J, Ishihama Y, Mann M (2003) Stop and go extraction tips for matrix-assisted laser desorption/ionization, nanoelectrospray, and LC/MS sample pretreatment in proteomics. Anal Chem 75:663–670

Part III

Imaging and Ultrastructural Analysis of Vesicle Trafficking in Cultured Cells

Chapter 8

Probabilistic Density Maps to Study the Spatial Organization of Endocytosis

Jean-Philippe Grossier, Bruno Goud, and Kristine Schauer

Abstract

Despite a large body of publications on endocytosis, only a few studies have focused on its spatial organization. To study how endocytosis is related to distinct cellular sites, we combine cell normalization by the "micropatterning technique" with the quantification of spatial organization by "probabilistic density mapping." Micropatterns of extracellular matrix proteins impose adhesive and non-adhesive areas to cultured cells and allow the control of adhesion geometry, shape, and cell organization. Probabilistic density maps provide a visual summary for 3D localization of the structures of interest and enable the extraction of robust statistics for quantification of cellular organization. Here, we provide a method to analyze and compare the spatial distribution of endocytosed ligands in micropatterned cells. This approach permits to establish the role of cellular adhesion on uptake mechanisms and to address the potential function of predefined sites of endocytosis.

Key words Cell asymmetry, Hot spots, Micropatterns, Spatial memory, Density mapping, Kernels

1 Introduction

Many studies have addressed endocytosis that is a fundamental process of eukaryotic cells to internalize macromolecules from their environment. Yet only a few investigations have dealt with the spatial organization of endocytosis. It has been noted in several cellular model systems that endocytosis does not occur randomly along the entire cell surface but is restricted to discrete sites. For instance, accumulation of clathrin-coated pits was observed at the leading edge of migrating cells [1]. Additionally, "hot spots" of endocytosis have been observed in several specialized cells, such as hepatocytes or neurons [2, 3]. One major problem to study how endocytosis is related to distinct cellular sites is the strong morphological cell-to-cell variation displayed by cultured cells. Cell morphology also varies over time as cells move. To precisely define cellular shape and morphology, micro-fabricated patterns of extracellular matrix proteins can be employed. Micropatterns impose

Andrei I. Ivanov (ed.), *Exocytosis and Endocytosis*, Methods in Molecular Biology, vol. 1174,
DOI 10.1007/978-1-4939-0944-5_8,

adhesive and non-adhesive areas to cultured cells, force them to adopt a certain shape and prevent their migration, mimicking the microenvironment found in tissues [4]. The reproducible cellular orientation induced by the micropattern not only normalizes cellular shape but also permits to define specific cellular sites, such as adhesive and non-adhesive cell surfaces. Additionally, average spatial information for a cell population can be extracted by the collation of several tens of cells [5].

A second challenge in studying the spatial organization of endocytic events is that they are numerous and dispersed throughout the cell. Classically, eulerian approaches are used to characterize individual uptake events. However, all events need to be considered to understand the behavior of the cell. Particularly, to reveal details of the spatial organization of uptake events, statistical methods such as probabilistic density mapping are required. Probabilistic mapping is a population-based, lagrangian method that focuses on aggregated system behavior. Thus, density maps provide information about the behavior of the majority of endocytosed molecules but give less accurate knowledge of individual uptake events. This mathematical method convolves each data point by blurring, in an inverse operation of the more widely known deconvolution, which takes a blurry image and sharpens it. Blurring is a mathematical representation that an observed structure should not only represent itself but also other nearby structures which were not observed. Previously, we have used this approach to determine the global spatial organization of various endomembranous compartments [6].

Here, we present a method that allows the quantification of the spatial organization of endocytosed ligands in micropatterned cells (Fig. 1). In brief, fluorescent microscopy images of labeled ligands are segmented and the 3D spatial coordinates of the structures are extracted. Typically, several hundred structures of a specific ligand are extracted from each cell and several tens of cells are collated. Then, coordinates are replaced by kernels and summed, resulting in an average three-dimensional density map. In addition to a visual summary, density maps are used to derive statistics for quantitative analysis of cell morphology. Probability contours admit an intuitive probabilistic interpretation, e.g., the 50 % probability contour defines the smallest region in which 50 % of the ligands are located.

Applying density mapping to transferrin (Tfn) and epidermal growth factor (EGF), two classical ligands of receptor-mediated endocytosis, we found an unexpected dorsal/ventral asymmetry in both clathrin-dependent and clathrin-independent endocytosis that predefined uptake of Tfn and EGF at distinct cellular sites (Fig. 2). Tfn was enriched in adhesive sites during uptake, whereas EGF endocytosis was restricted to the dorsal cellular surface [7]. This spatial separation was not due to distributions of corresponding

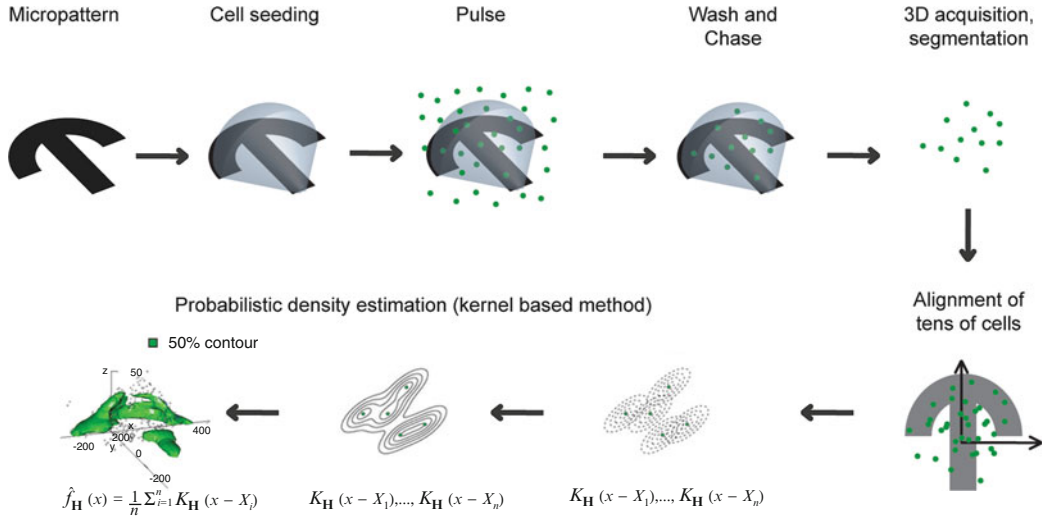

Fig. 1 Schema of the experimental procedure. Micropatterned coverslips are prepared using photolithography. Cells are cultured on micropatterns for three hours in serum free medium, pulsed with fluorescently marked ligands, washed and chased for different time points. After fixation, 3D images are acquired and 3D coordinates of fluorescently marked structures are extracted from several tens of cells by segmentation analysis. Coordinates are aligned using the micropattern and the probability density map is calculated: each of the coordinates is replaced by a kernel (normal distribution) and summed. To visualize the result, probability contours are calculated that represent smallest areas in which a given percentage of structures are found. The 50 % contour defines the smallest region in which 50 % of the endosomes are located and is used to indicate the characteristic distribution for each ligand

receptors but was regulated by the actin cytoskeleton. Together, this analysis revealed that cellular adhesion regulates endocytosis at distinct cellular sites that allows cells to sense their environment in an "outside-in" mechanism.

Potentially, this method can be employed to study the sites of endocytosis of different, fluorescently marked ligands (for instance, other growth factors, cytokines, lectins, LDL, toxins). Alternatively, antibodies can be employed to study the sites of endocytosis of various receptors.

2 Materials

2.1 Micropattern Preparation

1. Distilled water.
2. Phosphate-Buffered Saline (PBS), pH 7.4.
3. Ethanol, 96 %.
4. HEPES Buffer: 10 mM HEPES (4-(2-hydroxyethyl)-1-piperazineethanesulfonic acid), pH 7.4.

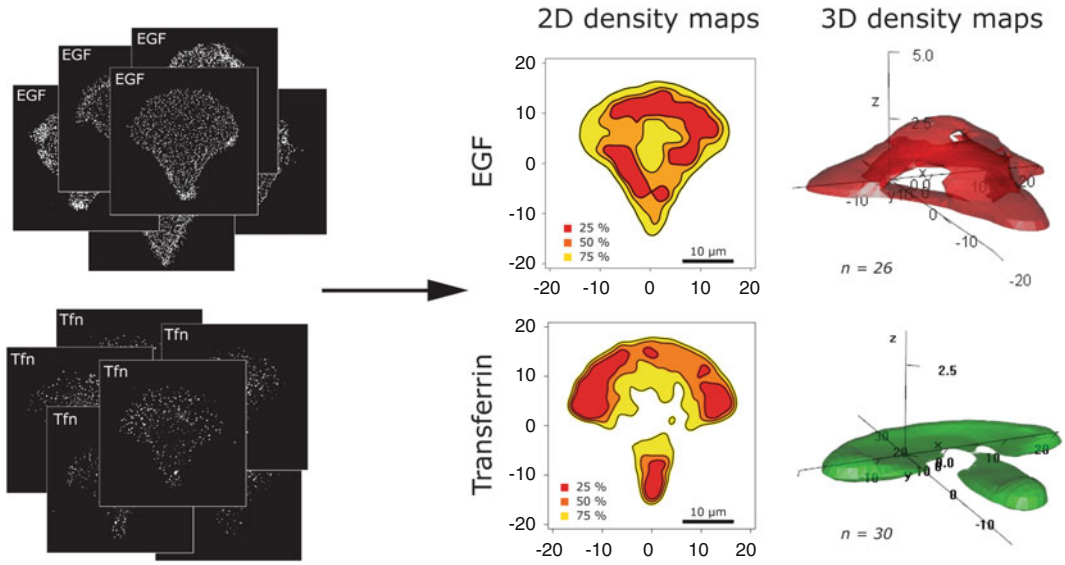

Fig. 2 Transformation of fluorescent images into probabilistic density maps. After normalization of cell shape by adhesion on a micropattern of the same geometry (such as a crossbow), several tens of cells are imaged by light microscopy. The reproducible cellular orientation induced by the micropattern allows the collation of several tens of cells and the construction of average density maps for the analyzed cell population. In contrast to classical, single particle-based, eulerian approaches, probabilistic mapping is a population-based, lagrangian method that focuses on aggregated system behavior. Density maps thus provide information about the behavior of the majority of endocytosed molecules but give less accurate knowledge of individual uptake events. The 2D density maps with the indicated percentile probability contours (25 %, 50 %, 75 %) represent the smallest regions in which the corresponding percentage of EGF (upper panel) or transferrin (Tfn, lower panel) is found after Z-projection of the data. These maps reveal that EGF and Tfn are found at different cellular locations at 1 min post-pulse. 3D density maps represent the "characteristic" volume (50 % contour) that indicates the smallest volume where 50 % of total EGF or Tfn signals are found. Probabilistic density maps reveal that EGF endocytosis is restricted to the dorsal cellular surface, whereas Tfn is enriched in adhesive sites during uptake

5. PLL-g-PEG Stock Solution: PLL-g-PEG (PLL(20)-g[3.6]-PEG(2) from Surface Solutions, Switzerland) dissolved at 1 mg/mL in HEPES buffer (stored at 4 °C for several months), pH 7.4.
6. PLL-g-PEG Solution: PLL-g-PEG Stock Solution diluted at 0.1 mg/mL in HEPES buffer (stored at 4 °C for few weeks), pH 7.4.
7. Photomask: from Delta Mask, Toppan Photomasks, or Microtronics Photomasks (*see* **Note 1**).
8. Glass coverslips (12–24 mm).
9. UV ozone oven (*see* **Note 2**).

2.2 Cell Seeding and Pulse-Chase Experiment

1. hTERT-RPE1 cells or other adherent cell lines.
2. Fibronectin (from bovine plasma, Sigma): 1 mg/mL in 0.05 M Tris–HCl, 0.5 M NaCl, pH 7.5.
3. Fluorescent fibrinogen: 1.5 mg/mL in water (Molecular Probe).
4. 12-Well plate.
5. Complete culture medium: DMEM/F12 (Gibco), 10 % fetal bovine serum.
6. Serum free medium: DMEM/F12 (Gibco), 20 mM HEPES.
7. EDTA–Trypsin (0.25 %).
8. Fluorescently labeled ligand: Alexa Fluor conjugate Transferrin or EGF from Molecular Probes.
9. Cell incubator (37 °C, 5 % CO_2).

2.3 Fixation and Mounting

1. Paraformaldehyde (PFA), 4 % (w/v) solution in PBS.
2. Quenching Solution: 0.05 M NH_4Cl in PBS.
3. Permeabilization Solution: 2 % BSA, 0.05 % Saponin in PBS.
4. DAPI.
5. Mowiol.
6. Glass slide.

2.4 Image Acquisition and Analysis

1. Epifluorescence microscope: 100× obj., piezo stage (0.2 µm step).
2. Image J [8] with "3D Object Counter Plugin."
3. Macro1 and Macro2 (*see* **Notes 9** and **10**).
4. R Software version 2.14.2 [9], with the following packages: ks [10], KernSmooth, mvtnorm, rgl, misc3d, tcltk (*see* **Note 8** for installation).
5. R source file and R script (*see* **Notes 11** and **12**).

3 Methods

3.1 Micropattern Preparation

This part is adapted from [11]. Every step must be handled with a minimal of dust. The method is summed up in Fig. 3. Alternatively, micropatterns might be purchased from Cytoo Company.

1. Wash coverslips in ethanol and let them dry.
2. Activate the coverslips by illumination under deep UV for 5 min at about 5 cm from the lamp.

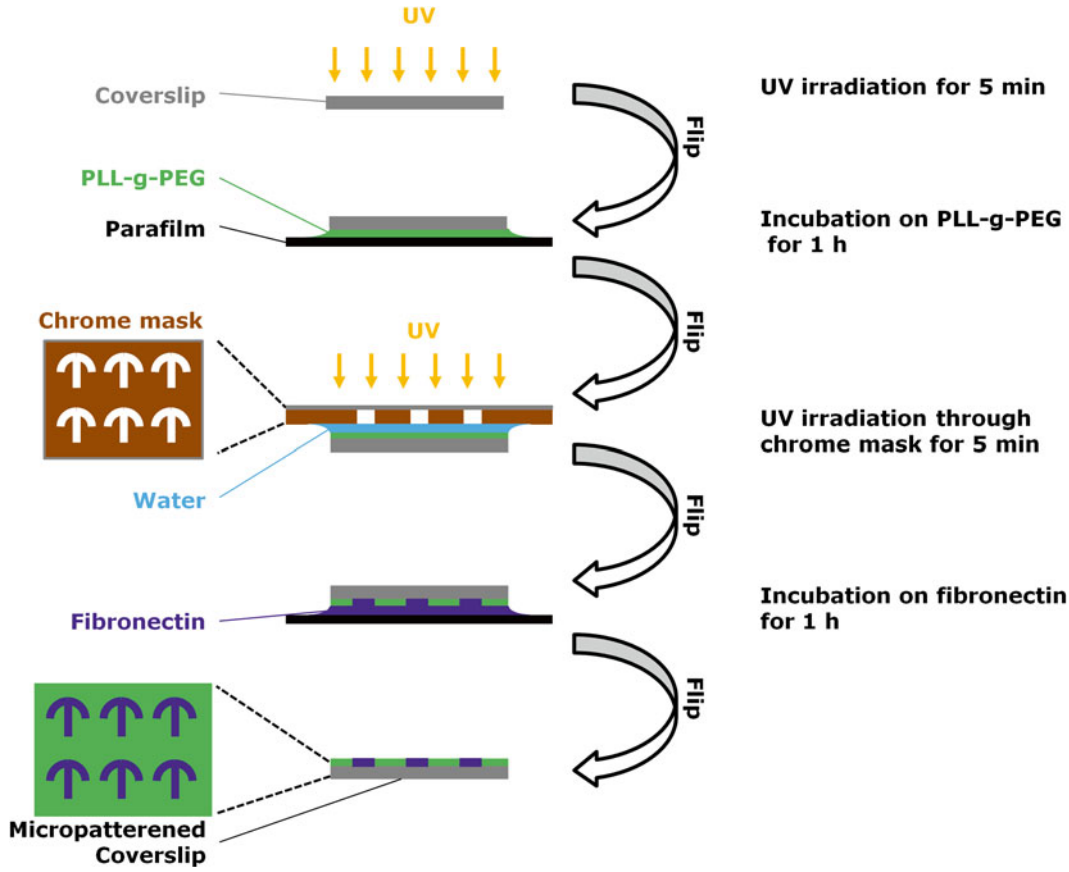

Fig. 3 Pattern production by photolithography. The surface of coverslips is first made repellent by exposure to deep UV irradiation and incubation with PLL-g-PEG. Then, pattern shapes are transferred to the PLL-g-PEG by exposing deep UV light trough a photomask that contains geometric features (patterns) defining regions where UV light can pass or not. Exposure of UV light on the pegylated surface will modify the PLL-g-PEG at regions of exposure and create functional groups to which proteins can bind. Incubation of the coverslip with fibronectin will result in patterns that correspond to the photoactivated areas, as non-activated PLL-g-PEG stays repellent

3. Incubate the coverslips on drops (15 µL for 12 mm coverslip) of PLL-g-PEG Solution on a Parafilm in a humid chamber for 1 h.
4. Wash the coverslips 2× in PBS and 1× in distilled water and let them dry.
5. Carefully wash the photomask with distilled water and then ethanol. Dry the photomask with filtered airflow.
6. Expose the photomask (chrome-coated side) to deep UV for 5 min, at about 5 cm from the lamp, to clean the surface.
7. Place the pegylated side of the coverslips on the chrome-coated side of the photomask with a water drop (*see* **Note 3**).

8. To ensure a better contact between the coverslips and the mask, and to avoid drying of water drops, place a thin glass slide (alternatively a western blot film, of the size of the photomask) on the coverslips and stick it to the mask with water drops alongside edges. Do not allow water to come in contact with the coverslips.
9. Expose the photomask-covered coverslips to deep UV for 5 min.
10. Remove the coverslips from the photomask by adding excess of water. The coverslips should quickly float (*see* **Note 4**).
11. The coverslips can be stored for 2 weeks at room temperature and protected from dust.
12. Incubate the coverslips in a solution of extracellular matrix proteins (50 μg/mL fibronectin, 5 μg/mL fluorescent fibrinogen diluted in water) on Parafilm in a humid chamber for 1 h under a laminar flow hood.
13. Experiment can be stopped at this point (*see* **Note 5**).

3.2 Cell Seeding and Pulse-Chase Experiment

1. Place micropatterned coverslips in Serum-Free Medium in a multi-well plate.
2. Wash subconfluent cell flask with PBS and detach cells with EDTA–trypsin.
3. Add Full Medium to the flask and count cells (*see* **Note 6**).
4. Add the cells on micropatterned coverslips to final density of 10,000 cells/cm^2 and place the plate in the incubator. Avoid shaking the plate to ensure an even cell seeding distribution.
5. Wait for between 5 and 15 min, until the cells start adhering to the micropatterns (check with a binocular scope). Wash carefully the coverslips (3–5 times) with Serum-Free Medium to remove non-micropatterned and floating cells (*see* **Note 7**).
6. Check that no more cells are floating otherwise wash again.
7. Place the plate in the incubator and let the cells spread for at least 3 h before starting any experiment/treatment.
8. Pulse the cells for 1 min at 37 °C with fluorescently marked ligand (i.e., Transferrin Alexa Fluor conjugate at 20 μg/mL or Alexa Fluor conjugate EGF at 1 μg/mL (the EGF-conjugate being a complex of biotin-EGF and labeled streptavidin, the effective concentration of EGF conjugate correspond to a final EGF concentration of 100 ng/mL).
9. Carefully wash the cells with ice cold PBS several times (*see* **Note 7**).
10. Chase the cells by incubating the cells in Serum Free Medium for various time points at 37 °C.

3.3 Fixation and Mounting

1. Fix the cells in 4 % PFA for 15 min at room temperature.
2. Incubate coverslips in Quenching Solution for 10 min.
3. Wash two times in PBS.
4. Permeabilize cells with Permeabilization Solution for 15 min.
5. Wash in PBS.
6. Incubate coverslip in a solution of DAPI diluted 1/5,000 in PBS for 5 min.
7. Wash in PBS and then in distilled water.
8. Mount coverslips on a glass slide with Mowiol.

3.4 Image Acquisition and Analysis

1. Acquire images using an epifluorescent microscope in 2D or 3D. Choose single and well-spread micropatterned cells for acquisition (at least 20 cells). Acquire micropattern images in the same conditions (field and z-stack) as for the channel of interest.
2. Proceed with a deconvolution step if required.
3. Determine the geometrical center (x_0, y_0, z_0) of the micropatterns using the macro1 for ImageJ (*see* **Note 9**). Save results as a excel spread sheet (*see* **Note 9** for format).
4. Segment channel(s) of interest to obtain a list of spatial coordinates (x_i, y_i, z_i) using classical segmentation algorithm (e.g., "3D object counter" in ImageJ, *see* **Note 10** for a macro to process several images in batch mode and for an output result example).
5. Open R software. It is recommended to set the working directory (enter `setwd("D:/DATA/...")` or go to `File->Change working directory...`) to a folder containing:
   - The pattern coordinate excel file (output of macro1).
   - A subfolder containing only the segmentation files (output of macro2).
   - The source R code file ("KDE_source.r", *see* **Note 11**).
6. To read and normalize data, copy-paste the following code in the R console:

```
source("KDE_source.r")      ## Or go to File>Source… and choose "KDE_source.r" file
dimension   <- 3            ## Set "3" for 3D data and "2" for 2D data
cal.xy      <- 0.0645       ## Set pixel size in micron
cal.z       <- 0.2          ## Set z step in micron
```

```
angle       <- -124          ## Set angle to
   rotate (in degree, clockwise) the data if
   required.
plot.micron <- TRUE ##  Set  plot  scale  in
   micron (TRUE) or in pixel (FALSE)
## Read and normalize data
patcoord <- read.patcoord()
segdata <- read.segdata()
segdata_norm <- normalize(segdata, patcoord)
```

7. To compute Kernel Density Estimation (KDE), copy-paste the following code in the R console:

```
x2d <- segdata_norm[,3:4]
x3d <- segdata_norm[,3:5]
n   <- nrow(x2d)
H2d <- Hpi(x2d, binned=n>100, pilot="samse")
fhat2d  <-  kde(x=x2d,  H=H2d,  xmin=c(xlim.
   est[1], ylim.est[1]), xmax=c(xlim.est[2],
   ylim.est[2]))
fhat2d$abs.cont.full <- contourLevels(fhat2d,
   prob=prob, approx=TRUE)
if(dimension == 3) {
H3d <- Hpi(x3d, binned=n>100, bgridsize=rep
   (31,3), pilot="samse")
fhat3d <- kde(x=x3d, H=H3d, xmin=c(xlim.est[1],
   ylim.est[1],  zlim.est[1]),  xmax=c(xlim.
   est[2], ylim.est[2], zlim.est[2]))
fhat3d$abs.cont.full <- contourLevels(fhat3d,
   prob=prob, approx=TRUE)
}
```

8. To plot a 2D density map in R, copy-paste the following code in the R console:

```
## Choose contour to plot, colors and PDF to
   save
ct        <- c(25, 50, 75)               ##
   Set contours to plot
cols      <- c("yellow", "orange", "red") ##
   Set colors
save.pdf  <- TRUE                        ##
   save pdf or not
```

```
save.path  <- "2Dexample.pdf"                ##
   pdf file name
plot2dKDE(fhat2d,  plot.micron,  ct,  cols,
   save.pdf, save.path, filled.cont=TRUE)
```

You should obtain a 2D density map as in Fig. 2.

9. To plot a 3D density map in R, copy-paste the following code in the R console:

```
## choose contour to plot and colors
ct        <- c(50)           ## Set contours
   to plot
cols      <- c("red")     ## Set colors
alpha1 <- 0.2                 ## Set minimum
   contour transparency
alpha2 <- 0.5                 ## Set maximum
   contour transparency
plot3dKDE(fhat3d,  plot.micron,  ct,  cols,
   alpha1, alpha2)
## Select the view you like and save a snap-
   shot (.png)
snapshot3d(file="3Dexample.png")
vv3d() ## to re initialize 3D view
```

You should obtain a 3D density map as in Fig. 2.

4 Notes

1. Use a photomask transparent to UV (wavelengths <200 nm) usually in fused silica or synthetic quartz.
2. Such ovens can be found, usually in large formats, in clean rooms. Smaller ones are often used to clean AFM tips. A small benchtop version can be found at Jelight (UVO cleaner, ref. 342-220). It is important to also order the ozone killer, or the oven will have to be placed under a chemical hood. We also recommend buying a fan to avoid overheating. Alternatively, it is possible for a very modest cost to build a homemade deep UV oven. Bulbs are available at Heraeus Noblelight GmH (NIQ 60/35 XL longlife lamp, = 185 and 254 nm, quartz tube, 60 W). Four bulbs are enough. Be careful to order controllers allowing frequent switches of the bulbs (EVG 65–80 W). A closed box has to be made containing bulb holders, allowing irradiation at a distance of about 10 cm. It is also recommended to add fans to the box to avoid overheating. Particular care has to be taken to avoid any direct exposition to deep UV light and to get rid of the ozone it produces.

3. The volume of water must be adjusted to the coverslip size in order to cover the entire coverslip surface but still keeping close together the photomask and the coverslip. 0.5 μL of water is enough to cover a 12 mm coverslip. Alternatively, an excess of water can be dropped at first (e.g., 5 μL for 12 mm coverslip). Once the coverslips are in place, excess of water is removed by pressing on them with a Kimwipes. At the end, coverslips should not be able to move anymore. The distance between the coverslip and the photomask is critical for micropattern printing resolution. Air bubbles between the mask and the coverslips must be prevented.
4. Use plastic tip and plastic tweezers to carefully remove the coverslips from the photomask, and be careful to not scratch the photomask. The life time of the photomask mostly depends on this step.
5. To stop the experiment at this point, wash the coverslips with PBS. Don't let them dry. Coverslips can be stored 24 h in PBS but it is recommended to proceed directly to the cell seeding.
6. Proceed as fast as possible. Long time in trypsin or centrifugation could impact cell spreading on micropatterns.
7. Watch out not drying the cells (the pegylated coverslip is highly hydrophobic). Typically, for a total volume of 1 mL in the well, wash gently the coverslip using 700 μL pipetting.
8. R software and package installation: R is an open source statistical data analysis platform for Unix, Windows, and Macintosh operating systems.
   (a) Install the R base distribution. This is freely available from the R project Web site http://www.r-project.org under the CRAN (Comprehensive R Archive Network) rubric. As recommended, most Windows and Macintosh users will find it easiest to download and install the pre-compiled binary versions of the base distribution, e.g., `R-2.10.1.pkg` (for Macintosh) or `R-2.10.1-win32.exe` (for Windows).
   (b) Install the required extension packages. There are two main ways to do this:
      - *Automatic*: This requires an Internet connection which allows for downloading in batch mode: networks with a proxy cache or firewall may not allow for this. Start `R`.
        – For Macintosh, select `Packages & Data -> Package Installer`. Make sure that `At User Level` is selected for `Install Location`. Choose the `CRAN (binaries)` under the

Packages repository label. Click Get List.

- For Windows, select Packages -> Install Packages.
- Choose the closest CRAN mirror site. This will bring up a list of all extension packages. Scroll down to select ks, and press Install. Repeat for the rgl and misc3d libraries.

- *Manual*: Go to the R project Web site -> CRAN. Choose a CRAN mirror site. Click on the Contributed extension packages link. This will bring up the list of all contributed packages. Look for mvtnorm. Download the appropriate binary file (.tgz for Macintosh, .zip for Windows) to the Desktop (or other desired location). Repeat for the ks, rgl, and misc3d libraries. Once all files have been downloaded, start R. To install these extension packages:
  - For Macintosh, select Packages & Data -> Package Installer. Then select Local Binary Package under Packages Repository label. Select mvtnorm and press Install.
  - For Windows, select Packages -> Install Packages from local zip files.
  - Install the extension packages in this order: mvtnorm, ks, rgl, misc3d.

(c) Start R and load the ks library. This can be done by selecting Packages & Data -> Package Manager (Macintosh) or Packages -> Load package (Windows), and then ks. Or it can be loaded by typing library(ks) into the command line window.

9. This macro requires the Plugin "Hough Circle" (http://rsbweb.nih.gov/ij/plugins/hough-circles.html). In imageJ, go to Plugins->New->Macro. Copy the following code in the text window. In the same window, go to Macro->Run Macro (ctrl + R). ImageJ will ask you to choose a folder which should contain only micropattern images. This macro contains a file extension filter currently set to ".tif" files that you may change to your favorite file format (e.g., ".stk," ".TIFF"). Once the macro is done, save the result table as a ".txt" or ".xls" file including columns headers and row numbers (go to Edit->Options->Input/Output...). The output table should look like the following:

	X	Y	Z
1	378.5	365.5	5
2	371.5	391.5	6
3	346.5	346.5	5
4	415.5	394.5	7

```
//Macro1: find center of micropatterns
//
//select a folder containing only pattern images
dirIn=getDirectory("Folder in which all pattern files will be analyzed:");
filesTmp  = getFileList(dirIn);
setBatchMode(true);
run("Input/Output...", "jpeg=100 gif=-1 file=.xls use_file copy_column save_column save_row");
//choose files with the .tif extension
files = filterFileNames(filesTmp,".tif",true);
for(i=0; i<files.length;i++)
{
        open(dirIn+files[i]);
        run("Find Edges", "stack");
//choose a focused Z slice
        mean0=0;
        z0=0;
        for (z=1; z<=nSlices; z++)
        {
                setSlice(z);
                getStatistics(area, mean, min, max, std, histogram);
                if (mean>mean0)
                {
                        mean0=mean;
                        z0=z;
        }}
//make a binary mask
        setSlice(z0);
        run("Duplicate...", "title=focus.tif");
        run("8-bit");
        run("Maximum...", "radius=1");
        run("Mean...", "radius=5");
        setAutoThreshold();
        run("Convert to Mask", " ");
        run("Close-");
        run("Fill Holes");
```

```
//find the center
    run("Find Edges");
    run("Hough Circles", "minimum=300 maximum=330 increment=20 number=1 threshold=60");
    selectWindow("1 Circles Found");
    setAutoThreshold();
    run("Convert to Mask");
    run("Set Measurements...", "  centroid redirect=None decimal=3");
    run("Analyze Particles...", "size=0-Infinity circularity=0.00-1.00 show=Outlines display exclude include
add");
    setResult("Z", i, z0);
    updateResults();
    while(nImages>0){
          selectImage(1);
          close();
    }
}
// end macro
print("end");
//function
function filterFileNames(filelist,extension,ignorecase)
{
            tmpfiles=newArray(filelist.length);
            count=0;
            pattern=extension;
            for(i=0;i<filelist.length;i++)
            {
                        strin=filelist[i];
                        if (ignorecase)
                        {
                                    strin=toLowerCase(strin);
                                    pattern=toLowerCase(pattern);
                        }
                        if (endsWith(strin,pattern))
                        {
                                    tmpfiles[count]=filelist[i];
                                    count++;
                        }
            }
            filteredList=newArray(count);
            for (i=0;i<count;i++)     filteredList[i]=tmpfiles[i];
            return filteredList;
}
```

10. Segmentation macro. This macro requires the plugin "3D Object Counter" (http://imagejdocu.tudor.lu/doku.php?id=plugin:analysis:3d_object_counter:start). In imageJ, go to `Plugins->New->Macro`. Copy the following code in the text window. In the same window, go to `Macro->Run Macro` (ctrl + R). ImageJ will ask you to choose a folder which should contain only images to segment. This macro contains an extension file filter currently set to ".tif" files that you may change to your favorite file format (e.g., ".stk," ".TIFF"). The macro creates as an output a folder containing a list of segmentation files.

```
//Macro2: Batch Mode Segmentation using 3D Object Counter

thr = 500; //set a threshold to separate objects from background

dirIn = getDirectory("image folder");

dirOut = dirIn+"results/";

File.makeDirectory(dirOut);

filesTmp = getFileList(dirIn);

setBatchMode(true);

run("Input/Output...", "jpeg=100 gif=-1 file=.xls use_file copy_column save_column save_row");

//choose files with the .tif extension

fileList     = filterFileNames(filesTmp,".tif",true);

setBatchMode(true);

run("Set 3D Measurements", "volume surface nb_of_obj._voxels nb_of_surf._voxels integrated_density

mean_gray_value std_dev_gray_value median_gray_value minimum_gray_value maximum_gray_value centroid

mean_distance_to_surface std_dev_distance_to_surface median_distance_to_surface centre_of_mass bounding_box

dots_size=5 font_size=10 store_results_within_a_table_named_after_the_image_(macro_friendly) redirect_to=none");

for(i=0;i<fileList.length;i++){

        if(File.isDirectory(dirIn+fileList[i])==false){

                open(dirIn+fileList[i]);

                run("3D object counter...", "threshold="+thr"+slice=15 min.=10 max.=17437500

exclude_objects_on_edges statistics");

                selectWindow("Statistics for "+fileList[i]);

                saveAs("Text",dirOut+fileList[i]);

                run("Close");

                close();

}}



// end macro

print("end");

//function

function filterFileNames(filelist,extension,ignorecase)

{

            tmpfiles=newArray(filelist.length);

            count=0;

            pattern=extension;

            for(i=0;i<filelist.length;i++)

            {

                        strin=filelist[i];

                        if (ignorecase)

                        {

                                    strin=toLowerCase(strin);

                                    pattern=toLowerCase(pattern);

                        }

                        if (endsWith(strin,pattern))

                        {

                                    tmpfiles[count]=filelist[i];

                                    count++;

                        }

            }
```

```
            filteredList=newArray(count);
            for (i=0;i<count;i++)     filteredList[i]=tmpfiles[i];
            return filteredList;
}
```

11. R source file for KDE computation. Copy and save this code as “KDE_source.r”.

```
## Load libraries
library(ks)
## Initialise variables
lwd <- 3
xlim <- c(-300,300)
ylim <- c(-300,300)
zlim <- c(-100,100)
xlim.est <- c(-400,400)
ylim.est <- c(-400,400)
zlim.est <- c(-100,100)
cont       <-seq(0,100,by=1)
cont.names <-paste(cont,"%",sep="")
prob       <-sort((100-cont)/100)
## Auxiliary functions
vv3d <-function()
{
 par3d(userMatrix=matrix(c(0.87, -0.48, 0.04, 0, 0.10, 0.26, 0.96, 0, -0.48, -0.83, 0.29, 0, 0.00, 0.00, 0.00,
1), byrow=TRUE, ncol=4), FOV=90)
}
kde.scale <- function(fhat, a=1)
{
 d <-nrow(fhat$H)
 if (length(a) < d) a <-rep(a,d)[1:d]
 fhat.scale <- fhat
 for (j in 1:d)
 {
  fhat.scale$x[,j] <- fhat$x[,j]*a[j]
  fhat.scale$eval.points[[j]] <- fhat$eval.points[[j]]*a[j]
 }
 fhat.scale$estimate <- fhat$estimate/prod(a)
 if (!is.null(fhat$abs.cont.full))
  fhat.scale$abs.cont.full <- fhat$abs.cont.full/prod(a)
```

```
  fhat.scale$H <- fhat$H*prod(a^2)
  return(fhat.scale)
}
################################################################################
## MAIN FUNCTIONS
################################################################################
## Select and read pattern coordinate file
read.patcoord <- function()
{
  path  <- choose.files(default = getwd(), caption = "Select pattern coordinates file", multi = FALSE)
  cat(paste\("npattern coordinates file: ",path,"\n"))
  patcoord <-read.table(path, header=T, row.names=1, sep="\t")
  return(patcoord)
}
## Select directory and read segmentation data
read.segdata <-function()
{
  path          <-choose.dir(default = getwd(),caption = "choose segmentation resultdirectory")
  cat(paste("\nsegmentation result directory: ",path,"\n"))
  segfiles <-dir(path)
  if(dimension == 3)
  {
    segdata  <-matrix(NA,0,5)
    for(i in 1:length(segfiles)){
      tmp     <- read.table(paste(path,"/",segfiles[i],sep=""), header=T, row.names=1, sep="\t")
      tmp     <- cbind(rep(i, nrow(tmp)),1:nrow(tmp), tmp[,c("X.1","Y","Z")])
      segdata <- rbind(segdata, tmp)
      }
    colnames(segdata) <- c("cell","Index","X","Y","Z")
  } else {
    segdata  <- matrix(NA,0,4)
    for(i in 1:length(segfiles)){
      tmp     <- read.table(paste(path,"/",segfiles[i],sep=""), header=T, row.names=1, sep="\t")
      tmp     <- cbind(rep(i, nrow(tmp)),1:nrow(tmp), tmp[,c("X.1","Y")])
      segdata <- rbind(segdata, tmp)
      }
```

```
    colnames(segdata) <-c("cell","Index","X","Y")
  }
  rm(tmp)
  return(segdata)
}
## Center and rotate coordinates according to the pattern
normalize <-function(segdata, patcoord)
{
  segdata_norm  <- segdata
  for(i in unique(segdata$cell)){
    tmp    <- subset(segdata, segdata$cell==i)[,3:ncol(segdata)]
    tmp    <- tmp -matrix(as.numeric(patcoord[i,1:ncol(tmp)]),nrow(tmp),dimension,byrow=T)
    segdata_norm[segdata$cell==i,3:ncol(segdata)]  <- tmp
  }
  if(dimension == 3) segdata_norm[,"Z"] <-cal.z/cal.xy * segdata_norm[,"Z"]
  ## Rotate coordinates
  theta <- angle*pi/180+pi
  rot<-matrix(c(cos(theta),sin(theta),-sin(theta),cos(theta)),2,2)
  rotmat<-rot %*% rbind(segdata_norm[,3],segdata_norm[,4])
  segdata_norm[,3] <- rotmat[1,]
  segdata_norm[,4] <- rotmat[2,]
  return(segdata_norm)
}
## Create 2D plots
plot2dKDE  <- function(fhat2d, plot.micron, ct, cols, save.pdf, save.path, filled.cont=TRUE)
{
  if(plot.micron)
  {
    scale.factor <- rep(cal.xy,3)
    xlim.disp    <- xlim*scale.factor[1]
    ylim.disp    <- ylim*scale.factor[2]
    zlim.disp    <- zlim*scale.factor[3]

  } else {
    scale.factor <- rep(1,3)
```

```
    xlim.disp    <- xlim
    ylim.disp    <- ylim
    zlim.disp    <- zlim
  }
  fhat <- kde.scale(fhat2d, a=scale.factor)
  ct.ind         <- which(c(cont.names) %in% paste(100-c(ct,0),"%", sep=""))
  cl             <- fhat$abs.cont.full[ct.ind]
  cl[length(cl)] <- 1.01*max(max(fhat$estimate), cl)
  col.len        <- length(cl)
  temp.cols      <- c("transparent", cols)
  cl             <- c(min(fhat$estimate)-0.01*abs(min(fhat$estimate)), cl)
  if(save.pdf) pdf(file=save.path)
  ## initialize plot
  par(mar=c(2,2,0.5,0.5))
  plot(fhat, disp="slice", abs.cont=0, add=FALSE, xlim=xlim.disp, ylim=ylim.disp, drawlabels=FALSE, asp=1)
  ## plot contours
  filled.cont = TRUE
  if (filled.cont)
    plot(x=fhat, abs.cont=cl[-1], asp=1, display="filled.contour2", lwd=lwd*(length(ct)<99), col=temp.cols,
drawlabels=FALSE, add=TRUE)  else
    plot(x=fhat, abs.cont=cl[-1], drawlabel=FALSE, display="slice", col=temp.cols[-1], lwd=lwd, add=TRUE)
  legend("bottomleft", title="", legend=paste(ct,"%"), lwd=lwd, col=rev(cols), bty="n", cex=1.2)
  sc.start <-100*scale.factor[1]
  lines(c(sc.start+10*scale.factor[1]/cal.xy, sc.start), c(ylim.disp[1],ylim.disp[1]),lwd=lwd)
  text(sc.start+5*scale.factor[1]/cal.xy,ylim.disp[1], expression(10*" "*mu*m), pos=3, cex=1.5)
  if(save.pdf) dev.off()
}
## Create 3D plots
plot3dKDE <-function(fhat3d, plot.micron, ct, cols, alpha1, alpha2)
{
  if(plot.micron)
  {
    scale.factor <- rep(cal.xy,3)
    xlim.disp    <- xlim*scale.factor[1]
    ylim.disp    <- ylim*scale.factor[2]
    zlim.disp    <- zlim*scale.factor[3]
```

```
  } else {
    scale.factor <- rep(1,3)
    xlim.disp    <- xlim
    ylim.disp    <- ylim
    zlim.disp    <- zlim
  }
  fhat <- kde.scale(fhat3d, a=scale.factor)
  ct.ind         <- which(c(cont.names) %in% paste(100-c(ct,0),"%", sep=""))
  cl             <- fhat$abs.cont.full[ct.ind]
  cl[length(cl)] <- 1.01*max(max(fhat$estimate), cl)
  col.len       <- length(cl)
  alphavec <- sort(c(alpha1,alpha2))
  if (alphavec[1]<0) alphavec[1] <- 0
  if (alphavec[2]>1) alphavec[2] <- 1
  if (length(ct)==1) {
  alphavec <- alphavec[2]
    } else    alphavec <- seq(alphavec[1], alphavec[2], length=length(ct))
  ## initialize plot
  open3d()
  wr <- par3d()$windowRect
  par3d(windowRect=c(wr[1],wr[2],wr[1]+350,wr[2]+300), zoom=0.3)
  ## plot contour (use vv3d() to reset to original view
  plot(x=fhat, abs.cont=rev(cl), alphavec=alphavec, xlim=xlim.disp, ylim=ylim.disp, zlim=zlim.disp, asp=c(1,1,1),
axes=FALSE, box=FALSE, xlab="", ylab="", zlab="", add=FALSE, col=cols)
  if(plot.micron) axis3d('z+-', at=round(seq(0,77.5, length=3)*scale.factor[3],2), pos=c(-100, 100,
0)*scale.factor[3]) else
    axis3d('z+-', at=seq(0,100, length=3)*scale.factor[3], pos=c(-100, 100, 0)*scale.factor[3])
  axis3d('x+', pos=c(NA, 100, 0)*scale.factor[1], size=3)
  axis3d('y+', pos=c(-100, NA, 0)*scale.factor[2], size=3)
  text3d(-120*scale.factor[3], 120*scale.factor[3], 50*scale.factor[3], "z", size=10)
  text3d(0, 150*scale.factor[1], 0, "x", size=10)
  text3d(-130*scale.factor[2], 0, 0, "y", size=10)
  vv3d()
}
###############################################################################
## END
###############################################################################
```

12. R script to compute and plot density maps:

```
################################################################################
##  INITIALISE, READ AND NORMALIZE DATA
################################################################################
source("KDE_source.r")      ## Or go to File>Source... and choose "KDE_source.r" file
dimension   <- 3            ## Set "3" for 3D data and "2" for 2D data
cal.xy      <- 0.0645       ## Set pixel size in micron
cal.z       <- 0.2          ## Set z step in micron
angle       <- 46           ## Set angle to rotate (in degree, clockwise) the data if required.
plot.micron <- TRUE
## Read and normalize data
patcoord <- read.patcoord()
segdata <- read.segdata()
segdata_norm <- normalize(segdata, patcoord)
################################################################################
##  COMPUTE 2D AND 3D KDE (Kernel Density Estimation)
################################################################################
x2d <- segdata_norm[,3:4]
x3d <- segdata_norm[,3:5]
n   <- nrow(x2d)
H2d <- Hpi(x2d, binned=n>100, pilot="samse")
fhat2d <- kde(x=x2d, H=H2d, xmin=c(xlim.est[1], ylim.est[1]), xmax=c(xlim.est[2], ylim.est[2]))
fhat2d$abs.cont.full <- contourLevels(fhat2d, prob=prob, approx=TRUE)
if(dimension == 3) {
H3d <- Hpi(x3d, binned=n>100, bgridsize=rep(31,3), pilot="samse")
fhat3d <- kde(x=x3d, H=H3d, xmin=c(xlim.est[1], ylim.est[1], zlim.est[1]), xmax=c(xlim.est[2], ylim.est[2],
zlim.est[2]))
fhat3d$abs.cont.full <- contourLevels(fhat3d, prob=prob, approx=TRUE)
}
```

```
##############################################################################

## CREATE 2D PLOT

##############################################################################

## Choose contour to plot, colors and PDFto save

ct        <- c(25, 50, 75)               ## Set contours to plot

cols      <- c("yellow", "orange", "red") ## Set colors

save.pdf  <- TRUE                        ## save pdf or not

save.path  <- "2Dexample.pdf"            ## pdf file name

plot2dKDE(fhat2d, plot.micron, ct, cols, save.pdf, save.path, filled.cont=TRUE)

##############################################################################

## CREATE 3D PLOT

##############################################################################

## choose contour to plot and colors

ct        <- c(50)                    ## Set contours to plot

cols      <- c("red")                 ## Set colors

alpha1 <- 0.2                         ## Set minimum contour transparency

alpha2 <- 0.5                         ## Set maximum contour transparency

plot3dKDE(fhat3d, plot.micron, ct, cols, alpha1, alpha2)

## Select the view you like and save a snapshot (.png)

snapshot3d(file="3Dexample.png")

vv3d() ## to re initialize 3D view

##############################################################################

## END

##############################################################################
```

References

1. Rappoport J, Simon S (2003) Real-time analysis of clathrin-mediated endocytosis during cell migration. J Cell Sci 116:847–855
2. Cao H, Krueger E, McNiven M (2011) Hepatocytes internalize trophic receptors at large endocytic “Hot Spots”. Hepatology 54:1819–1829
3. Gaffield M, Tabares L, Betz W (2009) Preferred sites of exocytosis and endocytosis colocalize during high- but not lower-frequency stimulation in mouse motor nerve terminals. J Neurosci 29:15308–15316
4. Gumbiner B (1996) Cell adhesion: the molecular basis of tissue architecture and morphogenesis. Cell 84:345–357
5. Thery M, Racine V, Piel M et al (2006) Anisotropy of cell adhesive microenvironment governs cell internal organization and orientation of polarity. Proc Natl Acad Sci U S A 103:19771–19776
6. Schauer K, Duong T, Bleakley K et al (2010) Probabilistic density maps to study global endomembrane organization. Nat Methods 7:560–566
7. Grossier JP, Xouri G, Goud B, Schauer K (2014) Cell adhesion defines the topology of endocytosis and signaling. EMBO J 33(1): 35–45
8. Schneider C, Rasband W, Eliceiri K (2012) NIH Image to ImageJ: 25 years of image analysis. Nat Methods 9:671–675
9. R Development Core Team (2013) R: a language and environment for statistical computing. Vienna, Austria
10. Duong T (2009) ks: Kernel smoothing, R package version 1.6.3
11. Azioune A, Storch M, Bornens M, Théry M, Piel M (2009) Simple and rapid process for single cell micro-patterning. Lab Chip 9 1640–1642

Chapter 9

Use of Kaede and Kikume Green–Red Fusions for Live Cell Imaging of G Protein-Coupled Receptors

Antje Schmidt, Burkhard Wiesner, Ralf Schülein, and Anke Teichmann

Abstract

The fusion of fluorescent proteins to G protein-coupled receptors (GPCRs) is an important tool to study, e.g., trafficking and protein interactions of these important drug targets. In the past, the green fluorescent protein and its derivatives have been widely used as fluorescent tags. More recently, it was reported that photoconvertible fluorescent proteins (PCFPs) such as Kaede or Kikume green–red protein could also be used as fluorescent tags for GPCRs. These proteins have the obvious advantage that their fluorescence can be switched once the GPCR of interest has reached a specific subcellular compartment. Here, we summarize the recent progress for live cell imaging of GPCRs using these PCFPs for trafficking, biosynthesis, and protein/protein interaction studies.

Key words G protein-coupled receptors, Kaede, Kikume green–red, Protein trafficking, Protein/protein interactions, Photoconvertible fluorescent proteins, Confocal laser scanning microscopy, Fluorescence correlation spectroscopy

1 Introduction

1.1 The Photoconvertible Fluorescent Fusion Proteins Kaede and Kikume Green–Red

The fusion of fluorescent tags to target proteins is widely used in experimental cell and molecular biology, e.g., to localize proteins or to analyze their protein/protein interactions. The first generation of fluorescent proteins were derived from the green fluorescent protein (GFP) from the hydrozoan medusa *Aequorea victoria* [1]. Despite some limitations, GFP is still one of the most frequently used fluorescence proteins. More recently, however, another family of fluorescence proteins were cloned from Anthozoa, the photoconvertible fluorescent proteins (PCFPs). These have become more and more popular because they opened completely new possibilities for live cell imaging of individual proteins in real time, e.g., to study their trafficking between subcellular compartments.

The archetypical PCFP is the Kaede protein, which was cloned by Ando et al. in 2002 from the stony coral *Trachyphyllia geoffroyi* [2]. The chromophore of Kaede consists of three amino

Andrei I. Ivanov (ed.), *Exocytosis and Endocytosis*, Methods in Molecular Biology, vol. 1174,
DOI 10.1007/978-1-4939-0944-5_9,

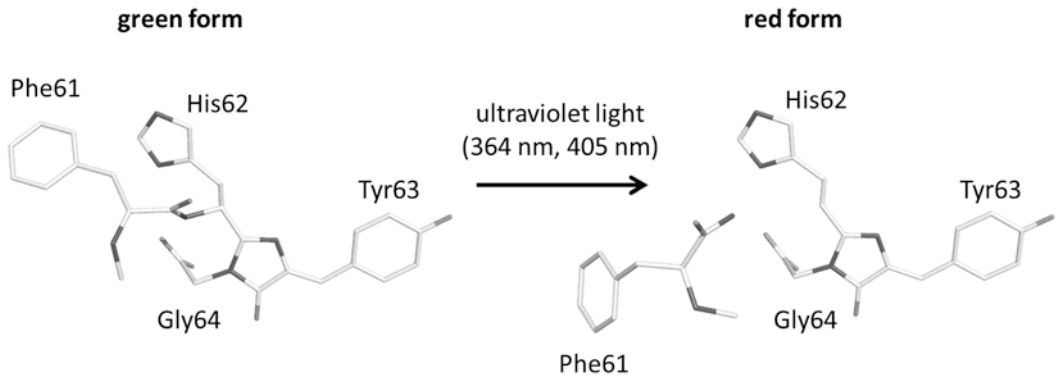

Fig. 1 Photoconversion mechanism for Kaede and KikGR. Kaede and KikGR possess a HYG chromophore. Photoconversion of the green fluorescent form is triggered by ultraviolet or violet radiation which induces cleavage between the amide nitrogen and α-carbon atoms of residue His62. As a consequence, a conjugated dual-imidazole ring system and a red fluorescent fluorophore is formed

acids, namely, His-Tyr-Gly. Excitation with UV light leads to rearrangements in the chromophore, thereby changing the excitation wavelength irreversibly from green to red (Fig. 1) [2, 3]. As many other anthozoan fluorescence proteins, Kaede tends to form tetramers because of electrostatic and hydrophobic interactions [4].

In 2005, Tsutsui et al. constructed a new PCFP, namely, Kikume green–red (KikGR) [5]. It was derived from a conventional fluorescent protein from *Favia favus* by introducing the Kaede chromophore. Even though the excitation and emission maxima of KikGR are similar to Kaede (Table 1), the fluorescence of KikGR was reported to be brighter and to undergo a more efficient photoconversion [5]. More recently, a monomeric version of KikGR (mKikGR) was generated using random mutagenesis and error-prone PCR [6]. PCFPs were originally used in their soluble form to analyze the fate of individual cell populations after photoconversion which can be performed also with the tetrameric proteins. If the PCFPs are used as fusion tags, e.g., for G protein-coupled receptors, however, monomeric variants may be preferable since they are less likely to influence the localization and protein/protein interactions of the target proteins. A comparison of the spectral and structural properties of Kaede, KikGR, and mKikGR is given in Table 1. Excitation and emission spectra of Kaede and mKikGR are shown for the native (green) and photoconverted (red) state in Fig. 2.

1.2 Trafficking of G Protein-Coupled Receptors

The heptahelical G protein-coupled receptors (GPCRs) form the largest group of plasma membrane receptors in eukaryotic cells and represent the most important drug targets. They are able to process a broad range of extracellular signals such as light, hormones, amino acids, nucleotides, and ions [7–9].

Table 1
Characteristics of the PCFP Kaede, KikGR, and mKikGR

	Kaede		KikGR		mKikGR	
Characteristics	**Green form**	**Red form**	**Green form**	**Red form**	**Green form**	**Red form**
Oligomerization	Tetrameric	Tetrameric	Tetrameric	Tetrameric	Monomeric	Monomeric
Number of amino acid	225	225	225	225	233	233
Excit./emiss. maxima (nm)	508/518	508/518	507/517	583/593	505/517	580/591
Molar extinction coefficient (M^{-1} cm^{-1})	98,800 (508 nm)	98,800 (508 nm)	53,700 (507 nm)	35,100 (583 nm)	47,100 (504 nm)	21,750 (579 nm)
Fluorescence quantum yield	0.88	0.88	0.70	0.65	0.53	0.64
Brightness[a]	86.9	86.9	37.6	22.8	25.0	13.9
pH sensitivity	p*K*a = 5.6	p*K*a = 5.6	p*K*a = 7.8	p*K*a = 5.5	p*K*a = 6.5	p*K*a = 5.2
Cytotoxicity[b]	No	No	No	No	No	No
Photoconversion (nm)	UV, 350–410 nm	No	UV, 350–410 nm	No	UV, 350–410 nm	No

The table summarizes the main characteristics of the photoconvertible fusion proteins Kaede, KikGR, and mKikGR. Data from Amalgaam Co., Ltd., Tokyo, Japan
[a]Brightness: Molar extinction coefficient × fluorescence quantum yield/1,000
[b]Toxicity when expressed in HeLa cells

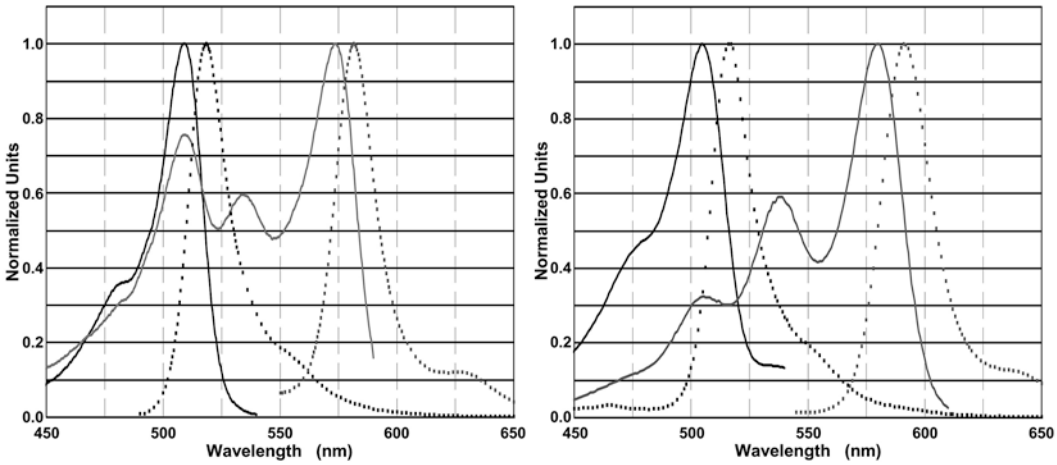

Fig. 2 Excitation and emission spectra of Kaede (*left panel*) and mKikGR (*right panel*). *Full lines* represent the excitation spectra (*black* = green form; *grey* = red form) and *dotted lines* the emission spectra (*black* = green form; *grey* = red form). Data from Amalgaam Co., Ltd., Tokyo, Japan

In terms of protein trafficking, the life cycle of a GPCR involves many subcellular compartments and is regulated by various interacting proteins [10]. Initially, the receptors are integrated into the membrane of the endoplasmic reticulum (ER). In the ER, GPCRs are folded and folding is checked by a quality control system. Only correctly folded GPCRs are allowed to leave the ER. They are transported via the Golgi apparatus to their target compartments, usually the plasma membrane. Misfolded GPCRs are retained in the ER by the quality control system and finally subjected to proteolysis via the ER-associated degradation (ERAD) pathway [11–13]. Misfolding of GPCRs due to mutations may lead to intracellular retention of the receptors by the quality control system and consequently to inherited diseases [14]. At the plasma membrane, GPCRs are usually internalized following ligand-induced activation and G protein coupling to terminate the signal transduction cascade. Several sorting processes take place after the internalization of GPCRs. They are either recycled to the plasma membrane for rapid resensitization or delivered to lysosomes for degradation [15, 16].

In the last decade, many GPCRs have been shown to form hetero- or homo-oligomeric complexes (*see*, e.g., the databases http://data.gpcr-okb.org or http://www.ssfa-gphr.de [17–21]). For both homo- and hetero-oligomeric receptors, positive and negative cooperative or allosteric effects on ligand binding have been described [22–24]. Homo- and hetero-oligomerization may also influence G protein selectivity of the receptors [25–28], their trafficking through the secretory pathway, and their internalization [29, 30]. The fact that GPCRs pass so many different subcellular compartments raises the question as to where these complexes are formed and whether they may undergo changes during the receptor's life cycles.

1.3 Using PCFP Fusions to Analyze GPCR Dynamics in Live Cells

Fluorescence microscopy and fluorescent-tagged GPCRs allow not only the localization of GPCRs in subcellular compartments of live cells but also their quantification.

1.3.1 Analysis of GPCR Trafficking/Recycling Using PCFP Fusions

Investigating the dynamics of GPCR trafficking between different compartments in real time is challenging when the individual pathways overlap and single-fluorescent fusion partners, such as GFP, are used. This problem can be overcome by using PCFPs: once the fusion protein of interest has reached a particular compartment, its fluorescence can be converted from green to red and trafficking to the target compartment can be analyzed by monitoring its new red fluorescence. This approach is especially useful to study GPCR recycling since the recycling pathway to the plasma membrane may overlap with that of the newly synthesized receptors. Using PCFPs as fusion partners, the receptors can be photoconverted from green to red once they have reached the endosomes and the fate of the red receptor population to either the plasma membrane (recycling) or the lysosomes (degradation) can be monitored. During the whole experiment the red receptor population can be easily differentiated from the newly synthesized green population [31]. In Fig. 3 the recycling of the C terminally Kaede-tagged corticotropin-releasing factor receptor type 1 (CRF_1R) is shown. Already 45 min after photoconversion, the red receptor population is detectable at the plasma membrane. A detailed description of the recycling assay using PCFP fusions is outlined in Subheading 3.1.

1.3.2 Analysis of GPCR Biosynthesis Using PCFP Fusions

Preventing the protein synthesis of specific target proteins or GPCRs by, e.g., antisense strategies (e.g., antisense oligonucleotides or RNA interference) is an important tool in cell biology and may be also of pharmacological relevance in the future [32]. The time-dependent biosynthesis of a protein and its inhibition is usually quantified using the incorporation of radiolabeled amino acids. Microscopical assays, in contrast, are challenging when using single fluorescent tags, since the newly synthesized proteins cannot be distinguished from the already existing population. However, PCFP fusions allow to perform "pulse chase microscopy" experiments and to quantify synthesis of proteins easily in real time in live cells.

To analyze and to quantify biosynthesis of a PCFP-tagged GPCR, the present green receptor population in the cells is completely photoconverted at time t_0. The preexisting receptor population thus shows a red fluorescence, whereas the newly synthesised receptors will appear in green and can be quantified over time. Monitoring biosynthesis microscopically is limited to single cells and can be performed in principle as described above for the recycling assay. If more quantitative data is required, measuring the reappearing green fluorescence by flow cytometry (FCM) will yield more reliable results, especially when analyzing substances which

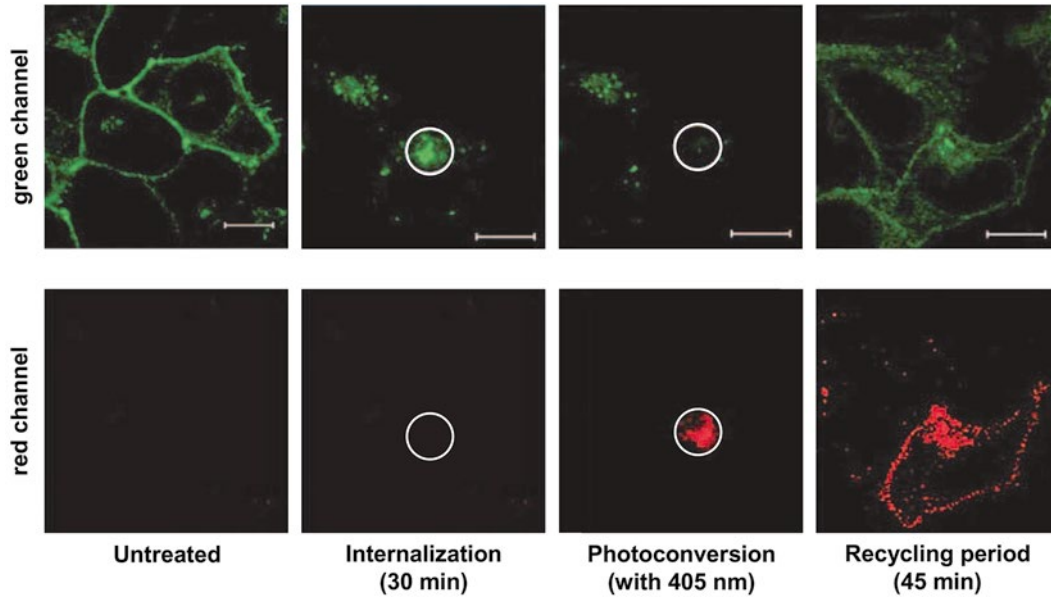

Fig. 3 Analysis of GPCR recycling using PCFP fusions. The corticotropin-releasing factor receptor type 1 (CRF_1R) was fused C-terminally with Kaede and was transiently transfected in HEK293 cells. By using a two-channel time series the fluorescence intensities of green Kaede and red Kaede were monitored. Receptors were internalized using saturating concentrations of the agonist sauvagine (100 nM). The fusion protein was photoconverted from green to red in a region of interest (ROI, *white circle*) representing endosomal compartments by UV irradiation (405 nm). Already 45 min after photoconversion the red Kaede fluorescence signals are detectable at the plasma membrane demonstrating receptor recycling. *Upper panel*: Green Kaede fluorescence signals. *Lower panel*: Red Kaede fluorescence signals

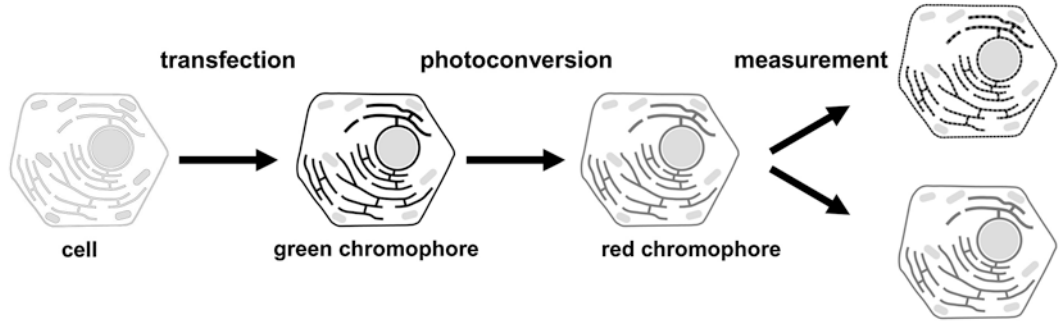

Fig. 4 Principle of the GPCR biosynthesis measurements using PCFP fusions. From *left* to *right* - HEK293 cells stably expressing a GPCR–PCFP fusion protein. Initially, the proteins are completely photoconverted from green to red with UV light (364 nm, 405 nm). Biosynthesis of the GPCR–PCFP fusion can be monitored by analyzing the reappearing green forms, either by LSM at a single-cell level or by FCM

inhibit biosynthesis [33]. In Fig. 4, the principle of the biosynthesis measurements using fusions of PCFPs to GPCRs is shown. A detailed description of an FCM analysis is given in Subheading 3.2.

1.3.3 Analysis of GPCR Interactions Using PCFP Fusions

To identify whether GPCRs form hetero- or homo-oligomers in live cells, assays using fluorescence resonance energy transfer (FRET) or bioluminescence resonance energy transfer (BRET) have been frequently applied. The major drawback of these methods is that they are dependent on the properties of the fluorescent tags. Therefore problems may result, e.g., from overlapping absorption and emission spectra and from the distances of the fluorophores. These techniques also yield qualitative rather than quantitative results for the oligomerization states of GPCRs. To address GPCR oligomerization in more detail, fluorescence correlation spectroscopy (FCS) can be performed using GPCR–PCFP fusions.

FCS is a powerful single-molecule detection methodology. It is useful to determine the concentration of GPCRs, their mobility, and interaction dynamics in live cells. Due to the fact that spatial resolution is limited in light microscopy, FCS measurements are based on light fluctuations emitted by very low concentrated fluorophores diffusing through a confocal volume. The detected intensity trace is used to derive the autocorrelation function of the fluorophore by correlating the intensity at a time point t with that of a time point $t+\tau$. When two different fluorophores fused to two different proteins are used, a cross-correlation function can be derived consequently leading to information about the interaction of the respective proteins. The interaction of GPCRs (homo- and hetero-oligomerization) using FCS can be measured, e.g., with the help of GFP and mCherry fusions. But also fusions of PCFPs to GPCRs can be used in case of homo-oligomerization. This methodology has the obvious advantage that a single GPCR–PCFP construct is sufficient for the experiments. Prior to the FCCS measurements, 50 % of the fluorophores need to be photoconverted by a suitable UV lamp yielding the required mixed green and red receptor population (Fig. 5). The cross-correlation function $G(\tau)$ can then be derived out of the detected green and red intensity fluctuations. The fluorescence signals of the green channel at a time t are correlated to the signals of the red channel at a time $(t+\tau)$ or vice versa. The normalized cross-correlation function (G_{ij}) with the interval time τ can be expressed as

$$G_{ij}(\tau) = \frac{\langle \delta F_i(t)\, \delta F_j(t+\tau) \rangle}{\langle F_i(t) \rangle \langle F_j(t) \rangle}, \quad i \neq j \tag{1}$$

$F_i(t)$ and $F_j(t)$ describe the fluorescence intensity at the time point t for species i and j, respectively, and $\delta F(t) = F(t) - \langle F(t) \rangle$ describes the fluctuation of the mean intensity. Cross-correlation of the green and red signals indicates co-diffusion through the confocal volume and thus interaction of the tagged receptors. In case of the photoconvertible fluorescence protein Kaede, the applicability to study GPCR interactions in live cells by FCS has

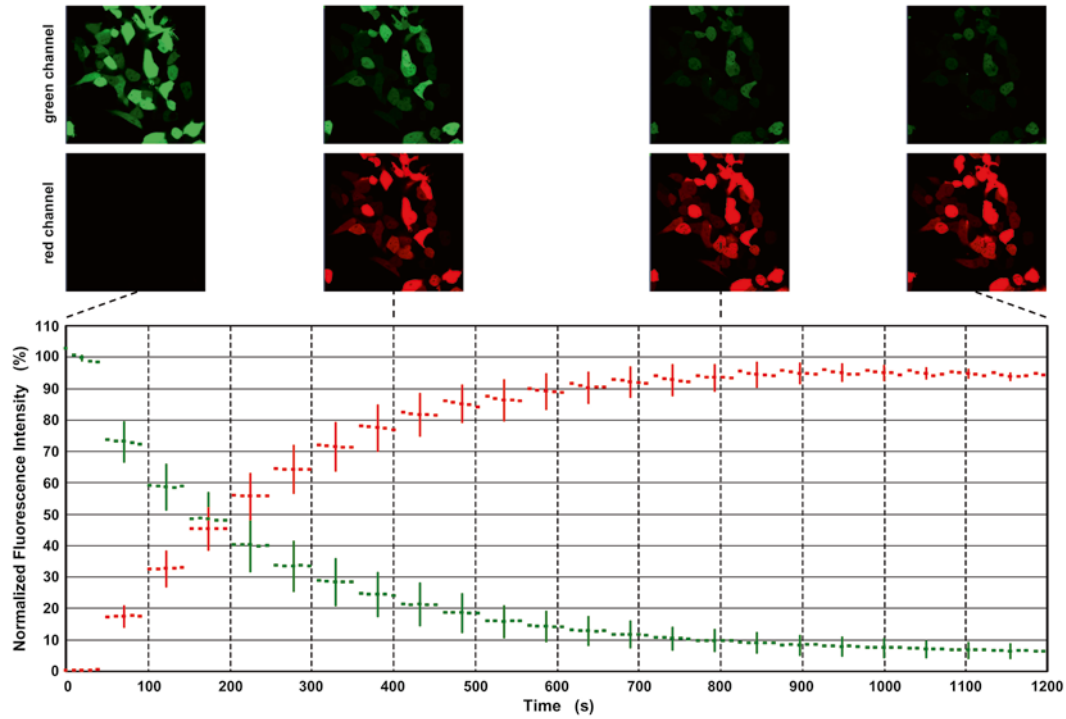

Fig. 5 Partial photoconversion of mKikGR in transiently transfected HEK293 cells. A two-channel time series was used to determine the illumination time for 50 % photoconversion of soluble mKikGR. *Upper images* and *black curves*: green mKikGR fluorescence signals; *lower images* and *grey curves*: red mKikGR fluorescence signals. Mean and SD, $N = 20$

been demonstrated by Schmidt et al. [31] and is described in detail in Subheading 3.3. A detailed description of the principle of this method is given in [34–36]. Representative auto- and cross-correlation curves of the Kaede-tagged CRF_1R demonstrating its oligomerization are shown in Fig. 6.

2 Materials

2.1 Construction of Kaede or mKikGR Fusion Proteins

Eucaryotic expression vector plasmids encoding Kaede or mKikGR for N- or C-terminal fusions can be purchased from MoBiTec (Göttingen, Germany), Amalgaam (Itabashi-ku, Tokyo), and MBL International (Woburn, USA), for example. In the case of GPCRs the cDNA of the PCFPs should be fused C-terminally, thereby replacing the stop codons of the GPCRs (*see* **Note 1**).

2.2 Transient and Stable Expression of GPCR–Kaede or GPCR–mKikGR Fusion Proteins in Mammalian Cells

1. Transfection reagents: Examples for commercially available transfection reagents working efficiently with many mammalian cell lines include Lipofectamine™ 2000 Reagent, TransFectin™ Lipid Reagent, or FuGENE® HD.
2. Dulbecco's modified Eagle medium (DMEM) with or without phenol red (*see* **Note 2**). Add 1 mM L-glutamine before use,

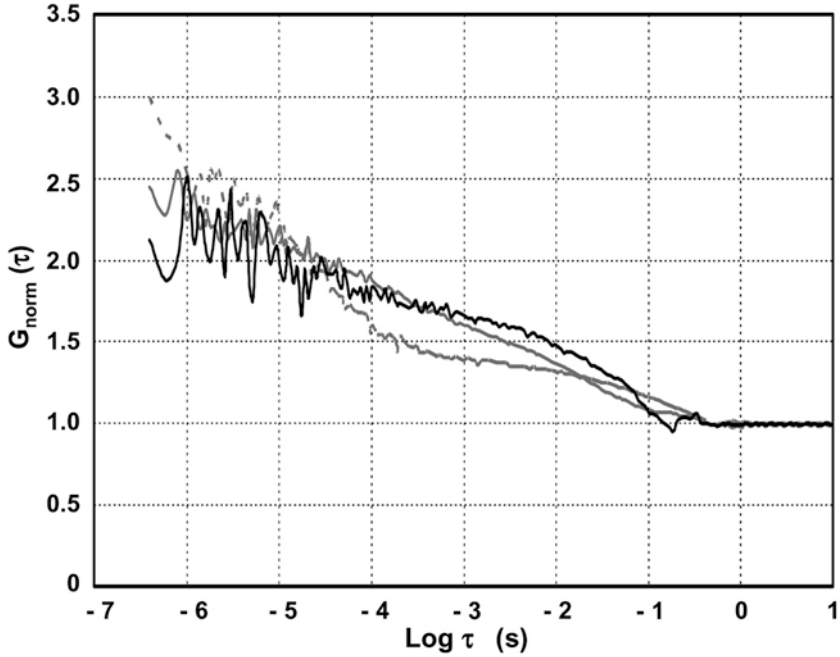

Fig. 6 FCS measurements of CRF_1R.Kaede in live transiently transfected HEK293 cells. The GPCR–Kaede fusion was expressed in transiently transfected HEK293 cells. Prior to the FCS measurements, approximately 50 % of the green GPCR–PCFP fusion proteins were photoconverted to red. Normalized auto- (AC, *grey* = gKaede, *dotted grey* = rKaede) and cross-correlation (CC, *black*) curves are shown

and store at 4 °C. Use within 2 weeks. DMEM GlutaMAX can also be used.

3. Krebs-Ringer HEPES (KRH) buffer: 125 mM NaCl, 3 mM KCl, 1 mM NaH_2PO_4, 1.2 mM $MgSO_4$, 2.4 mM $CaCl_2$, 22 mM $NaHCO_3$, 5.5 mM glucose, 10 mM HEPES; pH 7.4.
4. Dulbecco's phosphate-buffered saline (DPBS) solution: 137 mM NaCl, 2.7 mM KCl, 1.5 mM KH_2PO_4, 8.0 mM Na_2HPO_4, 0.9 mM $CaCl_2$, 0.5 mM $MgCl_2$; pH 7.4.
5. FCM tubes: Tubes for flow cytometric detection can be purchased in different sizes from several vendors, e.g., Cotech, Merck, or BD Biosciences.
6. Round cover slips (thickness between 125 and 170 μm, preferred diameter is 24–30 mm) or alternatively dishes having cover slips included.
7. Poly-L-lysine as solid substance or in sterile solution (100 mg/ml); storage for several months at 4 °C is possible.
8. Cell culture dishes in different diameter.
9. Holder for cover slips and heating unit for motorized or manual XY stage: Holders for cover slips, inserts, heating units, as well as heating/CO_2 incubation chambers are commercially available from PeCon GmbH (Erbach, Germany) or from Carl Zeiss Microscopy GmbH (Jena, Germany).

3 Methods

3.1 Analysis of GPCR Trafficking/Recycling Using PCFP Fusions and Confocal Laser Scanning Microscopy

The usage of GPCR–PCFP fusions allows the analysis of subcellular GPCR trafficking in real time. A detailed description of a recycling assay based on GPCR–PCFP fusions is given below. Internalized receptors are photoconverted in endosomes, and trafficking of the resulting red receptor population to either the plasma membrane (recycling) or the lysosomes (degradation) is monitored.

1. Seed cells in a cell culture dish with a thin plastic bottom (100,000–200,000 cells/dish) (*see* **Note 3**).
2. In case of transient transfection, transfect cells with plasmids encoding the GPCR–PCFP fusions 24 h after seeding (*see* **Note 4**).
3. Replace the medium by agonist-containing medium 24 h after transfection (or 24 h after seeding in case of stably transfected cells), and incubate the cells at 37 °C until the receptors are completely internalized (*see* **Note 5**).
4. Replace the agonist-containing medium by 500 ml pre-warmed (37 °C) DPBS containing an excess of a specific antagonist to prevent internalization of already recycled receptors.
5. Use objectives with magnifications of 63× or 100×. Add a small drop of oil onto the objective (inverted microscope). Use a heating/CO_2 incubation chamber in case of a longer detection period at 37 °C (e.g., for time series for more than 1 h) (*see* **Note 6**). Put the dish into the heating chamber fixed at the microscope stage (*see* **Note 7**).
6. Select a detection mode for two channels in "line scan". The settings to detect the green Kaede (or green mKikGR) and the red Kaede (or red mKikGR) fluorescence signals in the two channels are provided in Table 2.
7. Identify cells in which the GPCR–PCFP fusion is completely located in endosomes, and adjust the settings to record an image prior to photoconversion.
8. Select a region of interest (ROI) around a condensed endosomal compartment (*see* **Note 8**).
9. Completely photoconvert the fusion protein from green to red in the ROI using a UV laser (364 nm) or a diode laser (405 nm) (*see* **Note 9**).
10. Adjust the time period required to analyze receptor recycling, and define the number of scans to be recorded (e.g., 15 scans in 5-min intervals; *see* **Note 10**). Record the time series.

Table 2
LSM settings for the analysis of PCFPs

Fluorophore	Laser line (nm)	Main beam splitter	Scan mode	Channel	Emission filter
gKaede/gKikGR	488	MBS 488	Frame	1	BP 494–550
rKaede/rKikGR	561	MBS 561	Frame	2	BP 565–650
gKaede/gKikGR	488	MBS 488/561	Line	1	BP 494–550
rKaede/rKikGR	561	MBS 488/561	Line	2	BP 565–650
gKaede/gKikGR	488	MBS 488	Frame	1	BP 494–540
rKaede/rKikGR	543	MBS 543	Frame	2	BP 550–650
gKaede/gKikGR	488	MBS 488/543	Line	1	BP 494–540
rKaede/rKikGR	543	MBS 488/543	Line	2	BP 550–650

The table summarizes the excitation wavelengths, beam splitters, and emission filters for the analysis of the red and green fluorescent form of the photoconvertible fusion proteins Kaede and KikGR. Settings are shown using the "Multi-track" mode of the LSM in "Frame" and "Line" scanning option and different excitation wavelength for the red fluorescent form (543 nm and 561 nm, respectively). For the photoconversion from the green fluorescent to the red fluorescent form an additional laser line of 364 nm or 405 nm is necessary and the corresponding main beam splitter, respectively

11. Finally, the time-resolved increase or decrease of the red and green fluorescence signals of the GPCR–PCFP fusions is quantified in the subcellular compartments of interest. To this end, the recorded images are analyzed using either freeware (e.g., ImageJ) or the software provided by the microscope manufacturer (e.g., ZEN2010, Carl Zeiss Microimaging GmbH, Jena, Germany).

3.2 Analysis of GPCR Biosynthesis Using PCFP Fusion and FCM Measurements

The biosynthesis of GPCR–PCFP fusions can also be monitored microscopically at a single-cell level as described above. If more quantitative data are required, FCM measurements should be performed. A detailed description of the FCM methodology regarding this issue is given below.

1. Seed cells in 60 mm or 35 mm cell culture dishes (600,000 or 300,000 cells/dish, respectively) or in 6-well plates (300,000 cells/well) (*see* **Note 3**).
2. In case of transient transfection, transfect cells with plasmids encoding the GPCR–PCFP fusions 24 h after seeding (*see* **Note 4**).
3. Optional: Add substances influencing biosynthesis 24 h after transfection (or 24 h after seeding in the case of stably transfected cells).
4. Completely photoconvert the GPCR–PCFP fusions from green to red (*see* **Note 11**).
5. After defined time intervals, wash cells twice with DPBS (2 ml/60 mm dish; 1 ml/35 mm dish). After each washing step centrifuge at 700 × *g* for 5 min at 4 °C, remove the buffer, and add new buffer (resuspend by slight vortexing).

Table 3
FCM settings for the analysis of PCFPs

Flow cytometer: For example, FACSCalibur (Becton Dickinson GmbH, Heidelberg, Germany)							
Fluorophore	**Laser line (nm)**	**Beam splitter**	**Beam splitter**	**Flow velocity**	**Emission (nm)**	**Time limit (s)**	**Events**
gKaede/gKikGR	488	SP 560	–	Middle	530 ± 15	10	10,000
rKaede/rKikGR	488	SP 560	LP 640	Middle	585 ± 21	10	10,000

The table summarizes the main setting parameters for the analysis of Kaede and KikGR fluorescent signals at the flow cytometer, which can be used for the live cell imaging of G protein-coupled receptors. The necessary photoconversion from the green fluorescent to the red fluorescent form must be performed prior to the flow cytometer measurements

6. Resuspend cells in DPBS (*see* **Note 12**) for the FCM measurements.
7. Using the settings provided in Table 3, two-channel FCM experiments can be performed (*see* **Note 13**).
8. Time-resolved data for the synthesis of the GPCR–PCFP fusions (green signals) can be generated using the software provided by the system (*see* **Note 14**).

3.3 Analysis of GPCR Interactions Using PCFP Fusions and FCS Measurements

To quantify the (homo-) oligomerization of GPCRs, PCFP fusions and FCS measurements can be used. After photoconversion of 50 % of the GPCR–PCFP fusions, auto- and cross-correlation functions can be derived out of the green and red fluorescence signals. A description of this technique is given below.

1. Autoclave glass cover slips (Ø 30 mm) or wash them with 70 % (v/v) ethanol. Place dried cover slips in a petri dish (Ø 35 mm), and coat them with poly-L-lysine (20 mg/ml) for 20 min at room temperature to improve adherence of the cells (*see* **Note 15**). Remove the poly-L-lysine solution, and let the cover slips dry for 1 h.
2. Seed the cells on the cover slips (150,000–300,000 cells/dish) (*see* **Note 3**).
3. In case of transient transfection, transfect cells with plasmids encoding the GPCR–PCFP fusions 24 h after seeding (*see* **Note 4**).
4. Transfer cover slips to a holder, and cover cells with DPBS; avoid fluid leaks. Remove any remaining fluid from the bottom of the cover slip.
5. Use objectives suitable for FCS recordings. Place the holder with the cover slip on the microscopic stage.
6. Select a detection mode for two channels in the LSM mode of the microscope. The settings to detect the green Kaede

Table 4
LSM settings for the FCS measurements of PCFPs

Fluorophore	Laser line (nm)	Main beam splitter	Beam splitter	Channel	Emission filter	Acquisition time (s)	Repetitions
gKaede/ gKikume	488	MBS 488/561	NFT 565	2	BP 505–540	2	50
rKaede/ rKikume	561	MBS 488/561	NFT 565	1	LP 560	2	50
gKaede/ gKikume	488	MBS 488/543	NFT 545	2	BP 505–530	2	50
rKaede/ rKikume	543	MBS 488/543	NFT 545	1	LP 560	2	50

The table summarizes the excitation wavelengths, beam splitters, emission filters, and acquisition times for the FCS measurements of the photoconvertible fusion proteins Kaede and KikGR, which can be used for live cell imaging of G protein-coupled receptors. The necessary photoconversion from the green fluorescent to the red fluorescent form must be performed prior to the FCS recordings

(or green mKikGR) and the red Kaede (or red mKikGR) fluorescence signals in the two channels are provided in Table 2. Take the initial image using these settings (*see* **Note 16**).

7. After selection of a suitable cell, 50 % of the GPCR–PCFP fusions are photoconverted (*see* **Note 17**).
8. Focus to the apical or the basal membrane of the cell (lateral measurements are not useful). Use the FCS mode and select a point (cross hair) in the plasma membrane where the FCS recording should take place. Make sure that the fluorescence intensities are homogeneous in the surrounding area.
9. Use the parameters provided in Table 4 to perform the FCS recordings in the FCS mode of the LSM. Laser intensities should be as low as possible.
10. For the analysis of the FCS data, the software provided by the manufacturer of the microscope is used. The recorded intensity traces are transformed using the auto- and cross-correlation functions and subsequently fitted. In the case of integral membrane proteins like the GPCR–PCFP fusions, a two-dimensional diffusion equation should be used for fitting and the triplet state should be considered.
11. For each cell, the fitted single measurements (e.g., 50×2 s) are finally averaged by the microscope software. If single FCS recordings did not meet all the characteristics of a correlation function (e.g., conversion to 1), they can be excluded from the analysis (and from the average) (*see* **Note 18**).
12. Using the final average curves, protein–protein interactions can be determined out of the values of the amplitudes

(the amplitude of cross-correlation in relation with the lowest amplitude of the auto-correlation). Those values might be corrected once more.

13. FCS recordings should be conducted on at least 100 cells, and the final cross-correlation values describing protein–protein interactions should be displayed in a histogram.

4 Notes

1. GPCRs possess an extracellular N tail which must be translocated across the ER membrane during the ER insertion. This process may be impaired by N-terminal PCFP fusions. Moreover, the N tail of some GPCRs is involved in ligand binding and N-terminal fusions may also influence this process. Thus, PCFPs should be fused C-terminally. Even in this case, however, the functionality of a GPCR–PCFP fusion (ligand binding, second messenger formation) should be checked in comparison to the untagged receptor.
2. For LSM, medium without phenol red is preferred since light absorption is reduced compared to medium containing this pH indicator.
3. The LSM analysis of GPCR–PCFP fusions is usually carried out using non-confluent cells (30–50 % of confluence). Confluent cells, however, should be used for the analysis of polarized cells or cell/cell interaction mechanisms.
4. The various transfection methods (e.g., lipofection, electroporation, nucleofection, calcium phosphate precipitation) work well but depend on the cell type used. Transfections should always be optimized using different DNA concentrations. Nonetheless, the use of stable transfected cell clones is more comfortable and often leads to more convincing results since the cell clones have usually a more uniform expression pattern in comparison to transiently transfected cells. For all experiments, it is also recommended to adjust the time required for expression and proper sorting of the protein of interest. Plasma membrane staining of transiently transfected GPCR–PCFP fusions is usually observed 12–24 h after transfection. When proteins fold and assemble inefficiently, however, it may take up to 48–96 h until they can be detected at the cell surface.
5. For a receptor recycling experiment, receptors should be internalized completely. The time needed should be determined in initial experiments.
6. In case of using a heating chamber it should be preinstalled to reduce the temperature gradient between the microscope and

the microscope stage (including the heating chamber and the culture dish). Otherwise, a drift in *z* direction may occur. The "Definite Focus" option of the microscope should be used (if available) which helps to correct this drift. The focus may also be corrected manually, but in this case, time series should not be recorded using automated picture scanning procedures.

7. Try to use small volumes for the analysis to keep the amount of ligand as small as possible. However, the volume of ligand solution should be sufficiently large to guarantee its proper distribution. When the dish is mounted in a temperature-controlled insert, beware of evaporation of the medium. Evaporation can be reduced by capping the dish with a lid and by adjusting the LSM parameters quickly. If the ligands are added to the cells during time series, make sure that the lid can be removed quickly.
8. Upon ligand-induced internalization, most GPCRs are sorted into a condensed, perinuclear endosomal compartment, which can be easily marked using the ROI setting functions of the LSM software. If this perinuclear compartment is not detectable, the receptor of interest may recycle very rapidly from early endosomes to the plasma membrane. Be careful to adjust the ROI as small as possible to avoid photoconversions in other subcellular compartments (such as the ER).
9. The settings to photoconvert the PCFPs from green to red are given in Table 2. Depending on the properties of the LSM, photoconversion may be achieved using 364 or 405 nm excitation. The laser intensities and exposure time for complete photoconversion should be tested in initial experiments. When the settings are known, photoconversion can be included into the time series using the "bleaching" function of the LSM software.
10. The intervals for scanning in a time series should meet the experimental needs. In case of internalization or recycling analyses, the time to complete the experiment usually ranges from 10 to 60 min depending on the individual GPCRs. Note that prolonged or inappropriate frequent scanning may not only cause fluorophore bleaching but also affect cell viability (e.g., by lipid peroxidation). Thus intervals in the range of 1–5 min are recommended.
11. Complete photoconversion of the GPCR–PCFP fusions in the entire culture dish or a well plate exceeds the capabilities of an LSM. A conventional UV lamp is required in this case which is able to illuminate the whole culture dish with UV light of sufficient intensity. The exposure time necessary for complete photoconversion must be determined in initial experiments. The rate of photoconversion can be assessed using a conventional fluorescence microscope.

12. The buffer volume to detach the cells should be as small as possible (e.g., 400 ml for a 35 mm dish). Rinse cells with buffer several times to detach, and resuspend them. More adherent cells may necessitate the use of a cell scraper.
13. Cells expressing soluble forms of the original and photoconverted PCFPs (empty vector plasmids) are also required to eliminate the background and cross talk during the analysis. A drawback of this method is that cells cannot be used for additional studies after the experiment. This means that detection in defined time intervals is only possible using different, simultaneously treated culture dishes.
14. Data of the FCM device may also be exported as Excel files.
15. While coating cover slips with poly-L-lysine, avoid fluid excess beneath the glass since this would cause floating of the cover slip and coating of the wrong side. Moreover, an excess of fluid is difficult to remove by washing and might be released into the medium during cultivation consequently causing cell growth inhibition. It is recommended to use only 500 ml of the poly-L-lysine solution for 30 mm cover slips. Pre-coated cover slips should be used within a few days. After seeding of the cells, make sure that cover slips lie on the ground of the culture dish. Otherwise, cells will also grow on the bottom of the cover slip and thereby affect image quality. It is recommended to use 30 mm diameter cover slips since this size allows scanning of different areas of the cover slip when using objectives with higher magnification (smaller cover slips of, e.g., 10 mm in diameter allow only the center to be scanned under these conditions).
16. Due to the single-molecule detection mode of the FCS measurements, it is highly recommended to use cells expressing low levels of the GPCR–PCFP fusions. Therefore, standard configurations should be changed to cover weak fluorescent cells (i.e., open pinhole and high detector gain). Only cells which are visible under these optimized settings are suitable for FCS analyses (weak expression of the GPCR–PCFP fusions). Under optimal settings (only a few molecules are detected, but the value count/molecule is larger than 1), the recorded trace of fluctuations should not be adulatory since this could cause artefacts.
17. Since the quantum yields of the green and the red fluorescent forms of the PCFPs differ substantially and the amount of laser energy is usually unknown, it is recommended to monitor only the green channel during the photoconversion process. The cells need to be illuminated with 364 or 405 nm until the intensity of the green fluorescence is halved (try different steps with different energies).

18. The excluded values usually represent the initial curves which suffer from some bleaching characteristics or curves which do not converge to the value 1. Note that the detection time for FCS recordings depends on the diffusion time of the detected molecule. The rule of thumb is to detect 10,000 times longer than the particular diffusion time of the molecule itself (e.g., cytosolic protein detection approx. 10 s but membrane proteins approx. 100 s).

Acknowledgments

We thank Claudia Rutz for useful discussions and help in preparing the experiments. Jenny Eichhorst helped in analyzing the microscopic data and Bettina Kahlich in cell culture.

References

1. Prasher D, Eckenrode V, Ward W et al (1992) Primary structure of the Aequorea victoria green-fluorescent protein. Gene 111:229–233
2. Ando R (2002) An optical marker based on the UV-induced green-to-red photoconversion of a fluorescent protein. Proc Natl Acad Sci U S A 99:12651–12656
3. Rizo MA, Davidson MW, Piston WW (2010) Fluorescent protein tracking and detection: fluorescent protein structure and color variants. In: Goldmann RD, Swedlow JR, Spector DL (eds) Live cell imaging: a laboratory manual, 2nd edn. Cold Spring Harbor Laboratory Press, New York, USA, pp 3–34
4. Hayashi I, Mizuno H, Tong KI et al (2007) Crystallographic evidence for water-assisted photo-induced peptide cleavage in the stony coral fluorescent protein Kaede. J Mol Biol 372:918–926
5. Tsutsui H, Shimizu H, Mizuno H et al (2009) The E1 mechanism in photo-induced beta-elimination reactions for green-to-red conversion of fluorescent proteins. Chem Biol 16: 1140–1147
6. Habuchi S, Tsutsui H, Kochaniak AB et al (2008) mKikGR, a monomeric photoswitchable fluorescent protein. PLoS One 3:e3944
7. Drews J (2000) Drug discovery: a historical perspective. Science 287:1960–1964
8. Ma P, Zemmel R (2002) Value of novelty? Nat Rev Drug Discov 1:571–572
9. Salon JA, Lodowski DT, Palczewski K (2011) The significance of G protein-coupled receptor crystallography for drug discovery. Pharmacol Rev 63:901–937
10. Magalhaes AC, Dunn H, Ferguson SS (2012) Regulation of GPCR activity, trafficking and localization by GPCR-interacting proteins. Br J Pharmacol 165:1717–1736
11. Nejsum LN, Christensen TM, Robben JH et al (2011) Novel mutation in the AVPR2 gene in a Danish male with nephrogenic diabetes insipidus caused by ER retention and subsequent lysosomal degradation of the mutant receptor. NDT Plus 4:158–163
12. Schwieger I, Lautz K, Krause E et al (2008) Derlin-1 and p97/valosin-containing protein mediate the endoplasmic reticulum-associated degradation of human V2 vasopressin receptors. Mol Pharmacol 73:697–708
13. Vembar SS, Brodsky JL (2008) One step at a time: endoplasmic reticulum-associated degradation. Nat Rev Mol Cell Biol 9:944–957
14. Vassart G, Costagliola S (2011) G protein-coupled receptors: mutations and endocrine diseases. Nat Rev Endocrinol 7:362–372
15. Ferguson SS (2001) Evolving concepts in G protein-coupled receptor endocytosis: the role in receptor desensitization and signaling. Pharmacol Rev 53:1–24
16. Luttrell LM (2008) Reviews in molecular biology and biotechnology: transmembrane signalling by G protein-coupled receptors. Mol Biotechnol 39:239–264
17. Kreuchwig A, Kleinau G, Kreuchwig F et al (2011) Research resource: update and extension

of a glycoprotein hormone receptors web application. Mol Endocrinol 25:707–712

18. Kleinau G, Brehm M, Wiedemann U et al (2007) Implications for molecular mechanisms of glycoprotein hormone receptors using a new sequence-structure-function analysis resource. Mol Endocrinol 21:574–580
19. Khelashvili G, Dorff K, Shan J et al (2010) GPCR-OKB: the G protein coupled receptor oligomer knowledge base. Bioinformatics 26: 1804–1805
20. Skrabanek L, Murcia M, Bouvier M et al (2007) Requirements and ontology for a G protein-coupled receptor oligomerization knowledge base. BMC Bioinformatics 8:177
21. Albizu L, Cottet M, Kralikova M et al (2010) Time-resolved FRET between GPCR ligands reveals oligomers in native tissues. Nat Chem Biol 6:587–594
22. Urizar E, Montanelli L, Loy T et al (2005) Glycoprotein hormone receptors: link between receptor homodimerization and negative cooperativity. EMBO J 24:1954–1964
23. El-Asmar L, Springael JY, Ballet S et al (2005) Evidence for negative binding cooperativity within CCR5-CCR2b heterodimers. Mol Pharmacol 67:460–469
24. Mesnier D, Banères JL (2004) Cooperative conformational changes in a G-protein-coupled receptor dimer, the leukotriene B(4) receptor BLT1. J Biol Chem 279:49664–49670
25. George SR, Fan T, Xie Z et al (2000) Oligomerization of μ- and δ-opioid receptors: generation of novel functional properties. J Biol Chem 275:26128–26135
26. Charles AC, Mostovskay N, Asas K et al (2003) Coexpression of δ-opioid receptors with μ receptors in GH3 cells changes the functional response to μ agonists from inhibitory to excitatory. Mol Pharmacol 63:89–95
27. Mellado M, Rodríguez-Frade JM, Vila-Coro AJ et al (2001) Chemokine receptor homo- or heterodimerization activates distinct signaling pathways. EMBO J 20:2497–2507
28. Allen MD, Neumann S, Gershengorn MC (2011) Occupancy of both sites on the thyrotropin (TSH) receptor dimer is necessary for phosphoinositide signaling. FASEB J 25:3687–3694
29. Pin JP, Comps-Agrar L, Maurel D et al (2009) G-protein-coupled receptor oligomers: two or more for what? Lessons from mGlu and GABAB receptors. J Physiol 587:5337–5344
30. Terrillon S, Barberis C, Bouvier M (2004) Heterodimerisation of V1a and V2 vasopressin receptors determines the interaction with β-arrestin and their trafficking patterns. Proc Natl Acad Sci U S A 101:1548–1553
31. Schmidt A, Wiesner B, Weisshart K et al (2009) Use of Kaede fusions to visualize recycling of G protein-coupled receptors. Traffic 10:2–15
32. Juliano RL, Carver K, Cao C et al (2013) Receptors, endocytosis, and trafficking: the biological basis of targeted delivery of antisense and siRNA oligonucleotides. J Drug Target 21:27–43
33. Westendorf C, Schmidt A, Coin I et al (2011) Inhibition of biosynthesis of human endothelin B receptor by the cyclodepsipeptide cotransin. J Biol Chem 286:35588–35600
34. Elson EL (2001) Fluorescence correlation spectroscopy measures molecular transport in cells. Traffic 2:789–796
35. Rigler R, Mets U, Widengren J et al (1993) Fluorescence correlation spectroscopy with high count rate and low background: analysis of translational diffusion. Eur Biophys J 22:169–175
36. Haustein E, Schwille P (2003) Ultrasensitive investigations of biological systems by fluorescence correlation spectroscopy. Methods 29: 153–166

Chapter 10

HaloTag as a Tool to Investigate Peroxisome Dynamics in Cultured Mammalian Cells

Marc Fransen

Abstract

Peroxisomes are multifunctional organelles that can rapidly modulate their morphology, number, and function in response to changing environmental stimuli. Defects in any of these processes can lead to organelle dysfunction and have been associated with various inherited and age-related disorders. Progress in this field continues to be driven by advances in live-cell imaging techniques. This chapter provides detailed protocols for the use of HaloTag to fluorescently pulse-label peroxisomes in cultured mammalian cells. In contrast to the use of classical fluorescent proteins, this technology allows researchers to optically distinguish pools of peroxisomal proteins that are synthesized at different time points. The protocols can be easily adapted to image the dynamics of other macromolecular protein assemblies in mammalian cells.

Key words HaloTag, Protein labeling, Pulse-labeling, Live-cell imaging, Time-lapse microscopy, Protein trafficking, Organelle dynamics, Peroxisomes

1 Introduction

Over the past few decades, fluorescence microscopy has often become the first method of choice to study intracellular protein trafficking and organelle dynamics. Most live-cell imaging approaches make use of fluorescent proteins (FPs), such as green or red fluorescent protein (GFP or RFP), that are fused to a protein of interest (POI) or a signal sequence that targets the protein to a specific subcellular location by recombinant DNA techniques [1]. Although these fluorescent reporter proteins are excellent tools for monitoring protein localization and organelle dynamics, they do not allow researchers to optically distinguish pools of proteins and organelles that are synthesized at different time points. To overcome this problem, several alternative strategies have been developed. For example, one can employ (1) photoactivatable or photoswitchable FPs that are capable to change their spectral properties in response to irradiation with light of specific wavelengths [2], (2) fluorescent timer proteins that change their emission spectrum

Andrei I. Ivanov (ed.), *Exocytosis and Endocytosis*, Methods in Molecular Biology, vol. 1174,
DOI 10.1007/978-1-4939-0944-5_10,

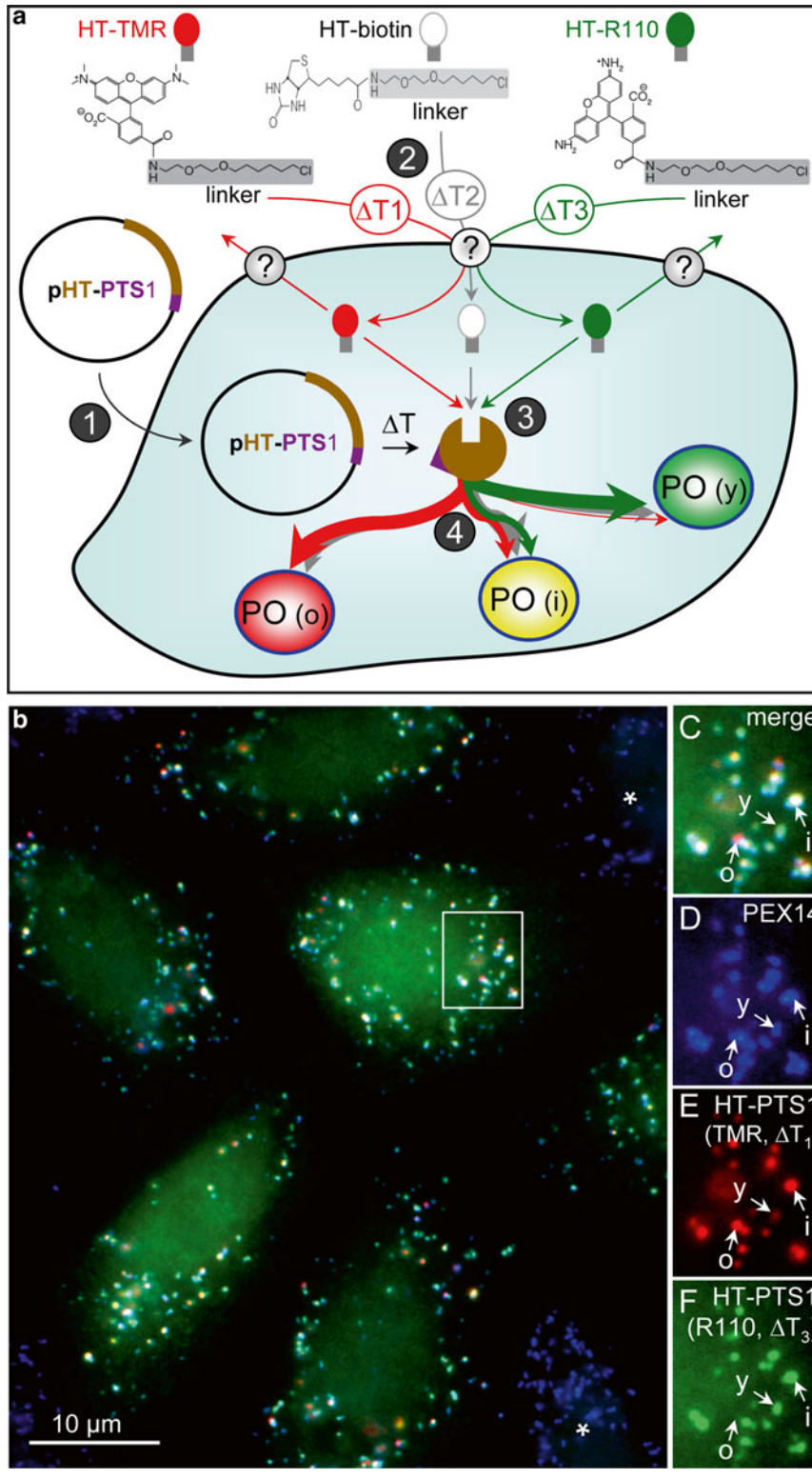

Fig. 1 Overview of the HaloTag protein-mediated pulse-labeling strategy to visualize peroxisomes in living mammalian cells. (**a**) Schematic overview of a dual-color labeling protocol. (1) Mammalian cells are transfected with a plasmid encoding a peroxisome-targeted HT-fusion protein (e.g., HT-PTS1). (2) The cells are sequentially incubated with HT-TMR, HT-biotin, and HT-R110. After each labeling reaction, the cells are extensively washed. The precise mechanisms of how these HT ligands are transported across the plasma membrane

over time [3], or (3) chemistry- or enzyme-based *in cellulo* labeling methods [4]. This chapter outlines detailed protocols for the use of a dehalogenase-based protein fusion tag, the HaloTag (HT), to study peroxisome dynamics in cultured mammalian cells [5, 6].

The HT labeling system consists of two components: the HT reporter protein and HT ligands [7]. The reporter protein is a genetically engineered bacterial monomeric haloalkane dehalogenase of 33 kDa, designed to irreversibly bind to synthetic chloroalkane derivatives, and the ligands are composed of a reactive chloroalkane linker and a functional group (e.g., fluorescent dyes, affinity handles) (Fig. 1a). As (1) eukaryotic cells lack any endogenous equivalent of the HT protein, (2) this reporter protein can be genetically fused to any POI, (3) the resulting fusion proteins bind with high efficiency and specificity to plasma membrane-permeable HT ligands, and (4) these ligands are not toxic for cells, the HT platform is an ideal technology for the imaging of spatial and temporal changes of specific intracellular structures [8, 9].

In the context of this chapter, it is important to point out that peroxisomes are dynamic cell organelles that play an important role in various cellular processes (for more details, see [10] and references therein) and that—as disturbances in peroxisome shape and number have been linked with various disease conditions [11–14]—the investigation of peroxisome morphology, distribution, and dynamics has become an exciting new field in cell biology and biomedical sciences [15]. This chapter discusses strategies and protocols that can be used to fluorescently pulse-label peroxisomes in living mammalian cells. The protocols cover all steps from cell culture and transfection to labeling and cell imaging. Importantly, as CHO-K1 and COS-7 are often the preferred cell lines to study peroxisome dynamics [5, 16, 17], and—in the author's laboratory—the Neon Transfection System (Promega) is regarded as one of the most reliable and efficient methods to transfect mammalian cells, these protocols are optimized for these particular settings. However, they can be easily adapted to study peroxisome dynamics in other mammalian cells or cell lines.

Fig. 1 (continued) are currently unknown (these ligands cannot freely cross the peroxisomal membrane). (3) Once inside the cell, the ligands can covalently bind to HT-PTS1. (4) The ligand-bound HT-PTS1 molecules are subsequently transported to and imported into peroxisomes (PO), whose import competence changes during their life-span. By employing this protocol, one can visualize peroxisomes of old (o), intermediate (i), and young (y) age. (**b**) Visualization of distinct peroxisome population in CHO-K1 cells. CHO-K1 cells, transiently transfected with a plasmid encoding HT-PTS1, were sequentially incubated with red fluorescent HT-TMR (0–44 h post-transfection), HT-biotin (44–68 h post-transfection), and green fluorescent HT-R110 (68–80 h post-transfection). The cells were fixed and immunostained for PEX14, a peroxisomal membrane protein (*blue color*). Non-transfected cells are indicated with an *asterisk*. Note that the diffuse green staining pattern observed in the transfected cells represents HT-R110-labeled HT-PTS1 that is not yet imported into peroxisomes. The scale bar represents 10 μm. (**c–f**) Enlargements of the outlined region in panel **b**. The positions of a young (y), "intermediate" (i), and old (o) peroxisome are indicated by *arrows*

2 Materials

All solutions, materials, and equipment coming into contact with living cells must be sterile, and aseptic techniques should be employed at all times.

2.1 HaloTag Components

1. Plasmids encoding peroxisome-targeted HT fusion proteins can be obtained from Promega (*see* **Note 1**) or created by conventional cloning strategies (*see* **Note 2**). The noncommercial plasmids pHT-PTS1 (*see* **Note 3**), pHT-HsCatalase (*see* **Note 4**), and pHT-HsPEX16 (*see* **Note 5**) are freely available from the author upon request.
2. HaloTag ligands (Promega): 5 mM Solution of HaloTag tetramethylrhodamine (HT-TMR, λex/λem: 555/585), 100 μM solution of HaloTag R110Direct (HT-R110, λex/λem: 498/528), and 5 mM solution of HaloTag biotin (HT-biotin) (*see* **Note 6**).

2.2 Cell Culture Components

1. Liquid nitrogen container for cell storage.
2. 37 °C Water bath.
3. Biological safety cabinet (*see* **Note 7**).
4. Humidified incubator (95 % air, 5 % CO_2, 37 °C).
5. Inverted light microscope (200-fold magnification).
6. Mammalian cell counter.
7. Vacuum aspiration system.
8. Biological waste container.
9. Cell-freezing device (cooling rate: 1 °C/min).
10. −80 °C Freezer.
11. Cryopreserved COS-7 cells (American Type Culture Collection CRL-1651) (*see* **Note 8**).
12. Cryopreserved CHO-K1 cells (American Type Culture Collection CCL-61) (*see* **Note 9**).
13. T-25 cell culture flasks.
14. Plastic pipettes (1, 5, and 10 ml).
15. Glass Pasteur pipettes.
16. Cryovials (2 ml).
17. Modified Eagle's medium-alpha (MEMα) with or without phenol red (store at 4 °C).
18. Heat-inactivated fetal bovine serum (FBS) (store at −20 °C).
19. Glutamax (100×): 200 mM L-Alanyl-L-glutamine dipeptide in 0.85 % (w/v) NaCl (store at −20 °C).
20. MycoZap antibiotics (500×) (store at −20 °C).

21. Cell culture-grade DMSO (store at room temperature).
22. Complete growth medium: MEMα, 10 % (v/v) FBS, 2 mM Glutamax, 1× MycoZap antibiotics (store at 4 °C).
23. Freezing medium: MEMα, 20 % (v/v) FBS, 2 mM Glutamax, 20 % DMSO (prepare fresh).
24. Thawing medium: MEMα, 20 % (v/v) FBS, 2 mM Glutamax (prepare fresh).
25. Dulbecco's phosphate-buffered saline without Ca^{2+} and Mg^{2+} (D-PBS): 8.06 mM Na_2HPO_4, 1.47 mM KH_2PO_4, 137.93 mM NaCl, 2.67 mM KCl (store at 4 °C).
26. Trypsin/EDTA (1×): 0.05 % (w/v) Trypsin, 0.68 mM EDTA, 5.5 mM glucose, 137.93 mM NaCl, 5.36 mM KCl, 6.9 mM $NaHCO_3$, 0.0002 % (w/v) phenol red (store at −20 °C).
27. Ethanol, 70 % (v/v).
28. MycoZap spray.
29. Liquid nitrogen.
30. Isopropyl alcohol, 100 % (v/v).

2.3 Transfection Components

1. Neon Transfection System: Pipette station, pipette, 10 µl tips, tubes, electrolyte buffer E, resuspension buffer R (Invitrogen).
2. Tabletop centrifuge equipped with a swing-out rotor for 15 ml conical tubes.
3. 15 ml conical tubes.
4. 1.5 ml microcentrifuge tubes.
5. Adjustable-volume pipettes (covering 1–1,000 µl) and pipette tips.
6. Cover glass bottom Fluorodish cell culture dishes—35 mm (FD35) (World Precision Instruments).
7. Plasmid DNA in deionized water (1 µg/µl) (*see* **Note 10**).

2.4 Fluorescence Imaging Components

1. Cell-M live-cell imaging station: Inverted motorized IX-81 microscope, temperature-controlled incubation chamber, CO_2-enrichment workhead, gas preheater and humidifier, motorized stage, insert for 35 mm dishes, 150 W Xenon-Arc lamp, 10× ocular lens, Universal Plan Super Apochromat oil immersion objectives with 60× and 100× magnification, U-MNIBA3 (excitation filter: 470–495; emission filter: 510–550; dichromatic mirror: 505) and U-MWIY2 (excitation filter: 545–580; emission filter: 610IF; dichromatic mirror: 600) filter cubes, CCD-FV2T digital black and white camera, Cell-M software (Olympus).
2. 5 % CO_2/air mixture.
3. Image analysis and particle detection software (Olympus).

3 Methods

All incubations are performed in a humidified incubator (95 % air, 5 % CO_2, 37 °C) unless specified otherwise.

3.1 Culturing of COS-7 and CHO-K1 Cells

Thawing and recovery protocol

1. Remove a vial of cells from the liquid nitrogen storage container and immediately place into a 37 °C water bath (*see* **Note 11**).
2. Wipe the vial with 70 % (v/v) ethanol immediately after thawing and before opening.
3. Transfer 500 μl of the thawed cell suspension to a T-25 cell culture flask containing 5 ml of thawing medium.
4. Confirm the next day by microscopy that the cells have attached to the growth surface of the flask, and replace the thawing medium with complete growth medium.

Subculturing protocol

5. Pre-warm D-PBS, trypsin/EDTA, and complete growth medium to 37 °C.
6. Remove all medium from the cell culture flask with a Pasteur pipette by vacuum aspiration, and wash the cells once with 5 ml of D-PBS.
7. Add trypsin/EDTA solution to the cells and swirl to cover the surface (1 ml/T-25 flask).
8. Aspirate the trypsin/EDTA solution, and incubate the cells for 2–5 min at room temperature or 37 °C (*see* **Note 12**).
9. Upon detachment, harvest the cells in complete growth medium (5 ml/T-25 flask) (*see* **Note 13**).
10. Pipette the cell suspension three times up and down to dislodge any remaining adherent cells.
11. Transfer the required amount of cells to a new T-25 cell culture flask, and add fresh medium to a final volume of 5 ml.
12. Refresh the cell culture medium every 3 days.
13. Repeat **steps 5–12** before the cells reach 100 % confluency.

Freezing protocol

14. Trypsinize cells (*see* **steps 5–10**) that are in a logarithmic growth phase (*see* **Note 14**).
15. Transfer the cell suspension to a 15 ml conical tube and centrifuge for 5 min at 500 × *g* at room temperature (cell suspensions from different T-25 flasks can be combined).
16. Remove the supernatant, and add freezing medium (0.5 ml/T-25 flask).

17. Transfer 1 ml aliquots of the cell suspension into 2 ml cryovials.
18. Transfer the vials to a cell-freezing container, which is filled with 100 % (v/v) isopropyl alcohol, and place the container in a −80 °C freezer overnight.
19. Transfer the vials to a liquid nitrogen cell storage container.

3.2 Electroporation of COS-7 and CHO-K1 Cells with the Neon Transfection System

Preparation of the cells

1. Cultivate the required number of cells (~5×10^4 cells/condition) in complete growth medium (*see* **Note 14**).
2. Trypsinize the cells (*see* Subheading 3.1, **steps 5–10**; use complete growth medium without antibiotics).
3. Transfer the cells to a 15 ml conical tube, and take an aliquot of the suspension for cell counting.
4. Pellet the cells by centrifugation at 500 × *g* for 5 min (at room temperature).
5. Resuspend the cells in 10 ml of D-PBS and pellet again (*see* **step 4**).
6. Carefully aspirate the supernatant, and resuspend the cells in resuspension buffer R at a final density of 5×10^6 cells/ml (*see* **Notes 15** and **16**).

Electroporation of the cells with plasmids encoding HaloTag fusion proteins

7. Place the Neon Electroporation device in a biological safety cabinet, and decontaminate the work surface and materials (e.g., pipettes) with 70 % (v/v) ethanol and MycoZap spray.
8. Set the pulse conditions on the device.
   - COS-7 → pulse voltage: 1,050 V; pulse width: 30 ms; pulse number: 2.
   - CHO-K1 → pulse voltage: 1,620 V; pulse width: 10 ms; pulse number: 3.
9. For each condition, add 2 ml of pre-warmed growth medium without antibiotics to an FD35 Fluorodish (*see* **Note 17**).
10. For each condition, pipette 2 µl of plasmid DNA (1 µg/µl) into a sterile 1.5 ml microcentrifuge tube (*see* **Notes 18** and **19**).
11. Gently transfer 20 µl of the cells to the microcentrifuge tubes containing the plasmid DNAs and pipette once up and down (*see* **Note 20**).
12. Fill a Neon tube with 3 ml of electrolyte buffer E, and insert the tube into the pipette station.
13. Mount a 10 µl Neon tip onto the Neon pipette (*see* **Note 21**).

14. Immerse the tip into a cell–DNA mixture, and slowly aspirate 10 μl of the sample. Make sure that there are no air bubbles in the tip.
15. Insert the pipette into the electrolyte buffer-containing tube in the pipette station, and press start on the touch screen.
16. After delivery of the electric pulse, remove the pipette from the pipette station and immediately transfer the sample from the tip to an FD35 Fluorodish.
17. Repeat **steps 14–16** (*see* **Note 22**).
18. Gently rock the Fluorodish back-forth and from side to side to assure an even distribution of the cells.
19. Discard the Neon tip in an appropriate biological hazardous waste container, and repeat **steps 12–18** for the remaining cell–DNA mixtures.
20. Incubate the cells in a humidified incubator (95 % air, 5 % CO_2, 37 °C) for at least 4 h (or overnight) to allow the cells to attach to the bottom of the Fluorodish (*see* **Note 23**).

3.3 Fluorescent Labeling of Cells Expressing an HT-Tagged Peroxisomal Protein

This section provides a detailed description of three different labeling protocols that can be used to fluorescently label peroxisomal HT-fusion proteins in COS-7 or CHO-K1 cells. These different protocols allow researchers to study various aspects of peroxisome dynamics in living cells, including protein targeting, the assembly of new peroxisomal structures, and the half-life of peroxisomal proteins. Importantly, as HT ligands cannot cross the peroxisomal membrane [5], the rapid labeling protocol cannot be used to pulse-label the preexisting pool of peroxisomal HT-fusion proteins that expose their tag to the matrix side of the organelle.

1. Pre-warm complete growth medium without phenol red to 37 °C (*see* **Note 24**).
2. Prepare a 10× working stock solution of HT ligand by diluting the commercial stock solution into pre-warmed complete growth medium lacking phenol red, and mix thoroughly (*see* **Notes 25–29**).
3. Aspirate the medium from the Fluorodish, and gently pipette 2 ml of pre-warmed FBS- and Glutamax-containing MEMα medium without phenol red onto the cells (repeat 1×).
4. Add 222 μl of the 10× HT ligand working stock solution to the Fluorodish, mix gently, and proceed to **steps 5**, **6**, or **10**.

Wash-free labeling protocol

5. Put the Fluorodish in the humidified incubator (95 % air, 5 % CO_2, 37 °C) until analysis (*see* **Notes 30** and **31**).

Rapid labeling protocol

6. Incubate the cells for 15 min in the humidified incubator (95 % air, 5 % CO_2, 37 °C).
7. Aspirate the ligand-containing medium, and gently pipette 2 ml of pre-warmed phenol red-free medium onto the cells (repeat 3×).
8. Repeat **steps 6** and **7** to wash out the unbound ligand.
9. Transport the sample to a fluorescence microscope for imaging (*see* **Note 31**).

Dual-color labeling protocol

10. Incubate the cells for the desired time period in the humidified incubator (95 % air, 5 % CO_2, 37 °C).
11. Aspirate the ligand-containing medium, and gently pipette 2 ml of warm fresh medium onto the cells (repeat 3×).
12. Incubate the cells for 15 min in the humidified incubator (95 % air, 5 % CO_2, 37 °C) to allow unbound fluorophores to diffuse out of cells.
13. Replace the medium with an equal volume of phenol red-free medium containing 5 μM HT-biotin, a non-fluorescent blocking ligand, to completely turn off fluorescent labeling of newly synthesized proteins.
14. Repeat **steps 10–12**.
15. Aspirate the medium from the Fluorodish, and gently pipette 2 ml of pre-warmed complete medium without phenol red onto the cells.
16. Add 222 μl of the second 10× fluorescent HT ligand working stock solution to the Fluorodish, mix gently, and proceed with **step 5**.

3.4 Live-Cell Imaging of Cells Expressing Fluorescently Labeled HT-Fusion Proteins

In the author's laboratory, a Cell-M live-cell imaging station (Olympus) is used to monitor the dynamics of fluorescently labeled peroxisomal HT-fusion proteins in mammalian cells. However, in case one has no access to instrumentation for live-cell imaging, one can always fix the cells at different time points and analyze the samples on a regular fluorescence microscope equipped with standard fluorescein or rhodamine filter sets and oil immersion objectives with 60× and 100× magnification.

1. Preheat the temperature-controlled incubation chamber to 37 °C (*see* **Note 32**).
2. Turn on the xenon-arc burner at least 15 min prior to starting imaging to give it time to stabilize.

3. Switch on the 5 % CO_2 enrichment accessory (*see* **Notes 33** and **34**).
4. Put a small drop of immersion oil on the objective, and place the Fluorodish in the dish holder (*see* **Note 35**).
5. Choose the appropriate configurations for the fluorophores to be imaged.
6. Adjust the light intensities according to the brightness of the sample (*see* **Note 36**).
7. Acquire multichannel images, time series, and/or *Z* stacks (*see* **Note 37**).
8. Analyze the images by using the image analysis and particle detection software (*see* **Note 38**).

4 Notes

1. www.promega.com/FindMyGene.
2. Plasmids designed for mammalian expression of N- or C-terminally tagged HT-fusion proteins are commercially available from Promega.
3. HT-PTS1 is a HaloTag reporter protein that is targeted to peroxisomes by genetically fusing it to PTS1, a targeting signal found at the extreme carboxy-terminus of most peroxisomal matrix proteins [10]. The protein has already been successfully used to demonstrate that (a) peroxisomes display an age-related heterogeneity with respect to their capacity to incorporate newly synthesized proteins (Fig. 1b–f), (b) peroxisomes do not exchange their matrix protein content, (c) the matrix protein content of preexisting peroxisomes is not evenly distributed over new organelles, and (d) peroxisomes in cultured mammalian cells have a half-life of approximately 2 days [5].
4. HT-HsCatalase is a HaloTag reporter protein that is targeted to peroxisomes by genetically fusing it to catalase, the most abundant peroxisomal antioxidant enzyme. The protein has already been successfully used to show that peroxisomal matrix and membrane proteins are targeted to distinct regions of peroxisomal structures [6].
5. HT-HsPEX16 is a HaloTag reporter protein targeted to peroxisomes by genetically fusing it to HsPEX16, a peroxisomal membrane protein involved in membrane biogenesis. The protein has already been successfully used to demonstrate that the turnover rate of at least some membrane proteins is much faster than that of matrix proteins and that its half-life can be extended by inhibiting the proteasome degradation pathway [5].

6. Aliquot and store at −20 °C. Avoid repeated freeze–thaw cycles, and protect from light.
7. Follow the biosafety guidelines of your institution.
8. COS-7 is a fibroblast-like cell line derived from African green monkey kidney tissue.
9. CHO-K1 is a fibroblast-like cell line derived from the ovary of a Chinese hamster.
10. Use your method of choice or one of the many commercially available kits for the preparation of transfection-quality plasmid DNA.
11. The cells should be thawed rapidly to prevent the formation of ice crystals that can cause cell lysis.
12. Regularly check on an inverted microscope if the cells start to detach (tap against the side of the flask to improve detachment; as over-trypsinization will decrease cell viability, the cells should only be exposed to trypsin/EDTA long enough to detach the cells).
13. As FBS contains trypsin inhibitors, adding this compound to MEMα will immediately inhibit further trypsin activity.
14. Ensure that the cells are healthy and actively growing (recommended confluency: 70–80 %; this corresponds to ~2×10^4 cells/cm^2).
15. As (a) depending on the method employed cell counting may be a time-consuming procedure and (b) storing the cell suspension for more than 15–30 min at room temperature may reduce cell viability and transfection efficiency, one can also directly resuspend the cell pellet from one T-25 flask in a final volume of 100 μl R1 buffer. This estimation will be reasonably accurate, providing that the guidelines given above are carefully followed.
16. Gently pipette the cell suspension ten times up and down to disperse cell clumps.
17. The addition of antibiotics and antimycotics to the culture medium can significantly reduce the viability of freshly transfected cells.
18. It is highly recommended to routinely include a mock-transfected condition as negative control.
19. In general, this amount of plasmid DNA yields excellent results. However, depending on the protein expressed, it may be necessary to increase or decrease the concentration of the plasmid DNA due to the fact that (a) the half-lives of some peroxisomal membrane proteins (e.g., Pex3p → $T_{1/2}$ = 2–6 h) strikingly differ from those of peroxisomal matrix proteins

($T_{1/2}$ = ~2 days) and (b) a high overexpression of peroxisomal membrane proteins may have unpredictable effects on peroxisome morphology [5, 18].

20. The volume of the plasmid DNA should not exceed 10 % of the total transfection volume (=10 μl/electroporation).
21. A detailed instruction manual of how to use the Neon device can be downloaded from the supplier's website (http://tools.invitrogen.com/content/sfs/manuals/neon_device_man.pdf).
22. This step is optional and depends on the time span over which the cells will be analyzed. For example, while high cell densities (e.g., 1×10^5 cells per dish) are not recommended for long-term experiments (e.g., they will be overgrown within 2–3 days), this will ensure that—for short-term imaging experiments—sufficient cells are present in selected fields of view at a final microscope magnification of 1,000-fold.
23. In general, this protocol yields a transfection efficiency of 70–80 %.
24. Phenol red can interfere with the collection of weak fluorescent signals, and as such it is better to omit this pH indicator dye from the culture medium.
25. Currently, many cell-permeable HT fluorescent ligands are commercially available from Promega. For historical and practical reasons, studies in the author's laboratory are routinely carried out with green fluorescent HT-R110 and red fluorescent HT-TMR ligands. Blue fluorescent HT-coumarin ligand (λex/λem: 362/450) was found to yield considerably weaker signals, and prolonged exposure to ultraviolet light resulted in phototoxicity problems.
26. The final labeling concentration of the HT ligands has to be optimized for each individual HT-fusion protein and will vary depending on its expression level and subcellular location. For example, as the volume density of peroxisomes has been estimated to be 1–4 % of that of the cytoplasm [19], translocation of a fluorescent protein from the cytoplasm to peroxisomes will strongly increase its local concentration and, hence, fluorescence intensity.
27. The recommended initial concentrations of the 10× working stock solutions of the HT-TMR ligand for the wash-free and rapid labeling protocols are 2.5 μM and 50 μM, respectively.
28. The recommended initial concentrations of the 10× working stock solutions of the HT-R110 ligand for the wash-free and rapid labeling protocols are 100 nM and 1 μM, respectively.

29. The use of a different cell line may also require optimization of the final HT ligand concentration. For example, we experienced that it is very difficult to label HT-fusion proteins in HepG2 cells, even at a high HT ligand concentrations (our unpublished data). A likely explanation for this observation may be that these cells express high levels of P-glycoprotein (ABCB1; MDR1), a multidrug resistance transporter that can effectively pump rhodamine analogues out of cells [20].
30. The first HT-labeled peroxisomes can be observed within 4–6 h.
31. After labeling, the cells can also be fixed with 4 % (w/v) paraformaldehyde or 100 % (v/v) precooled methanol (to –20 °C) and processed for immunostaining (without signal loss). The results of a typical dual-color labeling experiment are shown in Fig 1b–f.
32. This step is essential to ensure that the microscope is stable over the course of the experiment (changes in temperature may result in a thermal expansion or contraction of microscope components, and this may cause unwanted changes in focus position).
33. Many cell culture media, including MEMα, make use of the CO_2/bicarbonate reaction to buffer the pH of the medium (optimal pH range: 7.0–7.4).
34. It is essential to pre-humidify the 5 % CO_2/air mixture in order to prevent evaporation of the medium.
35. As peroxisomes are small organelles (0.5–1.5 μm in diameter), the preferred final magnification is 600× or 1,000×.
36. As cells are intrinsically sensitive to light, fluorescence live-cell imaging is always a trade-off between exposing the cells to enough light to capture clear images and limiting cell damage. In addition, over-illumination of the cells can lead to photobleaching of the fluorophores, especially during time-lapse experiments.
37. For long time-lapse experiments, one should also include an auto-focusing module.
38. Fluorescence microscopy images can also be analyzed with ImageJ, a freeware image processing and analysis program (http://rsbweb.nih.gov/ij/). Note that, for quantitative image analysis, the values of the pixels should not be saturated.

Acknowledgements

This work was supported by grants from the KU Leuven (OT/09/045) and the Research Foundation Flanders (G.0754.09).

References

1. Stepanenko OV, Stepanenko OV, Shcherbakova DM et al (2011) Modern fluorescent proteins: from chromophore formation to novel intracellular applications. Biotechniques 51:313–314
2. Lippincott-Schwartz J, Patterson GH (2009) Photoactivatable fluorescent proteins for diffraction-limited and super-resolution imaging. Trends Cell Biol 19:555–565
3. Subach FV, Subach OM, Gundorov IS et al (2009) Monomeric fluorescent timers that change color from blue to red report on cellular trafficking. Nat Chem Biol 5:118–126
4. Jung D, Min K, Jung J (2013) Chemical biology-based approaches on fluorescent labeling of proteins in live cells. Mol Biosyst 9: 862–872
5. Huybrechts SJ, Van Veldhoven PP, Brees C et al (2009) Peroxisome dynamics in cultured mammalian cells. Traffic 10:1722–1733
6. Delille HK, Agricola B, Guimaraes SC et al (2010) Pex11pβ-mediated growth and division of mammalian peroxisomes follows a maturation pathway. J Cell Sci 123: 2750–2762
7. Los GV, Encell LP, McDougall MG et al (2008) HaloTag: a novel protein labeling technology for cell imaging and protein analysis. ACS Chem Biol 3:373–382
8. Cong M (2012) HaloTag platform: from proteomics to cellular analysis and animal imaging. Curr Chem Genomics 6:6–7
9. Urh M, Rosenberg M (2012) HaloTag, a platform technology for protein analysis. Curr Chem Genomics 6:72–78
10. Fransen, M. (2012) Peroxisome dynamics: molecular players, mechanisms, and (dys)functions. ISRN Cell Biol, article ID 714192
11. Legakis JE, Koepke JI, Jedeszko C et al (2002) Peroxisome senescence in human fibroblasts. Mol Biol Cell 13:4243–4255
12. Waterham HR, Koster J, van Roermund CW et al (2007) A lethal defect of mitochondrial and peroxisomal fission. N Engl J Med 356: 1736–1741
13. Ebberink MS, Koster J, Visser G et al (2012) A novel defect of peroxisome division due to a homozygous non-sense mutation in the PEX11β gene. J Med Genet 49:307–313
14. Fransen M, Nordgren M, Wang B et al (2013) Aging, age-related diseases and peroxisomes. Subcell Biochem 69:45–65
15. Ribeiro D, Castro I, Fahimi HD et al (2012) Peroxisome morphology in pathology. Histol Histopathol 27:661–676
16. Schrader M, King SJ, Stroh TA et al (2000) Real time imaging reveals a peroxisomal reticulum in living cells. J Cell Sci 113:3663–3671
17. Koch A, Schneider G, Lüers GH et al (2004) Peroxisome elongation and constriction but not fission can occur independently of dynamin-like protein 1. J Cell Sci 117:3995–4006
18. Matsuzaki T, Fujiki Y (2004) The peroxisomal membrane protein import receptor Pex3p is directly transported to peroxisomes by a novel Pex19p- and Pex16p-dependent pathway. J Cell Biol 183:1275–1286
19. Beier K (1992) Light microscopic morphometric analysis of peroxisomes by automatic image analysis: advantages of immunostaining over the alkaline DAB method. J Histochem Cytochem 40:115–121
20. Saengkhae C, Loetchutinat C, Garnier-Suillerot A (2003) Kinetic analysis of rhodamines efflux mediated by the multidrug resistance protein (MRP1). Biophys J 85:2006–2014

Chapter 11

SNAP-Tag to Monitor Trafficking of Membrane Proteins in Polarized Epithelial Cells

Emily H. Stoops, Glen A. Farr, Michael Hull, and Michael J. Caplan

Abstract

In order to understand the mechanisms through which apical and basolateral membrane proteins achieve their subcellular distributions in polarized epithelial cells, it is critical to develop techniques that permit the selective observation of newly synthesized populations of these proteins. The SNAP tag system permits the detection and visualization of distinct spatially and temporally defined cohorts of tagged proteins. Thus, this technique is especially well suited to studying the trafficking routes pursued by newly synthesized proteins. The SNAP tag can be applied in the setting of fixed or live cell fluorescence microscopic analysis and can also be used in the context of various biochemical approaches. Here, we describe the use of the SNAP tag in association with confocal microscopy and SDS-PAGE to follow the biosynthetic pool of a membrane protein as it exits from the *trans*-Golgi network and makes its way to the plasma membrane.

Key words SNAP tag, Golgi block, Fluorescence microscopy, Biosynthetic route, Membrane trafficking, MDCK cells, Polarized epithelial cells

1 Introduction

Polarized epithelial cells direct distinct populations of membrane proteins to the apical and basolateral domains of their plasma membranes. This asymmetry is essential in order for these cells to perform their physiological functions, which include the net secretion or absorption of fluid and solutes. To both maintain and generate epithelial cell polarity, cells must sort membrane proteins into distinct transport carrier vesicles and target these vesicular carriers to the appropriate membrane. To dissect the biosynthetic routes taken by proteins destined for the apical or basolateral membrane, it is important to develop tools that permit the investigator to analyze specifically and exclusively the behaviors of newly synthesized proteins. The trafficking of newly synthesized proteins has been studied using a wide variety of techniques and reagents, including radioactive labeling, mutant forms of proteins that manifest

Andrei I. Ivanov (ed.), *Exocytosis and Endocytosis*, Methods in Molecular Biology, vol. 1174,
DOI 10.1007/978-1-4939-0944-5_11,

temperature-sensitive trafficking properties, and viral infection [1–3]. While these techniques have produced significant advancements in our understanding of biosynthetic trafficking, each is limited in its application. For example, radioactive pulse labeling cannot be used to mark newly synthesized proteins for the purposes of light microscopic analysis. Similarly, temperature-sensitive mutant forms of proteins that permit their biosynthetic trafficking to be temporally coordinated are quite rare. The SNAP tag is an elegant new tool with which to study the trafficking of a newly synthesized cohort of a specified protein.

The SNAP tag, invented by Kai Johnsson and his colleagues, is a recently developed, genetically encoded tag that supports a large number of applications and requires a limited amount of genetic manipulation [4, 5]. Similar to the Fluorescein Arsenical Hairpin (FlAsH) system [6, 7] and the HaloTag [8], the SNAP tag employs the small molecule-binding ability of a naturally occurring protein domain in order to render the protein of interest a substrate for highly selective chemical labeling. The SNAP tag is based upon the DNA repair protein O^6-alkylguanine-DNA alkyltransferase (AGT), which undergoes a covalent reaction with O^6-benzylguanine (BG). This reaction results in the irreversible transfer of the substituted benzyl group to the reactive thiol within the SNAP tag. The SNAP tag sequence can be appended to the sequence of any protein of interest, thus making the protein a substrate for this covalent modification. The Johnsson lab modified AGT to create the 21-kDa SNAP tag, whose reactivity with benzylguanine is 50-fold times that of wild-type AGT, which permits specific visualization of SNAP-tagged proteins over the background signal due to endogenous AGT [4]. The SNAP tag was also mutated to manifest decreased binding to DNA. Unlike conventional genetically encoded protein fusion tags, the SNAP tag is extremely versatile. It can be labeled with synthetic BG-based probes carrying a wide variety of substituents that can be tailored to each specific application. BG derivatives bearing fluorophores, biotin, or magnetic beads—all of which are commercially available from New England Biolabs—can be used to label SNAP-tagged proteins. BG-containing building blocks have also been used to create fluorogenic, photoactivatable, photoconvertible, Ca^{2+}-sensing, intramolecularly quenched, and live cell imaging-optimized probes [9–12].

The irreversible nature of the reaction between the SNAP tag and BG compounds ensures that this tag is well-suited to applications involving the study of newly synthesized proteins, as we have previously demonstrated with SNAP-tagged Na,K-ATPase α-subunit [13]. The preexisting pool of the SNAP-tagged protein of interest is first irreversibly blocked via incubation of cells with a membrane permeable unlabeled “BG-block” compound (Fig. 1a).

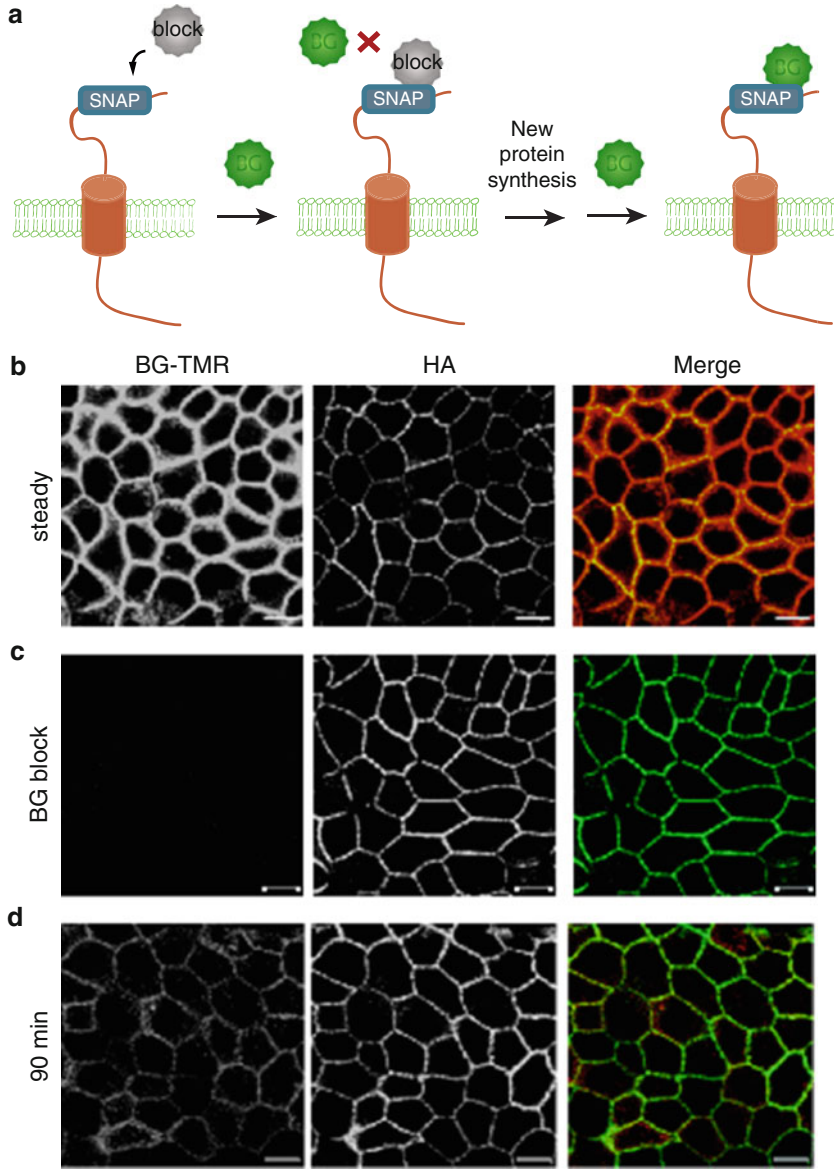

Fig. 1 Detection of newly synthesized SNAP-tagged Na,K-ATPase using fluorescence microscopy. (**a**) Schematic representation of the combination of BG-block and BG-fluorophore to detect newly synthesized protein. (**b**) Stably transfected MDCK cells expressing Na,K-ATPase α-subunit carrying the SNAP tag and an HA epitope tag were labeled with tetramethylrhodamine-conjugated BG (BG-TMR) and processed for immunofluorescence with anti-HA. (**c**) SNAP-Na,K-ATPase cells were incubated for 30 min with BG-block and then labeled as in **b**. (**d**) SNAP-Na,K-ATPase cells pretreated with BG-block were washed and incubated for 90 min at 37 °C to allow for new protein synthesis. The cells were labeled as in **b**. Bars, 10 μm. (**b**–**d**) ©Glen Farr et al., 2009. Originally published in *J Cell Biol*. doi:10.1083/jcb.200901021

After washing away any remaining unincorporated BG-block and waiting for a new cohort of protein to be synthesized, cells are labeled with fluorophore-conjugated BG. Since the reaction between BG and the SNAP tag is irreversible, the blocking preincubation step ensures that all of the "old" protein of interest in a cell is no longer available for subsequent labeling with BG molecules carrying detectable substituents. Treatment with the BG-block compound does not block subsequent labeling with BG compounds by causing protein degradation, as demonstrated by staining with an antibody against an HA epitope tag that is also present on the SNAP-tagged Na,K-ATPase construct (Fig. 1b). Only through the synthesis of a new cohort of the SNAP-tagged protein of interest will the cells acquire a pool of SNAP-tagged protein that can be labeled with BG compounds. By labeling samples at different time points after synthesis, membrane protein trafficking from the site of synthesis to the cell membrane can be tracked (Fig. 1c).

As a complement to the SNAP tag, directed mutagenesis was used to create the CLIP tag. The CLIP tag is an alternative AGT-based tag that binds to O^2-benzylcytosine (BC) substrates rather than BG substrates [14]. The orthogonal substrate specificities of the SNAP and CLIP tags allow for specific, simultaneous labeling of two distinct proteins. As with BG, a variety of BC derivatives are commercially available. Using a combination of nonfluorescent and fluorescent BG and BC, newly synthesized pools of a SNAP- and a CLIP-tagged protein can be followed simultaneously (Fig. 2).

In addition to fixed cell and live cell imaging by fluorescence microscopy, the SNAP tag can be detected by SDS-PAGE to address biochemical questions. Using the SNAP tag to detect the newly synthesized pool of the apical glycoprotein gp135, we observed this protein's maturation from its immature precursor form to its fully glycosylated mature form (Fig. 2b, total). Cell-impermeable BG reagents can be used when labeling SNAP tags placed on a membrane protein's extracellular domain to detect the surface population versus the total cell-associated pool at different time points (Fig. 2, [15, 16]). Using BG conjugated to beads (or BG-biotin in conjunction with streptavidin-conjugated beads), newly synthesized cohorts can also be purified to detect the time-dependent changes in their inventory of interacting partners [17]. The ability to isolate distinct spatial or temporal cohorts of protein and to detect labeled protein using multiple techniques make the SNAP tag an extremely powerful tool with which to answer a variety of biologically interesting questions relating to membrane protein biogenesis and sorting.

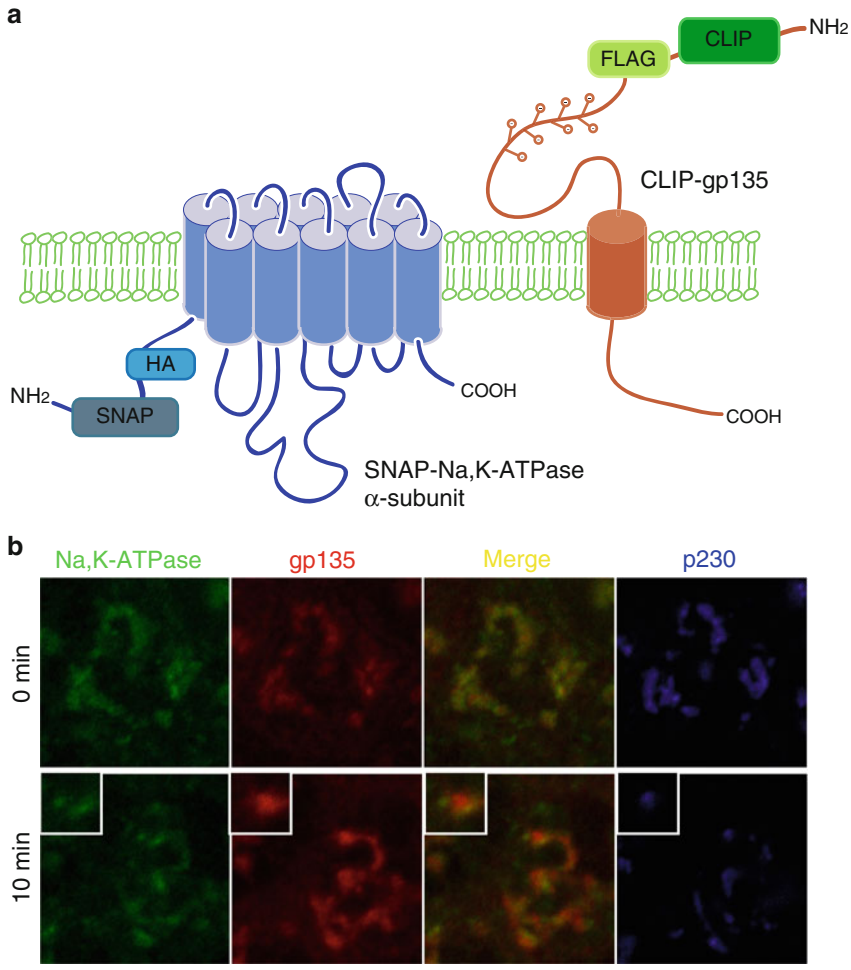

Fig. 2 Co-localization of newly synthesized SNAP-Na,K-ATPase and CLIP-gp135 in the Golgi complex. (**a**) The SNAP tag was engineered into the N-terminal intracellular tail of the Na,K-ATPase α-subunit. The CLIP tag, a mutated form of SNAP that binds to benzylcytosine substrates, was engineered into the N-terminal extracellular tail of gp135. (**b**) Live MDCK cells expressing SNAP-tagged Na,K-ATPase α-subunit and CLIP-tagged gp135 were pretreated with BG- and BC-block. The cells were subsequently washed and allowed to synthesize new protein for 30 min at 37 °C and then subjected to 19 °C Golgi block conditions for 80 min. Cycloheximide was added in the last 20 min of this incubation to chase any residual newly synthesized protein out of the ER. Following 0–10 min incubation at 37 °C, the cells were fixed, labeled with BG-Alexa488 and BC-547, and processed for immunofluorescence with an antibody directed against the Golgi marker p230. *Insets* in the 10 min images demonstrate separation of Na,K-ATPase and gp135 within the Golgi stack

Discussed here in detail is the combination of the SNAP and CLIP tag block/pulse protocol with a 19 °C temperature incubation that results in the accumulation of the newly synthesized protein pool in the Golgi complex shortly after its synthesis. Methods for detecting the resulting synchronized wave of protein exiting the Golgi by fluorescence microscopy or SDS-PAGE are described.

2 Materials

MDCK cells expressing a SNAP-tagged and/or CLIP-tagged protein are grown on Transwell filters (Corning Inc, Corning, NY) in α-Minimum Essential Medium (α-MEM, Gibco) supplemented with 10 % fetal bovine serum, pen–strep, and 2 mM L-glutamine (*see* **Note 1**). The cells are grown 4–5 days past confluence (*see* **Note 2**).

2.1 Golgi Block

1. SNAP-Cell Block (New England Biolabs, Ipswich, MA): Denoted here as BG-block. Dissolve in dimethylsulfoxide (DMSO) to 2 mM. Store at −20 °C for up to 3 months (*see* **Note 3**).
2. CLIP-Cell Block (New England Biolabs, Ipswich, MA): Denoted here as BC-block. Dissolve in DMSO to 2 mM. Store at −20 °C for up to 3 months (*see* **Note 3**).
3. CO_2-independent media (CIM) (Invitrogen, Eugene, OR): Store at 4 °C (*see* **Note 4**).
4. SNAP-Surface Block (New England Biolabs): Denoted here as Surface BG-block. Dissolve in DMSO to 4 mM. Store at −20 °C for up to 3 months.
5. Cycloheximide (CHX): Prepare stock solution at 300 mg/ml in DMSO. Aliquot and store at −20 °C. Avoid multiple freeze–thaw cycles.
6. Chase media (2×): 300 μg/ml CHX and 4 μM Surface BG-block in CIM. Prepare on day of use and preincubate at 19 °C.
7. Release media (1×): 150 μg/ml CHX in CIM. Prepare on day of use and preincubate at 37 °C.
8. PBS^{++}: PBS supplemented with 0.1 mM $CaCl_2$ and 1 mM $MgCl_2$. Store at room temperature.

2.2 Fluorescence Microscopy

1. Fixation buffer: 4 % paraformaldehyde in PBS^{++}. Store at −20 °C.
2. IF Blocking buffer (GSAP): PBS^{++} supplemented with 0.5 % BSA, 10 % goat serum, and 0.2 % saponin. Store at −20 °C.
3. SNAP-fluorophore (New England Biolabs). Dissolve in DMSO and store at −20 °C for up to 3 months (*see* **Note 5**).
4. CLIP-fluorophore (New England Biolabs). Dissolve in DMSO and store at −20 °C for up to 3 months (*see* **Note 5**).
5. Primary and secondary antibodies against common organelle markers or known interacting partners.
6. IF Washing buffer (BSAP): PBS^{++} containing 1 % BSA, 0.2 % saponin. Store at −20 °C.
7. Slides and coverslips.
8. Mounting media such as VECTASHIELD (Vector Laboratories, Burlingame, CA).

2.3 Biochemical Analysis

1. Lysis buffer: 50 mM Tris–HCl pH 7.5, 100 mM NaCl, 1 % Triton X-100, 1 mM DTT, and complete EDTA-free protease inhibitor cocktail tablet (1 tablet per 50 ml; Roche, Basel, Switzerland) in ddH_2O (*see* **Note 6**). Tris–HCl, NaCl, Triton (TNT)-containing buffer can be prepared in advance and stored at 4 °C. DTT and protease inhibitor should be added fresh on the day of the experiment (*see* **Note 7**).
2. SNAP-Surface 782 (New England Biolabs). Dissolve in DMSO to 1 mM (*see* **Note 8**).
3. Standard materials for SDS-PAGE and western blotting.

3 Methods

3.1 Golgi Block

1. Add fresh media to the cells approximately 16 h before starting the experiment.
2. Wash the cells twice with serum-free α-MEM (pre-warmed to 37 °C).
3. Incubate the cells for 30 min at 37 °C with BG-block (0.16 μM, *see* **Note 3**) in serum-free α-MEM to block all existing SNAP-tagged protein in the cell. If using, add BC-block (1.33 μM, *see* **Note 3**) to block all existing CLIP-tagged protein (*see* **Note 9**).
4. Set aside one sample as a BG/BC-block control and place in 4 °C PBS^{++} on ice.
5. Rinse remaining samples three times in α-MEM to wash away BG/BC-block. Return the cells to 37 °C incubator for 30 min to allow for new protein synthesis (*see* **Note 10**).
6. Wash the cells three times with 19 °C CIM. During the final wash, add 1 ml of CIM to the basolateral cup and 0.5 ml to the apical cup. Float plate in 19 °C water bath and incubate the cells for 1 h, making sure to position filters evenly throughout plate to enable floating (*see* **Note 11**).
7. Add 1 ml chase media (2×) to basolateral cup and 0.5 ml to apical cup, resulting in 1× concentration of cycloheximide and Surface BG-block (*see* **Note 12**). Incubate the cells for 20 additional minutes at 19 °C. During this period, new protein synthesis will be inhibited and protein synthesized during the previous two steps will be chased out of the endoplasmic reticulum. Additionally, the Surface BG-block will block any protein that may escape the Golgi block and reach the cell membrane prior to Golgi block release.
8. Remove one sample and place in 4 °C PBS^{++} on ice. This is the Golgi block control sample (*see* **Note 13**).
9. Wash remaining samples two times with release media (1×) to rapidly change temperature and rinse away Surface BG-block.

Float the cells in 37 °C water bath for desired chase times (*see* **Note 14**). For every time point, remove one filter and immediately wash with 4 °C PBS^{++} and place on ice.

10. Wash all samples two additional times in cold PBS^{++} on ice.
11. Use a razor blade to cut out filters from support structures and place filters cell-side up in the wells of a cell culture plate.
12. Proceed with processing for either fluorescence microscopy or SDS-PAGE.

3.2 Processing for Fluorescence Microscopy

1. Fix the cells in 250 µl ice-cold fixation buffer for 30 min on ice.
2. Permeabilize the cells in 500 µl GSAP for 15 min at room temperature.
3. Treat the cells with BG-fluorophore and (if using) BC-fluorophore diluted in GSAP to an optimized concentration. The cells can be simultaneously treated with primary antibodies, as desired (*see* **Note 15**). Incubate for 1 h at room temperature, or overnight at 4 °C. Protect from light for remainder of experiment.
4. Wash the cells 3× 5 min in BSAP on a rocker.
5. Treat the cells with secondary antibody diluted in GSAP, as required for any antibodies used in **step 3**.
6. Wash the cells 2× 5 min in BSAP and 2× 5 min in PBS^{++} on a rocker.
7. Mount filters cell side up on slides with VECTASHIELD mounting reagent. Place coverslip on top of filter. Aspirate excess mounting reagent and seal with clear nail polish.
8. For best results in polarized cells, use a confocal microscope to take *z*-stack images of each sample.

3.3 Processing for SDS-PAGE Surface vs. Total Labeling (Described for SNAP Tag Only)

1. Surface-label the cells with SNAP-Surface 782 (1 µM in PBS^{++}) at 4 °C for 1 h (*see* **Note 16**). Protect samples from light.
2. Wash the samples 3× 5 min PBS^{++} on a rocker at 4 °C.
3. Aspirate PBS^{++} from the cells. Add 500 µl of lysis buffer to the cells. Use a cell scraper to scrape the cells off of filter. Without removing filter, place dish on ice on a rocker for 30 min to allow for cell lysis.
4. Transfer lysate to a 1.5 ml microcentrifuge tube.
5. Spin down insoluble material for 10 min at 5,220 × *g* at 4 °C.
6. Save 250 µl of each lysate as the "surface-labeled" sample (*see* **Note 17**).
7. Label remaining lysate (~250 µl) again with 1 µM SNAP-Surface 782. Add SNAP-Surface 782 directly to lysate and incubate for 1 h at 4 °C (*see* **Note 18**). This sample serves as a measure of the total pool of newly synthesized SNAP-tagged protein.

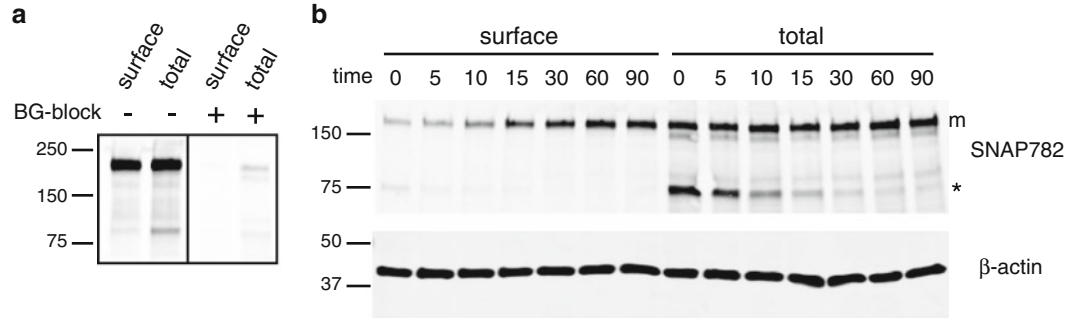

Fig. 3 Detection of newly synthesized SNAP-tagged gp135 by SDS-PAGE. (**a**) MDCK cells expressing a SNAP-tagged version of the apical protein gp135 were pretreated with or without BG-block for 30 min. The cells were labeled with an infrared fluorescent dye-conjugated BG (SNAP782) prior to cell lysis (surface). Aliquots of cell lysates were labeled again with SNAP782 (total). Following SDS-PAGE and western blotting, SNAP782 signal was detected using the Licor system. (**b**) SNAP cells were pretreated with BG-block and then newly synthesized protein was subjected to a 19 °C Golgi block incubation, after which the cells were warmed to 37 °C for 0–90 min. Surface and total protein were labeled with SNAP782 and detected as in **a**. Only mature protein (m) was detected in the surface-labeled pool, whereas mature protein and a lower molecular weight precursor form of gp135 with a molecular mass of ~75 kDa (denoted by an *asterisk*) were detected in the "total" sample. The precursor form disappeared over time, coincident with the arrival of the mature form in the surface pool

8. Prepare lysates for gel electrophoresis. Load surface and total samples on the same gel for side-by-side comparison and quantification using standard SDS-PAGE and western blot procedures (*see* **Note 19**).
9. Image SNAP-Surface 782 using a Licor Odyssey Infrared Imager (Fig. 3 and *see* **Note 20**).

4 Notes

1. We use polycarbonate filters with a pore size of 0.4 μm. For fluorescence microscopy, we use 12-well filter plates. For biochemical analysis, we use 6-well filter plates.
2. In our hands, samples used rapidly after cells fully polarize (4–5 days post-confluence for MDCK cells) produce a larger pool of newly synthesized protein following BG-block. This is particularly important when analyzing cells by fluorescence microscopy.
3. The optimal concentration of BG/BC-block varies with each SNAP/CLIP-tagged protein. A simple titration experiment can help to determine the appropriate concentration for each protein. Use the lowest concentration that blocks all existing signal. Over-saturating cells with BG/BC-block can result in inefficient removal of excess block during wash steps. This will limit the extent of protein recovery observed following BG/BC-block.

4. CO_2-independent media is a phosphate-based cell culture media that maintains a near physiological pH outside of the CO_2-regulated atmosphere of an incubator.
5. As with the concentration of BG-block, the best fluorophore-conjugated BG/BC reagent for use with each particular SNAP/CLIP-tagged protein construct varies. Each tagged protein should be tested with a panel of SNAP/CLIP tag reagents to determine the fluorophore and labeling conditions (concentration, duration) that provide the best signal-to-noise ratio. When performing SNAP + CLIP block/pulse experiments, use the combination of labeling reagents that provide the best signal. This may necessitate using the second-best reagent for one tag to achieve the best overall two-color imaging.
6. Metal chelating reagents, such as EDTA, have been shown to inhibit the reactivity of the SNAP tag and should not be used.
7. Although not required, addition of 1 mM DTT has been suggested to enhance the stability of the SNAP tag.
8. For biochemical applications we use SNAP-Surface 782 with the Licor Odyssey Infrared Imager to detect newly synthesized SNAP-tagged proteins. Alternatively, a Typhoon Imager with 532 and 633 nm excitation lasers can be used to detect SNAP reagents such as SNAP-Surface 488 or SNAP-Surface 594. SNAP-biotin can also be used for SNAP tag detection, but commercially available SNAP-biotin is cell-permeable and not suitable for surface versus total protein quantification. SNAP-biotin blots can be developed using streptavidin-HRP and standard enhanced chemiluminescence substrates. The SNAP reagents listed above are all offered by New England Biolabs.
9. We have observed that BG-block binds to SNAP-tagged protein with greater efficiency in serum-free media than in serum-containing media, enabling greater saturation of existing protein in the block condition.
10. Recovery times may vary with each protein of interest. Proteins with long turnover rates may require significantly longer incubation at 37 °C and/or 19 °C to build a large enough pool of protein to enable visualization by fluorescence microscopy. Biochemical methods are more sensitive and thus can detect the smaller pools of protein that are produced in shorter incubation intervals.
11. Use a thermometer to ascertain water bath temperature. Small fluctuations in temperature can result in an incomplete block of transport out of the Golgi.
12. Depending on the experimental goal and/or the trafficking of the protein of interest, Surface BG-block can be added exclusively to either the apical or basolateral cup. Surface BC-block is not commercially available. This step is only applicable in instances where the SNAP tag is attached to an extracellular-facing domain of the protein of interest.

13. Within reason, the samples should be processed through to fixation or lysis as soon as possible after moving to 4 °C PBS^{++}. After fixation, samples can be held in PBS^{++} on ice until all remaining samples are ready for labeling.
14. Appropriate release times will depend on the protein and experimental goals. A good initial start point is to look every 5 min for 30 min following Golgi block release.
15. Post-fixation labeling steps for fluorescence microscopy are performed with excised filters resting on Parafilm. 75 μl drops of BG-, BC-, or antibody-containing GSAP are spotted onto Parafilm in a moist chamber. Remove excess buffer from each filter by gently gliding it against the edge of its well. Wet the underside of the filter in label-containing buffer and then place filter cell side down on the drop of label-containing GSAP.
16. Surface labeling is performed with excised filters resting on Parafilm. Follow steps from **Note 15**, using 100 μl drops for the larger 6-well filters.
17. As noted in the introduction, surface versus total analysis of SNAP-tagged proteins can only be performed if the SNAP tag is engineered into an extracellular domain of the protein of interest. In addition to the ability to specifically label surface versus internal protein, an extracellular SNAP tag enables the study of endocytic protein trafficking or analysis of protein stability at the cell surface, among other experiments. Thus, if an external tag is unlikely to perturb the trafficking or function of a particular protein of interest, an external tag is recommended.
18. If desired, incubation can also be done overnight at 4 °C.
19. No additional labeling is needed to visualize SNAP-Surface 782. If a loading control or other marker is desired, the transfer membrane can be processed with primary antibody and a Licor-suitable secondary antibody according to standard western blot protocol. If using BG-biotin and streptavidin-HRP, the gel should be cut in an appropriate location before processing with a primary antibody directed against another protein that migrates in a different molecular weight range.
20. Unbound SNAP-Surface 782 will run off the gel with the dye front, allowing for specific detection of SNAP-tagged protein.

Acknowledgements

The authors would like to thank Dr. Ivan Correa for helpful discussions and support. This material is based upon work supported by NIH training grant 5T32GM007223-35 and National Science Foundation Graduate Research Fellowship Grant No. DGE-1122492 (E.H. Stoops) and NIH grants DK17433 and DK072612 (M.J. Caplan).

References

1. Rodriguez-Boulan E, Kreitzer G, Müsch A (2005) Organization of vesicular trafficking in epithelia. Nat Rev Mol Cell Biol 6: 233–247
2. Fölsch H, Mattila PE, Weisz OA (2009) Taking the scenic route: biosynthetic traffic to the plasma membrane in polarized epithelial cells. Traffic 10:972–981
3. Weisz OA, Rodriguez-Boulan E (2009) Apical trafficking in epithelial cells: signals, clusters and motors. J Cell Sci 122:4253–4266
4. Juillerat A, Gronemeyer T, Keppler A et al (2003) Directed evolution of O6-alkylguanine-DNA alkyltransferase for efficient labeling of fusion proteins with small molecules in vivo. Chem Biol 10:313–317
5. Keppler A, Kindermann M, Gendreizig S et al (2004) Labeling of fusion proteins of O6-alkylguanine-DNA alkyltransferase with small molecules in vivo and in vitro. Methods 32:437–444
6. Griffin BA, Adams SR, Tsien RY (1998) Specific covalent labeling of recombinant protein molecules inside live cells. Science 281:269–272
7. Machleidt T, Robers M, Hanson GT (2007) Protein labeling with FlAsH and ReAsH. Methods Mol Biol 356:209–220
8. Los GV, Encell LP, McDougall MG et al (2008) HaloTag: a novel protein labeling technology for cell imaging and protein analysis. ACS Chem Biol 3:373–382
9. Maurel D, Banala S, Laroche T, Johnsson K (2010) Photoactivatable and photoconvertible fluorescent probes for protein labeling. ACS Chem Biol 5:507–516
10. Kamiya M, Johnsson K (2010) Localizable and highly sensitive calcium indicator based on a BODIPY fluorophore. Anal Chem 82: 6472–6479
11. Sun X, Zhang A, Baker B et al (2011) Development of SNAP-Tag fluorogenic probes for wash-free fluorescence imaging. Chembiochem 12:2217–2226
12. Lukinavičius G, Umezawa K, Olivier N et al (2013) A near-infrared fluorophore for live-cell super-resolution microscopy of cellular proteins. Nat Chem 5:132–139
13. Farr GA, Hull M, Mellman I, Caplan MJ (2009) Membrane proteins follow multiple pathways to the basolateral cell surface in polarized epithelial cells. J Cell Biol 186:269–282
14. Gautier A, Juillerat A, Heinis C et al (2008) An engineered protein tag for multiprotein labeling in living cells. Chem Biol 15:128–136
15. Harder JL, Whiteman EL, Pieczynski JN, Liu C-J, Margolis B (2012) Snail destabilizes cell surface Crumbs3a. Traffic 13:1170–1185
16. Milenkovic L, Scott MP, Rohatgi R (2009) Lateral transport of smoothened from the plasma membrane to the membrane of the cilium. J Cell Biol 187:365–374
17. Morton MJ, Farr GA, Hull M, Capendeguy O, Horisberger J-D, Caplan MJ (2010) Association with beta-COP regulates the trafficking of the newly synthesized Na, K-ATPase. J Biol Chem 285:33737–33746

Chapter 12

FlAsH-PALM: Super-resolution Pointillist Imaging with FlAsH-Tetracysteine Labeling

Mickaël Lelek, Francesca Di Nunzio, and Christophe Zimmer

Abstract

Super-resolution light microscopy including pointillist methods based on single molecule localization (e.g., PALM/STORM) allow to image protein structures much smaller than the diffraction limit (200–300 nm). However, commonly used labeling strategies such as antibodies or protein fusions have several important drawbacks, including the risk to alter the function or distribution of the imaged proteins. We recently demonstrated that pointillist imaging can be performed using the alternative labeling technique known as FlAsH, which better preserves protein function, is compatible with live cell imaging, and may help reach single nanometer resolution. We applied FlAsH-PALM to visualize HIV integrase in isolated virions or infected cells, allowing us to obtain sub-diffraction resolution images of this enzyme's spatial distribution and analyze HIV morphology without altering viral replication. The technique should also prove useful to image delicate proteins in intracellular vesicles and organelles at high resolution. Here, we present a detailed protocol in order to facilitate the application of FLAsH-PALM to other proteins and biological structures.

Key words Super-resolution microscopy, Fluorescence, FlAsH-tetracysteine labeling, HIV

1 Introduction

1.1 Pointillist Super-resolution Light Microscopy

Fluorescence microscopy allows for highly specific and sensitive imaging of molecular structures, but has long been limited by diffraction to a resolution of ~200–300 nm. This prevented detailed analyses of the structure of biological complexes smaller than this limit, including most vesicles and viruses. Super-resolution methods developed during the past decade have overcome this barrier [1]. Among the most powerful super-resolution methods are those that rely on the accurate localization of single, stochastically fluorescing molecules, such as PALM and STORM [2–5]. However, most implementations of PALM/STORM-like methods

Mickaël Lelek and Francesca Di Nunzio have contributed equally to this chapter.

Andrei I. Ivanov (ed.), *Exocytosis and Endocytosis*, Methods in Molecular Biology, vol. 1174,
DOI 10.1007/978-1-4939-0944-5_12, © Springer Science+Business Media New York 2014

(also referred to here as pointillism) employ fluorescent labeling strategies that face several drawbacks.

1.2 Pros and Cons of Standard Fluorescence Labeling Schemes

The two most commonly used techniques to label proteins are (1) antibodies coupled to synthetic dyes and (2) fusions with fluorescent proteins [6]. These two strategies have different advantages and drawbacks. Briefly, antibodies are easy to use, and many bright synthetic dyes are available, enabling high accuracy fluorophore localization (necessary to achieve high resolution in pointillist microscopy). However, antibodies require fixation and permeabilization to penetrate the cells, which prevents live cell imaging. Furthermore, sufficiently specific antibodies may not be commercially available, and depending on fixation conditions, the imaged protein distributions may be artefactual [7]. In addition, the size of the antibodies itself poses a limit to resolution, especially when secondary antibodies are used. Resolution may be further restricted if antibodies have low affinity, such that only a fraction of the proteins are labeled [8].

By contrast, fluorescent protein fusion allows highly specific labeling and live cell imaging. However, fluorescent proteins are usually less bright than synthetic dyes, thereby restricting the achievable resolution. Furthermore, the relatively large size of the fluorescent protein (~25 kDa for GFP) can modify or destroy the function of the native protein. This is particularly problematic for microbial proteins, which are often sensitive to labeling. One example is type III secretion, where effector molecules are injected by bacteria into host cells through a thin molecular needle. Because the diameter of this needle is too small to accommodate GFP-fused effectors, this labeling approach cannot be used to study the secretion process [9]. Another example is the HIV integrase enzyme, which cannot be fused to GFP without disrupting viral replication [10, 11].

1.3 FlAsH Labeling

The FlAsH-tetracysteine labeling system provides an interesting alternative to antibodies and fluorescent protein fusions. In this system, the protein of interest is genetically modified by fusion of a small motif of approximately ten amino acids, containing four cysteines. A nonfluorescent membrane-permeant derivative of fluorescein containing two arsenic atoms, FlAsH, binds to this motif with high affinity, and becomes fluorescent upon binding [12]. Nonspecific binding to endogenous cysteine motifs can be minimized using 1,2-ethanedithiol (EDT) and/or optimized tetracysteine sequences [12, 13]. A key advantage of FlAsH labeling compared to fusions with fluorescent proteins is the much smaller size of the tag (<1 kDa). As a result, the function of the native protein is much better preserved. Indeed, tetracysteine-tagged effector molecules can be ejected by the type III secretion pathway

[9] and HIV with tetracysteine-tagged integrase infects target cells similarly to the wild-type virus [14]. The FlAsH labeling system is also compatible with live cell imaging [9, 12, 14, 15].

1.4 FlAsH-PALM and HIV

We demonstrated that FlAsH can be used successfully in pointillist super-resolution microscopy [16]. We showed that in presence of a suitable "photoswitching" buffer and laser irradiation, FlAsH exhibits stochastic blinking, and that single FlAsH-labeled proteins can be localized with high accuracy, compatible with ~30 nm resolution pointillist imaging. We then applied FlAsH-PALM to image the HIV integrase enzyme, both in isolated virions and inside infected cells, and obtained images with an estimated resolution <30 nm [16]. Using computational methods, we analyzed the shape of FlAsH-integrase clusters, which provided sub-diffraction resolution information about the viral morphology. Specifically, we were able to statistically discriminate between isolated mature and immature HIV virions based on the shape of their integrase distribution (conical and spherical, respectively), even though these virions have sizes well below the diffraction limit (<150 nm) [16]. In infected cells, the bulk of the integrase appeared to assume a conical morphology consistent with intact viral capsids. This provided optical evidence against the notion that capsid disassembly occurs immediately after virion entry into the cell and corroborated other lines of evidence that HIV capsids remain intact in the cytoplasm, including evidence that capsids interact with components of the nuclear pores [17–19].

1.5 Application to Intracellular Organelles

Although our demonstration of FlAsH-PALM was restricted to the HIV integrase [16], the method should be widely applicable and useful for many other proteins, especially those most sensitive to fusions with fluorescent proteins. We acknowledge, however, that the typical presence of high background fluorescence due to non-specific FlAsH labeling may pose a difficulty and compromise FlAsH-PALM resolution. In our HIV study, we circumvented this difficulty by labeling the viral protein before infecting the cells [16]. This strategy cannot be easily extended to proteins encoded by the cellular genome. Nevertheless, FlAsH has been used successfully to image endogenous proteins such as tubulin or actin in conventional microscopy, and optimizations of the tetracysteine-containing amino acid sequence to increase labeling affinity should help maintain high signal-to-noise ratio and resolution [13, 15]. With such improvements, FlAsH-PALM should also enable super-resolution studies of proteins in intracellular vesicles and organelles.

2 Materials

2.1 Microscopy System

We use a home-made microscopy system adapted to pointillist imaging, with the following main characteristics:

1. Inverted microscope (Ti-E Eclipse, Nikon, Japan). We used a microscope equipped with the Nikon perfect focus system (PFS), which features a near-infrared sensor and a piezoelectric device to measure and correct focus drift.
2. Objective lens with 100× magnification and a numerical aperture of 1.49 (CFI Apochromat, Nikon, Japan).
3. Immersion oil between coverslip and objective lens.
4. Additional 1.5× lens (Optovar) to diminish pixel size.
5. Two aligned lasers at wavelengths of 488 nm and 405 nm, with a power of 100 mW (Spectra-Physics Excelsior CW Lasers).
6. An electron multiplying charge coupled device (EM-CCD) camera for single fluorophore detection (Andor iXon DV887ECS-BV, Andor, Belfast, Ireland) with a pixel size of 16 × 16 μm. With the magnification specified above, this translates into a pixel size in the image domain of 106 × 106 nm. We use the full camera chip for image acquisition, providing a field of view of 54 × 54 μm.
7. An Acousto-Optical Tunable Filter (AOTF) (AA-opto electronics, Orsay, France) for fast modulation of laser power.
8. A PC that runs Micromanager (www.micro-manager.org) with custom-made plugins that drive the camera, lasers and the AOTF [20]. We used a Dell PC under Windows XP with 4 Gb of RAM and a 1 Tb hard drive.

2.2 Virus Production and Cell Infection

1. P4-CXCR4-CCR5 HeLa derived cells. These are reporter cells carrying the LacZ gene under the control of the HIV-1 LTR promoter, a system used to measure viral infectivity by luciferase assay [21].
2. LAIΔ Env-IN-C4 virus. This is the HIV construct containing the tetracysteine tag fused to the C-terminus domain of the integrase (IN) [14].

2.3 FlAsH-PALM Imaging

1. Fibronectin, at a final concentration of 100 μg/mL in phosphate-buffered saline (PBS) (needed to image free virions).
2. Paraformaldehyde (PFA) at a final concentration of 2 % in water (needed to fix free virions and infected cells).
3. Ammonium chloride (NH_4Cl) at a concentration of 50 mM in water (used to quench free aldehyde groups of PFA).
4. FlAsH bis-ethanedithiol (FlAsH-EDT2) at a final concentration of 0.5 μM (Invitrogen).
5. β-mercaptoethanol (β-ME) at a final concentration of 1 mM in water.
6. Tris (2 carboxyethyl)phosphine (TCEP) at a final concentration of 1 mM (*see* **Note 1**).
7. 10 μM 1,2-ethanedithiol (EDT) (*see* **Note 2**).

8. Photoswitching buffer: Pointillist microscopy requires that fluorophores stochastically switch between dark and fluorescent states and that only few fluorophores emit fluorescence simultaneously, so that each can be localized individually with high accuracy. Sufficiently long dark state lifetimes can be achieved in standard fluorophores using "photoswitching buffers" that deprive the sample of oxygen [22, 23] (*see* **Note 3**). To prepare the photoswitching buffer, we mix equal volumes of the following two solutions (*see* **Note 4**):
   (a) Saturated glucose solution: Fill a glass tank with 50 mL of PBS, pH 7.4 and place it on a mixed tray. Progressively add glucose powder. Add powder until solid particles remain in the solution even after 30 min of mixing. Filter the saturated glucose solution with a 0.2 μm sterile filter (Minisart filter-17761 1CK) in order to remove the insoluble particles (*see* **Note 5**).
   (b) Oxygen scavenger solution: to prepare 50 mL of oxygen scavenger buffer, fill a tube with a volume of PBS pH 7.4, add 0.5 mg/mL of glucose oxidase, add 40 μg/mL of catalase from bovine liver, add 0.5 mL of β-mercaptoethanol, add PBS until the solution in the tube reaches 50 mL. The remainder of each solution can be kept separately at 4 °C for several months and used for future experiments.
9. Fiducial markers: tetraspec fluorescent beads with 100 nm diameter (Invitrogen, reference T7279). These beads are used as fiducial markers to correct for mechanical drift during image sequence acquisition (*see* **Note 6**).
10. Computer and software for analysis:
   (a) Hardware: Computational processing is needed to obtain high-resolution images from the raw image sequences acquired by the microscope. Processing is typically done on a distinct computer than the computer driving the microscope. We used a PC with 16 Gb of RAM, a 200 Gb hard drive, and 12 CPUs.
   (b) Software: For detection and localization of molecules, we used a modified version of the software MTT [24], which runs under Matlab. Home-made Matlab-scripts were used for drift correction, visualization and analysis of super-resolution images (*see* **Note 7**).

3 Methods

This section describes: our protocol for production and labeling of HIV with FlAsH; coverslip cleaning and our procedure to prepare free virions; steps taken for infection of cells with FlAsH-labeled HI virions and cell fixation; our protocol for FlAsH-PALM imaging.

3.1 Production of Viruses

1. In order to produce tetracysteine-tagged HIV pseudotyped with the glycoprotein from vesicular stomatitis virus (HIV IN-C4/VSVG), co-transfect 293T cells with Calcium phosphate ($CaPO_4$) in Dulbecco's modified Eagle's medium (DMEM) with 10 % serum. We used as vector a plasmid containing the HIV genome with the exception of the envelope protein gene (LAIΔEnv-IN-C4) and a plasmid expressing the VSVG envelope plasmid (pHCMV-G) [25].
2. Change the medium 16–18 h post-transfection with the new DMEM without serum.
3. Harvest the virus 48 h post-transfection. Measure the virus yield by p24 ELISA according to the manufacturer's instructions (Perkin Elmer).

3.2 FlAsH Labeling

1. Label 1 mL of viral supernatant (0.5–1 μg/mL of p24 antigen of labeled virus) at room temperature by adding FlAsH-EDT2, β-ME, TCEP, and EDT (*see* **Notes 2** and **4**).
2. After 2 h, eliminate unbound FlAsH by ultracentrifugation at 110,000 × *g* for 30 min.
3. Resuspend pellets in 150 μL of PBS (the labeled virus is stable at −80 °C).
4. Check FlAsH labeling of viruses by spectrofluorescence at 485–570 nm.

3.3 Coverslip Cleaning

For FlAsH-PALM imaging, it is important to clean the coverslips in order to avoid spurious signal. We used either chemical cleaning or a plasma cleaner (*see* **Note 8**):

3.3.1 Chemical Cleaning

1. Wash coverslips in methanol-CH_3OH and acetone.
2. Rinse with milliQ water.
3. Repeat **steps 1** and **2** three times.
4. Place coverslips in a 1 M KOH solution.
5. Sonicate for 1 h.
6. Place the cleaned coverslips in a tube filled with PBS and covered with Parafilm to avoid contamination. The coverslips not used for imaging (see below) can be kept in the tube for later use.

3.3.2 Plasma Cleaner

1. Mount coverslips in a home-built ceramic support placed in the plasma cleaner for 5 min.
2. Keep coverslips inside a vacuum bell until first use in order to avoid contamination.
3. After removing each coverslip, place the remaining coverslips back into the vacuum tank.

3.4 Infection and Fixation of Cells

For imaging free virions, please skip this subsection and move to Subheading 3.5.

1. Seed cells on a coverslip in a 24-well plate for 24 h in DMEM/F12 medium without phenol red and 10 % of fetal bovine serum.
2. Infect the cells with 100 ng of p24 of FlAsH-labeled virus for 2 h at 37 °C.
3. Wash the cells in PBS.
4. Finally, fix the cells with PFA for 10 min at room temperature.
5. Wash the cells in PBS.
6. Add ammonium chloride (NH_4Cl) to the fixed cells for 10 min at room temperature to neutralize the PFA.
7. Wash cells in PBS.

3.5 Preparation of Free Virions

Alternatively to imaging of infected cells, FlAsH-PALM can also be used to image free virions [16]. To prepare these samples, proceed as follows:

1. In order to allow the virus to adhere to the cleaned coverslips, treat them with fibronectin for 30 min at 37 °C.
2. Wash with PBS to remove excessive fibronectin.
3. Let the coverslip dry for 30 min.
4. Deposit 50 μL of free labeled virions onto the coverslip and leave at 37 °C for 30 min.
5. In order to fix the free virions, follow **steps 4–7** from Subheading 3.4.

3.6 Sample Preparation for Imaging

In order to put cells in contact with the photoswitching buffer described in **Step 8** of Subheading 2.3, we use the following special glass mounting procedure:

1. Spread a sheet of Parafilm on a rectangular cover glass.
2. Heat the cover glass on a hotplate until the Parafilm becomes translucent. This allows the Parafilm to stick to the cover glass and to remove the air in between (*see* **Note 9**).
3. Remove the cover glass from the hotplate.
4. Create a square hole in the translucent Parafilm.
5. Heat again the perforated Parafilm fixed on cover glass. The coverslip support is now ready to receive the sample.
6. Add beads to the sample. These will be used to correct for spatial drift (*see* **Step 9** of Subheading 2.3 and **Note 6**).
   (a) Place the coverslip in a dish filled with 2 mL of PBS.
   (b) Add 3 μL of TetraSpec fluorescent beads.

(c) Mix samples in orbital shaker for 20 min at room temperature to allow the beads to stick to the coverslip.

(d) Remove the excess medium (containing PBS and non-sticking beads).

(e) Wash three times with PBS to remove non-sticking beads.

(f) Fill the dish with fresh PBS.

7. Add the photoswitching buffer (*see* **Step 8** of Subheading 2.3) in the rectangular hole of the Parafilm.
8. Use a round 12 mm diameter coverslip (cleaned as described in Subheading 3.3) to cover the rectangular hole and seal it onto the Parafilm with nail polish. This keeps the cells hermetically closed and in contact with the buffer.

3.7 FlAsH-PALM Imaging

1. Place the sample under the objective lens of the microscope.
2. Find the sample region of interest using a mercury lamp (at low power to avoid photobleaching).
3. Turn on excitation laser (488 nm) at full power (100 mW) to bleach out the already activated fluorophores and start acquiring a sequence of images. We used an exposure time of 100 ms for each image frame.
4. Once fluorescence has stabilized and only isolated fluorescent spots are visible, start pulsing the activation (405 nm) laser, while keeping the excitation laser (488 nm) continuously on. We used 10 ms pulses of the 405 nm laser at intervals of 500 ms and a power of only a few μW (*see* **Note 10**).
5. Acquire images until photobleaching of almost all fluorophores (this typically requires several thousands of images).
6. Save and transfer the acquired images to the analysis computer.
7. Process the sequence of raw, diffraction-limited images with algorithms to detect and localize individual fluorophores, correct for drift using the fiducial markers, and create high-resolution visualizations (Fig. 1). We used a modification of the generic particle and tracking software MTT [24], and home-made Matlab scripts, but other tools can be used as well (*see* **Note 7**).

4 Notes

1. These are reducing agents enabling the binding of FlAsH to the tetracysteine tag (FlAsH does not bind to oxidized cysteines).
2. The concentration of EDT used to compete for nonspecific binding is crucial. In our experiments we used 10 μM of EDT.

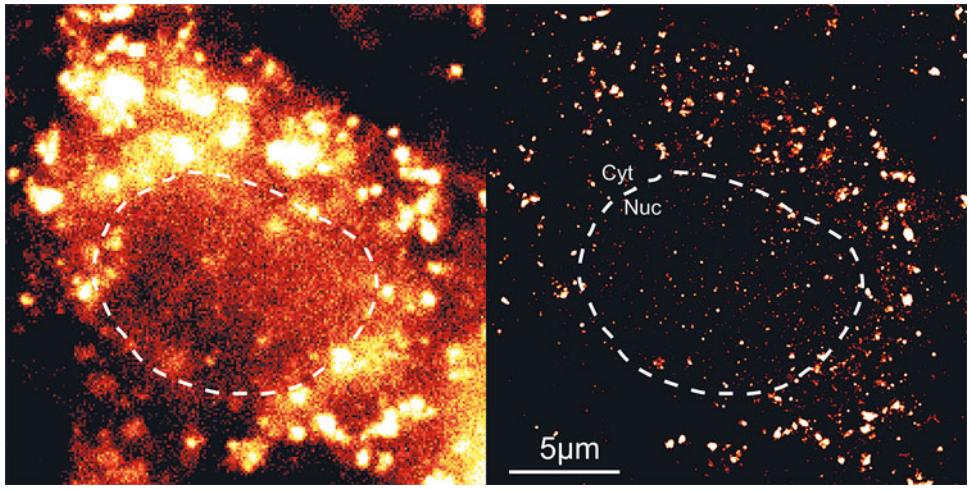

Fig. 1 FlAsH-PALM imaging of HIV-integrase in an infected cell. *Left*: raw, diffraction-limited image obtained at the beginning of image sequence acquisition. *Right*: high-resolution reconstruction of the same field of view using localizations calculated from 20,000 raw images of stochastically fluorescing FlAsH-tagged integrase molecules. The *dashed curve* outlines the cell nucleus. The field of view is 22 µm × 22 µm

For live cell imaging, EDT concentration can be maintained at 10–20 µM [32]. Note that this reagent is toxic and should be manipulated under a chemical hood.

3. More physiological buffers have been reported in pointillist microscopy with synthetic dyes, including ascorbic acid [26]. However, we tried FlAsH-PALM imaging with acid ascorbic at 100 µM, and could not observe FlAsH blinking with this buffer.
4. The photoswitching buffer contains β-mercaptoethanol, which is toxic. Preparation of the buffer and the sample should therefore be performed under a chemical hood.
5. Removing the insoluble aggregates from the saturated glucose solution is necessary in order to avoid spurious signal during FlAsH-PALM imaging.
6. Pointillist microscopy typically requires acquisition of thousands of images with diffraction-limited resolution to reconstruct one high-resolution image [4, 5, 27]. Lateral mechanical drift of the sample during this acquisition period can compromise image resolution and must therefore be corrected for. The standard correction method is to computationally subtract the drift from calculated molecule positions. For this purpose, the drift can be conveniently estimated by tracking the fiducial markers (**Step 9** of Subheading 2.3). The amount of fluorescent beads should be adjusted such that several beads are visible in the same focal plane as the sample region of interest. Alternatively, drift can also be corrected mechanically in real time using piezo-electric devices working in closed loops [28]

or can be estimated from the labeled molecules themselves without fiducial markers [29].

7. Several software tools are now available to reconstruct high-resolution pointillist images from raw diffraction-limited image sequences. Examples are QuickPALM [20], rapidSTORM [30], and GraspJ [31]. Available software tools differ in underlying algorithms as well as in the achieved resolution and computation times.
8. Cleaning the coverslips is very important for pointillist imaging, because any impurities can cause nonspecific signal. This is particularly important to reduce the background when imaging free virions. In our hands, the efficiency of both cleaning methods was similar. However, plasma cleaning is preferable over chemical cleaning if the coverslips are to be imaged more than a few days later, because in the latter case saline precipitates might appear, leading to spurious signal.
9. Take care to avoid air bubbles in the Parafilm close to the square hole, first because oxygen might diminish the efficiency of the photoswitching buffer and consequently FlAsH blinking, and second because bubbles can compromise the flatness of the coverslip and introduce optical aberrations.
10. After a few minutes of acquisition, the 405 nm laser power can be increased to compensate for the diminishing number of newly activated fluorophores due to photobleaching.

Acknowledgements

We acknowledge funding by Institut Pasteur, Région Ile-de-France (DIM Malinf), Fondation pour la Recherche Médicale (Equipe FRM 2010), Sidaction and ANRS. We thank Philippe Souque for comments on the manuscript.

References

1. Hell SW (2009) Microscopy and its focal switch. Nat Methods 6:24–32
2. Huang B, Babcock H, Zhuang X (2010) Breaking the diffraction barrier: super-resolution imaging of cells. Cell 143:1047–1058
3. Herbert S, Soares H, Zimmer C, Henriques R (2012) Single-molecule super-resolution microscopy: deeper and faster. Microscopy & Microanalysis 18:1419–1429
4. Betzig E, Patterson GH, Sougrat R et al (2006) Imaging intracellular fluorescent proteins at nanometer resolution. Science 313: 1642–1645
5. Rust MJ, Bates M, Zhuang X (2006) Sub-diffraction-limit imaging by stochastic optical reconstruction microscopy (STORM). Nat Methods 3:793–795
6. Giepmans BNG, Adams SR, Ellisman MH, Tsien RY (2006) The fluorescent toolbox for assessing protein location and function. Sci Signal 312:217
7. Schnell U, Dijk F, Sjollema KA, Giepmans BN (2012) Immunolabeling artifacts and the need for live-cell imaging. Nat Methods 9:152–158
8. Shroff H, Galbraith CG, Galbraith JA, Betzig E (2008) Live-cell photoactivated localization

microscopy of nanoscale adhesion dynamics. Nat Methods 5:417–423

9. Enninga J, Mounier J, Sansonetti P, Van Nhieu GT (2005) Secretion of type III effectors into host cells in real time. Nat Methods 2:959–965
10. Müller B, Daecke J, Fackler OT, Dittmar MT, Zentgraf H, Kräusslich HG (2004) Construction and characterization of a fluorescently labeled infectious human immunodeficiency virus type 1 derivative. J Virol 78:10803–10813
11. Engelman A, Englund G, Orenstein JM, Martin MA, Craigie R (1995) Multiple effects of mutations in human immunodeficiency virus type 1 integrase on viral replication. J Virol 69:2729–2736
12. Adams SR, Campbell RE, Gross LA et al (2002) New biarsenical ligands and tetracysteine motifs for protein labeling in vitro and in vivo: synthesis and biological applications. J Am Chem Soc 124:6063–6076
13. Martin BR, Giepmans BNG, Adams SR, Tsien RY (2005) Mammalian cell-based optimization of the biarsenical-binding tetracysteine motif for improved fluorescence and affinity. Nat Biotechnol 23:1308–1314
14. Arhel N, Genovesio A, Kim KA et al (2006) Quantitative four-dimensional tracking of cytoplasmic and nuclear HIV-1 complexes. Nat Methods 3:817–824
15. Andresen M, Schmitz-Salue R, Jakobs S (2004) Short tetracysteine tags to beta-tubulin demonstrate the significance of small labels for live cell imaging. Mol Biol Cell 15:5616–5622
16. Lelek M, Di Nunzio F, Henriques R et al (2012) Superresolution imaging of HIV in infected cells with FlAsH-PALM. Proc Natl Acad Sci U S A 109:8564–8569
17. Ganser BK, Li S, Klishko VY, Finch JT, Sundquist WI (1999) Assembly and analysis of conical models for the HIV-1 core. Science 283:80–83
18. Arhel N (2010) Revisiting HIV-1 uncoating. Retrovirology 7:96
19. Di Nunzio F (2013) New insights in the role of nucleoporins: a bridge leading to concerted steps from HIV nuclear entry until integration. Virus Res 178:187–196
20. Henriques R, Lelek M, Fornasiero EF, Valtorta F, Zimmer C, Mhlanga MM (2010) QuickPALM: 3D real-time photoactivation nanoscopy image processing in ImageJ. Nat Methods 7:339–340
21. Charneau P, Mirambeau G, Roux P, Paulous S, Buc H, Clavel F (1994) HIV-1 reverse transcription a termination step at the center of the genome. J Mol Biol 241:651–662
22. van de Linde S, Löschberger A, Klein T et al (2011) Direct stochastic optical reconstruction microscopy with standard fluorescent probes. Nat Protoc 6:991–1009
23. Heilemann M, van de Linde S, Schüttpelz M et al (2008) Subdiffraction-resolution fluorescence imaging with conventional fluorescent probes. Angew Chem Int Ed 47:6172–6176
24. Sergé A, Bertaux N, Rigneault H, Marguet D (2008) Dynamic multiple-target tracing to probe spatiotemporal cartography of cell membranes. Nat Methods 5:687–694
25. Yee JK, Miyanohara A, LaPorte P, Bouic K, Burns JC, Friedmann T (1994) A general method for the generation of high-titer, pantropic retroviral vectors: highly efficient infection of primary hepatocytes. Proc Natl Acad Sci U S A 91:9564–9568
26. Henriques R, Griffiths C, Hesper Rego E, Mhlanga MM (2011) PALM and STORM: unlocking live-cell super-resolution. Biopolymers 95:322–331
27. Hess ST, Girirajan TP, Mason MD (2006) Ultra-high resolution imaging by fluorescence photoactivation localization microscopy. Biophys J 91:4258–4272
28. Pertsinidis A, Zhang Y, Chu S (2010) Subnanometre single-molecule localization, registration and distance measurements. Nature 466:647–651
29. Geisler C et al (2012) Drift estimation for single marker switching based imaging schemes. Opt Express 20:7274–7289
30. Wolter S, Löschberger A, Holm T et al (2012) rapidSTORM: accurate, fast open-source software for localization microscopy. Nat Methods 9:1040–1041
31. Brede N, Lakadamyali M (2012) GraspJ: an open source, real-time analysis package for super-resolution imaging. Opt Nanoscopy 1:11
32. Gaietta GM, Deerinck TJ, Ellisman MH (2011) Labeling tetracysteine-tagged proteins with biarsenical dyes for live cell imaging. Cold Spring Harb Protoc 2011. doi: 10.1101/pdb.prot5547

Chapter 13

Analysis of Protein Dynamics with Tandem Fluorescent Protein Timers

Anton Khmelinskii and Michael Knop

Abstract

Fluorescent timers (FTs) are fluorescent proteins that change color with time. FTs can be used as tags to follow protein dynamics in living cells. Recently we described a novel class of FTs called tandem fluorescent protein timers (tFTs). Each tFT is a tandem fusion of two different conventional fluorescent proteins having distinct kinetics of fluorophore maturation. tFTs suitable for studying protein dynamics on different scales can be generated from a broad range of commonly used fluorescent proteins. Here we describe how to establish new tFTs and consider potential pitfalls. We detail a protocol for quantitative fluorescence microscopy imaging and analysis of intracellular protein dynamics with tFTs in the budding yeast *Saccharomyces cerevisiae*.

Key words Fluorescent proteins, Tandem fluorescent protein timers, tFT, Protein dynamics, Protein turnover, Protein degradation, Proteostasis, Quantitative fluorescence microscopy

1 Introduction

Fluorescent proteins (FPs) are invaluable tools in modern biological research. Since the discovery of the green fluorescent protein (GFP) [1–3], a plethora of FPs with diverse properties—both naturally occurring and engineered—has been described [4–6].

Conventional single-color FPs, which include the popular GFP variant known as enhanced GFP (EGFP), are widely used as protein tags to follow protein expression and localization in vivo. Upon folding, these FPs acquire the ability to fluoresce in a process termed fluorophore maturation, whereby amino acid residues located inside the β-barrel fold react to generate a conjugated electron system of p-orbitals that constitutes the fluorophore. Characteristic to each single-color FP is one major fluorescence emission peak, which defines its color.

Fluorescent timers (FTs) are peculiar FPs that change color during fluorophore maturation. The first FT, the E5 mutant of the

Andrei I. Ivanov (ed.), *Exocytosis and Endocytosis*, Methods in Molecular Biology, vol. 1174,
DOI 10.1007/978-1-4939-0944-5_13,

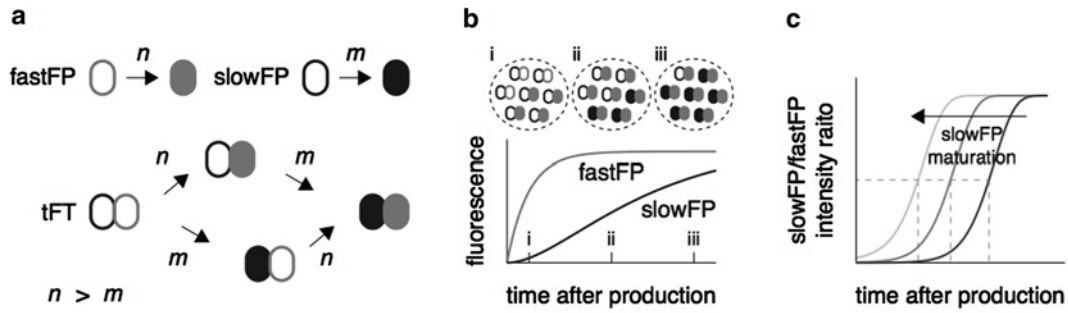

Fig. 1 Definition of tandem fluorescent protein timer (tFT). (**a**) A tFT is a tandem fusion of a fastFP, characterized by fast fluorophore maturation with rate constant *n*, and a slowFP, characterized by slow fluorophore maturation with rate constant *m*. (**b**) A pool of tFT molecules exhibits mostly only fastFP fluorescence early after production (time point [*i*]) and gradually acquires slowFP fluorescence (time points [*ii*] and [*iii*]). The color of the pool, represented by the slowFP/fastFP ratio of fluorescence intensities, provides a measure of time. (**c**) Theoretical curves of slowFP/fastFP ratios of fluorescence intensities over time (log scale) for tFTs composed of the same fastFP and different slowFPs with increasing fluorophore maturation rate constants (*arrow*). Each tFT provides a measure of protein age (time after production) in a specific time range centered at half maximum slowFP/fastFP ratio (*dashed lines*). Figure adapted from ref. 10

red fluorescent protein DsRed, is initially green fluorescent but becomes red fluorescent when fully matured [7]. This switch in color is caused by stepwise fluorophore maturation that occurs with reaction-specific rate constants and, therefore, provides a measure of time, making it possible to study temporal dynamics of intracellular processes with FTs. Although the strong tendency to oligomerize precludes the use of the DsRed-E5 timer as a protein tag, intracellular trafficking of proteins and organelles can be analyzed with monomeric FTs [8, 9].

Recently we expanded the definition of fluorescent timers to include the so-called tandem fluorescent protein timers (tFTs) [10]. A tFT is a tandem fusion of two single-color FPs that undergo fluorophore maturation with different kinetics, herein referred to as fastFP (faster maturation) and slowFP (slower maturation). It is because of the difference in maturation kinetics between the two FPs that a tFT changes color as a function of time, i.e., behaves as a timer (Fig. 1). The color of a tFT can be represented by the slowFP/fastFP ratio of fluorescence intensities and provides a measure of protein age. In a hypothetical case of an isolated pool of tFT molecules (instantaneously produced, not degraded), the slowFP/fastFP ratio is initially low, as only some fastFP molecules had time to mature, and monotonically increases with time as the pool ages until a plateau of complete maturation (Fig. 1). The situation is more complex in vivo, where various processes influence the lifetime of a protein. The average age of a protein in a cell is determined by the kinetics of production and degradation.

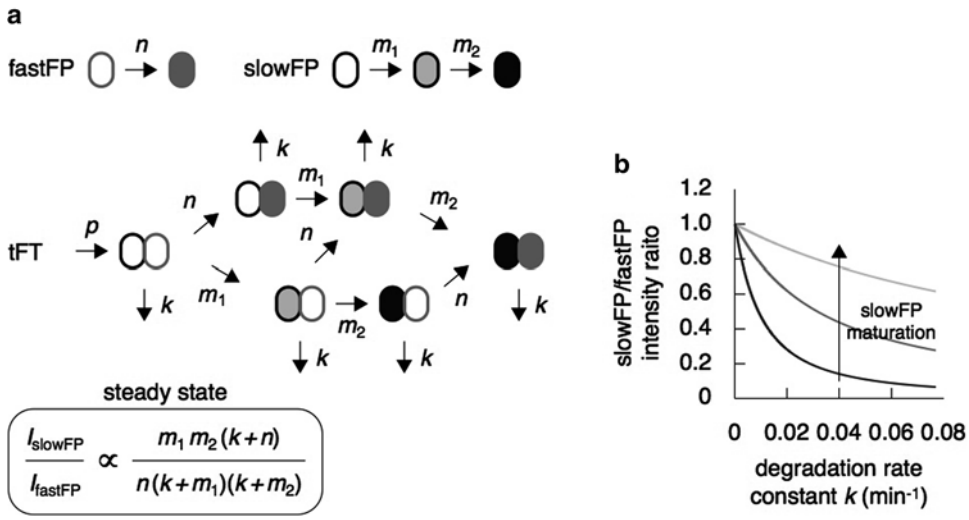

Fig. 2 SlowFP/fastFP ratio in steady state depends on tFT degradation kinetics. (**a**) Dynamics of a tFT produced with rate constant p and degraded with rate constant k. The tFT in this example is composed of a fastFP, which matures with rate constant n, and a slowFP that matures in a two-step process with maturation rate constants m_1 and m_2. Maturation of mCherry, a slowFP extensively used in this chapter, is more accurately described by a two-step process than a one-step process [10]. Note that all maturation intermediates are degraded with the same rate constant k. Solving a system of ordinary differential equations describing tFT dynamics reveals that in steady state the slowFP/fastFP ratio of fluorescence intensities is determined by the maturation properties of the tFT and depends on the degradation rate constant but not on the production rate constant [10]. (**b**) Theoretical curves of slowFP/fastFP ratios of fluorescence intensities as a function of degradation rate constant for tFTs composed of the same fastFP and different slowFPs with increasing fluorophore maturation rate constants (*arrow*). The curves are calculated according to the equation in (**a**), with $m_1 = m_2$ for simplicity, for a fastFP with a maturation half-time of 6 min and slowFPs with maturation half-times of 6, 20, and 60 min at each maturation step. The effect of protein dilution with cell division is included for a population doubling time of 90 min. Each curve is normalized to the maximum slowFP/fastFP ratio. Note that the maturation half-time $M_{1/2}$ is related to the maturation rate constant m as $M_{1/2} = \ln(2)/m$, and, similarly, the protein half-life $T_{1/2}$ is related to the degradation rate k constant as $T_{1/2} = \ln(2)/k$

On the subcellular level, the age of distinctly localized protein pools is additionally influenced by the kinetics of protein trafficking or, more generally, intracellular mobility. Protein tagging with tFTs can uncover qualitative aspects of intracellular protein dynamics and provide quantitative information on the kinetics of underlying processes. For example, for a tFT protein fusion with time-independent rate constants of production and degradation, the slowFP/fastFP intensity ratio in steady state is determined only by the degradation rate constant (Fig. 2). The slowFP/fastFP ratio decreases with increasing degradation kinetics as less slowFP can mature before destruction. This relationship can be used for comparative analysis of protein degradation kinetics and applied in high-throughput screens for regulators of protein stability [10].

The two single-color FPs composing a tFT are chosen based on fluorophore maturation kinetics, spectral characteristics, and oligomerization state. First and foremost, the two FPs must differ in fluorophore maturation kinetics. As the temporal range of processes that can be followed with a tFT is mostly determined by the maturation kinetics of the slowFP [10], the fastFP should be as fast maturing as possible, thus improving detection sensitivity. The slowFP should have a maturation half-time close to the duration of the process under investigation (Fig. 1). The two FPs should be spectrally separable, i.e., with clearly distinct emission spectra suitable for multicolor imaging, so that the fluorescence signals can be unequivocally attributed to each FP. Finally, both FPs should be monomeric. Because the oligomerization state of FPs is frequently determined in vitro, it is prudent to examine FP oligomerization in vivo in the relevant experimental system [11, 12]. Additionally, FPs with low pH sensitivity (i.e., a low p*K*a value) and high photostability and brightness are preferred [13]. Some of the brightest available single-color FPs can be used to generate tFTs suitable for sensitive measurements of intracellular protein dynamics in different organisms [10, 14].

In the first part of this chapter we describe a protocol to determine whether a particular pair of FPs functions as a timer. The protocol relies on the relationship between degradation kinetics of a tFT protein fusion and the corresponding slowFP/fastFP intensity ratio. The same procedure can be used to compare the degradation kinetics of different proteins tagged with an established tFT. In the second part of the chapter we describe a protocol for acquisition and processing of quantitative fluorescence microscopy images of yeast strains expressing tFT protein fusions. Visualizing protein distributions in terms of age can expose patterns of protein inheritance in asymmetric cell division, inform on protein exchange between subcellular compartments, and reveal local differences in activity of receptor-mediated signal transduction pathways [10, 14].

2 Materials

2.1 Yeast Culture Media and Plates

1. 24-Well and 96-well microtiter plates.
2. Gas-permeable adhesive seals for microtiter plates.
3. Microtiter plate shaker.
4. Rectangular plates (PlusPlates, Singer Instruments).
5. SC-Leu dropout powder mix: As previously described [15], mix thoroughly 5 g adenine, 20 g alanine, 20 g arginine, 20 g asparagine, 20 g aspartic acid, 20 g cysteine, 20 g glutamine, 20 g glutamic acid, 20 g glycine, 20 g inositol, 20 g isoleucine, 20 g lysine, 20 g methionine, 2 g para-aminobenzoic acid, 20 g phenylalanine, 20 g proline, 20 g serine, 20 g threonine,

20 g tyrosine, 20 g valine, 20 g histidine, 20 g uracil, 20 g tryptophan. All reagents can be obtained from Sigma-Aldrich. Store at room temperature, and protect from light.

6. SC Raf/Gal-Leu stock (2×): Add 6.7 g of yeast nitrogen base without amino acids (BD Difco), 2 g of SC-Leu dropout mix, 20 g of raffinose, 20 g of galactose, 100 mg of adenine, and 500 ml of distilled water to a 1 L bottle. Mix well, and filter sterilize (*see* **Note 1**).
7. SC Raf/Gal-Leu liquid medium: Mix one volume of the SC Raf/Gal-Leu stock with one volume of autoclaved distilled water.
8. SC Raf/Gal-Leu agar plates: Add 20 g of agar (BD Bacto), 500 ml of distilled water, and a magnetic stirring bar to a 1 L bottle. After autoclaving, add 500 ml of SC Raf/Gal-Leu stock preheated to ~65 °C. Mix thoroughly, and pour rectangular plates compatible with the pinning robot (*see* **Note 2**).
9. SC powder mix: Mix thoroughly 42.7 g of SC-Leu dropout mix with 4 g leucine. Store at room temperature, and protect from light.
10. SC glucose liquid medium: Dissolve 6.7 g of yeast nitrogen base without amino acids (BD Difco), 2 g of SC mix, 20 g of glucose, and 100 mg of adenine in 1 L of distilled water. Mix well, and filter sterilize.

2.2 Experimental Validation of Timer Behavior

1. Yeast strains carrying expression plasmids for different N-degron fusions or the empty plasmid (Table 1).
2. Disposable pin pads (96 long-pin RePads and 384 short-pin RePads, Singer Instruments).
3. Pinning robot (RoToR HDA, Singer Instruments).
4. Plate reader (Infinite M1000 Pro, Tecan).

2.3 Quantitative Fluorescence Microscopy for Analysis of Intracellular Protein Dynamics with tFTs

1. Yeast strains expressing proteins tagged with mCherry-sfGFP and the corresponding wild-type control strain that does not express any fluorescent proteins.
2. Bio-Conext (triethoxysilyl alkyl aldehyde, United Chemical Technologies): Dilute 1:1,000 in ethanol. Store at 4 °C.
3. Concanavalin A (Sigma-Aldrich): Dissolve in distilled water at concentration of 0.1 mg/ml. Store at 4 °C. Spin at 16,000 × *g* for 5 min at 4 °C before use.
4. 8-Well imaging chambers (Lab-Tek, Nunc) or 96-well imaging plates (Matrical) (*see* **Note 3**).
5. Wide-field epifluorescence microscope: DeltaVision Elite system (Applied Precision) consisting of an inverted epifluorescence microscope (IX71; Olympus) equipped with an LED light engine (SpectraX, Lumencor), 475/28 and 575/25

Table 1
N-degron constructs with different tFTs

Plasmid	Reference
p415-GAL1	[32]
p415-GAL1-Ubi-M*-mCherry-sfGFP (pDK70)	This manuscript
p415-GAL1-Ubi-I-mCherry-sfGFP (pMaM108)	[10]
p415-GAL1-Ubi-R-mCherry-sfGFP (pMaM107)	[10]
p415-GAL1-Ubi-M*-2×mCherry-sfGFP (pDK71)	This manuscript
p415-GAL1-Ubi-I-2×mCherry-sfGFP (pDK72)	This manuscript
p415-GAL1-Ubi-R-2×mCherry-sfGFP (pDK74)	This manuscript
p415-GAL1-Ubi-M*-mCerulean-Venus (pDK75)	This manuscript
p415-GAL1-Ubi-I-mCerulean-Venus (pDK76)	This manuscript
p415-GAL1-Ubi-R-mCerulean-Venus (pDK78)	This manuscript

excitation, and 525/50 and 624/40 emission filters (Semrock), a dual-band beam splitter 89021 (Chroma Technology), a 100× NA 1.4 UPlanSApo and 60× NA 1.42 PlanApoN oil immersion objectives (Olympus), an sCMOS camera (pco. edge 4.2, PCO), a motorized stage, and a temperature-controlled chamber (*see* **Note 4**).

6. Set of fluorescent reference slides (Applied Precision).

3 Methods

3.1 Experimental Validation of Timer Behavior

Here we describe a simple procedure to prove that a pair of selected FPs functions as a tFT in *S. cerevisiae*. The experiment requires at least two proteins that are degraded with different kinetics. We use synthetic proteins (N-degrons) that differ by a single amino acid residue, which determines the rate of degradation according to the N-end rule (Fig. 3) (*see* **Note 5**) [16]. Timer behavior is considered to be proven if yeast strains expressing N-degrons tagged with a potential tFT exhibit different slowFP/fastFP ratios of fluorescence intensities, such that the slowFP/fastFP ratio decreases with increasing degradation kinetics (Fig. 2) [10].

The protocol is illustrated with two different tFTs composed of the fast-maturing green fluorescent protein sfGFP [17] and the slower-maturing red fluorescent protein mCherry [18]. A tandem fusion of two FPs with similar maturation kinetics, the cyan fluorescent protein mCerulean [19] and the yellow fluorescent protein Venus [20, 21], is used for comparison. Whereas strains expressing N-degrons tagged with a tFT composed of mCherry and sfGFP

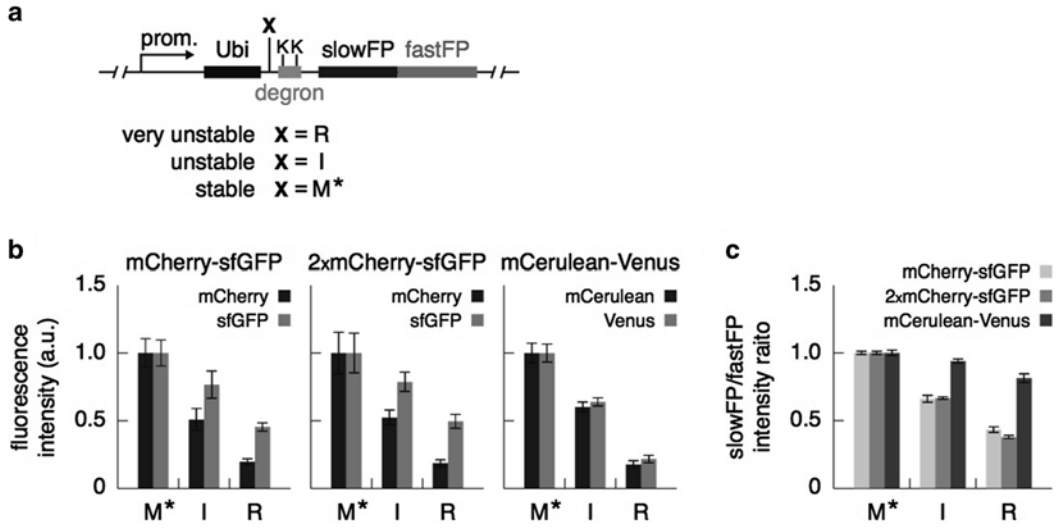

Fig. 3 Experimental validation of timer behavior. (**a**) N-degron constructs encode ubiquitin (Ubi) fusions. Co-translational cleavage of ubiquitin unmasks the N-terminal residue X. Fusions with destabilizing N-terminal residues (arginine (R) or isoleucine (I)) are targeted for proteasomal degradation. The stable fusion carries an N-terminal methionine residue (M) and two lysine (K)-to-arginine mutations in the degron sequence (*). (**b** and **c**) Fluorescence intensities and slowFP/fastFP intensity ratios of colonies expressing N-degron constructs with the indicated tFTs. 2×mCherry-sfGFP constructs carry two copies of the mCherry sequence, to improve detection in the mCherry channel, followed by sfGFP. All intensities were corrected for background and normalized to the intensity of the stable M* construct for each FP combination. Error bars indicated standard deviations ($n=8$ technical replicates of each colony placed next to each other on the same plate). The slowFP/fastFP intensity ratio decreases with increasing degradation kinetics for all combinations of FPs, proving that each functions as a tFT. However, the differences between the three N-degrons are less pronounced with the mCerulean/Venus timer because mCerulean and Venus mature with similar kinetics. Nevertheless, it is possible to conclude that Venus matures faster than mCerulean

should have clearly distinct mCherry/sfGFP ratios, N-degrons tagged with mCerulean-Venus are expected to have similar mCerulean/Venus intensity ratios.

The protocol starts after the following preparation steps have been carried out:

1. Obtain yeast codon-optimized DNA sequences of the selected FPs by full gene synthesis (*see* **Note 6**).
2. Construct the sequence encoding the tFT, with a flexible linker separating the two FPs (*see* **Note 7**).
3. Construct plasmids for expression of different N-degrons tagged with the tFT.
4. Generate strains, each carrying a different expression construct or the empty plasmid.

In this example, all constructs have been cloned into a centromeric plasmid (Table 1), are kept under selection on medium lacking leucine, and expressed under the control of the *GAL1* promoter on medium containing raffinose and galactose (*see* **Note 8**).

All strain manipulations should be performed under sterile conditions.

1. Distribute 150 µl of SC Raf/Gal-Leu liquid medium into each well of a 96-well microtiter plate, and inoculate sample strains from single colonies into individual wells, separated by wells with the control strain. Inoculate all the remaining wells with the control strain (*see* **Note 9**).
2. Seal the plate with a gas-permeable seal, mix on a microtiter plate shaker, and incubate at 30 °C for 1–2 days to allow growth until saturation.
3. Resuspend the cultures using a microtiter plate shaker. Transfer the strains from the 96-well plate onto an SC Raf/Gal-Leu agar rectangular plate in 384 format using the pinning robot and 96 long-pin pads, such that each strain is pinned four times (*see* **Note 10**). Incubate the agar plate at 30 °C for 1–2 days.
4. Transfer the colonies onto a new SC Raf/Gal-Leu agar rectangular plate using the pinning robot and 384 short-pin pads to smooth differences in colony size caused by the initial liquid to agar pinning. Incubate the new plate at 30 °C for 1–2 days.
5. Measure the fluorescence intensity levels of the colonies (except the two outermost rows and columns) (*see* **Note 9**) with a plate reader, using optimal excitation and emission wavelengths for each FP (*see* **Notes 11** and **12**).
6. Subtract from the fluorescence intensities of sample colonies the average fluorescence intensities of neighboring control colonies (background correction). Calculate the slowFP/fastFP ratios of intensities (Fig. 3).

3.2 Quantitative Fluorescence Microscopy for Analysis of Intracellular Protein Dynamics with tFTs

Dynamic processes on time scales between ~10 min and a few hours can be followed with a tFT composed of the fast-maturing monomeric green fluorescent protein sfGFP [17] and the slower-maturing monomeric red fluorescent protein mCherry [18]. Whereas sfGFP matures with a half-time of ~6 min, mCherry maturation can be described by a two-step process with maturation half-times of ~17 min (first step) and ~30 min (second step) in *S. cerevisiae* [10]. This makes the mCherry-sfGFP timer particularly suitable for studies of protein dynamics in this rapidly dividing organism.

Various applications only require single-time-point fluorescence imaging of strains expressing proteins of interests tagged with mCherry-sfGFP. For example, average mCherry/sfGFP intensity ratios of asynchronous populations, measured on whole-colony level (as described above) or on single-cell level with fluorescence microscopy (detailed below), are sufficient for comparing degradation kinetics of different proteins (or mutants of the same protein) or for comparing protein degradation kinetics

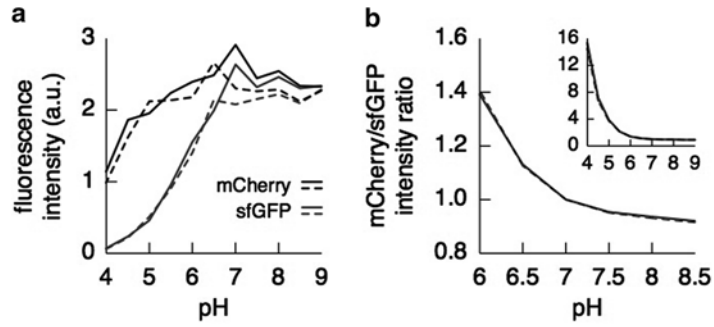

Fig. 4 pH sensitivity of the mCherry-sfGFP timer. (**a**) Fluorescence intensities of purified mCherry-sfGFP in solutions with indicated pH levels. Purified mCherry-sfGFP [10] was diluted to 20 μg/ml in buffers containing 50 mM Na_2HPO_4, 50 mM sodium acetate, and 50 mM glycine and with pH adjusted using NaOH or acetic acid. Fluorescence intensities were measured with a plate reader using optimal excitation and emission wavelength for each FP. All measurements are corrected for background by subtracting the fluorescence levels of the corresponding buffers. (**b**) Ratios of mCherry and sfGFP intensities from (**a**), normalized to the ratio at pH 7. Measurements from two independent experiments are marked with *solid* and *dashed lines*

in different conditions (genetic or environmental). Information on protein inheritance during cell division and intracellular protein trafficking can be extracted from local mCherry/sfGFP intensity ratios, measured for distinct subcellular protein pools with fluorescence microscopy [10].

Several aspects should be considered when analyzing protein dynamics with tFTs:

1. The two FPs composing a tFT can be affected differently by the intracellular environment. For example, sfGFP is more sensitive to pH than mCherry and the mCherry/sfGFP ratio of fluorescence intensities increases with decreasing pH (Fig. 4). In fact various tandem fusions of FPs, including a fusion of the red fluorescent protein mRFP1 and EGFP, can be used as indicators of intracellular pH [22, 23]. It is therefore not informative to directly compare mCherry/sfGFP intensity ratios of protein fusions localized to compartments with different pH (e.g., an acidic compartment such as the lysosome/vacuole and a pH neutral compartment such as the cytosol).
2. Genetic or environmental perturbations can similarly affect the behavior of a tFT. Moreover, because protein degradation is accomplished by two routes, effective degradation (destruction) and removal due to cell growth and division (dilution) [24], perturbations that affect population doubling time are expected to generally influence protein degradation kinetics measured with a tFT [10]. To control for such effects unrelated

Table 2
Modules for C-terminal protein tagging with the mCherry-sfGFP timer

Plasmid	Reference
pFA6a-mCherry-sfGFP-kanMX (pMaM17)	[10]
pFA6a-mCherry-sfGFP-natNT2 (pMaM61)	[10]
pFA6a-mCherry-sfGFP-hphNT1 (pMaM60)	[10]

to effective degradation, we typically analyze a series of tFT protein fusions with different stabilities (e.g., N-degron constructs described above) that provide a reference curve relating tFT ratios measured under different conditions or in different imaging sessions.

3. Protein dynamics can be influenced by tagging and expression levels [25]. Overexpression of some proteins results in rapid degradation of excess molecules that fail to assemble into complexes (e.g., ribosomal components [26]). Thus, unless overexpression is part of the experimental design, it is preferable to analyze protein fusions expressed at endogenous levels. We tag the proteins of interest with tFTs at endogenous chromosomal loci using conventional PCR targeting, with minor modifications of previously published protocols [27, 28]. Briefly, the mCherry-sfGFP module is amplified from one of the template plasmids for C-terminal tagging (Table 2) with a pair of ORF-specific primers (S2-ORF: the reverse complement of 55 bases downstream of the STOP codon (including STOP) of the gene, followed by 5′-ATCGATGAATTCGAGCTCG-3′; S3-ORF: 55 bases before the STOP codon (excluding STOP) of the gene, followed by 5′-CGTACGCTGCAGGTCGAC-3′). A high-fidelity DNA polymerase (e.g., Velocity DNA polymerase (Bioline)) is used for amplification to minimize the chance of introducing mutations into the tFT sequence during PCR, which could affect tFT fluorescence. Competent yeast cells are transformed following a modified lithium acetate method [29], using frozen competent cells, as described [27].

Here we detail a procedure for quantitative fluorescence microscopy imaging and analysis of yeast strains expressing proteins tagged with mCherry-sfGFP.

1. Distribute 1 ml of SC glucose liquid medium into each well of a 24-well microtiter plate, and inoculate strains from single colonies into individual wells (*see* **Note 13**). Incubate at 30 °C for 1–2 days to allow growth until saturation.
2. Prepare serial dilutions of each culture in a 24-well microtiter plate. Incubate at 30 °C for at least 12 h. At the end of this time

period, at least one of the dilutions should be in the exponential growth phase and have an optical density at 600 nm (OD_{600}) between 0.2 and 0.8 (~0.4×10^7 to 1.6×10^7 cells/ml).

3. Coat the wells of the imaging chamber/plate with concanavalin A: Cover the bottom of each well with Bio-Conext solution, incubate for 15 min, wash once with ethanol and once with distilled water, cover the bottom of each well with concanavalin A solution, incubate for 30 min, and wash twice with water.
4. Transfer exponentially growing cultures from the 24-well plate into the imaging chamber/plate (150 μl of culture at OD_{600} of 0.25 per well (~0.5×10^7 cells/ml)) (*see* **Note 14**). Place the wild-type control strain between sample wells (*see* **Note 15**). Let the cells settle and attach for at least 15 min before imaging (*see* **Note 16**).
5. Acquire fluorescence images (mCherry first, followed by sfGFP) and bright-field images (for cell identification) of multiple fields of view in each well (*see* **Notes 17** and **18**).
6. Acquire mCherry and sfGFP fluorescence images of a fluorescent slide to correct for uneven illumination of the field of view (flat-field correction) (*see* **Notes 19** and **20**).
7. Acquire mCherry and sfGFP fluorescence images of a fluorescent slide at different exposure times to determine the relationship between exposure time and fluorescence intensity levels of the imaging setup.
8. For each fluorescence channel, acquire multiple images without excitation light (dark images) with each exposure setting used in **steps 5**–7. Determine the average dark signal for each combination of channel and exposure time (*see* **Note 21**).
9. Subtract from all fluorescence images the average dark signal measured with the corresponding exposure settings. Correct the resulting images for lamp intensity fluctuations (*see* **Note 22**).
10. Perform flat-field correction on all sample and control fluorescence images: Calculate an average flat-field image for each fluorescence channel, smooth the average image by convolving with a Gaussian function, normalize to the maximum intensity in the image, and divide all sample and control fluorescence images by the flat-field image of the corresponding channel.
11. Determine the relationship between integrated image intensity and exposure time from the images acquired in **step 7** (and corrected following **steps 9** and **10**). Rescale the corrected sample and control images using this relationship to compensate for the different exposure times used during imaging acquisition.
12. Segment the cells (or the subcellular structures of interest) in the rescaled sample and control images (*see* **Note 23**). Record the mCherry and sfGFP intensities of each segmented object.

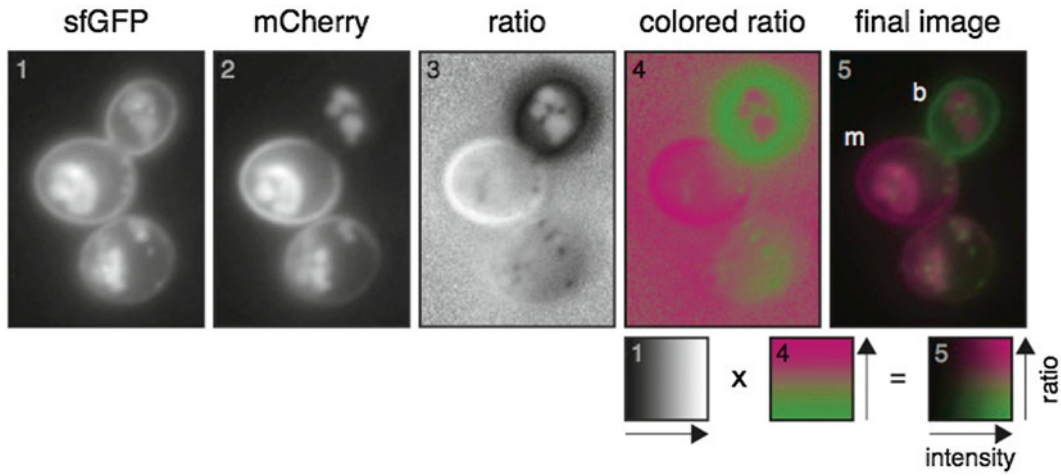

Fig. 5 Visualizing tFT protein dynamics with intensity-weighted ratiometric images. sfGFP (*1*) and mCherry (*2*) single-plane fluorescence microscopy images of cells expressing the plasma membrane proton pump Pma1 tagged with mCherry-sfGFP. The fluorescence images are corrected for uneven illumination and autofluorescence background. The mCherry/sfGFP ratiometric image (*3*) was color coded (*4*) and multiplied with the sfGFP image to obtain the sfGFP intensity-weighted ratiometric image (*5*). The final image shows that the plasma membrane pool of Pma1 is older in the mother cell (m) than in the bud (b). Two intracellular pools of Pma1 are observed: older Pma1 molecules in vacuoles and younger Pma1 molecules in punctate secretory compartments

13. Subtract from the fluorescence intensities of each object segmented in the sample images the median autofluorescence levels of cells from the corresponding control well (background correction). Determine the mCherry/sfGFP intensity ratio for each sample object.
14. Perform background correction on all sample images using the median cellular autofluorescence levels from the corresponding control well. Calculate intensity-weighted ratiometric images to visualize subcellular distributions of mCherry/sfGFP intensity ratios: divide each mCherry image by the corresponding sfGFP image to obtain a ratiometric grayscale image, convert the ratiometric image—color coded with a lookup table of choice—into RGB, and multiply each channel with the sfGFP image to obtain the final sfGFP intensity-weighted ratiometric image (Fig. 5).

4 Notes

1. Alternatively, sterilize the stock by autoclaving. However, autoclaving increases the fluorescence of the growth medium, and filter sterilization is preferred for imaging applications.
2. Pour plates (~50 ml of medium per plate) on a flat and perfectly horizontal surface, and ensure that plates are free of bubbles.

Leave plates drying with closed lids overnight at room temperature. Store at 4 °C.

3. Ensure that the thickness of the coverslip glass (typically ~170 μm) is compatible with the microscope objectives.
4. For systems equipped with a mercury arc lamp, consider that the intensity and stability of the illumination source decrease significantly with lamp age. We typically use mercury arc lamps between 20 and 100 h of their lifetime for quantitative fluorescence imaging.
5. Endogenous proteins with known degradation signals that can be exploited to manipulate degradation kinetics are suitable alternatives [10, 14].
6. We only optimize the sequences for frequency of codon usage.
7. We typically separate the two FPs in a tFT with a flexible linker composed of five glycine–alanine repeats. In our experience, the order of the two FPs does not influence the properties of a tFT [10]. However, tFT protein fusions, especially those undergoing fast degradation, are more likely to exhibit fastFP fluorescence than slowFP fluorescence. Therefore, we usually place the slowFP first, followed by the fastFP in tFT constructs used for protein tagging at the C-terminus. This arrangement eliminates the possibility that the absence of slowFP fluorescence is caused by premature stop codons introduced during the PCR step in the tagging procedure.
8. An inducible promoter such as the promoter of the *GAL1* gene is not a requirement of this protocol, and all constructs can be expressed from any strong constitutive promoter (e.g., the promoter of the *TDH3* gene, also known as the *GPD* promoter). However, constructs with inducible promoters have additional applications and can be used to characterize the maturation kinetics of a tFT in vivo [10].
9. After subsequent transfer to agar medium, fluorescence measurements of colonies in the outermost rows and columns will be discarded due to local differences in growth. We therefore inoculate all outermost wells with the control strain.
10. The strains can also be transferred from liquid to agar with manual pinning tools following previously described protocols [30]. Alternatively, spot the strains by pipetting 2–5 μl of each culture in a 96-spot grid.
11. On an Infinite M1000 Pro plate reader (Tecan), we normally use one of the central colonies to determine the optimal *z* position for measuring each plate, set the monochromators to the optimal (peak) emission and excitation wavelengths—with 10 nm bandwidth—for each FP, and perform the measurements using the 400 Hz frequency setting of the flash lamp, with ten flashes per colony and optimal gain settings for the detector.

12. Alternatively, the plates can be imaged on any system with wide-field illumination and camera-based detection. In this case, it is imperative to also acquire images of a fluorescent phantom (e.g., a plate with fluorescent agar medium) to correct sample images for uneven illumination (flat-field correction, detailed in the next protocol) before segmenting the colonies.
13. Use a 96-well microtiter plate for growing a large number of strains. Seal the plate with a gas-permeable seal, and mix on a microtiter plate shaker.
14. To unequivocally identify pairs of mother and bud cells, synchronize the strains with α-factor (2.5-h incubation at 30 °C with 10 μg/ml α-factor for *BAR1* strains or 1 μg/ml α-factor for *bar1*Δ strains). Attach the strains with concanavalin A to the imaging chamber during the last 30 min of synchronization, release from the G1 arrest by washing with fresh medium, and image between 45 and 90 min after release.
15. Cellular autofluorescence levels will be determined from images of the control strain for background correction of sample fluorescence intensities. We typically have one control well for every two sample wells. For strains with fluorescence levels close to autofluorescence, background correction can be improved by imaging sample and control cells mixed in the same well.
16. Optionally, let the cells settle for 15 min and carefully wash the wells once with SC glucose medium to remove unattached cells.
17. Adjust the exposure settings for each well to avoid overexposed images. Note that image quality is reduced by long exposure times (>2 s) due to cell and intracellular movements.
18. mCherry and sfGFP differ in their photostability. Bleaching during image acquisition can therefore alter the mCherry/sfGFP intensity ratio. To minimize bleaching, set the focus in the bright-field channel to the center of the cell layer. Acquire single-plane fluorescence images. Single-plane images are generally sufficient for relative comparisons of protein age and degradation kinetics. It is recommended to image first the dimmer, less photostable fluorescent protein. Thus acquire the mCherry channel first, followed by the sfGFP channel. Correcting for bleaching could be necessary in experiments that involve time-lapse imaging of a field of view. In such cases the correction factors can be determined from bleaching curves of each FP.
19. Any uniformly fluorescent sample can be used for flat-field correction. Instead of a fluorescent slide, we regularly image a solution of purified mCherry-sfGFP that is spiked with a few cells to help set the focal plane.

20. Ensure that the images are acquired at the same focal plane as the samples because the shape of the illumination field changes as a function of the focal plane. Set the exposure time such that the maximum intensity of the images is approximately at 70 % of the dynamic range of the camera. Acquire images of different fields of view to be able to remove the contribution of dust particles.
21. All image processing steps can be performed with freely available software such as ImageJ [31].
22. The DeltaVision system records the intensity levels of the illumination lamp for each image. Normalize all images to the maximum intensity level of an imaging session assuming a linear relationship between lamp intensity and fluorescence signal intensity. This step is particularly important for imaging setups with less stable sources of illumination (e.g., mercury arc lamp).
23. Segment the cells in the bright-field images, and apply the segmentation masks to the fluorescence images. Alternatively, perform the segmentation directly on the fluorescence images.

Acknowledgements

We thank Daniel Kirrmaier and Matthias Meurer for help with the experiments and Joseph D. Barry and Leopold Parts for comments and acknowledge support from the European Molecular Biology Organization to AK (EMBO ALTF 1124-2010) and from the Deutsche Forschungsgemeinschaft (SFB1036).

References

1. Shimomura O, Johnson FH, Saiga Y (1962) Extraction, purification and properties of aequorin, a bioluminescent protein from the luminous hydromedusan, *Aequorea*. J Cell Comp Physiol 59:223–239
2. Prasher DC, Eckenrode VK, Ward WW et al (1992) Primary structure of the Aequorea victoria green-fluorescent protein. Gene 111: 229–233
3. Chalfie M, Tu Y, Euskirchen G et al (1994) Green fluorescent protein as a marker for gene expression. Science 263:802–805
4. Tsien RY (1998) The green fluorescent protein. Annu Rev Biochem 67:509–544
5. Day RN, Davidson MW (2009) The fluorescent protein palette: tools for cellular imaging. Chem Soc Rev 38:2887
6. Chudakov DM, Matz MV, Lukyanov S, Lukyanov KA (2010) Fluorescent proteins and their applications in imaging living cells and tissues. Physiol Rev 90:1103–1163
7. Terskikh A, Fradkov A, Ermakova G et al (2000) "Fluorescent timer": protein that changes color with time. Science 290: 1585–1588
8. Subach FV, Subach OM, Gundorov IS et al (2009) Monomeric fluorescent timers that change color from blue to red report on cellular trafficking. Nat Chem Biol 5:118–126
9. Tsuboi T, Kitaguchi T, Karasawa S et al (2010) Age-dependent preferential dense-core vesicle exocytosis in neuroendocrine cells revealed by newly developed monomeric fluorescent timer protein. Mol Biol Cell 21:87–94
10. Khmelinskii A, Keller PJ, Bartosik A et al (2012) Tandem fluorescent protein timers for in vivo analysis of protein dynamics. Nat Biotechnol 30:708–714
11. Costantini LM, Fossati M, Francolini M, Snapp EL (2012) Assessing the tendency of fluorescent proteins to oligomerize under physiologic conditions. Traffic 13:643–649

12. Landgraf D, Okumus B, Chien P et al (2012) Segregation of molecules at cell division reveals native protein localization. Nat Methods 9: 480–482
13. Shaner NC, Steinbach PA, Tsien RY (2005) A guide to choosing fluorescent proteins. Nat Methods 2:905–909
14. Donà E, Barry JD, Valentin G et al (2013) Directional tissue migration through a self-generated chemokine gradient. Nature 503(7475):285–289
15. Sherman F (1991) Getting started with yeast. Methods Enzymol 194:3–21
16. Varshavsky A (2011) The N-end rule pathway and regulation by proteolysis. Protein Sci 20: 1298–1345
17. Pédelacq J-D, Cabantous S, Tran T et al (2006) Engineering and characterization of a superfolder green fluorescent protein. Nat Biotechnol 24:79–88
18. Shaner NC, Campbell RE, Steinbach PA et al (2004) Improved monomeric red, orange and yellow fluorescent proteins derived from *Discosoma sp.* red fluorescent protein. Nat Biotechnol 22:1567–1572
19. Rizzo MA, Springer GH, Granada B, Piston DW (2004) An improved cyan fluorescent protein variant useful for FRET. Nat Biotechnol 22:445–449
20. Nagai T, Ibata K, Park ES et al (2002) A variant of yellow fluorescent protein with fast and efficient maturation for cell-biological applications. Nat Biotechnol 20:87–90
21. Sheff MA, Thorn KS (2004) Optimized cassettes for fluorescent protein tagging in *Saccharomyces cerevisiae*. Yeast 21:661–670
22. Awaji T, Hirasawa A, Shirakawa H et al (2001) Novel green fluorescent protein-based ratiometric indicators for monitoring pH in defined intracellular microdomains. Biochem Biophys Res Commun 289:457–462
23. Gjetting SK, Ytting CK, Schulz A, Fuglsang AT (2012) Live imaging of intra- and extracellular pH in plants using pHusion, a novel genetically encoded biosensor. J Exp Bot 63:3207–3218
24. Alon U (2006) An introduction to systems biology. Chapman & Hall, New York, NY
25. Yewdell JW, Lacsina JR, Rechsteiner MC, Nicchitta CV (2011) Out with the old, in with the new? Comparing methods for measuring protein degradation. Cell Biol Int 35:457–462
26. Warner JR (1989) Synthesis of ribosomes in *Saccharomyces cerevisiae*. Microbiol Rev 53: 256–271
27. Knop M, Siegers K, Pereira G et al (1999) Epitope tagging of yeast genes using a PCR-based strategy: more tags and improved practical routines. Yeast 15:963–972
28. Janke C, Magiera MM, Rathfelder N et al (2004) A versatile toolbox for PCR-based tagging of yeast genes: new fluorescent proteins, more markers and promoter substitution cassettes. Yeast 21:947–962
29. Schiestl RH, Gietz RD (1989) High efficiency transformation of intact yeast cells using single stranded nucleic acids as a carrier. Curr Genet 16:339–346
30. Baryshnikova A, Costanzo M, Dixon S et al (2010) Synthetic genetic array (SGA) analysis in *Saccharomyces cerevisiae* and *Schizosaccharomyces pombe*. Methods Enzymol 470:145–179
31. Schneider CA, Rasband WS, Eliceiri KW (2012) NIH Image to ImageJ: 25 years of image analysis. Nat Methods 9:671–675
32. Mumberg D, Müller R, Funk M (1995) Yeast vectors for the controlled expression of heterologous proteins in different genetic backgrounds. Gene 156:119–122

Chapter 14

Synchronization of Secretory Cargos Trafficking in Populations of Cells

Gaelle Boncompain and Franck Perez

Abstract

In mammalian cells, secretory proteins are transported to their destination compartment via the secretory pathway. Cargos start their journey in the endoplasmic reticulum and then reach the Golgi complex where they are processed and sorted to be delivered to their target intracellular compartment. To analyze and visualize this flow of proteins, one needs to synchronize their transport. We recently developed the retention using selective hooks (RUSH) system enabling simultaneous and synchronous release of secretory cargos from the endoplasmic reticulum in a population of cells. Here, we describe how to subclone the gene coding for a cargo of interest into a RUSH plasmid and to monitor its synchronized transport along the secretory pathway in fixed samples and in living cells.

Key words Secretory pathway, Protein trafficking, Golgi-dependent transport

1 Introduction

To be delivered to their final destination, about one-third of newly synthetized proteins enter the secretory pathway in mammalian cells. After translation, secretory cargos are targeted to the endoplasmic reticulum (ER), and they reach then the Golgi complex where they are modified and sorted toward their destination compartment (e.g., plasma membrane, extracellular medium, lysosomes) [1, 2].

The easiest way to monitor the trafficking of a secretory cargo is to synchronize its transport. Over the last decades, several methods were developed to analyze the transport along the secretory pathway. These methods are mainly based on reversible temperature blocks: 15 °C to block proteins in the ER or 20 °C to accumulate proteins in the Golgi complex [3, 4]. Reversible perturbation using chemical molecules, such as brefeldin A [5] or monensin, is also frequently used, but these molecules have multiple targets and induce diverse effects that complicate the analysis. The main contribution to the field of anterograde trafficking was

Andrei I. Ivanov (ed.), *Exocytosis and Endocytosis*, Methods in Molecular Biology, vol. 1174,
DOI 10.1007/978-1-4939-0944-5_14,

brought by the thermosensitive mutant of VSVG (VSVGtsO45). This viral glycoprotein needs to trimerize to be exported from the ER and to enter the secretory pathway. At the restrictive temperature of 39.5 °C, this mutant is unable to trimerize and is blocked in the ER. Upon shifting to the permissive temperature of 32 °C, the protein folds properly and is transported through the Golgi complex toward the plasma membrane [6, 7]. The main drawbacks of these methods lie on the nonphysiological temperatures used and their difficult use for screening approaches. It also restricts the analysis to one type of secretory cargo.

To overcome these drawbacks, we developed a novel secretory assay named the retention using selective hooks (RUSH) system [8]. The RUSH system is a two-state secretion assay based on the retention of the cargo of interest in the ER and its synchronous release. It is based on the co-expression of two partners: the hook that stably resides in the ER and the reporter which is the secretory cargo to be studied. The interaction is mediated by streptavidin fused to the hook and a streptavidin-binding peptide (SBP) fused to the reporter (Fig. 1). In addition, a fluorescent protein (like EGFP, mCherry) is fused to the reporter to follow its transport using fluorescence imaging, in fixed and in living cells. At steady state upon expression, the reporter interacts with the hook and is blocked in the ER. To induce the synchronous release of reporter, biotin is added in the medium. Biotin binds to streptavidin and competes out the SBP tag releasing the reporter from the hook. The reporter is thus free to traffic toward its destination compartment. Depending on the topology of the protein, the retention can take place either in the lumen of the ER or at its cytoplasmic face. The choice of the ER hook is thus important to mediate the interaction between the hook and the reporter (Fig. 2). Since the RUSH system relies on the tagging of the reporter, prior knowledge about the fusion protein (e.g., with GFP) has to be taken into consideration. The place of the SBP tag and the fluorescent protein (if needed) must not affect the targeting of the cargo by masking some trafficking signals for instance.

This chapter describes the protocol to choose the appropriate location of the tags and the type of hook as well as the procedure to clone the gene of interest into the RUSH vector. It contains also protocols to detect and monitor the trafficking of the cargo of interest in fixed samples and in living cells.

2 Materials

2.1 Materials for Cloning

1. Restriction enzymes and CutSmart buffer from New England Biolabs (NEB).
2. Alkaline phosphatase from calf intestine and its 10× buffer from Roche.

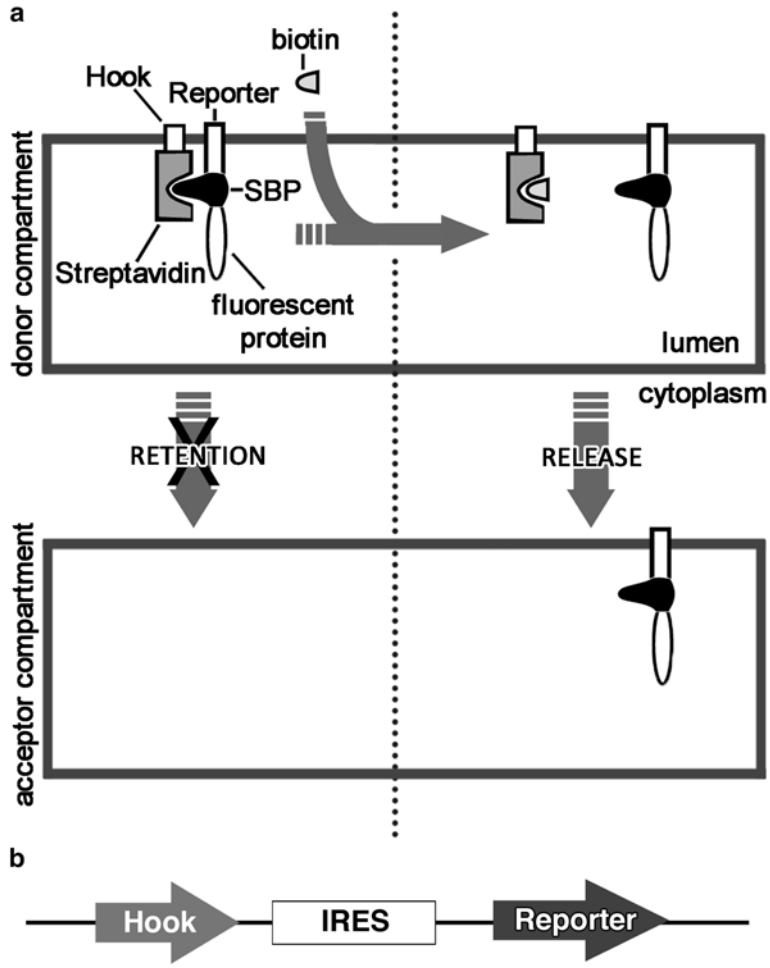

Fig. 1 Principle of the RUSH system. (**a**) The RUSH system is two-state secretory assay enabling retention of a cargo of interest in a donor compartment by interaction with a hook protein. Binding of the reporter to the hook is mediated by streptavidin fused to the hook and a streptavidin-binding peptide (SBP) fused to the reporter. Synchronous release of the reporter is induced by addition of biotin which competes out the SBP. The reporter is then free to traffic to its acceptor compartment. (**b**) A RUSH plasmid is a bicistronic expression vector. The hook protein is placed upstream of an internal ribosome entry site (IRES), and the reporter is placed downstream of the IRES. This orientation ensures that sufficient amount of hook is expressed to trap the reporter expressed in lower amount

3. T4 DNA ligase and its 10× ligation buffer from NEB.
4. TBE 10× buffer to prepare and migrate agarose gel: Weigh 108 g Tris base and 55 g of boric acid, add 40 mL of EDTA 0.5 M pH 8, and complete up to 1 L with distilled water. Store TBE 10× and 1× at room temperature.
5. 1 % Agarose gel: Weigh 1 g of ultrapure agarose, and add 100 mL of TBE 1× (dilute the TBE 10× in distilled water).

a

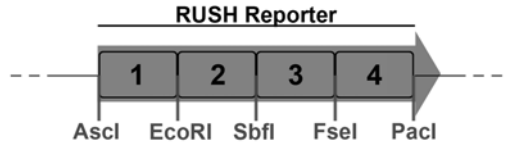

b

type of retention	topology of the protein X	cloning cassettes			
		1	2	3	4
luminal	soluble secreted	signal peptide	SBP	FP	X without signal peptide
		X with SP	SBP	FP	
	type I	signal peptide	SBP	FP	
	type II	X	SBP	FP	
cytoplasmic	type I	X with SP	SBP	FP	
	type II		SBP	FP	X

Fig. 2 Scheme of the RUSH reporter cassette and indication for the tagging. (**a**) The RUSH reporter cassette is divided into four cloning cassettes separated by restriction sites. (**b**) Depending on the topology of the cargo of interest (protein X) and on the type of retention (luminal or cytoplasmic) the gene is placed either in the first or in the fourth cloning cassette. Usually, the SBP tag is kept in the second cloning cassette and the fluorescent protein in the third one. *SP* signal peptide, *SBP* streptavidin-binding peptide, *FP* fluorescent protein

Boil with a microwave until the agarose is dissolved. Let the solution cool down a little bit, and add gel Green reagent 1 μL for 100 mL of agarose gel. Pour in a holder with adapted wells.

6. Nucleospin Gel and PCR Clean-up kit from Macherey-Nagel or equivalent.
7. *E. coli* DG1 thermocompetent bacteria or equivalent.
8. LB agar plates containing ampicillin.
9. NucleoSpin Plasmid Quickpure kit or NucleoBond Xtra Midi plus kit from Macherey-Nagel or equivalent for purification of DNA from liquid bacterial cultures.

2.2 Cell Seeding, Transfection, and Release with Biotin

1. Glass cover slips.
2. 24-Well plates.
3. Culture medium adapted to the cells.
4. Transfection reagent.
5. 100× Biotin stock solution (at 4 mM): Weigh 48 mg of D-biotin (Sigma, Cat. # B4501), and dissolve into 50 mL of culture medium. When biotin is completely dissolved, sterilize by filtration on a 0.22 μm membrane. Store at 4 °C for 3 months.

2.3 Cell Fixation and Immunofluorescence

1. 3 and 1 % paraformaldehyde (PFA) (from 16 % stock solution, Electronic Microscopy Sciences) solution prepared in PBS, pH 7.4.
2. Quenching solution: Weigh 2.67 g of NH_4Cl, and dissolve in 1 L of PBS pH 7.4. Store at room temperature.

3. Permeabilizing solution 10×: Weigh 4 g of bovine serum albumin (BSA) and 1 g of saponin. Adjust volume to 200 mL with PBS pH 7.4. Store aliquots at −20 °C.
4. Antibodies: Mouse monoclonal antibody directed to streptavidin (e.g., clone S10D4, Santa Cruz, sc-52234 used at 1:500). Mouse monoclonal antibody directed to SBP tag (e.g., clone 20, Millipore, MAB10764 used at 1:100).
5. Fluorophore-conjugated anti-mouse secondary antibodies (e.g., Jackson Immunoresearch).
6. Mounting medium: Weigh 6 g of glycerol and 2.4 g of Mowiol 4-88. Add 6 mL of distilled water, and incubate for 2 h at room temperature under agitation. Add 12 mL of 0.2 M Tris–HCl pH 8.5. Agitate for 2 h at 50 °C until it completely dissolved. Centrifuge for 15 min at 4,000 × *g*. Store aliquots at −20 °C for several months.

2.4 Videomicroscopy

1. Leibovitz's medium without phenol red (e.g., Life Technologies).
2. Glass-bottomed Petri dishes or Chamlide L-shape magnetic chamber (see below) with 25-mm glass cover slips, plastic tubing, and 1-mL syringes.
3. Inverted fluorescence microscope equipped with a thermostated incubation chamber.
4. Immersion oil.

3 Methods

3.1 Cloning the Gene of Interest in the RUSH Vector

Decide the orientation of tagging of the gene encoding the cargo of interest depending on its topology and on prior knowledge about fusion with tags or fluorescent proteins and about trafficking signals. The type of retention, luminal or cytoplasmic, is also an important parameter (*see* **Note 1**). To help the reader, please refer to Fig. 2. The RUSH reporter cassette is divided into four cloning cassettes where the gene of interest and its potential signal peptide, the SBP, and a fluorescent protein can be cloned.

1. Digest 5 μg of the RUSH plasmid to be used with the appropriate enzymes in NEB CutSmart buffer in a final volume of 50 μL for 1 h at 37 °C. The RUSH plasmids are available upon request to the authors [8, 9].
2. Dephosphorylate the vector by adding 5.7 μL of 10× alkaline phosphatase buffer and 2 μL of alkaline phosphatase to the digestion mix. Incubate for 30 min at 37 °C.
3. Purify the digested and dephosphorylated vector from agarose gel. We routinely use the NucleoSpin Gel and PCR Clean-up kit from Macherey-Nagel. Elute the 5 μg of prepared vector into 15 μL of elution buffer.

4. Prepare the insert (the gene of interest flanked with compatible restriction sites) either by PCR amplification or by gene synthesis. Digest 10 μg of the insert using the same enzymes as the ones used for the vector in NEB CutSmart buffer. Incubate for 1 h at 37 °C.
5. Purify the insert using the agarose gel extraction kit. Elute the digested insert in 25 μL of elution buffer.
6. Ligate the vector with the insert following the ratio of 1:3 (*see* **Note 2**). To do so, mix 50 ng of digested and dephosphorylated vector with the insert, 1 μL of 10× ligation buffer, and 0.5 μL of T4 DNA ligase in a final reaction volume of 10 μL. Incubate for 1 h at room temperature or overnight at 16 °C. Perform an autoligation control by preparing the same ligation mix without insert.
7. Transform *E. coli* bacteria. We routinely use chemically thermocompetent DG1 cells from Eurogentec. For these bacteria, prepare a tube with 25 μL of bacteria and 1.5 μL of ligation mix. Place on ice for 15 min. Perform the thermic choc for 45 s at 42 °C in liquid water bath. Incubate on ice for 5 min.
8. Add 300 μL of LB. Incubate at 37 °C for 30 min under agitation.
9. Plate on LB agar dishes containing ampicillin, since the RUSH plasmids bear an ampicillin resistance cassette. Incubate the plates overnight at 37 °C to let the colonies grow.

   Almost no colony should have developed on the plate corresponding to the autoligation control or at least a lot more colonies should be present on the plate with the ligation performed with the vector and the insert.
10. If the autoligation control is fully negative, directly pick one colony and amplify DNA using for example the NucleoSpin plasmid Quickpure kit or the NucleoBond Xtra Midi plus kit from Macherey-Nagel. Otherwise, pick a few colonies and carry out a plasmid mini-prep (Macherey-Nagel).
11. Check the gene encoding for the fusion protein (RUSH reporter) generated by restriction enzyme analysis and by sequencing.

3.2 Synchronous Release of the Cargo of Interest in Fixed Samples

Using the RUSH plasmid that you generated as described above, the retention and release of the cargo of interest can now be tested in cells and analyzed in fixed samples. By performing this end point assay, the efficiency of retention and the kinetics of transport can be evaluated.

1. Seed the adherent cells on 12-mm glass cover slips the day prior to transfection. Use 0.5 mL of culture medium for a well of 24-well plate.

2. Transfect the cells with the RUSH plasmid using the method adapted to the cells employed (*see* **Note 10**). As an example, we use HeLa cells and the calcium phosphate transfection method [10]. Transfect as many cover slips as necessary to perform incubation with biotin for different times. An important control is prepared using cells incubated with biotin since the transfection. In this condition, the hook and the reporter should not interact and thus the reporter should be localized at its target compartment (*see* **Notes 3** and **4**). Leave the other cover slips in medium without biotin.
3. The day after transfection, take one cover slip and keep it in medium without biotin. This cover slip will show the retention state of your cargo of interest.
4. Remove medium from the well, replace with 0.5 mL of medium containing biotin at 40 μM final (from a 100× biotin stock dissolved in medium), and incubate at 37 °C and CO_2 for the desired time. In a first experiment, 15 min, 30 min, 1 h, and 2 h of incubation with biotin should be sufficient to evaluate the kinetics of trafficking of the cargo of interest.
5. Fix the cells using a method suitable for the cells and the cargo studied. As an example, we routinely fix HeLa cells with 250 μL of 3 % PFA incubated for 15 min at room temperature.
6. Wash once with 1 mL of PBS.
7. Quench the free aldehydes using a quenching solution. Incubate for 5 min at room temperature.
8. Wash twice with 1 mL of PBS.
9. Add 250 μL of permeabilizing solution. Incubate for 5 min at room temperature.
10. Perform immunofluorescence to detect the hook using an antibody directed to streptavidin. If the reporter was fused to a fluorescent protein, its visualization does not require detection with an antibody (Fig. 3). If no fluorescent protein was used, an antibody directed to the SBP tag can be used.
11. Dilute the primary antibody in permeabilizing solution. Prepare a drop of 25 μL of the diluted antibody on a parafilm. Put the cover slip upside down in this drop; the cells should be in contact with the liquid. Incubate for 45 min at room temperature in a humid chamber to prevent desiccation.
12. Wash three times with permeabilizing solution.
13. Prepare the secondary antibody coupled to a fluorophore at the appropriate dilution. Incubate the cover slip upside down in a 25 μL drop of this secondary antibody for 30 min at room temperature.
14. Wash three times with permeabilizing solution.

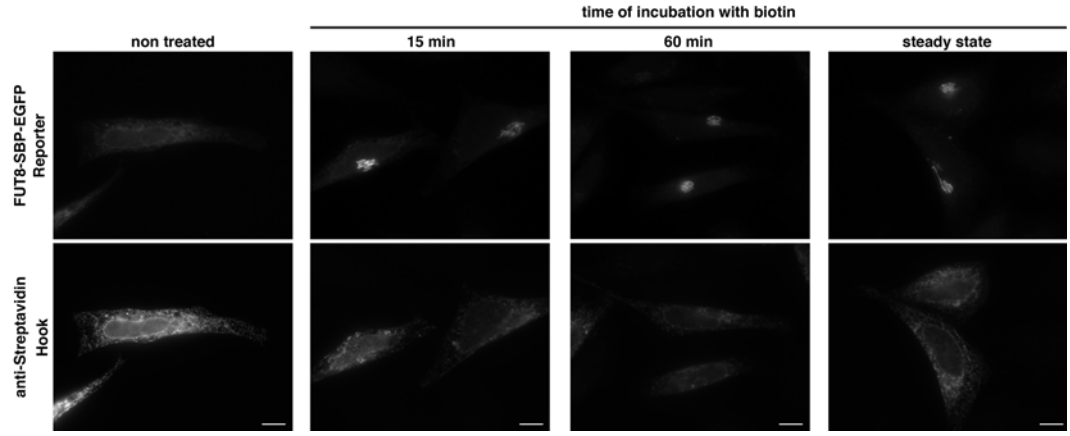

Fig. 3 Retention and release of the Golgi enzyme FUT8 (alpha-(1,6)-fucosyltransferase). HeLa cells transiently expressing the RUSH plasmid encoding for streptavidin-KDEL as a hook (luminal ER hook) and FUT8 as a reporter. Cells were incubated with biotin for 15 and 60 min and from the transfection (steady state with biotin). The retention state is shown in the cells not treated with biotin. The hook is detected by immunofluorescence using an antibody directed to streptavidin. The reporter is visualized using the intrinsic fluorescence of EGFP. Scale bar: 10 μm

15. Mount the cover slips on a glass slide with 5 μL of Mowiol containing DAPI. Take care to avoid air bubbles.
16. Let the mounting medium polymerize for a couple of hours before observation with a fluorescence microscope.

3.3 Detection of the Arrival at the Plasma Membrane of a Plasma Membrane Fated Cargo

A number of secretory cargos are destined to the plasma membrane. The method below describes a procedure to detect the arrival of this type of cargo at the plasma membrane by immunofluorescence on intact cells (Fig. 4).

1. Seed cells, transfect cells with the RUSH plasmid, and perform time course as described in the previous paragraph (*see* Subheading 3.2).
2. To perform a surface staining on intact cells, it is better not to fix the cells but to incubate the cells with the antibody directed to the surface protein at 4 °C (*see* **Note 5**). Fixation usually induces perforations in the plasma membrane resulting in entry of the antibodies and prevents specific detection of only the surface fraction of the protein.
3. The key parameter to perform good surface staining is to preincubate solutions on ice for several hours. Cool down on ice 100 mL PBS as well as a holder to incubate cover slips.
4. Wash cells twice with 1 mL ice-cold PBS.
5. Prepare diluted primary antibody directed to the extracellular part of the RUSH reporter in ice-cold PBS.

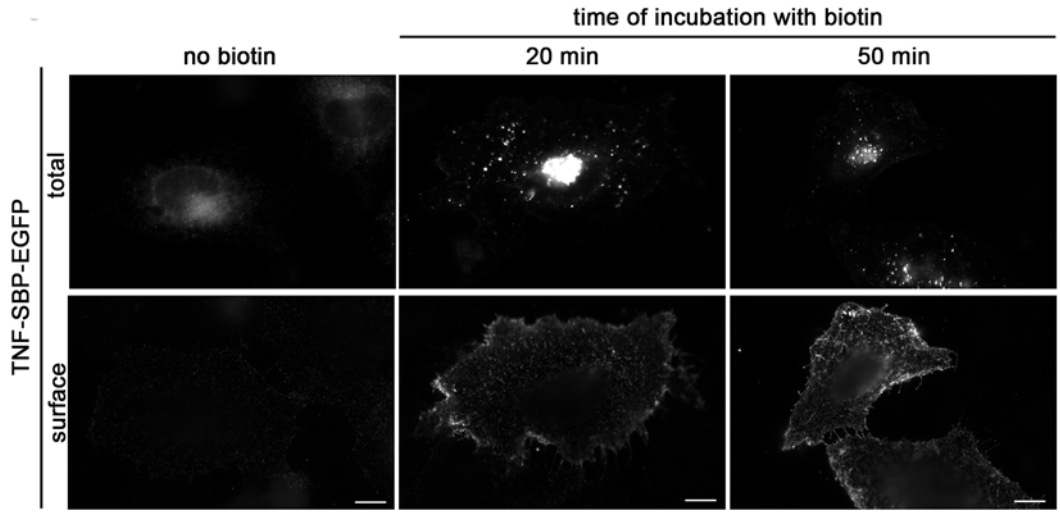

Fig. 4 Detection of the arrival of TNF-SBP-EGFP at the plasma membrane by surface immunolabelling. HeLa cells transiently expressing the RUSH plasmid encoding for streptavidin-KDEL as a hook (luminal ER hook) and TNF as a reporter. Cells were incubated with biotin for 20 and 50 min. The retention state is shown in the cells not treated with biotin (no biotin). Total TNF is observed using the intrinsic fluorescence of EGFP. Surface TNF is detected using an antibody directed to EGFP on intact cells. Scale bar: 10 μm

6. Place a 25 μL drop of diluted primary antibody on the ice-cold holder. Incubate the cover slip upside down on this drop for 45 min on ice.
7. Wash three times with 1 mL ice-cold PBS.
8. Fix with 250 μL of 1 % PFA for 15 min at room temperature. From here, the cells are fixed so that there is no need to work with ice-cold solutions.
9. Wash once with PBS. Quench the free aldehydes using a 50 mM NH_4Cl solution. Incubate for 5 min at room temperature.
10. Wash twice with PBS. At this step, if required, immunolabelling for an intracellular target could be performed (*see* **Note 6**).
11. Prepare the secondary antibody solution in PBS at the appropriate dilution.
12. Put the cover slip upside down in a 25 μL drop of secondary antibody. Incubate for 45 min at room temperature.
13. Wash three times in PBS.
14. Mount the cover slip in a 5 μL drop of Mowiol containing DAPI.
15. Let the mounting medium polymerize for a couple of hours before observation with a fluorescence microscope.

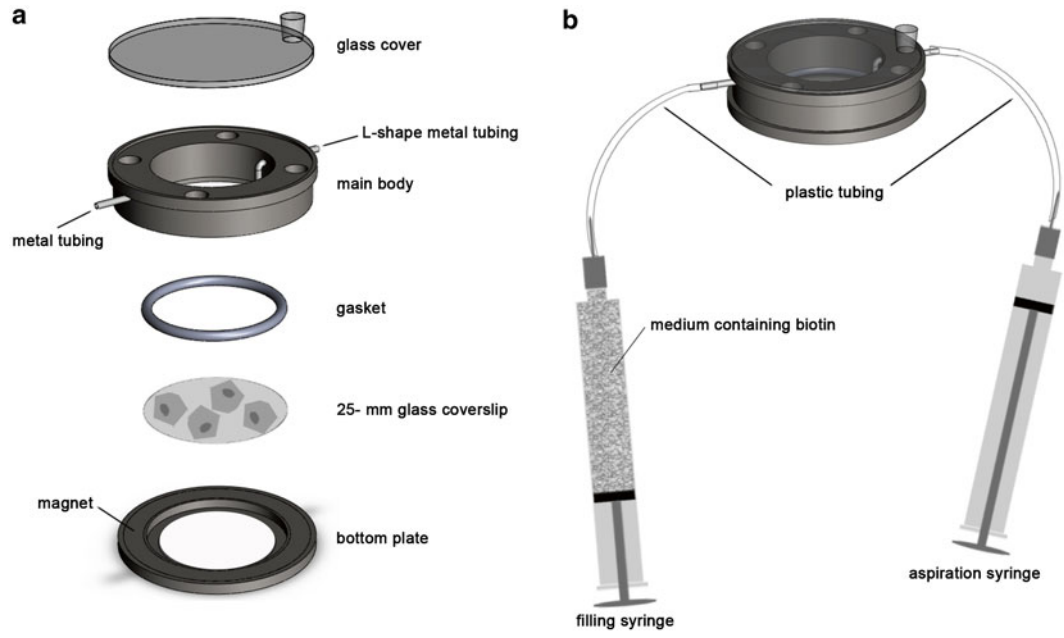

Fig. 5 Device for imaging the synchronous release of a cargo in living cells using magnetic L-shape Chamlide. (**a**) Components of the L-shape Chamlide. (**b**) Scheme of the assembled Chamlide and tubing to replace medium with medium containing biotin. Pictures adapted from www.chamlide.com (Live Cell Instruments)

3.4 Analysis of the Transport of the Reporter Using the RUSH System in Living Cells

The best way to visualize the different steps of the synchronized transport of the cargo of interest is to observe its release in real time. Since the RUSH system allows synchronization of the trafficking at physiological conditions for mammalian cells, release from the ER can easily be observed in living cells using time-lapse microscopy (*see* **Note 7**). This type of experiments requires adapted equipment, such as an inverted microscope equipped with a thermostated chamber driven by automatic software (e.g., Metamorph, Molecular Device). We performed such experiments using a spinning disk microscope (*see* **Note 8**).

1. Seed cells either on glass -bottomed Petri dishes adapted to videomicroscopy or magnetic chamber adapted to glass cover slips (such as L-shape Chamlide, Fig. 5). The L-shape Chamlide shows the advantage to be equipped with tubing to replace medium with medium containing biotin to induce a homogenous release. Below we describe the procedure that we use to perform time-lapse imaging with Chamlide magnetic chambers.
2. Transfect cells with the RUSH plasmid using an appropriate method.
3. The day after, transfer the cover slip into the Chamlide and assemble the chamber as depicted in Fig. 5.

4. Add 1 mL of pre-warmed Leibovitz's medium (without phenol red) (*see* **Note 9**).
5. Install the Chamlide on the stage of microscope.
6. Fill a 1-mL syringe with Leibovitz's medium containing biotin at 40 μM final. Place this syringe inside the thermostated chamber.
7. Connect the plastic tubing and syringes to the Chamlide.
8. Set up the focus and the acquisition parameters to visualize the reporter(s).
9. Mark positions of interest if you are able to perform multistage acquisition.
10. Acquire picture with a 30-s time interval and *z* stacks.
11. Let the microscope acquire about ten time points to visualize the retention state of the cargo of interest.
12. Between two time points, aspirate the medium contained in the chamber using the empty syringe connected to tubing.
13. Add 1 mL of Leibovitz's medium containing biotin using the previously filled and pre-warmed 1-mL syringe.
14. The next picture corresponds to time zero. Release of the reporter starts.
15. Continue time-lapse acquisition as long as necessary to visualize the trafficking of the cargo of interest.

4 Notes

1. Several ER hooks were developed [8]. Transmembrane proteins stably present in the ER (invariant chain of MHC and STIM-1) were tagged either in their luminal part or in their region cytoplasmically exposed to mediate either luminal or cytosolic retention. We also developed a soluble ER hook, streptavidin fused to the KDEL ER-retrieval peptide. Str-KDEL only mediates retention in the lumen of the ER. From our experiments, Str-KDEL is generally the most efficient luminal ER hook and the easiest to express due to its small size.
2. To estimate the relative amounts of vector and insert, load 1 μL of each on an agarose gel, migrate, and analyze fluorescence.
3. The hook should be localized in the ER both in the retention and in the release states. Immunofluorescence (using anti-streptavidin antibodies) to detect the hook is needed to check its location. If the hook follows the reporter in the retention state, retention will not occur properly and is probably due to a strong trafficking signal of the reporter. In this case, another hook has to be tried.

4. Some culture media (and/or serum) contain biotin that prevents the efficient retention of the reporter. We routinely use DMEM GlutaMax from Life Technologies that does not contain biotin. We identified OptiMEM, DMEM-F12, and RPMI-1640 from Life Technologies as media containing biotin. To overcome this problem, low amount of avidin (or streptavidin but it is more expensive) can be added in the medium to trap biotin contained in the medium and enable efficient retention. For example, we use 10^{-7} mol/L of avidin in OptiMEM and 0.4×10^{-8} mol/L in DMEM-F12 (both supplemented with 10 % serum). In this condition, the 40 μM biotin, added at $t = 0$, is still efficient to induce reporter release.
5. Incubation at 4 °C to perform surface immunolabelling has two effects: (1) to stop the anterograde trafficking of the cargo and (2) to inhibit endocytosis and thus prevent the internalization of the antibody.
6. In addition to surface immunolabelling on intact cells to detect the presence of the reporter at the plasma membrane, an intracellular staining against a subcompartment (e.g., the Golgi complex) can be performed. In this case, after incubation with the primary antibody and fixation with 1 % PFA, the cells had to be permeabilized using PBS pH 7.4 supplemented with BSA and saponin. Incubation with the antibody directed to the intracellular target is performed in permeabilizing solution at the appropriate dilution. Then, wash cells with permeabilizing solution and incubate with fluorophore-conjugated secondary antibodies.
7. Since the RUSH system is a fluorescence-based assay, several secretory cargos can be observed at the same time in the same cell. It facilitates the comparison of their mode of transport. To do so, fusion with different fluorescent proteins of different colors can be generated. Three-color imaging using tagBFP, EGFP, and mCherry combination can be realized to image the synchronous trafficking of three cargos.
8. During long-term acquisition (several hours) or medium changes, the focus of the fluorescence microscope could drift. Consequently, it is highly advantageous to equip the microscope with an autofocus module (e.g., Perfect Focus System). This module is very helpful when using the RUSH system in living cells, because medium has to be replaced with medium containing biotin while the sample is imaged under the microscope. This allows to follow retention and release states of the cargo of a same field in real time.
9. Note that the use of Leibovitz's prevents the user to fit a CO_2 device on the microscope stage since this medium is buffered. The addition of CO_2 to Leibovitz's medium can be toxic for living cells.

10. To overcome transient transfection of the RUSH plasmid and to obtain homogenous expression levels over the cell population, cells stably expressing the RUSH proteins can be established [8]. To achieve this, lentiviral transduction is highly efficient but has to be performed into two steps. First, establish a cell line stably expressing the hook and then transduce this cell line to express the reporter. For detailed protocols, read ref. 11.

References

1. Boncompain G, Perez F (2013) The many routes of Golgi-dependent trafficking. Histochem Cell Biol 140:251–260
2. Glick BS, Nakano A (2009) Membrane traffic within the Golgi apparatus. Annu Rev Cell Dev Biol 25:113–132
3. Matlin KS, Simons K (1983) Reduced temperature prevents transfer of a membrane glycoprotein to the cell surface but does not prevent terminal glycosylation. Cell 34:233–243
4. Saraste J, Kuismanen E (1984) Pre- and post-Golgi vacuoles operate in the transport of Semliki Forest virus membrane glycoproteins to the cell surface. Cell 38:535–549
5. Lippincott-Schwartz J, Yuan LC, Bonifacino JS, Klausner RD (1989) Rapid redistribution of Golgi proteins into the ER in cells treated with brefeldin A: evidence for membrane cycling from Golgi to ER. Cell 56:801–813
6. Kreis TE, Lodish HF (1986) Oligomerization is essential for transport of vesicular stomatitis viral glycoprotein to the cell surface. Cell 46: 929–937
7. Lafay F (1974) Envelope proteins of vesicular stomatitis virus: effect of temperature-sensitive mutations in complementation groups III and V. J Virol 14:1220–1228
8. Boncompain G, Divoux S, Gareil N et al (2012) Synchronization of secretory protein traffic in populations of cells. Nat Methods 9: 493–498
9. Boncompain G, Perez F (2012) Synchronizing protein transport in the secretory pathway. Curr Protoc Cell Biol 15:Unit15.19
10. Jordan M, Schallhorn A, Wurm FM (1996) Transfecting mammalian cells: optimization of critical parameters affecting calcium-phosphate precipitate formation. Nucleic Acids Res 24: 596–601
11. Boncompain G, Perez F (2013) Fluorescence based analysis of trafficking in mammalian cells. Methods Cell Biol 118:179–194

Chapter 15

Use of Transmembrane FRET to Investigate the Internalization of Glycosylated Proteins

Yoshimi Haga and Tadashi Suzuki

Abstract

The importance of glycans in various cellular events, especially intracellular and intercellular trafficking of proteins, has been reported in numerous studies. Here, we present a novel method to monitor endocytosis of proteins of interest bearing a specific glycan modification. Using a fluorescence resonance energy transfer technique, we investigated the role of glycan structure on the internalization of insulin-responsive glucose transporter GLUT4. We found that sialylated glycoforms of GFP-tagged GLUT4 appear to be internalized more slowly than non-sialylated GLUT4 upon insulin removal. This novel glycan imaging tool allows probing functional roles of specific glycan modifications in endocytosis of various proteins.

Key words FRET, Glycoform, Imaging, GFP, Azido sugar, Click chemistry

1 Introduction

N-glycosylation is one of the most common co- and posttranslational modifications of proteins. Recent advances in metabolic sugar engineering have proven to be a powerful tool for glycoproteomic analysis of a specific sugar modification [1–3]. In this technique, chemically modified sugars such as azide- or alkyne-modified sugars are incorporated into cellular glycans by means of the normal biosynthetic pathway and subsequently detected using click chemistry with a probe such as a FLAG tag, biotin, or fluorescent molecules [4–10]. However, the currently available techniques do face certain limitations. One of these limitations is that this method results in the labeling of all glycoproteins bearing the modified sugars; therefore, unless the protein of interest is isolated through laborious biochemical purification, analysis of a specific glycoprotein with the labeled sugar is not possible.

Recently, analyses of glycosyltransferase knockout mice have suggested that their pathological phenotypes are not always attributable to overall changes in sugar modifications, but rather the result of changes in glycan structures on a specific "target"

Andrei I. Ivanov (ed.), *Exocytosis and Endocytosis*, Methods in Molecular Biology, vol. 1174,
DOI 10.1007/978-1-4939-0944-5_15,

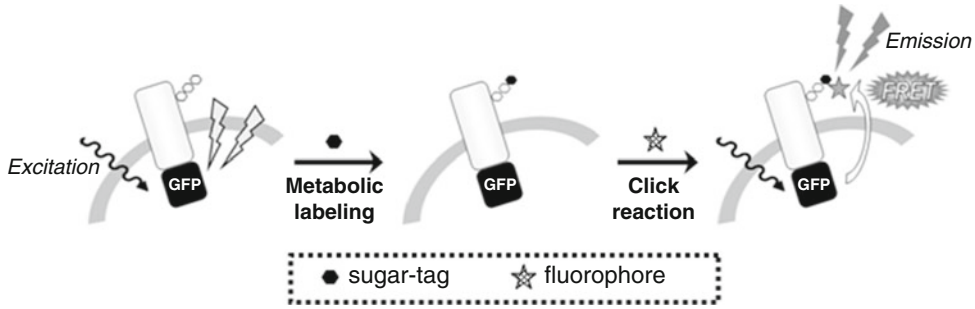

Fig. 1 FRET-based imaging of the glycosylation pattern of a specific glycoprotein. Glycans are metabolically labeled with azido sugars and click chemistry, and the target protein is conjugated with GFP. The specific glycoprotein can be visualized by FRET between GFP and the glycan-conjugated fluorophore (reproduced from [19])

glycoprotein [11–18]. Therefore, establishment of a novel technique to detect or monitor the glycosylation status of specific proteins in living cells is becoming an increasingly urgent issue.

To overcome the current problems, we combined the sugar-labeling technique with specific protein labeling, such as GFP fusion, to establish a method for detecting the glycoforms of a glycoprotein of interest. The rationale behind the idea is that if sugars can be labeled with a fluorescent probe which can be designed to be an acceptor for emission fluorescence released by GFP, we may be able to detect the glycoforms in a specific manner as intramolecular fluorescence resonance energy transfer (FRET) signals (Fig. 1).

Our analysis of the sialylated glycoform of glucose transporter GLUT4 indicated that glycan structure significantly affects the velocity of GLUT4 internalization [19]. In our imaging analysis, a clear difference in the internalization kinetics between the sialylated form (FRET) and the overall protein (GFP) was observed without any specific defects in the glycosylation pathway. This opens an avenue for direct measurements of the internalization kinetics of distinct protein glycoforms using an imaging technique.

2 Materials

1. Ac_4ManNAz (Molecular Probes, Eugene, OR).
2. Click-iT Alexa Fluor 555 DIBO alkyne (Molecular Probes).
3. Plasmids for the expression of GFP-tagged protein (*see* **Note 1**).
4. Glass-bottom dish (35-mm diameter).
5. FuGENE HD transfection reagent (Roche Applied Sciences, Indianapolis, IN).

6. Krebs–Ringer bicarbonate (KRB) buffer: 129 mM NaCl, 4.7 mM KCl, 1.2 mM KH_2PO_4, 5 mM $NaHCO_3$, 10 mM HEPES, 3 mM D-glucose, 2.5 mM $CaCl_2$, 1.2 mM $MgCl_2$, and 0.2 % BSA; pH adjusted to 7.4 with NaOH.
7. Human recombinant insulin.

3 Methods

1. Transfect cells of your choice (*see* **Note 2**) with the plasmids using the FuGENE HD transfection reagent, according to the manufacturer's protocol (*see* **Note 3**). Here, we used GLUT4-GFP (GFP-tagged GLUT4 glucose transporter) and HeLa cells.
2. Seed the cells onto a glass-bottom dish in appropriate medium and incubate in the absence or the presence of 100 μM Ac_4ManNAz for 2 days to incorporate azide-labeled sialic acid into the cellular glycans (*see* **Note 4**).
3. Prior to the imaging experiments, serum-starve the cells by incubating in KRB buffer with or without 100 μM Ac_4ManNAz for 3 h at 37 °C.
4. Stimulate cells with 100 nM insulin for 30 min.
5. Label cell surface azido sugars (SiaNAz) with 50 μM DIBO-555 in KRB buffer with 100 nM insulin for 5 min at 37 °C or for 1 h at 4 °C (*see* **Note 5**).
6. Wash the cells with KRB buffer three times.
7. Add pre-warmed KRB buffer, and acquire fluorescent images using laser scanning confocal microscopy (Fig. 2) or total internal reflection fluorescence (TIRF) microscopy equipped

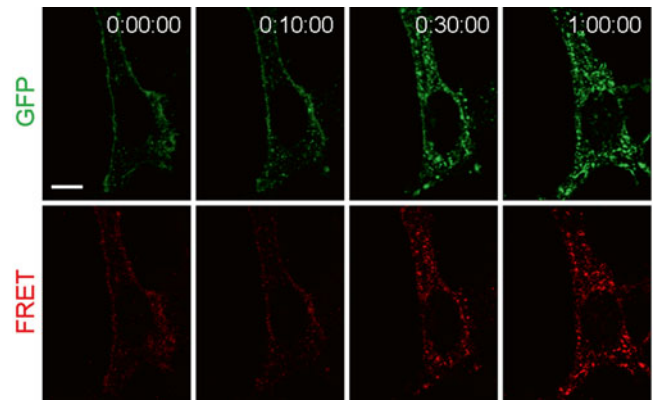

Fig. 2 Time-lapse imaging of sialylated GLUT4-GFP. HeLa cells transfected with GLUT4-GFP were treated with 100 μM Ac_4ManNAz, serum-starved, stimulated with insulin, and then labeled with DIBO-555 at 37 °C for 5 min. The cells were monitored by confocal microscopy. The time (h, min, s) is indicated at the top of each image. Scale bar: 10 μm

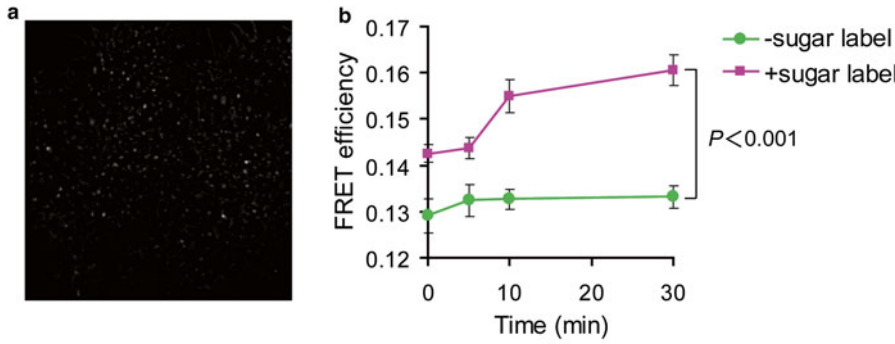

Fig. 3 Internalization analysis of sialylated GLUT4 using TIRF microscopy. (**a**) TIRF image showing the distributions of GLUT4-GFP. (**b**) Increased FRET efficiency after 5 min was observed, suggesting that more sialylated GLUT4 species were internalized at later time point (reproduced from [19])

with an incubator to maintain the cells at 37 °C throughout the experiments. To measure FRET, excite the sample at 488 nm and measure the fluorescence intensities of the donor (GFP) and acceptor (Alexa Fluor 555) using an appropriate filter set (*see* **Note 6**).

8. For endocytosis kinetics analysis, use TIRF images at each time point. In TIRF, only fluorophores very close (e.g., within ~100 nm) to the cover slip–sample interface are excited, thereby allowing the detection of events adjacent to the plasma membrane. Due to the technical problems, we used fixed cells for the quantitative analysis (Fig. 3), but if microscope setting allows, live imaging analysis should also be possible.
9. Subtract background from the fluorescence images in the GFP channel using the median filter of the MetaMorph software (Molecular Devices). Determine dot positions by setting the threshold for each image. The positions were then transferred to the corresponding image in the FRET channel, and the green and red pixel intensities were logged. Calculate the FRET efficiency as the ratio of red pixel/green pixel intensities.

4 Notes

1. A human GLUT4 cDNA was purchased from Open Biosystems (Huntsville, AL) and subcloned into pEGFP-N1 (Clontech, Mountain View, CA). GFP tag does not have to be on the cytosolic phase, but it is imperative that the tagging does not impair the function of protein. Elimination of nonspecific signal on FRET analysis is also very important (*see* **Note 6**).
2. In this particular case, cells have to be responsive to insulin.

3. For stable expression of GFP-tagged protein, maintain transfected cells in medium supplemented with a selection agent appropriate for the expression vector used (G418, neomycin, hygromycin, etc.), and isolate stably transfected cells using a FACS system.
4. The Ac_4ManNAz concentration is typically between 20 and 100 μM. The best working concentration should be determined empirically for each protein/cell line.
5. Place 100 μL of staining solution to cover the cells on the glass position of the glass-bottom dish.
6. As nonspecific FRET signals can also be detected, i.e., as bleed-through of GFP signal or autofluorescence, various careful control experiments are necessary before concluding that the signal detected is truly derived from intramolecular FRET. For instance, experiments with glycosylation-site mutants (N-to-Q mutants) will clarify if the detected signal is dependent on the glycosylation of the protein of interest. Other experiments such as acceptor photobleaching or emission spectra analysis are also imperative to confirm that the detected signal originates from FRET.

Acknowledgments

This work was partly supported by a Grant-in-Aid for Exploratory Research (25650041) from the Ministry of Education, Culture, Sports, Science and Technology of Japan (to T. S.) and a Grant-in-Aid for JSPS postdoctoral fellow (to Y. H.).

References

1. Dube DH, Bertozzi CR (2003) Metabolic oligosaccharide engineering as a tool for glycobiology. Curr Opin Chem Biol 7:616–625
2. Du J, Meledeo MA, Wang Z et al (2009) Metabolic glycoengineering: sialic acid and beyond. Glycobiology 19:1382–1401
3. Zaro BW, Yang YY, Hang HC, Pratt MR (2011) Chemical reporters for fluorescent detection and identification of O-GlcNAc-modified proteins reveal glycosylation of the ubiquitin ligase NEDD4-1. Proc Natl Acad Sci U S A 108:8146–8151
4. Saxon E, Bertozzi CR (2000) Cell surface engineering by a modified Staudinger reaction. Science 287:2007–2010
5. Vocadlo DJ, Hang HC, Kim EJ, Hanover JA, Bertozzi CR (2003) A chemical approach for identifying O-GlcNAc-modified proteins in cells. Proc Natl Acad Sci U S A 100:9116–9121
6. Hsu TL, Hanson SR, Kishikawa K et al (2007) Alkynyl sugar analogs for the labeling and visualization of glycoconjugates in cells. Proc Natl Acad Sci U S A 104:2614–2619
7. Baskin JM, Prescher JA, Laughlin ST et al (2007) Copper-free click chemistry for dynamic in vivo imaging. Proc Natl Acad Sci U S A 104:16793–16797
8. Laughlin ST, Baskin JM, Amacher SL, Bertozzi CR (2008) In vivo imaging of membrane-associated glycans in developing zebrafish. Science 320:664–667
9. Baskin JM, Dehnert KW, Laughlin ST, Amacher SL, Bertozzi CR (2010) Visualizing enveloping layer glycans during zebrafish early embryogenesis. Proc Natl Acad Sci U S A 107: 10360–10365
10. Dehnert KW, Beahm BJ, Huynh TT et al (2011) Metabolic labeling of fucosylated glycans in developing zebrafish. ACS Chem Biol 6:547–552
11. Taniguchi N, Miyoshi E, Gu J, Honke K, Matsumoto A (2006) Decoding sugar functions

by identifying target glycoproteins. Curr Opin Struct Biol 16:561–566

12. Muhlenhoff M, Manegold A, Windfuhr M, Gotza B, Gerardy-Schahn R (2001) The impact of N-glycosylation on the functions of polysialyltransferases. J Biol Chem 276:34066–34073
13. Wang X, Inoue S, Gu J et al (2005) Dysregulation of TGF-beta1 receptor activation leads to abnormal lung development and emphysema-like phenotype in core fucose-deficient mice. Proc Natl Acad Sci U S A 102:15791–15796
14. Wang X, Gu J, Ihara H et al (2006) Core fucosylation regulates epidermal growth factor receptor-mediated intracellular signaling. J Biol Chem 281:2572–2577
15. Partridge EA, Le Roy C, Di Guglielmo GM et al (2004) Regulation of cytokine receptors by Golgi N-glycan processing and endocytosis. Science 306:120–124
16. Ohtsubo K, Takamatsu S, Minowa MT et al (2005) Dietary and genetic control of glucose transporter 2 glycosylation promotes insulin secretion in suppressing diabetes. Cell 123: 1307–1321
17. Kitazume S, Imamaki R, Ogawa K et al (2010) Alpha2,6-sialic acid on platelet endothelial cell adhesion molecule (PECAM) regulates its homophilic interactions and downstream antiapoptotic signaling. J Biol Chem 285: 6515–6521
18. Lau KS, Partridge EA, Grigorian A et al (2007) Complex N-glycan number and degree of branching cooperate to regulate cell proliferation and differentiation. Cell 129:123–134
19. Haga Y, Ishii K, Hibino K et al (2012) Visualizing specific protein glycoforms by transmembrane fluorescence resonance energy transfer. Nat Commun 3:907

Chapter 16

A Method to Rapidly Induce Organelle-Specific Molecular Activities and Membrane Tethering

Toru Komatsu and Takanari Inoue

Abstract

In this chapter we describe a technique for rapid protein targeting to individual intracellular organelles. This method enables a real-time imaging-based study of cellular behavior in response to controlled induction of signaling events in a specifically targeted cellular compartment. We provide rationales and a step-by-step protocol for probe design and imaging of protein targeting along with two different applications of this technique. One application involves organelle-specific activation of small GTPases, while the other application involves membrane tethering of two different organelles. In the former case, we activate Rac1 and Ras at distinct intracellular locations in order to study compartmentalization of their signaling pathways, and in the latter example, we induce membrane tethering of the endoplasmic reticulum and mitochondria in order to study organelle–organelle communication. The described technique allows to rapidly perturb molecular activities and organelle–organelle communications at precise locations with specified timing and represents a powerful strategy to dissect spatiotemporally complex biological processes.

Key words Cell signaling, Fluorescence imaging, Synthetic biology, Small GTPases, Membrane lipid signaling, Organelle–organelle interaction, Endoplasmic reticulum

1 Introduction

Many cellular signaling pathways are precisely localized and rapidly induced in response to environmental stimulation. Elucidation of the nature and functions of complex signaling networks requires development of cellular probes that operate in the same time scale as the signaling events themselves, act in well-defined cellular domains, and can be activated at defined time points [1]. A major strategy employed for this purpose involves a chemically induced heterodimerization to trigger rapid-onset and specific perturbations of various signaling molecules in living cells [2–8]. Since most signaling events compose networks operating at multiple intracellular locations [9], it is important to specifically induce signaling in distinct cellular organelles, such as plasma membrane, the Golgi complex, mitochondria, the endoplasmic reticulum (ER), or lysosomes.

Andrei I. Ivanov (ed.), *Exocytosis and Endocytosis*, Methods in Molecular Biology, vol. 1174,
DOI 10.1007/978-1-4939-0944-5_16,

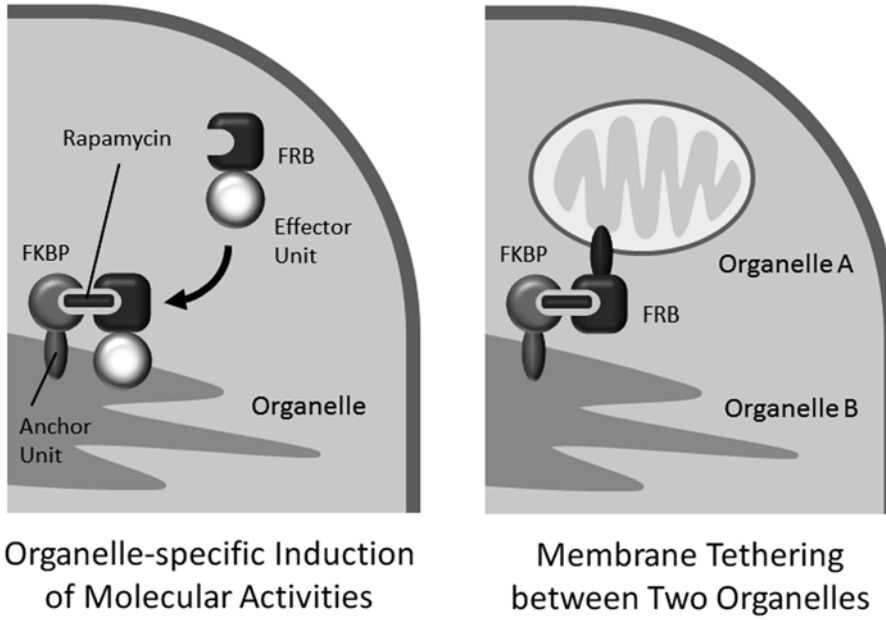

Fig. 1 Schematic illustration of the techniques described in this chapter

We achieved this goal in living cells via inducible dimerization of two engineered proteins triggered by addition of a chemical dimerizer and leading to the controlled organelle translocation of the proteins of interest. Specifically, we designed an anchoring unit that is attached to the cytoplasmic face of a specific organelle and an effector unit that is present in the cytosol and induces a signaling event upon translocation to the target membrane. Such translocation occurs via dimerization of the effector with the anchor, and it can induce site-specific signaling events on the organelle targeted by the anchoring unit (*see* Fig. 1, left). Furthermore, this technique can be used to dimerize two anchoring units (targeted to different organelles) in order to induce tethering of these organelles (*see* Fig. 1, right).

One commonly used example of a chemically induced dimerization system involves FK506-binding protein (FKBP) and FKBP-rapamycin-binding (FRB) domain, which can be dimerized by addition of rapamycin or its analogs such as indole rapamycin (*see* **Note 1**). Recent developments of this technique include photoactivatable dimerizers [10, 11], attempts to overcome a relative irreversibility of the standard FKBP–rapamycin–FRB system [12], and approaches to eliminate possible off-target effects of the method [13]. In this chapter, we describe the basic organelle-targeting technique and some of its cellular applications.

2 Materials

Prepare all solutions using analytical grade reagents under sterile conditions. Ensure that all relevant waste disposal regulations are followed when disposing waste materials.

2.1 Plasmid Design and Preparation

1. Vector DNAs: Plasmids for mammalian expression controlled by the cytomegalovirus (CMV) promoter. Single unit is encoded in a single plasmid (*see* **Note 2**).
2. cDNAs of proteins for the anchor unit and the effector unit.
3. Reagents for standard subcloning.

2.2 Cell Culture and Transfection (Preparation of Experiments)

1. Cultured cells (*see* **Note 3**): Maintain the cells at 37 °C in 5 % CO_2 atm at 90 % relative humidity in the appropriate cell culture medium.
2. Cell culture medium: Dulbecco's modified Eagle's medium (DMEM) supplemented with 10 % fetal bovine serum (FBS), 60 U/mL penicillin, and 60 U/mL streptomycin.
3. Cell transfection medium: DMEM supplemented with 10 % FBS without antibiotics (*see* **Note 4**).
4. DMEM without FBS: DMEM without FBS is used in transfection mixture preparation. Plasmid transfection can also be performed using Opti-MEM reduced serum medium.
5. Trypsin–EDTA (*see* **Note 5**).
6. Phosphate-buffered saline (PBS), pH 7.4.
7. Plasmids: Plasmid DNA is prepared at 1 μg/mL concentration in sterile water.
8. Transfection reagents: In the described experiments, we used Lipofectamine 2000 (Invitrogen), but other transfection reagents can also be used.
9. Polylysine-coated cover slips: Sterilize round glass cover slips (0.1–0.2 mm thickness and 25 mm diameter) with absolute ethanol, air-dry them, and apply 30 μL of poly-D-lysine solution (0.1 mg/mL) per each cover slip. Incubate for 30 min at room temperature, and wash twice with sterile PBS (*see* **Note 6**).
10. Metal frame: Serves as a chamber to hold cover slips for cell imaging (Fig. 2).

2.3 Fluorescence Microscopy

1. Chemical dimerizer: Prepare a 1,000× stock solution of a desirable chemical dimerizer in dimethylsulfoxide (DMSO) (*see* **Notes 7** and **8**). Since 100 nM of rapamycin is sufficient to induce dimerization, its stock solution should be prepared at 100 μM concentration. Other chemical dimerizers should be prepared by using appropriate organic synthesis.

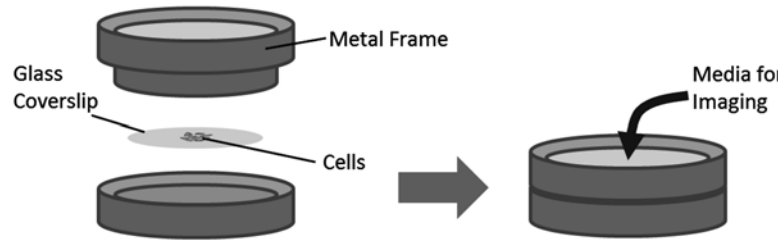

Fig. 2 Placement of cover slips in the metal frames

2. Physiological stimulant (such as growth factors or chemoattractants) (*see* **Note 9**): 1,000× Stock solution should be prepared following the manufacturer's instructions.
3. Fluorescent probes (such as calcium sensors and fluorescent lipids): 1,000× Stock solution should be prepared following the manufacturer's instructions (*see* **Note 10**).
4. Imaging media (*see* **Note 11**): PBS containing calcium and magnesium ions or phenol red-free DMEM.
5. Fluorescence microscope (*see* **Notes 12** and **13**): In our laboratory, live cell measurements are performed using a spinning-disc confocal microscope. Cyan fluorescent protein (CFP) and yellow fluorescent protein (YFP) are excited with a helium–cadmium laser and an argon laser (CVI-Melles Griot, NM, USA), respectively. These two lasers are fiber-coupled to the spinning disc confocal unit (CSU10; Yokogawa, Japan) equipped with dual-CFP/YFP dichroic mirrors. Appropriate filter sets for CFP and YFP are used to enable capture of fluorescence images with a CCD camera (Orca ER, Hamamatsu Photonics, Japan). Images are taken using a 40× objective lens mounted on an inverted microscope (Axiovert 200, Carl Zeiss, Germany). The microscope is operated by the MetaMorph software package (Molecular Devices, CA, USA).
6. Data analysis software.

3 Methods

3.1 Plasmid Design and Preparation

The dimerization system is composed of an anchoring unit and an effector unit. The anchoring unit is designed to localize on the cytosolic face of a specific organelle, and the effector unit is designed to induce specific signaling events on the surface of the organelle targeted by the anchor. Plasmids for the anchoring and the effector units should be prepared by using standard subcloning protocols.

1. Construct design for the anchoring unit:
   The design of the anchoring unit is based on proteins that are known to specifically localize in the target organelle. This unit also includes a fluorescent protein and one of the two dimerizing

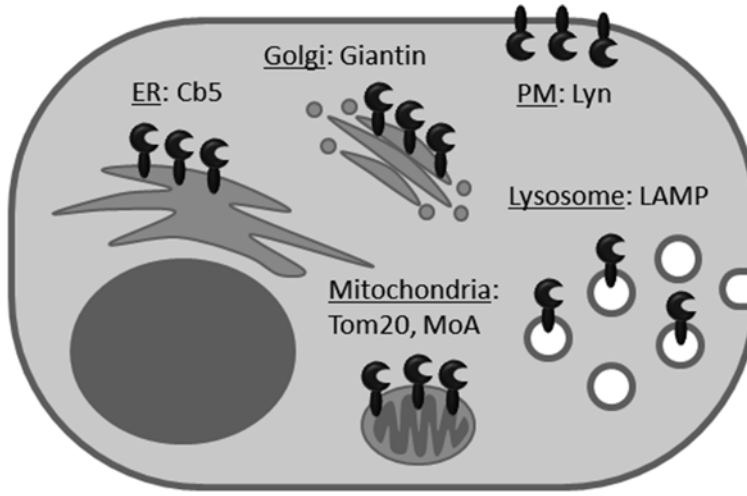

Organelle	Name	Constructs
Plasma Membrane (PM)	Lyn	Lyn *N*-terminus sequence (GCIKSKGKDSA)
Golgi	Giantin	Giantin (3131-3259)
Endoplasmic reticulum (ER)	Cb5	Cytochrome b5 (100-134)
Lysosome	LAMP	Lysosomal-associated membrane protein 1 (1-417)
Mitochondria	Tom20 MoA	Tom20 (1-33) Monoamine Oxidase A (490-527)

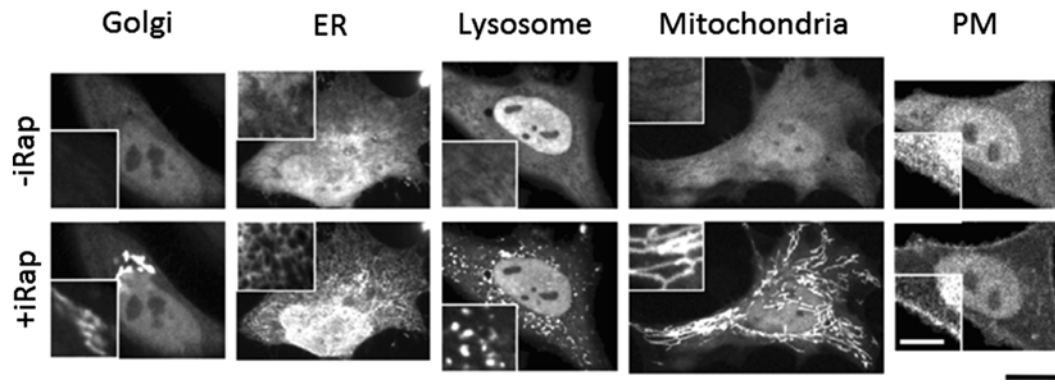

Fig. 3 Examples of the organelle-specific targeting constructs. Fluorescence images at the bottom show the translocation of cytosolic protein upon dimerization (+iRap) with the corresponding anchoring unit. Scale bar, 20 μm (scale bar in *insets*, 5 μm). The images are reproduced from [1] with permission

domains that are targeted to the cytosolic face of the organelle. The already designed organelle-targeting constructs are summarized in Fig. 3 [1]; however, it may be important to design novel organelle anchors. Here, we describe how to develop such a novel unit using the Golgi anchoring motif as an example.

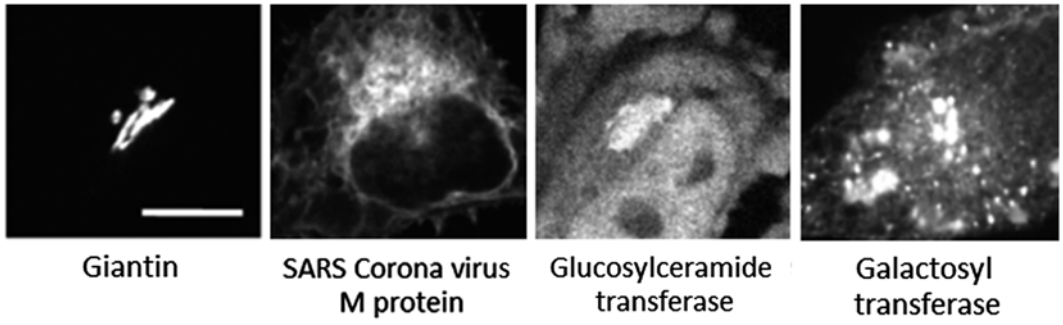

Fig. 4 Fluorescence images of candidate Golgi-targeting proteins. A giantin-based construct specifically localizes in the Golgi complex. By contrast, constructs based on SARS Corona virus M protein and glucosylceramide transferase demonstrate ER and cytosolic localization, respectively. Expression of a galactosyl transferase-based construct disrupts integrity of the Golgi complex. Scale bars, 20 μm. Reproduced from [1] with permission

Since it is impossible to predict the cellular localization of a particular protein based on its structural features, new anchors should be developed using a trial-and-error approach involving structural analysis of known organelle-resident proteins. To obtain motifs that specifically target the Golgi complex, we tried four different Golgi proteins and found that constructs derived from giantin work the best (Fig. 4). Giantin is a Golgi-specific structural protein [14] that is known to interact with multiple proteins to maintain the Golgi structure [15]. Since we intended to eliminate unwanted interactions between the anchoring unit and other proteins, we focused on the giantin sequence around its transmembrane domain (TMD). We found that a minimum sequence around the TMD is successfully targeted to the Golgi without disrupting morphology of this organelle. Therefore, this sequence was selected as the Golgi anchoring unit.

Next, we selected the dimerization domain and optimized the order of the dimerization domain and the fluorescent protein in the designed construct. These two parameters are known to affect the expression level of the anchor, the heterodimerization rate, and the structural features of the targeted organelle (***see*** **Note 14**). Specifically, we swapped FKBP with FRB and placed FKBP or FRB at the N-terminal or the C-terminal ends of either the fluorescent protein or the anchoring motif. A construct with the following order, FKBP–(fluorescent protein)–(giantin TMD), appears to be the most suitable for our purposes.

2. Construct design for the effector unit:
The effector unit can be designed to perturb cellular signaling mediated by small GTPases [1, 2, 16, 17] or phosphoinositides [3, 16, 18]. Here we describe the design of the effector construct

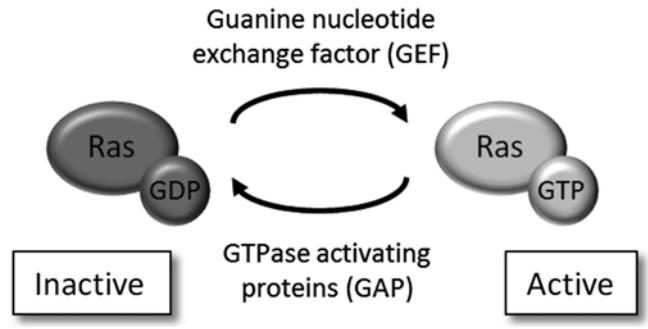

Fig. 5 The activity cycle of the Ras GTPase. Constitutively active Ras mutants have point mutations that block the GTP–GDP exchange. As a result, these mutants remain in the active state independently of cellular activities of their GEF and GAP

aimed to perturb GTPase signaling. GTPases are known to cycle between an active, GTP-bound and inactive, GDP-bound forms. The activation step is controlled by guanine nucleotide-exchanging factors (GEF), whereas the inactivation step is accelerated by GTPase-activating proteins (GAP) (Fig. 5). Based on this activation–inactivation cycle two different strategies for modulating GTPase signaling have been designed. One strategy is to create a constitutively active GTPase that is not regulated by GEF and GAP, and the other strategy is to use a specific GEF for the targeted GTPase. The first approach was used to recruit constitutively active forms of Rac1, Cdc42, and RhoA to the cellular membranes [2]. The second, more natural approach to activate endogenous GTPases was used to target Rac1 [2, 17], Ras [1], and Arf6 [16]. The design of the effector unit involves removing domains that determine effector compartmentalization to ensure its localization in the cytosol prior to dimerization. Afterwards, dimerization domains and fluorescent proteins are attached in various orders and pairings, and the activity of the constructs is tested.

3. Plasmid preparation:
   Prepare the plasmids according to standard subcloning protocols using the design strategy described above. Validate all plasmids by sequencing.

3.2 Cell Culture and Transfection (Preparation of Experiments)

1. To study organelle-specific cellular events and membrane tethering, select plasmid pairs containing appropriate anchoring and effector units. To study the morphology and functions of the targeted organelle, prepare required protein biosensors (*see* **Note 15**), antibodies for immunolabeling (*see* **Note 16**), and small molecular fluorescent probes, such as calcium sensors and fluorescent lipids (*see* **Note 17**).

2. Pre-warm culture media, DMEM with FBS and without antibiotics, trypsin, and DMEM without FBS at 37 °C.
3. Prepare the transfection mixture in a 1.5 mL sterile microcentrifuge tube. Its composition depends on the transfection reagents used. For Lipofectamine 2000 transfection, dilute up to 2 μg (normally 0.3–1.2 μg) of plasmid DNA and 4.5 μL Lipofectamine in 100 μL DMEM without FBS. If multiple constructs are transfected, their ratio should be optimized by testing expression of each construct.
4. Incubate the transfection mixture for 20 min at room temperature.
5. In the meantime, prepare glass cover slips coated with poly-D-lysine.
6. Trypsinize cells, transfer them into 15 mL tube using 10 mL of the culture medium, and spin them down (1,000 × *g* for 3 min).
7. Resuspend the cells into 1 mL culture media for transfection (per condition).
8. Add 1 mL of resuspended cells to 100 μL of the transfection mixture, and mix them well by gentle pipetting.
9. Add 50 μL of the cell suspension onto each cover slip.
10. Leave the cover slips in the incubator for 1 h (*see* **Note 18**).
11. Aspirate the media, and add 1 mL of fresh culture media for transfection.
12. Acquire images 24 or 48 h post-transfection.

3.3 Fluorescence Microscopy

1. Wash cover slips twice with PBS, and place them into metal frames filled with the imaging medium. The medium should not contain chemical dimerizer that should be added only during the fluorescence imaging.
2. Use confocal microscopy for image acquisition. Usually a single Z-point (preferably around the center of the cells), where the translocation and following signaling events can be clearly visualized, is selected for the imaging. For short imaging times (<30 min), neither incubation at 37 °C nor CO_2 are necessary, but these conditions are desirable for longer imaging in order to preserve cell viability.
3. Under the microscope, select the cell(s) for monitoring in the live imaging mode. These cells should contain all the constructs required for the perturbation and monitoring, which should be confirmed by checking appropriate fluorescence signals. Cells that are unusually dim or bright, or that show aberrant localization of the construct, should not be selected (*see* **Note 19**).
4. Start the image acquisition in a time-lapse mode. The time frame should be determined depending on the event to be monitored.

Usually, translocation is completed within 10 s after addition of chemical dimerizer, so images are generally acquired every 10 or 15 s.

5. After time-lapse imaging has been started, add the chemical dimerizer. It is important to minimize the focus drift during addition of chemical dimerizer. We achieve this by removing half of the medium (500 μL in the case of imaging in 1 mL volume) from the dish by mechanical pipette, mixing it with the chemical dimerizer, and then gently returning it back into the dish (*see* **Note 20**). Then, the dimerizer rapidly reaches cells by diffusion, so the translocation should begin immediately. The microscope operating software should be used to monitor the timing of stimuli for subsequent data analysis.
6. Acquire images until the event of interest is completed.

3.4 Data Analysis

1. Use the image acquisition software or other image analysis software for the data analysis. Evaluate translocation of constructs and biosensors by taking regions of interest (ROIs) and calculating the fluorescence signal intensity in these regions (Fig. 6, top and middle).
2. Alternatively, quantify the probe translocation by measuring the decrease of its fluorescence intensity in the cytosol (*see* Fig. 6, bottom). The latter approach is useful to examine protein translocation to irregular compartments or small or thin organelles, where quantification may be difficult due to cellular movement. For example, translocation of Ras-binding protein to the Golgi complex can be examined by monitoring the increase in fluorescence intensity of the Golgi. On the other hand, translocation to the plasma membrane is better analyzed by monitoring the decrease in the cytosolic fluorescence, because the plasma membrane is thin, and its fluorescence measurements suffer from high noise level due to ROI drift.

3.5 Examples of Applications

1. Compartmentalization of Ras signaling:
Ras localizes on various membranes of living cells, and its activation has been observed at the plasma membrane and/or the Golgi complex in T cells, depending on the type of stimulus [9]. To distinguish between different membrane pools of Ras, we designed the organelle-specific anchoring units together with the effector unit consisting of a guanine nucleotide exchange factor for Ras (RasGEF). This allowed us to investigate the output of compartmentalized Ras signaling.

   We detected formation of membrane ruffles a few minutes after targeting of active Ras to the plasma membrane (Fig. 7). Oppositely, targeting of active Ras to the Golgi complex did not cause changes in plasma membrane dynamics. This data suggests that local activation of Ras at the plasma membrane,

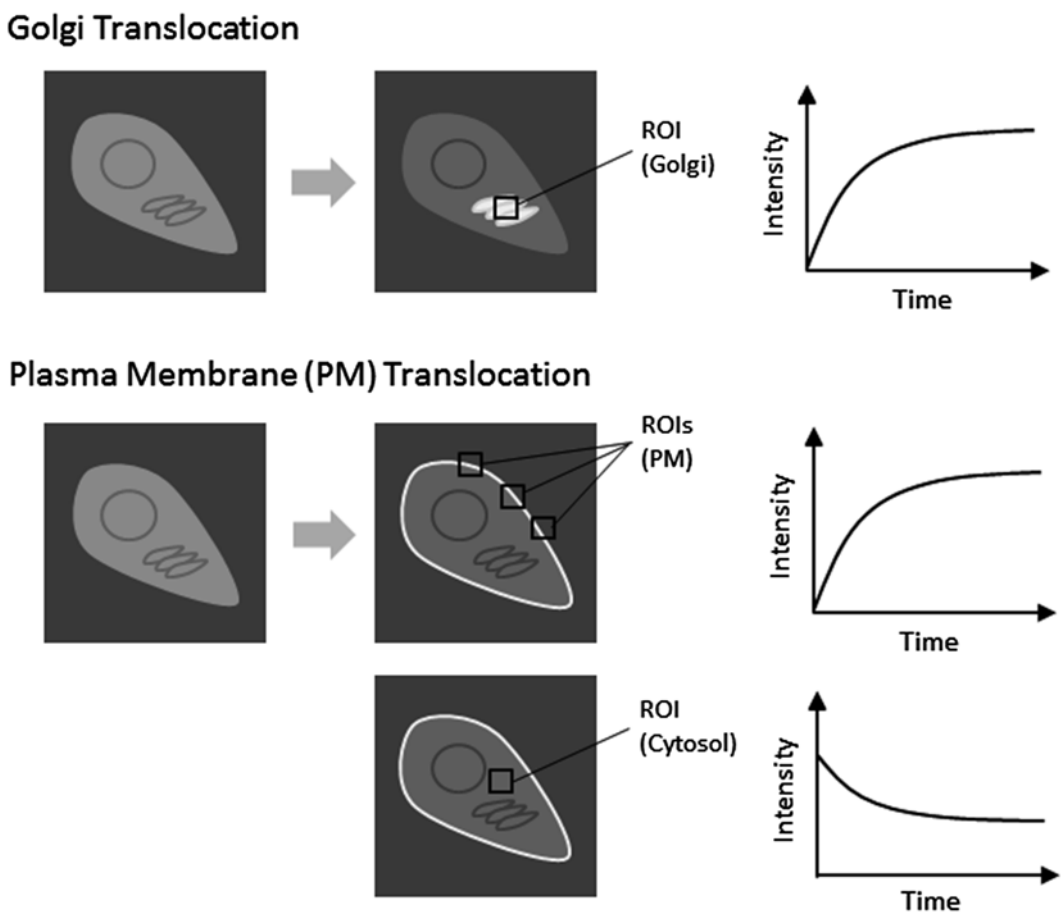

Fig. 6 Quantification of the probe translocation to the cellular membranes. Due to limited expression of the constructs containing fluorescent protein, their translocation from the cytosol to the target compartment results in a decrease of fluorescence in cytosol. In case of the thin plasma membrane, such translocation can be quantitated by using the average of multiple ROIs to reduce the error or by monitoring the decrease in fluorescence intensity in the cytosol

but not at the cell interior (Golgi), regulates remodeling of the cortical actin filaments. The same system has been used to study downstream signaling, such as ERK phosphorylation.

3.5.1 Membrane Translocation During Organelle–Organelle Tethering

To rapidly link mitochondria and ER (thus mimicking mitochondria-associated membranes, MAMs [19]) in living cells, we expressed the anchoring units for both ER and mitochondria and then induced their heterodimerization to connect the two membranes. As shown in Fig. 8, addition of the dimerizer to cells co-expressing two anchoring units induced a rapid transformation of the typical meshwork-like structure of ER to a tubular shape that is more typical of mitochondria. The resulting synthetic MAMs showed an accumulation of fluorescent dye-labeled phosphatidylserine [20] at the interface between the two organelles, indicating the formation of the unique membrane structures.

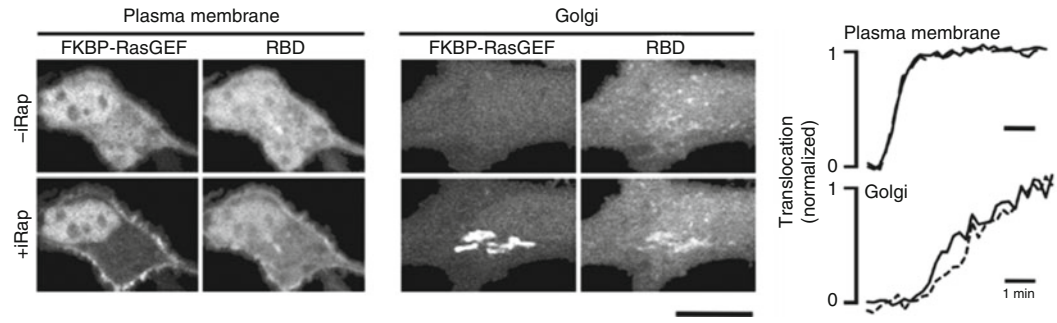

Fig. 7 Observation of the compartmentalized Ras signaling. Recruitment of FKBP-RasGEF to the plasma membrane or the Golgi complex upon addition of chemical dimerizer (+iRap) resulted in Ras activation only on the corresponding organelle, which can be monitored by translocation of the fluorescent protein modified with Ras-binding domain (RBD). Membrane ruffling is observed only after Ras activation to the plasma membrane. Scale bar, 20 μm. Reproduced from [1] with permission

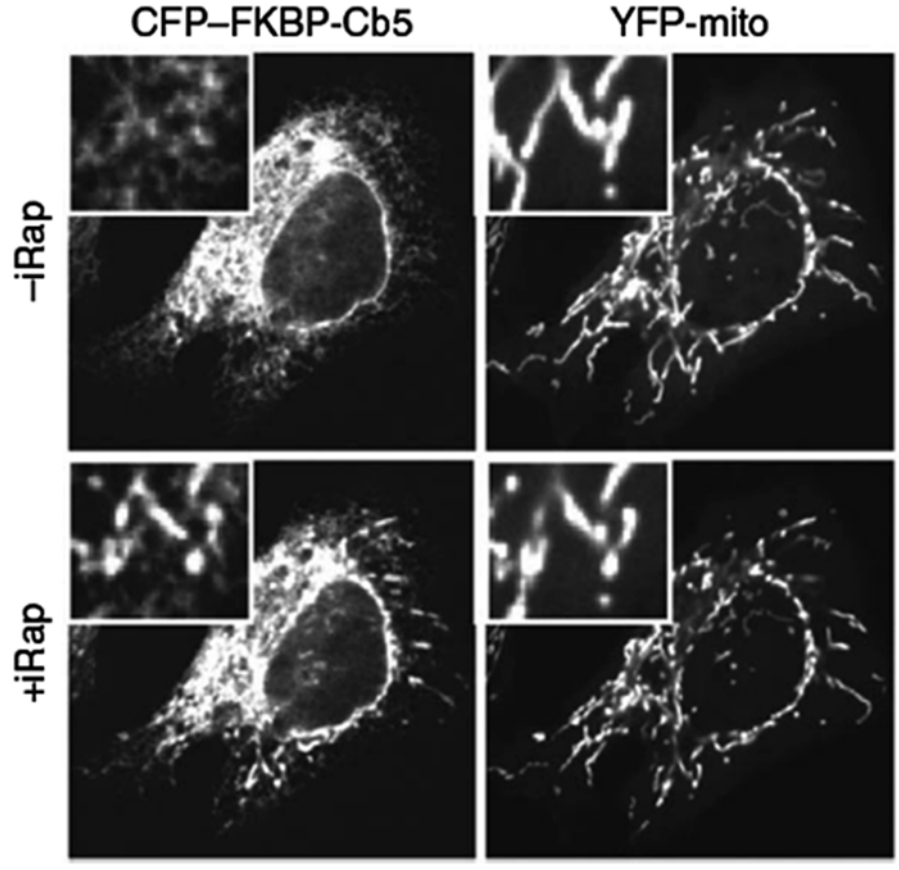

Fig. 8 Tethering of mitochondrial and ER membranes. After addition of the chemical dimerizer (+iRap), ER structure (imaged with CFP-FKBP-Cb5) shows a dramatic transformation reflecting formation of a novel interface between the ER and mitochondria (imaged with YFP-mito). Reproduced from [1] with permission

4 Notes

1. Dimerization systems that are orthogonal to the rapamycin-based system have been reported, such as gibberellin-based heterodimerization. When using the rapamycin-induced system, one should be aware that rapamycin can inhibit mTOR activity, thereby perturbing downstream signaling events [21]. However, these downstream effects of mTOR activation require hours to develop; therefore, they will unlikely interfere with cellular events that occur on a time scale of seconds to minutes. There are alternative chemical dimerizers, such as iRap, which does not affect the mTOR signaling [4].
2. In order to visually confirm the transfection and quantify the translocation, each construct should contain a fluorescent protein, such as CFP, YFP, or mCherry, in addition to the dimerization domain. Since both the anchoring and the effector units are required for perturbation, cells are transfected with a mixture of two constructs that contain the respective dimerization domains and differently colored fluorescent proteins. If the signaling events need to be monitored with fluorescent protein-based biosensors, these sensors are also expressed in the cells. In this case, the anchoring unit is designed without a fluorescent protein to allow tagging this fluorescence protein with the biosensor.
3. The system can be applied to any cultured cells as long as the constructs can be expressed. For example, the tethering systems appeared to be useful in model neutrophils to study the role of phosphoinositide signaling in chemotaxis [15]. In this chapter, we focus on commonly used mammalian cell lines, such as HeLa, NIH3T3, HEK 293, and COS7 cells, for all of which the system has been successfully used.
4. The use of the lipofection reagents with antibiotics can cause cytotoxicity due to the internalization of antibiotics. Therefore, transfection should be performed in the antibiotic-free medium.
5. The optimal concentration of trypsin is determined by the tightness of cellular adhesion. Most cell types can be detached with 0.05 % trypsin, but highly adherent cells such as MDCK require 0.25 % trypsin.
6. Alternatively, commercially available glass-bottomed dishes or chambered cover slips pre-coated with poly-D-lysine can be used.
7. The final concentration of DMSO in the cell culture medium will be 0.1 %. This level of DMSO is well tolerated by the majority of cell lines. For the DMSO-sensitive cell lines (such as neural cells) the final vehicle concentration can be reduced. Adding the same concentration of DMSO to all appropriate controls is essential.

8. The stock solutions should be divided into single-use aliquots that are stored at −20 °C to avoid repeated freeze-and-thaw cycles. During the experiment, the aliquots should be kept on ice before use.
9. Since membrane targeting experiments are usually performed to better understand different steps of the signaling pathways induced by external stimuli, such as growth factors, it is desirable to compare the effects of chemical dimerizers with the effects of physiological stimuli. Such stimuli may also be used as a positive control for cellular responses and biosensors.
10. Many lipophilic sensors are difficult to solubilize and being introduced into the cell. To prepare stock solutions of such sensors, the manufacturer's instructions should be strictly followed. In general, lipid solutions in organic solvents are dried and then reconstituted in buffers containing defatted BSA with rigorous vortexing, and the resulting BSA–lipid complexes are diluted to the appropriate concentration before adding to the cells.
11. Since growth factors and nutrients in FBS can cause nonspecific signaling in the transfected cells, the imaging experiments should be performed in the FBS-free medium.
12. A confocal microscope is more suitable than an epifluorescence microscope to monitor and quantify protein translocation. Any confocal microscope can be used as long as it can detect differently colored fluorescent proteins independently, and the image acquisition speed is fast enough relatively to the targeted cellular response.
13. A multi-positioning scanner on the microscope makes it possible to monitor signaling events in multiple cells on the dish simultaneously. Monitoring a larger number of cells is desirable in order to increase the reliability of results and identify both false-positive and false-negative events.
14. These effects can be evaluated by measuring fluorescence intensities of the constructs, the responses to chemical dimerizers, the fluorescence images of co-expressed organelle markers, and viability of the transfected cells. Different responses may be due to differences in protein stability and/or the steric environment of the FKBP–FRB interaction.
15. Fluorescent biosensors can be used to visualize signaling events induced by the organelle-specific manipulations described above. Several biosensors are available to monitor live cell activity of small GTPases. For example, Ras activation can be examined by a fluorescent protein attached to the Ras-binding domain (RBD) that specifically interacts with active Ras [22]. Additionally, several FRET-based biosensors for small GTPases have been developed [23].

16. If the appropriate biosensor is not available, the downstream signaling events can be studied by immunofluorescence labeling with phospho-specific antibodies. Since transfection efficiency can vary from cell to cell, and some cells might show either high or low level of construct expression, the signaling events should be analyzed in the cells with moderate level of expressed reporters.
17. A key question in studying organelle-to-organelle communications is how the interaction causes redistribution of the molecules of interest. Phospholipids are important messengers, and their translocation during organelle–organelle interactions can be studied by using the membrane-tethering system and commercially available fluorescently conjugated lipids [20]. For example, we used fatty acid-labeled phosphatidylserine (Avanti Polar Lipids, Inc., AL, USA) to monitor phospholipid translocation at junctional sites of ER and mitochondria upon organelle tethering.
18. The incubation time should be exactly 1 h.
19. During the search for cells to image, care should be taken to limit light exposure, and avoid photobleaching of the constructs or photodamages of the cells.
20. This also helps to preserve the temperature before and after addition of the chemical dimerizers to avoid the focus drift arising from temperature changes.

Acknowledgements

We are grateful to Robert DeRose for constructive comments. This work was supported in part by the National Institute of Health (NIH) (GM092930 to TI) and by JST (10216 to TI and 10602 to TK) and JSPS (24655147 to TK). TK is a recipient of a research grant from the Mochida Memorial Foundation for Medical and Pharmaceutical Research.

References

1. Kukelyansky I, Komatsu T, McCaffery JM et al (2010) Organelle-specific, rapid induction of molecular activities and membrane tethering. Nat Methods 7:206–208
2. Inoue T, Heo WD, Grimley JS, Wandless TJ, Meyer T (2005) An inducible translocation strategy to rapidly activate and inhibit small GTPase signaling pathways. Nat Methods 2:415–418
3. Suh BC, Inoue T, Meyer T, Hille B (2006) Rapid chemically induced changes of PtdIns(4,5)P2 gate KCNQ ion channels. Science 314:1454–1457
4. Miyamoto T, DeRose R, Suarez A et al (2012) Rapid and orthogonal logic gating with a gibberellin-induced dimerization system. Nat Chem Biol 8:465–470
5. Castellano F, Montcourrier P, Chavrier P (2000) Membrane recruitment of Rac1 triggers phagocytosis. J Cell Sci 113:2955–2961
6. Castellano F, Chavrier P (2000) Inducible membrane recruitment of small GTP-binding proteins by rapamycin-based system in living cells. Meth Enzymol 325:285–295

7. Crabtree GR, Schreiber SL (1996) Three-part inventions: intracellular signaling and induced proximity. Trends Biochem Sci 21:418–422
8. DeRose R, Miyamoto T, Inoue T (2013) Manipulating signaling at will: chemically-inducible dimerization (CID) techniques resolve problems in cell biology. Pflugers Arch 465:409–417
9. Mor A, Philips MR (2006) Compartmentalized Ras/MAPK signaling. Annu Rev Immunol 24: 771–800
10. Umeda N, Ueno T, Pohlmeyer C, Nagano T, Inoue T (2011) A photocleavable rapamycin conjugate for spatiotemporal control of small GTPase activity. J Am Chem Soc 133:12–14
11. DeRose R, Pohlmeyer C, Umeda N, Nagano T, Kuo S, Inoue T (2012) Spatio-temporal manipulation of small GTPase activity at subcellular level and timescale of seconds in living cells. J Vis Exp 61:e3794
12. Lin Y-C, Nihongaki Y, Liu T-Y, Razavi S, Sato M, Inoue T (2013) Rapidly reversible manipulation of molecular activity with dual chemical dimerizers. Angew Chem Int Ed 52:6450–6454
13. Phua SC, Pohlmeyer C, Inoue T (2012) Rapidly relocating molecules between organelles to manipulate small GTPase activity. ACS Chem Biol 7:1950–1955
14. Linstedt AD, Hauri HP (1993) Giantin, a novel conserved Golgi membrane protein containing a cytoplasmic domain of at least 350 kDa. Mol Biol Cell 4:679–693
15. Lesa GM, Seemann J, Shorter J, Vandekerckhove J, Warren G (2000) The amino-terminal domain of the Golgi protein giantin interacts directly with the vesicle-tethering protein p115. J Biol Chem 275: 2831–2836
16. Ueno T, Falkenburger BH, Pohlmeyer C, Inoue T (2011) Triggering actin comets versus membrane ruffles: distinctive effects of phosphoinositides on actin reorganization. Sci Signal 4:ra87
17. Lin B, Wang J, Ueno T, Harwell A, Inoue T, Levchenko A (2012) Synthetic spatially graded Rac activation drives directed cell polarization and locomotion. Proc Natl Acad Sci 109:E3668
18. Inoue T, Meyer T (2008) Synthetic activation of endogenous PI3K and Rac identifies an AND-gate switch for cell polarization and migration. PLoS One 3:e3068
19. Hayashi T, Rizzuto R, Hajnoczky G, Su TP (2009) MAM: more than just a housekeeper. Trends Cell Biol 19:81–88
20. Kobayashi T, Arakawa Y (1991) Transport of exogenous fluorescent phosphatidylserine analogue to the Golgi apparatus in cultured fibroblasts. J Cell Biol 113:235–244
21. Sabers CJ, Martin MM, Brunn GJ et al (1995) Isolation of a protein target of the FKBP12-rapamycin complex in mammalian cells. J Biol Chem 270:815–822
22. Bivona TG, Quatela S, Philips MR (2006) Analysis of Ras activation in living cells with GFP-RBD. Methods Enzymol 407:128–143
23. Hodgson L, Pertz O, Hahn KM (2008) Design and optimization of genetically encoded fluorescent biosensors: GTPase biosensors. Methods Cell Biol 85:63–81

Chapter 17

A Novel Pair of Split Venus Fragments to Detect Protein–Protein Interactions by In Vitro and In Vivo Bimolecular Fluorescence Complementation Assays

Kazumasa Ohashi and Kensaku Mizuno

Abstract

Protein–protein interactions are critical components of almost every cellular process. The bimolecular fluorescence complementation (BiFC) method has been used to detect protein–protein interactions in both living cells and cell-free systems. The BiFC method is based on the principle that a fluorescent protein is reassembled from its two complementary non-fluorescent fragments when an interaction occurs between two proteins, each one fused to each fragment. In vivo and in vitro BiFC assays, which use a new pair of split Venus fragments composed of VN210 (amino acids 1–210) and VC210 (amino acids 210–238), are useful tools to detect and quantify various protein–protein interactions (including the cofilin–actin and Ras–Raf interactions) with high specificity and low background fluorescence. Moreover, these assays can be applied to screen small-molecule inhibitors of protein–protein interactions.

Key words Bimolecular fluorescence complementation (BiFC), Split Venus, Protein–protein interaction, High-throughput screening, Cofilin, Actin

1 Introduction

Numerous biological processes are regulated by protein–protein interactions. Thus, analysis of protein–protein interactions is essential to understand the molecular mechanisms of cellular activities and functions. Many methods have been developed to detect protein–protein interactions. In cell lysates, protein–protein interactions are analyzed using co-immunoprecipitation and immunodetection methods using antibodies [1]. The yeast two-hybrid system is a useful tool for large-scale screening of interacting proteins [1]. Fluorescence resonance energy transfer (FRET) [2, 3] and fluorescence cross-correlation spectroscopy (FCCS) [4] enable the visualization of protein–protein interaction real-time dynamics in living cells. The bimolecular fluorescence complementation (BiFC) method can be used to visualize protein–protein interactions in living cells and for quantitative analyses of such interactions

Andrei I. Ivanov (ed.), *Exocytosis and Endocytosis*, Methods in Molecular Biology, vol. 1174,
DOI 10.1007/978-1-4939-0944-5_17,

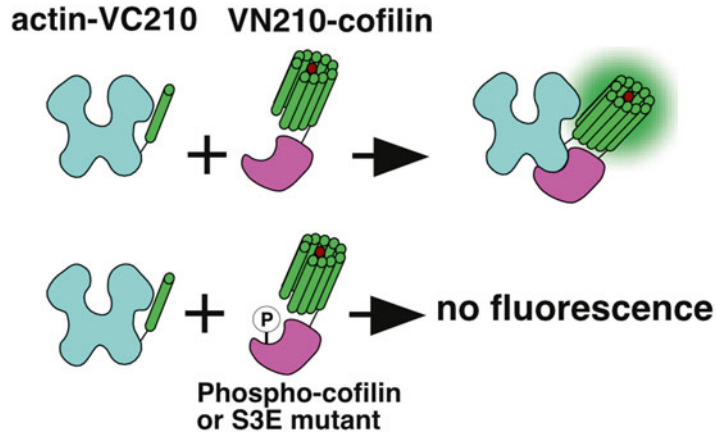

Fig. 1 Schematic representation of the BiFC method to detect the interaction between actin and cofilin. A fluorescent Venus protein is reassembled from its two complementary non-fluorescent fragments (VN210 and VC210), whose association depends on the interaction between cofilin and actin fused to each fragment. Incubation of actin-VC210 with VN210-cofilin wild type recovers fluorescence, while incubation with the actin-non-binding VN210-phospho-cofilin or VN210-cofilin (S3E) does not recover fluorescence. Reproduced from ref. 13, with the permission of BioTechniques

in cell-free assays [5–8]. These methods have also been used to screen for protein–protein interaction inhibitors, which are promising therapeutic drug candidates [9].

The BiFC method is based on the complementary reconstruction of a fluorescent protein from its split non-fluorescent fragments (probes). The two non-fluorescent fragments are fused to two proteins that are thought to interact. An interaction between the two proteins fused to each probe facilitates the reconstitution of the fluorescent protein (Fig. 1) [5–8]. A pair of green fluorescent protein (GFP) fragments, split at a site between 157 and 158, were reported as the first BiFC probes, which complementarily reassembled to recover fluorescence, depending on the interaction of leucine zipper peptides fused to each GFP fragment [5]. Since then, various BiFC probes have been developed using other fluorescent proteins, and multicolor BiFC probes have also emerged recently [8, 10]. Compared to FRET, the BiFC method is more sensitive and selective for the visualization of protein–protein interactions. Due to the remarkable stability and almost irreversible association of the fluorescent protein complex after the reassembly of the split fragments and its sequential accumulation, BiFC can even detect weak protein–protein interactions effectively [8]. Moreover, the BiFC method does not require exogenous dyes or coloring reagents for staining, and the fluorescence can be detected with a standard fluorescence microscope. However, the use of the BiFC method is

limited in terms of visualization of the dynamics of protein–protein interactions in living cells because of the high stability of the reassembled complex and the amount of time required for the fluorophore maturation [8].

Several pairs of GFP split fragments and its variants, including cyan fluorescent protein (CFP), yellow fluorescent protein (YFP), and Venus, have been developed [8, 11]. The pair of YFP fragments that split at position 155 is currently the most popular, although fragment pairs that split near positions 144 or 173 have also been used [8, 11]. To detect the interaction between actin and cofilin (an actin-severing and -depolymerizing factor [12]) by using the BiFC method, a series of combinations of the N- and C-terminal fragments of Venus fused upstream or downstream of actin and cofilin were systematically screened [13]. Venus was used because of its strong fluorescence intensity and its fast and efficient maturation property [14]. Of the numerous pairs of Venus fragments examined, a new pair, VN210 (an N-terminal fragment of Venus consisting of amino acids 1–210) and VC210 (a C-terminal fragment of Venus consisting of amino acids 210–238), which were fused upstream of cofilin and downstream of actin, respectively, was the most effective combination for visualizing the specific interaction between actin and cofilin (Fig. 1) [13]. This pair of split Venus fragments was also effective for detecting the specific interaction between active Ras and Raf oncogenes and the interaction between calmodulin and its target M13 peptide (a calmodulin-binding sequence of the myosin light chain) [13]. In vivo and in vitro BiFC assays using this new pair of split Venus fragments appear to have broad utility for measuring protein–protein interactions with high sensitivity and low background fluorescence.

In this chapter, the method to construct the BiFC probes and their use for in vivo and in vitro BiFC assays are described. An application of the BiFC method to screen protein–protein interaction inhibitors is also described [15].

2 Materials

2.1 Construction of Expression Plasmids for BiFC Probes

1. cDNAs: Venus (gift from Dr. A. Miyawaki, Riken; Wako, Japan), human cofilin (Accession No. X95404), mouse β-actin (Accession No. X03672).
2. EGFP-C1 plasmid (Clontech; Mountain View, CA, USA).

2.2 In Vivo BiFC Assay

1. HeLa cells (Riken Cell Bank; Tsukuba, Japan).
2. Growth medium for HeLa cells: Dulbecco's modified Eagle's medium (DMEM: Life Technologies; Carlsbad, CA, USA) supplemented with 10 % fetal bovine serum (FBS), 100,000 U/L penicillin, and 10 mg/L streptomycin.

3. 35-mm Glass-bottom dishes.
4. Lipofectamine 2000 reagent (Life Technologies).
5. Opti-MEM (Life Technologies).
6. Phosphate-buffered saline (PBS): 2.7 mM KCl, 1.5 mM KH_2PO_4, 137 mM NaCl, 8.1 mM Na_2HPO_4, pH 7.4.
7. 4 % Paraformaldehyde in PBS.
8. Lysis buffer A: 50 mM HEPES–NaOH, 150 mM NaCl, 1 % NP-40, 1 mM dithiothreitol, 5 % glycerol, 10 μg/mL leupeptin, 1 mM phenylmethylsulfonyl fluoride (PMSF), pH 7.4.

2.3 Construction of Baculovirus Expression Plasmids

1. pFastBac: A donor plasmid to a baculovirus shuttle vector (Life Technologies).
2. Luria-Bertani (LB) agar plate containing 50 μg/mL kanamycin, 7 μg/mL gentamicin, 10 μg/mL tetracycline, 100 μg/mL X-gal, and 40 μg/mL isopropyl-β-D-1-thiogalactopyranoside (IPTG).
3. LB agar: 10 g/L Bactotrypton, 10 g/L NaCl, 5 g/L yeast extract, 1.5 % agar.
4. Yeast Trypton (2×): 16 g/L Bactotrypton, 10 g/L NaCl, 5 g/L yeast extract.
5. Solution I (glucose solution): 50 mM Glucose, 25 mM Tris–HCl, pH 8.0, 10 mM ethylenediaminetetraacetic acid (EDTA), pH 8.0.
6. Solution II (alkaline-SDS solution): 0.2 M NaOH, 1 % sodium dodecyl sulfate (SDS).
7. Solution III (K-acetate solution): 3 M Potassium acetate containing 28.5 % (v/v) glacial acetic acid.
8. TE buffer: 10 mM Tris–HCl, pH 8.0, 1 mM EDTA, pH 8.0.
9. RNase A (10 μg/mL) (Sigma-Aldrich; St. Louis, MO, USA).
10. DH10Bac competent cells (Life Technologies).

2.4 Production of Recombinant Baculovirus and Expression of BiFC Probe Proteins

1. SF9 cells (Life Technologies).
2. SF900II medium (Life Technologies).
3. Growth medium for insect cells: SF900II medium supplemented with 5 % FBS.
4. Cellfectin Reagent (Life Technologies).
5. Lysis buffer B: 40 mM Tris–HCl, 100 mM NaCl, 0.1 % NP-40, 1 mM dithiothreitol, 5 % glycerol, 10 μg/mL leupeptin, 1 mM PMSF, pH 7.4.

2.5 Purification of Recombinant BiFC Probe Proteins

1. Ni-NTA agarose (Qiagen; Valencia, CA).
2. Poly-Prep chromatography columns, 0.8×4 cm (Bio-Rad; Hercules, CA).

3. Wash buffer: 40 mM Tris–HCl, 100 mM NaCl, 0.1 % NP-40, 5 mM imidazole, 1 mM dithiothreitol, pH 7.4.
4. Elution buffer: 0.2 M imidazole in wash buffer.
5. PD-10 column (GE Healthcare; Little Chalfont, England).
6. Gel filtration/BiFC reaction buffer: 50 mM Tris–HCl, 100 mM NaCl, 0.1 mM $MgCl_2$, 1 mM dithiothreitol, 5 % glycerol, pH 7.5.
7. Coomassie Brilliant Blue staining kit (Nacalai Tesque; Kyoto, Japan).
8. Bradford protein assay kit (Bio-Rad).

2.6 In Vitro BiFC Assay and Screening of Inhibitors

1. Gel filtration/BiFC reaction buffer: As described above.
2. Micro quartz cell (Hitachi High-Tech; Tokyo, Japan).
3. Glass-bottom 96-well black microtiter plate.
4. A library of chemical compounds: SCADS inhibitor kits were provided by the Screening Committee of Anti-cancer Drugs through a Grant-in-Aid for Scientific Research from the Ministry of Education, Culture, Sports, Science and Technology, Japan. Other chemical compounds were donated by Dr. M. Oikawa (Yokohama City University, Yokohama, Japan).

3 Methods

The in vivo and in vitro BiFC methods are described using a pair of split Venus fragments, VN210 (Venus 1–210) and VC210 (Venus 210–238), to measure the protein–protein interactions, utilizing the cofilin–actin interaction as an example (*see* **Note 1**). The construction of the expression plasmids for BiFC probes and in vivo BiFC assays are first described, along with evaluations of their efficiency and specificity. Then, the method of in vitro BiFC assays, using the purified BiFC probe proteins, is presented. Finally, the procedure of the screening of protein–protein interaction inhibitors using the in vitro BiFC assay is detailed.

3.1 Construction of the Expression Plasmids for BiFC Probes and In Vivo BiFC Assays

To reassemble a fluorescent protein from its fragments in BiFC assays, each fragment of a fluorescent protein must be properly positioned and oriented in the three-dimensional structure of the protein complex of the BiFC probes. Therefore, the first step of performing a BiFC assay is to test which pair of the probes out of eight possible combinations (VN210 or VC210 fused to the N- or the C-terminal end of each of the two proteins of interest; *see* Subheading 3.1.2) will most effectively reconstruct a fluorescent protein. In addition, to determine whether the recovery of fluorescence from Venus fragments can accurately reflect the specific interaction between the two proteins conjugated to Venus

fragments, it is necessary to confirm that the BiFC probe encoding a binding-deficient mutant protein (e.g., a phospho-mimic mutant of cofilin) does not recover fluorescence.

3.1.1 Construction of the Expression Plasmids for BiFC Probes

1. The cDNAs coding for the split Venus fragments (VN210 and VC210) are amplified by PCR, using Venus cDNA as a template and the primers containing restriction enzyme sites (Fig. 2). The VN210 cDNA encodes amino acid residues from 1 (Val) to 210 (Asp) of Venus. The VC210 cDNA encodes amino acid residues from 210 (Asp) to 238 (Lys) of Venus. In the case where the cDNA for the protein of interest is fused downstream of VC210, the VC210 cDNA encodes amino acid residues from 210 (Asp) to 227 (Ala).
2. To construct the expression plasmids encoding the BiFC probes, the cDNAs coding for the interacting proteins of interest (e.g., cofilin and actin) are fused downstream or upstream of the cDNA coding for VN210 or VC210, using the linker sequence GGGAATTCG (including an *Eco*RI site) or TCT AGA (*Xba*I site). As an example, a set of four sequences of cofilin probes is presented in Fig. 2. The initiation Met codon is added in front of the first codon of all cDNAs. The cDNAs coding for the BiFC probes are subcloned into a pEGFPC1 mammalian expression vector by substituting for the EGFP cDNA region (*see* **Note 2**).

3.1.2 In Vivo BiFC Assays to Evaluate the Efficiency of the BiFC Probes

To detect the specific protein–protein interactions by BiFC assays, the fluorescence recovery from Venus fragments must depend on the interaction between the proteins of interest (X and Y) fused to each fragment. Evaluation of the self-reassembly of various pairs of Venus fragments is shown in ref. 13. To evaluate the efficiency and specificity of the BiFC probes conjugated to the proteins of interest, the pair of putative BiFC probes is coexpressed in HeLa cells and the recovered fluorescence of Venus is analyzed using a fluorescence microscope or a fluorescence spectrophotometer.

1. Culture HeLa cells in DMEM supplemented with 10 % FBS (*see* **Note 3**).
2. Place 5×10^4 cells in 35 mm glass-bottom dishes for observation with a high-aperture oil immersion objective lens (*see* **Note 4**).
3. The next day, cotransfect the cells with the expression plasmids coding for the BiFC probes. To evaluate which pair of probes most effectively permits the reconstruction of a fluorescent protein, cotransfect HeLa cells with the plasmids coding for the eight possible combinations of VN210- and VC-210-fused proteins: VN210-X+VC210-Y, VN210-X+Y-VC210, X-VN210+VC210-Y, X-VN210+Y-VC210, VC210-X+VN210-Y, VC210-X+Y-VN210, X-VC210+VN210-Y, and X-VC210+

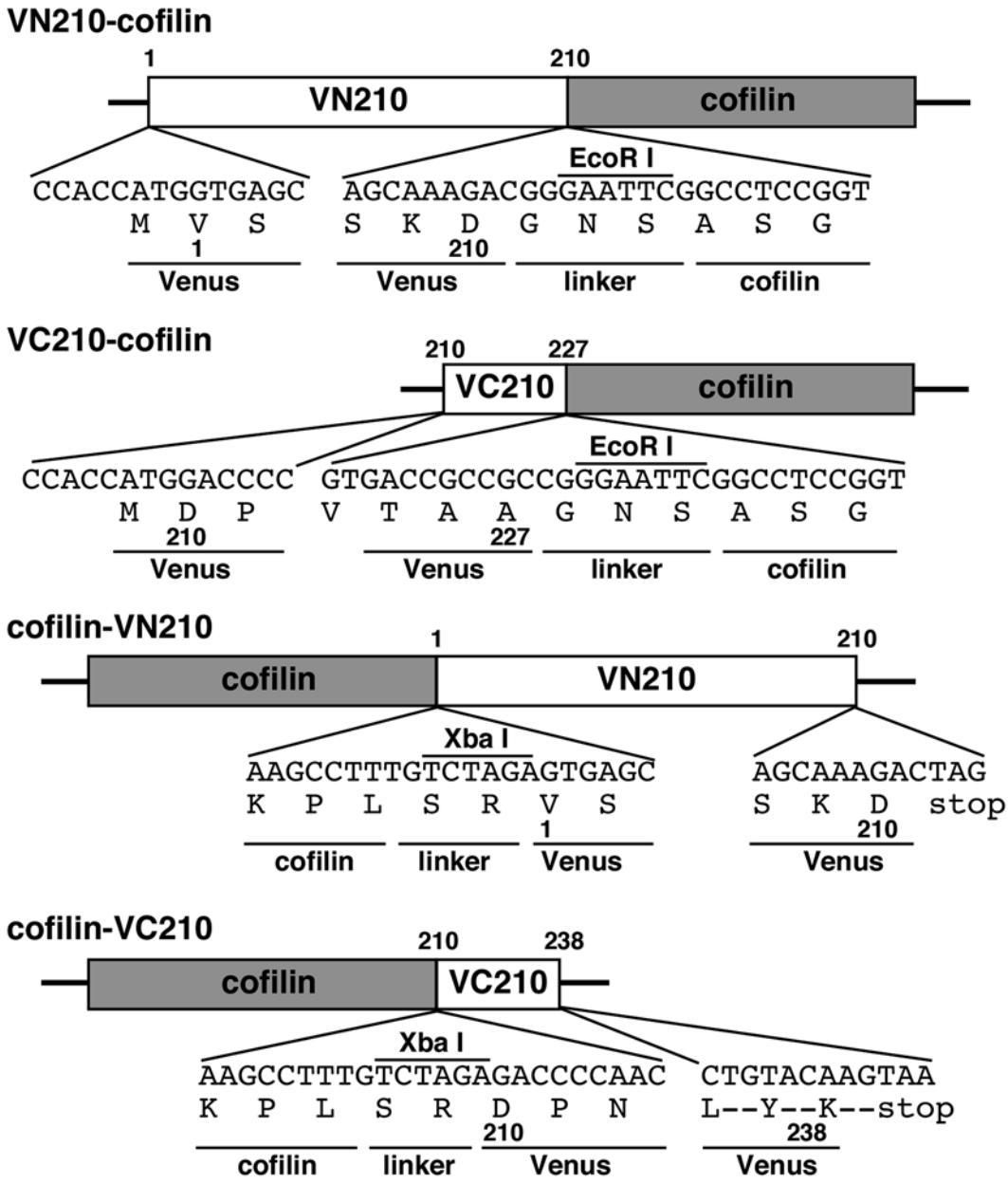

Fig. 2 Construction of the BiFC probe cDNA plasmids. Four cDNA sequences coding for the BiFC probe proteins, consisting of VN210 or VC210 Venus fragments fused to the N- or the C-terminus of cofilin, are schematically shown. The cDNA sequences and the translated amino acids surrounding the linker regions are presented. The *numbers* below the amino acids indicate the Venus amino acid positions. Note that the initiation residue Met is conventionally designated as 0 in the GFP and GFP-related proteins

Y-VN210, where VN210-X/Y and X/Y-VN210 indicate VN210 fused to the N- and C-terminal end of the protein X or Y, respectively. For transfection, dilute 0.5 μg of each plasmid encoding VN210- and VC210-fused protein into 100 μL of Opti-MEM

and add 3 μL of Lipofectamine 2000 reagent to another 100 μL of Opti-MEM. Incubate the diluted Lipofectamine 2000 reagent for 5–10 min.

4. Combine the diluted plasmid DNA with the diluted Lipofectamine 2000 reagent, mix gently, and incubate for 30 min at room temperature.
5. Change a HeLa cell culture medium to 0.8 mL of Opti-MEM, and add the transfection preparations of DNA and Lipofectamine 2000 to the HeLa cells.
6. After 3 h of incubation at 37 °C in a CO_2 incubator, change the medium to growth medium and incubate the cells at 37 °C in a CO_2 incubator.
7. After 16 h of incubation, analyze the fluorescence in living cells using an inverted fluorescence microscope with a 40× or a 63× high-aperture oil immersion objective lens and the filter set for Venus (YFP) fluorescence. The fluorescence can also be detected after fixation with 4 % paraformaldehyde.
8. Alternatively, the fluorescence can be measured using a fluorescence spectrophotometer. Lyse the cells with 100–200 μL of lysis buffer A, and remove the cell debris by centrifugation.
9. Measure the fluorescence in a micro quartz cell with excitation at 505 nm and emission at 545 nm.
10. If the fluorescence is detected, it is important to show that the fluorescence obtained from the pair of the BiFC probes is brighter than the fluorescence observed from the negative control pair of the BiFC probes, which contains the binding-deficient mutation on the protein of interest. If the fluorescence is not detected or if there is no difference in fluorescence between the wild-type (WT) and the binding-defective mutant probes, the linker sequences between the Venus fragments and the interacting proteins should be reconsidered or other pairs of Venus split fragments should be examined [13].

Figure 3 shows the results of the in vivo BiFC assay using the analysis of the interaction between actin and cofilin as a representative example. Cofilin binds to actin, and its actin-binding activity is inhibited by cofilin phosphorylation at Ser-3 [16]. The strong fluorescence of complemented Venus is observed in cells cotransfected with actin-VC210 and VN210-cofilin (WT), but only a weak signal is observed in cells cotransfected with actin-VC210 and VN210-cofilin (S3E), a phospho-mimetic mutant with replacement of the serine-3 residue by the glutamic acid residue (Fig. 3a). Moreover, coexpression of LIM-kinase 1 (LIMK1), a protein kinase phosphorylating cofilin at Ser-3 [17], with actin-VC210 and VN210-cofilin (WT) causes a decrease in Venus fluorescence (Fig. 3b, arrows) compared to a LIMK1-nonexpressing

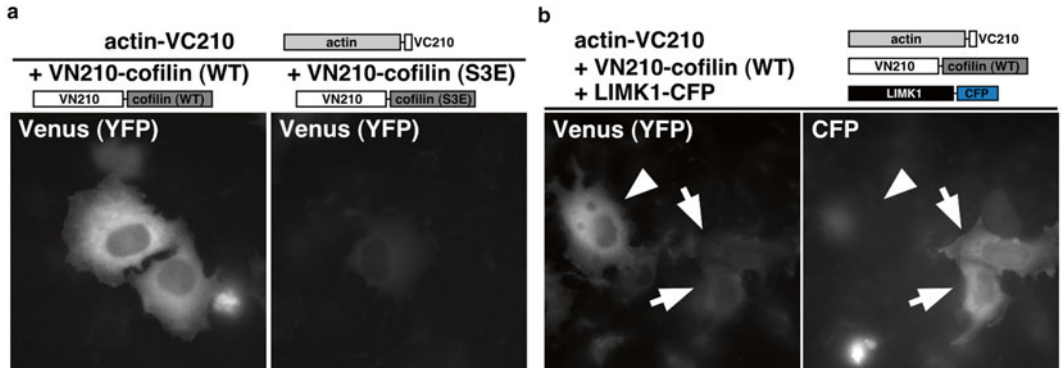

Fig. 3 Detection of the actin–cofilin interaction using the in vivo BiFC assay. (**a**) Venus fluorescence images of HeLa cells co-expressing actin-V210 and VN210-cofilin (WT) or VN210-cofilin (S3E). (**b**) Effect of inactivation of the actin-binding activity of cofilin by coexpression of LIMK1-CFP on the fluorescence recovery in vivo. The fluorescence images of Venus (**a**) or Venus and CFP (**b**) were observed in living cells by fluorescence microscopy using a 63× oil immersion lens. Reproduced from ref. 13, with the permission of BioTechniques

cell (Fig. 3b, an arrowhead). These are examples of experiments used to evaluate whether the BiFC assays properly reflect the specific interaction between the proteins of interest.

3.2 In Vitro BiFC Assays Using the Purified Recombinant BiFC Probes

The in vitro BiFC assay requires a relatively large amount of purified recombinant BiFC probe proteins. There are many methods for expressing recombinant proteins, including systems using insect cells and *E. coli*. In this chapter, we describe the method of protein expression using insect cells and the baculovirus expression system because the insect cell expression system tends to produce functional recombinant proteins more effectively compared to the bacterial expression system (*see* **Note 5**). The qualities of the in vitro BiFC assay are its high sensitivity and the convenience of detection using a fluorescence spectrophotometer. Because the complementary association of the split Venus fragments is almost irreversible, the complemented Venus is sequentially accumulated during the reaction. The self-complementation of the split Venus fragments can be suppressed by controlling the concentrations of the BiFC probe proteins.

3.2.1 Construction of the Baculovirus Expression Plasmids

1. Insert the cDNAs coding for His_6-tagged BiFC proteins into the multi-cloning site of a pFastBac donor plasmid. To purify the BiFC probe proteins by Ni-NTA agarose, a sequence coding for 6× histidine is added downstream of the cDNA coding for BiFC probe proteins in the expression plasmids.
2. Purify the pFastBac plasmids according to a standard method [18].
3. Transform the *E. coli* DH10Bac strain with the recombined pFastBac donor plasmids according to a standard method [18].

Plate the transformed cells on LB agar plates containing 50 μg/mL kanamycin, 7 μg/mL gentamicin, 10 μg/mL tetracycline, 100 μg/mL X-gal, and 40 μg/mL IPTG (*see* **Note 6**).

The DH10Bac *E. coli* strain contains the Bacmid plasmid with Tn7 recombination sites for accepting the expression cassette of the pFastBac plasmid. The competent cells of DH10Bac can be prepared by a standard method or can be obtained commercially.

4. Incubate the plates for 36–48 h at 37 °C until white colonies can be distinguished. The success of the recombination between a donor plasmid and Bacmid in DH10Bac is determined by the presence of white colonies.
5. Select some white colonies and culture them in 5 mL of 2 × YT containing 50 μg/mL kanamycin, 7 μg/mL gentamicin, and 10 μg/mL tetracycline (*see* **Note 7**).
6. Collect the culture solution in a 1.5 mL tube, pellet the transformed *E. coli* at 5,000 × *g* for 3 min at 4 °C, and discard the supernatant.
7. Resuspend the *E. coli* pellet in 100 μL of solution I (*see* **Note 8**).
8. Add 200 μL of room-temperature solution II, and mix gently to lyse cells.
9. Add 150 μL of ice-cold solution III, and mix gently.
10. Centrifuge at 15,000 × *g* for 10 min at 4 °C.
11. Transfer the supernatant to a new 1.5 mL tube.
12. Add 0.8 volume of isopropanol to precipitate the Bacmid DNA, and mix gently.
13. Centrifuge at 15,000 × *g* for 10 min at 4 °C, and discard the supernatants.
14. Rinse with 80 % ethanol, and vacuum dry for 3 min.
15. Dissolve the precipitate with 50 μL of TE, and add RNase A (final concentration of 10 μg/mL). The Bacmid DNA is now ready for the SF9 insect cell transfection.

3.2.2 Production of Recombinant Baculovirus

1. Culture SF9 cells in the insect cell growth medium.
2. In a 35 mm tissue culture dish, seed 1×10^5 SF9 cells per well in 2 mL of insect cell growth medium and culture for 1 h at 27 °C.
3. Add 1 μg of Bacmid DNA to 100 μL of SF900II medium, and add 6 μL of Cellfectin reagent to another 100 μL of SF900II medium.
4. Combine the diluted Bacmid DNA with the diluted Cellfectin reagent. Mix gently, and incubate for 30 min at room temperature.

5. Change the growth medium in the wells containing SF9 cells to 0.8 mL of SF900II medium.
6. Add the DNA–Cellfectin complexes to the cells.
7. Culture the cells at 27 °C for 5 h.
8. Replace the transfection medium containing the DNA–Cellfectin complexes with 2 mL of growth medium in each well.
9. Culture the cells at 27 °C for 72 h.
10. Collect the culture medium and the cells in a 1.5 mL tube by pipetting.
11. Centrifuge at 15,000 × *g* for 10 min at 4 °C.
12. Transfer the supernatant in a new 1.5 mL tube. The supernatants are used as the first virus solution.

3.2.3 Amplification of Recombinant Baculovirus

1. Dilute SF9 cells to 5×10^5 cells/mL in 10 mL of growth medium in a 50 mL tube.
2. Culture the cells to 1×10^6 cells/mL, and add 100 μL of the first virus solution.
3. Culture the infected cells in suspension on a shaker (120 rpm) at 27 °C for 2–3 days.
4. Centrifuge the 50 mL tube at 5,000 × *g* for 10 min at 4 °C.
5. Collect the supernatant as the amplified virus solution. Use the cell pellets to check the amount of the recombinant protein expressed in the cells. Store the amplified virus solution at 4 °C.

3.2.4 Expression of Recombinant BiFC Probe Proteins

1. Grow SF9 cells in suspension to up to 1×10^6 cells/mL in 200 mL of growth medium in a 500 mL shaker flask.
2. Add 2 mL of the amplified virus solution (*see* **Note 9**).
3. Culture the infected cells in suspension on a shaker (120 rpm) at 27 °C for 2–3 days.
4. Transfer the cultured cells to a centrifuge tube, and pellet the cells at 3,000 × *g* for 10 min at 4 °C.
5. Resuspend the cell pellets with 40 mL of cold PBS and transfer to a 50 mL tube.
6. Pellet the cells at 3,000 × *g* for 10 min at 4 °C, and discard the supernatant.
7. Add 10 mL of ice-cold lysis buffer B, suspend, and lyse with ten times sonication at 5–10 W for 15 s on ice.
8. Centrifuge at 10,000 × *g* for 10 min at 4 °C.
9. Recover the supernatants and filter with a 0.45 μm pore size filter before purification using a Ni-NTA agarose column.

3.2.5 Purification of Recombinant BiFC Probe Proteins

The method of His_6-tagged recombinant protein purification is described, taking VN210-cofilin-His_6 and actin-VC210-His_6 as examples.

1. Transfer 0.5 mL of Ni-NTA agarose (bed volume) into Poly-Prep chromatography columns (0.8 × 4 cm).
2. Equilibrate the Ni-NTA agarose with 10 mL of wash buffer.
3. Apply 10 mL of the cell lysates prepared in Subheading 3.2.4 onto the column.
4. Wash the column with 10 mL of the wash buffer.
5. Successively apply 0.25 mL of elution buffer (0.2 M imidazole) and then 0.5 mL of elution buffer five times. Collect the eluates each time. Sample 20 μL of these fractions to check the purity of the eluted protein.

   Check the amount and the purity of the eluted proteins by SDS-polyacrylamide gel electrophoresis (PAGE) followed by Coomassie Brilliant Blue staining. The second fraction should contain the majority of the eluted proteins.
6. Remove the imidazole in the eluted proteins by gel filtration using a PD-10 desalting column. Equilibrate the PD-10 column with 25 mL of the gel filtration/BiFC reaction buffer.
7. Apply 0.5 mL of the fraction No. 2 eluted from the Ni-NTA column onto the PD-10 column, and collect the eluates as fraction No. 1. Then, add 0.5 mL of the gel filtration buffer onto the PD-10 column 16 times and collect the eluates each time. The recombinant protein should be eluted by fraction No. 6 or No. 7.
8. Measure the absorbance of the fractions at 280 nm to estimate the protein concentration. Then, to more accurately determine the protein concentration in the fractions, use a Bradford protein assay kit.
9. Apply 1–4 μg of proteins from the peak fractions to SDS-PAGE, and stain the proteins with Coomassie Brilliant Blue to determine the purity of the protein.

   The SDS-PAGE analyses of the purified recombinant BiFC probe proteins, VN210-cofilin (WT)-His_6, VN210-cofilin (S3E)-His_6, and actin-VC210-His_6, are presented in Fig. 4a as examples [13].
10. Store the BiFC probe proteins at –80 °C.

3.2.6 In Vitro BiFC Assay

To analyze the protein–protein interaction by the in vitro BiFC assay quantitatively, the purified BiFC probe proteins are mixed in vitro and the fluorescence recovery of complemented Venus is measured using a fluorescence spectrophotometer. Because it is easy to control the concentration of the probe proteins in the in vitro BiFC assay, the background fluorescence derived from the

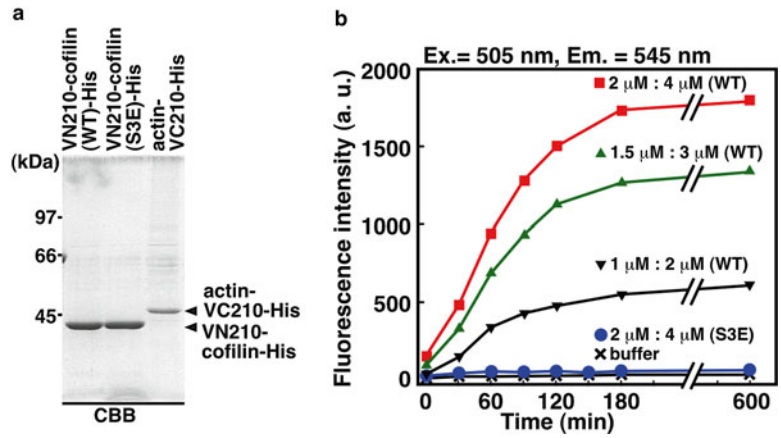

Fig. 4 Detection of the actin–cofilin interaction using the in vitro BiFC assay. (**a**) SDS-PAGE of the purified BiFC probe proteins. His_6-tagged proteins expressed in SF9 cells were purified with Ni-NTA agarose, separated on SDS-PAGE, and stained with Coomassie Brilliant Blue (CBB). (**b**) Detection of the cofilin–actin interaction by in vitro BiFC assay. Purified actin-VC210 were combined with VN210-cofilin (WT or S3E) at indicated concentrations [actin-VC210:VN210-cofilin (WT or S3E)] at 30 °C in a micro quartz cell. The time course of fluorescence intensity was measured by a fluorescence spectrophotometer. a.u., arbitrary units. Reproduced from ref. 13, with the permission of BioTechniques

self-reassembly of Venus fragments can be reduced. The conditions of the reaction, including the concentration of probe proteins, incubation time, temperature, and buffer, should be optimized for each pair of interacting proteins. The procedures of the in vitro BiFC assay using VN210-cofilin and actin-VC210 probes are described herein.

1. In a micro quartz cell, combine actin-VC210 and VN210-cofilin (WT) or VN210-cofilin (S3E) at the micro-molar range in 100 μL of reaction buffer.
2. Measure the fluorescence intensity at time 0 and then every 30 min for several hours with excitation at 505 nm and emission at 545 nm at 30 °C in a fluorescence spectrophotometer. As shown in Fig. 4b [13], when actin-VC210 is incubated with VN210-cofilin (WT), the fluorescence intensity is gradually increased and saturates after 180 min. The rate of increase in fluorescence intensity depends on the concentration of the probes. When actin-VC210 is incubated with VN210-cofilin (S3E), no fluorescence is recovered, even after 600 min of incubation, in contrast to VN210-cofilin (WT), indicating that the recovery of fluorescence reflects the specific interaction between actin and an active (non-phosphorylated) form of cofilin. Thus, the in vitro BiFC assay system described herein is useful and specific for detecting the protein–protein interaction with low background fluorescence.

3.3 High-Throughput Screening of Protein–Protein Interaction Inhibitors

The in vitro BiFC assay can be applied to a high-throughput screening of chemical compounds that inhibit or promote protein–protein interactions (Fig. 5a). The procedures of the screening for small-molecule inhibitors of the actin–cofilin interaction are described [15].

1. Add 1 μL of DMSO (control) or DMSO solution containing each of the chemical compounds tested at a final concentration of 6.6–10 μM into each well of a 96-well glass-bottom black microtiter plate in duplicate before addition of the BiFC probe proteins (*see* **Note 10**).
2. Add up to 30 μL of actin-VC210 and VN210-cofilin (WT) into each well of the 96-well plate with final concentrations of 1.5 μM and 3 μM, respectively.

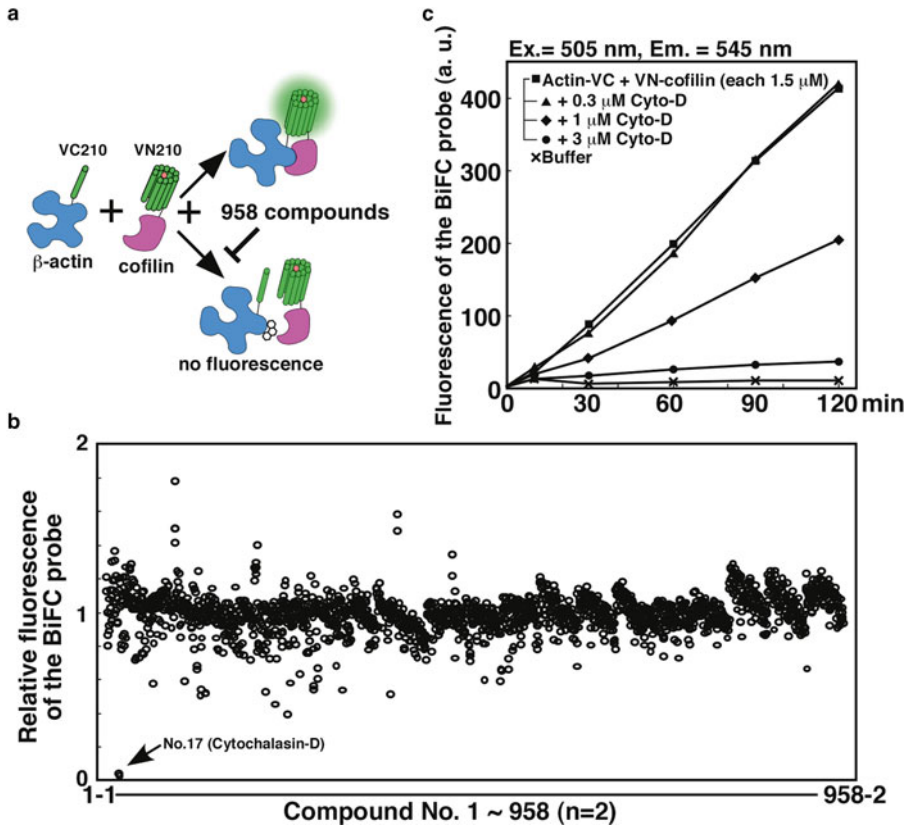

Fig. 5 Screening of actin–cofilin interaction inhibitors using the in vitro BiFC assay. (**a**) Schematic representation of the BiFC assay used for screening of inhibitors. (**b**) Results of the screening of actin–cofilin interaction inhibitors. The purified actin-VC210 (1.5 μM) and VN210-cofilin (3 μM) probes were incubated with a library of 958 chemical compounds (6.6–10 μM) at 30 °C in 96-well microtiter plates. The relative fluorescence intensity recovered is shown and compared to the value of control (DMSO) reactions. Experiments were performed in duplicate. The compound No. 17 is cytochalasin-D (Cyto-D). (**c**) The inhibitory effect of Cyto-D on the actin–cofilin interaction. The BiFC probes were incubated in the presence of the indicated concentrations of Cyto-D. The time course of the fluorescence recovery was measured by a fluorescence spectrophotometer. a.u., arbitrary units. Reproduced from ref. 15, with the permission of BBRC

3. Incubate at 30 °C, and measure the fluorescence intensity at 0 and 120 min with excitation at 505 nm and emission at 545 nm in a microplate fluorescence spectrophotometer.

   Figure 5b shows the result of the screening for 958 compounds. Cytochalasin-D (Cyto-D) was identified as an inhibitor of the actin–cofilin interaction [15]. Cyto-D suppressed the recovery of Venus fluorescence from the pair of actin-VC210 and VN210-cofilin in a dose-dependent manner, as measured by the in vitro BiFC assay (Fig. 5c).

4 Notes

1. Venus is used because of its strong fluorescence intensity and its fast and efficient maturation property compared to YFP [14]. The use of GFP or other GFP variants would probably result in a lower efficiency of the BiFC assays.
2. Other general mammalian expression vectors can be used for the assay.
3. Widely used mammalian cells (COS, HEK293, etc.) can be used in this assay.
4. The use of a high-aperture oil immersion objective lens is recommended for the observation of the fluorescence from the complemented Venus, because the fluorescence may be too weak to be detected using a dry lens.
5. The VN210 and VC210 BiFC probe proteins derived from *E. coli* can be complemented [13]. If the interacting proteins derived from *E. coli* maintain their binding activity, the recombinant BiFC probe proteins from *E. coli* can be used for in vitro BiFC assays.
6. Do not overlay the X-gal and IPTG solutions on the LB agar plate. X-gal should be mixed in the LB agar. Otherwise, the blue color of the colonies will be too weak to be detected.
7. The expression efficiency of the recombinant protein in SF9 cells is different between the clones. The selection of the Bacmid clones with high expression levels is recommended.
8. To avoid the degradation of a large Bacmid DNA, the recombinant Bacmid DNA is prepared by the alkaline-SDS method, rather than with the method using an affinity resin.
9. The amplified virus solution is generally added to the suspension of SF9 cells (1×10^6 cells/mL) at a ratio of 1:100 (v/v). However, checking the optimum ratio of the virus solution to the number of SF9 cells (multiplicity of infection, MOI) is recommended.
10. The assay should be performed in duplicate or triplicate to ensure accuracy and reproducibility of the experiments.

Acknowledgments

We are grateful to Atsushi Miyawaki for providing Venus cDNAs, Takao Yamori for supplying the SCADS inhibitor kits, and Masato Oikawa for providing a library of chemical compounds. We also thank Tai Kiuchi, Kazuyasu Shoji, and Kaori Sampei for suggestions. This work was supported by a grant-in-aid for Scientific Research from the Ministry of Education, Culture, Sports, Science and Technology of Japan.

References

1. Phizicky EM, Fields S (1995) Protein-protein interactions: methods for detection and analysis. Microbiol Rev 59:94–123
2. Miyawaki A (2003) Visualization of the spatial and temporal dynamics of intracellular signaling. Dev Cell 4:295–305
3. Miyawaki A (2011) Development of probes for cellular functions using fluorescent proteins and fluorescence resonance energy transfer. Annu Rev Biochem 80:357–373
4. Bacia K, Kim SA, Schwille P (2006) Fluorescence cross-correlation spectroscopy in living cells. Nat Methods 3:83–89
5. Ghosh I, Hamilton AD, Regan L (2000) Antiparallel leucine zipper-directed protein reassembly: application to the green fluorescent protein. J Am Chem Soc 122:5658–5659
6. Hu CD, Chinenov Y, Kerppola TK (2002) Visualization of interactions among bZIP and Rel family proteins in living cells using bimolecular fluorescence complementation. Mol Cell 9:789–798
7. Kerppola TK (2006) Visualization of molecular interactions by fluorescence complementation. Nat Rev Mol Cell Biol 7:449–456
8. Kerppola TK (2009) Visualization of molecular interactions using bimolecular fluorescence complementation analysis: characteristics of protein fragment complementation. Chem Soc Rev 38:2876–2886
9. Michnick SW, Ear PH, Manderson EN et al (2007) Universal strategies in research and drug discovery based on protein-fragment complementation assays. Nat Rev Drug Discov 6:569–582
10. Kodama Y, Hu CD (2012) Bimolecular fluorescence complementation (BiFC): a 5-year update and future perspectives. Biotechniques 53:285–298
11. Nagai T, Sawano A, Park ES et al (2001) Circularly permuted green fluorescent proteins engineered to sense Ca^{2+}. Proc Natl Acad Sci U S A 98:3197–3202
12. Bamburg JR (1999) Proteins of the ADF/cofilin family: essential regulators of actin dynamics. Annu Rev Cell Dev Biol 15:185–230
13. Ohashi K, Kiuchi T, Shoji K et al (2012) Visualization of cofilin-actin and Ras-Raf interactions by bimolecular fluorescence complementation assays using a new pair of split Venus fragments. Biotechniques 52:45–50
14. Nagai T, Ibata K, Park ES et al (2002) A variant of yellow fluorescent protein with fast and efficient maturation for cell-biological applications. Nat Biotechnol 20:87–90
15. Shoji K, Ohashi K, Sampei K et al (2012) Cytochalasin D acts as an inhibitor of the actin-cofilin interaction. Biochem Biophys Res Commun 424:52–57
16. Mizuno K (2013) Signaling mechanisms and functional roles of cofilin phosphorylation and dephosphorylation. Cell Signal 25:457–469
17. Yang N, Higuchi O, Ohashi K et al (1998) Cofilin phosphorylation by LIM-kinase 1 and its role in Rac-mediated actin reorganization. Nature 393:809–812
18. Green MR, Sambrook J (2012) Molecular cloning a laboratory manual, 4th edn. Cold Spring Harbor Laboratory Press, Cold Spring Harbor, NY

Chapter 18

Real-Time Investigation of Plasma Membrane Deformation and Fusion Pore Expansion Using Polarized Total Internal Reflection Fluorescence Microscopy

Daniel R. Passmore, Tejeshwar Rao, and Arun Anantharam

Abstract

Polarized Total Internal Reflection Fluorescence Microscopy (pTIRFM) allows for real-time observation of plasma membrane deformations. The technique provides insights into the dynamics of biological processes requiring rapid and localized changes in membrane shape. Such processes include exocytosis, endocytosis, cytokinesis, and cell motility. In this chapter, we describe how to implement a polarization-based TIRF imaging system to monitor exocytosis in adrenal chromaffin cells.

Key words Exocytosis, Membrane, Deformation, TIRF, pTIRF, Chromaffin, Fusion, Polarization, Granule

1 Introduction

Total Internal Reflection Fluorescence Microscopy (TIRFM) is used to visualize the plasma membrane–cytosol interface using an exponentially decaying evanescent field. This field selectively illuminates a narrow optical slice from the coverslip–sample interface through the cellular membrane. Fluorophore excitation is restricted to this thin cross section, thereby reducing background fluorescence, increasing spatial resolution, and improving the signal-to-noise ratio. TIRFM has been extensively used to study the dynamics of fluorescently tagged secretory granules during exocytosis to better understand the mechanism of granule fusion [1–8]. However, this method alone cannot provide information on the changing topology of the plasma membrane that occurs during, and potentially before, fusion [9, 10]. For this, polarization-based TIRFM or pTIRFM is required. In pTIRFM, a polarized evanescent field is used to excite an oriented fluorescent membrane probe [11–13]. Lipophilic carbocyanine dyes have been shown to intercalate with their transition dipole moments aligned roughly parallel to the membrane plane [14].

Andrei I. Ivanov (ed.), *Exocytosis and Endocytosis*, Methods in Molecular Biology, vol. 1174,
DOI 10.1007/978-1-4939-0944-5_18,

For the experiments described in this chapter, membranes labeled with carbocyanine dye (e.g., 1,1′-Dioctadecyl-3,3,3′,3′-Tetramethylindodicarbocyanine, 4-Chlorobenzenesulfonate, or diD) are sequentially exposed to orthogonally polarized excitations. When the electric field of the excitation laser is parallel to the plane of incidence (perpendicular to the coverslip) it is referred to as p-polarized (p-pol), and when the electric field is perpendicular to the plane of incidence (parallel to the coverslip) it is s-polarized (s-pol). Microscopic deviations in the plasma membrane from planar to nonplanar are detected by taking the ratio of the p-pol and s-pol emission images (P emission$/S$ emission, or P/S). The amplitude of the P/S can be predicted by computer simulations [11]. These show that it is quite sensitive to even small deformations. Therefore, P/S is the main parameter used to detect and follow membrane deformations occurring during exocytosis. The linear combination $P+2S$ approximately reports total diD emission from a particular location on the membrane. In theory, this is proportional to the amount of dye at any x–y–z location convolved with the evanescent field intensity [11]. The interpretation of $P+2S$ is more ambiguous than for P/S because of countervailing tendencies arising from the specific membrane geometry. Computer simulations indicate that $P+2S$ will increase if the geometry results in more diD-labeled membrane close to the glass interface. $P+2S$ decreases if the dye diffuses into a post-fusion membrane indentation placing it away from the substrate, and thereby in weaker evanescent field intensity. This chapter describes how pTIRFM is implemented and utilized to study the rapid, localized changes in membrane shape that occur during fusion and fusion pore dilation in a bovine adrenal chromaffin cell.

2 Materials

Prepare all solutions using sterile, autoclaved deionized water and analytical grade reagents. Prepare and store all reagents at room temperature except stock glucose solution. Store dyes away from direct light. Diligently follow all waste disposal regulations when disposing of waste materials.

2.1 pTIRF Setup Components

1. IX81 Inverted Microscope (Olympus, Center Valley, PA, USA).
2. iXon3 EMMCD Camera (Andor Technology, Belfast, UK; catalog number, 897).
3. 43 Series Ar-Ion Laser (CVI Milles Griot Laser Optics, Albuquerque, NM, USA; catalog number, 543-AP-A01).
4. Sapphire 561 LP Diode Laser (Coherent, Santa Clara, CA, USA).
5. Achromatic optically coated plano-concave lenses (focal length 100, 250 mm).

6. Achromatic optically coated plano-convex lenses (focal length 50, 125 mm).
7. Mounted Achromatic Quarter-Wave Plate (Thorlabs, Newton, NJ, USA; catalog number AQWP05M-600).
8. 420–680 nm Polarizing Beamsplitter Cube (Thorlabs; catalog number PBS201).
9. Six Station Neutral Density Wheel (Thorlabs; catalog number FW1AND).
10. HQ412lp Dichroic Filter (Chroma Technology Corp, Bellows Falls, VT, USA; catalog number NC255583).
11. z488/561rpc Dichroic Filter Cube (Chroma Technology Corp).
12. z488/561_TIRF Emission Filter Cube (Chroma Technology Corp).
13. Stepper-motor Driven Smart Shutter (Sutter Instruments, Novato, CA, USA; catalog number IQ25-1219).
14. 2D (X–Y) Scanning Galvanometer Mirror System (Thorlabs; catalog number GVSM002).

2.2 Imaging Solutions and Perfusion Components

1. Basal Physiological Saline Solution (PSS) solution: 145 mM NaCl, 5.6 mM KCl, 0.5 mM $MgCl_2$, 2.2 mM $CaCl_2$, 15 mM HEPES, 5.6 mM Glucose, pH 7.4.
2. Depolarizing PSS solution: 95 mM NaCl, 56 mM KCl, 0.5 mM $MgCl_2$, 2.2 mM $CaCl_2$, 15 mM HEPES, 5.6 mM Glucose, pH 7.4.
3. DiD Membrane Dye (Invitrogen, Grand Island, NY, USA).
4. Rhodamine 6G Chloride (Invitrogen).
5. QMM Quartz Micro Manifold (ALA Scientific Instruments, Farmingdale, NY, USA; catalog number ALA QMM-4).
6. VC3 Channel Focal Perfusion System (ALA Scientific Instruments; catalog number ALA VC3X4PP).
7. 10 PSI Pressure Regulator (ALA Scientific Instruments; catalog number ALA PR10).
8. Manipulator (Thorlabs; catalog number TS 5000-150).
9. MetaMorph Imaging Software (Molecular Devices, Sunnyvale, California, USA).

3 Methods

This procedure assumes the use of an Ar-ion (488 nm) laser for conventional TIRFM, and a Sapphire (561 nm) laser for polarization-based TIRFM. Different combinations of lasers are possible without significantly changing the setup procedure.

It also assumes that optics for TIRF is already positioned on the air table in the optimum positions for fluorophore excitation and imaging. It describes how polarization optics added to an existing TIRF microscope set-up enables imaging of cell membrane deformations. The procedure for isolating healthy bovine adrenal chromaffin cells is not discussed. Excellent references are available elsewhere [15, 16].

3.1 Implementing Polarization-Based TIRFM Imaging

1. Power on the 488 nm laser (used for conventional TIRF imaging), galvanometer mirrors, and any other necessary microscope components. Focus the laser beam onto the back focal plane (BFP) of the objective (*see* **Note 1**). Enter TIR by changing the position of the X-galvanometer mirror (*see* **Note 2**).
2. Using mirrors, adjust the 561 nm beam so that it is co-linear with the 488 nm beam. Position an achromatic concave lens to expand the 561 nm beam as shown in Fig. 1. The beam is focused to the BFP using a pair of convex lenses.
3. Verify that the 561 nm laser beam is aligned for TIR (*see* **Note 2**).
4. The 561 nm laser beam is linearly polarized as it emerges from the laser aperture. Circularly polarize the beam by centering a quarter-wave (QW) plate in its path.
5. Place a polarization cube downstream of the circularly polarized beam. Polarization cubes pass light with horizontal electric field orientations and reflect the vertical component.
6. Insert a mirror into the vertically polarized beam path. To recombine the beams, position a second mirror in the horizontally polarized beam path. Place a second polarization cube where the paths meet and adjust mirrors as necessary so that beam paths are co-linear.
7. Insert a motorized shutter in each of the two polarized beam paths (*see* **Note 3**).
8. Combine the p-pol and s-pol beams with the 488 nm beam using a dichroic mirror. The three beams should all be focused on the BFP and emerge collimated from the objective.
9. Enter TIR by changing the position of the X-galvanometer mirror (*see* **Note 2**).

3.2 Imaging with pTIRF

1. Power on lasers, imaging equipment, camera, and start the acquisition software. Verify laser alignment and that TIR can be achieved with both laser lines. Load perfusion reservoirs with basal PSS and depolarizing PSS.
2. Before imaging transfected chromaffin cells, prepare a rhodamine sample to normalize *P* and *S* emission image intensities. In a glass-bottom dish, add 10 mM rhodamine in 2 mL PSS. Sequentially excite the rhodamine sample with p-pol and s-pol beams (*see* **Note 4**).

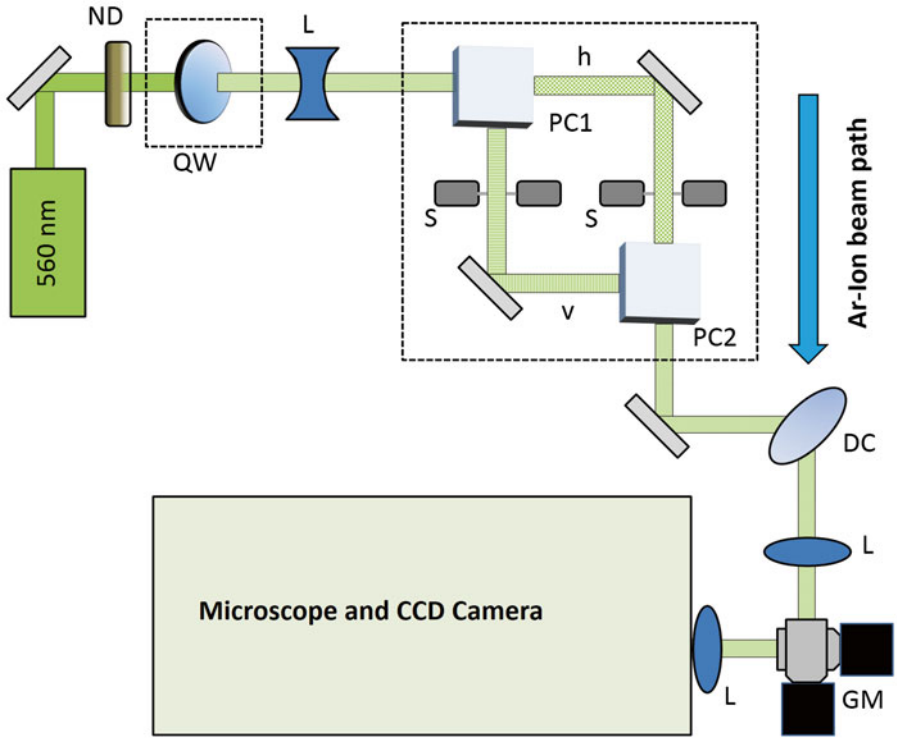

Fig. 1 Illustration of the pTIRFM optical assembly. A quarter-wave plate (QW) is placed in front of the 561 nm laser to circularly polarize the beam. The first lens (L) in the path is concave and expands the beam. The first polarization cube (PC1) separates the circularly polarized light into linear vertical (v) and horizontal (h) components. These polarized beam components are selected separately by two shutters (S). A second polarization cube (PC2) combines the two polarized beams. The two 561 nm beams are then joined with a 488 nm laser beam via a dichroic mirror (DC). The 488 nm beam path is not shown. Further downstream are convex lenses used in focusing the beam at the objective BFP. The combined beams are steered into a side illumination port of the microscope by a pair of galvanometer mirrors (GM). The optical components which allow for polarization selection are highlighted by *dashed boxes*

3. Prepare a 10 mM diD solution in ethanol.
4. Remove transfected chromaffin cells from the incubator. Replace culture media with PSS. Rinse twice. To stain the cell membranes with diD, directly add 10 μL of the diD solution to 2 mL of basal PSS in the culture dish. Agitate the dish gently for 5 s and then rinse the dish three times with basal PSS.
5. Place the dish containing the cells on the objective. Find a cell that is transfected with a fluorescently labeled cargo protein, such as NPY-pHluorin, and stained with diD (*see* **Note 5**).
6. Position the tip of the local perfusion needle so that it is roughly 100 μm away from the cell.
7. Acquire a full chip with the CCD camera and select a region of interest for the time-lapse image acquisition (*see* **Note 6**).

8. Activate the *Z*-dimension auto-focus hardware (*see* **Note 7**).
9. Set the perfusion to trigger with the start of image acquisition unless perfusing manually (*see* **Note 8**).
10. Start the image acquisition and shutter between the 488 nm, p-pol, and s-pol laser lines. The 488 nm excitation will excite the fluorescently tagged protein and the polarized beams will excite membrane-embedded diD (Fig. 2).

3.3 Analyzing Emission Images

1. Export images for off-line analysis (*see* **Note 9**). For background subtraction, find an average of pixel intensities in an off-cell area for each image stack (i.e., *P*, *S*, and NPY-pHluorin). Then subtract that value from all images in that stack (*see* **Note 10**).
2. Calculate a P/S image stack by dividing each frame pixel-by-pixel in the *P* emission stack by the corresponding frame in the *S* emission stack. Normalize P/S from diD emissions to the ratio obtained with rhodamine. Similarly, calculate a $P+2S$ image stack. No normalization is necessary to obtain $P+2S$.
3. To calculate P/S and $P+2S$ at sites of fusion, identify localized increases in emission intensity of NPY-pHluorin in the acquired images. Because of the pH sensitivity of pHluorin, its emission will increase when the fusion pore opens. Center an ROI at such regions. Apply the same ROI (same size and x–y location) to the P/S and $P+2S$ image stacks (*see* **Note 11**). Determine the average pixel value within the ROI for each frame in the image stack (Fig. 3).
4. Computer simulations are performed off-line to aid in the interpretation of P/S and $P+2S$ intensity versus time measurements, and to determine how these parameters relate to the simple geometries of a dilating fusion pore [11] (*see* **Note 12**).

4 Notes

1. During laser alignment, start with the X-Y galvanometer mirrors at the "0" position, with the beams focused on the BFP. They should emerge collimated from the objective and travel perpendicular to the sample plane. A well-defined Gaussian beam profile should appear on the ceiling centered directly above the objective if the 488 nm laser is focused at the BFP. A beam which appears as a cross or crescent shape instead of a round spot on the ceiling above the objective is most likely not traveling through the center of one of the lenses on the optical table. Remove all lenses and realign the lasers. Many inverted microscopes with a condenser have an iris diaphragm centered over the objective. The closed diaphragm makes a convenient target to aim for when determining if the lasers are traveling through the center of the microscope optical axis.

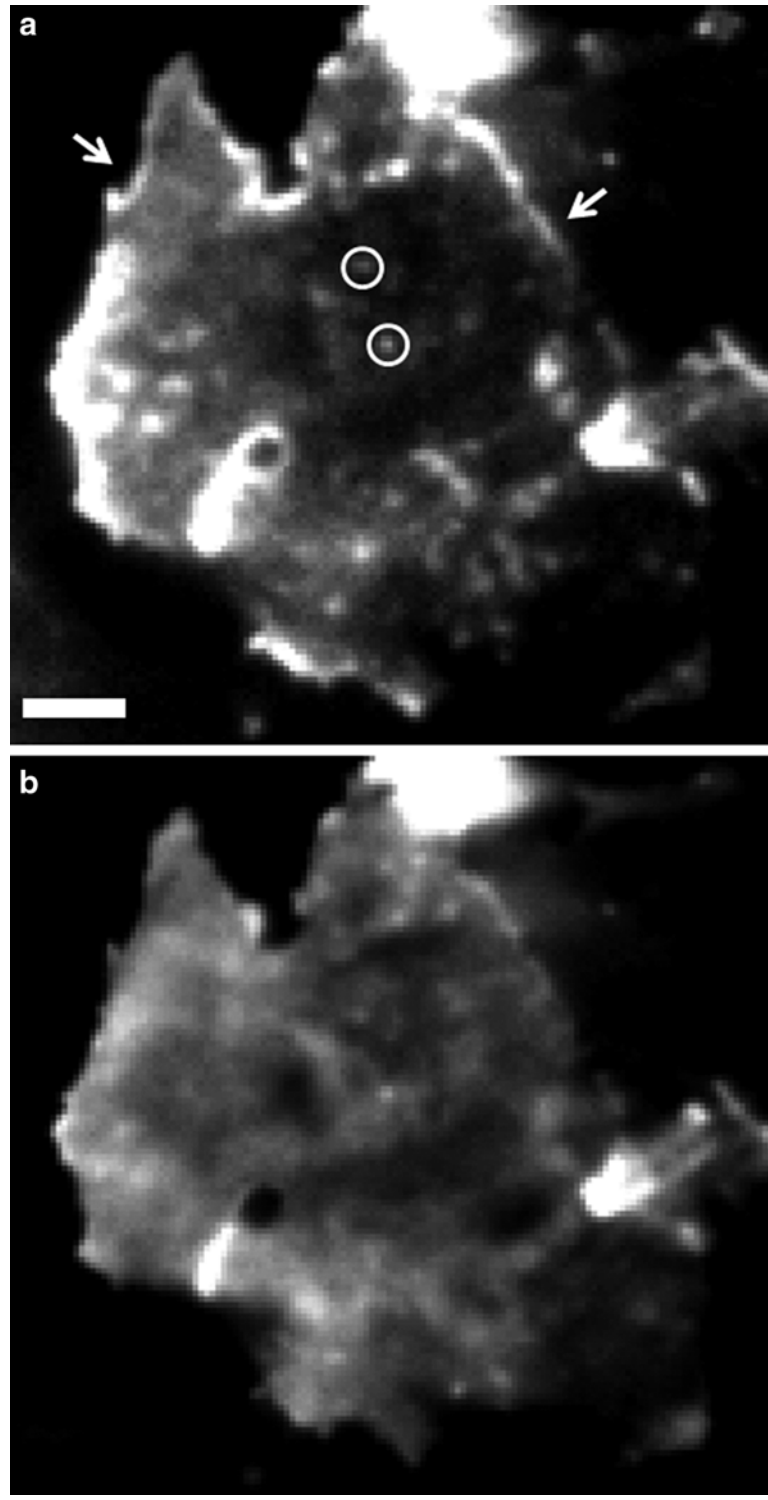

Fig. 2 Images of a diD-stained chromaffin cell obtained using pTIRFM. (**a**) P emission and (**b**) S emission images of membrane-embedded diD. The P emission highlights cell edges (*arrows*) and other nonplanar areas on the membrane (*circles*). The S emission image exhibits more uniform fluorescence over most of the cell footprint (i.e., the part of the cell visualized in TIRF). Scale bar, 3 μm

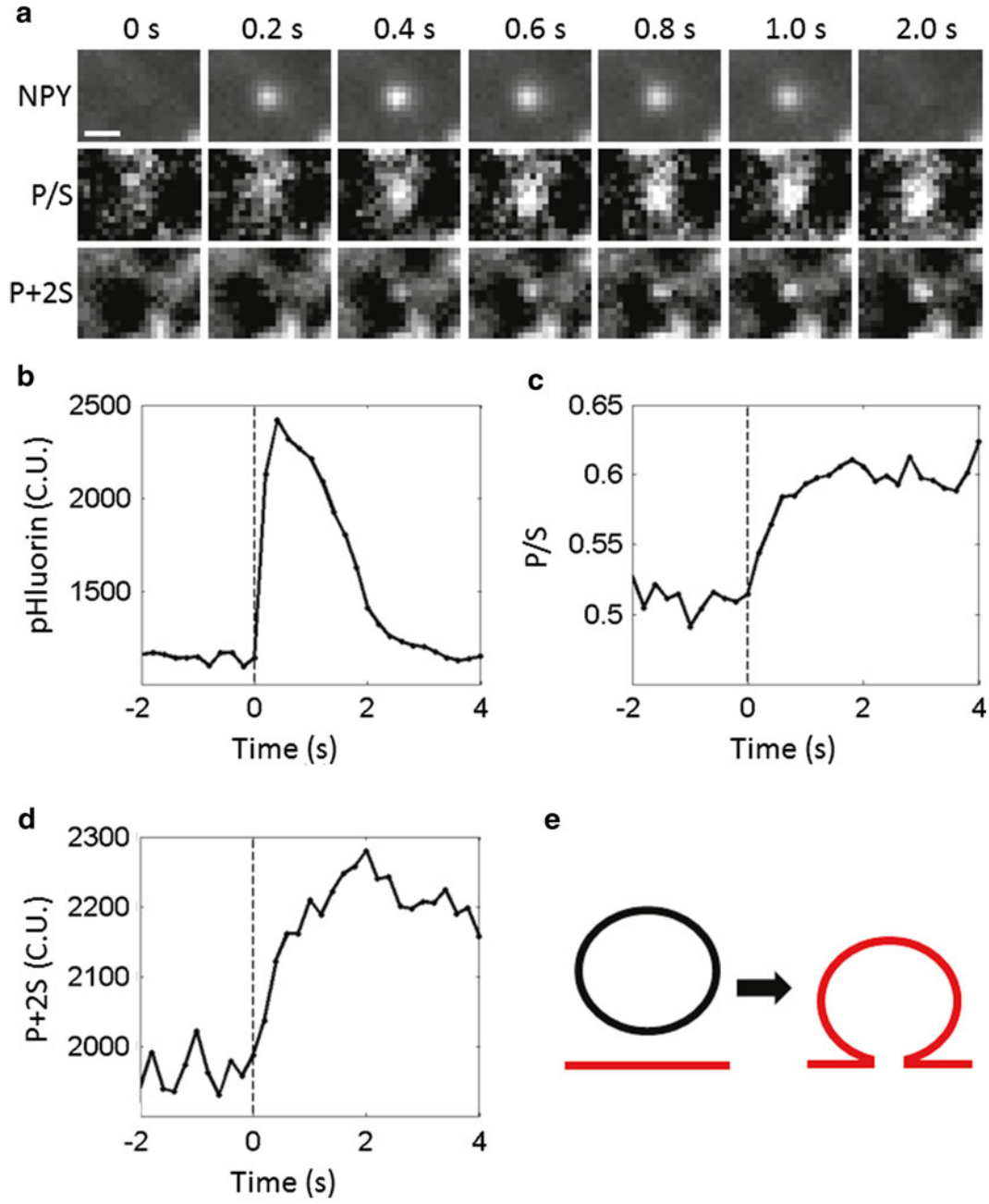

Fig. 3 Exocytosis visualized with pTIRFM. (**a**) Time-lapse images of an individual fusion event. *P/S* and *P+2S* images were calculated and aligned to the NPY-pHluorin image. Time 0 designates the frame immediately preceding fusion of the granule. (**b**) The pHluorin emission intensity increases when the granule interior is exposed to the extracellular solution, and decreases as the pHluorin-labeled cargo is released. (**c**, **d**) *P/S* and *P+2S* emission intensities increase with fusion. (**e**) Illustration showing one possible interpretation for the results obtained in (**a**)–(**d**). Scale bar, 1 μm

2. Adjust the X-galvanometer mirror (the mirror located in the equivalent sample plane) so that the laser beam is moved off-axis and emerges from the objective at progressively steeper angles to the objective normal. To verify that TIR is achieved, place a dish containing fluorescent microspheres in PSS on the objective. Only the fluorescent beads closest to the cover glass should be evident. If floating microspheres are visible, the angle between incident light and the objective normal is insufficient. If the field of illumination in TIR is shifted with respect to the field of illumination in epi-, then the galvanometer mirrors are not in the equivalent sample plane. To find the equivalent sample plane, move a notecard in the beam path until the edge of the notecard, as observed through the eyepiece, comes into focus. Reposition the X-galvanometer mirror so that it is located the equivalent sample plane.
3. These shutters allow for rapid selection between p-pol and s-pol excitation. Use a polarizing filter to verify the electric field orientation in each beam path.
4. The p-pol and s-pol intensity at the objective should be roughly equivalent. To ensure this is the case, place a dish containing rhodamine on the stage and bring it into focus. Shutter between p-pol and s-pol excitations and measure the emission intensity. The ratio of the resulting emission intensities (P/S) should be close 1. If not, add a neutral density filter in one polarized beam path to selectively attenuate its intensity or rotate the quarter-wave plate.
5. For reasons that are unclear, not every cell is equally well-stained with diD. Transfection efficiency can vary depending on the method used, but as a rule, it is much lower than staining efficiency. Therefore, start an experiment by looking for transfected cells first. Then look for transfected cells that are also stained with diD. Only choose cells which exhibit distinct differences in diD emission when illuminated with polarized light. The distinction between the cell edges and cell footprint will be vividly highlighted when switching between p-pol and s-pol beams, respectively. A cell which does not show such differences is not used for experiments.
6. Imaging with the full chip of a camera will reduce acquisition speed. Cells occupy only a small portion of the viewing field. Therefore, a small ROI encompassing only the cell of interest is necessary.
7. Review the auto-adjusted focus and reset if necessary. Autofocus is often necessary when imaging for more than 60 s.
8. Perfuse cells with basal PSS for at least 10 s before exposing them to depolarizing PSS. This is to ensure that exocytosis occurs as a result of depolarization and not as a result of perfusion alone.

If a cell fails to respond to stimulation, lift the perfusion needle above the culture dish and verify that the perfusion system is flowing at an adequate speed. Clean the perfusion system with ethanol followed by deionized water after every imaging session to avoid hard-to-remove salt deposits.

9. Calculations for image processing may be performed with ImageJ, but utilizing scripts in a flexible programming language such as Matlab can greatly increase analysis throughput by automating the task.
10. One may also choose to subtract a flat background value from all pixel values in an image stack.
11. There is sometimes a slight offset between the center of intensity of the fusing granule and the membrane deformation. In such cases, center the ROI over the parameter (pHluorin, P/S or $P+2S$) of greatest interest.
12. The computer simulations take into account the radius of the spherical indentation, diD labeling in both the indentation and planar areas, convolution with a point-spread function to simulate the optical resolution limit, the evanescent field depth, and angle between diD dipoles and the normal to the plane of the membrane [11].

Acknowledgements

This work is supported by a National Scientist Development Grant (13SDG14420049) from the American Heart Association and start-up funds from Wayne State University, both to A.A.

References

1. Toomre D, Steyer JA, Keller P, Almers W, Simons K (2000) Fusion of constitutive membrane traffic with the cell surface observed by evanescent wave microscopy. J Cell Biol 149:33–40
2. Taraska JW, Perrais D, Ohara-Imaizumi M, Nagamatsu S, Almers W (2003) Secretory granules are recaptured largely intact after stimulated exocytosis in cultured endocrine cells. Proc Natl Acad Sci U S A 100: 2070–2075
3. Zenisek D, Davila V, Wan L, Almers W (2003) Imaging calcium entry sites and ribbon structures in two presynaptic cells. J Neurosci 23: 2538–2548
4. Lang T, Wacker I, Steyer J et al (1997) Ca2+-triggered peptide secretion in single cells imaged with green fluorescent protein and evanescent-wave microscopy. Neuron 18:857–863
5. Steyer JA, Horstman H, Almers W (1997) Transport, docking and exocytosis of single secretory granules in live chromaffin cells. Nature 388:474–478
6. Degtyar VE, Allersma MW, Axelrod D, Holz RW (2007) Increased motion and travel, rather than stable docking, characterize the last moments before secretory granule fusion. Proc Natl Acad Sci U S A 104:15929–15934
7. Allersma MW, Bittner MA, Axelrod D, Holz RW (2006) Motion matters: secretory granule motion adjacent to the plasma membrane and exocytosis. Mol Biol Cell 17:2424–2438
8. Allersma MW, Wang L, Axelrod D, Holz RW (2004) Visualization of regulated exocytosis with a granule-membrane probe using total internal reflection microscopy. Mol Biol Cell 15:4658–4668

9. Chernomordik LV, Zimmerberg J, Kozlov MM (2006) Membranes of the world unite! J Cell Biol 175:201–207
10. Chernomordik LV, Kozlov MM (2003) Protein-lipid interplay in fusion and fission of biological membranes. Annu Rev Biochem 72:175–207
11. Anantharam A, Onoa B, Edwards RH, Holz RW, Axelrod D (2010) Localized topological changes of the plasma membrane upon exocytosis visualized by polarized TIRFM. J Cell Biol 188:415–428
12. Sund SE, Swanson JA, Axelrod D (1999) Cell membrane orientation visualized by polarized total internal reflection fluorescence. Biophys J 77:2266–2283
13. Axelrod D (1989) Fluorescence polarization microscopy. Methods Cell Biol 30:333–352
14. Axelrod D (1979) Carbocyanine dye orientation in red cell membrane studied by microscopic fluorescence polarization. Biophys J 26:557–574
15. Wick PW, Senter RA, Parsels LA, Holz RW (1993) Transient transfection studies of secretion in bovine chromaffin cells and PC12 cells: generation of kainate-sensitive chromaffin cells. J Biol Chem 268:10983–10989
16. O'Connor DT, Mahata SK, Mahata M, Jiang Q, Hook VY, Taupenot L (2007) Primary culture of bovine chromaffin cells. Nat Protoc 2:1248–1253

Chapter 19

Nanocones to Study Initial Steps of Endocytosis

Sangmoo Jeong and Milos Galic

Abstract

Vesicle endocytosis at the plasma membrane is associated with a precise temporal choreography in the recruitment of cytosolic proteins that sense, generate, or stabilize locally curved membrane regions. To dissect the role of membrane curvature sensing from other co-occurring events during the initial steps of endocytosis, we developed a method to artificially induce nanoscale deformations of the PM in living cells that is based on cone-shaped nanostructures (i.e., Nanocones). When cultured on Nanocones, cells create stable inward plasma membrane deformations to which curvature-sensing proteins are recruited. Here, we provide a detailed protocol how to use Nanocones to study recruitment during the initial steps of endocytosis in cells by fluorescence and electron microscopy.

Key words Nanocones, Plasma membrane, Membrane curvature, Endocytosis, Endocytic vesicles

1 Introduction

Membrane deformation is the result of forces applied to the plasma membrane (PM) against surface tension and membrane rigidity [1]. In cells, such forces are generated by oligomerization of membrane-associated proteins [2], clustering of trans-membrane proteins [3], asymmetric insertion of an active helix into the lipid bilayer [4], forces applied by the underlying cytoskeleton [5], and asymmetric lipid distribution [6]. Once formed, curved PMs trigger binding of curvature-sensing proteins [7]. However, many curvature-sensing proteins have been shown to directly alter the forces applied to the PM [8, 9], thus creating a causality dilemma: is protein recruitment the cause or the consequence of PM curvature? To separate curvature-sensing from curvature-induction in living cells, we developed a method to induce nanoscale plasma deformations that is based on cone-shapes nanostructures, which we named Nanocones [5]. Cells cultured on a Nanocone-coated substrate are exposed to constant focal forces (at the basal membrane) that trigger inward plasma membrane deformation independent of curvature-inducing proteins (Fig. 1a).

Andrei I. Ivanov (ed.), *Exocytosis and Endocytosis*, Methods in Molecular Biology, vol. 1174,
DOI 10.1007/978-1-4939-0944-5_19,

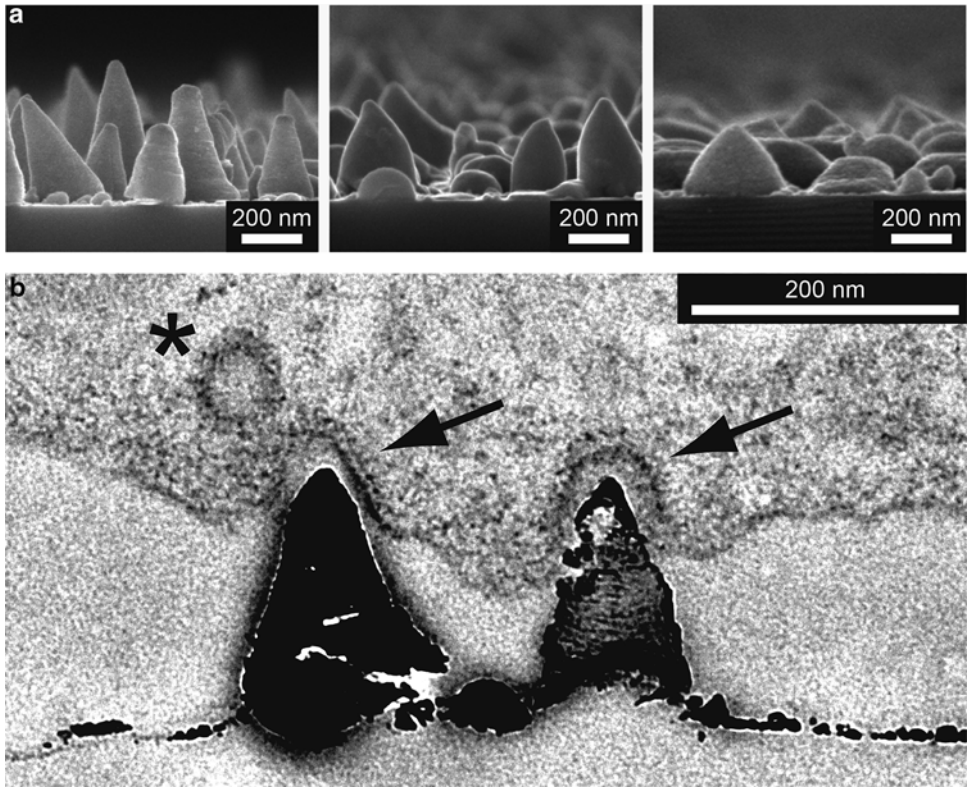

Fig. 1 Endocytic vesicles form at Nanocone-induced PM deformations in living cells. (**a**) Subtle changes in the annealing protocol causes changes in the shape of Nanocones. The *left image* shows the Nanocones fabricated with the optimized protocol. The *center image* shows the Nanocones fabricated at lower temperature (220 °C). The *right image* shows the Nanocones fabricated at higher oxygen concentration (5 %). (**b**) Nanocones deform the plasma membrane in living cells. Transmitted Electron Micrograph showing the cross section of a 3T3 cell cultured on a Nanocone-coated glass slide. Note the accumulation of Clathrin at the *top* of Nanocones (*arrows*) and the presence of a Clathrin-coated vesicle to the *top left* (*asterisk*). Scale bars (**a**, **b**), 200 nm

As Nanocones are transparent, this does not only allow the characterization of protein aggregation to curved membranes by electron microscopy but also the analysis of recruitment kinetics of curvature-sensing proteins to curved sites in living cells by fluorescence microscopy [5].

Kinetic analysis of protein localization during endocytosis has shown that the temporal order of protein recruitment is broadly consistent between yeast and mammalian cells [10, 11]. While this canonical model has elucidated the kinetics of proteins recruitment during endocytosis, it has also raised numerous questions about how forces at the PM are generated and coordinated during endocytosis. For example, how are the F-BAR domain proteins FCHo1 and FCHo2 polarized in the early stages of the invagination process? Current approaches to study curvature-sensing proteins

include crystal structure analysis [9], binding of curvature-sensing proteins to vesicles of different diameters [7], and tubulation of lipid vesicles [9]. In these assays, proteins are probed for their ability to sense or induce membrane curvature in vitro. These elegant approaches have substantially advanced our understandings on the molecular mechanisms of curvature-sensing and induction. However, since the lipid composition of the PM inner leaflet is not well defined, these assays do not show whether recruitment of curvature-sensing proteins is selective to particular curved membranes within the cell. Furthermore, dynamic measurements of curvature-sensing proteins in cells suggest that many of the relevant membrane binding events are short lived and selective to particular lipids within the PM [10]. Nanocones may complement these in vitro approaches and provide insights into how curvature-sensing proteins assemble and disassemble in their physiological setting (most known curvature-sensing proteins form oligomers when they bind to curved membranes). Creating PM curvature using Nanocones may thus be used to address questions such as how individual curvature-sensing proteins dynamically compete when binding to curved PMs, and help to resolve the role of specific proteins described to sense and/or induce PM curvature during early steps of endocytosis.

We found that subtle variations in the annealing protocol alter size, density, and shape of the Nanocones [12] and generate PM curvature with a range of diameters at the basal plasma membrane (Fig. 1b). The method presented here has been optimized to study curvature-dependent processes during the early phase of endocytosis using fluorescence and electron microscopy. It provides a step-by-step description for the fabrication of micro-pattern of Nanocones with a tip diameter of ~30–50 nm (*see* Subheading 3.1), a detailed portrayal how Nanocone-coated glass slides are prepared and used in fluorescence (*see* Subheading 3.2) and electron microscopy (*see* Subheadings 3.3 and 3.4), as well as comments on critical steps along the way (*see* Subheading 4).

2 Materials

2.1 Nanocone Production

1. 22 × 22 mm Square cover glass (0.13–0.17 mm thickness).
2. Tin (99.99 %).
3. Acetone (>99.5 %).
4. Methanol (>99.8 %).
5. Ethanol (>99.5 %).
6. Nitric Acid (68 %).
7. Ultrasonic bath (Branson Ultrasonics, Danbury, CT, USA).
8. Electron beam evaporator (custom-made).

9. Furnace (Lindberg/Blue M 1,200 °C Split-Hinge Tube Furnace, Thermo Scientific, Asheville, NC, USA).
10. Mass flow controller (150 MM Flowmeter, PRAXAIR, Danbury, CT, USA).

2.2 Pattern Generation (Optional)

1. Spin Coater (Laurell, North Wales, PA, USA).
2. Chrome Mask (custom-made pattern, Photo Sciences Inc., Torrance, CA, USA).
3. Photoresist.
4. UV exposure tool (KarlSuss MA-6 Aligner, SUSSMicroTec, Garching, Germany).
5. Photoresist developer (Microposit MF-26A, Shipley, Coventry, UK).
6. Isopropanol (>99.5 %).
7. Plasma Cleaner (PYREX, Sigma Aldrich, St. Louis, MO, USA).

2.3 Fluorescence Microscopy

1. Lab-Tek chambered Glass slides (Nunc, Thermo Scientific, Ashville, NC, USA).
2. Poly-L-lysine (30,000–60,000 MW).
3. 0.1 M borate buffer: add 1.55 g boric acid, 2.4 g sodium tetraborate to 500 mL ddH_2O and adjust pH to 8.5.
4. Nail polish.
5. High Vacuum Grease.

2.4 Electron Microscopy

1. 8 % EM grade glutaraldehyde in ddH_2O (EMS, Hatfield, PA, USA).
2. 16 % EM grade paraformaldehyde in ddH_2O (EMS).
3. 0.1 M HEPES, NaCacodylate buffer pH ~7.4 (EMS).
4. Embedding resin (EMbed 812 Kit, EMS).
5. 1 % OsO_4 in ddH_2O.
6. 1 % Uranyl acetate in ddH_2O.
7. EtOH (100 %).
8. Propylene oxide.
9. Hydrofluoric acid (49 %).
10. Microtome (Ultracut S, Leica, Wetzlar, Germany).
11. Transmission electron microscope (JEM-1230, JEOL, Peabody, MA, USA).
12. Sonicator (VCX130, SONICS, Newtown, CT, USA).
13. Critical Point Dryer (Tousimis, Rockville, MD, USA).

14. Sputter Coater (Denton Desk 11, Denton Vacuum, Moorestown, NJ, USA).
15. Scanning electron microscope (Sigma FE-SEM, Zeiss, Oberkochen, Germany).

3 Methods

3.1 Fabrication of Nanocones on Glass Slides

1. Wash glass slides (*see* **Note 1**) in an ultrasonic bath of acetone (at 40 kHz) for 5 min, and then rinse 3 times in ddH_2O.
2. Wash the glass slides in an ultrasonic bath of methanol (at 40 kHz) for 5 min, and then rinse 3 times in ddH_2O.
3. Wash the glass slides in an ultrasonic bath of ethanol (at 40 kHz) for 5 min, and then rinse 3 times in ddH_2O (*see* **Note 2**).
4. To create a litographic pattern (Fig. 2a), spin-coat photoresist on the cleaned glass slides (*see* **Note 3**).

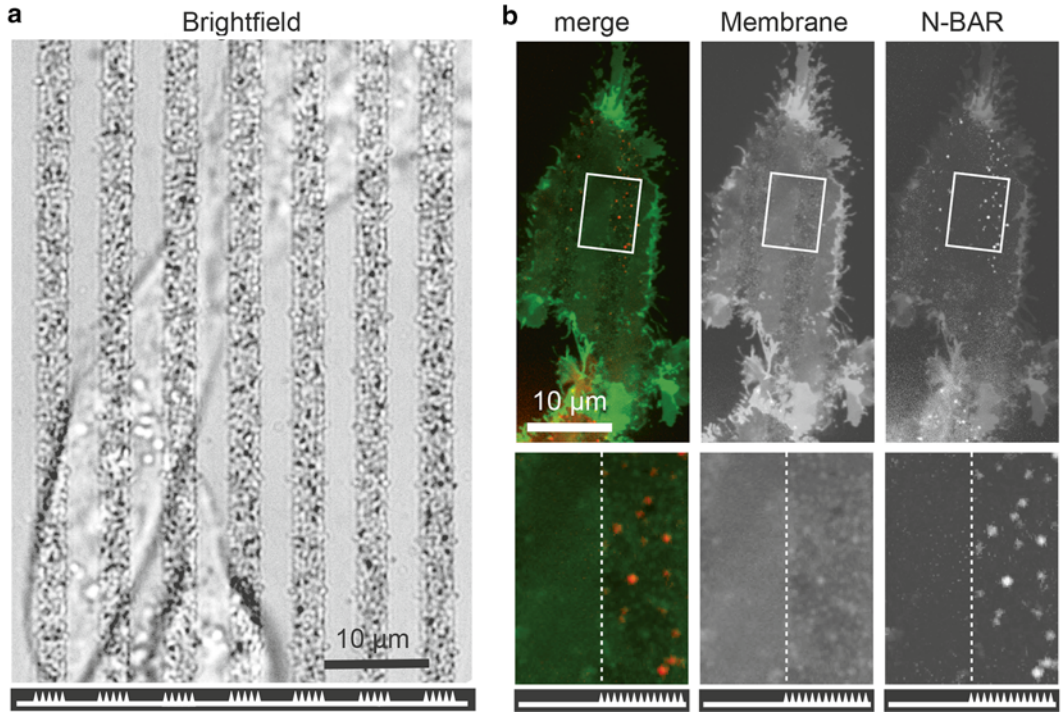

Fig. 2 Lithographic micro-pattern to generate stripes of Nanocones. (**a**) Bright light image of 3T3 cells cultured on glass slides patterned with 3 µm wide micro-stripes coated with Nanocones. Note that the transmitted light over Nanocones is only slightly dimmer. The localization of Nanocones is depicted as jagged pattern below the image. (**b**) A curvature-sensing protein is recruited to curved PM sections over Nanocones. Cells were cultured on 3 µm wide stripes of Nanocones and transfected with a membrane marker (*green*), and a fluorescently tagged N-BAR domain protein (*red*, Nadrin2). Magnifications of individual channels are shown below the image. Note the formation of puncta over stripes of Nanocones. Scale bars (**a**, **b**), 10 µm

5. Take a chrome mask with the pattern of choice (e.g., stripes), put it on top of the coated glass slides, and expose for 2 s to UV light (365 nm wavelength).
6. Dip exposed glass slides into photoresist developer for 1 min.
7. Rinse with isopropanol for 5 min. Sites that were exposed to UV are now protected with photoresist.
8. Deposit tin as a layer of 30–35 nm thick nano-islands on the cleaned substrate by electron-beam evaporation (*see* **Note 4**). The deposition rate is approximately 5–10 Å/s under the pressure of less than 1e–6 Torr (*see* **Note 5**).
9. To remove photoresist mask, place glass slide in acetone for 5 min followed by oxygen plasma stripping (*see* **Note 6**).
10. Rinse 3 times in ddH_2O.
11. Use air-pistol to blow glass on slides containing stripes of tin nano-islands in order to dry these nano-islands.
12. Transfer the glass slides with the stripes of tin nano-islands to a quartz tube mounted in a furnace.
13. Pump and purge the quartz tube with nitrogen gas several times (*see* **Note 7**).
14. To create the desired ~100 ppm oxygen needed for annealing (=99.99 % nitrogen vs. 0.01 % oxygen), the flow rates of nitrogen and oxygen are adjusted individually using two separate mass flow controllers.
15. After the gas flow rates are stabilized, the glass slides in the furnace are annealed at a temperature of ~400 °C for at least 90 min (*see* **Note 8**).
16. Wash the Nanocone-coated glass slides 3 times for 30 min in ddH_2O (*see* **Note 9**).
17. Check if annealing was successful by SEM. The Nanocones are now ready for use.

3.2 Imaging Cells Cultured on Nanocones Using a Fluorescence Microscope

1. Prepare 0.1 mL/mL poly-L-lysine (PLL) in 0.1 M borate buffer (pH ~8.5).
2. Prepare container for live-cell microscopy: Glue Nanocone-coated glass slides with nail polish to the plastic housing of Lab-Tek chambers of which the glass slides has previously been removed (*see* **Note 10**).
3. Dry the nail polish on a heating block at ~60 °C for >4 h (*see* **Note 11**).
4. Wash the Nanocone-coated glass slides 3 times for 30 min in ddH_2O.
5. Sterilize using UV from tissue culture hood for 15–30 min.

6. To increase cell adhesion, coat the slides with PLL overnight.
7. Wash 3 times for 30 min in ddH_2O.
8. Cells can now be plated, transfected with fluorescently tagged protein of interest, and imaged on an inverted microscope (Fig. 2b). Same rules as for normal fluorescent microscopy apply (*see* **Note 12**).
9. After imaging is finished, rinse sample 3 times with ddH_2O.
10. Aspirate ddH_2O and plasma-clean the Nanocone-coated glass slides for 10 min (*see* **Note 13**). If no plasma cleaner is available, remove cells in nitric acid for 30 min (*see* **Note 14**).

3.3 Imaging Cells Cultured on Nanocones by TEM

1. Prepare fixation solution containing a final concentration of 2 % glutaraldehyde (from 8 % stock) and 4 % paraformaldehyde (from 16 % stock) in 0.1 M HEPES, Na Cacodylate buffer pH ~7.4 (*see* **Note 15**).
2. Prepare fresh EMbed 812 following the manufacturer's protocol.
3. Warm fixative to room temperature.
4. Replace medium with the fixative and leave the cells in fixative for >10 min (*see* **Note 16**).
5. Wash 3 times in ddH_2O.
6. Incubate sample with 1 % uranylacetate in ddH_2O overnight.
7. Dehydrate samples as follows: 1× 50 % EtOH (in ddH_2O) for 5 min; 1× 70 % EtOH for 5 min; 1× 95 % EtOH for 10 min; 2× 100 % EtOH for 15 min.
8. Move the samples to Propylene Oxide (PO) for 15 min.
9. Infiltrate sample as follows: 1:1 (EMbed 812/PO) for 1 h; 2:1 (EMbed 812/PO) overnight; 100 % EMbed 812 for 3 h; 100 % EMbed 812 for 2 h.
10. Polymerize EMbed 812 at 65 °C overnight.
11. Dissolve glass and Nanocones in 49 % hydrofluoric acid (10 min) (*see* **Note 17**).
12. Wash the samples 3 times with ddH_2O.
13. Embed the samples a second time in 100 % EMbed 812 (to cover the side where the glass and Nanocones have been) and polymerize at 65 °C overnight.
14. Cut on microtome 70 nm thick sections orthogonally to the plane of the glass slide.
15. If desired, post-process samples (e.g., immuno-gold), then mount on a grid and image on a transmission electron microscope using 5–30,000× magnification.

3.4 Imaging Cells Cultured on Nanocones by SEM

1. Fix the cells in the fixative as described above.
2. Replace the fixative with 1× PBS.
3. Unroof the cells via brief sonication: use two 5 s pulses of 40 % intensity with a 1/8 in. microprobe that is placed 1 cm above the sample (*see* **Note 18**).
4. Wash the cells with ddH_2O.
5. Dehydrate the cells as follows: 50 % EtOH (in ddH_2O) for 20 min, 70 % EtOH for 20 min, 90 % EtOH for 20 min, and 100 % EtOH (twice) for 20 min each.
6. Critical point drying with liquid CO_2.
7. Mount sample on holder and sputter-coat with 100 Å of Au/Pd.
8. Visualize samples on a scanning electron microscope.

4 Notes

1. Nanocones can be deposited on any substrate as long as it can be heated to 400 °C. While a transparent substrate is required for an inverted microscope (due to the light path), any other materials can be considered on an upright microscope.
2. The described washing steps are critical to remove potential deposits of fat and/or dirt residues from the glass slide required for proper deposition of tin droplets and subsequent annealing to the substrate.
3. All steps involving photo-lithography should be conducted in a room equipped with filtered lighting that contains no ultraviolet or blue light.
4. Increased thickness of tin deposition prior to annealing increases the size while reducing the density of individual Nanocones. Note that bigger Nanocones will reduce the transparency of the sample after annealing, could interfere with cell attachment and may also cause penetration of the basal membrane.
5. Note that changes in the electron power alter the deposition rate of the tin film. To calibrate the system, measure the thickness of the tin layer (i.e., deposition rate) for a constant evaporation time via SEM.
6. To remove all residues, we recommend to always combining the wet strip (i.e., acetone) with a brief plasma strip.
7. To prevent premature oxidation of tin droplets, make sure the oxygen concentration is lower than 0.1 % (i.e., <1,000 ppm).
8. Longer annealing time increases the transparency of the Nanocones.

9. These washing steps are critical to remove toxic remains from the production.
10. If reversible attachment of a container to Nano-coated glass slides is desired, vacuum grease can be used.
11. Proper drying and extensive washing are essential to avoid release of potentially toxic substances from the nail polish into the medium. For some types of nail polish, drying may require more than 4 h.
12. Nanocones are not compatible with PALM/STORM-type super-resolution microscopy as the tin oxide nanostructures alter the point-spread function of light.
13. Nanocones can be reused up to 5 times with no significant drop in efficiency. However, drying of cells on Nanocones should be avoided, since this drastically reduced the efficiency of cell removal.
14. This should be done in a ventilated fume hood. Labtek chambers should be removed prior to addition of nitric acid.
15. Once prepared the fixation solution should be stored at 4 °C and used within 1 week. In our hands, the use of 4 % paraformaldehyde (without glutaraldehyde) was less efficient in preserving biological structures.
16. When replacing medium with the fixative, drying the sample or creating excessive flow-stress on the sample should be avoided. The cells can be stored in the fixative for up to 24 h at 4 °C.
17. Exposure to hydrofluoric acid for 30 min will dissolve the Nanocones, leaving only a thin outline (~10 nm) of the Nanocone shape. This can be used to analyze structures with low electron-density in the proximity of the Nanocones that would otherwise be overshadowed by the electrodense tinoxide of the Nanocones.
18. The degree of unroofing of cytosolic material depends on the distance of the cell to the microprobe. Position the probe at one edge of the sample and identify the area with the ideal degree of structural integrity on the SEM.

Acknowledgments

S. J. acknowledges support from the Korea Foundation for Advanced Studies (KFAS) for graduate fellowship. M. G. was supported by fellowships from the Swiss National Science Foundation (No. PBBSP3-123159), Novartis Jubilaeumsstiftung, Stanford Deans Postdoctoral Fellowship and grants from the German Research Foundation (Cluster of Excellence EXC 1003, Cells in Motion, CiM, Münster, Germany).

References

1. Peskin CS, Odell GM, Oster GF (1993) Cellular motions and thermal fluctuations: the Brownian ratchet. Biophys J 65:316–324
2. Hinshaw JE, Schmid SL (1995) Dynamin self-assembles into rings suggesting a mechanism for coated vesicle budding. Nature 374:190–192
3. McMahon HT, Gallop JL (2005) Membrane curvature and mechanisms of dynamic cell membrane remodelling. Nature 438:590–596
4. Gallop JL, Jao CC, Kent HM et al (2006) Mechanism of endophilin N-BAR domain-mediated membrane curvature. EMBO J 25:2898–2910
5. Galic M, Jeong S, Tsai FC et al (2012) External push and internal pull forces recruit curvature-sensing N-BAR domain proteins to the plasma membrane. Nat Cell Biol 14:874–881
6. Kooijman EE, Chupin V, Fuller NL et al (2005) Spontaneous curvature of phosphatidic acid and lysophosphatidic acid. Biochemistry 44:2097–2102
7. Bhatia VK, Madsen KL, Bolinger PY et al (2009) Amphipathic motifs in BAR domains are essential for membrane curvature sensing. EMBO J 28:3303–3314
8. Takano K, Toyooka K, Suetsugu S (2008) EFC/F-BAR proteins and the N-WASP-WIP complex induce membrane curvature-dependent actin polymerization. EMBO J 27:2817–2828
9. Peter BJ, Kent HM, Mills IG et al (2004) BAR domains as sensors of membrane curvature: the amphiphysin BAR structure. Science 303:495–499
10. Taylor MJ, Perrais D, Merrifield CJ (2011) A high precision survey of the molecular dynamics of mammalian clathrin-mediated endocytosis. PLoS Biol 9:e1000604
11. Kaksonen M, Toret CP, Drubin DG (2005) A modular design for the clathrin- and actin-mediated endocytosis machinery. Cell 123:305–320
12. Jeong S, McDowell MT, Cui Y (2011) Low-temperature self-catalytic growth of tin oxide nanocones over large areas. ACS Nano 5:5800–5807

Chapter 20

A Novel Permeabilization Protocol to Obtain Intracellular 3D Immunolabeling for Electron Tomography

Nuria Jiménez and Jan A. Post

Abstract

Electron tomography (ET) is a very important high-resolution tool for 3D imaging in cell biology. By combining the technique with immunolabeling, ET can provide essential insights into both cellular architecture and dynamics. We recently developed a protocol to achieve 3D immunolabeling of intracellular antigens without the need for uncontrolled permeabilization steps that cause random, extensive cell membrane disruption. Here we describe this novel method based on well-controlled permeabilization by targeted laser cell perforation. Mechanical permeabilization of the plasma membrane can be applied at specific sites without affecting other parts of the plasma membrane and intracellular membranes. Despite the relatively small opening created in the plasma membrane, the method allows specific 3D immunolocalization of cytoplasmic antigens in cultured cells by a pre-embedment protocol. The approach is unique and leads to a superior ultrastructural preservation for transmission electron microscopy and electron tomography.

Key words Chemical fixation, Cultured cells, Electron microscopy, Electron tomography, Pre-embedment immunolabeling, Targeted laser cell perforation

1 Introduction

In the last decades unravelling of the architecture of cells has gained a boost because of the application of electron tomography. To understand the 3D organization of cells it is a necessity to identify cytoplasmic structures and macromolecules unequivocally, and frequently this identification is based on immunolabeling. In case of electron tomography (ET) this identification should be done in 3D throughout the entire specimen/cell. Immunolabeling of cytosolic antigens implies bringing antibodies and probes into the cytosol. Until now, in transmission electron microscopy (TEM) and ET studies, this has been achieved by chemical or mechanical rupture of the plasma membrane [1–3]. An obvious drawback of this approach is that the applied permeabilization steps destruct the plasma membrane and other cellular membranes in an

Andrei I. Ivanov (ed.), *Exocytosis and Endocytosis*, Methods in Molecular Biology, vol. 1174,
DOI 10.1007/978-1-4939-0944-5_20,

uncontrolled manner. As a result of this ultrastructural details will be randomly lost, thereby limiting the applicability of the labeled specimen for high-resolution studies [4].

Therefore we developed a novel method to permeabilize the plasma membrane in a well-controlled manner, known as targeted laser cell perforation (tLCP) [5]. To set up the protocol we used human umbilical vein endothelial cells (HUVECs). We grew cells on a substratum compatible with correlative light and electron microscopy (CLEM; *see* **Note 1**), in our case Aclar, which is suitable for chemical and cryo-fixation [6, 7]. After mild chemical fixation of the cells we permeabilized the plasma membrane by perforating a single tunnel across the cell using a laser at a "dispensable" place in the current study: the nuclear area. Cells were then immunolabeled for caveolin, an endothelial antigen well represented in HUVECs [4] and subsequently processed for TEM and ET.

2 Materials

2.1 HUVEC Culture for tLCP

1. HUVECs cultured to "cobblestone" state as described before [8].
2. Pieces (ca. 1 cm^2) of Aclar® 33C (51 μm thick; Electron Microscopy Sciences), engraved with grids (nine grids/piece) and position marks using a focused ion beam exactly as published [7].
3. Glass-bottom culture dishes (35 mm diameter).
4. Matrigel™ (BD Biosciences).
5. Phase contrast microscope (Leica DMIL).

2.2 Standard Chemical Fixation Prior to tLCP

1. Primary fixative: Formaldehyde (from paraformaldehyde) at 4 % (wt/vol) in 0.2 M HEPES buffer, pH 7.2.
2. Washing buffer: PHEM buffer (60 mM PIPES, 25 mM HEPES, 10 mM EGTA, and 2 mM MgCl, pH adjusted to 6.9).

2.3 Targeted Laser Cell Perforation

1. Perforation buffer: PHEM buffer.
2. PALM CombiSystem (Carl Zeiss MicroImaging) equipped with (1) an Axiovert 200 M Zeiss inverted microscope (Carl Zeiss AG); (2) a three-chip charge-coupled device colour camera (HV-D30; Hitachi Kokusai Electric Inc.); (3) PALM Robo Software (v4.0; Carl Zeiss MicroImaging); (4) a 40× objective LD Plan Neofluar, 40×/0.6 (Carl Zeiss AG); and (5) a frequency tripled solid state (FTSS) laser (wavelength 355 nm; pulse energy >90 μJ; pulse duration <2 ns; pulse frequency max. 100 pulses/s; beam divergence 3 mrad).

2.4 Immunolabeling

1. Quenching solution: 0.02 M Glycine in PHEM buffer.
2. Blocking solution: 0.5 % (vol/vol) gelatin from cold-water fish skin in PHEM buffer.
3. Caveolin-specific antibody obtained in rabbit (BD Transduction Laboratories).
4. Alexa Fluor 555 goat antibody to rabbit (Molecular Probes) for immunofluorescence.
5. Protein A conjugated to 5 nm gold (Department of Cell Biology, Medical School, Utrecht University, The Netherlands), for immuno-gold labeling.

2.5 Fluorescence Microscopy

1. 4′,6-Diamidine-2′-phenylindole dihydrochloride (DAPI) stock in distilled water (2 mg/mL).
2. Tweezers.
3. Glass slides and cover slips.
4. Mounting medium: Prolong Gold (Invitrogen).
5. Wide-field fluorescence microscope (Provis AX70; Olympus) equipped with a Nikon DXM1200 digital camera (Nikon Instruments, Europe) with the Nikon ATC-1 software.

2.6 Cell Post-fixation, Osmication, Dehydration, Embedding, and Sectioning After Immuno-Gold Labeling

1. Cacodylate buffer: 0.1 M Sodium cacodylate buffer, pH 7.4.
2. Fixative: 2 % Formaldehyde, 2.5 % glutaraldehyde in 0.08 M sodium cacodylate buffer, containing 0.25 mM $CaCl_2$ and 0.5 mM $MgCl_2$ pH 7.4.
3. Post-fixative: 1 % OsO_4 (EMS) and 1.5 % $K_4[Fe(CN)_6]$ in 0.08 M sodium cacodylate buffer, pH 7.4.
4. 1 % Low-molecular-weight tannic acid ($(C_{14}H_{10}O_9)n$; EMS) in 0.1 M sodium cacodylate buffer, pH 7.4.
5. 1 % OsO_4 in distilled water.
6. Ethanol dehydration series.
7. Epon (Fluka, Steinheim, Germany).
8. Single-edge razor blades.
9. Tweezers.
10. Stereomicroscope.
11. Ultracut microtome (Leica).
12. One-slot EM copper grids (Veco/Stork) coated with Formvar and carbon.
13. Colloidal gold particles (20 nm).

2.7 Transmission Electron Microscopy and Electron Tomography

1. Tecnai-12 microscope (FEI Company, Eindhoven, The Netherlands) with a side-entry Megaview II camera (Olympus Soft Imaging Systems, Münster, Germany).

2. Tecnai-20 microscope (FEI Company, Eindhoven, The Netherlands) equipped with a bottom-mounted slow-scan CCD camera (Tem-Cam F214; TVIPS GmbH) and a motorized goniometer.
3. A Model 2020 Advanced Tomography Holder (E.A. Fischione Instruments Inc.).
4. Xplore3-D software package (FEI Company).
5. IMOD software package [9, 10].

3 Methods

All the steps are performed at room temperature, unless otherwise indicated. At every step, cells should be fully covered by the corresponding fluid to prevent drying out. Work in fume hood when using fixatives or Epon.

3.1 HUVEC Culture for tLCP (See Note 2)

1. Isolate and culture HUVECs from human umbilical cords following a recently developed protocol [8] (*see* **Note 3**).
2. Attach 1 cm^2 squares of engraved Aclar (*see* **Note 4**) to the cover slip of glass-bottom culture dishes using Matrigel as "glue" [7].
3. Sterilize culture vessels containing the Aclar by UV light [7].
4. Seed passage 1 HUVECs on the culture vessels, and let cells reach the "cobblestone" state following the previously published protocol [8].

3.2 Standard Chemical Fixation Prior to tLCP

1. Before cell perforation and subsequent immunolabeling and post-processing, fix cells by conventional chemical fixation (*see* **Note 5**). Add primary fixative 1:1 to the culture medium, and keep for 5 min before removing the fixative.
2. Fix the cells with fresh fixative for 30 min.
3. Wash cells twice with PHEM buffer (5 min each).

3.3 Targeted Laser Cell Perforation

1. Add fresh PHEM buffer. Be sure that the cells are covered by the buffer during the cell perforation.
2. Place the glass-bottom culture dish without lid on the stage of the Axiovert 200 M Zeiss inverted microscope (PALM CombiSystem).
3. Image HUVECs on Aclar by phase contrast. Use a 10× objective to visualize position marks on the engraved Aclar, thus finding the grids and quadrants of interest.
4. Zoom in a quadrant of interest with 40× objective, and focus cells sharply (*see* **Note 6**).

5. Assign the center of the nuclei of the cells present in the field (ca. 25 "cobblestone" HUVECs) using the PALM Robo Software (*see* **Note 7**).
6. Set the UV laser intensity at ~35–40 % (*see* **Note 8**), and activate laser.
7. The system will dissect and catapult then a small part of the assigned nuclei creating a small hole in the cells (Figs. 1 and 2a, b).
8. Typically the whole operation (focus, assignation, and dissection/catapulting) takes less than 2 min per field.
9. Write down which quadrants contain the perforated cells at every Aclar piece. These will be the cells of interest that will have to be found back for fluorescence and electron microscopic analysis.

3.4 Immunolabeling

All washing and incubations should be performed on a rotating shaker at 5 rpm.

1. Wash cells two times with PHEM buffer (5 min each).
2. Quench free aldehyde groups with quenching solution (5 min).
3. To avoid nonspecific binding of antibodies, incubate cells for 30 min with blocking solution.
4. Incubate samples for 2 h with 2.5 μg/mL caveolin-specific antibody diluted in blocking solution (*see* **Note 9**).
5. Wash five times with PHEM buffer (2 min each).
6. Incubate cells for 2 h at room temperature with either the secondary antibody for fluorescence microscopy (*see* **Note 10**) or the protein A conjugated to 5 nm gold for electron microscopy/tomography. Antibody and protein A conjugate are diluted in blocking solution.
7. Wash cells five times with PHEM buffer (2 min each).

3.5 Fluorescence Microscopy (See Note 10)

1. Incubate cells for 5 min with 5 μg/mL DAPI in distilled water in order to stain nuclei.
2. Wash two times with distilled water (5 min each).
3. Retrieve Aclar pieces out of the glass-bottom dish using tweezers. Avoid touching the engraved areas.
4. Mount Aclar between glass slide and cover slip with Prolong Gold, with cells facing cover slip.
5. Leave to cure in darkness before analysis.
6. Image cells using a wide-field fluorescence microscope. We captured pictures with the 20× objective using the Nikon ATC-1 software with a typical exposure time of 1/6 s (Figs. 1c, b and 2a).

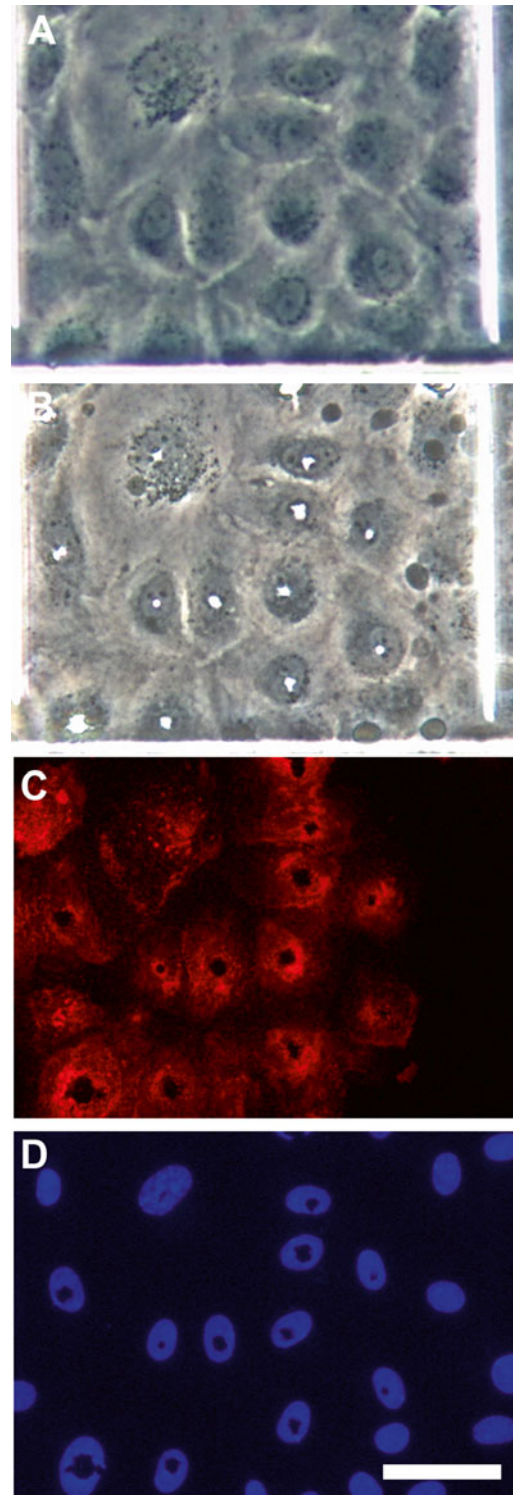

Fig. 1 Effects of targeted laser cell perforation on cell morphology. HUVECs were observed by phase-contrast microscope (**a**, **b**) or by fluorescence microscope (**c**, **d**) before (**a**) or after cell permeabilization by tLCP (**b**–**d**). Note that all the panels show the same cells. The cell perforation is observed as a *white point* by phase-contrast microscopy (**b**) or as a *black hole* in the nuclei by fluorescence microscopy (**d**; nuclei stained with DAPI, *blue*). Note that the cells which have

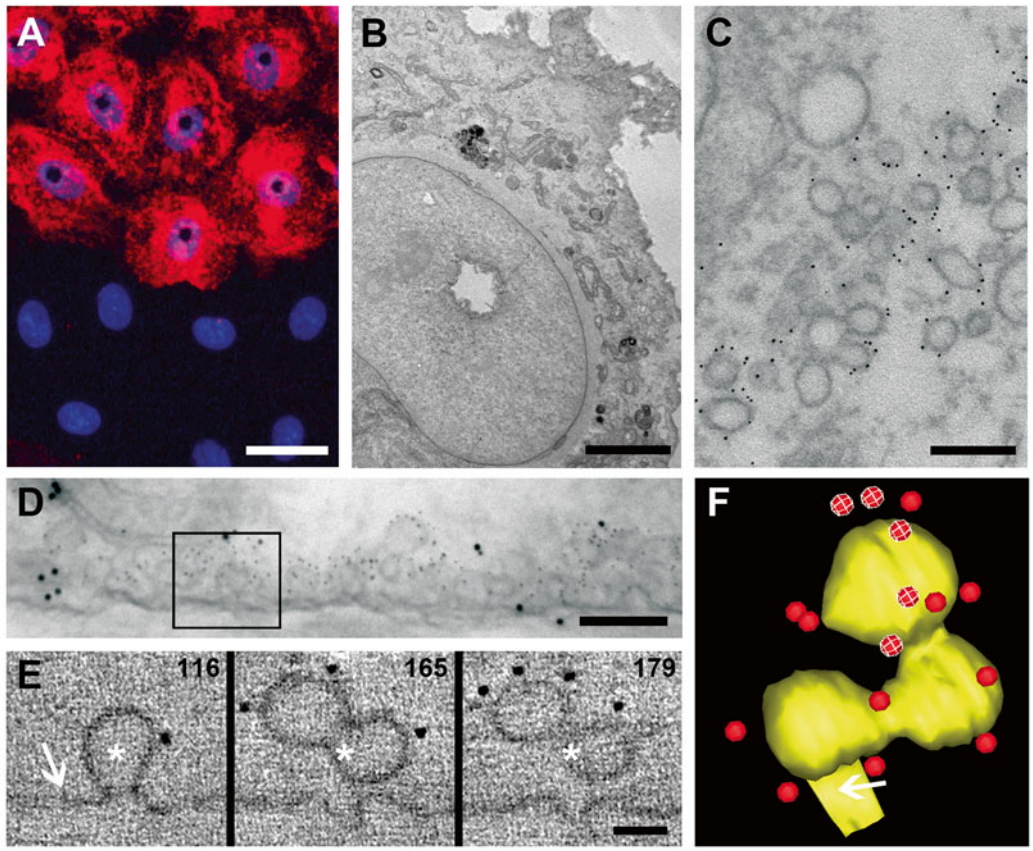

Fig. 2 Caveolae labeling in HUVECs subjected to targeted laser cell perforation. (**a**) Immunofluorescence labeling. Cells with a perforated nucleus (*blue*, with a *black hole*) show labeling (*red*) throughout the cytoplasm, while non-perforated cells (intact *blue* nuclei) are negative. (**b** and **c**) 2D TEM micrographs of 50 nm thick sections of HUVECs cut in parallel to the base of the cell monolayer. The cellular perforation is visible as a hole in the nucleus (**b**). Cellular membranes are well preserved, and the numerous caveolae present show immuno-gold (5 nm) labeling (**c**). (**d**) 2D TEM micrograph of a 350 nm thick section of a HUVEC cut in perpendicular to the cell monolayer. Multiple caveolae labeled with 5 nm gold are present. The large gold particles (20 nm) are the fiducials used for alignment of the tilt series. (**e**) Virtual slices (thickness ~4 nm) extracted from the tomogram calculated for the area *squared* in (**d**). *Asterisks* are on the same *XY* coordinate, and *numbers* indicate the slice location in *Z*. *Arrow* points to the same location of the plasma membrane as in (**f**). (**f**) 3D model of caveolar structures present in the area *squared* in (**d**). A cluster of caveolae (*yellow*) invaginated from the plasma membrane (*yellow*, *arrow*) is surrounded by several gold particles (*red*) that label for caveolin. Some of the gold particles are orderly arranged in a curve following the curvature of the membrane (*red* with *white lines*). Scale bars: (**a**) 25 μm, (**b**) 3 μm, (**c**, **d**) 200 nm, and (**e**) 50 nm. This figure is modified from Fig. 1 in Jiménez and Post, 2012 [5], with permission from Traffic

Fig. 1 (continued) been perforated are immunolabeled for caveolin (**c**; *red* cytoplasmic labeling), while the cells without cell perforation (**c**; *right area*) are negative. The *white vertical lines* visible by phase contrast (**a**, **b**) are part of the engraved quadrant on Aclar. Scale bar, applicable to all panels, 50 μm

3.6 Cell Post-fixation, Osmication, Dehydration, Embedding, and Sectioning After Immuno-Gold Labeling

After immunolabeling cells are post-fixed and processed for TEM and ET studies.

1. Wash cells two times with cacodylate buffer (5 min each).
2. Fix the cells for 2 h using formaldehyde/glutaraldehyde fixative (*see* **Note 11**).
3. Wash cells two times with cacodylate buffer (3 min each).
4. Fix the cells for 90 min on ice in the darkness with post-fixative.
5. Wash ten times with cacodylate buffer (3 min each).
6. Incubate for 30 min with tannic acid solution.
7. Wash five times with distilled water (3 min each).
8. Incubate with 1 % OsO_4 in distilled water (*see* **Note 12**).
9. Wash ten times with distilled water (3 min each).
10. Dehydrate using a range of ethanol according to standard protocols.
11. Add absolute ethanol:Epon mixture (1:1) three times for 10 min.
12. Add freshly prepared Epon, and leave on rotating shaker (20–30 rpm) for 6 h.
13. Under a stereomicroscope, divide the piece of Aclar in as many parts as engraved grids using tweezers and razor blades (*see* **Note 13**).
14. Put the pieces of Aclar, with cells upwards, on the appropriate support, for either regular or flat embedding, containing fresh Epon.
15. Add labels to the blocks.
16. Leave to polymerize at 60 °C for 48 h.
17. After cooling down, trim the block and remove the Aclar. The engraved lines and position marks will be transferred to the surface of the block and will aid to find the perforated cells.
18. Trim the blocks further for either parallel or perpendicular sectioning (with respect to the cell monolayer) of the cells of interest.
19. Cut 50 nm (for TEM) or 350 nm (for ET) thick sections with ultramicrotome according to standard procedures.
20. Collect sections on copper slot grids coated with Formvar and carbon.
21. Seed colloidal gold particles (20 nm) onto one side of the grids for ET to serve as fiducial markers in the alignment of the tilt series.

3.7 Transmission Electron Microscopy and Electron Tomography (See Note 14)

1. We perform TEM using a Tecnai-12 at 100 kV (50 nm thick sections for routine 2D studies; Fig. 2b, c) or 120 kV (350 nm thick sections for analysis of sections prior to ET; Fig. 2d).
2. Localize areas of interest for tomography (Fig. 2d).
3. Map these cellular areas (for us, containing caveolin-positive structures) and pre-irradiate to minimize Epon shrinkage during the tilt series acquisition.
4. Take double-angle tilt series of the regions of interest. In our case, we record series automatically at 200 kV using a Tecnai-20 microscope with associated equipment and software (for detail on tilt series acquisition *see* ref. 4).
5. Align the digital images, reconstruct tomograms (by weighted-back projection), and merge orthogonal single-axes tomograms. For this we use the IMOD software package [9, 10].
6. Perform 3D modelling and analysis of immunolabeled structures of interest (Fig. 2e, f). We do this by manual segmentation as previously reported [4].

4 Notes

1. Application of CLEM is indispensable in this method. A number of cells are subjected to tLCP on a light microscope; these will be the cells of interest which will have to be tracked back for the study by electron microscopy/tomography.
2. This method is not restricted to HUVECs; however, the procedures described are optimized for this cell type. Other cell types might need slightly adapted protocols.
3. Isolation and culture of HUVECs is not the subject of this contribution. Extensive information on this can be found at Jiménez et al. [8]. In this chapter, we only refer to general aspects of the culture in relation to the development of the current protocol.
4. We use gridded Aclar as substratum to grow cells; however, other CLEM-compatible substrates might work as well.
5. The tLCP method can also be applied to cryo-fixed cells; for specific details on this variant of the method, *see* [5].
6. A good optical focusing is critical; samples over- or under-focused result in no or inappropriate cell perforation. Under phase contrast, a good perforation is seen as a white point in the cells (Fig. 1); a black point means damage in Aclar but not perforation in cells (due to under-focusing).
7. The system should have been previously calibrated on an irrelevant area to ensure that the laser perforates the nuclei exactly at the assigned point.

8. We advise users to test the best laser intensity in an unimportant zone of the sample before working with the cells of interest. Laser application should ensure a limited but sufficient nucleus ablation (ca. 2–5 μm in diameter).
9. Users should optimize conditions for the antibody of interest. Double labeling is possible, provided an appropriate choice of antibodies and probes.
10. The tLCP method is meaningful for high-resolution imaging; however, we show results obtained by fluorescence microscopy in order to illustrate how the technique works.
11. If the experiment needs to be postponed to the next day, this is a suitable step to stop. Cells can be left overnight at 4 °C in fixative.
12. The consecutive incubations with OsO_4, tannic acid, and OsO_4 will improve the sample contrast for EM applications [11].
13. White plastic background will help viewing the grids by stereomicroscope. The use of direct and indirect light sources (for example cold fingers) might facilitate this step. Ensure that the Aclar pieces are always with cells upwards, that the grids (containing perforated cells) do not get damaged by the tweezers, and that the cells are at any time covered by fluid Epon.
14. The immunolabeling is distributed in 3D over the cell volume. But, obviously, the samples are appropriate for both TEM (2D) and ET (3D) studies.

Acknowledgements

We thank F. Kindt for assistance during cell microdissection, M. de Winter for engraving quadrants on Aclar, and A. Verkleij (in memoriam) for supporting our creativity. This work was funded by Cyttron Consortium II (LSH framework: FES0908) and FEI Company.

References

1. Morphew MK (2007) 3D immunolocalization with plastic sections. Methods Cell Biol 79: 493–513
2. Humbel BM, de Jong MD, Muller WH, Verkleij AJ (1998) Pre-embedding immunolabeling for electron microscopy: an evaluation of permeabilization methods and markers. Microsc Res Tech 42:43–58
3. Stirling JW (1990) Immuno- and affinity probes for electron microscopy: a review of labeling and preparation techniques. J Histochem Cytochem 38:145–157
4. Lebbink MN, Jimenez N, Vocking K, Hekking LH, Verkleij AJ, Post JA (2010) Spiral coating of the endothelial caveolar membranes as revealed by electron tomography and template matching. Traffic 11:138–150
5. Jimenez N, Post JA (2012) A novel approach for intracellular 3D immuno-labeling for electron tomography. Traffic 13:926–933

6. Jimenez N, Humbel BM, van Donselaar E, Verkleij AJ, Burger KN (2006) Aclar discs: a versatile substrate for routine high-pressure freezing of mammalian cell monolayers. J Microsc 221:216–223
7. Jimenez N, Van Donselaar EG, De Winter DA, Vocking K, Verkleij AJ, Post JA (2010) Gridded aclar: preparation methods and use for correlative light and electron microscopy of cell monolayers, by TEM and FIB-SEM. J Microsc 237:208–220
8. Jiménez N, Krouwer VJ, Post JA (2013) A new, rapid and reproducible method to obtain high quality endothelium in vitro. Cytotechnology 65:1–14
9. Kremer JR, Mastronarde DN, McIntosh JR (1996) Computer visualization of three-dimensional image data using IMOD. J Struct Biol 116:71–76
10. Mastronarde DN (1997) Dual-axis tomography: an approach with alignment methods that preserve resolution. J Struct Biol 120: 343–352
11. Jimenez N, Vocking K, van Donselaar EG, Humbel BM, Post JA, Verkleij AJ (2009) Tannic acid-mediated osmium impregnation after freeze-substitution: a strategy to enhance membrane contrast for electron tomography. J Struct Biol 166: 103–106

Chapter 21

VIS2FIX: Rapid Chemical Fixation of Vitreous Sections for Immuno-Electron Microscopy

Matthia A. Karreman and Elly G. van Donselaar

Abstract

Immuno-electron microscopy uniquely allows high-resolution localization of proteins in their cellular context. Usually, affinity labeling with an electron-dense marker, e.g., small gold particles, is performed on sections of chemically fixed cells or tissues. In this chapter, we describe two novel protocols, the VIS2FIX methods, for chemical fixation of sections of cryo-immobilized biological samples. This method involves production of thin sections of high-pressure frozen cells that are statically adhered to a TEM grid. Subsequent steps involve chemical fixation of the samples by either the $VIS2FIX_{H}$ ("H" for "hydrated") or the $VIS2FIX_{FS}$ ("FS" for "freeze substitution") techniques. Following chemical fixation, the samples are ready for immunolabeling. The described methods are fast and efficient, yield excellent preservation of intracellular structures, and offer the possibility to maintain lipids in the sample.

Key words Transmission electron microscopy (TEM), Immunolabeling, Immuno-electron microscopy, Chemical fixation, Cryo-immobilization, THP-1 monocytes, Human umbilical vein endothelial cells (HUVEC), High-pressure freezing (HPF)

1 Introduction

The majority of the currently available information about the ultrastructure of cells and tissues is derived from studies performed using electron microscopy (EM). Nowadays, this technique remains to be an indispensible tool to study the cell architecture at unparalleled resolution. Cryo-immobilization is the method of choice for the immobilization of biological material since it results in the most accurate preservation of the sample [1]. When performed at ~2,000 bar, such as with high-pressure freezing (HPF), the rate of ice crystal formation is reduced, allowing to vitreously freeze the samples up to a depth of approximately 200 μm [2–5].

Targeting the structure of interest with affinity labeling, however, requires the specimen to be stable at room temperature. While increasing the temperature of the vitreously frozen sample, it is crucial to circumvent the formation of ice crystals that damage

Andrei I. Ivanov (ed.), *Exocytosis and Endocytosis*, Methods in Molecular Biology, vol. 1174,
DOI 10.1007/978-1-4939-0944-5_21,

the fine ultrastructure of the sample. To achieve this, the vitreous ice in frozen material is replaced for an organic solvent by means of freeze substitution (FS), and next the temperature in the sample is raised [6, 7]. Upon increasing the temperature, the sample can be chemically stabilized by fixatives that are added to the FS medium. The sample may then be infiltrated with resin, which is subsequently polymerized to create a solid block. Alternatively, the specimen can be stepwise rehydrated following FS [8] and processed according to the Tokuyasu method, which entails cryo-protecting the sample with sucrose and subsequent freezing in liquid nitrogen [9–11]. Following processing the sample according to either of these methods, sections are produced that are sufficiently thin for the electron beam to penetrate. The sections are mounted on TEM grids, and immunolabeling can be performed on-section.

The samples used for these procedures are generally several hundreds of micrometers in size, demanding long substitution, fixation, and infiltration times. For this reason, processing from high-pressure frozen samples can easily take 5–10 workdays to complete. Here, we outline a new and high-speed approach for the chemical stabilization of cryo-immobilized material: VIS2FIX [12]. Vitreous sections (VIS) are processed according to either of the two different protocols (VIS2FIX$_{H}$ or VIS2FIX$_{FS}$), resulting in chemically fixed (FIX) samples. Compared to the >1,000× thicker sample blocks employed in other protocols, markedly shorter infiltration and fixation times are required by the thin specimen fixed by the VIS2FIX methods. For VIS2FIX, vitreous sections are produced from the high-pressure frozen samples. Ribbons of sections are statically adhered to a TEM grid and chemically stabilized according to the VIS2FIX$_{FS}$ method or the VIS2FIX$_{H}$ method. VIS2FIX$_{FS}$ entails a quick freeze substitution and subsequent rehydration of the sections. The other method, VIS2FIX$_{H}$, is even simpler and shorter. Here, sections adhered to TEM grids are placed on frozen fixative in buffer. Subsequently, the fixative is melted, simultaneously chemically stabilizing the sections. Following VIS2FIX fixation, the sections are ready for immunolabeling or for staining and TEM imaging.

The VIS2FIX methods provide a number of advantages over conventional chemical fixation. First, these techniques are quick and each sample section may be fixed in a different manner. This allows efficient optimization of the fixation procedure for each immunolabeling experiment. Second, VIS2FIX fixed samples are suitable for immunolabeling of the fixation-sensitive antigens such as caveolin [12]. This could be because the VIS2FIX methods cross-link thin sections, instead of large 3D sample blocks, thereby reducing shielding of the epitopes. Third, use of osmium tetroxide in the VIS2FIX$_{H}$ method results in the retention of (neutral) lipids in the section, making this method uniquely suitable for immuno-electron microscopy (immuno-EM) studies in trafficking and lipidomics [12]. Finally, we would like to propose combining the VIS2FIX with

cryo-electron microscopy of vitreous sections [13, 14]. As a result, a vitreous section can be fixed according to the VIS2FIX methods and labeled for the molecule of interest. The region of interest can be retrieved in a succeeding serial section that is then imaged in close-to-native state with cryo-electron microscopy.

In this chapter, we provide a step-by-step protocol of cryo-immobilization by HPF, the required preparation steps for the VIS2FIX methods, and the immunolabeling procedure. Furthermore, we share tips and tricks for vitreous sectioning, the VIS2FIX fixation procedure, and some other experimental maneuvers.

2 Materials

Millipore-filtered water should be used for the preparation of the reagents. The fixatives and dehydration series should all be prepared on the day the experiment is performed.

2.1 High-Pressure Freezing

1. Trypsinization buffer: 0.05 % Trypsin, 0.02 % EDTA in phosphate-buffered saline (PBS) or in Hanks' Buffered Salt Saline (HBSS) in case of trypsinization of human umbilical vein endothelial cells.
2. Copper Specimen Tubes (Leica).
3. High Pressure Freezing apparatus (EMPACT, Leica).
4. Tube Cutter (Leica).

2.2 Vitreous Sectioning and Transfer of the Grids

1. Trimming diamond knife (Trimtool 45, Diatome).
2. Cryo diamond knife (35–45° angle, Diatome).
3. Cryo-ultramicrotome (UC6/FC6, Leica).
4. CRION antistatic device (Leica) (*see* **Note 1**).
5. Micro-manipulator with bended-tip cross-over tweezers (Leica).
6. Sapphire Disc (SD) Holder (from the SD FS Unit, Leica).
7. Cold Rings (Bottom Plates, Leica).
8. Aclar Ring: Cut out a circle with a diameter of 35 mm from a 200 μm thick aclar foil (Electron Microscopy Sciences), and create a hole in the center (9 mm in diameter) (*see* **Note 2**).
9. Aclar Disc: Cut out a circle with a diameter of 35 mm from a 200 μm thick aclar foil (*see* **Note 2**).
10. Tin (Universal Container, Leica).
11. Large tweezers.
12. Small petri dishes, 35 mm in diameter (*see* **Note 2**): Petri dishes of this size are used throughout the procedure, unless otherwise indicated.
13. TEM grids with formvar film, carbon coated and freshly glow-discharged.

2.3 VIS2FIX Fixation

The concentration of each component in the fixative can be altered depending on the material to be fixed and the immunolabeling conditions (*see* **Note 3**).

1. $VIS2FIX_{FS}$ fixative: 0.1 % Uranyl acetate (UA, from powder, SPI; *see* **Note 4**), 0.1–0.5 % glutaraldehyde (GA, from 10 % GA in acetone, Electron Microscopy Sciences), and 0.01–0.5 % osmium tetroxide (OsO_4, from crystals, Electron Microscopy Sciences; *see* **Note 5**). Prepare the fixative on ice in dried acetone (*see* **Notes 6** and 7), then place the fixative as quick as possible in the automatic freeze substitution (AFS) apparatus at −90 °C, and shield it from light.
2. Rehydration steps for the $VIS2FIX_{FS}$: 0–0.5 % GA in 95, 90, 80, 70, 50, 30, and 10 % acetone in water. Prepare 5 mL volumes of each of the seven different rehydration steps. Hereto, use GA from a 10 % GA in acetone (Merck) to prepare **steps 1–5**. To prepare the final two rehydration steps, use 8 % GA in water (EM grade, Polysciences, Inc).
3. PHEM buffer (pH 6.9): 60 mM PIPES, 25 mM HEPES, 10 mM EGTA, and 2 mM $MgCl_2$ in water. To prepare 100 mL double-concentrated PHEM buffer, dissolve 3–4 small pellets of NaOH in 75 mL water. Add 3.63 g of PIPES to the solution, and mix. Check the pH with a pH paper; it should be 7.0. Sequentially add 1.19 g HEPES, 0.08 g $MgCl_2$, and 0.76 g EGTA. In between adding these reagents, mix the solution thoroughly. Check the pH with a pH meter, and adjust it to pH 6.9. Transfer the solution to a measuring cylinder, and fill it up to 100 mL with water.
4. $VIS2FIX_H$ fixative: 0.2 % UA (SPI Supplies; *see* **Note 8**), 0.01–0.2 % GA (from 8 % GA in water, Polysciences, Inc), and 0.01–0.5 % OsO_4 (from crystals, Electron Microscopy Sciences; *see* **Note 9**) in PHEM buffer. Prepare the fixative on ice, and keep it on ice and in the dark until usage.
5. AFS apparatus (Leica) (*see* **Note 10**).
6. Bended fine-tip tweezers (Fig. 1a, left) to transfer the grids.
7. Large tweezers (Fig. 1a, right) to move the setups and the fixatives.
8. A small transfer tool, a bended piece of metal (Fig. 1b), used to hold $VIS2FIX_H$ fixative steady and fully horizontal while transferring it to and from the AFS room.
9. Flow-through ring (Leica), trimmed with a razorblade to a height of ±6 mm.
10. Reagent bath (Leica), trimmed with a razorblade to a height of ±10 mm.
11. Reagent bath (Leica), trimmed with a razorblade to a height of ±6 mm.

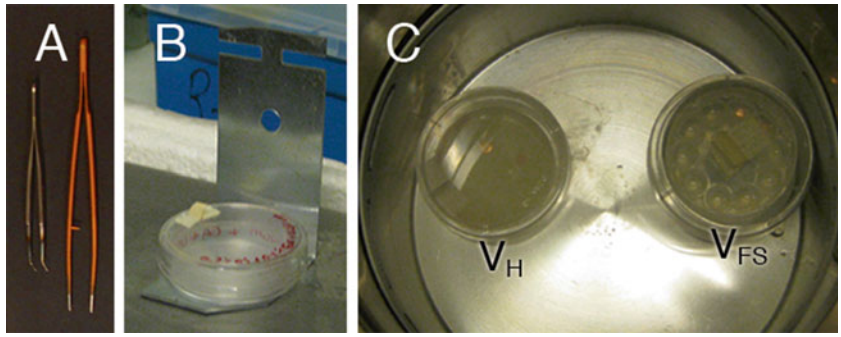

Fig. 1 Setting up the VIS2FIX experiment. (**a**) Tweezers employed for the VIS2FIX methods. *Left*: Fine-tip tweezers that were bended to facilitate removing the grids from the SD holder and placing them on fixative. Larger tweezers (*right*) are used for handling the fixative and transfer setups. (**b**) A simple piece of bended metal functions as a transfer tool to stably move the $VIS2FIX_H$ fixative in and out of the AFS. (**c**) A top view of the AFS substitution chamber, showing the $VIS2FIX_H$ (V_H, *left*) setup and the $VIS2FIX_{FS}$ (V_{FS}, *right*) setup. The TEM grids, placed for demonstration purposes, are mounted on the fixatives

2.4 Immunolabeling

1. Quenching solution: 0.02 M Glycine in PHEM buffer.
2. Blocking buffer: 1 % Bovine serum albumin (BSA) in PHEM buffer.
3. Primary antibodies, diluted in blocking buffer: The dilution is dependent on the choice of antibody but is generally in the range of 2–20 μg/mL. Dilute the primary antibody fresh on the day of the experiment, and keep on ice until use.
4. Washing buffer: 0.1 % BSA in PHEM buffer.
5. Bridging antibodies, if required, diluted in blocking buffer: Diluted stocks can be prepared, stored at 4 °C, and used for 2 months if 0.02 % sodium azide is added.
6. Protein A-gold (Cell Microscopy Centre, Utrecht Medical Centre, the Netherlands): 5–15 nm gold conjugated to protein A, diluted in blocking buffer. Protein A-gold should be diluted just prior to use, preferably in the last washing step preceding the incubation.
7. 1 % GA in PHEM buffer, prepare from 8 % aqueous GA (EM grade, Polysciences, Inc).
8. 2 % Aqueous uranyl oxalate, pH 7.0, prepared from aqueous UA (*see* **Note 8**) and 0.3 M oxalic acid: Pass through a 0.22 μm pore filter before use, and store at 4 °C in a small glass vial with a screw cap. Replace the air in the vial with nitrogen gas.
9. 0.4 % UA in 1.8 % methylcellulose, prepared from aqueous UA (*see* **Note 8**) and 2 % methylcellulose in water. Store at 4 °C.
10. Drying loops: Loops (4 mm in diameter) made from remanium wire (0.3 mm in diameter), attached to 1 mL pipette tips.

3 Methods

While handling the grids with the frozen sections and while moving the cooled transfer or fixative setups, it is highly important to use tweezers that were cooled down in liquid nitrogen. This prevents heat transfer to the samples or the fixatives.

3.1 High-Pressure Freezing

1. Culture the cells according to the supplier's instructions. In the case of adherent cells, perform **steps 2** and **3**. For cells in suspension, proceed with **step 4**.
2. Disassociate the monolayer by placing trypsin/EDTA solution on the cells for the short time (*see* **Note 11**).
3. Stop the trypsinization process by adding an excess of culture medium to the cells.
4. Transfer the cells in suspension to a 15 or a 50 mL tube, depending on the volume of cells in medium.
5. Spin the cells down for 5 min at 1,200 × *g* at 37 °C.
6. Resuspend the pellet in a small volume of cell culture medium, and keep at 37 °C.
7. Mix a small volume (e.g., 10 μL) of cells in medium 1:1 with 30 % dextran. This volume is sufficient to freeze 3–5 samples (**steps 8** and **9**), which takes approximately 10 min. For the next set of samples, prepare a fresh mixture with dextran. Keeping the cells in this mixture for only a short time prevents the cells from taking up dextran.
8. Load the copper specimen tubes with the cells in the mixture of culture medium and dextran. Use a stainless steel wire (0.25 mm diameter) to plunge the tube.
9. High-pressure freeze the copper tubes at a pressure of ~2,000 bar.
10. Store the tubes with the high-pressure frozen samples in liquid nitrogen until cryo-sectioning.

3.2 Preparation of the VIS2FIX Experiment

Before vitreous sectioning, a number of preparations steps are required to successfully perform the VIS2FIX experiments.

1. Prepare the fixatives (*see* Subheading 2.3).
2. For the $VIS2FIX_{FS}$, place the flow-through ring in the reagent bath (height: 10 mm). Position these on top of two cold rings in a tin, and transfer the setup to the AFS substitution chamber (Fig. 1c, right). Cool down the machine to –90 °C. Cool down the $VIS2FIX_{FS}$ fixative in the AFS. Pipet 3 mL of cooled fixative into the flow-through ring, and cover with a lid of petri dish.
3. For the $VIS2FIX_{H}$, place a petri dish and a tin with three cold rings in the substitution chamber of the AFS. Cool the machine

down to −90 °C if it is not already at this temperature. Later in the protocol, the petri dish will be used during the transfer of the fixative setup to protect the sections from humidity in the air upon their removal from the AFS substitution chamber. Pipet 800 µL of fixative solution in the reagent bath (height: 6 mm), and keep on ice (*see* **Note 12**). In a closed petri dish, carefully transfer the reagent bath with fixative solution to the AFS (−90 °C). In this cold environment, the fixative immediately freezes. Position the reagent bath in the tin, on top of three cold rings (Fig. 1c, left). Then cover the tin with a petri dish lid to protect the fixative from the moist air.

4. Place a tin with a raised bottom (part of an SD FS Unit) or, if this part is not available, a tin housing three cold rings to cool down with the AFS (*see* Subheading 3.3, **step 17**).
5. Place the SD holder, used to store the grids with the mounted sections, in a closed petri dish on the raised plateau in the front part of the cryo-ultramicrotome's cryo-chamber (*see* **Note 13**) (Fig. 2a).
6. Assemble the transfer setup, which is a tin that holds three cold rings, an aclar disc, an aclar ring, and that is covered with a petri dish lid (Fig. 2a). Place it in the cryo-ultramicrotome next to the SD holder.
7. Cool down the cryo-ultramicrotome to −150 °C.

3.3 Vitreous Sectioning and Grid Transfer

1. In a cryo-ultramicrotome, cooled down to −150 °C (*see* **Note 14**), trim the front of the tubes until a shiny black face is obtained (*see* **Note 15**).
2. Trim 100 µm from the sides of the sample, so that a square block face is achieved (*see* **Note 16**).
3. Mount a TEM grid with a carbon-coated and glow-discharged formvar film (*see* **Note 17**) in the tweezers of the micromanipulator, so that it is parallel to the knife edge (*see* **Notes 18–20**) (Fig. 2b, c).
4. Rotate the grid away from the knife edge by turning the tweezers towards yourself, resulting in an almost side view of the grid (Fig. 2d). This position prevents the grid from interfering with the sectioning, but it still allows the grid to be slightly charged by the antistatic device, improving subsequent adhering of the sections.
5. Produce a ribbon of 60–80 nm thick (*see* **Note 21**) glossy-looking sections that has approximately the length of the TEM grids' diameter (3 mm). The ribbon of sections can be manipulated with a hair mounted on a long wooden skewer (*see* **Note 22**).
6. Hold the section in place, and turn of the discharge mode of the antistatic device.

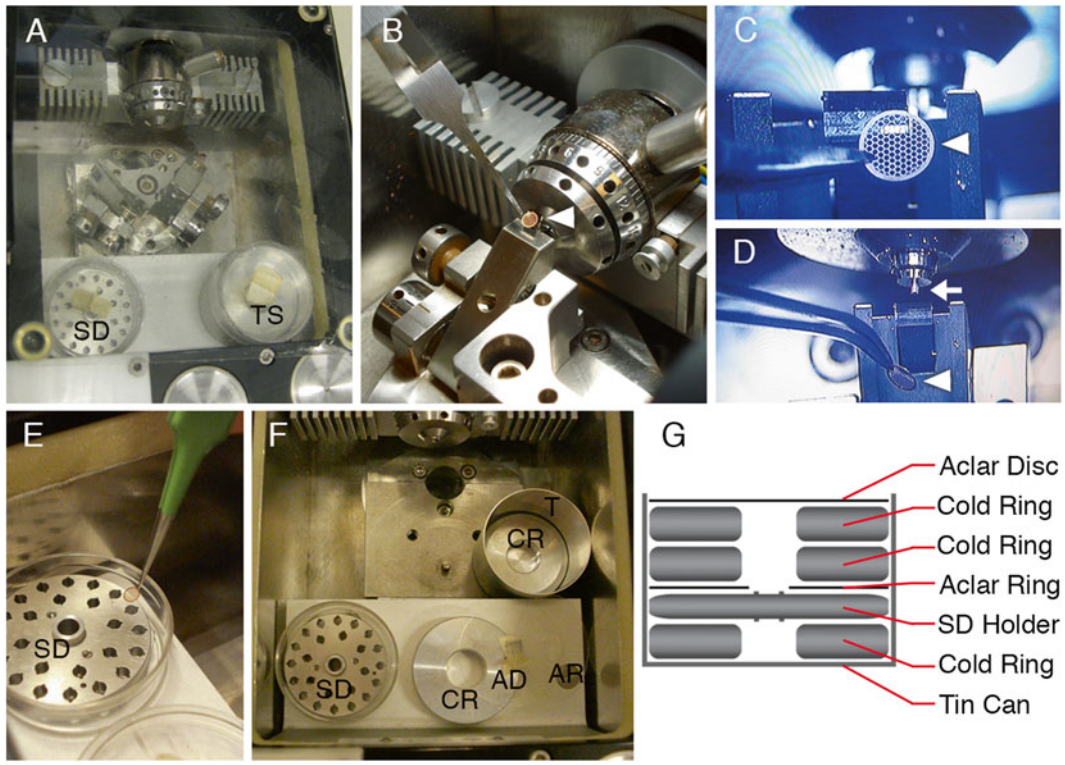

Fig. 2 Vitreous sectioning and sample transfer. (**a**) Top view of the cryo-chamber of the cryo-ultramicrotome. The SD holder (SD) and transfer setup (TS) are placed on the raised plateau in the front of the cryo-chamber. While cooling the microtome down, a perspex cover is placed over the cryo-chamber. (**b**) Side view of the diamond knife and the TEM grid (*arrowhead*) held by the micromanipulator tweezers inside the cryo-chamber of the cryo-ultramicrotome. (**c**) A selected and enlarged view of the cryo-chamber of the cryo-ultramicrotome, showing the knife edge, the TEM grid (*arrowhead*), and the bended tip of the micromanipulator tweezers. (**d**) During sectioning, the TEM grid (*arrowhead*) is tilted away from the knife edge (*see* **step 19**). The trimmed sample (*arrow*) is also visible. (**e**) The grids with the adhered sections are placed in the SD holder (SD) and then protected from the air by mounting the petri dish lid. (**f**) Before transfer to the AFS, the grids with the sections in the SD holder (SD) are placed in the tin (T), in between a cold ring (CR), an aclar ring (AC), two more cold rings, and an aclar disc (AD). (**g**) A cartoon of the transfer setup, indicating the order in which the various components should be mounted

7. Rotate the grid back to be parallel to the knife face (*see* **Note 23**, Fig. 2b, c), and position the ribbon of sections above the grid, so that it overlaps with as little grid bars as possible (*see* **Note 20**) (Fig. 2c).
8. Statically adhere the sections to the grid using the "charge" mode of the CRION (*see* **Note 24**).
9. Move the tweezers away from the knife, and rotate them as shown in Fig. 2d.
10. Remove the grid from the micromanipulator tweezers (*see* **Note 25**).

11. Place the grid carefully in the SD holder, which sits in a petri dish on the raised plateau in the cryo-ultramicrotome (Fig. 2e). Shield the grids from the moist air by again covering the petri dish with a lid.
12. Following obtaining the desired number of grids, remove the diamond knives and the sample from the microtome chamber.
13. Mount the transfer setup, which shields the sections from the humid air and keeps them at low temperature while moving the samples from the cryo-ultramicrotome to the AFS. To build the transfer setup, a cold ring, the SD holder with the grids, an aclar ring, two more cold rings, and finally an aclar disc are placed in a tin (Fig. 2f, g).
14. Wheel the AFS apparatus close to the cryo-ultramicrotome (Fig. 3a).
15. Use large tweezers (Fig. 1a, right) to lift out the transfer setup with the grids from the cryo-chamber of the cryo-ultramicrotome, and swiftly and gently place it in the AFS (Fig. 3b).
16. Remove the aclar disc and the two cold rings from the transfer setup. The components of the transfer setup can be removed from the AFS substitution chamber (Fig. 3c, top).
17. Transfer the SD holder, still covered with the aclar ring (*see* **Note 26**), to a holder with a raised bottom (from SD FS Unit (Leica), depicted in top left corner of Fig. 3b). The SD holder is now at the same height as the fixatives in the reagent baths, which are resting on three cold rings in the tins.
18. Use bended fine-tip tweezers to transfer the grids to the fixative setups (Fig. 3c).

3.4 VIS2FIX$_{FS}$: Freeze Substitution

1. Following sectioning and transfer to the AFS, float the grids, section side down, on the fixative in the compartments of the flow-through ring (*see* **Notes 27–29**).
2. Start the FS program. The program first holds the samples at −90 °C for 15 min, then raises the temperature to −60 °C in 13 min (maximum slope), and keeps the sections at this temperature for 15 min. Next, the temperature is raised further to −20 °C in 18 min (maximum slope). After 15 min at −20 °C, the temperature is finally increased to 0 °C in 9 min (maximum slope) (*see* **Notes 30** and **31**).
3. Stepwise rehydrate the sections (*see* Subheading 2.3, **item 2**). These steps can either be performed in the AFS, at 0 °C, or on ice. Remove the majority of the fixative, and sequentially rinse the sections twice, for 2 min, with each of the solutions from the rehydration series (*see* **Note 32**) (Fig. 3d).
4. Wash three times with water, and then place the flow-through ring with the grids in a petri dish filled with water at room temperature.

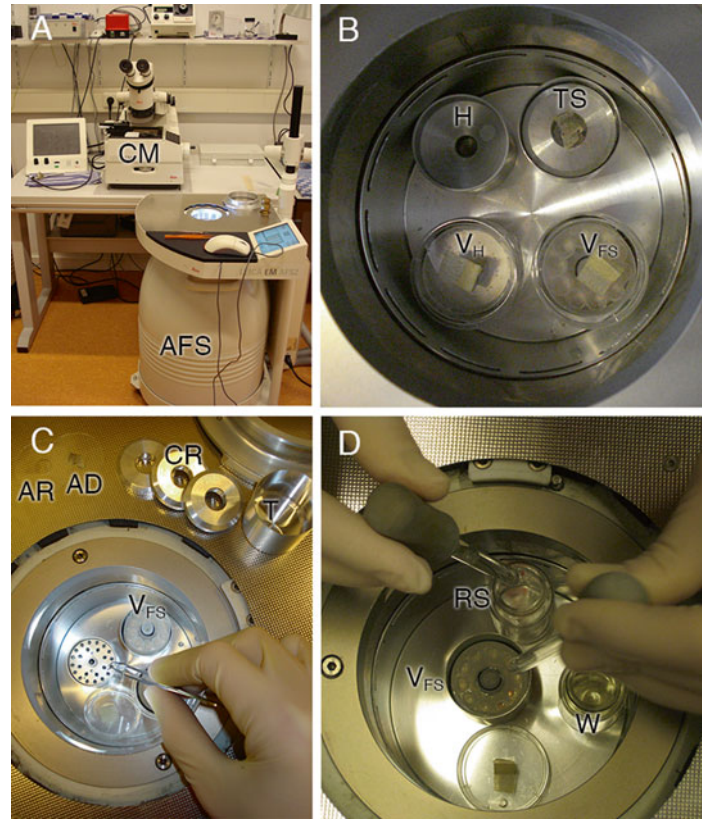

Fig. 3 Section fixation and rehydration. (**a**) To minimize the risk of contamination of the sections during transfer, the AFS apparatus (AFS) is moved very close to the cryo-ultramicrotome (CM). (**b**) A top view of the AFS substitution chamber, at −90 °C, just after placing the transfer setup (TS). The holder with the raised bottom (H), the VIS2FIX$_H$ (V_H), and the VIS2FIX$_{FS}$ (V_{FS}) were already cooled down with the AFS. (**c**) After disassembling the transfer setup, its components, that is, the aclar ring (AR), the aclar disc (AD), the three cold rings (CR), and the tin (T), can be removed from the AFS substitution chamber. The grids, in the SD holder mounted on the holder ("H" in **b**), can now be transferred to the fixative(s). (**d**) Following FS, during VIS2FIX$_{FS}$, the sections can be rehydrated. The rehydration solutions (RS) are added to the setup via the central tube of the flow-through ring in the VIS2FIX$_{FS}$ setup (V_{FS}). The used fixation/rehydration solutions are removed, without letting the grids fall dry, via the same route and disposed of in a separate waste vial (W)

5. Carefully, one by one, remove the grids from the flow-through ring with bended-tip tweezers.
6. Dry the back of the grid on moist filter paper (*see* **Note 33**).
7. Wash the grids seven times for 1 min on drops of water which are placed on a strip of parafilm on the workbench.
8. Store the grids (Subheading 3.6) or continue with immunolabeling and/or post-contrasting (Subheading 3.7).

3.5 VIS2FIX$_H$: Hydrated

1. Following vitreous sectioning and transfer of the samples to the AFS (*see* Subheading 3.3), place the grids section side down on the frozen VIS2FIX$_H$ fixative (*see* **Note 34**).
2. Place the reagent bath, with the frozen fixative and the grids, in the precooled petri dish.
3. Carefully lift out the petri dish with the fixative and the grids using the transfer tool as a lever (Fig. 1b).
4. Place the VIS2FIX$_H$ setup, the petri dish with the fixative and the grids, on a hot plate that is pre-warmed to 40 °C.
5. Gently circle the VIS2FIX$_H$ setup over the hot plate. Moving it around ensures constant warming of the fixative.
6. Upon partial melting of the fixative, the grids start to move around on the liquid (*see* **Note 35**). When all the grids are floating, quickly place the VIS2FIX$_H$ set-up on ice and continue the fixation for an additional 10 min (*see* **Note 36**).
7. When intended for storage, wash the sections ten times for 1 min on drops of water that are placed on a strip of parafilm. When aiming to directly continue with immunolabeling, wash the sections ten times for 1 min on drops of PHEM buffer.

3.6 Storage of VIS2FIX Fixed Sections

1. Wrap a small strip of parafilm around a glass slide, and attach it with scotch tape.
2. Float the grids, section side down, on a 1:1 mixture of 2.3 M sucrose in PHEM buffer and 1.8 % methylcellulose on ice. This sucrose/methylcellulose solution is generally used to pick up cryo-sections produced from cryo-protected frozen samples prepared according to the Tokuyasu method [15].
3. Gently remove the grids from the drop of sucrose/methylcellulose, ensuring that part of the mixture sticks to the grid.
4. The grids are placed on the parafilm-wrapped glass slide with the residual sucrose/methylcellulose drop and the sections facing downward.
5. Place the glass slide in a petri dish (90 mm in diameter), seal it with parafilm, and store at 4 °C. Similar to Tokuyasu sections, the samples can be stored for several months [16].
6. To release the grids after storage, a drop of PHEM buffer can be pipetted carefully next to the dried drop of sucrose/methylcellulose. The PHEM buffer will dissolve the drop, and the grids can be lifted off the glass slide. Before starting the immunolabeling procedure, wash the sections ten times on PHEM buffer to ensure that all residual sucrose/methylcellulose is removed.

3.7 Immunolabeling

The immunolabeling procedure is performed at room temperature. The grids are floated section side down on drops of solutions that are placed on strips of parafilm.

1. Wash the sections five times for 2 min in quenching buffer to reduce the free aldehyde groups in the sample.
2. Incubate the sections for 15 min on blocking buffer to minimize unspecific labeling (*see* **Note 37**).
3. Incubate the sections for an hour on 5 μL droplets of primary antibody. A petri dish lid can be placed over a series of droplets, including previous washing steps. This creates a moist environment which prevents the labeling droplets from drying out. Incubation times can be increased to improve labeling efficiency.
4. Remove the unbound antibody by washing the sections: one time quickly and five times for 2 min on drops of washing buffer.
5. Target the primary antibody (*see* **Note 38**) by incubating the sections for 20 min on 7 μL droplets of protein A-gold (*see* **Note 39**).
6. Wash the sections on PHEM buffer: three times very briefly and seven times for 2 min.
7. Stabilize the labeling by fixing the samples, in a fume hood, for 5 min on 1 % GA in PHEM buffer.
8. Wash the sections ten times for 1 min on drops of water (*see* **Note 40**).
9. Stain the sections for 5 min with 2 % aqueous uranyl oxalate (pH 7).
10. Wash the sections twice briefly on drops of water.
11. Briefly wash, and then incubate the sections at 0 °C on droplets of 0.4 % UA in 1.8 % aqueous methylcellulose.
12. After 5 min, pick up the grids from the droplet with a drying loop. Quickly reduce the 0.4 % UA in methylcellulose to thin film by pulling the loop sideways, briefly, over filter paper lying on top of a small strip of parafilm (*see* **Note 41**). A long stroke will result in a thinner film, and that may cause the membranes in the sample to collapse.

4 Notes

1. In order to statically adhere the vitreous sections to the TEM grid, it is crucial that the antistatic device has a charge/discharge option. For our purposes we employed the CRION, but other setups with similar characteristics (e.g., homemade devices) may also be employed.

2. To facilitate handling, a partially folded piece of tape was mounted on the surface of the aclar disc and aclar ring and to the lids of the petri dishes.
3. In our experience, choosing weaker fixatives limits the amount of material retained in the section. Although the ultrastructural quality is not optimal in these cases, the epitopes are more easily accessible for the antibody during the immunolabeling procedure. Therefore, for some epitopes, e.g., membrane-bound proteins, weaker fixatives may yield higher labeling efficiency. These conditions, however, are not suitable for the labeling of weakly bound antigens or those that diffuse freely through the cytosol or nucleoplasm. Weak fixatives may fail to cross-link these antigens, which will then be lost in subsequent washing steps.
4. Always prepare the UA in acetone fresh on the day of the experiment. Prepare a solution of 0.2 % UA (wt/v) in dried acetone (*see* **Note 6**), and let it stir in the dark for >30 min before usage.
5. OsO_4 crystals quickly dissolve in acetone. Prepare a stock solution of 2 % OsO_4 in dried acetone. Aliquots can be stored in liquid nitrogen.
6. To prevent water contamination in the dried acetone, special precautions should be taken when storing the stock bottle. After use, replace the air in the bottle with nitrogen gas. Seal the lid of the bottle with parafilm, and place the bottle in a canister containing water-absorbing beads. Close the canister with a lid and seal with parafilm.
7. The choice of FS medium is based on the previous finding [17] that acetone limits the extraction of phospholipids from the sample during the substitution procedure.
8. Prepare the solution from a stock solution of 4 % aqueous UA that was passed through a millipore filter and stored at 4 °C.
9. Prepare a stock solution of 4 % aqueous OsO_4 by letting the crystals dissolve in water for ≥12 h in the dark at room temperature. The solution can be stored at 4 °C, protected from light and air, to prevent oxidation. Hereto, the vials with the stock solutions are sealed with parafilm, placed in a container that is also sealed with parafilm, and stored in a separate fridge that contains only OsO_4. We strongly discourage speeding up the process of dissolving OsO_4 in water by heating the solution. The stock of OsO_4 in water will remain usable for a maximum of 2 weeks following preparation. It is however very important to always check the color of the solution before usage: when the OsO_4 is oxidized, it will become more grayish or even black, and in this case it should not be used anymore.

10. We employed a Leica AFS2, since its large substitution chamber allows for placing multiple VIS2FIX setups. The Leica AFS1 houses an opening, in the middle of the substitution chamber, through which the liquid nitrogen container can be filled and which holds the temperature range tubes. The presence of this opening restricts the free space in the chamber and does not allow for placing petri dish lids on the tins.
11. For optimal preservation of the ultrastructure of the cells, it is important to keep the trypsinization process as short as possible. For the disassociation of MDCK-II cells we trypsinized for 10 min, whereas for human umbilical vein endothelial cells less than 1 min was sufficient.
12. The hydrophobicity of the reagent bath makes it difficult to distribute the small volume of fixative equally over the bottom. Therefore, first 2 mL of fixative is transferred, which covers the entire bottom of the bath. Next, twice remove carefully 600 μL of fixative, leaving an end volume of 800 μL in the reagent bath. Subsequent handling of the reagent bath should be done as gentle as possible to prevent accumulation of the fixative in a single drop.
13. The SD holder can hold 24 sapphire discs or, for this application, grids. It is recommended not to perform the VIS2FIX procedure with more than 24 samples/grids simultaneously due to the complexity of some steps. However, when required, an additional SD holder in a petri dish can be placed in the cryo-chamber of the microtome.
14. For trimming the samples, we employed a Trimtool 45 diamond knife: the knife angle is 45°, and corners of the knife face are not a straight 90° angles, like with a conventional cryo-diamond knife, but angled 45°. This results in a pyramid-shaped block face with an inclining angle of 45°. Trimming the samples and trimming can be performed at 100 mm/s with a feed of 200 nm.
15. Freezing the sample with the Leica EMPact requires mounting the tube in a Specimen Tube Holder (Leica). Following freezing, the samples need to be cut out of their holders. Employing the Leica tube cutter to release the samples may locally create ice crystals, caused by recrystallization through increased pressure and mechanical damage to extremities of the tube. To get rid of these damaged areas, the first 400 μm of the cutout tubes should therefore be trimmed away.
16. Employing a Trimtool 45 diamond knife (*see* **Note 14**), a block face of the appropriate dimensions can be achieved by using the interface between the sample and the tube as the onset point for trimming.

17. Grids with homemade formvar films do not need to be freshly prepared on the day of the experiment. Glow-discharging the carbon-coated grids ensures a hydrophilic surface that enables the adhering of the sections.
18. We changed the tweezers of the Leica micromanipulator with Dumont N5 tweezers that we especially altered for this purpose. The tip of the N5 tweezers was bended so that the grid is parallel to the knife face when mounted in the micromanipulator (Fig. 2b, c). The sliding lock tweezer (Dumont L5) that came with the micromanipulator was more challenging to open and close, especially when water condensed on the lock.
19. To facilitate mounting of the grid, the tweezers can be rotated in the micromanipulator (Fig. 2d). Mount the grid by gently moving it in between the legs of the tweezers and positioning it at the tip. To allow flexibility to move the grid in this manner, the tweezers should be adjusted to not press close too tight.
20. Grids with a hexagonal or a square mesh provide better support for the formvar film and thus the sections. However, parts of the section that are adhered on top of the grid bars cannot be imaged with TEM. To maximize the visibility of the ribbon of sections, the grid should be positioned so that the produced ribbon of sections will be parallel to, and, importantly, in between the grid bars (Fig. 2c).
21. The optimal thickness of the sections may vary depending on the type of sample and, importantly, the choice of fixative for VIS2FIX. A fixative mixture containing more potent fixatives, or higher concentrations of fixative, may allow for thinner sections: more material will be maintained in the section following fixation. When a weaker fixative mixture is employed to stabilize the sections, it may be required to produce thicker vitreous sections to achieve similar results.
22. The hairs that are mounted on the long wooden skewer can be of various origins. Employing one's own eyebrow hairs or eyelashes is popular, and also hairs of Dalmatian dogs have proven to be very strong. In our hands, the best results were achieved with guinea pig hairs. The hairs have a convenient angle and are very flexible and strong; they have a very thin tip and are slightly sticky, which facilitates holding on to the section.
23. The reflection of the formvar film may interfere with visualizing the ribbon of sections. Tilting the grid slightly towards the knife edge changes the angle of the reflection so that it is less dominant.
24. A critical step is to verify if the sections are properly adhered by trying to lift the sections from the grid. If the ribbon is statically adhered, this is not possible. During the charging, the adhering of the sections can be observed.

25. To preserve the alignment of the micromanipulator tweezers relative to the knife edge, the grids are transferred to the SD holder using another set of fine-tip tweezers.
26. Upon placing the SD holder in the tin, the aclar ring remains on top of the tin, since it does not fit inside. The aclar ring can then be safely removed, exposing the grids. Removing the aclar ring at an earlier stage may cause the grids to "jump" to the ring due to static charge. In our experience, the gentle lift-off achieved as described above is the safest approach to remove the ring from the SD holder.
27. The viscosity of acetone is higher at –90 °C compared to higher temperatures. This allows floating the grids on the fixative solution. Upon raising the temperature, the grids will eventually sink to the bottom of the flow-through ring. Sometimes, the grids will instantly sink upon transferring them to the fixative. When this happened, we neither observed a difference in fixation efficiency nor in the preservation of the section.
28. To facilitate floating the grids on the fixative solution, we employed tweezers of which the tip was bended perpendicular to the plane of the tweezer's legs, similar to the tweezers employed during vitreous sectioning (Fig. 1a, left).
29. The flow-through ring has ten compartments and can hold an equal amount of grids. If required, up to three VIS2FIX$_{FS}$ setups fit into the cold chamber of the AFS2, maximizing the number of samples to be fixed in a single FS procedure to 30.
30. In the design for the FS schedule, the maximum temperature increase that was allowed by the AFS was a limiting factor. Different FS schedules of different lengths were investigated, and the described schedule was the shortest one we have tested. However, we believe that it may be possible to reduce the length of the FS procedure even more, for instance by shortening the time periods that the temperature is kept at –90, –60, and –20 °C.
31. The fixative can be altered at any time. It is recommended to remove any osmium tetroxide present in the fixative mixture before raising the temperature above –60 °C. To change the primary fixative, the majority of the fixative can be removed from the flow-through ring by pipetting it out of the center tube. Fresh fixative can then be added, and these steps can be repeated as washing steps aiming to minimize the residual primary fixative. During all steps of the described protocol it is of great importance not to let the grids fall dry.
32. Lower concentrations of GA can be used during the rehydration, or it can be completely left out. However, even the lowest concentration of GA we tested, 0.01 %, aids in the preservation of the biological material in the section.

33. Using moist filter paper to dry the back of the grids minimizes the risk of the sections on the front of the grid to fall dry. If the grids are not dried, they will not float on drops of water, which is required for the next washing steps and immunolabeling procedure. If the back of the grids become wet during any future step, they need to be dried as described above.
34. $VIS2FIX_H$ fixation entails simultaneous melting and chemical stabilizing the sections on a hot plate (*see* **steps 3–5**). This process should in theory introduce ice crystals into the specimen, but we have observed this not to take place in our experiments. The conditions in the AFS substitution chamber, the comparatively high temperature (−90 °C) and the absence of water vapor, together create an environment that allows for sublimation: the transition of frozen water to gas. We postulate that recrystallization is prevented due to sublimation of the unbound water in the section. Therefore it may be important to leave the grids for several minutes in the SD holder before placing them section side down on the frozen fixative.
35. Due to the temperature difference between the frozen fixative and the outside air, water will condense on the petri dish. This obscures the view of the fixative, making it difficult to monitor the melting process. It is tempting to rub away the condensed water. However, this may create static charge, which makes the grids "jump" to the lid of the petri dish. Generally it takes 4–5 min for the fixative to melt, and this experience can be used as a guideline in monitoring the melting of the fixative. After 4 min, the petri dish lid can be gently wiped clean. By that time the condensation process is limited due to the increased temperature of the fixative, and subsequent cleaning of the lid is not necessary. Furthermore, 4 min is sufficient for the fixative to partly melt and become sticky: this prevents the sections from "jumping."
36. When OsO_4 is added to the fixative mixture, it is important to shield the fixative from light. Following melting, the fixative should thus be placed on ice *and* kept in the dark.
37. Depending on the choice of antibody, unspecific binding can be further reduced by employing different blocking agents, e.g., cold fish gelatin, BSA-c, or both. Otherwise, the blocking steps can be increased in time.
38. When protein A-gold has none or only minor affinity for the primary antibody, a bridging antibody can be employed. In this case, the bridging antibody is incubated for 20 min following **step 4**, followed by one brief and next five 2-min washing steps. After this, continue with **step 5**.
39. The dilution of the protein A-gold is batch dependent. Instead of protein A-gold, gold-conjugated antibodies can also be employed.

40. Instead of PHEM buffer, PBS can also be employed for the earlier steps in the labeling procedure. In this case, the sections should be thoroughly washed in water to completely remove the buffer. Phosphate will cause uranyl acetate to participate during the next step of the protocol.
41. Here, two layers of thin filter paper (e.g., coffee filter) or a single thick (Whatman, No. 50) filter paper can be employed. The parafilm strip underneath the filter paper is to prevent the spillage of UA, which should be disposed of carefully.

Acknowledgements

This work was supported by Technology Foundation Stichting Technologische Wetenschappen, Innovatiegerichte Onderzoekprogramma's Genomics (IOP Genomics, SenterNovem), and the Dutch FSHD Foundation. We thank D. Zeuschner for providing the pictures shown in Figs. 1b, 2c, d, and 3d.

References

1. Moor H, Mühlethaler K (1963) Fine structure in frozen-etched yeast cells. J Cell Biol 17: 609–628
2. Moor H (1987) Theory and practice of high pressure freezing. Springer, Berlin
3. Dubochet J, Richter K, Roy HV et al (1991) Freezing: facts and hypothesis. Scanning Microsc Suppl 5:S11–S16
4. Studer D, Graber W, Al-Amoudi A et al (2001) A new approach for cryofixation by high-pressure freezing. J Microsc 203: 285–294
5. Sartori N, Richter K, Dubochet J (1993) Vitrification depth can be increased more than 10-fold by high-pressure freezing. J Microsc 172:55–61
6. Fernández-Morán H (1960) Low-temperature preparation techniques for electron microscopy of biological specimens based on rapid freezing with liquid helium II. Ann N Y Acad Sci 85: 689–713
7. Humbel BM, Marti T, Müller M (1983) Improved structural preservation by combining freeze substitution and low temperature embedding. Beitr Elektronenmikrosk Direktabb Oberfl 16:585–594
8. Van Donselaar EG, Posthuma G, Zeuschner D et al (2007) Immunogold labeling of cryosections from high-pressure frozen cells. Traffic 8:471–485
9. Bernhard W, Viron A (1971) Improved techniques for the preparation of ultrathin frozen sections. J Cell Biol 49:731–746
10. Tokuyasu KT (1973) A technique for ultracryotomy of cell suspensions and tissues. J Cell Biol 57:551–565
11. Tokuyasu KT (1980) Immunochemistry on ultrathin frozen sections. Histochem J 12:381–403
12. Karreman MA, van Donselaar EG, Gerritsen HC et al (2011) VIS2FIX: a high-speed fixation method for immuno-electron microscopy. Traffic 12:806–814
13. Dubochet J, McDowall AW, Menge B et al (1983) Electron microscopy of frozen-hydrated bacteria. J Bacteriol 155:381–390
14. Al-Amoudi A, Norlen LPO, Dubochet J (2004) Cryo-electron microscopy of vitreous sections of native biological cells and tissues. J Struct Biol 148:131–135
15. Liou W, Geuze HJ, Slot JW (1996) Improving structural integrity of cryosections for immunogold labeling. Histochem Cell Biol 106:41–58
16. Griffith JM, Posthuma G (2002) A reliable and convenient method to store ultrathin thawed cryosections prior to immunolabeling. J Histochem Cytochem 50:57–62
17. Weibull C, Christiansson A (1986) Extraction of proteins and membrane lipids during low temperature embedding of biological material for electron microscopy. J Microsc 142:79–86

Part IV

Analysis of Exocytosis and Endocytosis in Model Organisms

Chapter 22

Chemical Genomics: Characterizing Target Pathways for Bioactive Compounds Using the Endomembrane Trafficking Network

Cecilia Rodriguez-Furlán, Glenn R. Hicks, and Lorena Norambuena

Abstract

The plant endomembrane trafficking system is a highly complex set of processes. This complexity presents a challenge for its study. Classical plant genetics often struggles with loss-of-function lethality and gene redundancy. Chemical genomics allows overcoming many of these issues by using small molecules of natural or synthetic origin to inhibit specific trafficking proteins thereby affecting the processes in a tunable and reversible manner. Bioactive chemicals identified by high-throughput phenotype screens must be characterized in detail starting with understanding of the specific trafficking pathways affected. Here, we describe approaches to characterize bioactive compounds that perturb vesicle trafficking. This should equip researchers with practical knowledge on how to identify endomembrane-specific trafficking pathways that may be perturbed by specific compounds and will help to eventually identify molecular targets for these small molecules.

Key words Chemical genomics, Screening, Organelle markers, Multidrug treatments, Exocytosis, Endocytosis

1 Introduction

Plant endomembrane macromolecular trafficking can be functionally divided into the secretory and the endocytic pathways. The secretory route delivers cargoes to the plasma membrane (PM), cell wall, extracellular space, and vacuole. While anterograde transport is the route for newly synthesized materials, retrograde transport functions to preserve the integrity of the compartments by maintaining organelle-specific resident proteins including components of the trafficking machinery [1]. Endocytosis and secretory trafficking converge in a continuum of endosome compartments [2], and these two trafficking modes are highly coordinated and subjected to sophisticated regulation [3]. Such tight regulation

Andrei I. Ivanov (ed.), *Exocytosis and Endocytosis*, Methods in Molecular Biology, vol. 1174,
DOI 10.1007/978-1-4939-0944-5_22,

of endomembrane trafficking is essential for maintenance of many cellular processes that directly affects development and survival of the organism.

The structural and functional complexity of plant endomembrane system represents a significant challenge for its study using conventional genetics. Forward and reverse genetic approaches struggle with lethal phenotypes, genetic redundancy, pleiotropic phenotypes, and limiting possibility to perturb in vivo pathways in a conditional manner. By contrast, chemical genomics has proven to be a powerful tool to overcome the above-mentioned problems [4]. Chemical genomics refers to an experimental approach that uses small bioactive molecules of natural or synthetic origin to modify or disrupt functions of specific proteins leading to alterations of biological processes [5]. A chemical genomic approach involves three major steps: (1) screening for bioactive small molecules, (2) characterization of the phenotypic effects of candidate compounds, and (3) identification of their molecular targets [6].

The first (1) step consists of high-throughput screening of small compound libraries in order to identify candidate molecules that alter membrane traffic-related processes and induce a cell phenotype that can be easily observed and scored [7, 8]. The selected set of compounds can then be subjected to the step (2) aimed to identify specific endomembrane trafficking pathways perturbed by the candidate chemical compounds.

Detailed characterization of the effects of the candidate compounds on endomembrane trafficking will provide a rational for selecting most promising compounds for their future studies. This step is critical given that hundreds of small molecules can be identified from a high-throughput screen. As a general approach to characterize chemical modulators of endomembrane trafficking involves asking the following questions:

1. Does this compound affect endocytosis or exocytosis/secretion?
2. Does it affect general mechanisms of protein trafficking or it inhibits targeting to a specific compartment?
3. Does it affect cargo trafficking or the compartment biogenesis?

At this point, we are still going to deal with a large number of compounds, which will require to use a systematic approach for their characterization. These characterization steps performed after the primary screening are crucial in order to focus only on the most promising lead compounds for target identification. Although identifying the modes of action (step 2 above) of the bioactive compounds is often the most time-consuming step of chemical genomics, it is rarely discussed in the literature.

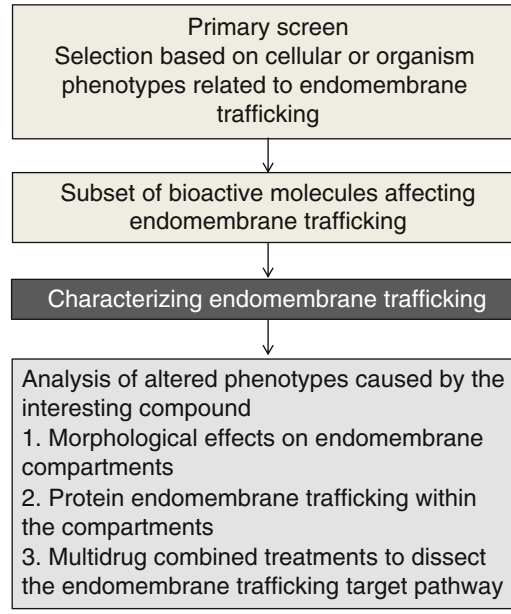

Fig. 1 General workflow for characterizing endomembrane trafficking pathways targeted by chemical compounds. The starting point in this workflow consists of a subset of small bioactive molecules previously selected by a high-throughput screening based on cellular or organism phenotypes related to endomembrane pathways alterations. The selected molecules are re-screened in order to identify their targets within among different endomembrane trafficking pathways

In this chapter, we present a workflow for characterization of endomembrane trafficking effects (step 2) of bioactive compound that have been identified by chemical genomics during the primary high-throughput screening (step 1). This characterization step is necessary to unravel the link between phenotypes at the cellular and organismal levels (Fig. 1). We propose the use of endomembrane compartment-specific markers tagged with fluorescent proteins to identify compounds affecting exocytosis, endocytosis, recycling, or vacuolar morphogenesis [8–11]. We also describe co-treatments of candidate compounds with drugs that perturb known steps of endomembrane trafficking [8, 9, 11]. Such well-known compounds are essential for prioritizing lead compounds for the subsequent target identification (step 3). Even without their cognate targets, novel bioactive compounds have contributed new knowledge about endomembrane protein trafficking pathways and their involvement in plant development and responses to environmental stimulus [6, 8, 9, 11].

2 Materials

2.1 Materials for Plant Growth

1. *Plants*. Arabidopsis plants that express GFP or YFP fusion protein markers of different endomembrane compartments (plant sources are listed and referred in Table 1).
2. *Growth culture media*. MS media containing 0.44 % Murashige and Skoog medium (1,650 mg/L Ammonium nitrate,

Table 1
Fluorescent fusion-protein markers and their corresponding endomembrane compartment locations

Protein fusion	Organelle	References
VHA-a1::VHA-a1:GFP	TGN	[20]
SYP61::SYP61:CFP	TGN/early endosome	[21]
SYP22::SYP22:YFP	PVC/tonoplast	[22]
35S::MAN-GFP	Golgi	[23, 24]
35S::NAG1:GFP	Golgi	[24]
UBQ::ARA7:GFP	PVC/late endosome	[25]
35S::ROP6:GFP	PM	[24]
35S::ROP2:GFP	PM/endosome	[26, 27]
35S::BR1:GFP	PM/endosome	[27]
AUX1::AUX1:YFP	PM/endosome	[13, 28]
35S::GFP:PIP2A	PM	[28]
UBQ::Vti12:YFP	TGN	[29]
35S::GFP:KDEL	ER	[30]
35S::ARA6:GFP	Endosomes	[24]
SNX1::SNX1:GFP	Endosomes	[31]
35S::BOR1:GFP	PM/endosome	[32]
35S::Ale:GFP	Lytic vacuole	[33]
35S::GFP:CHI	Protein storage vacuole	[33]
35S::GFP:dTIP	Tonoplast	[33]
UBQ::SYP32:YFP	Golgi	[25]
UBQ::VAMP711:YFP	Tonoplast	[25]
UBQ::abF2a(Rha1):YFP	PVC/late endosome	[25]
PIN1::PIN1:GFP		[34, 35]
PIN2::PIN2-GFP		[35]

The table lists GFP or YFP fusion markers for different endomembrane compartments and their correspondent bibliographic references

6.20 mg/L Boric acid, 332.20 mg/L Calcium chloride (anhydrous), 0.0250 mg/L Cobalt chloride hexahydrate, 0.0250 mg/L Cupric sulfate pentahydrate, 37.260 mg/L Disodium EDTA dihydrate, 27.80 mg/L Ferrous sulfate heptahydrate, 2.0 mg/L Glycine, 180.70 mg/L Magnesium sulfate (anhydrous), 16.90 mg/L Manganese sulfate monohydrate, 100 mg/L myo-Inositol, 0.50 mg/L Nicotinic acid, 0.830 mg/L Potassium iodide, 1,900 mg/L Potassium nitrate, 170.0 mg/L Potassium phosphate monobasic, 0.50 mg/L Pyridoxine hydrochloride, 0.250 mg/L Sodium molybdate dihydrate, 0.10 mg/L Thiamine hydrochoride 8.60 mg/L Zinc sulfate heptahydrate) with 1 % sucrose, 0.05 % MES, 0.01%, 0.7 % phytoagar; pH 5.7.

2.2 Chemical Treatments

1. Cycloheximide, 50 mM stock in dimethylsulfoxide (DMSO), stored at −20 °C.
2. Wortmannin, 30 mM stock in DMSO, stored at −20 °C.
3. Latrunculin B, 30 mM stock in DMSO, stored at −20 °C.
4. Oryzalin, 10 mM stock in DMSO, stored at −20 °C.
5. Brefeldin A, 5 mg/mL stock in absolute ethanol, stored at −20 °C.
6. Tyrphostin A23, 30 mM stock in DMSO, stored at −20 °C.

3 Methods

3.1 Characterization of the Effects of Small-Molecular Compounds on Endomembrane Trafficking by Using Intracellular Markers

Below, we outline the secondary screen that uses compounds selected from the primary screening. The aim of this screen is to understand how the selected compounds affect endomembrane trafficking. The effects of bioactive compounds on the morphology of endomembrane compartments and vesicle trafficking can be monitored by using fluorescent-fusion marker proteins. Table 1 shows a list of either GFP or YFP fusion protein markers for different membrane compartments. Figure 2 shows some representative phenotypes observed with these markers after plant exposure to a bioactive compound Sortin2 previously characterized as stimulator of endocytosis [9].

3.1.1 A Standard Secondary Compound Screen Using Fluorescently Tagged Markers of Different Endomembrane Compartments

1. Stratify sterilized seeds in darkness for 48 h at 4 °C prior to plating and start growing them at 22 °C under standard conditions of humidity and 16 h light/8 h dark photoperiod.
2. Sow seeds from transgenic lines expressing the marker proteins fused to GFP on MS (liquid or solid) containing different concentrations of the selected compound. The concentration range should be based on the results of the primary screen and should span the range from tenfold lower to fivefold higher the concentration used in the primary screen.

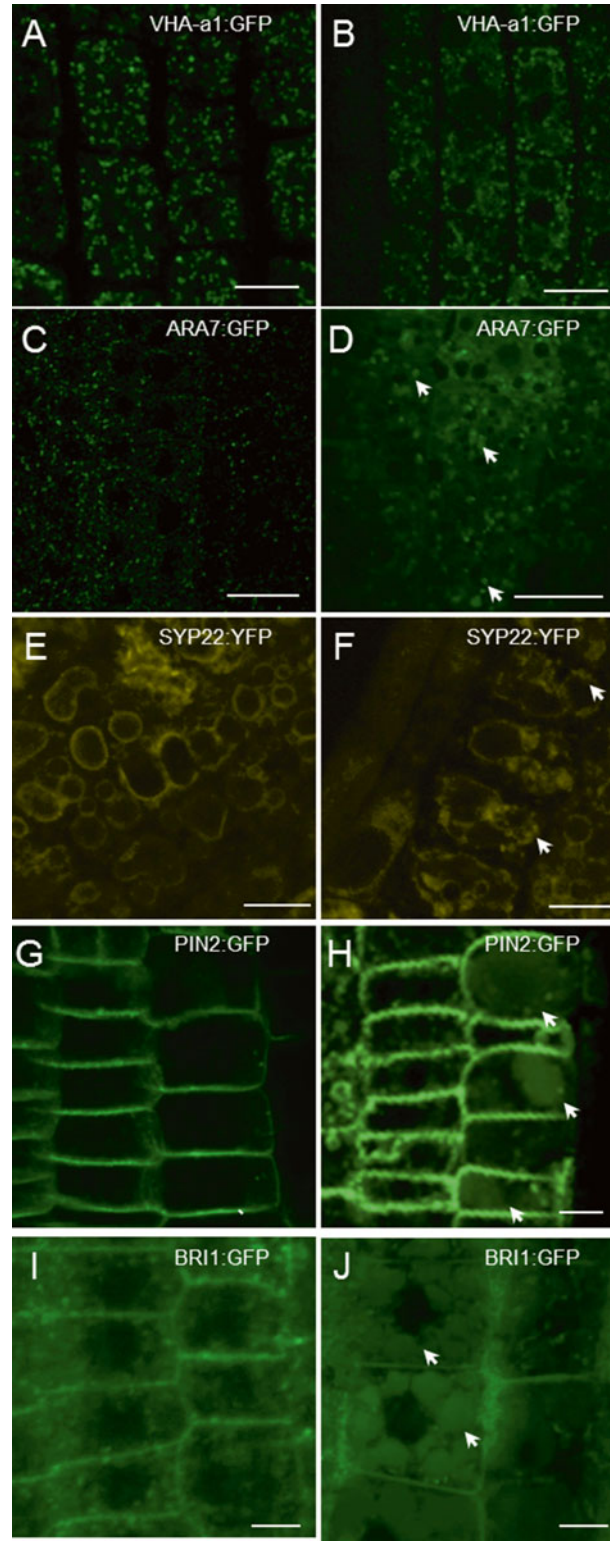

Fig. 2 Sortin2 affects morphology and targeting of fluorescent fusion markers of endomembrane trafficking. Scale bar, 10 μm. Reproduced from Pérez-Henríquez P, Raikhel NV, Norambuena L, Endocytic trafficking towards the vacuole plays a key role in the auxin receptor SCF(TIR)-independent mechanism of lateral root formation in A. thaliana. Mol Plant, 2012, 5 (6):1195–1209 with permission of Oxford University Press

3. Incubate the plates for 7 days at 22 °C. If the chemical compound causes any alteration on seed germination or growth, the treatment could be performed using 7-day-old plants.
4. Pull out the seedling carefully and mount it on a slide with water and cover it with a coverglass.
5. Image different tissues of interest by fluorescent microscopy to visualize morphology of different endomembrane compartments in the presence and the absence of the selected compounds. Although this analysis can be done using a conventional confocal microscope, the initial screens can be greatly accelerated by the use of a high-throughput confocal microscope such as the Pathway HT (BD Biosciences). After the high-throughput imaging, more detailed analysis of different tissues (cotyledons, hypocotyls and roots) can be performed by confocal microscopy in order to better characterize morphological changes on the specific endomembrane compartments (*see* **Notes 1** and **2**).

3.2 Characterizing the Effects of the Dual Treatment with Novel and Well-Characterized Chemical Modulators of Endomembrane Trafficking

The following procedure is aimed to dissect possible mechanisms of action of novel bioactive molecules by examining their activity in the presence of well-known modulators of endomembrane trafficking.

1. Transfer four or six 7-day-old transgenic seedlings expressing the fluorescent marker of interest to 1 mL of liquid MS media containing a Chemical A and incubate for 30 min. After this pretreatment perform a co-treatment for 6 h using the Chemical A together with a compound under study, Chemical B. Include appropriate controls, one involving the Chemical A alone and the other involving only the Chemical B. Finally include a control treatment containing an equivalent amount of the solvent (the most common solvent used in chemical compound libraries is DMSO, *see* **Note 1**).
2. Place the seedlings on slides and examine the effects of the treatments using confocal microscopy. This approach can be useful to identify possible targeting pathways and dissect the effects of the chemical compounds on the particular endomembrane system (*see* **Note 3**). For example, compounds of interest can perturb vesicular trafficking between endomembrane compartments by modifying either the dynamic behavior of compartments or their morphology in characteristic ways [12]. Figure 3 highlights the phenotypes of multidrug treatments with a bioactive compound, Sortin2, that helps to characterize its specific activity in affecting the endocytic pathway from the plasma membrane to the vacuole [9].

3.2.1 Examples of Dual Compound Treatments

1. To investigate the contribution of de novo protein synthesis preincubate the samples for 30 min with 50 μM of the protein synthesis inhibitor, cycloheximide (CHX) [13]. Thereafter, perform 6 h treatment with a combination of 50 μM CHX and

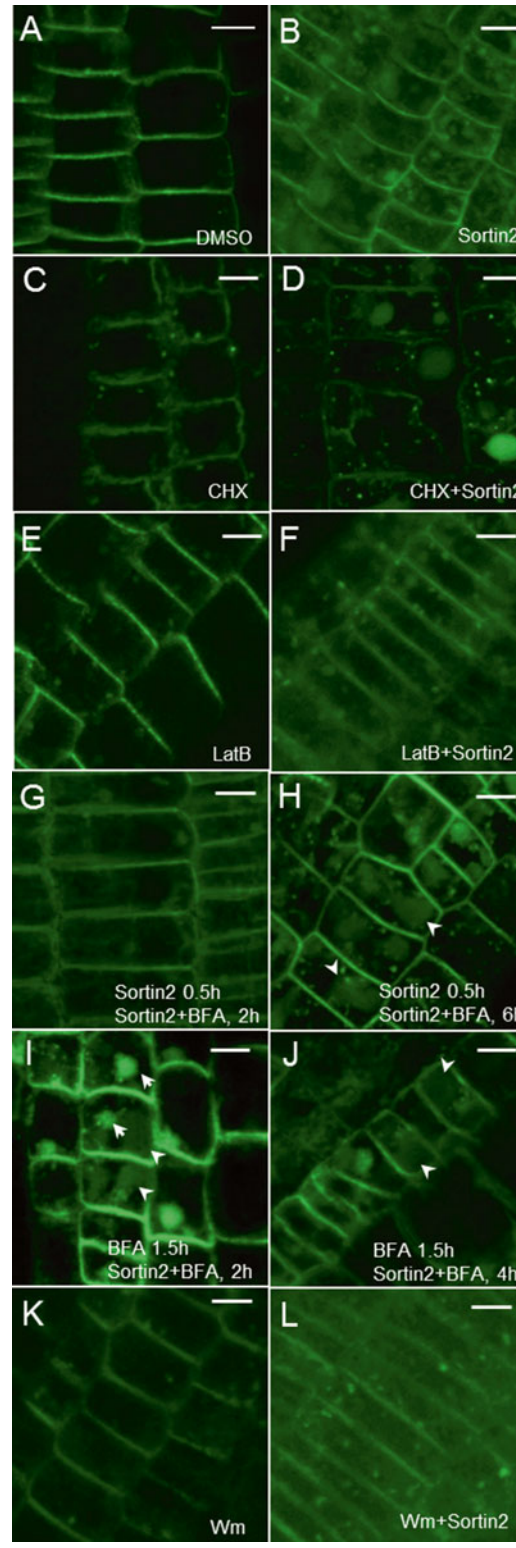

Fig. 3 Combined drug treatments reveal that Sortin2 alters PIN2 trafficking from the endosomes to the vacuole. Seven-day-old Arabidopsis plants expressing PIN2-GFP marker were subjected to the following treatments: (**a**) Control condition containing DMSO only; (**b**) treatment for 2 h with Sortin2 (50 μg/mL);

a chemical compound of interest. Include DMSO only and CHX only controls [14].

2. To test if the activity of the compound of interest depends on integrity of different cytoskeletal structure, perform the following sets of experiments (*see* **Note 2**). In the first experiment, preincubate the samples for 30 min with 20 μM of the actin-depolymerizing drug Latrunculin B (LatB) and then perform 6 h co-treatment with 20 μM LatB and the compound of interest [13, 14]. In the second experiment, preincubate the samples for 30 min with 10 μM of the microtubule depolymerizing drug, Oryzalin, and perform 6 h co-treatment with 10 μM Oryzalin and the compound of interest [13, 15].
3. To dissect the roles of the compound of interest on the endocytic pathway from the PM to endosomes use known inhibitors of endomembrane trafficking and fusion such as Brefeldin A (BFA), Wortmannin, and Tyrphostin A23(*see* **Notes 4** and **5**) [13, 16]. In the first experiment, pretreat the samples for 1.5 h with 50 μM BFA followed by the 2 h co-treatment with 50 μM BFA and the compound of interest [9]. In the second experiment, pretreat the samples for 1 h with 50 μM Wortmannin (Wm) followed by the 2 h co-treatment with 50 μM Wm and the compound of interest [9, 17]. Wm is a specific inhibitor of the phosphatidyl-inositol 3-kinase that induces homotypic fusion of the PVC/MVB resulting in ring-like structures altering trafficking to the vacuole [18]. Finally, pretreat the samples for 30 min with 30 μM Tyrphostin A23 followed by the 1 h co-treatment with 30 μM Tyrphostin A23 and the compound of interest [9].

Fig. 3 (continued) (**c**) treatment for 6.5 h with CHX (50 μM); (**d**) preincubation for 0.5 h with CHX followed by 6 h co-treatment with CHX and Sortin2; (**e**) treatment for 6.5 h with LatB (20 μM); (**f**) preincubation for 0.5 h with LatB followed by 6 h co-treatment with LatB and Sortin2; (**g**, **h**) pretreatment for 0.5 h with Sortin2 (50 μg/mL) followed by co-treatment with BFA (50 μM) and Sortin2 for 2 h (**g**) and 6 h (**h**). Vacuole accumulations are indicated by arrowheads. (**i**, **j**) Pretreatment for 1.5 h with BFA followed by co-treatment with BFA and Sortin2 for 2 h (**i**) and 4 h (**j**). Accumulation of BFA bodies and vacuole is indicated by *arrows* and *arrowheads*, respectively. (**k**) Treatment for 6.5 h with Wm (15 μM); (**l**) pretreatment 0.5 h with Wm followed by 6.5 h co-treatment with Wm plus Sortin2. Scale bar, 10 μm. Reproduced from Pérez-Henríquez P, Raikhel NV, Norambuena L, Endocytic trafficking towards the vacuole plays a key role in the auxin receptor SCF(TIR)-independent mechanism of lateral root formation in A. thaliana. Mol Plant, 2012, 5 (6):1195–1209 with permission of Oxford University Press.

4 Notes

1. Chemical compounds for high-throughput screening obtained from the commercial libraries are typically dissolved in 100 % DMSO. Arabidopsis seedlings appear to grow normally in MS supplemented with up to 1 % DMSO. Therefore, DMSO should always be included as a control to ensure that this solvent does not perturb responses to tested compounds or induce any off-target phenotype. The DMSO concentration in control and experimental groups should be identical.
2. Since cytoskeleton-disrupting drugs have dramatic effects on vesicle trafficking, these compounds should not be selected for the secondary screen. To test if the selected compound displays any effect on actin or microtubule organization and/or their dynamics, you can use specific fluorescent cytoskeleton markers, such as MAP4::GFP for microtubules, Talin::GFP, or ABD2::YFP for actin [19]. This step will help to avoid selecting molecules that can indirectly affect endomembrane trafficking.
3. The drugs combination for the multidrug treatments should be selected based on the subcellular phenotype and the putative target pathway that you want to characterize (reviewed in ref. [12]).
4. Multidrug treatments can also include a 1–2 h preincubation with the compound of interest followed by 2–6 h co-treatment that includes a known modulator of the trafficking pathway. This will help to observe the effects of the compound of interest on the specific trafficking pathway.
5. Experiments involving wash-out of the studying compound can also be helpful, since this should rapidly reverse the compound-induced effects on endomembrane trafficking. This step will help to avoid selecting small molecules that irreversible bind to intracellular targets thereby impairing different physiological functions in vivo and inducing toxicity and lethal phenotypes.

Acknowledgements

This work was supported by Fondecyt 1120289 and FONDEF IDeA CA12I10206.

References

1. Zouhar J, Rojo E, Bassham DC (2010) Retrograde transport from the prevacuolar compartment to the trans-Golgi network. Plant Sci 178:90–93
2. Viotti C, Bubeck J, Stierhof Y-D et al (2010) Endocytic and secretory traffic in Arabidopsis merge in the trans-Golgi network/early endosome, an independent and highly dynamic organelle. Plant Cell 22:1344–1357
3. Contento AL, Bassham DC (2012) Structure and function of endosomes in plant cells. J Cell Sci 125:3511–3518
4. Hicks GR, Raikhel NV (2012) Small molecules present large opportunities in plant biology. Annu Rev Plant Biol 63:261–282
5. Blackwell HE, Zhao Y (2003) Chemical genetic approaches to plant biology. Plant Physiol 133:448–455
6. Robert S, Raikhel NV, Hicks GR (2009) Powerful partners: Arabidopsis and chemical genomics. Arabidopsis Book 7:21
7. Surpin M, Rojas-Pierce M, Carter C et al (2005) The power of chemical genomics to study the link between endomembrane system components and the gravitropic response. Proc Natl Acad Sci U S A 102:4902–4907
8. Drakakaki G, Robert S, Szatmari A-M et al (2011) Clusters of bioactive compounds target dynamic endomembrane networks in vivo. Proc Natl Acad Sci U S A 108:17850–17855
9. Pérez-Henríquez P, Raikhel NV, Norambuena L (2012) Endocytic trafficking towards the vacuole plays a key role in the auxin receptor SCF(TIR)-independent mechanism of lateral root formation in *A. thaliana*. Mol Plant 5: 1195–1209
10. Ung N, Brown MQ, Hicks GR et al (2013) An approach to quantify endomembrane dynamics in pollen utilizing bioactive chemicals. Mol Plant 6:1202–1213
11. Rivera-Serrano EE, Rodriguez-Welsh MF, Hicks GR et al (2012) A small molecule inhibitor partitions two distinct pathways for trafficking of tonoplast intrinsic proteins in Arabidopsis. PLoS One 7:e44735
12. Swarup R, Kargul J, Marchant A et al (2004) Structure-function analysis of the presumptive Arabidopsis auxin permease AUX1. Plant Cell 16:3069–3083
13. Urbina D, Pérez-Henríquez P, Norambuena L (2012) The use of multidrug approach to uncover new players of the endomembrane system trafficking machinery. In: Hicks GR, Stéphanie R (eds) Plant chemical genomics, vol 1056, Methods in molecular biology. Humana Press, New York
14. Takano J, Tanaka M, Toyoda A et al (2010) Polar localization and degradation of Arabidopsis boron transporters through distinct trafficking pathways. Proc Natl Acad Sci U S A 107:5220–5225
15. Robert S, Bichet A, Grandjean O et al (2005) An *Arabidopsis* endo-1,4-beta-D-glucanase involved in cellulose synthesis undergoes regulated intracellular cycling. Plant Cell 17:3378–3389
16. Robinson DG, Jiang L, Schumacher K (2008) The endosomal system of plants: charting new and familiar territories. Plant Physiol 147:1482–1492
17. Konopka CA, Backues SK, Bednarek SY (2008) Dynamics of *Arabidopsis* dynamin-related protein 1C and a clathrin light chain at the plasma membrane. Plant Cell 20:1363–1380
18. Wang J, Cai Y, Miao Y et al (2009) Wortmannin induces homotypic fusion of plant prevacuolar compartments. J Exp Bot 60:3075–3083
19. Wang YS, Motes CM, Mohamalawari DR et al (2004) Green fluorescent protein fusions to Arabidopsis fimbrin 1 for spatio-temporal imaging of F-actin dynamics in roots. Cell Motil Cytoskeleton 59:79–93
20. Sanderfoot AA, Kovaleva V, Bassham DC et al (2001) Interactions between syntaxins identify at least five SNARE complexes within the Golgi/prevacuolar system of the Arabidopsis cell. Mol Biol Cell 12:3733–3743
21. Robert S, Chary SN, Drakakaki G et al (2008) Endosidin1 defines a compartment involved in endocytosis of the brassinosteroid receptor BRI1 and the auxin transporters PIN2 and AUX1. Proc Natl Acad Sci U S A 105:8464–8469
22. Nebenfuhr A, Gallagher LA, Dunahay TG et al (1999) Stop-and-go movements of plant Golgi stacks are mediated by the acto-myosin system. Plant Physiol 121:1127–1142
23. Grebe M, Xu J, Mobius W et al (2003) Arabidopsis sterol endocytosis involves actin-mediated trafficking via ARA6-positive early endosomes. Curr Biol 13:1378–1387
24. Geldner N, Denervaud-Tendon V, Hyman DL et al (2009) Rapid, combinatorial analysis of membrane compartments in intact plants with a multicolor marker set. Plant J 59:169–178
25. Fu Y, Xu T, Zhu L et al (2009) A ROP GTPase signaling pathway controls cortical microtubule ordering and cell expansion in *Arabidopsis*. Curr Biol 19:1827–1832

26. Geldner N, Hyman DL, Wang X et al (2007) Endosomal signaling of plant steroid receptor kinase BRI1. Genes Dev 21:1598–1602
27. Cutler SR, Ehrhardt DW, Griffitts JS et al (2000) Random GFP::cDNA fusions enable visualization of subcellular structures in cells of *Arabidopsis* at a high frequency. Proc Natl Acad Sci U S A 97:3718–3723
28. Ovečka M, Berson T, Beck M et al (2010) Structural sterols are involved in both the initiation and tip growth of root hairs in Arabidopsis thaliana. Plant Cell 22:2999–3019
29. Boevink P, Oparka K, Santa Cruz S et al (1998) Stacks on tracks: the plant Golgi apparatus traffics on an actin/ER network. Plant J 15:441–447
30. Jaillais Y, Fobis-Loisy I, Miege C et al (2006) AtSNX1 defines an endosome for auxin-carrier trafficking in *Arabidopsis*. Nature 443: 106–109
31. Takano J, Miwa K, Yuan L et al (2005) Endocytosis and degradation of BOR1, a boron transporter of Arabidopsis thaliana, regulated by boron availability. Proc Natl Acad Sci U S A 102:12276–12281
32. Fluckiger R, De Caroli M, Piro G et al (2003) Vacuolar system distribution in *Arabidopsis* tissues, visualized using GFP fusion proteins. J Exp Bot 54:1577–1584
33. Benkova E, Michniewicz M, Sauer M et al (2003) Local, efflux-dependent auxin gradients as a common module for plant organ formation. Cell 115:591–602
34. Xu J, Scheres B (2005) Dissection of Arabidopsis ADP rybosilation factor 1 function in epidermal cell polarity. Plant Cell 17: 525–536
35. Abas L, Benjamins R, Malenica N, Paciorek T, Wisniewska J, Moulinier-Anzola JC, Sieberer T, Friml J, Luschnig C (2006) Intracellular trafficking and proteolysis of the Arabidopsis auxin-efflux facilitator PIN2 are involved in root gravitropism. Nat Cell Biol 8(3):249–256

Chapter 23

Application of RNAi Technology and Fluorescent Protein Markers to Study Membrane Traffic in *C. elegans*

Jachen A. Solinger, Dmitry Poteryaev, and Anne Spang

Abstract

RNA interference (RNAi) is a powerful tool to study the intracellular membrane transport and membrane organelle behavior in the nematode *Caenorhabditis elegans*. This model organism has gained popularity in the trafficking field because of its relative simplicity, yet being multicellular. *C. elegans* is fully sequenced and has an annotated genome, it is easy to maintain, and a growing number of transgenic strains bearing markers for different membrane compartments are available. *C. elegans* is particularly well suited for protein downregulation by RNAi because of the simple but efficient methods of dsRNA delivery. The phenomenon of systemic RNAi in the worm further facilitates this approach. In this chapter we describe methods and applications of RNAi in the field of membrane traffic. We summarize the fluorescent markers used as a readout for the effects of gene knockdown in different cells and tissues and give details for data acquisition and analysis.

Key words *C. elegans*, Confocal microscopy, Embryo, Endocytosis, Endoplasmic reticulum, GFP, Membrane dynamics, Membrane trafficking, Protein transport, RNAi

1 Introduction

Only recently the potential of *C. elegans* as a model for membrane traffic and membrane dynamics was recognized. Comparing *C. elegans* to yeast, flies, mice, and cultured mammalian cell lines, the worm has great advantages as well as some weaknesses. It cannot beat yet yeast when it comes to easiness and speed of creating transgenic lines and knockouts, although some progress is being made [1, 2]. However *C. elegans* is a multicellular organism with differentiated tissues, which is closer to humans in terms of orthologous genes, cell organization, and intracellular interactions. The functions of genes should ideally be studied in a context of a whole organism. These studies are very difficult or sometimes impossible in vertebrates and of course not possible by definition in isolated cells in culture. *C. elegans*, in contrast, offers such an opportunity.

Andrei I. Ivanov (ed.), *Exocytosis and Endocytosis*, Methods in Molecular Biology, vol. 1174,
DOI 10.1007/978-1-4939-0944-5_23,

The phenomenon of RNA interference (RNAi) has initially been discovered in plants but was developed as a powerful tool for gene silencing in *C. elegans*. The biological role of RNAi seems to be to confer resistance to viruses, since the enzymatic machinery of RNAi is triggered by viral double-stranded (ds) RNA. RNAi may also protect against the self-propagation of transposons. RNAi in worms is still a much less complicated technique than in higher organisms.

Different delivery methods of dsRNA in *C. elegans* have been described in detail [3, 4]. Additionally we advise the reader to consult the web resource devoted to *C. elegans* biology and methods, including RNAi: www.wormbook.org. Therefore, we shall concentrate on RNAi in the context of membrane traffic and the analysis of phenotypes related to membrane transport and dynamics. We would like to emphasize that, when it comes to choosing a specific technique, RNAi by feeding or soaking, although simple, are inferior in penetrance to RNAi by injection of dsRNA in a few ways. Generally, RNAi by injection causes stronger gene downregulation, often persisting more than one generation (if not lethal). The strength of RNAi can be more readily adjusted, by injecting more or less concentrated dsRNA. The effect of RNAi by feeding can be adjusted by the length of incubation on the respective plate (1–3 days) during development of the worms. This is particularly useful in case of sterility caused by dsRNA, and observation of embryonic or postembryonic phenotypes is desirable [5]. On the other hand, in genome-wide (*see* **Note 1**) screens, there is no easy alternative to RNAi by feeding a bacterial library [6]. The growing number of null alleles (gene knockouts), produced by two consortia, will allow a faster progress in understanding the regulation of membrane traffic in *C. elegans* (*see* Subheading 2.5). There are, however, several caveats in their use (*see* **Note 2**), making RNAi still indispensable, even in the foreseeable future, when the worm could make it to the "yeast" stage and for virtually all predicted open reading frames a strain with a null allele will exist.

Studying membrane traffic and organelle behavior by RNAi requires appropriate and solid readouts (*for examples, see* Table 1). This is easily achieved by using transgenic strains bearing fluorescent proteins marking specific membrane organelles and/or cargo [7]. The most popular markers are listed in Table 2 and are discussed below. Synthetic fluorescent compounds marking organelles and traffic pathways have also their use, although their application is limited in *C. elegans* (*see* **Note 3**). They are listed in Table 3.

Nowadays, virtually all aspects of membrane transport such as exo- and endocytosis [8–10], intracellular [11] and intercellular [12] transport, and mitosis and cytokinesis [5, 13] sparked considerable interest in *C. elegans*.

Table 1
Telltale signs of RNAi phenotypes having a trafficking defect

Phenotype	Visualization method	Possible defect	Examples
The animals are dumpy, that is, short and fat	Dissecting binocular (Bino)	Endocytic pathway (End)	[10]
Molting defects: The larvae are unable to shed the old cuticle during molting	Bino, Nomarsky optics (DIC)	End, secretion (Sec)	[28]
Cuticular defects	Bino, DIC	Sec	[12]
Vacuolated intestine	Bino, DIC	End, Sec	[11]
Swiss cheese phenotype: Embryonic blastomeres display "holes" in the cytoplasm	DIC	End	[29]
Glo: Gut birefringent granules are absent or severely reduced in number	Polarization optics or fluorescent binocular/ microscope (Fl)	End	[26]
Coelomocytes with too big or too small endocytic vacuoles	DIC	End	[30]
Weak eggshell, osmotically sensitive embryos, permeable eggshell		Sec, End	[31]
Increased or decreased yolk granule size in oocytes/embryos	DIC or Fl (for VIT-2::GFP strain)	End	[10, 32]
Rme receptor-mediated endocytosis defective: Body cavity filled with GFP, while oocytes/embryos are devoid of GFP	Fl, in VIT-2::GFP strain	End (*direct evidence*)	[10]
Cup coelomocyte uptake defective: Body cavity is filled with GFP	Fl, in ssGFP-expressing strains	End (*direct evidence*)	[30]

2 Materials

2.1 dsRNA Production

1. Thermal cycler for PCR.
2. Reagents for performing PCR: Normal Taq polymerase, without proofreading activity, is acceptable.
3. Oligonucleotides targeting a coding segment within a gene of interest. Both forward and reverse primers must have a T7 RNA polymerase promoter sequence at 5′ ends.
4. In vitro transcription kit (Promega T7 RiboMAX Express).

2.2 Worm Maintenance and Handling

1. Dissecting binocular; worm picks made from iridium–platinum wire flattened at the picking end.

Table 2
List of fluorescent protein fusions marking specific membrane compartments in different *C. elegans* tissues

Fusion protein	Compartment marked	Reference
Oocytes and early embryos		
GFP::SP12 (signal peptidase complex subunit)	ER	[5]
GFP:PH$^{PLC1}\delta^1$ (PH domain of phospholipase Cδ)	PI(4,5)P_2 in plasma membrane	[33]
CAV-1::GFP (caveolin)	Caveolin-containing granules (localization depends on the cell cycle)	[34]
GFP::RAB-35	Recycling endosomes	[35]
VIT-2::GFP (yolk protein 170)	Yolk granules/endocytic compartments	[10]
GFP::MAN1	Inner nuclear membrane	[36]
mCherry::RAB-6.1	Golgi-derived cortical granules	[37]
GFP::RAB-6.2	Golgi-derived cortical granules	[37]
Coelomocytes		
pmyo-3::ssGFP (secreted soluble GFP expressed in muscles)	Endocytic pathway (excluding lysosomes)	[30]
phsp::ssGFP (heat shock-inducible ssGFP)	Endocytic pathway (excluding lysosomes): Used in pulse-chase experiments (*see* **Note 7**).	[27]
pmyo-3::dsRed2	Accumulates in lysosomes	[38]
GFP:PH$^{PLC1}\delta^1$	PI(4, 5)P_2 in plasma membrane	[38]
GFP::RAB-5	Early endosomes	[38]
GFP::RME-1 (EPS15 homology domain protein)	Plasma membrane/endocytic recycling compartment	[18]
RME-8::GFP, RME-8::RFP (DnaJ-domain protein)	Endosomes (presumably both early and late)	[39, 40]
RAB-7::GFP	Late endosomes	[29]
CUP-5::GFP (putative Ca^{2+} channel)	Late endosomes/lysosomes	[40]
2xFYVE::GFP	PI(3)P (endosomes)	[41]
Mannosidase II::GFP	Golgi	[40]
Cytochrome b5::GFP	Smooth ER	[38]
ARF-6::RFP (Arf family small GTPase)	ARF-6-dependent ERC	[41]
MTM-6, MTM-9::GFP (myotubularins)	ARF-6/RME-1 endocytic recycling pathway	[41]
Intestine		
GFP::CHC-1 (clathrin heavy chain)	Clathrin at the plasma membrane and vesicles	[42]
GFP/RFP::RME-1	Basolateral and apical recycling endosomes	[11]
GFP/RFP::RAB-11.1	Basolateral recycling endosomes	[11]
GFP/mCherry::ALX-1 (Alix)	Basolateral recycling endosomes and multivesicular bodies (MVBs)	[43]
ARF-6::GFP/mCherry	Recycling endosomes	[44]

(continued)

Table 2
(continued)

Fusion protein	Compartment marked	Reference
GFP/RFP::RAB-10	Endosomes, Golgi	[11]
GFP/RFP::RAB-8	Endosomes, Golgi	[45]
MANS::GFP (mannosyl transferase)	Golgi	[11]
GFP/RFP::RAB-5	Early endosomes	[11]
GFP::VPS-27 (Hrs ortholog)	MVBs	[43]
GFP/RFP::RAB-7	Late endosomes	[11]
GFP::GLO-1 (gut granule-specific Rab GTPase)	Lysosomal related gut granules	[26]
hTfR::GFP (transferrin receptor)	Clathrin-dependent uptake and recycling	[11]
hTAC::GFP (alpha-chain of the IL-2 receptor)	Clathrin-independent endocytic pathway	[11]
Hypodermal epithelium		
VHA-5::RFP, VHA-8::YFP (V0 and V1 subunits of vacuolar H+-ATPase)	Apical membrane stacks, MVBs	[12]
WRT-2::GFP (Hedgehog-related protein)	Apical secretion pathway	[12]
Neurons		
GFP::RAB-3	Exocytic vesicles	[46]
GFP::RAB-27	Exocytic vesicles	[46]
Muscles		
COGC-3, COGC-1::GFP (conserved oligomeric Golgi complex)	Golgi	[47]
RFP::SP12	ER	[47]
YFP::TRAM (translocon-associated membrane protein)	ER	[47]
Signal peptide-GFP-ER retention signal KDEL	ER	[48]
TOM-70::YFP/CFP	Mitochondrial outer membrane	[48]
GFP::DRP-1 (dynamin-related protein)	Mitochondrial scission sites	[48]
Engulfing cells (*phagocytosis*)		(*see* [49])
mCherry::CHC-1, CHC-1::GFP	Clathrin at the plasma membrane and phagosomes	[50]
APA-2::GFP (AP2 complex)	Plasma membrane and phagosomes	[50]
DYN-1::YFP (dynamin)	Very early phagosomes	[51]
LST-4::mCherry/GFP	Early phagosomes	[50]
GFP::RAB-5	Early phagosomes	[52]
GFP::RAB-7	Late phagosomes/phagolysosomes	[52]
lifeACT::RFP	Filamentous actin	[52]
PIKI-1::GFP (PI3Kinase)	Maturing phagosomes	[53]
GFP::MTM-1 (myotubularin)	Maturing phagosomes	[53]
GFP::UNC-108/RAB-2	Late phagosomes	[54]
GFP/mCherry::RAB-14	Late phagosomes	[54]

(continued)

Table 2
(continued)

Fusion protein	Compartment marked	Reference
Markers with ubiquitous expression		
DYN-1::CFP/GFP (dynamin)	Plasma membrane	[51, 55]
VPS-27::GFP (Hrs ortholog)	MVBs	[56]
SNX-1::GFP	Retromer pathway	[57]
VPS-29::GFP	Retromer pathway	[57]
LGG-1::GFP (microtubule-associated anchor protein)	Autophagosomes	[58]
MAA-1::GFP (membrane-associated Acyl-CoA-binding protein)	Endosomes, Golgi	[59]
LMP-1::GFP (LAMP-1)	Lysosomes	[40]
ARL-8::mCherry (Arf-like GTPase)	Lysosomes	[60]
ASP-1::mCherry (aspartic protease)	Lysosomal lumen	[60]

Table 3
Small fluorescent dyes for membrane traffic research in *C. elegans*

Dye	Reported application	Method of delivery	Example
FM4-64 (Invitrogen)	Plasma membrane, endocytic pathway in embryos, endocytosis in the gut.	Laser puncture of the eggshell and bathing (at 32 μM), injection into body cavity or feeding (40 μM)	[31]
BSA-Texas Red (Invitrogen)	Endocytic pathway in coelomocytes.	Injection into body cavity (0.1–1 mg/mL)	[27]
LysoTracker (Invitrogen)	Lysosomes in many tissues.	Feeding (2 μM, calculated for NGM plate volume)	[29, 26]
LysoSensor-dextran (Invitrogen)	Lysosomes in the gut and coelomocytes.	Injection into body cavity (at 5 mg/mL)	Poteryaev, unpublished
Dehydroergosterol (Sigma-Aldrich)	Cholesterol transport, many tissues.	Feeding; *see* [61] for details	[61]
Acridine Orange (Molecular Probes)	Acidic compartments (lysosomes).	Soaking (0.1 mg/mL)	[26]

2. Mouth pipets, made from 100×1.5 mm glass capillaries: One end is pulled and broken in a Pasteur pipet fashion.
3. NGM agar plates seeded with *E. coli* strain *OP50* (available from CGC http://www.cgc.cbs.umn.edu/).
4. M9 buffer: 2.2 mM KH_2PO_4, 4.2 mM Na_2HPO_4, 85.6 mM NaCl, 1 mM $MgSO_4$, pH 6.5 (does not need to be adjusted).

2.3 Worm Microinjection

1. Inverted DIC microscope (such as Axiovert from Zeiss, with a free-sliding stage with centered rotation) equipped with 10× and 40× objectives, micromanipulator (Luigs and Neumann/Narishige/Zeiss), and microinjecting device with needle holder (Eppendorf Femtojet/Narishige).
2. Needle puller (Sutter Instrument).
3. Microcapillary loading tips (Microloaders, Eppendorf).
4. Needle-breaking device: A microcapillary glued onto 24×60 mm glass cover slip and covered with mineral oil.
5. Heavy mineral oil (Sigma-Aldrich).
6. Injection pads: 24×60 mm glass cover slips with dried drops of 0.8 % agarose in water.
7. Pulled borosilicate glass capillaries with filaments (injection needles): We use capillaries from World Precision Instruments (1B120F-4, outer/inner diameter 1.2/0.68 mm, length 100 mm).

2.4 Microscopy

1. Microscope objective slides, cover slips.
2. Agarose pads for microscopy of worms or embryos (prepared freshly): 2 % Agarose in water is melted, and a drop of it is put on the objective slide. Flatten the agarose immediately with a second slide. Remove the second slide just before use.
3. Levamisole (Tetramisole hydrochloride, Sigma) 10 mM solution in M9.
4. We also had good experiences using polystyrene beads to immobilize the worms, although this method asks for 10 % agarose pads that need to be prepared in advance [14].
5. Confocal laser scanning microscope/multiphoton/spinning disk confocal microscope/epifluorescent microscope equipped with deconvolution software.
6. Image analysis and procession software (either the software packages at the confocal microscope workstation or freeware such as ImageJ http://rsbweb.nih.gov/ij/).

2.5 C. elegans strains

1. Many strains are available from *C. elegans* Genetics Center (CGC) at low cost. Check http://www.cgc.cbs.umn.edu/ for availability.
2. Also check the National Bioresource Project for the nematode http://www.shigen.nig.ac.jp/c.elegans/index.jsp.
3. Otherwise contact the researchers who produced the strain you need. The *C. elegans* research community has traditionally maintained high ethical standards in dissemination of materials.

3 Methods

3.1 Candidate Gene Approach

RNAi is a method of reverse genetics. That is, you move from a gene towards its function. Consider the following points when using the so-called candidate gene approach. The candidate gene approach, in a context of RNAi in *C. elegans*, can be defined as the study of the influence of a gene downregulation on a certain biological process, such as membrane traffic in our case.

1. The trafficking defects that you are aiming to observe should be relatively easy and unambiguously scored. For example, if you can score a phenotype using just a fluorescent binocular, viewing worms on plate, and spending only seconds or minutes for each RNAi experiment, you can easily go for a high-throughput screen (and forget about the candidate approach). If, however, you are only able to detect a desired phenotype (for instance cytokinesis failure or change in the behavior of a membrane organelle) by spending hours cutting worms and making movies at the microscope, then the number of your candidates is quite limited.
2. Each tissue in *C. elegans* has certain advantages and disadvantages in respect of RNAi (*see* Subheading 3.2). When picking up a candidate gene, try to get a clue about its expression pattern. This can be found in the following databases: http://www.wormbase.org, http://nematode.lab.nig.ac.jp, and http://elegans.bcgsc.bc.ca/home/. Naturally, the function of a gene in membrane traffic should be studied only in tissues where it is expressed.
3. A candidate gene may have homologs (paralogs) in the *C. elegans* genome. It is helpful if it also has homologs in other model organisms and something is known about their functions. Not always a *C. elegans* protein functions in the same pathway as its closest yeast or mammalian counterpart [5]. Therefore, all *C. elegans* paralogs should be tested.

3.2 Choosing the Tissue in Which to Study the Phenotype of a Gene Knockdown

3.2.1 Germline

RNAi has the fastest and generally strongest effect in oocytes and early embryos by injection of dsRNA into hermaphrodites or by feeding *E. coli* expressing dsRNA. The oocytes and early blastomeres are ideally suited for imaging many trafficking events, since they are the biggest cells in the worm. The fast embryonic divisions facilitate monitoring membrane-bound organelle behavior linked to the cell cycle. A downside of this system is the phenomenon of germline silencing of extrachromosomal reporter arrays. The integrated arrays, which are not silenced, are more difficult to produce. Thus, there are only a few markers available so far. However, this will change in the near future.

Grant and Hirsh [10] established the oocyte as a model to study the receptor-mediated endocytosis in *C. elegans* and screened

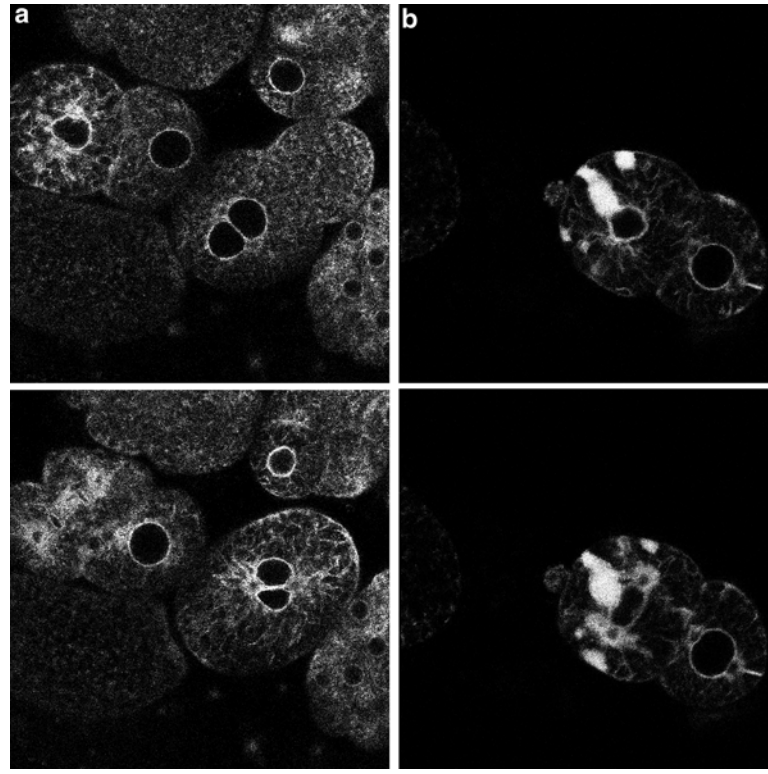

Fig. 1 The dynamics of ER during embryonic cell divisions in *C. elegans*. Time-lapse confocal microscopy of RNAi-treated GFP::SP12-expressing embryos. During the prophase and metaphase of mitosis, ER forms "sheets" which disappear during late anaphase/telophase. Each division this cycle is repeated. A Cdc48/p97 homolog is required for ER transitions. (**a**) Control RNAi. The simultaneous RNAi of two Cdc48 homologs C41C4.8 and C06A1.1 resulted in the wild-type ER behavior during early cell division and does not interfere with ER cycling. (**b**) Knockdown by RNAi of the third Cdc48 homologue (K04G2.3) causes the ER to collapse. Reproduced modified with permission from [5]

for novel genes involved in this process. They used the GFP fused to yolk protein, which is synthesized in the gut of the adult hermaphrodites and taken up by maturing oocytes, to dissect the endocytic pathway. We studied cell cycle-linked dynamics of the endoplasmic reticulum (ER) in early embryo using the ER marker SP12::GFP [5] (Fig. 1). RNAi was the main method to show the involvement of several proteins in rapid change of ER morphology. Oocytes and early embryos are the only cells in which one can study the effects of RNAi if it leads to embryonic lethality.

The germline is also amenable to EM analysis because of the possibility to dissect and fix gonads [15]. Intracellular structures and vesicles can be observed, and specific factors can be localized by immuno-EM [16, 17].

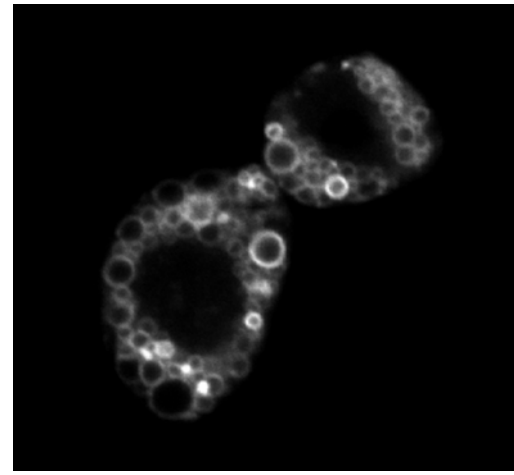

Fig. 2 A pair of coelomocytes displaying GFP::RAB-7 on the membranes of late endosomes. Live imaging in the anesthetized worm. Scale bar, 10 μm

3.2.2 Coelomocytes

Coelomocytes are six specialized scavenger cells residing in the body cavity (pseudocoelom), which are highly active in fluid-phase endocytosis. Coelomocytes have become a focus of endocytic transport research because of several advantages: their endocytic compartments are unusually big, making them easy to image (Fig. 2); transgenic animals with reporters under coelomocyte-specific promoters are easy to make; endocytic tracers are readily taken up from the body cavity. Delivery methods of the endocytic tracers to the body cavity include direct microinjection or secretion of a fluorescent reporter protein (such as soluble GFP) by muscle cells [8].

There is no need to dissect the worm for imaging of coelomocytes. In most cases, the animals are just immobilized by levamisole and put on a slide with an agarose pad.

The effects of RNAi in coelomocytes are seen in the F_1 progeny of the animals exposed to dsRNA (regardless of delivery method). Several endocytosis-related genes have proven to be difficult to RNAi in coelomocytes compared to germline. We recommend microinjection of dsRNA, since especially for coelomocytes, this method is most effective. The biggest collection of endocytic effectors and pathway markers is available for the coelomocytes. Coelomocytes are suited for knockdown of the genes, which are not essential for viability.

3.2.3 Hypodermal Epithelium

The epithelium is a favored model to study the intracellular membrane transport in polarized cells. *C. elegans* provides an in vivo model to elucidate the mechanisms involved in apical exocytosis. For instance, Liegeois and co-workers have chosen to analyze apical secretion of cuticle proteins by the epidermis [12]. The cuticle includes glycosylated collagens, glycosyl phosphatidylinositol-linked

cuticlins, and lipid-modified Hedgehog-related peptides. The abnormal cuticle, therefore, may result from defects of secretion from the epithelium. This phenotype can be used as a readout in RNAi screens and would be suitable for a high-throughput approach.

3.2.4 Intestine

The worm intestine consists of large epithelial cells, which, in addition to the digestive function, serves as storage depot for the worm. Furthermore, the intestine regulates the fluid balance in the body and synthesizes and secretes the yolk for the oocytes. Naturally, secretion, endocytosis, and transcytosis are very important for the function of the intestine. Several laboratories successfully used RNAi to target the traffic-related genes in the intestine (*see* **Note 4**), some on a genome-wide scale.

Targeting the traffic-related genes by RNAi results in several easily distinguishable phenotypes in the gut, such as failure of yolk secretion from the gut, which will appear as Rme (receptor-mediated endocytosis defective) phenotype, defects in transport of apical and/or basolateral fluid-phase markers [10, 18], and vacuolization of the gut (Fig. 3).

Intestinal cells provide also an easy target to RNAi. In the intestine, RNAi by feeding is as efficient as RNAi by microinjection. The effects can be frequently seen in the P_0 generation. A number of fluorescent protein reporters are available, and the intestine is easily accessible to small fluorescent dyes, which can be delivered by feeding.

3.2.5 Muscles

Several aspects of membrane organelle behavior and transport have been studied in *C. elegans* muscles, employing a number of markers under muscle-specific promoters (Table 2). Muscle cells are easy to target for RNAi by any methods. However, RNAi as a method to interfere with the membrane transport in this tissue have not been used yet.

3.2.6 Neurons

Neurons are notoriously difficult to RNAi. In the generic wild-type strain (Bristol N2), the majority of neuronal genes known to have uncoordinated phenotypes when mutated are impossible to knock down by RNAi. This can be overcome by using a mutant hypersensitive to RNAi, such as *rrf-3*. Alternatively, overexpression of SID-1 improves sensitivity to dsRNA in neurons by improving the passive uptake of dsRNA [19]. However, most of these strains have other defects and should be used with caution. Usually, *C. elegans* researchers rely on genetic mutants to study intracellular transport in neurons.

3.3 Telltale Signs of RNAi Phenotypes Having Trafficking Defects

There are several classes of phenotypes, which are frequently associated with defects in secretory or endocytic pathways (besides sterility and embryonic/larval lethality, which are not specific at all). They are easy to spot, often already with the dissecting binocular. These phenotypes may help you in the initial extensive analysis of the RNAi experiments (Table 1).

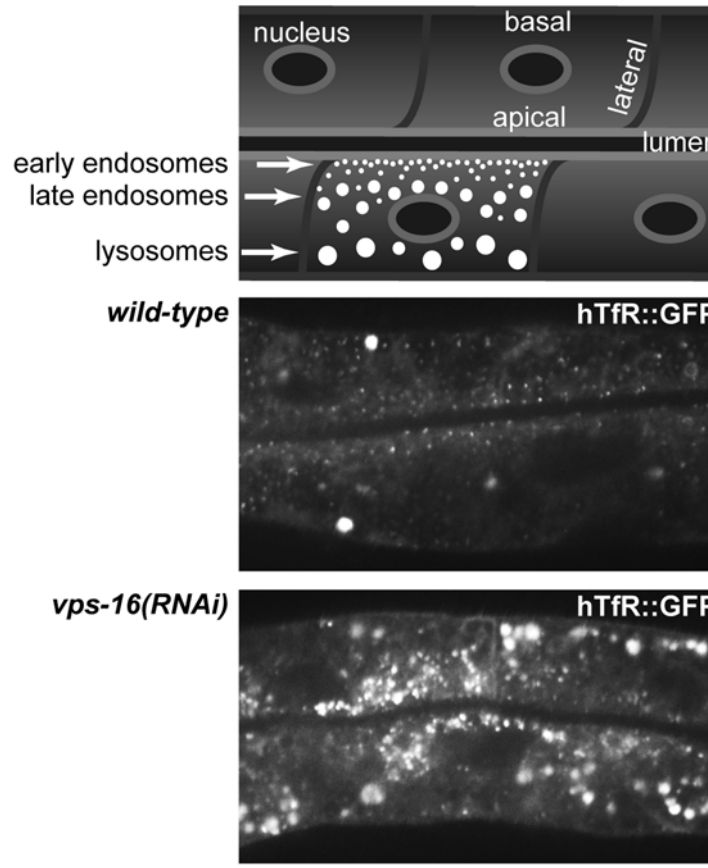

Fig. 3 Endosomal pathway in intestinal epithelial cells in *C. elegans*. Live imaging of wild-type and RNAi worms showing dramatic changes in the endosomal pathway upon knockdown of CORVET and HOPS tethering complexes (subunit VPS-16). The fluorescence marker shown is human transferrin receptor (hTfR) fused to GFP [11] that labels recycling endosomes as well as the degradative pathway leading to lysosomes. The downregulation of endosomal tethers CORVET and HOPS leads to accumulation of early endosomes near the lumen and late endosomes/lysosomes at the basal side of the cells

3.4 RNAi by Injection and Observation of Phenotype in Early Embryos Using Confocal Microscopy

3.4.1 dsRNA Preparation

Use a PCR fragment of the gene of interest as a template for dsRNA synthesis. Choose a fragment that corresponds to a coding segment of a gene. The length can be from 200 to 1,000 bp. Within this range, longer fragments may target mRNA more efficiently. The source of DNA for PCR amplification may be either the total genomic DNA, cDNA, individual cosmid, or plasmid clones. Order forward and reverse primers that contain the T7 RNA polymerase promoters at their 5′-end. Thus, both sense and antisense strands are transcribed and anneal to each other yielding a dsRNA. Treat the transcription reaction product with phenol–chloroform and precipitate with isopropanol. Remove DNA template by DNase digestion (*see* **Note 5**). Dissolve dsRNA in TE buffer. The typical

concentration range is 1–5 μg/μL. RNAi of essential genes involved in the secretion pathway often lead to sterility. Therefore, the dsRNA concentration must be gradually reduced down to 0.2 μg/μL to observe phenotypes in early embryos [5]. To target two or more genes simultaneously, mix the dsRNAs in equal proportion. Beware that the efficiency of knockdown may be reduced compared to the efficiency of targeting each gene individually [20].

3.4.2 Preparing Needles for Injection

Load the injection needle with 2 μL of dsRNA solution using microloader tips. Insert the needle into the holder, and supply pressure to the injection system. Position the needle in the center of view (10× objective). Withdraw the needle, put the needle breaking device, and focus at the lateral side of the microcapillary. Bring the injection needle in focus again, and move close to the breaking capillary at a sharp angle. Use the sliding stage or the micromanipulator to touch slightly the capillary with the tip of the needle. Push "inject" button immediately. The flow of liquid should be visible. If not, repeat breaking. If the opening is too small, the needle will not work and clog immediately in the worm. If the opening is too big, your worms will die because of the big holes in their bodies.

3.4.3 Worm Mounting

Scoop 1–5 worms from the feeding plate with a wormpick, and transfer them on the injection pad in a drop of injection oil. The worms should stick to the dry agarose. The number of animals to inject depends on your experience. To prevent the fatal dehydration of the worms, the time between sticking them on the pad and rehydrating after injection should be within 2–3 min.

3.4.4 Injection

Focus on the worms with 10× objective. Switch to 40× objective, and bring the needle in the worm proximity. With a swift movement (best achieved by manually sliding the stage) insert the needle into the worm. For RNAi, the exact location of the needle is not critical. Try to hit the distal gonadal arm, gut, or body cavity. Avoid hitting the head. Push inject button. The injected part of the worm should be visibly inflating. Take the needle out, push the "clean/flush" button to partially rehydrate the injected worm, and clean the needle itself. Proceed to the next worm on the same pad or move back to the dissecting binocular for worm recovery.

3.4.5 Recovery

Allow animals to rehydrate after injection for 10 min by adding a drop of M9 buffer on the pad. Transfer animals with a mouth pipet to NGM agar plates with an OP50 lawn.

For RNAi in the, e.g., SP12:GFP strain, inject a suitable number of L4 larvae or young hermaphrodites with dsRNAi at 1 mg/mL in injection buffer. For a single experiment the number of animals surviving the injection should be at least 10–20.

Allow the effect of RNAi to develop overnight. The earliest time point at which the animals can be analyzed is 14–16 h post-injection. Sometimes 24 h is needed for the full effect of RNAi to take place.

3.4.6 Preparing Specimens for Microscopy

Inspect the animals: the hermaphrodites should be alive, should respond to touch, and should not spill guts. For imaging oocytes and embryos in utero, transfer worms to the object slide with an agarose pad in a drop (10 μL) of 10 mM levamisole. Levamisole is used to immobilize and anesthetize the worms without killing them. Cover the specimen with a cover slip, which has a thin layer of Vaseline spread on the edges. This provides the sealing and shields the worms from excessive pressure.

To image single embryos, transfer the hermaphrodites to a drop of M9 with levamisole in an hourglass. Using fine hypodermic needles (26G) as scissors, cut the worms open. The levamisole causes muscle contraction, thus helping to expel eggs from the uterus. Transfer the eggs to the agarose pads with a mouth pipet. You can also take the cut worms along; the last embryos will be released from the uterus on slide. Seal the slide as above.

The confocal microscope should be on and running before you prepare your specimen. Some gene knockdowns lead to a permeable eggshell and osmotic sensitivity. This greatly reduces the time window for your experiment. Use your wild-type worms expressing the same fluorescent marker to figure out the best settings and parameters for imaging.

The "trouble" of keeping the worms alive and intact can be avoided by using fixation and antibody staining (many fluorescent proteins can also be imaged well after fixation without having to use antibodies) [21]. The negative aspect of this method is that sometimes vesicular structures and membranes are changed or disrupted by the fixation procedure.

3.4.7 Imaging

Locate the worms or the embryos with low magnification objective (10 or 20×) using transmitted light. For imaging with laser use the oil-immersion 63× NA 1.32 objective (or similar). Adjust the imaging parameters so that they do not interfere with embryonic viability within the time frame of the experiment (*see* **Note 6**). When imaging the dynamics of an organelle, such as ER in oocytes/early embryos, the optimal imaging parameters are critical for the interpretation of a phenotype.

Time between frames in time-lapse recording. This should be below 20 s. Ideally, the scan should last for about 1 s, but this is only possible with multiphoton custom-built microscopes or with spinning disk confocal microscopes. With a conventional confocal microscope, too short intervals between scans can also lead to excessive photobleaching of fluorophores and photodamage of the cell.

Scan average. The imaging of fine membrane structures like ER in the early embryo (Fig. 1) requires substantial averaging of the scans to improve the signal-to-noise ratio. Because of the rapid dynamics of ER, certain restrictions apply. Use line average instead of frame average in the scan mode. The number of average should not increase 8 per line.

Use the highest frame resolution (normally $1{,}024 \times 1{,}024$ or $1{,}024 \times 512$ pixels).

Photomultiplier (PMT) gain and offset. Increasing the PMT gain can improve your specimen viability and reduce photobleaching, since lesser laser power is required. Offset increase helps to reduce background and unfocused fluorescence. For representative SP12::GFP imaging the gain and offset are pulled almost to the maximum (*see also* [22] for a description of time-lapse microscopy with *C. elegans*).

3.4.8 Post-filming Image Procession

As a golden rule, try to optimize the imaging parameters, such as PMT gain and offset and scan average during imaging, rather than trying to improve the poor-quality images by graphic software. Linear and especially nonlinear filters should be applied with caution such as not to obscure or misrepresent the original information. Confocal images often benefit from the use of a sharpening filter. Gaussian blur is eliminating the random pixel noise and sometimes helpful to better represent continuous structures, such as ER sheets. All manipulations of the original image should be clearly indicated when reporting the experimental conditions. The details of confocal images postproduction can be found in [23].

4 Notes

1. One caveat of using a bacterial feeding library for RNAi on a genome-wide scale is that a significant number of clones are missing, contain empty insert, or cannot be re-grown upon delivery of the library. Thus, the total loss can be up to 24 % [24]. If you plan to use individual clones from the library, always confirm the presence of a correct insert by PCR and sequencing of a plasmid. We routinely do bacterial colony PCRs with T7 primers for controls.
2. The knockout technology in *C. elegans* is based upon isolation of random deletions. Often, the produced alleles eliminate only a portion of the gene target or that are in frame with the coding sequence. Without further evidence, such alleles must be presumed to retain some function. If a knockout allele is maternal embryonic lethal, it precludes the study of the corresponding gene function at later developmental stages. By varying the strength of RNAi it is possible to

circumvent this problem. If a gene of interest has a paralog whose function is redundant, RNAi may frequently target both genes simultaneously (providing that there is a stretch of about 100 nucleotides with 80 % identity). In the knockout strain, in which only one of the paralogs is deleted, the other may compensate for the biological function.

3. The main problem of the delivery of a fluorescent dye to the embryos is the impermeable eggshell. Therefore, it must be punctured with a laser pulse, making the embryo accessible to a dye in the bathing solution. Somatic tissues can be accessed if a dye is fed to the animal or injected into the body cavity [25].
4. Hermann and co-workers [26] have proposed the gut granules as model system for understanding the formation of specialized, lysosome-related organelles, such as melanosomes and platelet granules in mammals. The gut granules could provide a simple model for several congenital lysosome-related organelle disorders in humans.
5. DNase treatment is not absolutely necessary but facilitates the transcription product analysis by gel electrophoresis.
6. A sudden embryonic arrest during image acquisition always raises a red flag. Check if this happens as well in RNAi-treated embryos using the same dsRNA during the transmitted light imaging. If this is not the case, you have induced an arrest due to photodamage. Lower the laser strength, acquisition time, and frequency. Normally it should be possible to image the embryos with the confocal microscope for more than 1 h without apparent damage. The following parameters work well for us: argon laser (488 nm) at 25 % power, time lapse recording with 20s-intervals, and scan duration 10 s. It is a good idea to image the wild-type or control RNAi-treated embryos with the same parameters and leave them on slide overnight. If you see that embryos progressed in development or even hatched the next day, your experimental conditions are optimal.
7. The strain expressing secreted soluble GFP under heat shock-inducible promoter is used as a tool to probe the lysosomal degradation pathway in coelomocytes. During an in vivo pulse-chase experiment, the worms are shifted to 33 °C for 30 min and then returned to ambient temperature (20–25 °C). The heat shock at 33 °C results in the secretion of a finite pulse of GFP into the pseudocoelom. The fate of the GFP can then be followed as a function of time. If the pathway to the lysosome or the lysosomal function is compromised, the GFP fails to be degraded (or is degraded much slower) in the coelomocytes. In the wild type, no GFP is detected after 24 h post-heat shock [27].

Acknowledgements

Protocols were based on many works published by members of the worm research community. We apologize for any omissions in reference. We would like to acknowledge funding by the Biozentrum of the University of Basel and the Swiss National Science Foundation.

References

1. Dickinson DJ, Ward JD, Reiner DJ, Goldstein B (2013) Engineering the Caenorhabditis elegans genome using Cas9-triggered homologous recombination. Nat Methods 10:1028–1034
2. Robert VJP (2012) Engineering the *Caenorhabditis elegans* genome by Mos1-induced transgene-instructed gene conversion. Methods Mol Biol 859:189–201
3. Timmons L (2006) Delivery methods for RNA interference in *C. elegans*. Methods Mol Biol 351:119–125
4. Ohkumo T, Masutani C, Eki T, Hanaoka F (2008) Use of RNAi in *C. elegans*. Methods Mol Biol 442:129–137
5. Poteryaev D, Squirrell JM, Campbell JM, White JG, Spang A (2005) Involvement of the actin cytoskeleton and homotypic membrane fusion in ER dynamics in *Caenorhabditis elegans*. Mol Biol Cell 16:2139–2153
6. Lehner BB, Tischler JJ, Fraser AGA (2005) RNAi screens in *Caenorhabditis elegans* in a 96-well liquid format and their application to the systematic identification of genetic interactions. CORD Conf Proc 1:1617–1620
7. Isik M, Berezikov E (2013) Biolistic transformation of *Caenorhabditis elegans*. Methods Mol Biol 940:77–86
8. Fares H, Grant B (2002) Deciphering endocytosis in *Caenorhabditis elegans*. Traffic 3:11–19
9. Koushika SP, Nonet ML (2000) Sorting and transport in C. elegans: a model system with a sequenced genome. Curr Opin Cell Biol 12:517–523
10. Grant B, Hirsh D (1999) Receptor-mediated endocytosis in the Caenorhabditis elegans oocyte. Mol Biol Cell 10:4311–4326
11. Chen C-H, Schweinsberg PJ, Vashist S, Mareiniss DP, Lambie EJ, Grant BD (2006) RAB-10 is required for endocytic recycling in the *Caenorhabditis elegans* intestine. Mol Biol Cell 17:1286–1297
12. Liégeois S, Benedetto A, Garnier J-M, Schwab Y, Labouesse M (2006) The V0-ATPase mediates apical secretion of exosomes containing Hedgehog-related proteins in *Caenorhabditis elegans*. J Cell Biol 173:949–961
13. Skop AR, Bergmann D, Mohler WA, White JG (2001) Completion of cytokinesis in *C. elegans* requires a brefeldin A-sensitive membrane accumulation at the cleavage furrow apex. Curr Biol 11:735–746
14. Kim E, Sun L, Gabel CV, Fang-Yen C (2013) Long-term imaging of *Caenorhabditis elegans* using nanoparticle-mediated immobilization. PLoS One 8:e53419
15. Ackema KB, Sauder U, Solinger JA, Spang A (2013) The ArfGEF GBF-1 is required for ER structure, secretion and endocytic transport in *C. elegans*. PLoS ONE 8:e67076
16. Paupard MC, Miller A, Grant B, Hirsh D, Hall DH (2001) Immuno-EM localization of GFP-tagged yolk proteins in C. elegans using microwave fixation. J Histochem Cytochem 49:949–956
17. Witte K, Schuh AL, Hegermann J et al (2011) TFG-1 function in protein secretion and oncogenesis. Nat Cell Biol 13:550–558
18. Grant B, Zhang Y, Paupard MC, Lin SX, Hall DH, Hirsh D (2001) Evidence that RME-1, a conserved *C. elegans* EH-domain protein, functions in endocytic recycling. Nat Cell Biol 3:573–579
19. Calixto A, Chelur D, Topalidou I, Chen X, Chalfie M (2010) Enhanced neuronal RNAi in *C. elegans* using SID-1. Nat Methods 7: 554–559
20. Ahringer J (2006) Reverse genetics. WormBook.1.47.1
21. O'Connell KF, Golden A (2014) Confocal imaging of the microtubule cytoskeleton in *C. elegans* embryos and germ cells. Methods Mol Biol 1075:257–272

22. Boyd L, Hajjar C, O'Connell K (2011) Time-lapse microscopy of early embryogenesis in *Caenorhabditis elegans*. J Vis Exp. doi:10.3791/2852
23. Halder G, Paddock SW (1999) Presentation of confocal images. Methods Mol Biol 122: 373–384
24. Lamitina T (2006) Functional genomic approaches in *C. elegans*. Methods Mol Biol 35:127–138
25. Hutter H (2006) Fluorescent reporter methods. Methods Mol Biol 351:155–173
26. Hermann GJ, Schroeder LK, Hieb CA et al (2005) Genetic analysis of lysosomal trafficking in *Caenorhabditis elegans*. Mol Biol Cell 16: 3273–3288
27. Fares H, Greenwald I (2001) Regulation of endocytosis by CUP-5, the *Caenorhabditis elegans* mucolipin-1 homolog. Nat Genet 28: 64–68
28. Frand AR, Russel S, Ruvkun G (2005) Functional genomic analysis of C. elegans molting. PLoS Biol 3:e312
29. Nicot A-S, Fares H, Payrastre B et al (2006) The phosphoinositide kinase PIKfyve/Fab1p regulates terminal lysosome maturation in *Caenorhabditis elegans*. Mol Biol Cell 17: 3062–3074
30. Fares H, Greenwald I (2001) Genetic analysis of endocytosis in *Caenorhabditis elegans*: coelomocyte uptake defective mutants. Genetics 159: 133–145
31. Rappleye CA, Paredez AR, Smith CW, McDonald KL, Aroian RV (1999) The coronin-like protein POD-1 is required for anterior-posterior axis formation and cellular architecture in the nematode *Caenorhabditis elegans*. Genes Dev 13:2838–2851
32. Poteryaev D, Spang A (2005) A role of SAND-family proteins in endocytosis. Biochem Soc Trans 33:606–608
33. Audhya A, Hyndman F, McLeod IX et al (2005) A complex containing the Sm protein CAR-1 and the RNA helicase CGH-1 is required for embryonic cytokinesis in *Caenorhabditis elegans*. J Cell Biol 171:267–279
34. Sato K, Sato M, Audhya A, Oegema K, Schweinsberg P, Grant BD (2006) Dynamic regulation of caveolin-1 trafficking in the germ line and embryo of *Caenorhabditis elegans*. Mol Biol Cell 17:3085–3094
35. Sato M, Sato K, Liou W, Pant S, Harada A, Grant BD (2008) Regulation of endocytic recycling by *C. elegans* Rab35 and its regulator RME-4, a coated-pit protein. EMBO J 27: 1183–1196
36. Franz C, Askjaer P, Antonin W et al (2005) Nup155 regulates nuclear envelope and nuclear pore complex formation in nematodes and vertebrates. EMBO J 24:3519–3531
37. Kimura K, Kimura A (2012) Rab6 is required for the exocytosis of cortical granules and the recruitment of separase to the granules during the oocyte-to-embryo transition in *Caenorhabditis elegans*. J Cell Sci 125:5897–5905
38. Patton A, Knuth S, Schaheen B, Dang H, Greenwald I, Fares H (2005) Endocytosis function of a ligand-gated ion channel homolog in *Caenorhabditis elegans*. Curr Biol 15: 1045–1050
39. Zhang Y, Grant B, Hirsh D (2001) RME-8, a conserved J-domain protein, is required for endocytosis in *Caenorhabditis elegans*. Mol Biol Cell 12:2011–2021
40. Treusch S, Knuth S, Slaugenhaupt SA, Goldin E, Grant BD, Fares H (2004) *Caenorhabditis elegans* functional orthologue of human protein h-mucolipin-1 is required for lysosome biogenesis. Proc Natl Acad Sci U S A 101: 4483–4488
41. Dang H, Li Z, Skolnik EY, Fares H (2004) Disease-related myotubularins function in endocytic traffic in *Caenorhabditis elegans*. Mol Biol Cell 15:189–196
42. Sato K, Ernstrom GG, Watanabe S et al (2009) Differential requirements for clathrin in receptor-mediated endocytosis and maintenance of synaptic vesicle pools. Proc Natl Acad Sci U S A 106:1139–1144
43. Shi A, Pant S, Balklava Z, Chen CC-H, Figueroa V, Grant BD (2007) A novel requirement for C. elegans Alix/ALX-1 in RME-1-mediated membrane transport. Curr Biol 17: 1913–1924
44. Shi A, Liu O, Koenig S, Banerjee R, Chen CC-H, Eimer S, Grant BD (2012) RAB-10-GTPase-mediated regulation of endosomal phosphatidylinositol-4,5-bisphosphate. Proc Natl Acad Sci U S A 109:2306–2315
45. Shi A, Chen CC-H, Banerjee R et al (2010) EHBP-1 functions with RAB-10 during endocytic recycling in *Caenorhabditis elegans*. Mol Biol Cell 21:2930–2943
46. Mahoney TR, Liu Q, Itoh T et al (2006) Regulation of synaptic transmission by RAB-3 and RAB-27 in *Caenorhabditis elegans*. Mol Biol Cell 17:2617–2625
47. Kubota Y, Sano M, Goda S, Suzuki N, Nishiwaki K (2006) The conserved oligomeric Golgi complex acts in organ morphogenesis via glycosylation of an ADAM protease in *C. elegans*. Development 133:263–273

48. Labrousse AM, Zappaterra MD, Rube DA, van der Bliek AM (1999) *C. elegans* dynamin-related protein DRP-1 controls severing of the mitochondrial outer membrane. Mol Cell 4: 815–826
49. Li Z, Lu N, He X, Zhou Z (2013) Monitoring the clearance of apoptotic and necrotic cells in the nematode *Caenorhabditis elegans*. Methods Mol Biol 1004:183–202
50. Chen D, Jian Y, Liu X et al (2013) Clathrin and AP2 are required for phagocytic receptor-mediated apoptotic cell clearance in *Caenorhabditis elegans*. PLoS Genet 9:e1003517
51. Kinchen JM, Doukoumetzidis K, Almendinger J et al (2008) A pathway for phagosome maturation during engulfment of apoptotic cells. Nat Cell Biol 10:556–566
52. Huang J, Wang H, Chen Y, Wang X, Zhang H (2012) Residual body removal during spermatogenesis in *C. elegans* requires genes that mediate cell corpse clearance. Development 139:4613–4622
53. Lu N, Shen Q, Mahoney TR, Neukomm LJ, Wang Y, Zhou Z (2012) Two PI 3-kinases and one PI 3-phosphatase together establish the cyclic waves of phagosomal PtdIns(3)P critical for the degradation of apoptotic cells. PLoS Biol 10:e1001245
54. Guo P, Hu T, Zhang J, Jiang S, Wang X (2010) Sequential action of *Caenorhabditis elegans* Rab GTPases regulates phagolysosome formation during apoptotic cell degradation. Proc Natl Acad Sci U S A 107:18016–18021
55. Pant S, Sharma M, Patel K, Caplan S, Carr CM, Grant BD (2009) AMPH-1/Amphiphysin/Bin1 functions with RME-1/Ehd1 in endocytic recycling. Nat Cell Biol 11:1399–1410
56. Roudier N, Lefebvre C, Legouis R (2005) CeVPS-27 is an endosomal protein required for the molting and the endocytic trafficking of the low-density lipoprotein receptor-related protein 1 in *Caenorhabditis elegans*. Traffic 6:695–705
57. Chen D, Xiao H, Zhang K (2010) Retromer is required for apoptotic cell clearance by phagocytic receptor recycling. Science 327: 1261–1264
58. Meléndez A, Tallóczy Z, Seaman M, Eskelinen E-L, Hall DH, Levine B (2003) Autophagy genes are essential for dauer development and life-span extension in *C. elegans*. Science 301: 1387–1391
59. Larsen MK, Tuck S, Faergeman NJ, Knudsen J (2006) MAA-1, a novel acyl-CoA-binding protein involved in endosomal vesicle transport in *Caenorhabditis elegans*. Mol Biol Cell 17: 4318–4329
60. Nakae I, Fujino T, Kobayashi T et al (2010) The arf-like GTPase Arl8 mediates delivery of endocytosed macromolecules to lysosomes in *Caenorhabditis elegans*. Mol Biol Cell 21: 2434–2442
61. Matyash V, Geier C, Henske A et al (2001) Distribution and transport of cholesterol in *Caenorhabditis elegans*. Mol Biol Cell 12: 1725–1736

Chapter 24

Visualization of Clathrin-Mediated Endocytosis in Live *Drosophila* Egg Chambers

Anupma Jha and Linton M. Traub

Abstract

In oviparous animals, clathrin-dependent endocytosis is often critical to stockpile a necessary supply of yolk within the maturing oocyte, which enables subsequent embryonic development. In the physically linked chains of maturing egg chambers within the *Drosophila melanogaster* ovary, a distinct, morphologically discernable subset undergoes a massive burst clathrin-mediated endocytosis to accumulate yolk in a process termed vitellogenesis. Here, we describe how to prepare isolated ovaries to follow endocytosis, and detail approaches to follow live uptake of soluble reporters into vitellogenic *Drosophila* egg chambers.

Key words *Drosophila melanogaster*, Oocyte, Endocytosis, Receptor, Clathrin, Yolk, Vesicle, Vitellogeneisis

1 Introduction

Clathrin-mediated endocytosis is an evolutionarily ancient mechanism to convey selected transmembrane proteins and surface constituents into the interior of eukaryotic cells within small membrane-bound vesicles. The process occurs in both unicellular and multicellular organisms and operates on a time scale of seconds to minutes [1]. Although mostly studied in isolated or cultured adherent cells [1–3], clathrin-mediated endocytosis can be effectively followed in intact plants [4] or animals [5, 6], as well as in whole organs or individual tissues [7]. One suitable and experimentally tractable whole organ to follow clathrin function is the ovary of dipteran insects. In fact, the seminal conceptualization of clathrin-mediated endocytosis as a mechanism of selective vesicle-mediated transport from the cell surface came from careful ultrastructural analysis of blood-fed mosquito egg chambers [8]. The fruit fly *Drosophila melanogaster* utilizes a similar, although not identical, clathrin-mediated uptake process during egg maturation within the ovary. The object is to stock each maturing egg chamber

Andrei I. Ivanov (ed.), *Exocytosis and Endocytosis*, Methods in Molecular Biology, vol. 1174,
DOI 10.1007/978-1-4939-0944-5_24,

with a reserve of yolk to support the proper development of the embryo following fertilization, before the organism can feed alone. One reason why this internalization process in *Drosophila* is well suited for experimental investigation is because a short but massive wave of endocytosis occurs over a restricted time window, between developmental stages 8 and 11 [9–11], which takes approximately 18 h [12]. In this chapter, we describe how to prepare *Drosophila* ovaries to follow the clathrin-mediated endocytosis of tracers into the oocyte [13].

2 Materials

2.1 Drosophila Culture and Dissection

1. Suitable stain(s) of *Drosophila melanogaster* (*see* **Note 1**).
2. Active dry yeast (*see* **Note 2**).
3. Thick glass microscope slides (25 × 75 × 1.5 mm) with either single or double well depression (Erie Scientific).
4. Dumont #5SF fine stainless steel forceps (World Precision Instruments) (*see* **Note 3**).
5. Mechanical micropipettes (Gilson Pipetman or equivalent).
6. Disposable petri (35 mm) dish.
7. Glass Pasteur pipettes.
8. Flystuff Flypad anesthesia apparatus (Genesee) connected to a carbon dioxide gas cylinder.
9. 1× phosphate buffered saline (PBS).
10. Schneider's Drosophila Medium (Invitrogen/Life Technologies).

2.2 Isolated Ovary Endocytosis Assays

1. Pre-prepared trypan blue solution (0.4 % in PBS).
2. Polypropylene 1.5 ml microfuge tubes.
3. Paraformaldehyde (4 %) prepared in PBS from a 16 % EM grade paraformaldehyde stock (Electron Microscopy Sciences).
4. Alexa Fluor 488 phalloidin (Invitrogen/Life Technologies).
5. Hoechst 33258 (bisbenzimide) DNA stain. A 10 mg/ml stock solution is prepared in DMSO and kept in the dark at 4 °C. The working stain is a 2 μg/ml solution of Hoechst 33258 in PBS.
6. The glutathione *S*-transferase (GST)—monomeric cherry red fluorescent protein (mcRFP)—*Drosophila* receptor associated protein (RAP) (designated GST-mcRFP-RAP) fusion protein, purified from *E. coli* as previously described [13]. The encoding plasmid is available from our laboratory upon request. The GST fusion protein is purified by standard affinity

chromatographic procedures using glutathione-Sepharose, and we have a parallel GST-mcRFP fusion protein as a similarly fluorescent negative control.

7. Regular (25 × 76 mm) precleaned glass microscope slides.

3 Methods

All dissection procedures are performed at room temperature unless specifically indicated otherwise.

3.1 Fly Preparation

1. One-to-two days before the planned dissection, supplement new fly medium containing vials with a small dollop of freshly prepared yeast paste (*see* **Note 4**) using a spatula.
2. Transfer sufficient recently eclosed adults of the appropriate strain or genotype of *Drosophila melanogaster* into yeast containing vials (*see* **Note 5**) and incubate at 26.5 °C until required. Both males and females are included in the vial.

3.2 Ovary Dissection

1. Anesthetize flies either using a carbon dioxide diffuser tray, such as the Flypad, or by placing the vial in a 4 °C refrigerator for a few minutes to immobilize the animals.
2. Place a 100–200 μl drop of either PBS or Schneider's Drosophila medium (*see* **Note 6**) at room temperature into the well of a glass slide positioned on the stage of a stereo dissecting microscope.
3. Select a female with a large distended abdomen. In yeasted vials, females are easily differentiated from males by the conspicuously swollen abdomen in addition to the characteristic difference in the abdominal stripe location and coloration (Fig. 1).
4. First, kill the chosen fly by removing and discarding the head with a pair of forceps.
5. Grasp the female, wings down and legs up, using one pair of Dumont #5SF forceps on the anterior abdomen, at a position just where the abdomen joins the thorax (Fig. 1) and transfer into the drop of PBS/Schneider's (*see* **Note 7**) under the stereo dissecting microscope.
6. Using another pair of Dumont #5SF forceps in your dominant hand, grasp the posterior-most region of the abdomen (Fig. 1) and gently pull away from the immobilized fly body (*see* **Note 8**). Under most circumstances, the last segment draws out tubular gut material that is discarded. Sometimes, the pair of ovaries neatly exits the abdomen with this first dissection step. If not, they can be carefully extracted with clean forceps or expelled by gently pressing on the abdomen from the anterior side and moving the forceps very slowly toward the posterior side.

Fig. 1 Handling positions for the dissection of *Drosophila* to isolate whole ovaries. Ventral (**a**) and lateral (**b**) views of a typical *Drosophila melanogaster* female, with the location of sites for placement of forceps indicated. The upside-down fly is initially grasped at the anterior side of the abdomen (*red arrows*). Once firmly restrained under the stereo dissecting microscope, the final posterior abdominal segment (*yellow arrow*) is clamped with forceps and gently separated from the body of the female

7. The isolated pair of ovaries looks somewhat reminiscent of bulbs of garlic (Fig. 2). Notice that the immature, anterior end, which contains the diminutive sausage-shaped germarium (housing the germ line and somatic stem cell compartments) and the early-stage egg chambers, has a transparent glassy appearance. These chambers are very small compared with the milky-white, opaque mature eggs at the posterior side of the ovary.
8. Minimize repeated contact between the forceps with the ovaries to avoid inadvertently damaging the chambers during handling.

3.3 Endocytosis Assays

3.3.1 Light Microscopy Assays

1. For trypan blue uptake experiments, a small drop of 0.4 % trypan blue in PBS (~100–200 μl) at room temperature is placed into a well depression on a glass slide.
2. Transfer the freshly dissected ovaries gently into the drop and incubate for 1–15 min at room temperature (*see* **Note 9**).

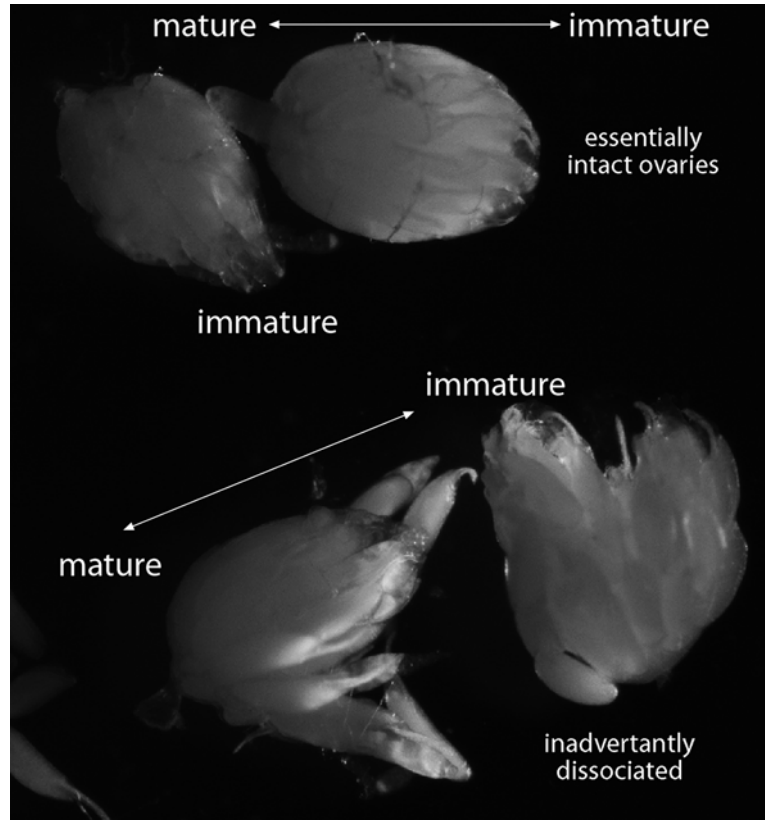

Fig. 2 Isolated *Drosophila* ovaries. Comparative images of a pair of largely intact ovaries versus a pair damaged during dissection, leading to separation of the ovarioles and release of individual egg chambers

3. At the appropriate time point, remove the ovaries and immediately transfer to a small, open-topped round container (for example, a 35 mm petri dish) containing ~1–2 ml PBS (*see* **Note 10**). Excess trypan blue can be effectively removed by gently swirling the dish.
4. Under the dissecting microscope, vitellogenic stage egg chambers in the washed preparations are identified by hemispherical or bullet-shaped blue stain accumulation at the posterior end (Fig. 3), which is the location of the germ line oocyte (*see* **Note 11**). Higher magnification views reveal time-dependent concentration of the dye first in small, cortical punctate structures (clathrin-coated vesicles and endosomes) and then, later, also in larger, more central organelles (maturing yolk granules) (*see* **Note 12**). In healthy egg chambers, neither the surrounding somatic follicle cells that ensheath the oocyte (*see* **Note 13**) nor the anterior 15 germ line nurse cells (Fig. 3b) should take up trypan blue (*see* **Note 14**).

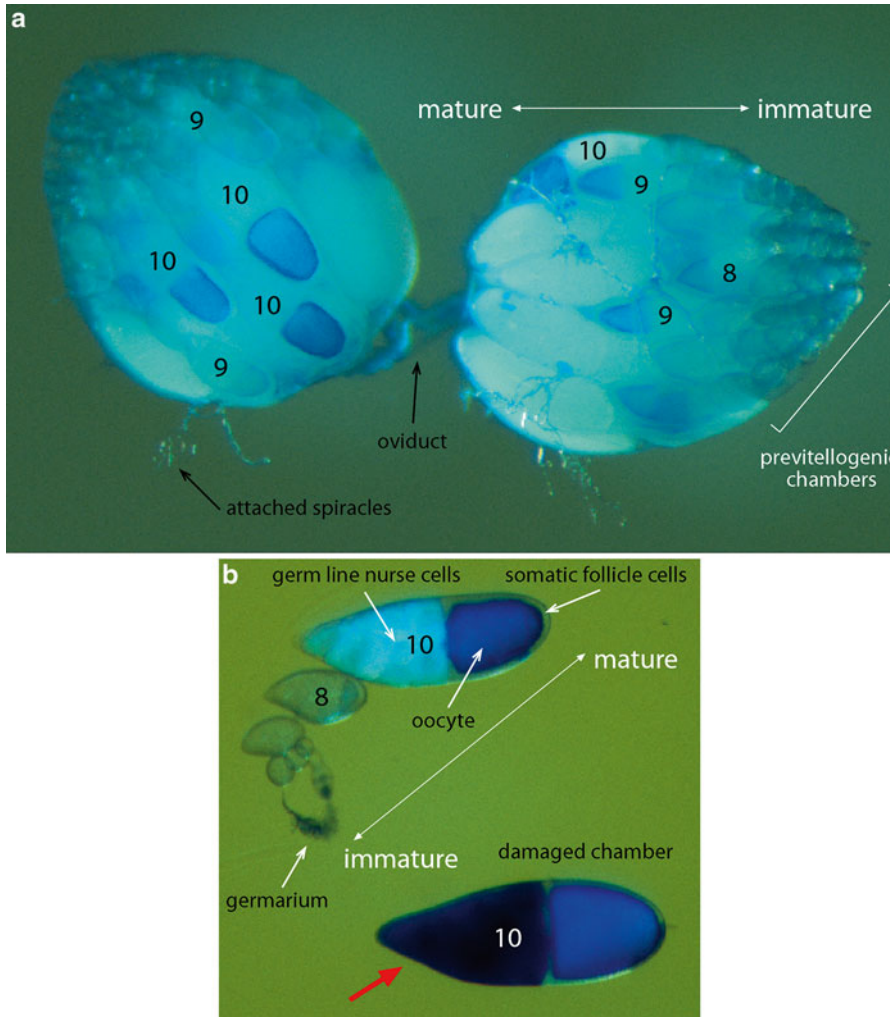

Fig. 3 Selective endocytic uptake of trypan blue by vitellogenic egg chambers. (**a**) Example of a pair of intact ovaries after the trypan blue internalization assay. Highly selective clathrin-mediated endocytosis into stage 8-to-stage 10 vitellogenic oocytes is evident. Notice the glassy previtellogenic egg chambers are considerably smaller. Developmental stages of selected egg chambers are indicated. (**b**) Higher magnification view of an individual ovariole also showing distinctive uptake of trypan blue into vitellogenic chambers. The specific localization of the germ line derived 15 nurse cells and the posterior oocyte, surrounded by a somatic epithelial sheet of follicle cells (*see* **Note 11**), is indicated. An example of a damaged stage 10 egg chamber, with intense trypan blue staining of the nurse cells, is indicated (*red arrow*)

3.3.2 Fluorescence Microscopy Assays

1. For internalization assays utilizing a soluble fluorescent endocytic tracer, we use purified recombinant GST-mcRFP-RAP (*see* **Note 15**).
2. Dissect the required *Drosophila* ovaries into a drop of Schneider's Drosophila medium. Carefully transfer intact ovaries to a 1.5 ml polypropylene microfuge tube containing ~1.5 ml Schneider's medium and keep on ice until incubation with the GST-fusion proteins (*see* **Note 16**).

3. Incubate the dissected ovaries with GST-mcRFP-RAP in PBS for 2-30 min at room temperature. In parallel, GST-mcRFP can be used as a negative control (*see* **Note 17**).
4. After the desired incubation period, use a Pasteur pipette to carefully aspirate and discard the fluorescent tracer solution.
5. Wash the ovaries by gently adding 0.5–1.0 ml PBS to the tube containing the ovaries and then placing it on an orbital shaker for ~5 min (*see* **Note 18**).
6. Remove the PBS wash by aspiration and replace with 4 % paraformaldehyde in PBS. Return the tube to the orbital shaker for 30 min.
7. Aspirate the paraformadehyde fixative using a Pasteur pipette. If no counterstaining is to be performed, the preparation is ready to be mounted on glass slides for microscopic analysis.
8. Alternatively, for DNA and/or actin labeling (Fig. 4d), the egg chambers are permeabilzed and blocked by adding 1.0 ml of a solution of 2 % BSA, 0.3 % Triton X-100, and 5 % normal goat serum in PBS. Place the tube with the ovaries on the orbital shaker for 30 min.
9. After aspirating and discarding the blocking solution ovaries, stain with Alexa Fluor 488 phalloidin conjugate diluted in blocking buffer at room temperature for 1 h (*see* **Note 19**).
10. Remove the phalloidin solution with a Pasteur pipette and wash the ovaries three times for 15 min in ~1.5 ml PBS, 0.3 % Triton X-100.
11. Incubate the washed ovaries with ~250 μl Hoechst stain for 5 min to label the nuclei (*see* **Note 20**).
12. Aspirate the stain and give the stained ovaries two final washes in 1.5 ml PBS for 10 min each.
13. Mount the ovaries in Gelvatol mounting medium. Place a small (~20–30 μl) drop of Gelvatol in the center of a precleaned glass slide and add some ovaries from the microfuge tube using the Dumont #5SF forceps or a wide-bore Pasteur pipette. Cover with a regular glass cover slip. As the cover slip is pressed gently and flattened over the ovary preparation, the individual ovarioles tend to separate apart for better visualization. Carefully remove excess mounting medium using a Kimwipe.
14. Visualize selective GST-mcRFP-RAP internalization into the egg chambers with either a wide-field epifluorescence or confocal fluorescence microscope (Fig. 4). Typically, the endocytosed mcRFP-RAP is present only within vesicular elements (coated vesicles and maturing endosomes) within vitellogenic oocytes (*see* **Note 21**), and is not internalized by either follicle cells or nurse cells.

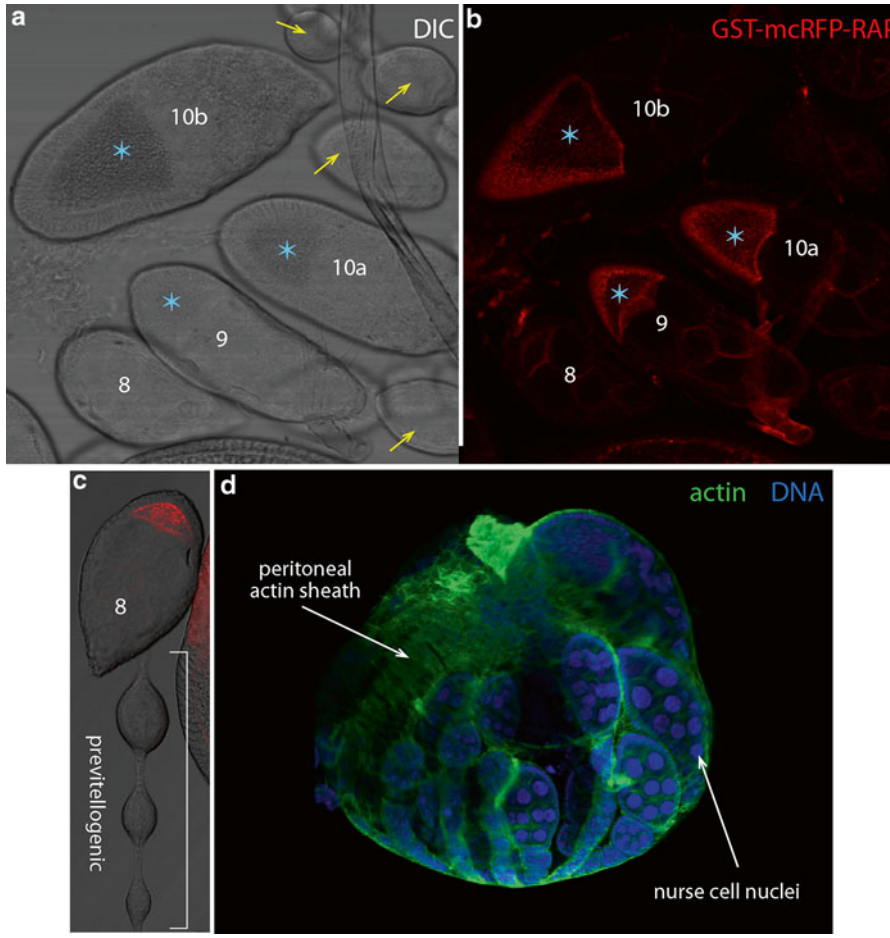

Fig. 4 Selective uptake of fluorescent GST-mcRFP-RAP by vitellogenic egg chambers. Differential interference contrast (DIC) (**a**) and corresponding single confocal fluorescent optical (**b**) sections of fixed and mounted ovaries that were preincubated with GST-mcRFP-RAP. The developmental stages of vitellogenic egg chambers are indicated. Despite some nonspecific background staining, the clathrin-mediated endocytosis tracer is selectively concentrated only within oocytes of vitellogenic egg chambers. Adjacent previtellogenic egg chambers (*yellow arrows*) are identified that do not internalize the GST-mcRFP-RAP ligand. (**c**) Merged DIC and fluorescence confocal image of an individual dissociated ovariole, showing clear failure of pre-vitellogenic egg chambers to internalize GST-mcRFP-RAP through clathrin-mediated endocytosis, while the ligand is concentrated in vesicles and endosomes of the oocyte in the stage-8 chamber. Obvious sequential physical attachment of the previtellogenic chambers is evident. (**d**) Example of whole intact ovary morphology after counterstaining with Alexa Fluor 488 phalloidin to label actin microfilaments and with Hoechst stain to label DNA

4 Notes

1. Any normally fertile strain of *Drosophila melanogaster* can be utilized for these experiments; we use the Canton-S strain as the wild type. Other *Drosophila* species can be analyzed similarly with these methods as well [14].
2. This is not the same as the yeast extract used for the preparation of bacterial growth media. It is dried live yeast, as used for

baking. The dry yeast powder is reconstituted with water and a spatula to the consistency of thick peanut butter. Be sure not to cover the entire horizontal surface of the solid fly medium with yeast paste.

3. These delicate forceps are easily damaged at the tips. Handle with care and always store with a tip protector (a 20 μl plastic micropipette tip works well).
4. The characteristic anatomy of the fly ovary ensures that in recently yeast-fed females, generally several endocytically active egg chambers will always be present. This is because flies, like mosquitoes, have egg production coupled to the environmental nutritional status.
5. If females from old or non-yeast fed vials are used, the representation of egg chambers undergoing active clathrin-mediated endocytosis drops dramatically. Ovaries from these females consist primarily of developmentally arrested immature stages and mature eggs.
6. Schneider's insect medium contains nutritional supplements not found in PBS. However, the endocytic uptake experiments are of short duration and we have not found significant differences between the two. Nevertheless, if live cell imaging is being attempted [15], Schneider's medium must be used. Some procedures using *Drosophila* egg chambers [15] call for the dissection to be done in Halocarbon oil 27 (Sigma catalogue number H8773), which preserves the mid-stage (vitellogenic) egg chambers better. Again, however, given the limited duration of the uptake experiments, we have not found this necessary.
7. If the thorax is clamped with the forceps instead of the abdomen, there is a good possibility of unintentionally detaching the entire abdomen when the posterior segment is grasped and pulled. Also, never grasp the female fly in the middle region of the abdomen. The ovary is the largest organ in the female fly, and, in fattened females, the pair of ovaries occupy much of the interior volume of the abdomen.
8. Some investigators prefer to isolate the ovaries without submerging the female in a drop of liquid. The positioning of the forceps is the same for this technique, but the gentle pulling of the last segment of the abdomen away from the body is simply done while suspending the fly under the dissecting microscope with the other pair of forceps. The ovaries are easily expelled from the abdominal cuticle after removing the posterior-end portion by gently but smoothly moving the forceps from the thorax region toward the posterior. Typically, the pair of ovaries pops out of the posterior wound and usually adheres to the forceps.

The isolated ovaries are then immediately placed into a drop of PBS or Schneider's medium in the well of a glass slide.

9. Initially, the trypan blue uptake procedure entailed direct microinjection into the female abdomen followed by ovary dissection [10]. Under these conditions, peripheral yolk granules are labeled within 5 min [10]. However, similar uptake kinetics occur in freshly dissected ovaries.
10. The drop of trypan blue is very intense dark blue and it is frequently difficult to see the submerged ovaries. If necessary, carefully aspirate off most of the dye with a Pasteur pipette to enable moving the ovaries with minimal damage.
11. The egg chambers have a characteristic a stereotyped morphology: The 16 germ-line cells are encapsulated by a polarized somatic layer of cells, termed the follicle epithelium. The most posterior of the germ-line cells is the oocyte proper, and this is physically connected to the 15 other nurse cells through cytoplasmic channels called ring canals.
12. Trypan blue is not really a selective marker for clathrin-mediated endocytosis, but rather a bulk fluid phase uptake reporter. However, because the vast majority of endocytic activity is clathrin and dynamin (termed Shibire in *Drosophila* [16]) dependent [17, 18], and the trypan blue accumulates exclusively within forming yolk granules of intact vitellogenic egg chambers, this dye serves practically as a proxy for clathrin-dependent events.
13. Given the complex architecture and morphology of each egg chamber, it may seem odd that rapid internalization of an endocytic tracer occurs in an oocyte surrounded by a polarized sheet of somatic epithelial cells. During the early stages of egg chamber development, this laterally adherent follicular epithelium prevents access of yolk, as all stages of egg chambers are bathed in the same yolk protein precursor-rich hemolymph. However, with the onset of vitellogenesis, the follicle cells necessarily become "patent," the formed gaps between individual follicle cells allowing yolk (and experimental tracer) access to the oolemma between the basolateral surfaces of the follicle cells.
14. Since trypan blue is a vital dye, it is also informative in revealing (unintended) damage to the ovaries and egg chambers during the dissection procedure. Endocytically internalized trypan blue is characteristically localized asymmetrically at the posterior pole of the oocyte (Fig. 3a), and only in a subset egg chambers within each ovariole. Blue dye in any other pattern is indicative of gross cellular damage (Fig. 3b). With increasing practice, damage to the isolated ovaries can be minimized.

15. RAP was initially characterized in mammals and is a dedicated endoplasmic reticulum lumenal chaperone for members of the low density lipoprotein receptor superfamily [19]. However, the protein can be expressed in bacteria and used as a pseudo-ligand for uptake experiments in *Drosophila* since the principal receptor that clusters yolk protein precursors in the oolemma is Yolkless, a transmembrane protein evolutionarily related to lipoprotein receptors [20].
16. Because of the substantial size of intact ovaries, they sediment rapidly under gravity. To effectively remove solutions from the microfuge tube during this procedure, allow the ovaries to collect at the base of the vertical tube to prevent damage or accidental aspiration of the egg chambers.
17. Additionally, a suitable negative control for clathrin-mediated internalization experiment in *Drosophila* oocytes is the female-sterile *yolkless* (*yl*) strain [9]. Homozygous null *yolkless* females fail to form productive endocytic clathrin-coated structures in the oocyte because of a lack of the Yolkless receptor. Alternatively, the Shibire strain can be utilized at the non-permissive temperature [17, 18].
18. Washing should be done carefully but thoroughly with the tube placed horizontally, because without proper but gentle washing the fluorescent reporter proteins can give false non-specific signals following fixation.
19. Counterstaining with fluorescent phalloidin stains the actin-rich peritoneal sheath that surrounds the ovary and, at higher magnification, the cortical actin cytoskeleton in germ line and somatic cells.
20. The Hoechst stain reveals the nuclei, especially the polyploid nuclei of the 15 germ line nurse cells in each egg chamber (Fig. 4d).
21. The fluorescence-based internalization assays can also be coupled with fly strains that express fluorescently tagged clathrin [13] for live, two color imaging of clathrin-mediated endocytosis [15].

Acknowledgements

This work was supported by NIH grant R01 GM106963-16 to LMT.

References

1. Taylor MJ, Perrais D, Merrifield CJ (2011) A high precision survery of the molecular dynamics of mammalian clathrin mediated endocytosis. PLoS Biol 9:e1000604
2. Anderson RG, Vasile E, Mello RJ, Brown MS, Goldstein JL (1978) Immunocytochemical visualization of coated pits and vesicles in human fibroblasts: relation to low density lipoprotein receptor distribution. Cell 15:919–933
3. Hanover JA, Willingham MC, Pastan I (1984) Kinetics of transit of transferrin and epidermal growth factor through clathrin-coated membranes. Cell 39:283–293
4. Fan L, Hao H, Xue Y et al (2013) Dynamic analysis of *Arabidopsis* AP2 s subunit reveals a key role in clathrin-mediated endocytosis and plant development. Development 140:3826–3837
5. Grant B, Hirsh D (1999) Receptor-mediated endocytosis in the *Caenorhabditis elegans* oocyte. Mol Biol Cell 10:4311–4326
6. Scholpp S, Brand M (2004) Endocytosis controls spreading and effective signaling range of Fgf8 protein. Cur Biol 14:1834–1841
7. Perry MM, Gilbert AB, Evans AJ (1978) Electron microscope observations on the ovarian follicle of the domestic fowl during the rapid growth phase. J Anat 125:481–497
8. Roth TF, Porter KR (1964) Yolk protein uptake in the oocyte of the mosquito *Aedes aegypti*. L. J Cell Biol 20:313–332
9. DiMario PJ, Mahowald AP (1987) Female sterile (1) *yolkless*: a recessive female sterile mutation in *Drosophila melanogaster* with depressed numbers of coated pits and coated vesicles within the developing oocytes. J Cell Biol 105:199–206
10. Mahowald AP (1972) Ultrastructural observations on oogenesis in *Drosophila*. J Morphol 137:29–48
11. Schonbaum CP, Perrino JJ, Mahowald AP (2000) Regulation of the vitellogenin receptor during *Drosophila melanogaster* oogenesis. Mol Biol Cell 11:511–521
12. King RC (1970) Ovarian development in *Drosophila melanogaster*. Academic, New York
13. Jha A, Watkins SC, Traub LM (2012) The apoptotic engulfment protein Ced-6 participates in clathrin-mediated yolk uptake in *Drosophila* egg chambers. Mol Biol Cell 23:1742–1764
14. Lamnissou K (1997) Ovarian defects in hybrids of the species pair *Drosophila virilis* and *Drosophila texana*. Dev Genet 20:47–52
15. Prasad M, Jang AC, Starz-Gaiano M, Melani M, Montell DJ (2007) A protocol for culturing *Drosophila melanogaster* stage 9 egg chambers for live imaging. Nat Protoc 2:2467–2473
16. van der Bliek AM, Meyerowitz EM (1991) Dynamin-like protein encoded by the *Drosophila* shibire gene associated with vesicular traffic. Nature 351:411–444
17. Kessell I, Holst BD, Roth TF (1989) Membranous intermediates in endocytosis are labile, as shown in a temperature-sensitive mutant. Proc Natl Acad Sci U S A 86:4968–4972
18. Tsuruhara T, Koenig JH, Ikeda K (1990) Synchronized endocytosis studied in the oocyte of a temperature-sensitive mutant of *Drosophila melanogaster*. Cell Tissue Res 259:199–207
19. Herz J, Goldstein JL, Strickland DK, Ho YK, Brown MS (1991) 39-kDa protein modulates binding of ligands to low density lipoprotein receptor-related protein/a2-macroglobulin receptor. J Biol Chem 266:21232–21238
20. Schonbaum CP, Lee S, Mahowald AP (1995) The *Drosophila* yolkless gene encodes a vitellogenin receptor belonging to the low density lipoprotein receptor superfamily. Proc Natl Acad Sci U S A 92:1485–1489

Chapter 25

A Novel Extraction Protocol to Probe the Role of Cholesterol in Synaptic Vesicle Recycling

Jeffrey S. Dason and Milton P. Charlton

Abstract

Cholesterol helps to stabilize membrane fluidity and many membrane proteins interact with cholesterol and are functionally clustered in cholesterol rich "rafts." Synaptic vesicle (SV) membranes are enriched in cholesterol in comparison to other organelles. Attempts to study the function of this high cholesterol content have been hampered by the inability to extract cholesterol from SVs in live presynaptic terminals. Here, we describe a method to extract vesicular cholesterol using a temperature-sensitive *Drosophila* dynamin mutant, *shibire-ts1* (*shi*), to trap SVs on the plasma membrane. Trapped SVs are more accessible to cholesterol extraction by the cholesterol chelator, methyl-β-cyclodextrin (MβCD). This method can likely be extended to extract other lipids from SVs and could also be used to add lipids. We speculate that this method could be used on mammalian preparations in conjunction with dynamin inhibitors.

Key words Cholesterol, Presynaptic, Drosophila, Endocytosis, Exocytosis, Dynamin, Dynasore, Lipids, Shibire, Neuromuscular junction

1 Introduction

Cholesterol is found in both plasma and synaptic vesicle (SV) membranes [1]. The cholesterol content of membranes can be controlled by diet [2, 3] and by inhibitors of cholesterol synthesis [4, 5]. However, acute changes in membrane cholesterol allow for immediate comparison of physiology in normal and depleted states. This can be accomplished by the application of cyclodextrins, which are toroidal molecules that have a hydrophobic interior and hydrophilic exterior. There are many cyclodextrins available that vary in ring size and functional subgroups. One cyclodextrin, methyl-β-cyclodextrin (MβCD), can extract cholesterol from the plasma membrane of cells including presynaptic terminals (Fig. 1c), and its extraction from the plasma membrane affects several aspects of neurotransmitter release [4, 6–8]. However, SVs in presynaptic terminals are not readily

Andrei I. Ivanov (ed.), *Exocytosis and Endocytosis*, Methods in Molecular Biology, vol. 1174,
DOI 10.1007/978-1-4939-0944-5_25,

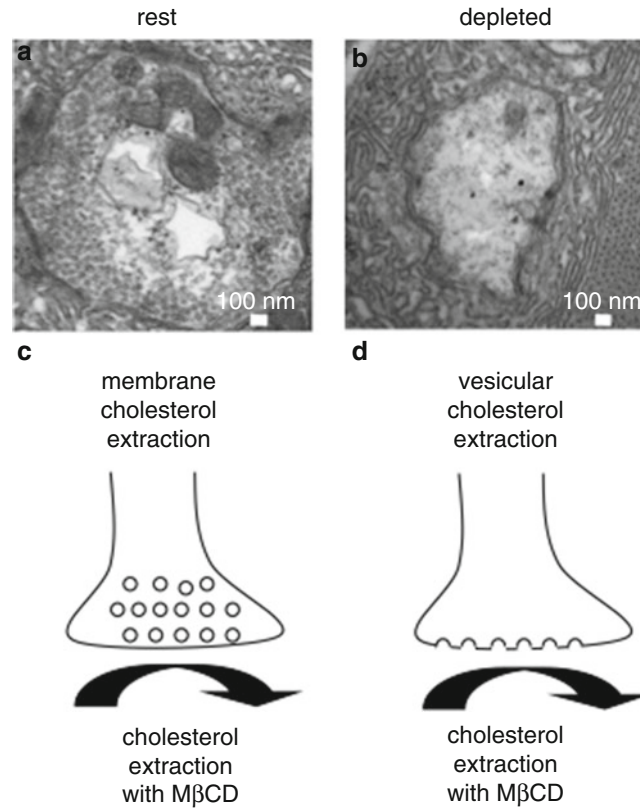

Fig. 1 Synaptic vesicles are more accessible to cholesterol extraction by MβCD when trapped on the plasma membrane. (**a**) Numerous SVs are present in presynaptic terminals of *shi* mutants at rest. (**b**) The entire SV pool can be trapped on the plasma membrane when *shi* mutants are stimulated at 10 Hz for 12 min at non-permissive temperatures (30 °C). (**c**) MβCD normally extracts cholesterol from the plasma membrane of presynaptic terminals. (**d**) However, when SVs are trapped on the plasma membrane, vesicular cholesterol is more accessible to extraction by MβCD. This figure was adapted from [8] with permission from Journal of Neuroscience

accessible to MβCD. Here, we describe techniques to make the interior of SVs accessible to biochemical manipulation in live presynaptic terminals.

SVs can be reversibly trapped on the plasma membrane of presynaptic terminals following exocytosis in the *Drosophila* temperature-sensitive dynamin mutant, *shibire-ts1* (*shi*) (Fig. 1a, b; [8–10]). The failure of dynamin at non-permissive temperatures prevents SV endocytosis thereby trapping SVs on the plasma membrane following exocytosis. The inactivation of dynamin is reversible and SVs re-form once returned to permissive temperatures.

Here, we describe a method in which we exploit the *shi* mutant to trap SVs on the plasma membrane, where they are more accessible to cholesterol extraction by MβCD (Fig. 1d). We previously used this technique to ask whether vesicular cholesterol is essential

for SV endocytosis [8], whether membrane pools of cholesterol readily intermingle [8], and whether vesicular cholesterol is required for actin-dependent clustering of SV proteins during recycling [11].

2 Materials

2.1 Fly Stocks

1. Cornmeal agar with dry yeast (cornmeal 0.09 g/ml, agar 0.005 g/ml, yeast extract 0.005 g/ml, corn syrup 0.11 ml/ml, whole-milk powder 0.02 g/ml, 99 % propionic acid 0.002 ml/ml, 85 % phosphoric acid 0.0002 ml/ml). Fly stocks grow on this medium in uncrowded conditions at 22 °C (*see* **Note 1**).
2. The temperature-sensitive *shibire-ts1* (*shi*) mutant [12] from the Bloomington *Drosophila* Stock Center (Bloomington, IN, USA).
3. SynaptopHluorin (n-Syb-pH) flies (*+;+;UAS-n-Syb-pH, elaV^{3E1}-GAL4/TM6b*) from Graeme Davis laboratory (University of California, San Francisco, USA; [13]). n-Syb-pH is a pH sensitive GFP molecule fused to synaptobrevin that can be used to measure SV cycling [14].

2.2 Solutions

1. HL6 saline for recording and imaging: 15 mM $MgCl_2$, 24.8 mM KCl, 23.7 mM NaCl, 10 mM $NaHCO_3$, 20 mM Na^+ isethionic acid, 5 mM BES, 80 mM Trehalose-$2H_2O$, 5.7 mM L-Alanine, 2 mM L-Arginine-HCl, 14.5 mM glycine, 11 mM L-Histidine, 1.7 mM L-Methionine, 13 mM L-Proline, 2.3 mM L-Serine, 2.5 mM L-Threonine, 1.4 mM L-Tyrosine, 1 mM L-Valine, 0.0001 mM TPEN, 1 mM $CaCl_2$, pH 7.2 [15].
2. High K^+ saline to induce depolarization: 25 mM NaCl, 90 mM KCl, 10 mM $NaHCO_3$, 5 mM HEPES, 30 mM sucrose, 5 mM trehalose, 10 mM $MgCl_2$, 2 mM $CaCl_2$, pH 7.2 [16].
3. Methyl-β-cyclodextrin (MβCD), 10 mM solution in HL6 saline freshly prepared for each experiment (*see* **Note 2**).
4. Schneider's insect medium (Sigma-Aldrich).
5. A proportional temperature controller and a mini heating module (Scientific Systems Design Inc.) to perfuse saline at the higher temperature onto the preparation.

2.3 Electrophysiology

Experiments were conducted with standard electrophysiology equipment.

1. An Axoclamp-2A (Axon Instruments) and a MacLab/4S data acquisition system (ADInstruments) to record electrical signals. Any microelectrode electrometer amplifier would suffice.
2. A Grass S48 stimulator and Grass S105 stimulation isolation unit for electrical nerve stimulation.
3. An upright Nikon microscope (Optiphot-2).

4. Recording and stimulating electrodes were pulled on a Model P-87 Sutter micropipette puller (Sutter Instrument Co.). Borosilicate glass with filament (Sutter Instrument; 10 cm length, O.D.:1.5 mm, O.D.:0.86 mm) were used for intracellular recording electrodes. Kimax-51 glass (Fisher Scientific; catalogue number: 12-141-2; 100 mm length; both ends open) was used to make suction electrodes.

2.4 FM1-43 Imaging

1. FM1-43 (Invitrogen Molecular Probes) is a lipophilic dye used to measure SV cycling. Other FM dyes such as FM4-64 can also be used.
2. Advasep-7 (Sigma-Aldrich) ([17]; *see* **Note 3**).
3. A Leica TCS SL confocal laser-scanning microscope with either a 40× (0.8 NA) or 63× (0.9 NA) water dipping objective. However, this technique can be adapted to other image acquisition systems.

2.5 SynaptopHluorin Imaging

1. A Bio-Rad MRC 600 confocal scan head on a Nikon microscope (Optiphot) with a 40× (0.7 NA) water dipping objective. However, this technique can be adapted to other image acquisition systems.

3 Methods

3.1 Drosophila shi Larvae

1. Select a wandering third-instar larva and dissect in Schneider's insect medium under a dissecting microscope.
2. Place a larva on a dissection dish dorsal side up and pin on the anterior and posterior ends.
3. Cut larva longitudinally between the two dorsally located trachea using fine dissection scissors.
4. Use fine forceps to gently remove the intestine and fat bodies.
5. Pin each corner of the larva to expose the ventral body musculature.
6. Carefully cut the segmental nerves and remove the CNS.

3.2 Trapping SVs on the Plasma Membrane

1. Perform all recordings and imaging in HL6 saline.
2. Make a suction electrode by pulling a sharp electrode and break the tip using a diamond knife. Heat-polish the electrode, so that the inner diameter is approximately 10–12 μm in diameter.
3. Use electrical stimulation to trap SVs on the plasma membrane. Use a suction electrode to suck up and then stimulate a cut segmental nerve. Stimulate for 12 min at 10 Hz at nonpermissive temperature (30 °C) to trap the entire SV population on the plasma membrane [8].

4. Alternatively, apply high K^+ depolarization for 10 min at non-permissive temperature (30 °C) to trap SVs on the plasma membrane [8].
5. This approach can likely be modified for mammalian preparations using dynamin inhibitors (*see* **Notes 4** and **5**).

3.3 Measuring the Effects of Cholesterol Extraction on Synaptic Transmission

1. Impale the ventral longitudinal muscle fiber 6 (abdominal segment 3) of a dissected larva with a sharp glass electrode filled with 3 M KCl (~40 MΩ) to measure spontaneously occurring miniature excitatory junction potentials (mEJPs) and stimulus-evoked excitatory junction potentials (EJPs).
2. Stimulate cut segmental nerves using a suction electrode. Stimulate nerve at 0.05 Hz to obtain baseline EJPs.
3. Increase the temperature of the saline to non-permissive temperature (30 °C) using a proportional temperature controller and a mini heating module to perfuse saline at the higher temperature onto the preparation. Stimulate at 10 Hz for 12 min to trap the entire SV population on the plasma membrane. The EJPs will become progressively smaller until synaptic transmission fails owing to the depletion of the SVs (Fig. 2c).
4. Add 10 mM MβCD to the saline to extract cholesterol from membranes. A cholesterol–MβCD complex can be used to add cholesterol (*see* **Notes 6–8**). This assay can also be adapted to add or extract other lipids (*see* **Notes 9** and **10**). Furthermore, exposure of the lumen of vesicles to extracellular space would allow access to intravesicular domains of SV proteins (*see* **Note 11**).
5. Dissolve 10 mM MβCD in HL6 saline and apply at different times to target cholesterol removal from the plasma or SV membranes.
6. Apply 10 mM MβCD prior to SV trapping to extract cholesterol from the plasma membrane (Fig. 2a).
7. Apply 10 mM MβCD during or following SV trapping to extract cholesterol from SV membranes and plasma membranes (Fig. 2b).
8. Determine the effects of extracting cholesterol by measuring the recovery of synaptic transmission in *shi* mutants at permissive temperatures (22 °C; Fig. 2c).

3.4 Measuring the Effects of Cholesterol Extraction on SV Cycling Using FM1-43

1. Trap SVs on the plasma membrane using high K^+ depolarization for 10 min at non-permissive temperatures (30 °C; [8]).
2. Add 10 mM MβCD to the high K^+ saline to extract cholesterol from trapped SVs (Fig. 3a). Alternatively, add 10 mM MβCD prior to trapping to extract cholesterol from the plasma membrane only (Fig. 3d).
3. Wash off MβCD while SVs are still trapped (i.e., the temperature must remain at 30 °C).

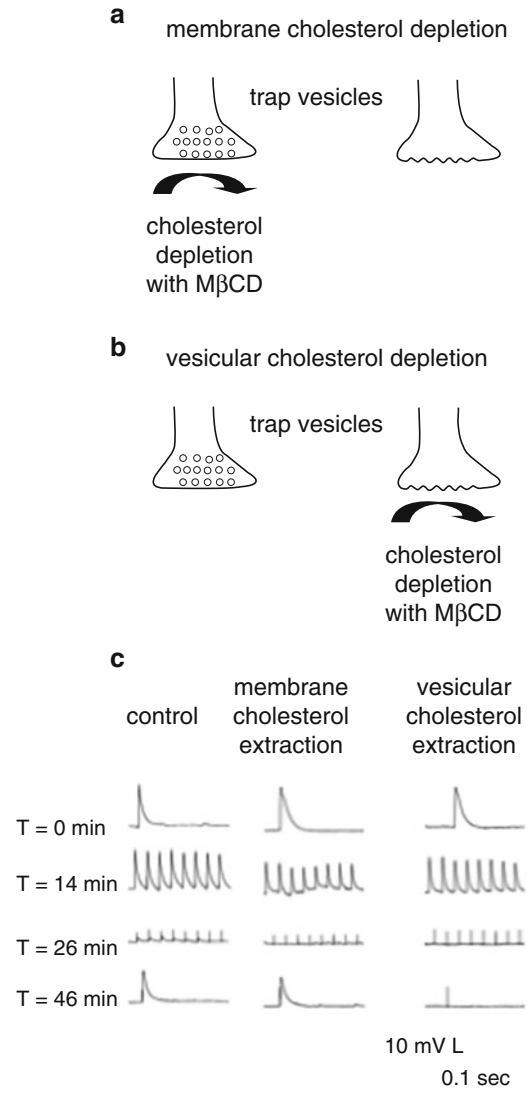

Fig. 2 Measuring synaptic transmission following cholesterol extraction. (**a**, **b**) Schematics demonstrating how to extract cholesterol from the plasma membrane prior to SV trapping (**a**) or from SVs that are trapped (**b**). (**c**) EJPs were recording from preparations that were initially stimulated at 0.05 Hz ($T = 0$ min). SVs were then trapped by stimulating at 10 Hz for 12 min at non-permissive temperatures (30 °C; $T = 14$ min). At $T = 26$ min, there was no EJP in response to stimulation indicating that all SVs were trapped on the plasma membrane. The temperature was then returned to 22 °C and the preparation was stimulated at 0.05 Hz to assess recovery. EJP amplitude returned to baseline levels within 20 min of returning to 22 °C. Extraction of cholesterol from SVs, but not the plasma membrane, blocked this recovery. This figure was adapted from [8] with permission from Journal of Neuroscience

Fig. 3 (continued) *Arrows* indicate when images were taken. (**b**, **c**, **e**, **f**) Representative images of *shi* preparations loaded with FM1-43 following high K^+ stimulation and then subsequently unloaded with high K^+ stimulation. Extraction of cholesterol from SVs, but not the plasma membrane, impaired endocytosis. Scale bar, 10 μm. This figure was adapted from [8] with permission from Journal of Neuroscience

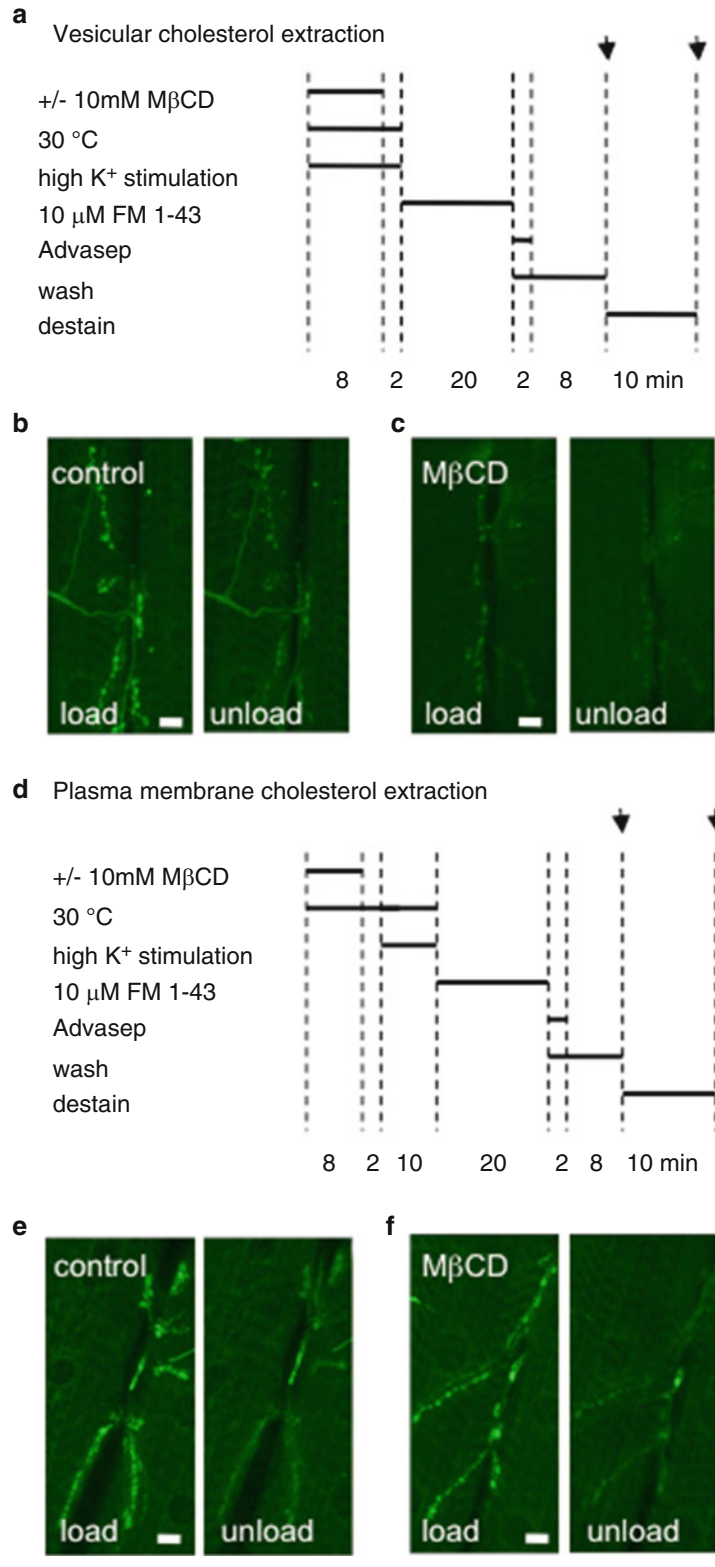

Fig. 3 FM1-43 as a probe to measure the effects of cholesterol extraction on SV recycling. (**a**, **d**) Experimental protocol for determining the effects of vesicular cholesterol extraction (**a**) and plasma membrane cholesterol extraction (**d**). Note that FM1-43 and MβCD are never applied at the same time (*see* **Note 12**).

4. Incubate the preparation with 10 μM FM1-43 (or other FM dyes) for 20 min at permissive temperatures (22 °C) to measure SV re-formation. FM dyes and MβCD must not be applied at the same time (*see* **Note 12**).
5. Wash the preparation extensively in Ca^{2+} free HL6 for 10 min (include 75 μM Advasep-7 for the first 2 min of the wash).
6. Take an image of the neuromuscular junctions as a measure of FM1-43 loading (Fig. 3b, c, e, f).
7. Induce exocytosis using high K^+ depolarization for 10 min at 22 °C and take another image to determine the amount of FM1-43 unloading (Fig. 3b, c, e, f).

3.5 Measuring the Effects of Cholesterol Extraction on SV Cycling Using SynaptopHluorin

1. Cross male *+;+;UAS-n-Syb-pH, elaV^{3E1}-GAL4/TM6b* flies to female *shi;+;+* flies and select non-tubby male larvae (*shi;+;UAS-n-Syb-pH,elaV^{3E1}-GAL4/+*) from F1 progeny for experiments.
2. Take an image of a string of boutons from a *shi;+;UAS-n-Syb-pH,elaV^{3E1}-GAL4/+* preparation prior to stimulation (Fig. 4).
3. Stimulate cut segmental nerves using a suction electrode. Stimulate nerves at 10 Hz for 12 min at non-permissive temperatures (30 °C) to trap all SVs on the plasma membrane (Fig. 4). Take an image every minute to measure changes in fluorescence. Increased fluorescence indicates SV exocytosis.
4. Take images at regular intervals at permissive temperatures (22 °C) during the recovery phase (Fig. 4). A decrease in fluorescence indicates SV recycling.
5. Apply 10 mM MβCD while SVs are trapped to test the effects of cholesterol extraction from SVs.
6. Apply 10 mM MβCD prior to SV trapping to test the effects of extracting cholesterol from plasma membranes.

4 Notes

1. *Drosophila*, like other insects, cannot synthesize cholesterol directly, but do contain cholesterol in addition to other sterols [18, 19]. They acquire cholesterol from their diet and also produce it from the conversion of other sterols [3, 20]. Thus, the amount of cholesterol in *Drosophila* membranes can be modified by altering the amount of dietary cholesterol [2, 3]. Our fly food medium contained a source of cholesterol (whole milk powder), and thus, our larvae should have significant amounts of cholesterol.
2. Application of 10 mM MβCD to third-instar larval fillet preparations for 10–30 min reduces cholesterol levels by 30–40 % [8] without disrupting gross presynaptic or postsynaptic structure (Fig. 5). Cholesterol levels from larval fillet preparations

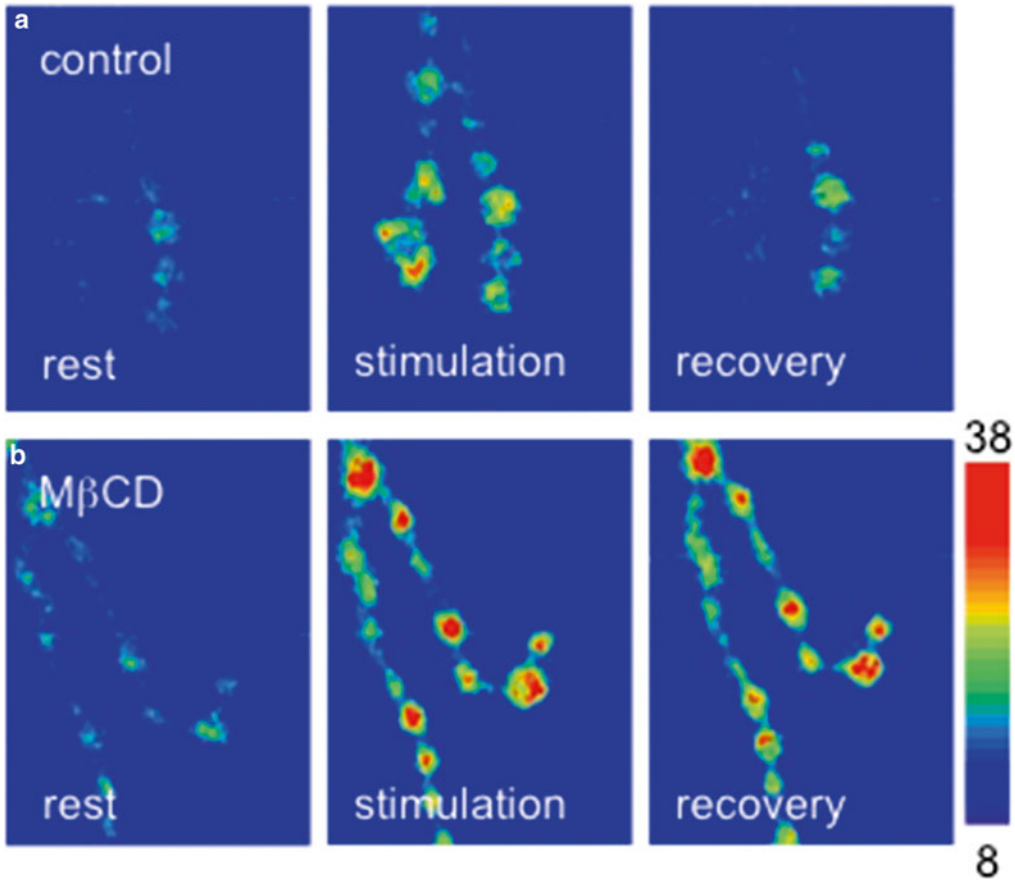

Fig. 4 SynaptopHluorin can be used to measure the effects of cholesterol extraction on SV recycling. (**a**) Representative images of *shi;+;UAS-n-Syb-pH,elaV^{3E1}-GAL4/+* preparations at rest, stimulated at 10 Hz for 12 min at non-permissive temperatures (30 °C), and then allowed to recover with no stimulation at permissive temperatures (22 °C). (**b**) Representative images of *shi;+;UAS-n-Syb-pH,elaV^{3E1}-GAL4/+* preparations under the same three conditions as above but in the presence of MβCD. Extraction of cholesterol from SVs impaired recycling. This figure was adapted from [8] with permission from Journal of Neuroscience

can be measured using an Amplex Red Cholesterol Assay kit [8]. However, this technique measures cholesterol in both the muscle and presynaptic terminals, not SVs specifically.

3. Advasep-7, a cyclodextrin that does not extract cholesterol, reduces background fluorescence [17] by removing extracellular FM1-43 during washing.
4. We believe the technique of SV trapping can be extended to other preparations, including mammalian ones. Recently, a number of dynamin inhibitors have been developed. The dynamin inhibitor, Dynasore, blocks SV recycling in other preparations [21, 22] and causes rundown of neurotransmitter release at the *Drosophila* larval neuromuscular junction (NMJ) during high frequency stimulation [23]. Our preliminary experiments

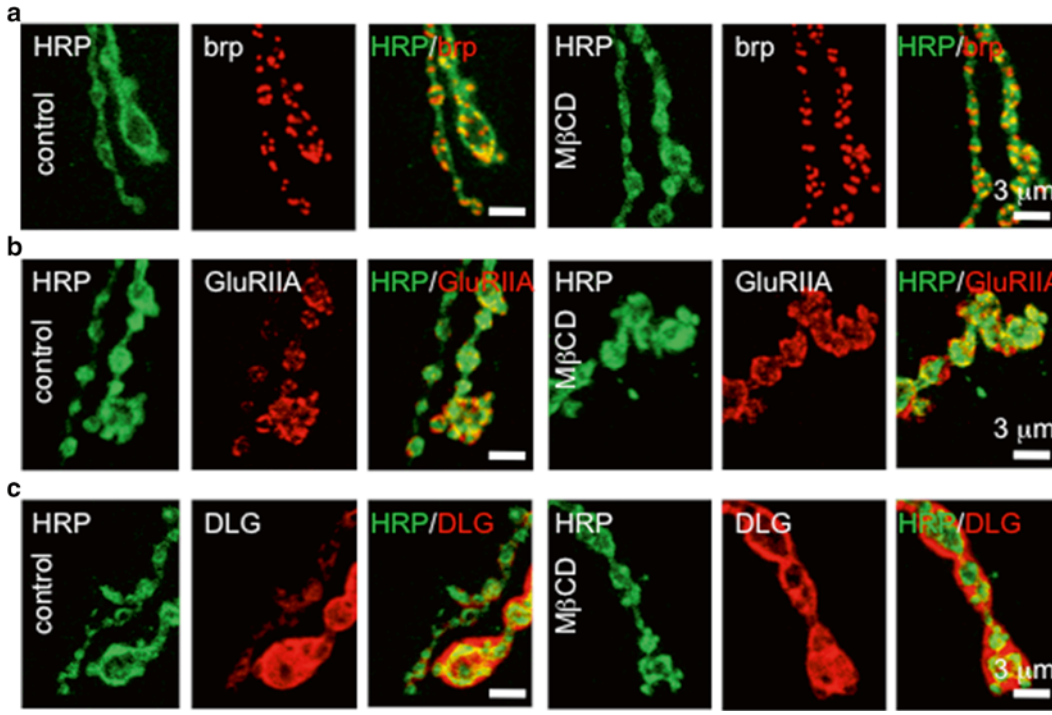

Fig. 5 Cholesterol extraction does not disrupt presynaptic or postsynaptic structure. (**a–c**) Fixed preparations were stained with FITC-conjugated anti-HRP antibody (a neuronal plasma membrane marker; *green*) and an anti-bruchpilot (brp; an active zone protein), an anti-GluRIIA (postsynaptic glutamate receptors) or anti-DLG (PSD-95; a postsynaptic scaffolding protein) antibody (*red*). Unstimulated *shi* preparations contain numerous active zones (as indicated by brp staining) and postsynaptic glutamate receptors when incubated with or without 10 mM MβCD for 20 min at 22 °C and then fixed at 22 °C. In addition, DLG (PSD-95) localization was not disrupted

using Dynasore on the *Drosophila* larval NMJ indicated that Dynasore enhanced spontaneous neurotransmission. We observed increased muscle contraction and spontaneously occurring EJP-like responses in wild-type preparations following Dynasore application (Fig. 6). Dynasore has been reported to increase neurotransmitter release and resting intracellular Ca^{2+} at the frog NMJ [24]. An increase in resting intracellular Ca^{2+} would explain the burst of spontaneous activity we observed. Thus, Dynasore has other nonspecific effects in addition to inhibition of endocytosis that would make its effects at some synapses difficult to interpret.

5. Several other dynamin inhibitors have been developed and are commercially available from several sources. For instance the "Dynamin Inhibitors Toolbox" (Abcam, ab120468 http://www.abcam.com/Dynamin-Inhibitors-Toolbox-ab120468.html) contains three different structure groups and control compounds that target the PH domain or the GTPase allosteric site on dynamin. We have not tried these on synapses.

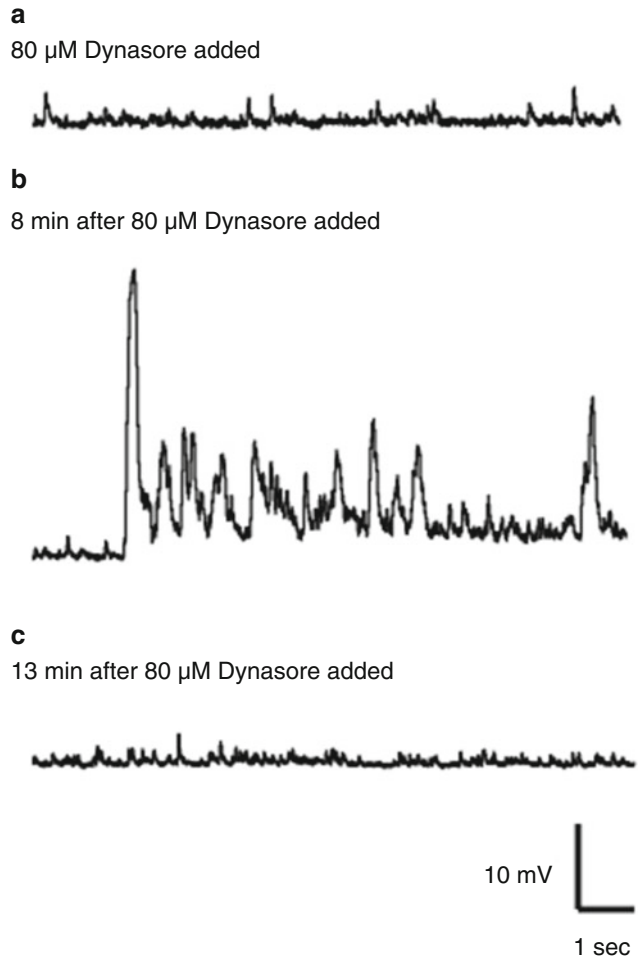

Fig. 6 Dynasore enhances spontaneous neurotransmission. (**a**) Representative trace showing spontaneously occurring mEJPs from a wild-type *Drosophila* larval NMJ. (**b**) Following the application of 80 μM Dynasore, periodic bursts of synaptic activity was observed in unstimulated preparations. (**c**) This increase in spontaneous neurotransmitter release disappears over time

6. Cholesterol can be added to membranes by applying a 1:10 cholesterol–MβCD complex. The 1:10 cholesterol–MβCD complex is prepared by dissolving 38.7 mg of cholesterol in 1 ml of chloroform. This solution is then separated into 10 aliquots of 100 μl. The solution is then evaporated with nitrogen. 10 ml of HL6 with 10 mM MβCD is added to each aliquot before use.
7. 1:10 cholesterol–MβCD complex can be used for rescue experiments. We found that this complex restores cholesterol levels and function in preparations in which plasma membrane cholesterol has previously been extracted [6, 8]; function was not restored when vesicular cholesterol was extracted.

8. The 1:7 cholesterol–MβCD complex, which neither donates nor extracts cholesterol, can be used as a control to demonstrate cholesterol-specific effects of MβCD. If no effect is observed following the addition of the 1:7 cholesterol–MβCD complex, then the effects of MβCD are likely to due to cholesterol extraction.
9. The effects of adding cholesterol can be studied using the 1:10 cholesterol–MβCD complex. This can be extended to other lipids such as ergosterol. However, we found that ergosterol is not very soluble in 10 mM MβCD solutions. A β-cyclodextrin with a greater affinity for ergosterol may be required.
10. This approach can also be extended to extract other lipids from SVs using other lipid-extracting agents. For instance there are numerous cyclodextrins available that might have affinities appropriate to extract or donate other lipids.
11. The technique of SV trapping can also be used to expose the intravesicular domains of SV proteins for experimentation. For instance the function of intravesicular domains of pumps, channels, and other proteins involved in exocytosis and endocytosis could be investigated by chemical modification, by antibody binding, or by chromophore-assisted light inactivation (CALI).
12. MβCD binds to lipophilic dyes such as FM1-43 [8] and prevents uptake of FM1-43 by SVs. Thus, experiments must be designed so that FM dyes and MβCD are not applied at the same time. It's extremely likely that MβCD will also bind to other lipophilic or hydrophobic molecules. This must be considered when using MβCD in combination with other drugs or inhibitors. For instance if a lipophilic drug must remain while MβCD is applied, one could use the MβCD to deliver the drug from an MβCD–drug complex while extracting cholesterol.

Acknowledgements

This work was supported by a grant from CIHR, Canada MOP-82827 (M.P.C.).

References

1. Takamori S, Holt M, Stenius K et al (2006) Molecular anatomy of a trafficking organelle. Cell 127:831–846
2. Huang X, Warren JT, Buchanan J et al (2007) Drosophila Niemann-Pick type C-2 genes control sterol homeostasis and steroid biosynthesis: a model of human neurodegenerative disease. Development 134:3733–3742
3. Shreve SM, Yi SX, Lee RE Jr (2007) Increased dietary cholesterol enhances cold tolerance in *Drosophila* melanogaster. Cryo Lett 28: 33–37
4. Wasser CR, Ertunc M, Liu X, Kavalali ET (2007) Cholesterol-dependent balance between evoked and spontaneous synaptic vesicle recycling. J Physiol 579:413–429

5. Linetti A, Fratangeli A, Taverna E et al (2010) Cholesterol reduction impairs exocytosis of synaptic vesicles. J Cell Sci 123:595–605
6. Zamir O, Charlton MP (2006) Cholesterol and synaptic transmitter release at crayfish neuromuscular junctions. J Physiol 571:83–99
7. Smith AJ, Sugita S, Charlton MP (2010) Cholesterol-dependent kinase activity regulates transmitter release from cerebellar synapses. J Neurosci 30:6116–6121
8. Dason JS, Smith AJ, Marin L, Charlton MP (2010) Vesicular sterols are essential for synaptic vesicle cycling. J Neurosci 30:15856–15865
9. Koenig JH, Ikeda K (1989) Disappearance and reformation of synaptic vesicle membrane upon transmitter release observed under reversible blockage of membrane retrieval. J Neurosci 9:3844–3860
10. Macleod GT, Marin L, Charlton MP, Atwood HL (2004) Synaptic vesicles: test for a role in presynaptic calcium regulation. J Neurosci 24:2496–2505
11. Dason JS, Smith AJ, Marin L, Charlton MP (2014) Cholesterol and F-actin are required for clustering of recycling synaptic vesicle proteins in the presynaptic plasma membrane. J Physiol 592:621–633
12. Grigliatti TA, Hall L, Rosenbluth R, Suzuki DT (1973) Temperature-sensitive mutations in *Drosophila melanogaster*. XIV. A selection of immobile adults. Mol Gen Genet 120: 104–114
13. Poskanzer KE, Marek KW, Sweeney ST, Davis GW (2003) Synaptotagmin I is necessary for compensatory synaptic vesicle endocytosis in vivo. Nature 426:559–563
14. Miesenböck G, De Angelis DA, Rothman JE (1998) Visualizing secretion and synaptic transmission with pH-sensitive green fluorescent proteins. Nature 394:192–195
15. Macleod GT, Hegstrom-Wojtowicz M, Charlton MP, Atwood HL (2002) Fast calcium signals in Drosophila motor neuron terminals. J Neurophysiol 88:2659–2663
16. Verstreken P, Ohyama T, Bellen HJ (2008) FM 1-43 labeling of synaptic vesicle pools at the *Drosophila* neuromuscular junction. Methods Mol Biol 440:349–369
17. Kay AR, Alfonso A, Alford S et al (1999) Imaging synaptic activity in intact brain and slices with FM1-43 in *C. elegance*, lamprey, and rat. Neuron 24:809–817
18. Rietveld A, Neutz S, Simons K, Eaton S (1999) Association of sterol- and glycosylphosphatidylinositol-linked proteins with *Drosophila* raft lipid microdomains. J Biol Chem 274:12049–12054
19. Phillips SE, Woodruff EA 3rd, Liang P et al (2008) Neuronal loss of *Drosophila* NPC1a causes cholesterol aggregation and age-progressive neurodegeneration. J Neurosci 28: 6569–6582
20. Behmer ST, Nes WD (2003) Insect sterol nutrition and physiology: a global perspective. Adv Insect Physiol 31:1–72
21. Macia E, Ehrlich M, Massol R et al (2006) Dynasore, a cell-permeable inhibitor of dynamin. Dev Cell 10:839–850
22. Newton AJ, Kirchhausen T, Murthy VN (2006) Inhibition of dynamin completely blocks compensatory synaptic vesicle endocytosis. Proc Natl Acad Sci U S A 103:17955–17960
23. Rodal AA, Blunk AD, Akbergenova Y et al (2011) A presynaptic endosomal trafficking pathway controls synaptic growth signaling. J Cell Biol 193:201–217
24. Douthitt HL, Luo F, McCann SD, Meriney SD (2011) Dynasore, an inhibitor of dynamin, increases the probability of transmitter release. Neuroscience 172:187–195

Chapter 26

Microfluidic Devices for Imaging Trafficking Events In Vivo Using Genetic Model Organisms

Sudip Mondal and Sandhya P. Koushika

Abstract

Miniature devices are powerful new tools that can be used to address multiple questions in biology especially in investigating an individual cell or organism. The primary step forward has been the ease of soft lithography fabrication which has allowed researchers from different disciplines, with incomplete technical knowledge, to develop and use new devices for their own research problems. In this chapter, we describe a simple fabrication process that will allow investigators to make microfluidic devices for in vivo imaging studies using genetic model organisms such as *C. elegans*, *Drosophila* larvae, and zebrafish larvae. This microfluidic technology enables detailed studies on multiple cellular and subcellular phenomena including intracellular vesicle trafficking in living organisms over different developmental stages in an anesthetic free environment.

Key words Microfluidics, PDMS, Soft lithography, *C. elegans*, *Drosophila*, Zebrafish, In vivo imaging

1 Introduction

Microfabricated devices are being increasingly used as a tool to study a variety of biological questions ranging from cellular dynamics in subcellular microdomains in single cells [1] to spatiotemporal dynamics of morphogen gradients during *Drosophila* embryonic development [2]. The successful use of such devices requires well-controlled liquid environments for the preparation and manipulation of samples with minimal human intervention [3, 4]. Simpler and slightly larger devices with channels in the micron scale have been used to study cellular and subcellular dynamics in single cells [5–8], in tissues [9], and in the model organisms *C. elegans* [10–16], *Drosophila* [2, 12, 17–20], zebrafish [12, 21, 22], etc. (reviewed by Hwang and Lu [23]). One class of studies use high-resolution in vivo imaging in living organisms that typically requires complete immobilization of the animal. Unlike animals immobilized using anesthetics, appropriate fluidic platforms can provide a more

Andrei I. Ivanov (ed.), *Exocytosis and Endocytosis*, Methods in Molecular Biology, vol. 1174,
DOI 10.1007/978-1-4939-0944-5_26,

physiological environment for short and longer term in vivo assays that exploit genetic model systems [11]. A large number of microfluidic devices have been developed for *C. elegans* that have achieved on-chip immobilization using various techniques such as channel geometry [24–26], suction [27, 28], flexible polydimethylsiloxane (PDMS) membranes [10, 11, 29], low temperature [28], temperature-sensitive gels [30, 31], anesthetic gases [32], and laser-induced heat knockdown [33]. These immobilization techniques have shown minimal adverse effects on *C. elegans* physiology and have been used for carrying out high-resolution imaging [11, 31, 32, 34], conducting nano-axotomy [10, 29], following calcium dynamics in neurons [26], in vivo organelle trafficking in neurons [11, 18], cell migration during early development [11], and tracking synaptogenesis [25]. Fluidic devices in combination with computer-controlled valve systems have established high-throughput platforms for *C. elegans* that have been used in screening chemical compounds that alter electropharyngeograms [35, 36], in assessing cellular morphology in neuronal regeneration studies [27], and in screening for mutants with altered gene expression levels [37]. Additional examples include the use of a single-layer device for semiautomated *C. elegans* genetic screens to identify genes regulating tryptophan hydroxylase expression [37]. The advantage of such approaches is illustrated in this last study where a typically labor-intensive large manual screen was semiautomated and in conjunction with an image analysis algorithm resulted in isolation of several new mutants [37].

Designing and fabricating novel platforms using microfabrication technology have permitted researchers to perform experiments that were extremely challenging earlier. Currently available technologies and instrumentation can deliver high-resolution device features that are useful for sample sizes in the scale of submicrons to millimetres [4, 23]. Using such approaches, robust microfluidic control systems have been developed that can regulate a large number of sequential and parallel processes without human intervention [20, 25, 27, 28, 37]. Most of these technologies rely on high-resolution fabrication processes that require sophisticated instrumentation and skilled personnel to achieve the necessary precision required for their successful use. Hence, it is important that simpler fabrication steps be used to enable scientists with limited technical training and/or access to high-end instrumentation to apply microfluidic techniques to biological problems of their choice.

Collecting in vivo data from stable intact organisms to study multiple cellular and subcellular events has always been a challenge and often the most desirable outcome. Events such as vesicle trafficking and fusion, growth cone dynamics, cell division, and endocytosis at the cell surface are all problems which a large number of biologists study. The devices described in this chapter are

particularly suited to addressing nearly all of the above phenomena that occur in the time scale of seconds to a few hours [11, 38–42]. We ourselves have not investigated events that occur at faster time scales such as vesicle fusion, but nonetheless there is per se no barrier to the use of microfluidic devices to collect such data. Some phenomena that are particularly accessible for study include slow organelle transport [43, 44], cargo dynamics in wild-type and mutant/disease models [44], tracking retrograde cargo [45], developmental neuronal branching, axon guidance towards its target [39], growth cone formation [46], tracking intracellular dynamics such as microtubule transport, or contributions from the extracellular matrix during axon outgrowth [47, 48]. The device technology described can also help in tracking endocytic events such as uptake of artificial nanoparticles to probe intracellular viscoelastic properties in early embryos [49] or DNA nanomachine probes that map spatiotemporal pH changes in vivo [50].

In this chapter, we outline procedures for fabricating simple microfluidic devices which use relatively inexpensive equipment that can be set up in any standard biology laboratory, including those that lack access to cleanroom facilities. By removing the need for precise alignment of features in the two-layer bonding step, these simple devices described below eliminate the need for expensive equipment which is often essential for critical alignment steps in more complex devices. We have adapted the technology of fabricating flexible PDMS membranes to demonstrate successful immobilization of *C. elegans*, *Drosophila* larvae, and zebrafish larvae [11, 12]. Using this technology, investigators will be able to immobilize whole organisms with minimal adverse effects on their health and also permit repeated immobilization of the same organism for in vivo studies up to the time scale of a few hours. These devices are fabricated using optically transparent materials, thus allowing acquisition of both bright-field and fluorescent images from an animal immobilized inside the device. The microfluidic chips described are best used with inverted imaging platforms for high-resolution time-lapse observations. We also describe a protocol for acquiring high-resolution vesicle trafficking data from neurons of a living organism when immobilized under a flexible PDMS membrane. Modifications of this basic protocol can be used to acquire data across different time scales or using different markers.

2 Materials

Prepare all solutions using distilled water, and store all chemicals under ambient conditions unless mentioned otherwise. Use a dedicated fabrication area to reduce dust and equipped with a yellow

light to avoid exposure of photosensitive chemicals. Exposure to light can cause permanent damage to the photosensitive chemicals used in fabrication (*see* **Note 1**).

2.1 Photolithography of SU8

1. Mask design and printing: Prepare CAD-based design features for the microfluidic device.
2. Print the photomask using a high-resolution photo-plotter with a minimum resolution of 10 μm on transparencies.
3. Substrates: Silicon wafers (p type and ⟨100⟩ orientation).
4. Diamond scriber.
5. 20 % KOH: 20 g of KOH pellets dissolved in 80 ml distilled water (*see* **Note 2**).
6. Compressed nitrogen gas line with a blower gun for blow drying.
7. HMDS: Hexamethyldisilazane, ≥99 % (Sigma, St. Louis, USA).
8. Negative photoresist SU8-2025 and SU8-2050 (MicroChem Corp., MA, USA) at room temperature (*see* **Note 3**).
9. Hot plate that can attain the maximum temperature of 150 °C.
10. Spin coater: Vacuum chuck of a spinner connected to a vacuum pump for holding small silicon wafers while pouring photoresist and spinning the substrates at high speed (*see* **Note 4**).
11. UV light source: Collimated mercury-arc light source (Oriel Instruments, Newport) for ultraviolet (UV) wavelengths with a dichroic mirror for 350–400 nm light wavelengths.
12. Resist developer: SU8 photo-resist developer (Microchem Corp., MA, USA).
13. Isopropyl alcohol (IPA).

2.2 Soft Lithography of PDMS from the SU8 Pattern

1. Trichloro(1H,1H,2H,2H-perfluorooctyl)silane, 97 % (Sigma, St. Louis, USA).
2. PDMS mixture: Sylgard 184 base and curing agent (Dow Corning, MI, USA).
3. Degasing chamber: Desiccator connected to a rotary pump for degasing the PDMS mixture that removes all trapped bubbles formed during mixing or pouring on silicon wafers with SU8 features.
4. Baking oven: Hot air convection oven (that can attain 100 °C) to bake the PDMS cast on silicon wafers with SU8 features.
5. A sharp surgical blade.
6. Harris micro puncher (Sigma, St. Louis, USA) with an inner diameter of 1.0 mm.
7. Harrick plasma cleaner (Harrick Plasma, NY, USA) with a maximum power of 18 W.

8. 1.5 Grade thin glass cover slip of size 22 × 22 mm square shape.
9. Stereomicroscope with 10–50× magnification to inspect devices for fabrication defects.

2.3 Initial Characterization of the Fabricated Device

1. Compressed gas: A compressed nitrogen gas connection through a three-way stopcock.
2. S Basal: 5.85 g NaCl, 1 g K_2HP_4, 6 g KH_2PO_4, and 1 ml cholesterol (5 mg/ml in ethanol) dissolved in 1 l of distilled water, sterilized by autoclaving, and stored at 4 °C.
3. 1 M Potassium citrate: 20 g Citric monohydrate and 293.5 g tri-potassium citrate monohydrate dissolved in 1 l distilled water, sterilized by autoclaving, and stored at 4 °C.
4. Trace metal solution: 1.86 g Disodium EDTA, 0.69 g $FeSO_4{\cdot}7H_2O$, 0.2 g $MnCl_2{\cdot}4H_2O$, 0.29 g $ZnSO_4{\cdot}7H_2O$, and 0.025 g $CuSO_4{\cdot}5H_2O$ dissolved in 1 l distilled water, sterilized by autoclaving, and stored at 4 °C. Cover the solution with aluminium foil to avoid exposure to light.
5. 1 M $CaCl_2$: 55.5 g $CaCl_2$ dissolved in 1 l of H_2O, sterilized by autoclaving, and stored at 4 °C.
6. 1 M $MgSO_4$: 24.65 g $MgSO_4$ dissolved in 1 l of H_2O, sterilized by autoclaving, and stored at 4 °C.
7. S Medium: Mixture of 100 µl of 1 M potassium citrate, 100 ml of trace metal solution, 30 µl of 1 M $CaCl_2$, 30 µl of 1 M $MgSO_4$, and 10 ml of S Basal. Store the solution at 4 °C.
8. Tygon tube with ~1.6 mm inner diameter (Sigma, St. Louis, USA).
9. 18 Gauge syringe needles cut to a length of 8 mm.

2.4 Immobilizing C. elegans in PDMS Devices

1. S medium (as mentioned in Subheading 2.3).
2. Each model organism is grown using standard protocols. We describe the steps for *C. elegans* [51] below (for other model systems *see* Subheading 2.5).
3. OP50 bacteria grown overnight in LB diluted in half using S medium.
4. Stereomicroscope with magnification from 15 to 50× (e.g., Nikon SMZ645) to pick single organisms for experiments.
5. Compressed nitrogen gas line connected with the device through a variable pressure regulator and a three-way stopcock.
6. Inverted compound microscope equipped with a fluorescent filter set depending on the fluorescent protein tag used.
7. Camera of appropriate sensitivity to image bright field and/or fluorescence.

2.5 Immobilizing Drosophila and Zebrafish Larvae in PDMS Devices

1. *Drosophila* larvae [52] or zebrafish [53] grown using standard protocols as applicable for each model organism.
2. 1× PBS buffer.
3. First instar *Drosophila* larvae in 1× PBS buffer.
4. Dechorionated staged zebrafish larvae in 1× PBS buffer.
5. A low-magnification stereomicroscope such as Nikon SMZ645.
6. An inverted compound microscope with optics for imaging bright field and fluorescence such as Olympus IX71.

2.6 High-Resolution In Vivo Imaging of Organelle Transport in Genetic Model Organisms

1. Larval stage 1 (L1) and young adult (YA) transgenic *C. elegans* strain grown on NGM plates. *Drosophila* larvae [52] or zebrafish [53] grown using standard protocols. These strains typically express a fluorescent protein attached to another protein or by itself to mark the biological process under study. Typically in our laboratory we use markers for organelles to track their motion.
2. 1× M9 buffer.
3. Clean microfluidic device with compressed gas line connected with the device through a variable pressure regulator and a three-way stopcock.
4. Inverted microscope equipped with excitation laser and fluorescence collection using a sensitive camera.
5. ImageJ software to analyze particle motion using kymographs from the time-lapse images.

2.7 Cleaning and Storage of PDMS Devices for Future Use

1. Distilled water.
2. 70 % Alcohol.
3. 30 ml Syringe connected with a tube and metal coupler.
4. Desiccator to store device in dust-free environments.

3 Methods

We have designed simple double-layer microfluidic devices for immobilizing various model organisms that do not require precise alignment during fabrication [12]. These devices can be used to study cellular and subcellular processes in *C. elegans*, *Drosophila* larvae, and zebrafish larvae. In this chapter, we review the utility of such microfluidic devices for high-resolution bright-field and/or fluorescence imaging to carry out in vivo studies using the above model organisms. Our devices are fabricated using soft lithography molding of PDMS from SU8 photoresist patterns created on silicon substrates using optical photolithography. One can use the SU8 pattern on a silicon substrate ("SU8 master") over ~100 times

(until the SU8 patterns delaminate or deform) to obtain identical devices by repeating the soft lithography fabrication steps. Device designs are decided based on experimental needs and the model system under study. The dimensions are carefully chosen to fit the model organism, wherein width of the device is decided by the photomask design while its height is determined by the photoresist thickness. Our devices utilize the principle of double-layer PDMS fabrication with a thin layer of flexible PDMS membrane separating the two layers. Higher pressure in the top control channel layer deflects the thin flexible PDMS membrane and immobilizes the organism allowing it to be probed using optical imaging. On releasing the membrane, the organism is free from the trap and shows normal locomotion usually within 5 min. The animals survive post-immobilization and show normal growth when maintained under standard growth conditions. Carry out all experiments at room temperatures in the range of 20–22 °C unless mentioned otherwise.

3.1 Photolithography of SU8

1. Design the photomask using a computer-based design software such as AutoCAD, Solidworks, or Clewin. For *C. elegans* devices, set the width of the design at approximately 300 μm to allow enough space for a freely moving worm to swim inside the device. Keep the length of the channel around 10 mm to accommodate a ~2 mm central trapping region distant from both the inlet and outlet reservoirs by ~3 mm for ease in the punching steps (described in Subheading 3.2). For *Drosophila* or zebrafish, design a 5 mm wide central flow channel layer and 5 mm wide central trapping region in the control channel layer that is distant from the inlet and outlet reservoirs by about 2.5 mm. Print the design using a high-resolution laser printer (~10,000 dpi) to obtain smooth features on the mask.
2. Cut a polished silicon wafer into a 30 × 30 mm square shape for each device design using a diamond scriber. Take at least two such pieces, one each for the flow layer and the control layer.
3. Clean both wafer pieces using 20 % KOH for 1 min, rinse in deionized water, and blow dry using a blower nozzle attached to a compressed nitrogen cylinder.
4. Bake both silicon pieces on a hot plate at 150 °C for 30 min to dehydrate them. Cool down the silicon pieces to room temperature before using them for the next step.
5. Place one of the silicon pieces on the vacuum chuck of the spinner unit, and turn on the vacuum pump to hold it on place. Pipette ~20 μl of HMDS on the wafer, and spin coat the chemical at 5.9 × *g* for 5 s followed by 213 × *g* for 30 s. Pour ~2 ml of SU8-2050 on the silicon substrate to cover it completely. Spin the wafer at 5.9 × *g* for 5 s followed by 94.8 × *g* for 30 s

to produce a resist height of ~80 μm to fabricate the SU8 features for adult *C. elegans*, *Drosophila* larvae, and zebrafish larvae. In order to fabricate devices for early *C. elegans* larvae, spin coat silicon wafers using SU8-2025 at 5.9 × *g* for 5 s followed by 148.1 × *g* for 30 s to produce a resist height of ~35 μm. Turn off the vacuum, remove the wafer from the vacuum chuck, and leave it on a flat surface for 5 min.

6. Place the second silicon piece on the vacuum chuck, and turn on the vacuum pump to hold it in place. Repeat the steps above to coat the piece with HMDS. Pour ~2 ml of SU8-2050 on the silicon substrate to cover it completely. Spin the wafer at 5.9 × *g* for 5 s followed by 94.8 × *g* for 30 s to produce a resist height of ~80 μm to fabricate the SU8 features for the control layer.
7. Place both silicon pieces with SU8 coating on the hot plate to bake them at 65 °C for 1 min followed by 95 °C for 10 min. Turn off the hot plate, and allow the hot plate to cool down to room temperature while the silicon pieces continue to be kept on the hot plate. Leave the pieces at room temperature for an additional 10 min (*see* **Note 5**). Inspect the baked SU8-coated surface for bubbles. Do not use a defective SU8 resist-coated substrate with bubbles for UV exposure since it can lead to discontinuous channels after resist development.
8. Turn on the ultraviolet light source 15 min before use to stabilize the light source for photolithography exposure (Fig. 1a and *see* **Note 6**).
9. Mount one of the silicon wafers with 80 μm resist height, and expose it to UV light through the photomask #1 (for flow

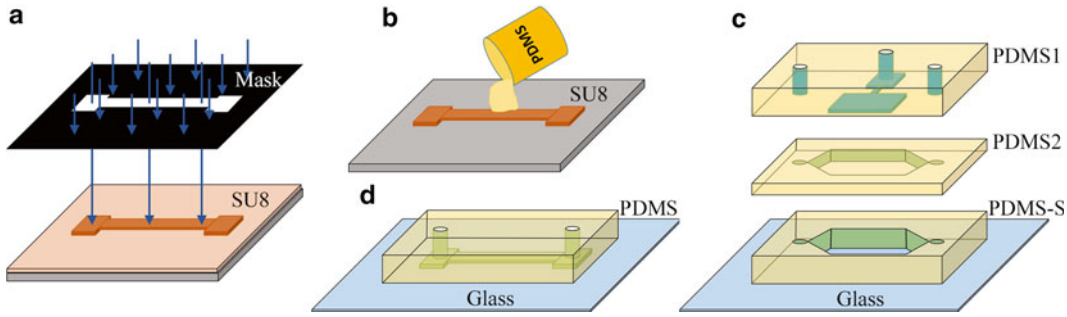

Fig. 1 Photolithography and soft lithography fabrication of microfluidic devices for model organisms. (**a**) Ultraviolet photolithography on SU8 photoresist through a user-defined photomask creates a master mould in SU8. (**b**) PDMS is mixed and poured on the SU8 mould to fabricate identical device dimensions repeatedly. (**d**) The devices are punched for access holes and bonded on to a glass cover slip for high-resolution imaging using plasma cleaning. (**c**) Shows a schematic diagram of the *Drosophila*/zebrafish device with a top control layer (PDMS1), a PDMS flow layer (PDMS2), and a thick spacer layer (PDMS-S) bonded to a glass cover slip

layer) for 15 s. Expose the second silicon piece for 15 s through the photomask #2 (for control layer). Leave both exposed silicon wafers at room temperature for 5 min.

10. Develop the wafers in the SU8 developer one by one till all the resist is developed, leaving only the pattern of the device on the flat silicon substrates. Wash the pattern using IPA, and blow dry using a blower nozzle attached to a compressed nitrogen cylinder to remove the solvent from the substrates. Incomplete development leaves white residues on the substrate. If such residue is present, repeat the above development step until the SU8 layer is completely developed.
11. Bake the silicon pieces at 120 °C for 15 min to hard bake the pattern. Turn off the hot plate, and allow it to cool down to room temperature with the silicon substrates continuing to be present on the hot plate. Leave the pieces at room temperature for an additional 10 min.

3.2 Soft Lithography of PDMS from the SU8 Pattern

1. Blow dry the SU8-patterned surfaces using a blower nozzle connected to a compressed nitrogen gas cylinder to remove any dust. Keep both silicon substrates with the SU8 patterns inside a vacuum desiccator. Take 50 μl of trichloro (1H,1H,2H,2H-perfluorooctyl)silane solution in a small plastic cup, and place it inside the desiccator. Close the lid of the desiccator to prevent entry of air or exit of vapor, and leave the wafers inside the silane vapor for ~2 h (*see* **Notes 7** and **8**).
2. Mix 15 g of PDMS base and 1.5 g of PDMS curing agent in a plastic cup. Stir the mixture well to ensure proper mixing. Degas the mixture using a vacuum desiccator for ~30 min to remove all the bubbles formed during stirring.
3. Hold the silicon piece with the SU8 pattern for the flow layer on the vacuum chuck of the spinner unit. Pour ~1 g of the PDMS mix on top of the SU8 pattern gently to avoid any bubble formation. For SU8 features with ~35 μm height for early *C. elegans* larvae devices, spin the PDMS on the wafer at $5.9 \times g$ for 5 s followed by $53.3 \times g$ for 30 s. Spin the PDMS on substrates with ~80 μm SU8 features for adult *C. elegans*, *Drosophila* larvae, and zebrafish larvae devices at $5.9 \times g$ for 5 s followed by $23.7 \times g$ for 30 s to obtain a thicker PDMS layer. In case you find additional bubbles, degas the wafer inside the vacuum desiccator as described in Subheading 3.2, **step 2**, to remove these bubbles. Keep the wafer with the spin-coated PDMS layer at room temperature for 5 min.
4. Keep the silicon wafer with the SU8 pattern for the control layer inside a petri dish, and pour ~10 g of the PDMS mix on the silicon. Adjust the amount of PDMS to obtain a height of ~8 mm on top of the silicon (height is adjusted by pouring

appropriate amount of PDMS) (Fig. 1b). Degas the PDMS if bubbles are formed during the pouring step as in Subheading 3.2, **step 2**.

5. Bake both silicon pieces with the PDMS layers at 65 °C for 4 h.
6. Take out the PDMS layer on the control mould, and allow it to cool down to room temperature. Cut the PDMS layer around the mould using a sharp blade. Peel it off from the silicon surface gently to avoid delamination and deformation of the SU8 features. Pour ~1 ml IPA on the wafer to ease the peeling process if necessary (Fig. 1d).
7. Punch access holes on the control layer channel inlet using the Harris micro-puncher.
8. Simultaneously expose the bottom surface of the bulk PDMS mould (PDMS1, Fig. 2a) and the top surface of the spin-coated PDMS layer of the flow layer (PDMS2, Fig. 2a) with 18 W air plasma for 2 min in a Harrick plasma chamber. Take out the pieces, and place the two exposed surfaces in contact within 30 s. Apply gentle pressure to remove air trapped at the interface.
9. Bake the bonded device at 65 °C for 2 h.
10. Take out the PDMS device, and cool it down to room temperature. Cut out the PDMS device from the silicon wafer with flow layer attached on top. Punch two access holes at the inlet and outlet reservoirs for the flow layer using the Harris puncher.
11. For *Drosophila* and zebrafish, make a PDMS spacer layer by casting a layer of PDMS on a plain glass ($22 \times 22 \times 1$ mm) of height ~500 μm and 900 μm, respectively (Fig. 1c). Bake the PDMS layer at 65 °C for 4 h. Cut the PDMS into the shape of the flow layer design from the center of the PDMS layer with a sharp surgical blade. Expose the top surface of the spacer layer and the bonded PDMS block to 18 W air plasma for 2 min. Take out the PDMS block and the buffer layer from the plasma chamber, and place the two surfaces in contact with each other immediately. Press the device with gentle pressure to avoid any air bubbles between the layers, and bake it at 65 °C for 2 h. Take out the device from the oven, and punch access holes for both the inlet and outlet.
12. Treat the PDMS device and a clean glass cover slip (grade 1.5) with 18 W air plasma for 2 min. Take out the device for *C. elegans* (Subheading 3.2, **step 10**) or *Drosophila*/zebrafish (Subheading 3.2, **step 11**) and the glass from the plasma chamber. Place the two exposed surfaces in contact with each other within 30 s. Press the PDMS top surface gently to avoid air bubbles at the interface (Fig. 2a).

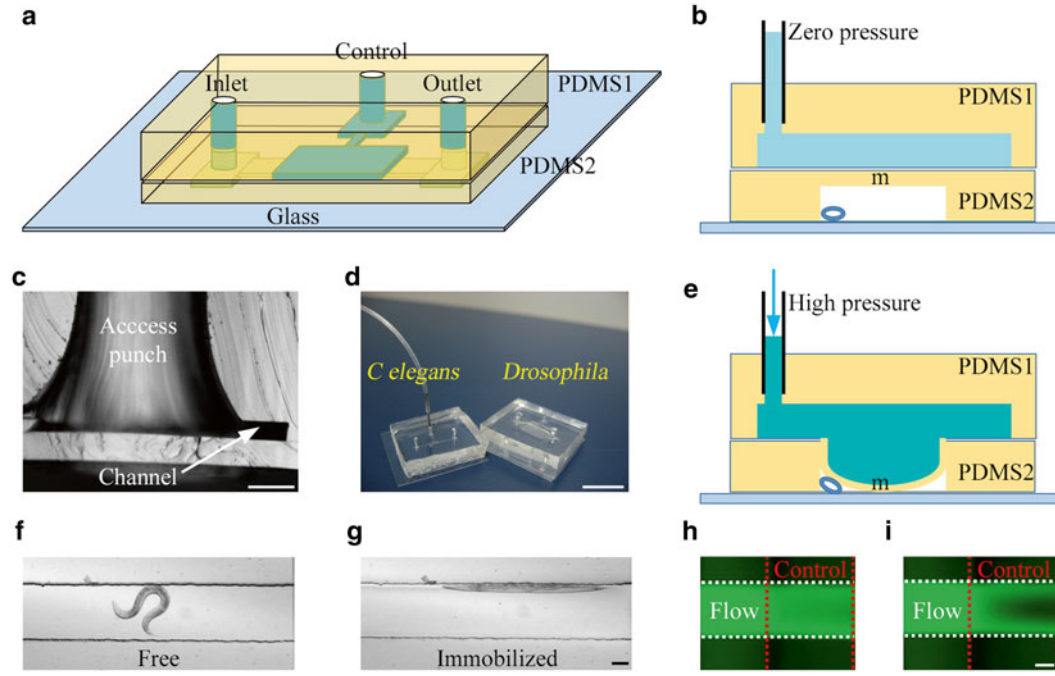

Fig. 2 Double-layer microfluidic devices for immobilization of genetic model organisms. (**a**) Schematic of a double-layer PDMS device bonded to a thin glass cover slip. Organisms are inserted into the flow channel (PDMS2, *bottom layer*) through the inlet. The control channel (PDMS1, *top layer*) is connected to a high-pressure line to deflect the flexible PDMS membrane that subsequently immobilizes the organism beneath the flexible membrane and inside the flow layer. Organisms initially move freely in the flow channel and under no pressure from the control channel (**b**) and immobilized under the flexible PDMS membrane (m) when pressure is applied to the control channel (**e**). (**c**) Shows the cross section of the channel and the access punch into the inlet reservoir of the top layer. (**d**) Images of PDMS devices for *C. elegans* and *Drosophila* larvae bonded to a glass cover slip. (**f** and **g**) Shows bright-field images of a free and immobilized adult *C. elegans*, respectively. (**h** and **i**) Shows displacement of fluorescein solution in the flow channel ("flow") when pressure is applied on the flexible PDMS membrane through the control channel ("control"). Scale bar, 200 μm (**c**), 10 μm (**d**), 100 μm (**g** and **i**)

13. Bake the device at 65 °C for 2 h.
14. Take the device out of the oven, and cool it to room temperature. Store the device in a dust-free environment such as a sealed desiccator.

3.3 Initial Characterization of the Fabricated Device

1. Inspect the device under a stereomicroscope to test for device defects such as improper bonding, channel blocks, improper punching, and biological contamination before proceeding to the next step (Fig. 2c, d) (*see* **Note 9**).
2. Place the device on an inverted compound microscope under a low magnification (4× or 10× lens).
3. Bring tubing (inner diameter 1.6 mm) with a metal coupler glued to one end and with the other end connected to a compressed nitrogen gas cylinder placed close to the microscope stage. Fill this tube with a ~10 cm distilled water column

through the metal coupler, and connect it to the control channel layer through the punched hole (Fig. 2a).

4. Turn on the gas pressure valve to ~5 psi, and observe the liquid column slowly migrate inside the control channel. Watch the control channel under a microscope; the water column will displace the air present in the control channel. Keep the pressure on until all air is displaced and the whole channel is filled with the water column.
5. In the absence of any defect, water should not leak from the control channel into the flow channel up to an applied pressure of 20 psi on the water column in the control layer. We have tested our devices up to 20 psi which is sufficient to immobilize all tested model systems under the flexible PDMS membrane (*see* **Note 10**).
6. Turn off the control pressure line, and fill the flow channel with S medium solution for 10 min prior to the experiment. This primes the flow channel with the same medium used during the experiment (*see* **Note 11**).
7. Test the ability of the membrane to deform by manually turning on and off the pressure line attached to the control layer. No bubbles should form in the flow channel during this test (Fig. 2b, e, h, i).

3.4 Immobilizing C. elegans in PDMS Devices

1. Collect 10–20 healthy *C. elegans* worms of a defined stage growing on an NGM plate using a sterile platinum pick or a drop of S medium solution. Place the collected animals in a 1.5 ml centrifuge tube with S medium.
2. Pipette in single worms along with ~2–5 μl volume of the S medium solution (*see* **Notes 12** and **13**).
3. Dispense the volume of liquid gently into the microfluidic device through the inlet reservoir (Fig. 2a). Watch the device entrance for a swimming worm using an inverted compound microscope with a bright-field light source and low-magnification objectives (4× or 10×) (*see* **Note 14**).
4. Stop pipetting pressure when a single worm is visible inside the device around the inlet reservoir. Adjust the pipetting pressure slowly to push the worm into the middle of the fluidic channel under the flexible PDMS membrane (Fig. 2f).
5. Turn on the three-way stopcock slowly when the worm is under the membrane to deflect the flexible PDMS membrane down towards the flow channel to immobilize the worm (*see* **Note 15**).
6. Turn on the final pressure (~14 psi) to immobilize the worm completely (Fig. 2g). Avoid single-step high-pressure immobilization trapping since it traps *C. elegans* in random orientation. Immobilization using incremental increase in pressure

provides sufficient time for the animal to be oriented along its length (Fig. 2g). We found it easier to track subcellular processes/organelles in *C. elegans* oriented along its length as the cells and the axons we imaged were in focus over longer lengths (*see* **Note 16**).

7. Choose the objective with the desired magnification and numerical aperture for high-resolution imaging. Use oil on the objective while using high NA oil immersion objectives.
8. Capture bright-field or fluorescent images for single or multiple frames with defined exposure times (Fig. 3a, b).

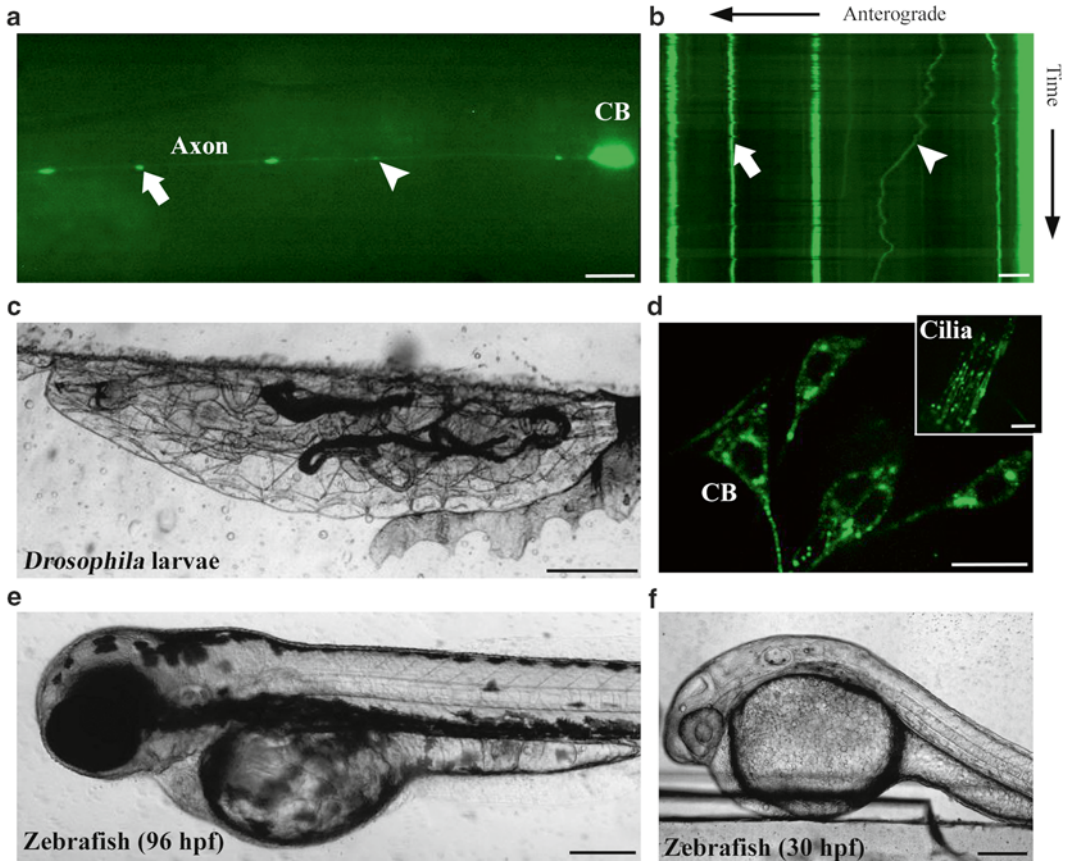

Fig. 3 High-resolution fluorescent and bright-field images from genetic model systems. (**a**) Shows a high-resolution fluorescent image of the anterior lateral mechanosensory neuron of *C. elegans* immobilized in a microfluidic device. (**b**) Time-lapse images are acquired from such neurons and converted to kymographs (time vs. distance) to analyze transport parameters. The *arrow* and the *triangle* show a stationary and moving mitochondrion, respectively. Similar devices are used to immobilize *Drosophila* larvae (**c**), 96 hpf zebrafish (**e**), and 30 hpf zebrafish (**f**). (**d**) Shows high-resolution fluorescent images of synaptotagmin-eGFP-marked cargo in sensory neurons of *Drosophila*. The *inset* shows the image of the sensory cilia in the same animal. Scale bar, 5 μm (**a**, *inset* in **d**), 10 μm (**b**, **d**), and 200 μm (**c**, **e**, and **f**)

9. After acquiring necessary images, shut off the fluorescent light arriving at the sample, and move the objective to a low-magnification bright-field settings as described in **step 3** above. Turn off the pressure in the control channel using the three-way stopcock (*see* **Note 17**).
10. Observe the organism under the membrane in the flow channel. In 5–10 min the organism will be freely moving in the flow channel (*see* **Note 18**).
11. Pipette 5–10 μl of buffer through the inlet channel to push the animal to the outlet reservoir. Collect the animal along with buffer at the outlet reservoir using a pipette.
12. Repeat **steps 2–11** to acquire data for the next worm. Alternatively the same worm can be retrapped and imaged for up to 1–2 h by trapping every 10 min after which the health of the animals deteriorates. Younger *C. elegans* larvae (L2, L3) cannot be retrapped in such short intervals. Add extra oil for the high NA oil immersion objective if necessary to avoid air bubbles during imaging (*see* **Note 19**).

3.5 Immobilizing Drosophila and Zebrafish Larvae in PDMS Devices

1. Pick a single first instar *Drosophila* larvae or a manually dechorionated zebrafish embryo using 1× PBS buffer and a wide-bore pipette tip under a low-magnification stereomicroscope.
2. Mount a microfluidic device fabricated with the appropriate height for the organism on an inverted compound microscope. Insert a single animal inside the microfluidic device through the inlet reservoir using 1× PBS buffer. Adjust the pipetting pressure to position the animal under the flexible PDMS membrane.
3. Watch the animal swimming in the buffer under the microscope using low magnification.
4. Turn on the pressure in the control channel slowly to the desired value (0.25–0.5 psi) such that the animal is immobilized under the membrane. Single-step high-pressure immobilization traps the animal in random orientation. Immobilization using incremental increase in pressure provides sufficient time for the animal to be oriented along its anterior–posterior axis (Fig. 3c, e). We found it easier to track subcellular processes/organelles in animals with this orientation for biological processes we imaged.
5. Release the pressure on the control channel after imaging, and watch the animal become free. Ensure that the animal moves/swims normally in buffer within 5–10 min after release from the trap.

6. Pipette 1× PBS into the inlet reservoir to remove the animal from the microfluidic channel through the outlet reservoir.
7. Pick the next animal, and repeat the above steps with each subsequent animal.

3.6 High-Resolution In Vivo Imaging of Organelle Transport in Genetic Model Organisms

1. Immobilize single L1 and YA *C. elegans* under the flexible PDMS membrane of a microfluidic device with channel height 35 μm and 80 μm, respectively, as mentioned in Subheading 3.4. Immobilize first instar *Drosophila* larvae under appropriate device as discussed in Subheading 3.5. These strains express a fluorescent protein either alone or tagged to another protein to mark the biological process under study. Typically in our laboratory we use markers for organelles to track their motion.
2. Mount the device on a high-resolution confocal fluorescence microscope.
3. Turn on a blue laser to image green fluorescence from GFP-labelled mitochondria (Fig. 3a, b) or RAB-3::GFP-marked presynaptic vesicles (Fig. 4a, b), respectively, in the neuronal process near the cell body of a mechanosensory neuron. Switch to appropriate objective to capture the desired bright-field or fluorescent images from device-immobilized *Drosophila* or zebrafish larvae (Fig. 3c–f).
4. Move the microscope stage to bring the axon in best focus and in the middle of the field of view (FOV). At optimum condition organelles will fluoresce as distinct particles in the neuronal process (Fig. 3a).
5. Adjust the laser power and detector gain to optimize fluorescence signal from moving organelles when acquired at ~2–5 frames per second (FPS).
6. Acquire 300 images for 70 s from the same portion of the axon for GFP::RAB-3-marked vesicles (Fig. 4a, b). Choose appropriate exposure times, frame rates, and imaging conditions for different cellular and subcellular processes.
7. Remove the animal by flushing the worm through the inlet.
8. Insert a new organism in respective devices, and repeat **steps 1–6** to acquire fluorescent images from the second animal.
9. Open all the image frames from a single worm using ImageJ software. Adjust brightness and contrast of the images for easy visualization of the GFP::RAB-3-marked vesicles or GFP-marked mitochondria.
10. Draw a line along the bright neuronal process in the first image frame, and analyze all frames using multiple-kymograph plug-in (Fig. 4a, c).

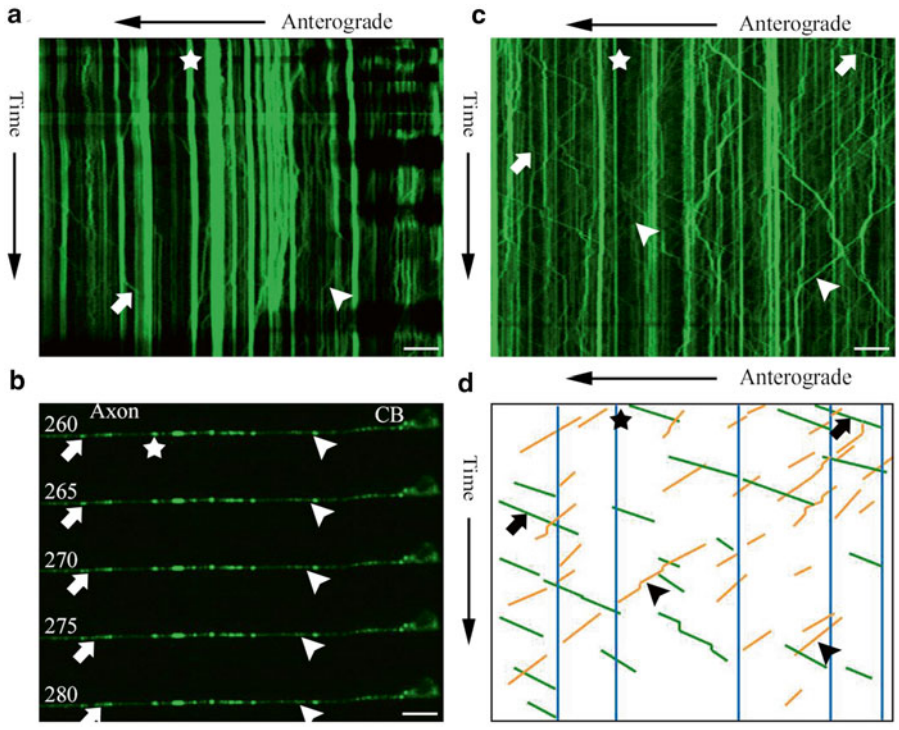

Fig. 4 In vivo imaging of GFP::RAB-3-marked presynaptic vesicles in *C. elegans* immobilized in microfluidic device. (**a**) Shows the kymograph of all 300 frames acquired from a posterior lateral mechanosensory (PLM) neuron of a *jsIs609* larval stage 1 (L1) worm. Anterograde, retrograde, and stationary particles are labelled with *arrowhead*, *arrow*, and *star*, respectively. The worm is immobilized under a flexible PDMS membrane inside a microfluidic device of channel height 35 μm. Images are acquired at five frames per seconds using 100× objective (oil immersion, numerical aperture 1.4). (**b**) Shows a montage of five frames indicating the position of vesicles. (**c**) Kymograph of GFP::RAB-3-marked vesicle transport from a young adult (YA) animal immobilized inside a microfluidic device with channel height of 80 μm. (**d**) Shows the traces of some of the vesicle trajectories from the kymograph. Scale bar, 5 μm

11. Trace every single-organelle paths using segmented lines in every kymograph (Fig. 4d). Analyze segmented lines for characteristics such as instantaneous velocity, pause frequency, and pause duration. Count the total number of lines through a thin neuronal process segment to calculate flux of particles in a movie [11].
12. Calculate average values for parameters from segmented values.

3.7 Cleaning and Storage of PDMS Devices for Future Use

1. Switch the high-magnification oil objective to a low-magnification air objective. Wipe the oil from the device using alcohol. Clean the oil from the high NA oil objective.
2. Turn off the pressure in the control layer, and then release the residual pressure in the main line. Observe the freely moving organism in the flow channel of the device.
3. Connect a syringe to the inlet, and flush the flow channel with S medium to push the organism out of the device. Collect the waste with the animal at the outlet reservoir.

4. Flush 100–200 μl of 70 % alcohol through the device using a syringe. Blow air through the device using a new syringe. Filter the alcohol if necessary to avoid entry of any particles inside the flow channel.
5. Wipe the device with alcohol, unplug the coupler for the control layer, and store the device inside a desiccator (*see* **Note 20**).

4 Notes

1. Set up microfabrication equipment in a room with stable ambient temperature, a yellow light source, and minimal dust. Keep the instruments as far from the room entrance as possible to minimize accumulation of dust particles on the devices during fabrication process. Presence of dust on the SU8 layer can lead to a break in the channel features after developing. The problem can be partially eliminated by carefully placing the photomask on the SU8 layer so that the dust does not directly contact the region under the transparent area in the photomask during the UV exposure step.
2. Wear eye protection and gloves during the fabrication process. Be aware that intense UV is harmful for your eyes and skin. Many of the chemicals used in this procedure are toxic to humans, and one needs to take adequate precautions when using them. Follow precautions listed in the MSDS and institutional rules for chemical handling.
3. Do not expose SU8 photoresist and SU8 developer to white light. Aliquot SU8 photoresist in small dark color/foil-wrapped bottles (~100 ml) to avoid any contamination with dust, bubbles, or high-intensity light. Bring SU8 to room temperature before use. Maintain a constant temperature in the fabrication process room to avoid variation in fabrication parameters during UV exposure and developing steps.
4. It is very difficult to clean SU8 photoresist from the lab bench or equipment. Wrap the spin coater with an aluminium foil to avoid any direct spills on equipment. Replace the foil before each use to keep the spin coater clean. Place a paper pad on the lab bench to avoid PDMS spills. Replace the pad after every fabrication process to keep the bench top clean.
5. Avoid fast-temperature ramps with SU8 fabrication. Ramp the temperature in the hot plate from 65 °C to 95 °C (~1–5 °C/s) and during cooling down to ambient temperature by changing the set temperature in the hot plate. Do not place SU8-coated substrates directly from room temperature on a hot plate at 95 °C. Allow the wafer to equilibrate at room temperature to avoid exposure of the resist material to high temperature while it is still hot due to previous baking step at 95 °C.

6. Too much roughness in the flow layer SU8 features can cause the PDMS layer to rupture when peeling off from the mould. We find that one of the main reasons for increased edge roughness is low-quality photo-plotting or improperly optimized UV exposure caused by a diverging beam and/or a larger gap between the sample and the photomask. A diverging beam results in two different beam diameters when observed at two separate distances. Adjust the beam such that you have an identical beam diameter at two separate distances from the lamp source. This is achieved by aligning the beam collimator system in the lamp housing as directed in the equipment manual. Use a soda lime glass slab on top of the photomask after placing it on the SU8-coated surface during UV exposure to avoid any gap between the photomask and the SU8 layer during UV exposure.
7. Silane vapor is very toxic and should be used only in a well-ventilated room. Leave the container for long-term incubation with the silicon wafers in a closed container such as desiccator and preferably under a fume hood.
8. We find that the SU8 mould can be used for 6–9 months. Repeat the silane vapor coating of the SU8 mould when PDMS begins sticking to the silicon substrate and peeling becomes difficult with time and multiple uses. Avoid excess silane treatment since it interferes with the spin-coated PDMS layer that will result in uneven thickness. An optimally coated surface will form a nice droplet with a 5–10 μl volume of water.
9. During initial device inspection, the integrity of the flexible PDMS membrane is tested by the application of ~5 psi pressure. Under this pressure, (a) an improperly bonded device delaminates and starts leaking, (b) a weak flexible membrane ruptures and the water column leaks from the control layer into the flow layer, (c) improper punching will cause leaks around the metal coupler (as mentioned in Subheading 3.3), and (d) biological or dust contamination will appear like foreign bodies inside the device channels.
10. One major reason for membrane rupture is low height of PDMS coated on control features. To increase the membrane thickness lower the spin speed during the PDMS coating step.
11. Prime the device sufficiently with S medium and 1× PBS for *C. elegans* devices and *Drosophila*/zebrafish devices, respectively, to get rid of trapped air in the flow channel. Insufficient priming can cause air bubble formation during experiments. A bubble in the flow channel can block the smooth flow of organisms during the experiment.
12. Prepare a fresh batch of S medium every week to avoid contamination of the medium and the device during the experiment.

13. Dilute a saturated OP50 bacterial solution in S medium just before the start of an experiment. Use the diluted solution within a week from its preparation.
14. Pick worms with minimal volume of buffer to keep the worms closer to the end of the pipette tip. Apply gentle pressure on the pipette to allow the worms to swim down the device inlet entry point into the flow channel. View the device inlet with a low-magnification objective (4× or 10×) to be able to see the worm moving down inside the device. Stop pipetting pressure when the worm is free inside the inlet reservoir. Load the pipette tip with fresh buffer, and apply gentle pressure to move the worm to the center of the device under the membrane.
15. Turn on the membrane pressure in small steps using a three-way stopcock to allow the animal (*C. elegans*, *Drosophila* larvae, and zebrafish larvae) to straighten along the side wall of the device as the flexible PDMS membrane is pushed down into the flow channel. When the organism is straight, increase the pressure in the control layer to immobilize the organism completely under the membrane.
16. Optimize both the immobilization pressure for the animal under study and the device dimensions. We observe poor image quality arising from inefficient immobilization. Often this is due to lower pressure applied on the flexible PDMS membrane. However higher pressure can damage the organism. Very high pressure often leads to rupture of the body wall muscle or cuticle, damaging the animal permanently. Very high pressure can damage the yolk in zebrafish larvae. Thus small changes in channel width, height, and flexible membrane thickness are best optimized for each organism and mutant genotype under investigation.
17. Minimize the time required to image the organism from the time when it is immobilized to reduce the effect of applied pressure on organism health and possible effects on the biological process under study.
18. Allow up to 10 min after releasing the organism from the trap to regain normal locomotion. Flush the animal with ~5–10 μL of buffer. We find it much easier to flush a healthy animal from the device compared to a sick or a dead animal. Damaged animals often stick to the device wall and have low resistance to buffer flow due to their straightened body shape.
19. The glass cover slip at the bottom of the device is in contact with the index matching oil while using a high NA oil immersion objective. Clean the glass bottom of the device thoroughly with alcohol to enable repeated use of the same device. This is especially critical for high-resolution imaging. An unwanted spot of the dried oil or dust contamination will blur or deform

the image in subsequent applications which is especially noticeable in high-resolution imaging.

20. Since one cannot clean the distilled water in the control layer channel, one needs to check for the presence of contamination before reuse. In case one finds contamination in the flow channel, do not use this device for high-resolution imaging. Foreign particles floating in the distilled water inside the control layer channel interfere with imaging. Typically one device can be used for 3 weeks before the contamination is visible inside the control layer and one needs to discard then. Such devices are discarded.

Acknowledgements

We thank Prof. Krishanu Ray (DBS-TIFR) for providing us with *Drosophila* stocks, Shikha Ahlawat for *jsIs609* imaging, Tarjani Agarwal for maintaining a *Drosophila* cage, and Dr. Vatsala Thirumalai (NCBS-TIFR) and Surya Prakash for providing us with zebrafish larvae. This work was funded by the DBT postdoctoral fellowship (S. M.), DST Fast-track scheme (S. M.), and a DBT grant (S. P. K.). S. P. K. is an HHMI International early career scientist.

References

1. Takayama S, Ostuni E, LeDuc P, Naruse K, Ingber DE, Whitesides GM (2001) Subcellular positioning of small molecules. Nature 411:1016
2. Lucchetta EM, Lee JH, Fu LA, Patel NH, Ismagilov RF (2005) Dynamics of Drosophila embryonic patterning network perturbed in space and time using microfluidics. Nature 434:1134–1138
3. Whitesides GM, Ostuni E, Takayama S, Jiang X, Ingber DE (2001) Soft lithography in biology and biochemistry. Annu Rev Biomed Eng 3:335–373
4. Sivagnanam V, Gijs MA (2013) Exploring living multicellular organisms, organs, and tissues using microfluidic systems. Chem Rev 113:3214–3247
5. Huang B, Wu H, Bhaya D et al (2007) Counting low-copy number proteins in a single cell. Science 315:81–84
6. Di Carlo D, Wu LY, Lee LP (2006) Dynamic single cell culture array. Lab Chip 6:1445–1449
7. Kobel S, Valero A, Latt J, Renaud P, Lutolf M (2010) Optimization of microfluidic single cell trapping for long-term on-chip culture. Lab Chip 10:857–863
8. Le Gac S, van den Berg A (2012) Single cell electroporation using microfluidic devices. Methods Mol Biol 853:65–82
9. Steinmeyer JD, Yanik MF (2012) High-throughput single-cell manipulation in brain tissue. PLoS One 7:e35603
10. Guo SX, Bourgeois F, Chokshi T et al (2008) Femtosecond laser nanoaxotomy lab-on-a-chip for in vivo nerve regeneration studies. Nat Methods 5:531–533
11. Mondal S, Ahlawat S, Rau K, Venkataraman V, Koushika SP (2011) Imaging in vivo neuronal transport in genetic model organisms using microfluidic devices. Traffic 12:372–385
12. Mondal S, Ahlawat S, Koushika SP (2012) Simple microfluidic devices for in vivo imaging of C. elegans, Drosophila and zebrafish. J Vis Exp 67:pii: 3780
13. Gilleland CL, Rohde CB, Zeng F, Yanik MF (2010) Microfluidic immobilization of physiologically active Caenorhabditis elegans. Nat Protoc 5:1888–1902
14. Xian B, Shen J, Chen W et al (2013) WormFarm: a quantitative control and measurement device toward automated

Caenorhabditis elegans aging analysis. Aging Cell 12:398–409

15. Yang J, Chen Z, Yang F, Wang S, Hou F (2013) A microfluidic device for rapid screening of chemotaxis-defective Caenorhabditis elegans mutants. Biomed Microdevices 15:211–220
16. Rezai P, Salam S, Selvaganapathy PR, Gupta BP (2012) Electrical sorting of Caenorhabditis elegans. Lab Chip 12:1831–1840
17. Kanodia JS, Liang HL, Kim Y et al (2012) Pattern formation by graded and uniform signals in the early Drosophila embryo. Biophys J 102:427–433
18. Ghannad-Rezaie M, Wang X, Mishra B, Collins C, Chronis N (2012) Microfluidic chips for in vivo imaging of cellular responses to neural injury in Drosophila larvae. PLoS One 7:e29869
19. Levario TJ, Zhan M, Lim B, Shvartsman SY, Lu H (2013) Microfluidic trap array for massively parallel imaging of Drosophila embryos. Nat Protoc 8:721–736
20. Chung K, Kim Y, Kanodia JS, Gong E, Shvartsman SY, Lu H (2011) A microfluidic array for large-scale ordering and orientation of embryos. Nat Methods 8:171–176
21. Wielhouwer EM, Ali S, Al-Afandi A et al (2011) Zebrafish embryo development in a microfluidic flow-through system. Lab Chip 11:1815–1824
22. Pardo-Martin C, Allalou A, Medina J, Eimon PM, Wahlby C, Fatih Yanik M (2013) High-throughput hyperdimensional vertebrate phenotyping. Nat Commun 4:1467
23. Hwang H, Lu H (2013) Microfluidic tools for developmental studies of small model organisms—nematodes, fruit flies, and zebrafish. Biotechnol J 8:192–205
24. Hulme SE, Shevkoplyas SS, Apfeld J, Fontana W, Whitesides GM (2007) A microfabricated array of clamps for immobilizing and imaging C. elegans. Lab Chip 7:1515–1523
25. Allen PB, Sgro AE, Chao DL et al (2008) Single-synapse ablation and long-term imaging in live C. elegans. J Neurosci Methods 173:20–26
26. Chronis N, Zimmer M, Bargmann CI (2007) Microfluidics for in vivo imaging of neuronal and behavioral activity in Caenorhabditis elegans. Nat Methods 4:727–731
27. Rohde CB, Zeng F, Gonzalez-Rubio R, Angel M, Yanik MF (2007) Microfluidic system for on-chip high-throughput whole-animal sorting and screening at subcellular resolution. Proc Natl Acad Sci U S A 104:13891–13895
28. Chung K, Crane MM, Lu H (2008) Automated on-chip rapid microscopy, phenotyping and sorting of C. elegans. Nat Methods 5:637–643
29. Zeng F, Rohde CB, Yanik MF (2008) Sub-cellular precision on-chip small-animal immobilization, multi-photon imaging and femtosecond-laser manipulation. Lab Chip 8:653–656
30. Krajniak J, Lu H (2010) Long-term high-resolution imaging and culture of C. elegans in chip-gel hybrid microfluidic device for developmental studies. Lab Chip 10:1862–1868
31. Krajniak J, Hao Y, Mak HY, Lu H (2013) C.L.I.P.-continuous live imaging platform for direct observation of C. elegans physiological processes. Lab Chip 13:2963–2971
32. Chokshi TV, Ben-Yakar A, Chronis N (2009) CO_2 and compressive immobilization of C. elegans on-chip. Lab Chip 9:151–157
33. Chuang HS, Chen HY, Chen CS, Chiu WT (2013) Immobilization of the nematode Caenorhabditis elegans with addressable light-induced heat knockdown (ALINK). Lab Chip 13:2980–2989
34. Caceres Ide C, Valmas N, Hilliard MA, Lu H (2012) Laterally orienting C. elegans using geometry at microscale for high-throughput visual screens in neurodegeneration and neuronal development studies. PLoS One 7:e35037
35. Hu C, Dillon J, Kearn J et al (2013) NeuroChip: a microfluidic electrophysiological device for genetic and chemical biology screening of Caenorhabditis elegans adult and larvae. PLoS One 8:e64297
36. Lockery SR, Hulme SE, Roberts WM et al (2012) A microfluidic device for whole-animal drug screening using electrophysiological measures in the nematode C. elegans. Lab Chip 12:2211–2220
37. Lee H, Crane MM, Zhang Y, Lu H (2013) Quantitative screening of genes regulating tryptophan hydroxylase transcription in Caenorhabditis elegans using microfluidics and an adaptive algorithm. Integr Biol (Camb) 5:372–380
38. Orozco JT, Wedaman KP, Signor D, Brown H, Rose L, Scholey JM (1999) Movement of motor and cargo along cilia. Nature 398:674
39. Norris AD, Lundquist EA (2011) UNC-6/netrin and its receptors UNC-5 and UNC-40/DCC modulate growth cone protrusion in vivo in C. elegans. Development 138:4433–4442
40. Alan JK, Lundquist EA (2012) Analysis of Rho GTPase function in axon pathfinding using

Caenorhabditis elegans. Methods Mol Biol 827:339–358

41. Ou G, Vale RD (2009) Molecular signatures of cell migration in C. elegans Q neuroblasts. J Cell Biol 185:77–85
42. Dai J, Ting-Beall HP, Sheetz MP (1997) The secretion-coupled endocytosis correlates with membrane tension changes in RBL 2H3 cells. J Gen Physiol 110:1–10
43. Wang X, Schwarz TL (2009) Imaging axonal transport of mitochondria. Methods Enzymol 457:319–333
44. Plucinska G, Paquet D, Hruscha A et al (2012) In vivo imaging of disease-related mitochondrial dynamics in a vertebrate model system. J Neurosci 32:16203–16212
45. Murthy K, Bhat JM, Koushika SP (2011) In vivo imaging of retrogradely transported synaptic vesicle proteins in Caenorhabditis elegans neurons. Traffic 12:89–101
46. Simpson HD, Kita EM, Scott EK, Goodhill GJ (2012) A quantitative analysis of branching, growth cone turning, and directed growth in zebrafish retinotectal axon guidance. J Comp Neurol 521:1409–1429
47. Roossien DH, Lamoureux P, Van Vactor D, Miller KE (2013) Drosophila growth cones advance by forward translocation of the neuronal cytoskeletal meshwork in vivo. PLoS One 8:e80136
48. Wolman MA, Sittaramane VK, Essner JJ, Yost HJ, Chandrasekhar A, Halloran MC (2008) Transient axonal glycoprotein-1 (TAG-1) and laminin-alpha1 regulate dynamic growth cone behaviors and initial axon direction in vivo. Neural Dev 3:6
49. Daniels BR, Masi BC, Wirtz D (2006) Probing single-cell micromechanics in vivo: the microrheology of C. elegans developing embryos. Biophys J 90:4712–4719
50. Surana S, Bhat JM, Koushika SP, Krishnan Y (2011) An autonomous DNA nanomachine maps spatiotemporal pH changes in a multicellular living organism. Nat Commun 2:340
51. Brenner S (1974) The genetics of Caenorhabditis elegans. Genetics 77:71–94
52. Ashburner M, Roote J (2007) Maintenance of a Drosophila laboratory: general procedures. CSH Protoc 2007:pdp ip35
53. Avdesh A, Chen M, Martin-Iverson MT (2012) Regular care and maintenance of a zebrafish (Danio rerio) laboratory: an introduction. J Vis Exp. (69): e4196

Chapter 27

The "In Situ" Proximity Ligation Assay to Probe Protein–Protein Interactions in Intact Tissues

Arianna Bellucci, Chiara Fiorentini, Michela Zaltieri, Cristina Missale, and PierFranco Spano

Abstract

The proximity ligation assay (PLA) is a sensitive and specific technique to visualize proteins, their posttranslational modifications and activation state as well as protein–protein interactions.

The assay is based on the employment of proximity probes, composed by oligonucleotide-conjugated antibodies, to recognize a couple of specific targets. The binding of probes in close proximity allows for their hybridization by connector oligonucleotides, that can form a circular DNA strand. These DNA circles can then be amplified by polymerase chain reaction. Finally, the conjugation of fluorescence-labelled oligonucleotides with the amplification product allows for the localized detection of individual or interacting proteins in cells and tissues.

Here, we describe the use of "in situ" PLA to visualize the localization of protein–protein interactions in intact tissues.

Key words Protein–protein interaction, "In situ" proximity ligation assay (PLA), Intact tissue, Confocal microscopy

1 Introduction

The "in situ" proximity ligation assay (PLA) was developed to provide visualization of proteins and of their posttranslational modifications and activation state. However, PLA also allows for the localized detection of endogenous protein–protein interactions in fixed cells and intact tissues [1–4]. In the latter case, the assay is based on the detection of interacting proteins by a couple of "proximity probes" encompassed by a target-specific antibody, which can either be covalently or non-covalently conjugated with an oligonucleotide sequence. When the probes bind to a couple of ligands located in close proximity (<16 nm) the conjugated-oligonucleotides can be hybridized with two connector oligonucleotides which are then ligated to form a circular DNA molecule [2]. This latter, can be then amplified by polymerase chain reaction (PCR) and hybridized

Andrei I. Ivanov (ed.), *Exocytosis and Endocytosis*, Methods in Molecular Biology, vol. 1174,
DOI 10.1007/978-1-4939-0944-5_27,

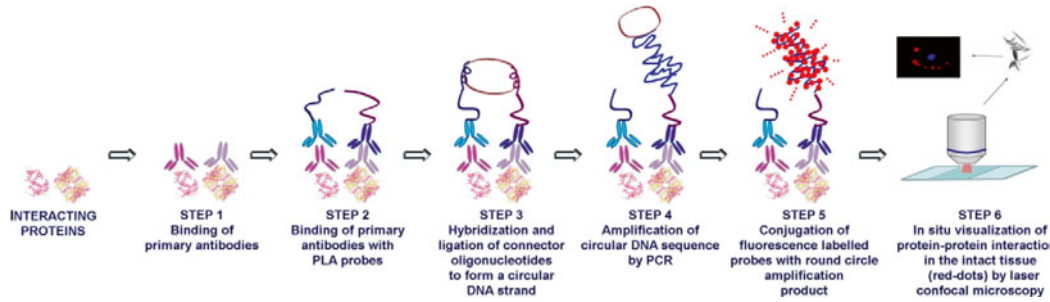

Fig. 1 Schematic representation of detection of protein–protein interactions in fixed tissue or cell cultures by indirect "in situ" PLA. *STEP 1*: the interacting target proteins are recognized by two specific primary antibodies. *STEP 2*: a couple of oligonucleotide-conjugated secondary antibodies (PLA-probes) recognizing the primary antibodies used to bind targeted proteins is added to the sample. *STEP 3*: when the targeted proteins are located in close proximity, the PLA probes can be hybridized to connector oligonucleotides to form a round circle which is then stably ligated to the target template by DNA ligase to form a circular oligonucleotide. *STEP 4*: the circular oligonucleotide is then amplified by PCR during the rolling circle amplification step. *STEP 5*: the resulting product is finally hybridized with fluorescence-labelled oligonucleotides. *STEP 6*: laser confocal microscopy allows for the "in situ" visualization of protein–protein interactions as *red dots* in the slide mounted tissue sections

in turn with fluorescence-labelled complementary oligonucleotides. Hence, at the end of the assay, the interaction of endogenous target proteins can be visualized "in situ" by confocal microscopy [5].

Differently from other standardized methods for detection of protein–protein interactions, such as co-immunoprecipitation (Co-IP) (*see* **Note 1**) or bioluminescence resonance energy transfer (BRET) and fluorescence resonance energy transfer (FRET), which usually fail to reveal the cellular context of molecules, "in situ" PLA allows for the visualization of tissue-, cellular-, and subcellular-specific endogenous antigen interactions. In addition, the assay offers the possibility to investigate the distribution of protein–protein complexes in both physiological and pathological conditions [6, 7] and the way is open toward novel potential applications in the proteomic field.

The "in situ" PLA method can be performed either directly (direct targeting "in situ" PLA), by using primary oligonucleotide-conjugated antibodies, or indirectly (indirect targeting "in situ" PLA) (Fig. 1) by using proximity PLA probes recognizing the primary antibodies bound to the target proteins (*see* **Note 2**).

Recently, we described that indirect targeting "in situ" PLA is an optimal method to visualize localization of endogenous interacting proteins in tissue and in particular, to detect the redistribution of specific protein complexes in the brain [7]. To perform this study we first evaluated the distribution of our target proteins of interest: alpha-synuclein and the dopamine transporter (DAT) by double fluorescence immunohistochemistry in the mouse brain tissue (Fig. 2a).

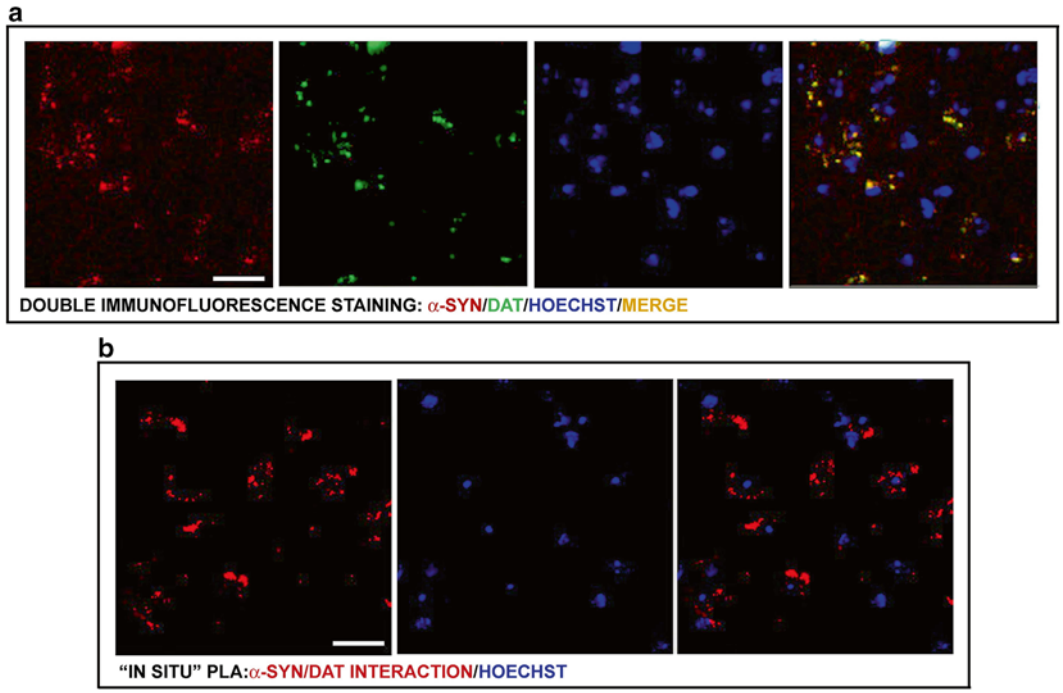

Fig. 2 Double fluorescence immunohistochemical protein labelling and "in situ" PLA-positive signal. (**a**) Visualization of alpha-synuclein (*red*) and DAT (*green*) in the striatum by using 30 μm PFA-fixed cryostat coronal brain sections of C57BL/6 J mice. (**b**) Visualization of DAT/alpha-synuclein complexes by "in situ" PLA in the striatum by using 30 μm PFA-fixed cryostat coronal brain sections of C57BL/6 J mice. *Red dots* are indicative of areas where the two proteins are interacting. Scale bars, 40 μm (panel **a**) and 25 μm (panel **b**)

Then, we optimized the "in situ" PLA protocol to visualize alpha-synuclein/DAT interaction "in situ" on mouse striatal brain sections (Fig. 2b).

Below, we describe an optimized method to perform indirect targeting "in situ" PLA to visualize the localization of interacting proteins in fixed intact tissue and we provide an exhaustive list of advantages and disadvantages linked to the employment of this technique when compared with widely used methods for detection of protein–protein interactions.

2 Materials

Tissue samples must be fixed in ice-cold 4 % paraformaldehyde (PFA) solution (*see* **Note 3**). The experiment can be performed either by using free-floating sections or by open droplet reactions on slide-mounted sections. In the latter case, all the incubations must be performed in a humidity chamber to prevent evaporation. Furthermore, the optimal volume of working solution for the reaction area must be previously determined by the operator.

Before performing "in situ" PLA to visualize protein–protein interactions it is strongly recommended to perform a series of preliminary analysis in the tissue of interest (*see* **Note 4**).

2.1 "In Situ" PLA

Prepare all the solutions in deionized water and store them at 4 °C.

1. Phosphate Buffer Saline (PBS)*:* 137 mM NaCl, 2.7 mM KCl, 10 mM Na_2HPO_4, 2 mM KH_2PO_4 pH 7.4.
2. 4 % PFA solution pH 7.4: 4 % (w/v) PFA in PBS pH 7.4.
3. 18 % Sucrose solution: 18 % (w/v) sucrose in PBS pH 7.4.
4. Storage Buffer: PBS with 0.1 % BSA.
5. Tris Buffered Saline with Tween-20 (TBS-T): 50 mM Tris–HCl, 138 mM NaCl, 2.7 mM KCl, pH 7.4 containing 0.05 % Tween-20.
6. Saline Sodium Citrate (SSC) buffer 20× stock solution: 3 M Na-Citrate, 0.3 M NaCl, pH 7.0.
7. SSC-T buffer A: 2× SSC buffer containing 0.05 % Tween-20.
8. SSC-T buffer B: 1× SSC buffer containing 0.05 % Tween-20.
9. SSC buffer C: 0.2× SSC buffer.
10. SSC buffer D: 0.02× SSC buffer.
11. PLA probe mix: to prepare oligonucleotide-linked antibodies incubate 100 nM oligonucleotide-streptavidin complexes with 100 nM of biotinylated antibody solution for 1 h at RT. Then directly dilute the deriving PLA probes in PLA solution containing 50 ng/μl RNase A, 2.5 ng/μl poly(A), 2.5 mM cysteine, 5 mM EDTA, and 0.05 % Tween-20 in TBS.
12. Ligation mix: 10 mM Tris-acetate pH 7.5, 10 mM magnesium acetate, 50 mM potassium acetate, 0.05 U/μl T4 DNA ligase, 250 mM NaCl, 250 ng/μl BSA, and 0.05 % Tween-20 in H_2O.
13. Amplification mix: 50 mM Tris–HCl pH 7.5, 10 mM $MgCl_2$, 10 mM $(NH_4)_2SO_4$, 250 μM dNTPs, 250 ng/μl BSA, and 0.05 % Tween-20.
14. Detection mix: 2× SSC, 7.5 ng/μl poly(A), 250 ng/μl BSA, 0.05 % Tween-20 containing 5 nM of fluorescence-labelled probe (Alexa).

2.2 Microscopy

1. Microscope slides: 1–1.2 mm thick microscope slides and 0.13–0.16 mm thick coverslips.
2. Mounting solution: optimal PLA signal detection in tissue can be achieved by using the VECTASHIELD mounting medium (Vector Laboratories, Burlingame, CA, USA).
3. Laser confocal microscope: Laser confocal microscopes must be equipped with 40× and 60× oil objectives and 543/633 HeNe and 405 Diode excitation lasers plus image acquisition

software. Optimal image acquisitions may be achieved by using a Zeiss LSM 510 Laser Scanning Microscope in combination with LSM Image Browser software (Carl Zeiss, Advanced Imaging Microscopy, Jena, Germany).

4. Image analysis software: Image J (http://rsbweb.nih.gov/ij/) (NIH, Bethesda, MD, USA).

3 Methods

3.1 Indirect Targeting "In Situ" PLA

1. Isolate tissue samples in ice-cold PBS solution and gently wash them with PBS to remove blood. Place tissue in ice-cold freshly made 4 % PFA solution at 4 °C for 24–48 h depending on the size of tissue samples (*see* **Note 5**). Tissue slices (15–30 μm thick) can now be obtained by vibratome sectioning. When choosing to perform cryostat sectioning put tissue samples in 18 % sucrose solution at 4 °C for 24 h for cryoprotection, quickly freeze tissue at −20 °C and cut sections (15–30 μm thick). Use either free-floating or slide-mounted tissue sections (*see* **Note 6**).
2. Set up the PLA experiment in order to have the following samples in duplicate: (a) a sample of interest; (b) a negative control without one of the primary antibody recognizing the target protein of interest; (c) a negative control consisting of a knock-out of one of the targeted proteins; (d) a positive control representing a tissue or cultured cell sample with well-documented interactions between the two targeted proteins.
3. Choose primary antibodies (monoclonal or polyclonal) of IgG-class specific for the targeted proteins (*see* **Note 7**). Mix and dilute the primary antibodies in blocking solution made up by storage buffer containing antibody specific blocking sera and 0.3–0.03 % Triton X-100. Remove the blocking solution and immediately add primary antibodies to samples. Incubate either overnight at 4 °C or for at least 90 min at room temperature (RT).
4. Remove primary antibodies and wash the samples three times for 5–10 min with washing buffer under gentle orbital shaking. Add the PLA probe solution and incubate up to 2 h at either RT or 37 °C. The length of the PLA probe oligonucleotide sequence (*see* **Note 8**) and the concentration of proximity probes must be optimized by the operator in order to avoid unspecific trapping.
5. Prepare the hybridization solution by diluting 125 nM of connector oligonucleotides in the ligation mix. Remove the PLA probe solution, wash the samples at least twice for 5–10 min in TBS-T and incubate them in hybridization solution for 15 min at 37 °C.

6. Wash the samples three times for 5–10 min in TBS-T. Incubate them with the ligation mix supplemented with 0.05 U/μl of T4 DNA ligase for 30 min at 37 °C.
7. Remove the ligation mix and wash the samples three times for 5–10 min in TBS-T. During the last wash prepare the amplification solution by adding 0.125 U/μl phi29 DNA polymerase. Add this solution to samples and incubate them for 90 min at 37 °C.
8. From this stage, the tissue sections must be protected from light to prevent quenching of fluorescence-labelled oligonucleotides. Remove the amplification solution and wash the samples twice for 5–10 min with TBS-T under gentle agitation. Add detection mix containing fluorescence-labelled probes to hybridize the round circle amplification product and incubate for 30 min at 37 °C.
9. Wash the samples twice in TBS-T for 5–10 min and then once for 5–10 min in H_2O. Incubate the sections in 1 μM Hoechst 33342 diluted in H_2O for 1 min at RT.
10. Before performing these washing steps freely floating sections must be mounted on microscope slides. Final washing remove the excess of detection reagents to avoid the formation of unspecific background. The sections must be consequently washed in the following solutions:

    SSC-T A buffer for 5 min

    SSC-T B buffer for 5 min

    SSC C buffer for 5 min

    SSC D buffer for 5 min

    70 % Ethanol for 1 min

    At the end of this step let the sections dry.
11. Slide-mounted sections must be covered with a minimal volume of the appropriate mounting medium (2–3 μl) for laser confocal microscopy and covered with coverslip. Slides should be protected from light and can be stored at 4 °C for several days or at −20 °C for longer periods.
12. Examine the results of PLA by laser confocal microscopy with 40× and 60× oil objectives. Excitation of samples must be obtained either by using 543 or 633 HeNe laser for detection of PLA signal and Diode 405 for detection of Hoechst signal. Optimal height of sections' scanning is about 1 μm. Sequential Z-stuck scanning is useful to appreciate the size of protein complexes. Acquire a minimum of 10 high resolution images from each specimen and analyze them by Image J to calculate the density of PLA puncta. At the first image analysis set threshold manually to discriminate the PLA signal from background fluorescence. Then, apply this threshold setting to all

the following image analysis. Use the built in macro "Analyze particles" to count all the objects in the thresholded image. Discard objects larger than 5 μm to remove nuclei signal, and count the remaining objects as PLA puncta. Density of PLA signal can be estimated by dividing total positive area for the number of positive PLA puncta.

4 Notes

1. Co-immunoprecipitation (Co-IP), a widely used biochemical method to study protein–protein interactions, is based on the use of an antibody to pull down the protein of interest and all interacting proteins. A list of advantages and disadvantages linked to the usage of Co-IP versus "in situ" PLA to detect protein–protein interactions is provided below:

Advantages of Co-IP:

- Low-cost and easy-to-use technique. When appropriate controls are used, Co-IP represents a valid technique for demonstrating protein–protein interaction.
- Allows for detection of native protein complexes in cell lines or tissues in which they are endogenously expressed by using a specific antibody. In these conditions any artificial effects of tags or protein overexpression are avoided.
- The proteins of interest can be expressed in heterologous expression systems with a plasmid encoding a tagged bait protein that circumvents the need for a specific antibody.
- Specificity of this technique can be increased by performing subcellular fractionation step prior to performing Co-IP if the interaction takes place in a specific organelle.
- Analyses of the proteins involved in the complex evaluated by western blot or by mass spectrometry can reveal new interacting partners of a known bait protein.

Disadvantages of Co-IP:

- Low expression levels and the difficulties of obtaining highly specific antibodies recognizing the protein of interest represent the main problem.
- High risk of detecting nonspecific interactions due to the presence of highly abundant contaminant proteins. In addition, the presence of eluted antibody light and heavy chains may interfere with detection of target proteins during western blot analysis.
- Larger molecular complexes might be difficult to analyze.
- Data obtained in transfected cells should be interpreted with caution since they represent artificial systems possible lacking

of appropriate molecular chaperones, escort proteins, or co-receptors. Moreover, artificial protein–protein interactions could be detected due to non-physiological expression levels or interactions with tag.

- The native cellular environment that may affect the integrity of the protein complexes is loss.
- Co-IP of highly hydrophobic membrane proteins or extreme levels of protein expression require solubilization, that itself induces protein–protein aggregation. By contrast, interaction with proteins could occur due to incomplete solubilization.
- Difficulties in identifying less-stable interactions because of the requirement of extensive washing to eliminate nonspecifically bound proteins. However, cross-linking techniques in combination with Co-IP could be applied to stabilize labile protein–protein interactions through covalent bonds.
- It does not allow for the localized visualization of protein–protein interactions "in situ" in intact tissue.

2. When the targeted proteins are localized intracellularly, it is desirable to use cell permeabilization to allow for better penetration of primary antibodies (for instance, 20 % methanol and/or 0.3 % Triton X-100). Please avoid the use of heat-induced or RT antigen retrieval as these techniques may change epitopes' conformations, thus causing detection of false positives or precluding the visualization of protein complexes.
3. When starting from freshly frozen tissue samples, the tissue sections can be cut by a cryostat and then fixed in ice-cold 4 % PFA for 5 min.
4. Perform (a) Co-IP experiments to assay the interaction between the targeted proteins in the tissue of interest; (b) double immunofluorescence staining coupled to confocal microscopy to evaluate the distribution of the targeted proteins in the tissue of interest. This will give the operator an idea about localization and interactions of these proteins in the intact tissue; (c) choose proper negative controls to minimize the possibility of false positive results. For instance, when working with animal tissues, the animals with knockout of one of the targeted proteins would represent an optimal negative control.
5. Tissues with higher amount of blood or fat may require longer fixation time.
6. The use of free-floating sections allows for better penetration and binding of primary antibodies and proximity probes but may lead to false positive results. The use of slide-mounted sections allows for consumption of less reagents. Please note that when working with slide-mounted sections it is recommended to delimit the reaction area with a PAP pen.

7. When using "in situ" PLA to detect interactions between two trans-membrane proteins it is important that the primary antibodies chosen for the assay recognize epitopes of both proteins located on the same face of the plasma membrane.
8. Since the distance between the epitopes is a powerful determinant of PLA efficiency, the length of the PLA probe could be modified to improve the specificity of the assay either by reducing the detection distance or by increasing such a distance (e.g., longer DNA sequences to detect substrates belonging to a multi-protein complex).

Acknowledgements

This work was supported by the Regione Lombardia, Italy NEDD Project (CUPH81J09002660007).

References

1. Fredriksson S, Gullberg M, Jarvius J et al (2002) Protein detection using proximity-dependent DNA ligation assays. Nat Biotechnol 20:473–477
2. Soderberg O, Leuchowius KJ, Gullberg M et al (2008) Characterizing proteins and their interactions in cells and tissues using the in situ proximity ligation assay. Methods 45: 227–232
3. Weibrecht I, Leuchowius KJ, Clausson CM et al (2010) Proximity ligation assays: a recent addition to the proteomics toolbox. Expert Rev Proteomics 7:401–409
4. Soderberg O, Leuchowius KJ, Kamali-Moghaddam M et al (2007) Proximity ligation: a specific and versatile tool for the proteomic era. Genet Eng (N Y) 28:85–93
5. Soderberg O, Gullberg M, Jarvius M et al (2006) Direct observation of individual endogenous protein complexes in situ by proximity ligation. Nat Methods 3:995–1000
6. Trifilieff P, Feng B, Urizar E et al (2011) Increasing dopamine D2 receptor expression in the adult nucleus accumbens enhances motivation. Mol Psychiatry 51:111–118
7. Bellucci A, Navarria L, Falarti E et al (2011) Redistribution of DAT/alpha-synuclein complexes visualized by "in situ" proximity ligation assay in transgenic mice modelling early Parkinson's disease. PLoS One 6:e27959

Chapter 28

Probing the Role of the Actin Cytoskeleton During Regulated Exocytosis by Intravital Microscopy

Oleg Milberg, Muhibullah Tora, Akiko Shitara, Taishin Takuma, Andrius Masedunskas, and Roberto Weigert

Abstract

The actin cytoskeleton plays a fundamental role in controlling several steps during regulated exocytosis. Here, we describe a combination of procedures that are aimed at studying the dynamics and the mechanism of the actin cytoskeleton in the salivary glands of live rodents, a model for exocrine secretion. Our approach relies on intravital microscopy, an imaging technique that enables imaging biological events in live animals at a subcellular resolution, and it is complemented by the use of pharmacological agents and indirect immunofluorescence in the salivary tissue.

Key words Intravital microscopy, Exocytosis, Actin cytoskeleton, Membrane trafficking, Salivary glands

1 Introduction

Exocytosis is the process by which proteins are delivered by membranous carriers to the surface of cells and released into the extracellular space [1]. Proteins can be sorted to undergo either constitutive exocytosis, which occurs in all cell types, or regulated exocytosis, which occurs only in specialized secretory cells following the stimulation of specific cell surface receptor [2]. Activation of those receptors elicits a series of signaling pathways that lead to docking and fusion of the membranous carriers into the plasma membrane [1]. This multistep process is controlled by several molecules including the actin cytoskeleton and its regulators, which have been shown to play multiple roles by either promoting or inhibiting the various exocytic steps [3, 4].

Our lab has developed a methodology to study how regulated exocytosis occurs in the exocrine organs in live rodents by using intravital microscopy (IVM) [5, 6]. Specifically, we focused on studying the dynamics of the large secretory granules in the acinar

Andrei I. Ivanov (ed.), *Exocytosis and Endocytosis*, Methods in Molecular Biology, vol. 1174,
DOI 10.1007/978-1-4939-0944-5_28,

cells of the submandibular salivary glands (SSGs) that in resting conditions are localized at the apical plasma membranes (APM) [7]. We showed that upon stimulation of the β-adrenergic receptors, secretory granules fuse with the APM and recruit an actomyosin complex that plays three major functions: (1) to provide a scaffold to protect the granules from the hydrostatic pressure generated by fluid secretion, (2) to regulate the process of membrane integration of the secretory granule into the APM, and (3) to act as a barrier to prevent compound exocytosis from occurring in vivo [7, 8].

Uncovering the molecular machinery regulating the assembly of the actin cytoskeleton during regulated exocytosis in vivo is our ultimate goal. To this end, we employ a series of strategies based on in vivo transient transfection of fluorescently tagged probes for the actin cytoskeleton, transgenic animal models, and selective delivery of pharmacological inhibitors. Specifically, we use rats for non-viral based delivery of plasmid DNA and selected transgenic mouse models expressing (1) the F-actin probe Lifeact tagged with either GFP or RFP [9, 10], (2) the membrane-targeted peptide mTomato [7], and (3) cytoplasmic GFP [7]. In addition, we complement data obtained using intravital microscopy with indirect immunofluorescence of cryosections of the SSGs, to gain a larger perspective of the molecules involved in the exocytic process. The goal of this chapter is to provide investigators interested in studying the actin cytoskeleton with a basic set of modular protocols that will enable investigating F-actin dynamics and its regulation in vivo. Although the procedures described in here are tailored towards regulated exocytosis, they can be easily adapted to other areas of cell biology.

2 Materials

2.1 Animals and Surgical Tools

1. Sprague–Dawley rats, 150–250 g body weight (Harlan Laboratories, Frederick, MD).
2. RFP- and GFP-Lifeact [9] and GFP mice [7] 20–25 g body weight (*see* **Note 1**).

2.2 In Vivo Transient Transfection

1. SZX7 Stereo microscope mounted on an adjustable arm (Olympus America, Center Valley, PA).
2. Custom-made stereotactic device for salivary duct cannulation [11].
3. Polyethylene PE-5 cannula (0.008″I.D.×0.020″O.D.) (Strategic Applications Incorporated, Libertyville, IL).
4. Histoacryl tissue adhesive (TissueSeal, Ann Arbor, MI).
5. 1 mL Plastic syringes.
6. 30G 1/2 in. needle.

7. In vivo-jet PEI polyethyleneimine (PEI) (Polyplus Transfection, New York, NY).
8. Plasmid DNA purified from maxi-prep kit (Qiagen, Valencia, CA) (*see* **Note 2**).

2.3 Cardiac Perfusion Fixation

1. 1 M HEPES Buffer pH 7.3 (Quality Biological, Inc., Gaithersburg, MD).
2. 4 % Formaldehyde.
3. 0.05 % Glutaraldehyde.
4. Ultrapure water.
5. Monoject 60 mL syringes, SURFLO winged infusion set 25G × ¾″ (Terumo, Somerset, NJ), 3-way valve (*see* **Note 3**).
6. 70 % EtOH.
7. Surgical instruments: Operating scissors (11.5 cm straight); #7 curved tip tweezers (one with blunt and one with sharper tips), 25 cm curved tip forceps, microscissors (World Precision Instruments, Sarasota, FL) (*see* **Note 4**).

2.4 Cryosectioning and Immunostaining

1. O.C.T compound (Tissue-Tek, Torrance, CA).
2. Disposable Base Molds (Electron Microscopy Sciences, Hatfield, PA).
3. Liquid nitrogen and isopentane.
4. Cryostat (Leica CM1900, Buffalo Grove, IL).
5. Cryostat blade.
6. Histobond Silane coated microscope slides (VWR, Radnor, PA).
7. #1.5 coverslips (Corning, Corning, NY).

2.5 Microscope and Imaging Setup

1. Inverted confocal microscope (Olympus IX-81 with a Fluoview1000 scanner, Olympus America, Center Valley, PA) equipped with a motorized stage [12].
2. Custom-made immobilization stage [12].
3. Stage insert for 35 mm dishes to accommodate a 40 mm glass coverslip (Olympus America, Center Valley, PA) [11].
4. Glass 40 mm round coverslips, # 1.5 (Bioptechs, Butler, PA).
5. Objective heater (Bioptechs, Butler, PA).
6. Gauze sponges 4″ × 4″ (Tyco Healthcare, Gosport, UK) to be used as blankets.
7. Disposable Foot Warmers (Heat Factory, Vista, CA).
8. IX81 inverted confocal microscope, equipped with a Fluoview-1000 scanning unit (Olympus America, Center Valley, PA).

9. Plan-Apo 60×, 1.2 NA, water-immersion objective. Plan-Apo 60×, 1.42 NA, oil objective (Olympus America, Center Valley, PA) UPLSAPO 10×.

2.6 Imaging Software

1. For processing time-lapse imaging: Metamorph (Molecular Devices, Sunnyvale, CA), ImageJ (NIH, Bethesda, MD). For 3D reconstructions: Imaris (Bitplane, South Windsor, CT).

3 Methods

The procedures described here have been developed to: (1) investigate the dynamics of F-actin recruitment at the apical plasma membrane in the SSGs upon stimulation of exocytosis using IVM, and (2) to study the machinery regulating the recruitment of actin using a complementary pharmacological approach and indirect immunofluorescence. IVM relies on the use of fluorescently tagged proteins that can be either expressed in adult animals or introduced into mouse germ lines. In adult animals, genes can be delivered to selected organs using different approaches: One example being the administration of transgenes to the rat submandibular salivary glands through the salivary duct (Wharton's duct) by using either non-viral or viral methods [13, 14]. Focusing specifically on non-viral delivery, we express fluorescently tagged Lifeact in the acinar cells by mixing plasmid DNA with polyethyleneimine (PEI), a molecule extensively used for in vivo siRNA delivery [15]. Here, we described the details for the in vivo transfection of fluorescently tagged Lifeact, but the procedure can be easily adapted to transfect any other construct.

In mice, due to the reduced size of the Wharton's duct, the same approach has been more difficult to implement without damaging the organ. However, this issue has been overcome by the generation of mice expressing either GFP- or RFP-Lifeact [9]. With respect to the rats, transgenic mice offer the possibility to image F-actin dynamics in every cell population in the tissue and ensure homogeneous expression levels of the transgene. On the other hand, in rats, fluorescent Lifeact can be co-transfected with other markers or with constructs that may affect regulated exocytosis, thus providing information on the molecular machinery underlying this process.

In both experimental systems, mice and rats, we have been able to visualize F-actin dynamics upon stimulation of regulated exocytosis by a subcutaneous injection of isoproterenol (ISOP). In addition, we have developed a procedure to extract quantitative information about the kinetics of F-actin assembly in vivo. Finally, we have complemented the imaging in both species with the use of pharmacological agents that perturb the dynamics of the actin cytoskeleton, and with a procedure to label for several intracellular markers by using indirect-immunofluorescence. Finally, the procedures described below can be used in a modular fashion, as illustrated in

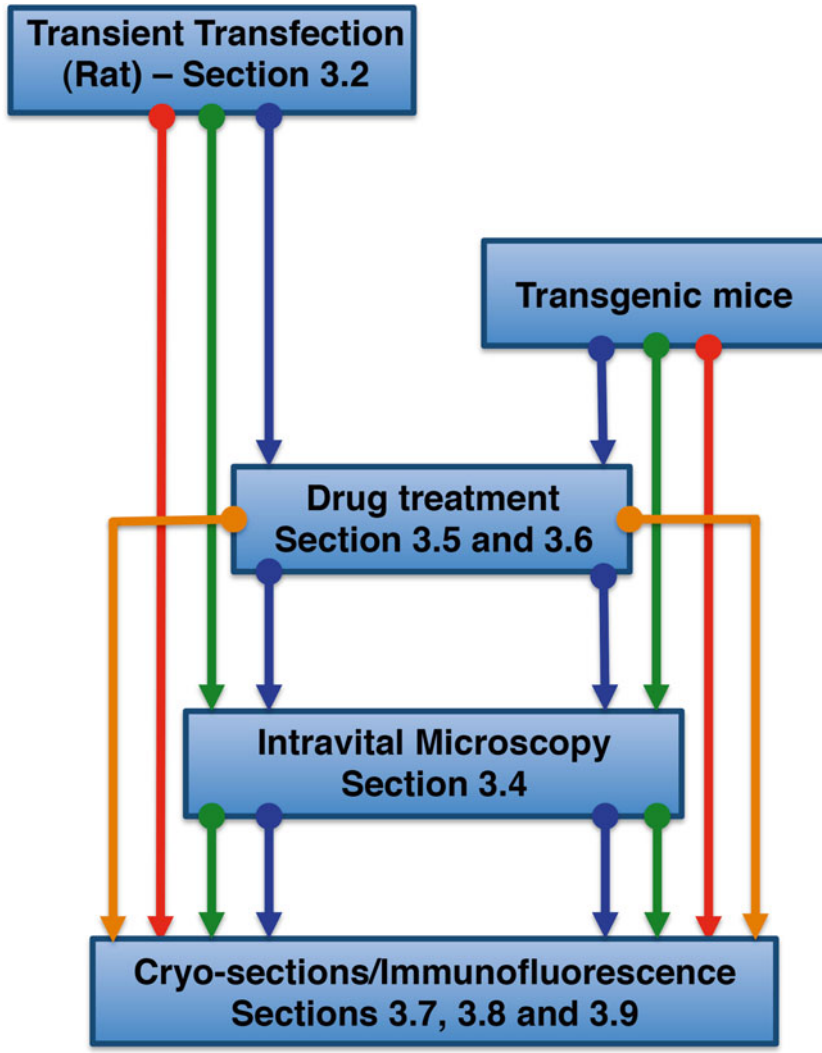

Fig. 1 General layout of procedures for probing the dynamics and regulation of the actin cytoskeleton in the SSGs of mice and rats, which can be extended to other subcellular structures. Intravital microscopy (IVM) experiments with mice and rats follow similar protocols, differing mainly in that introduction of fluorescent probes into rats is accomplish through transient transfection, while transgenic mice would serve for a similar purpose. The SSGs can further be treated pharmacologically to perturb the regulation of F-actin assembly and also fixed and immuno-stained to investigate the involvement of molecules that may regulate F-actin dynamics during regulated exocytosis

the diagram in Fig. 1, in order to better suit the specific questions that the investigator seeks to address.

3.1 Animal Preparation

The procedures to prepare both mice and rats for IVM, which include pre-anesthesia, anesthesia, surgical procedures, and positioning of the animals on the microscope stage, have been extensively described elsewhere [11].

3.2 Transfection of Fluorescently Tagged Lifeact via Cannulation of the SSGs

1. Place the anesthetized rat on a stereotactic device [11] with mandibles held open and the tongue bent back into the mouth to prevent the obstruction of the airways.
2. Move the stereotactic device under the stereomicroscope and tilt it to approximately a 45° angle. Adjust the focus to visualize the area below the tongue. The two orifices of the Wharton's duct will appear as two small flaps.
3. Grab the PE-5 cannula with a pair of tweezers close to the tip. Gently push the orifice with the tip of the cannula until it gets inserted into the duct (*see* **Note 5**). Do the same for both orifices, if transfecting both glands.
4. Apply a small drop of Histoacryl tissue glue around the cannulated orifices, and let it dry.
5. Prepare the transfection mixture. Typically, efficient transfection is achieved by using 12–24 μg of plasmid DNA/gland. Mix 50 μl of 10 % glucose with the plasmid DNA and adjust the volume to 100 μl (solution 1). Mix 50 μl of 10 % glucose with 7.5 μl of Jet PEI and adjust the volume to 100 μl (solution 2). Mix solution 1 and solution 2 and incubate them for 30 min at room temperature.
6. Aspirate the transfection mixture with a syringe (30-gauge needle) and make sure that no air bubbles are released when injecting the fluid. Connect the needle to the cannula without piercing the tubing.
7. Inject the transfection mixture gradually over a 5 min time period by applying gentle pressure on the plunger.
8. Remove the cannula and the syringe from the mouth and allow the animal to recover in the cage. A warm environment should be provided to facilitate the recovery and the animal should be monitored for at least 2 h.
9. After 12–48 h from the injection, perform IVM (*see* **Note 6**).

3.3 Intravital Microscopy

1. Set up the microscope with a 60× objective (oil or water) connected to an objective heater to maintain the temperature at 37–38 °C.
2. Set up the stage and position the animal with the glands exposed and immobilized as previously described for rats [11] and mice [16].
3. Set imaging parameters to approximately 320 × 320 pixels and 4 microseconds per pixel (resulting in a scanning speed of 0.4 s/frame) and with a 0.2 μm/pixel spatial scale (field of view of approximately 50 μm × 50 μm). In order to image the assembly of F-actin around the secretory granules, the optical thickness should be set between 0.9 and 1.2 μm.

To excite GFP-Lifeact and the RFP-Lifeact use a wavelength of 488 nm (peak power 0.5 mW) and 561 nm (peak power 1 mW), respectively.

4. Use epifluorescence illumination to locate the cells expressing the transgene.
5. Image the cell by confocal microscopy and select the appropriate focal plane, which should include the apical plasma membrane that is enriched with Lifeact (Fig. 2).
6. Acquire an image to be used as a reference to correct for changes in focus and shifts in the xy direction that are due to the motion artifacts.
7. Inject 0.1 mg/kg of ISOP sub-cutaneously (SC) and image in time lapse mode for 10–15 min.
8. After 1–2 min, a Lifeact "ring" appears around the secretory granules (Fig. 2). Within 40–60 the ring shrinks in diameter and disappears, designating the completion of the integration of the secretory granule into the APM.
9. Manually correct for any shift in the xyz directions.
10. Save the images in the appropriate format to be used with the available image processing software.

3.4 Optimization of the Administration of the Drugs Affecting the Actin Cytoskeleton

1. Before performing IVM to study the effect on regulated exocytosis of a drug that perturbs the actin cytoskeleton, it is necessary to determine the conditions for its administration (i.e., concentration and incubation time). To this end we use a mouse that expresses cytoplasmic GFP [7] and that enables the visualization of the secretory granules. The rationale for using this mouse is that when the cytoskeleton is impaired the secretory granules do not collapse normally, and instead form large vacuoles due to the stimulation of compound exocytosis. This is a quick assay that can rapidly determine the concentration of the drug necessary to perturb regulated exocytosis (*see* **Note 7**).
2. Surgically expose both glands as previously described [11, 16].
3. Install on the exposed glands a small circular ring (0.5–0.75 cm thick) made from cutting a 1 mL syringe (Fig. 3a). Secure the ring having its edges covered by the skin.
4. Pour the inhibitor into the ring (*see* **Note 8**).
5. After 20 min stimulate exocytosis by injecting SC 0.1 mg/kg ISOP.
6. After 20 min stop the process by performing intra-cardiac perfusion of the fixative (*see* Subheading 3.7) (*see* **Note 9**).
7. Excise the glands and fix further in 4 % formaldehyde for 1 h at R.T.

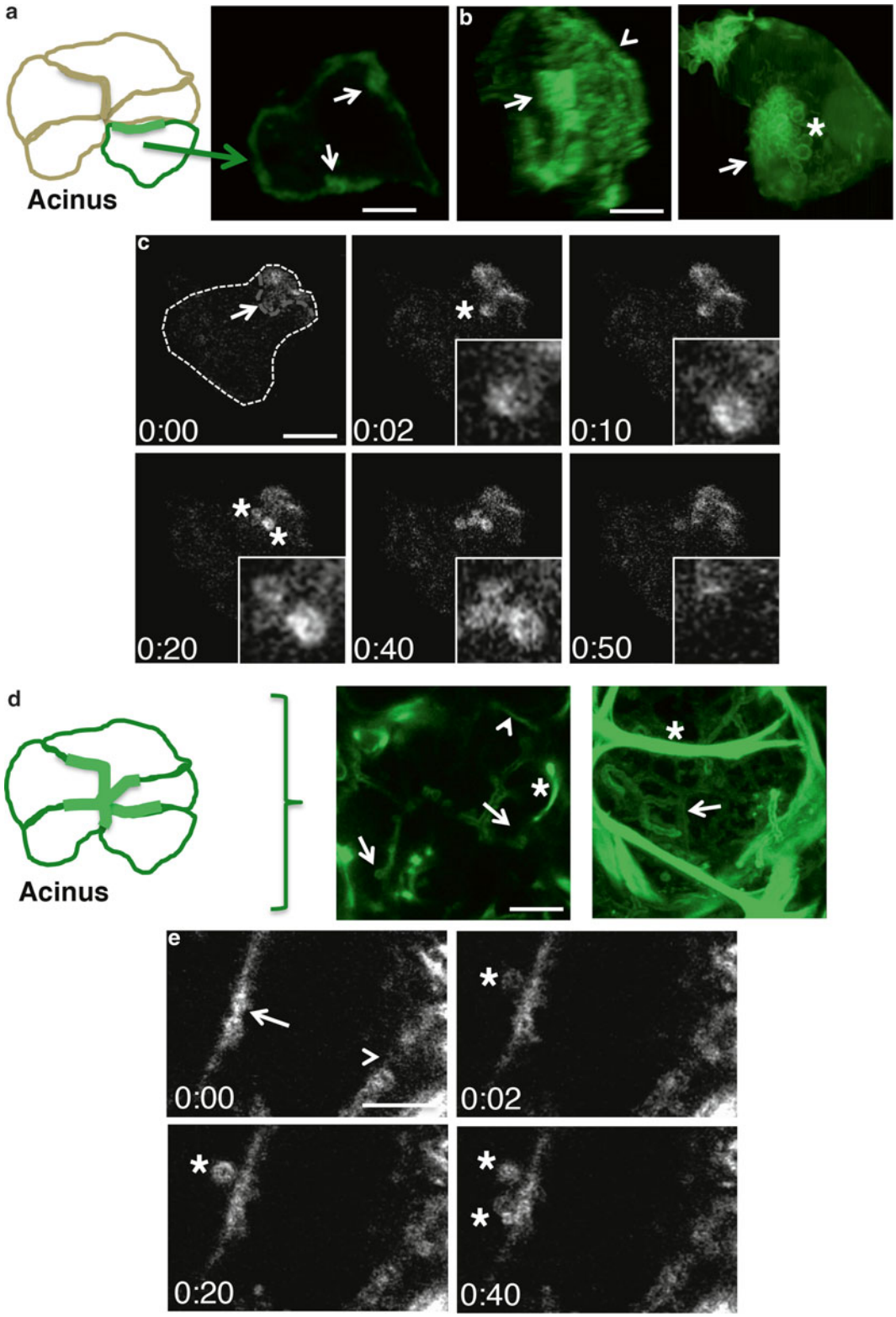

Fig. 2 Lifeact dynamics in transfected rats (**a–c**) and transgenic mice (**d**, **e**). (**a–c**) Transient transfection typically results in one transfected cell per acinus (**a**, *left diagram*). Rats were transfected with GFP-Lifeact and individual acinar cells were imaged before (**a** *right panel*, **b** *left panel*) or after (**b** *right panel*, **c**) SC injection of ISOP. Single slice (**a**) or volume rendering of 3D stacks (**b**) show the basolateral (*arrow*) and the apical (*arrowhead*)

8. Image the glands by confocal microscopy to assess any effect on regulated exocytosis (Fig. 3b). Drugs disrupting the cytoskeleton will generate large vacuoles [7].
9. Label the actin cytoskeleton to determine the efficacy of the drug (*see* Subheading 3.8).

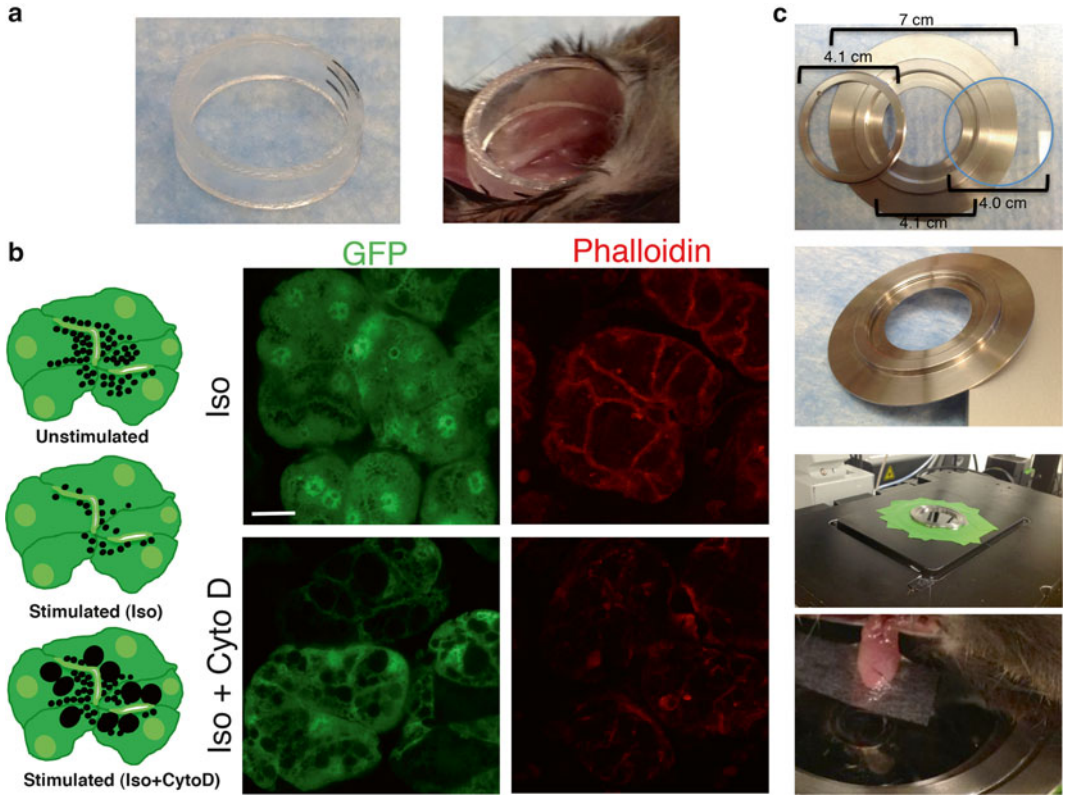

Fig. 3 Set up for bathing the salivary glands in pharmacological inhibitors. (**a**) Bathing ring cut from a 1 mL syringe, and example of its insertion into the anesthetized animal. (**b**) The exposed SSGs of anesthetized GFP mice were bathed in either saline (*upper panels*) or 10 μM cytochalasin D (*lower panels*) for 20 min followed by stimulation of exocytosis for 10 min. SSGs were fixed by perfusion, and labeled for phalloidin. The animals treated with cytochalasin D displayed large vacuoles as a result of swelling and compound exocytosis due to actin depolymerization (as shown, by phalloidin staining). Scale bar, 10 μm. (**c**) Stainless steel chamber used for bathing SSGs in pharmacological drugs during intravital imaging

Fig. 2 (continued) plasma membrane and the secretory granules (*asterisk*). (**c**) Time-lapse series of the dynamics of Lifeact recruitment around granules. The broken line highlights the cell border, whereas the *arrow points* to the apical plasma membrane (*green line*); *asterisks* are placed near Lifeact rings around the secretory granules. Scale bars, 5 μm. (**d**, **e**) In transgenic mice, GFP-Lifeact is expressed in all the acinar cells (**d**, *left diagram*). Single slide (**d**, *center*) and max projection of a 3D stack (**d**, *right*) show the basolateral (*arrow*) and the apical (*arrowhead*) plasma membrane and the myoepithelial cell (*asterisk*) that also express GFP-Lifeact. (**e**) Time-lapse series of recruitment and loss of Lifeact (*left*). Apical plasma membrane (*arrow*) and secretory granules (*asterisks*) are shown. Scale bar, 5 μm

3.5 IVM of Salivary Glands Exposed to Drugs Affecting the Actin Cytoskeleton

1. Place the animal with the exposed glands onto the microscope stage using the bathing chamber (Fig. 3c) (*see* **Note 10**).
2. Fill the chamber with the drug in saline at the appropriate concentration (*see* **Note 11**).
3. After 20 min begin imaging and stimulate exocytosis by SC injection of 0.1 mg/kg ISOP (*see* **Note 12**).
4. At the end of the imaging session, intracardiac fixation and immunofluorescence can be performed (*see* Subheadings 3.6 and 3.7).

3.6 Intra-cardiac Perfusion of the Fixative in the Live Animal

1. Place the fixative and saline in a water bath at 37 °C (*see* **Note 13**).
2. Place a Styrofoam board inside of a plastic container, which is capable of holding excess fluids and blood.
3. Place the anesthetized animal ventral side up and pin its feet in a stretched out position.
4. Load two 60 mL syringes with the pre-warmed saline and fixative and connect them to the 3-way valve (*see* **Note 14**).
5. Wet the skin on the ventral side of the animal with 70 % EtOH.
6. Remove the skin from the ventral side of the animal. Make an incision in the skin starting at the navel and proceed to cut up towards the mouth (be careful not to cut through the membrane underneath). At the shoulder joints, cut laterally to allow the skin to be peeled open and repeat at the lateral incision at the pelvic girdle. Use forceps and fingers to peel back the skin layer and pin it to the board.
7. Remove the abdominal membrane to reveal the internal organs and the lower part of the sternum: At the navel, gently cut the membrane upwards. Then, cut membrane flaps laterally and pin them to the board.
8. Clamp the end tip of the sternum with the curved tip forceps and proceed to cut up the sides of the rib cage while pulling the sternum towards the mouth to reveal the thoracic cavity.
9. Insert a needle into the left ventricle of the heart, cut the right atrium and proceed to fix the animal by first injecting pre-warmed saline at 1–2 mL/min until the blood flowing from the atrium becomes clear. Inject pre-warmed fixative at 1–2 mL/min (*see* **Note 15**).

3.7 Whole Mount Staining of the Tissue

1. Once the animal is thoroughly fixed (*see* **Note 16**), excise the glands and place them in 4 % formaldehyde for 1 h at room temperature. Then, slice the glands in half and fix them again in 4 % formaldehyde for an additional 30 min.
2. Place the sliced tissue in block solution (composed of 10 % FBS in PBS, 0.02 % saponin and 0.02 % NaN_3) overnight at 4 °C.

3. Incubate with the primary antibody in the presence of saponin for the required length, wash the primary, and incubate with a secondary antibody mixed with fluorescently labeled phalloidin (*see* **Note 17**).
4. Wash three times with block solution and store in block at 4 °C until ready to image (*see* **Note 18**).

3.8 Cryosections and Labeling Procedures

1. Dispense the OTC compound into the disposable base molds without creating any bubbles.
2. After intra-cardiac fixation, excise the glands, cut them in half, and fully immerse them in the OTC compound.
3. Carefully bring the bottom of the disposable base molds to the surface of liquid nitrogen and hold them there until the OTC compound fully freezes (*see* **Note 19**).
4. Place the frozen gland embedded in OTC into the cryostat and cut sections (10–15 μm in thickness).
5. Quickly place the sections on the silane coated side of the slide and once the sections have fully melted and adhered to the slide, move them to room temperature (*see* **Note 20**).
6. Proceed to stain and/or mount and image the sections.

3.9 Quantitative Analysis of the Lifeact Recruitment Around the Secretory Granules

1. Import the raw time-lapse series into ImageJ (Fig. 4).
2. Use the Stackreg plugin (rigid body option) to stabilize the frames and eliminate shift in the XY plane (*see* **Note 21**).
3. Use the rectangular region selection tool to crop the image series.
4. Save the image series as a Tiff image sequence and import it into Metamorph using the quick build stack option.
5. Identify secretory granule fusion profiles on which Lifeact is recruited and highlight the edges of those areas using the region tool (*see* **Note 22**) (Fig. 4).
6. Use the display region measurements tool to view the integrated fluorescence intensity of the ROIs in all the frames of the time-lapse series.
7. Select the parameters to record for data logging including:
   (a) Integrated fluorescence intensity
   (b) ROI label
   (c) Frame number
8. Record the raw data in an excel file using the log data tool.
9. Normalize the raw data for the fluorescence intensity just before the onset of Lifeact recruitment (*see* **Note 23**) and plot the data versus time elapsed (Fig. 4).

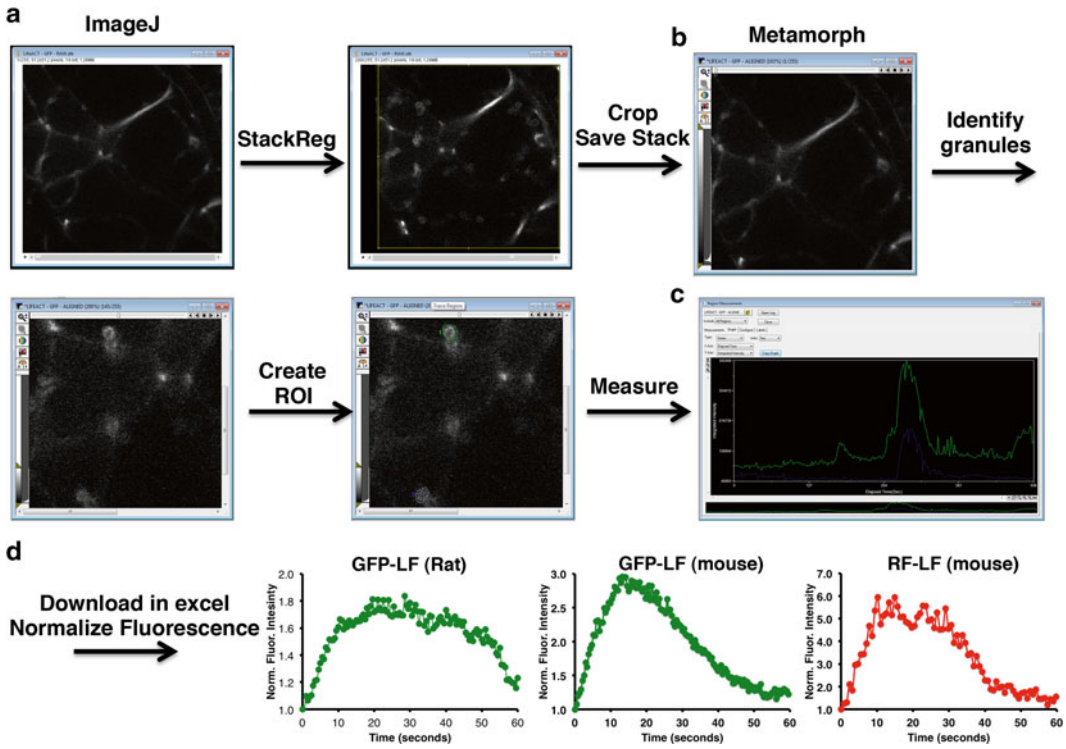

Fig. 4 Analysis of the Lifeact recruitment around the secretory granules. (**a**) Time series in tiff format are processed with ImageJ. Images in the series are aligned by applying the plug-in Stackreg. (**b**) After processing the stabilized series is cropped to eliminate the discarded areas, saved as tiff series, and opened with Metamorph. The secretory granules coated with Lifeact are highlighted and ROI are created with the region function. (**c**) The integrated fluorescence intensities are measured and plotted as a function of time using the "region measurement" function. This allows to identify the beginning of the exocytic events that will be used to normalize the fluorescence intensity. (**d**) The data are exported in excel files and processed to generate the curves. A comparison between GFP-Lifeact transfected in rats and transgenic mice expressing GFP- or RFP-Lifeact is shown

4 Notes

1. We use both males and female mice since we did not notice any gender difference in either the extent or the kinetics of the exocytic events.
2. We noticed that cDNAs cloned in Clontech vectors give the best transfection yield. Alternatively, cDNA can be delivered in rats by using adenoviral vectors. PEI targets the plasmid DNA primarily to acinar cells, whereas adenovirus drives the transgene expression to both acinar and ductal cells.
3. Connect the 3-way valve with the two 60 mL syringes and winged infusion set.

4. Instruments should be cleaned and sterilized before use.
5. Do not apply too much pressure, as the mucosa can be ruptured, damaging the duct, and causing bleeding from the mucosa.
6. Before performing IVM, determine the yield of transfection on a separate set of rats. Some variability may occur depending on the quality of the plasmid preparation, the batch of PEI, and the operator. After 12–48 h from the transfection expose the salivary glands, as previously described [11], excise, and place them in ice-cold saline. The tissue can be imaged for maximum 30 min after the excision. Select 10 random fields of view per gland using a 10× dry objective and acquire the images by confocal microcopy using a large pinhole (5–10 μm optical slice). Score the number of cells per field of view and divide them by the area. Typically, both GFP- and RFP-Lifeact are expressed in 5–10 cells/mm^2.
7. We have previously established that to block the collapse of the secretory granules the optimal conditions are 10 μM cytochalasin D or 10 μM of latrunculin A in saline for 20 min. We will use these drugs as an example but the same approach can be used for any other molecule.
8. Make sure that the glands are fully bathed in the drug. If the chamber is leaky, keep adding more inhibitor for the length of the experiment. The dose of the drug and the length of the incubation have to be established depending on the goal of the experiment. Finally, keep the animal warm with a heat lamp.
9. Perfusion of the fixative in mice and rats gives the quickest fixation of the SSGs, which ensures the best structural preservation.
10. The bathing chamber is made of stainless steel to provide a frame for holding a coverslip that enables imaging the exposed glands of the live animal, and to create a reservoir that ensures a constant exposure of the tissue to the drug.
11. Make sure that the glands are fully bathed in the drug. The dose and the length of the incubation have to be established depending on the goal of the experiment. It is important to maintain the body temperature of the animal by exposing it to a heat lamp. However, closely monitor for excessive heating that may provoke the evaporation of the drug. If this occurs, add fresh drug as necessary.
12. The time to wait before stimulating exocytosis may vary depending on the concentration and penetration rate of the drug.
13. Fixative is composed of 4 % formaldehyde, 0.05 % glutaraldehyde, and 200 mM HEPES buffer at pH 7.3 to be made fresh right before use.

14. Make sure the tubing is primed and that no air bubbles are pushed through the syringe. Also, push a few mL of saline through the needle to clear the line of any fixative prior to starting the procedure.
15. Saline can be injected within 30 s to 1 min in mice and about within 1–1.5 min in rats. It is best to start injecting the fixative while the animal is still alive and therefore it is important to rapidly perform the steps between the opening of the chest cavity and injecting into the heart. Finally, avoid inserting the needle too far into the left ventricle, as it could penetrate the wall of the heart between the right atrium and left ventricle, which would reduce the pressure in the vascular system.
16. Over-fixation may cause excessive background due to the glutaraldehyde, and can also interfere with the labeling.
17. Proper conditions for the primary and secondary antibody have to be determined for each case. As for the phalloidin, we recommend to incubate 0.5 U/ml in block solution for 30 min at RT.
18. Samples cannot be stored for more than 1 week.
19. Be careful not to crack the tissue or to drop it into the liquid nitrogen while the OTC compound is still freezing. Alternatively, place the base molds on top of frozen isopentane, which is placed in liquid nitrogen, since the freezing is quick, yet more gentle and better preserves the membranes.
20. Make sure to move the slides to room temperature within 30 s after their first contact with the sections. Avoid leaving the slides too long in the cryostat to prevent distorting the sections.
21. If necessary, crop the image and repeat the Stackreg alignment on a smaller area to ensure proper XY stabilization. Measurements will be inaccurate without proper image alignment.
22. Fusion profiles of Lifeact are identifiable as rings of intense fluorescence that form and collapse over 40–60 s and can reach up to 1 μm in diameter.
23. The onset of recruitment can be identified as a sharp increase in integrated fluorescence intensity within the selected region of interest.

Acknowledgments

This research was supported by the Intramural Research Program of the NIH, National Institute of Dental and Craniofacial Research.

References

1. Sollner TH (2003) Regulated exocytosis and SNARE function. Mol Membr Biol 20:209–220
2. Burgess TL, Kelly RB (1987) Constitutive and regulated secretion of proteins. Annu Rev Cell Biol 3:243–293
3. Porat-Shliom N, Milberg O, Masedunskas A, Weigert R (2013) Multiple roles for the actin cytoskeleton during regulated exocytosis. Cell Mol Life Sci 70:2099–2121
4. Eitzen G (2003) Actin remodeling to facilitate membrane fusion. Biochim Biophys Acta 1641:175–181
5. Pittet MJ, Weissleder R (2011) Intravital imaging. Cell 147:983–991
6. Weigert R, Porat-Shliom N, Amornphimoltham P (2013) Imaging cell biology in live animals: ready for prime time. J Cell Biol 201:969–979
7. Masedunskas A, Sramkova M, Parente L et al (2011) Role for the actomyosin complex in regulated exocytosis revealed by intravital microscopy. Proc Natl Acad Sci U S A 108:13552–13557
8. Masedunskas A, Porat-Shliom N, Weigert R (2012) Regulated exocytosis: novel insights from intravital microscopy. Traffic 13:627–634
9. Riedl J, Flynn KC, Raducanu A et al (2010) Lifeact mice for studying F-actin dynamics. Nat Methods 7:168–169
10. Riedl J, Crevenna AH, Kessenbrock K et al (2008) Lifeact: a versatile marker to visualize F-actin. Nat Methods 5:605–607
11. Masedunskas A, Sramkova M, Parente L, Weigert R (2013) Intravital microscopy to image membrane trafficking in live rats. Methods Mol Biol 93:153–167
12. Masedunskas A, Weigert R (2008) Intravital two-photon microscopy for studying the uptake and trafficking of fluorescently conjugated molecules in live rodents. Traffic 9:1801–1810
13. Adriaansen J, Perez P, Goldsmith CM, Zheng C, Baum BJ (2008) Differential sorting of human parathyroid hormone after transduction of mouse and rat salivary glands. Human Gene Ther 19:1021–1028
14. Kawakami S, Higuchi Y, Hashida M (2008) Nonviral approaches for targeted delivery of plasmid DNA and oligonucleotide. J Pharm Sci 97:726–745
15. Aigner A (2006) Gene silencing through RNA interference (RNAi) in vivo: strategies based on the direct application of siRNAs. J Biotechnol 124:12–25
16. Masedunskas A, Porat-Shliom N, Tora M, Milberg O, Weigert R (2013) Intravital microscopy for imaging subcellular structures in live mice expressing fluorescent proteins. J Vis Exp (79). doi:10.3791/50558

Chapter 29

Measurement of Dynamic F-Actin Changes During Exocytosis

Peter Thorn

Abstract

Exocytosis requires the fusion of vesicle membrane to the cell membrane. It is tightly regulated and orchestrated in space and time by diverse cellular mechanisms. It has long been recognized that one of these mechanisms is an essential role played by the cytoskeleton. In particular, accumulating evidence shows that the F-actin network is engaged during the final stages of vesicle interactions with the cell membrane. Using a combination of methods it is now possible to gain insights into F-actin dynamics and reveal its role during exocytosis. Here, we describe the use of two-photon and confocal microscopy to visualize F-actin changes at the cell membrane during exocytosis.

Key words F-actin, Exocytosis, Confocal, Two-photon, Microscopy

1 Introduction

The potential involvement of F-actin in the exocytic process has been suggested from observations of the positioning and changes in F-actin structure [1–3] and in changes to proteins linked to F-actin [4, 5], that are associated with secretion. Further work showed that manipulation of F-actin polymerization affected secretion [6–8].

Since this work there is now a body of data demonstrating that F-actin remodeling as a factor in controlling secretion from a range of cell types including: chromaffin cells [9], pancreatic beta cells [10, 11], pancreatic acinar cells [12–15], lacrimal acinar cells [16], type 2 alveolar cells [17], endothelial cells [18], and neurons [19]. However, there is not a unified view on the role that F-actin plays in the control of the mechanisms of secretion. There is evidence in some cells that F-actin changes precede exocytosis [2, 4] with a view that these changes might be necessary for the secretory granules to make contact with the plasma membrane [20]. However, in cells where secretory granules are large enough to be imaged it has been shown that F-actin remodels to coat the granules [18, 21] in a step that occurs post-fusion [14, 22]. The role of this F-actin coat is

Andrei I. Ivanov (ed.), *Exocytosis and Endocytosis*, Methods in Molecular Biology, vol. 1174,
DOI 10.1007/978-1-4939-0944-5_29,

unclear but has been suggested to stabilize the fused granule [13] or to play a more active role in expulsion of granule content [17, 18].

Methodologically, much of this work involves phalloidin staining in fixed tissues. The earlier work, using methods to live-cell identify F-actin, had concerns that this might affect actin polymerization and stability. New probes, such as Lifeact short amino acid fluorescent reporter [23] which, as we have shown among others, does not appear to affect cell function [24], are now being used to reveal the behavior and role of F-actin during exocytosis [25].

2 Materials

2.1 Cell Preparation

1. Wild-type mice on either CD1 or C57BL/6 genetic background. Typically the mice are used at 6–8 weeks old and 25–30 g body weight.
2. Transgenic Lifeact-EGFP mice were obtained as a gift from Professor Roland Wedlich-Soldner [26]. These transgenic mice were produced on a 128SV/C57BL/6 background using a cytomegalovirus enhancer, chicken actin promoter to drive expression of Lifeact-GFP in all tissues.
3. Na-rich extracellular solution: 135 mM NaCl, 5 mM KCl, 10 mM glucose, 2 mM $MgCl_2$, 2 mM $CaCl_2$, and 10 mM HEPES, pH adjusted to pH 7.4 with NaOH. To make 200 ml of this solution, weigh 1.58 g NaCl, 0.074 g KCl, 0.041 g $MgCl_2$, 0.06 g $CaCl_2$, 0.476 g HEPES, and 0.36 g glucose.
4. Collagenase (with either Worthington Biochemical CLSPA or Sigma Collagenase type 1) dissolved in the Na-rich extracellular solution at a concentration of 250 units/ml. Aliquot and store at –20 °C.

2.2 Experimental Cell Procedures

1. Sulforhodamine B, a typical long-wavelength dye dissolved at 400 μM in Na-rich extracellular solution. For a shorter emission dye we use 8-Methoxypyrene-1,3,6 trisulfonate (MPTS) at 400 μM final concentration in Na-rich extracellular solution.
2. Lysine fixable FITC-dextran with 3,000 and 10,000 MW. Make up a stock solution of the dextran in distilled water and dilute it in the Na-rich extracellular solution to give a final concentration of 2 mg/ml.

2.3 Fixation and Processing for Confocal Immunofluorescence

1. 80 mM PIPES buffer, adjusted to pH 7.4 with KOH.
2. Phosphate buffered solution (PBS) without Ca^{2+} or Mg^{2+}.
3. 4 % Paraformaldehyde (PFA) in either PBS or Na-rich extracellular solution. PFA is made up fresh from powder every day, with a stock of 8 % (w/v) in distilled water (depolymerised by vigorous stirring, heating to 65–70 °C and adding 3 drops of 1 M NaOH—the solution should clear completely within minutes) that is then diluted 50:50 with a double-strength

Na-rich solution or PIPES buffer. This gives a final concentration of 4 % PFA.

4. Triton-X 100, 0.1 % (w/vol) solution in PBS.
5. Alexa-488 or Alexa-633 phalloidin (Invitrogen Life Science). To make a working solution, dilute the phalloidin stock 1:200 in PBS.

3 Methods

3.1 Preparation of Tissue Samples

1. Mice should be humanely euthanized according to the animal protocol approved by the Institutional IACUC (this study was approved by the Anatomical Biosciences Ethics Committee of the University of Queensland).
2. Quickly dissect out the pancreas, which lies along the spleen and small intestine. The dissection does not have to be precise, and the aim is not to isolate the whole pancreas. Place the dissected part of the pancreas (approximately 1 cm × 1 cm size) into a 35 mm plastic dish.
3. Inject 0.75 ml of collagenase (in Na-rich extracellular solution). The injection is intended to inflate the pancreatic tissue and it may take multiple attempts of injection (recovering the collagenase solution back into the syringe each time) before the tissue inflates. This injection step should take less than 2 min.
4. Place the fragment of pancreas in a 1.5 ml eppendorf tube and incubate for 5–7 min (dependent on the strength of the particular batch of collagenase) at 37 °C.
5. Daw the tissue up through a 1 ml pipette where the pipette tip has been cut to enlarge the opening to around 2 mm in diameter. Vigorously triturate the tissue up and down through the 1 ml pipette which should lead to the breaking down of the tissue into smaller fragments.
6. Collect these pancreatic fragments in a 15 ml tube. As fragments are taken out of the eppendorf tube, fresh Na-rich extracellular solution should replace the removed volume. Trituration and removal of these smaller fragments should be performed within 5 min.
7. The 15 ml tube, containing the smaller tissue fragments, should now have a fluid volume of approximately 5 ml and should be filled up to 10 ml with extracellular solution and centrifuged at moderate g (e.g., 1,000 × *g*) for 3 min (*see* **Note 1**).
8. Discard the supernatant and gently resuspend the pellet in 3 ml of Na-rich extracellular solution.
9. Gently resuspend the pellet and triturate through a 1 ml pipette, this time with the normal tip opening. Around 30 gentle up-down triturations are needed to further break up the tissue (*see* **Note 2**).

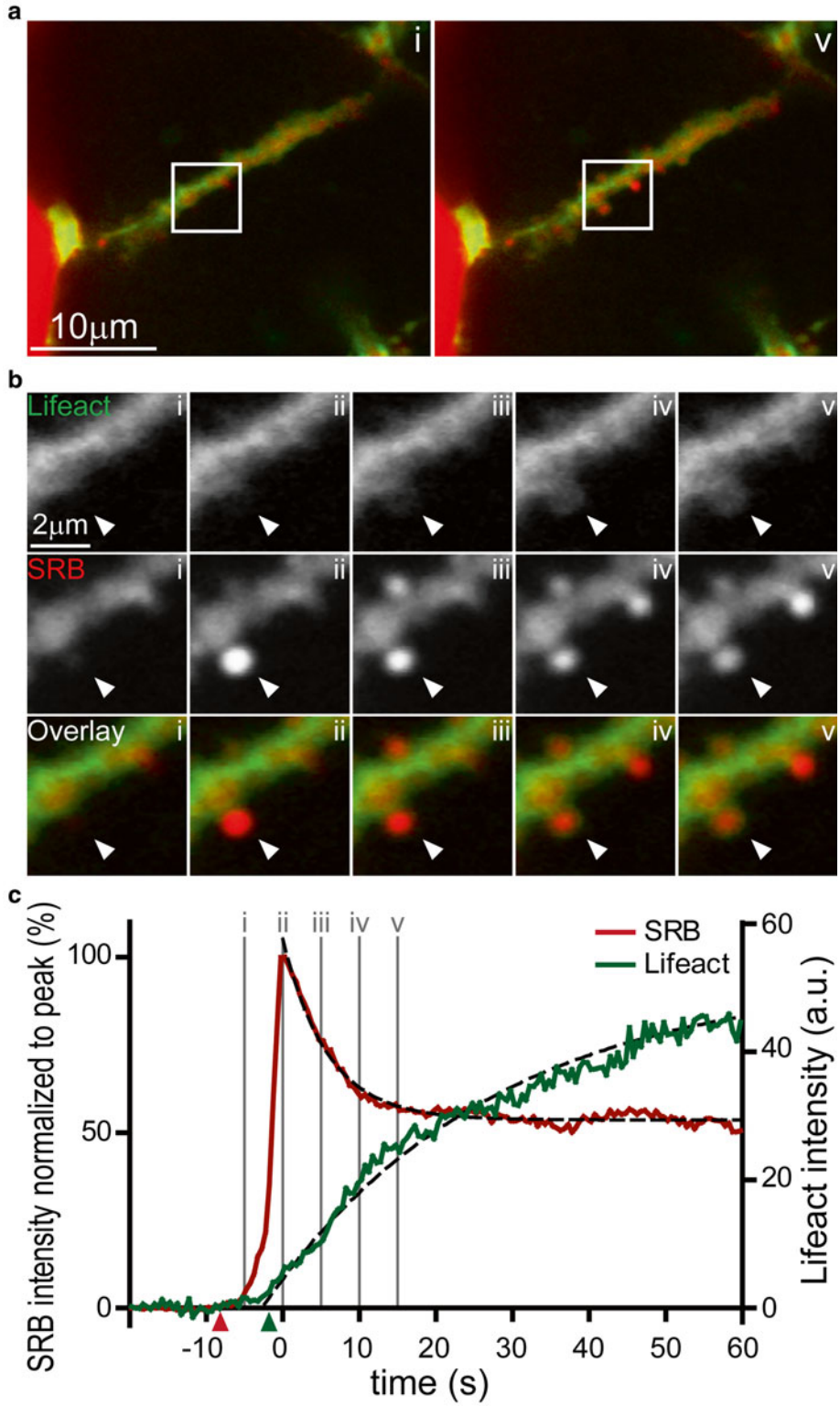

Fig. 1 Two-photon imaging of exocytic fusion and F-actin coating in pancreatic acinar cells. (**a**) Images show a lumen lying diagonally between two acinar cells identified with SRB (*red*) and Lifeact-EGFP (*green*). (**a**, i) is taken before the appearance of exocytic events at the time point indicated "i" on the graph of fluorescence intensity over time in panel (**c**). (**a**, v) is an image at a time point after stimulation. A number of exocytic events can be seen as bright spots of SRB fluorescence along the lumen; the time point "v" is indicated on the lower graph (**c**).

10. After trituration, fill up the tube with Na-rich extracellular solution to 10 ml, centrifuge again, discard the supernatant and resuspend the pellet in 3 ml of Na-rich extracellular solution.
11. The final stage is further gentle trituration and then the cell/tissue fragment preparation is ready for use (*see* **Notes 3** and **4**).

3.2 Two-Photon Imaging of Live Cells

After preparation of the pancreatic fragments, allow a small aliquot to adhere to poly-L-lysine coated coverslips for 1 min with subsequent cell washing in Na-rich extracellular solution. These coverslips can be used for either live-cell or fixed-cell imaging experiments.

1. We use a custom-made, video-rate, 2-photon microscope with a Sapphire-Ti laser [27], and usually a 60× oil immersion objective (NA 1.42, Olympus), providing an axial resolution (full width, half maximum) of ~1 μm (*see* **Note 5**).
2. We image exocytic events using extracellular Sulforhodamine B excited by femtosecond laser pulses at 850 nm, with fluorescence emission detected at 550–700 nm (*see* **Note 6**).
3. Mount coverslip-attached pancreatic tissue into a temperature-adjustable chamber, add SRB-containing Na-rich solution and mix well prior to imaging. Visually inspect the sample through the oculars and select better looking cells and cell clusters.
4. Perform two-photon imaging with resolution of 15 pixels/μm and data acquisition approximately 2 frames per second. These parameters are manually adjustable with our homemade setup but are usually computer-controlled on commercial machines.
5. We have recently switched to using the ScanImage control software, which provides a robust platform for image acquisition [28]. In addition, it has the functionality to control a range of peripherals which we use for example in the computer control of the Z focus.
6. Images are acquired and viewed in real time (*see* **Note 7**). During cell stimulation we can clearly observe exocytic events as the sudden appearance of bright spots of fluorescence as the extracellular dye enters the fusing granules. With the Lifeact-EGFP animals changes in the F-actin structures are simultaneously observed (Fig. 1). We use the 850 nm excitation

Fig. 1 (continued) (**b**) is an image sequence from the region (*box* in **a**) of Lifeact-EGFP and SRB and the overlay, for two exocytic events. The images were taken at the time points i, ii, iii, iv, and v as indicated on the graph in panel (**c**). (**c**) is a graph of fluorescence changes over time taken from a region of interest placed over the lower exocytic event (indicated by an *arrowhead*). SRB fluorescence, normalized to the peak, rises rapidly and then decays to a plateau. The simultaneously recorded Lifeact-EGFP signal rises slowly as F-actin coats the granule. The *black dotted lines* were mono-exponential fits to the data with τ values of 6.9 s (SRB) and 29.4 s (Lifeact-EGFP). Figure taken, with permission, from Jang et al. [24]

wavelength (the same as for SRB excitation, which means that both channels are captured simultaneously) and collect the emitted light at 450–520 nm (*see* **Note 8**).

7. Perform image analysis using either Metamorph or ImageJ. A typical analysis would involve selecting small (~1 μm) regions of interest to measure the average changes of fluorescence intensity associated with the single exocytic events. In the analysis we typically subtract the background fluorescent signals. For analysis of the SRB recordings, we normalize all records to the amplitude of the first peak response. In the case of the Lifeact-EGFP imaging, the signal intensity is expressed in arbitrary units.

3.3 Fluorescence Labeling and Imaging of Fixed Tissues

1. Fix the cells in freshly prepared 4 % paraformaldehyde in PBS for 30 min at room temperature.
2. Wash the cells in a PBS that does not contain Ca^{2+} or Mg^{2+}. The washing is repeated 3 times over a period of 5 min.
3. Permeabilize the cells with 0.5 % Triton-X 100 in PBS for 10 min at room temperature. Wash two times with Ca^{2+}/Mg^{2+}-free PBS.
4. Label F-actin with Alexa 488 or Alexa 633 conjugated phalloidin applied for 15–30 min at room temperature.
5. For a counter-immunolabeling apply a blocking solution (typically donkey serum and fish skin gelatin) for 1 h.
6. Wash the cells one time with Ca^{2+}/Mg^{2+}-free PBS before adding the primary antibody (dilutions need to be determined empirically) for 1 h.
7. Wash the cells three times with Ca^{2+}/Mg^{2+}-free PBS before adding the secondary antibody for 1 h.
8. Wash the cells three times with Ca^{2+}/Mg^{2+}-free PBS, followed by mounting (e.g., in the Prolong Antifade reagent) on glass slides.
9. Fixed specimens can be imaged with any confocal microscope. We use an Olympus BX61 upright confocal laser scanning microscope, with a 63× objective lens (NA 1.3), and an optical slice depth of ~1 μm. Images are collected with the appropriate filters and captured in sequential tracks to minimize cross talk to less than 2 % (*see* **Notes 6** and **7**).

4 Notes

1. The centrifugation settings are not critical. The aim of each centrifugation steps is to obtain a loose pellet of the pancreatic tissue.
2. The second two steps of trituration are determined by specific requirements for the final pancreatic fragments. If you need a

preparation composed of predominantly single cells, more triturations will be required. Conversely, do fewer triturations if preparations with larger multicellular tissue fragments are needed. We generally work with tissue fragments composed by 10–100 cells, which provides good compromise between workability of the preparation (i.e., penetration of antibodies in immunofluorescence studies) and preservation of cell polarity and tissue structures, such as acinar lumens.

3. We have found that the preparation can be fragile immediately after the trituration and that it is beneficial therefore to leave it for approximately 10 min before performing experiments.
4. In our hands, this acute preparation remains viable for at least 3 h at room temperature.
5. The utility of two-photon imaging in these experiments is twofold. Firstly, it enables us to work with tissue fragments and position the plane of focus deep within the tissue. This means that the cells of interest are entirely surrounded by neighboring cells, which exactly recapitulates their spatial position in the intact pancreas. Secondly, the method we use to track exocytosis relies on bathing the whole preparation in the fluorescent dye. Confocal microscopy would excite the entire volume of dye and lead to problems with out-of-focus fluorescence. In contrast, two-photon microscopy only excites the dye in the plane of focus, and thus the entry of fluorescent dye into each fusing granule appears as a bright spot of fluorescence on the dark background of the cell interior.
6. The settings for image acquisition are in accordance with a common process for optimizing image collection. The main parameters to be aware of on the illumination side are the intensity of illumination, the speed of acquisition and the amount of averaging. Together these variables dictate the amount of light that irradiates the specimen. Too little light will lead to poor excitation and very low emitted signal. Too much light will lead to possible problems with photo-bleaching of the dye and photo-damage of the tissue.
7. For collection of the emission signal it is important to adjust the detector gain (and possibly offset) to maximize the spread of the signal intensities across the acquisition scale. The optimum is for the darkest regions to be closest to zero and the brightest regions to be close to saturation (e.g., close to 255 on an 8 bit scale).
8. We usually quantitatively analyze our images which requires careful planning during image acquisition. When comparing a control sample with a test sample, it is critical to image both samples at the same settings.

Acknowledgements

This work was supported by an Australian Research Council Grant DP110100642 and National Health and Medical Research Council Grants APP1002520and APP1020764.

References

1. Orci L, Gabbay KH, Malaisse WJ (1972) Pancreatic beta-cell web: its possible role in insulin secretion. Science 175:1128–1131
2. Burgoyne RD, Cheek TR (1987) Reorganization of peripheral actin-filaments as a prelude to exocytosis. Biosci Reps 7: 281–288
3. Aunis D, Bader MF (1988) The cytoskeleton as a barrier to exocytosis in secretory-cells. J Exp Biol 139:253–266
4. Vitale ML, Delcastillo AR, Tchakarov L, Trifaro JM (1991) Cortical filamentous actin disassembly and scinderin redistribution during chromaffin cell stimulation precede exocytosis, a phenomenon not exhibited by gelsolin. J Cell Biol 113:1057–1067
5. Roth D, Burgoyne RD (1995) Stimulation of catecholamine secretion from adrenal chromaffin cells by 14-3-3-proteins is due to reorganization of the cortical actin network. FEBS Lett 374:77–81
6. Matter K, Dreyer F, Aktories K (1989) Actin involvement in exocytosis from pc12 cells – studies on the influence of botulinum-c2 toxin on stimulated noradrenaline release. J Neurochem 52:370–376
7. Pendleton A, Koffer A (2001) Effects of latrunculin reveal requirements for the actin cytoskeleton during secretion from mast cells. Cell Motil Cytoskeleton 48:37–51
8. Shupliakov O, Bloom O, Gustafsson JS et al (2002) Impaired recycling of synaptic vesicles after acute perturbation of the presynaptic actin cytoskeleton. Proc Natl Acad Sci U S A 99:14476–14481
9. Burgoyne RD, Morgan A, Osullivan AJ (1989) The control of cytoskeletal actin and exocytosis in intact and permeabilized adrenal chromaffin cells – role of calcium and protein kinase C. Cell Signal 1:323–330
10. Thurmond DC, Gonelle-Gispert C, Furukawa M, Halban PA, Pessin JE (2003) Glucose-stimulated insulin secretion is coupled to the interaction of actin with the t-SNARE (target membrane soluble N-ethylmaleimide-sensitive factor attachment protein receptor protein) complex. Mol Endocrinol 17:732–742
11. Tomas A, Yermen B, Min L, Pessin JE, Halban PA (2006) Regulation of pancreatic beta-cell insulin secretion by actin cytoskeleton remodelling: role of gelsolin and cooperation with the MAPK signalling pathway. J Cell Sci 119: 2156–2167
12. Valentijn KM, Gumkowski FD, Jamison JD (1999) The subapical actin cytoskeleton regulates secretion and membrane retrieval in pancreatic acinar cells. J Cell Sci 112:81–96
13. Nemoto T, Kojima T, Oshima A, Bito H, Kasai H (2004) Stabilization of exocytosis by dynamic f-actin coating of zymogen granules in pancreatic acini. J Biol Chem 279: 37544–37550
14. Turvey MR, Thorn P (2004) Lysine-fixable dye tracing of exocytosis shows f-actin coating is a step that follows granule fusion in pancreatic acinar cells. Pflugers Arch 448:552–555
15. Jungermann J, Lerch MM, Weidenbach H et al (1995) Disassembly of rat pancreatic acinar cell cytoskeleton during supramaximal secretagogue stimulation. Am J Physiol 268:G328–G338
16. Jerdeva GV, Wu KJ, Yarber FA et al (2005) Actin and non-muscle myosin ii facilitate apical exocytosis of tear proteins in rabbit lacrimal acinar epithelial cells. J Cell Sci 118:4797–4812
17. Miklavc P, Hecht E, Hobi N et al (2012) Actin coating and compression of fused secretory vesicles are essential for surfactant secretion – a role for Rho, formins and myosin II. J Cell Sci 125:2765–2774
18. Nightingale TD, White IJ, Doyle EL et al (2011) Actomyosin II contractility expels von Willebrand factor from Weibel-Palade bodies during exocytosis. J Cell Biol 194:613–629
19. Morales M, Colicos MA, Goda Y (2000) Actin-dependent regulation of neurotransmitter release at central synapses. Neuron 27:539–550
20. Oheim M, Stuhmer W (2000) Tracking chromaffin granules on their way through the actin cortex. Eur Biophys J 29:67–89
21. Valentijn JA, Valentijn K, Pastore LM, Jamieson JD (2000) Actin coating of secretory granules during regulated exocytosis correlates with the release of RAB3D. Proc Natl Acad Sci U S A 97:1091–1095

22. Sokac AM, Co C, Taunton J, Bement W (2003) Cdc42-dependent actin polymerization during compensatory endocytosis in *Xenopus* eggs. Nat Cell Biol 5:727–732
23. Riedl J, Crevenna AH, Kessenbrock K et al (2008) Lifeact: a versatile marker to visualize F-actin. Nat Methods 5:605–607
24. Jang Y, Soekmadji C, Mitchell JM, Thomas WG, Thorn P (2012) Real-time measurement of F-actin remodelling during exocytosis using Lifeact-EGFP transgenic animals. PLoS One 7:e39815
25. Wen PJ, Osborne SL, Zanin M et al (2011) Phosphatidylinositol(4,5)bisphosphate coordinates actin-mediated mobilization and translocation of secretory vesicles to the plasma membrane of chromaffin cells. Nat Commun 2:491
26. Riedl J, Flynn KC, Raducanu A et al (2010) Lifeact mice for studying F-actin dynamics. Nat Methods 7:168–169
27. Thorn P, Fogarty KE, Parker I (2004) Zymogen granule exocytosis is characterized by long fusion pore openings and preservation of vesicle lipid identity. Proc Natl Acad Sci U S A 101:6774–6779
28. Pologruto TA, Sabatini BL, Svoboda K (2003) Scanimage: flexible software for operating laser scanning microscopes. Biomed Eng 17:13

INDEX

Andrei I. Ivanov (ed.), *Exocytosis and Endocytosis*, vol. 1174,
DOI 10.1007/978-1-4939-0944-5, © Springer Science+Business Media New York 2014

F

G

H

I

K

L

M

N

O

P

Q

R

S

T

U

V

Z